Strained and Unstrained Sandwich Compounds: From Small Molecules to Polymers

A Thesis Submitted to the College of

Graduate Studies and Research

in Partial Fulfillment of the Requirements

for the Degree of Doctor of Philosophy

in the Department of Chemistry

University of Saskatchewan

Saskatoon

Canada

By

Bidraha Bagh

Permission to Use

In presenting this thesis in partial fulfilment of the requirements for a Postgraduate degree from the University of Saskatchewan, I agree that the Libraries of this University may make it freely available for inspection. I further agree that permission for copying of this thesis in any manner, in whole or in part, for scholarly purposes may be granted by the professor or professors who supervised my thesis work or, in their absence, by the Head of the Department or the Dean of the College in which my thesis work was done. It is understood that any copying or publication or use of this thesis or parts thereof for financial gain shall not be allowed without my written permission. It is also understood that due recognition shall be given to me and to the University of Saskatchewan in any scholarly use which may be made of any material in my thesis.

Requests for permission to copy or to make other use of material in this thesis in whole or part should be addressed to:

Head of the Department of Chemistry

University of Saskatchewan

Saskatoon, Saskatchewan (S7N 5C9), Canada

ABSTRACT

The synthesis and characterization of aluminum, gallium, and indium dichlorides decorated with the bulky Mamx [Mamx = 2,4-*t*Bu_2-6-(Me_2NCH_2)C_6H_2] ligand are described. The salt-metathesis reaction of (Mamx)ECl_2 (E = Al, Ga) with dilithioferrocene and dilithioruthenocene yielded strained [1]ferrocenophanes ([1]FCPs) and [1]ruthenocenophanes ([1]RCPs), respectively, with aluminum and gallium as bridging elements. Galla[1]ruthenocenophane was isolated from the reaction mixture, while other aluminum- and gallium-bridged [1]FCPs and [1]RCPs spontaneously ring-open polymerized under conditions of their formation reactions and produced metallopolymers. Galla[1]ruthenocenophane was polymerized using Karstedt's catalyst, which yielded poly(ruthenocenylgallane). Aluminum- and gallium-bridged bis(ferrocenyl) species were prepared by reacting lithioferrocene with respective dichlorides. DFT calculations were performed to study the structure and reactivity of these new [1]metallocenophanes. Particularly, the role of the bulky Mamx ligand and its influence on the high reactivity of these strained sandwich species was investigated. (Mamx)$InCl_2$ was reacted with dilithioferrocene and resulted in indium-bridged [1]FCP, [1.1]FCP and oligomers. However, the reaction of (Mamx)$InCl_2$ with dilithioferrocene, substituted with two isopropyl groups *ortho* to lithium atoms, resulted in inda[1]ferrocenophane selectively. However, this inda[1]ferrocenophane could not be isolated as it spontaneously polymerized under conditions of its formation reaction.

The synthesis and characterization of aluminum and gallium dichlorides decorated with the slim *p*-$SiMe_3$Ar′ [*p*-$SiMe_3$Ar′ =5-Me_3Si-2-(Me_2NCH_2)C_6H_3] and Mpysm [Mpysm = (2-C_5H_4N)Me_2SiCH_2] ligands are described. These dichlorides were utilized

to synthesize group-13-bridged [1.1]FCPs and bis(ferrocenyl) species. Bis(ferrocenyl) species with $SiMe_2$- and $SiEt_2$-bridges were described as well. Two similar species, bis(1'-bromoferrocenyl)dialkylsilane (alkyl = Me, Et) were also prepared. The reaction of bis(1'-lithioferrocenyl)dialkylsilane with tin and gallium dichlorides resulted in unsymmetrically bridged [1.1]FCPs as well as poly(ferrocene)s with two different elements as altering bridges. These poly(ferrocene)s consist of a series of linear and cyclic species. Using either crystallization or column chromatography, some species were isolated. The reactions of dilithioferrocene with dialkyltin dichlorides also yielded polymers that contained a mixture of linear and cyclic species. Some species were isolated by column chromatography. These [1.1]FCPs, bis(ferrocenyl) species and other isolated species with heavier group 13 and/or group 14 element bridges contained two or more iron redox centers. The electronic communication between these redox centers were investigated using several electrochemical methods.

ACKNOWLEDGMENTS

I am grateful to my supervisor Dr. Jens Müller for his support, guidance and encouragement during my studies as a Ph.D. student.

I would like to thank the University of Saskatchewan and Department of Chemistry for providing me with the opportunity to study here; the members of my advisory committee for their support and the staffs at the Saskatchewan Structural Science Centre and the Department of Chemistry. In particular, I am grateful to Dr. Ian J. Burgess for his help with electrochemical studies and Dr. Keith C. Brown for his help with NMR measurements.

I would like to acknowledge all present and past members of the Müller group for their help and support. In particular, I would like to acknowledge Nora C. Breit for her support and inspiration.

I am grateful to my parents Provat and Rina Bagh, sister Mutiny and cousin Ritu for their support and encouragement for such a long time. I would like to acknowledge my friends Dr. Partha Pratim Jana, Dr. Aurab Chakrabarty, Dr. Sougat Misra and Dr. Satyajit Haldar for their moral support.

TABLE OF CONTENTS

LIST OF FIGURES

LIST OF SCHEMES

Scheme page

LIST OF CHARTS

LIST OF TABLES

LIST OF ABBREVIATIONS

Abbreviation

AC ……...…… alternating current

Ar' …….. 2-[(dimethylamino)methyl]phenyl

cod ……...…….. 1,5-cyclooctadiene

Cp …… cyclopentadienyl

CV ……...…….. cyclic voltammetry

dba ……...……. dibenzylideneacetone

DLS ……...…… dynamic light scattering

DSC ……. differential scanning calorimetry

FCP …… ferrocenophane

Fc ……...…… $(C_5H_5)Fe(C_5H_4)$

fc ……..……...……. $(H_4C_5)_2Fe$

GPC …….. gel permeation chromatography

Mamx ……...…….. 2,4-di-*tert*-butyl-6-[(dimethylamino)methyl]phenyl

MCP …… metallocenophane

Me_2Ntsi …….. [(dimethylamino)dimethylsilyl]bis(trimethylsilyl)methyl

Mpysm …… [dimethyl(2-pyridyl)silyl]methyl

pmeda ……. *N*,*N*′,*N*′,*N*″-pentamethyldiethylenetriamine

p-SiMe_3Ar' …….. 5-trimethylsilyl-2-[(dimethylamino)methyl]phenyl

Pytsi ……...……. [dimethyl(2-pyridyl)silyl]bis(trimethylsilyl)methyl

RCP …… ruthenocenophane

ROP ……...……. ring-opening polymerization

tmeda …… *N*,*N*,*N*′,*N*′-tetramethylethylenediamine

VT NMR …….. variable temperature nuclear magnetic resonance

CHAPTER 1
INTRODUCTION

Over last hundred years, strained cyclic organic compounds have captured immense devotion of scientists from different fields because of their usage as monomers in ring-opening polymerization (ROP) to yield organic polymers. As a consequence, strained cyclic organic compounds have been studied extensively. However, strained cyclic organometallic molecules containing transition metals such as metallacyclophanes are less studied, but have attracted considerable attention in past two decades. Metallacyclophanes are a class of sandwich compounds where the two π-hydrocarbons of the sandwich moiety are bridged by some elements. A particular type of metallacyclophane is [n]metallocenophane (**1**; Figure 1-1) where two cyclopentadienyl (Cp) anions of the sandwich unit are π-bound to the transition metal M in η^5-fashion and σ-bound to n bridging elements. The first strained metallacyclophane, a [2]ferrocenophane (FCP) with the bridging moiety C_2Me_4 (**2**; Figure 1-1), was discovered in 1960 by Rinehart Jr. et al. and it was suggested that analogous [1]FCPs would be too strained to exist.[1] Maybe as a result of this suggestion, serious investigation in this field was hindered for more than a decade; however in 1975, Osborne et al. finally synthesized [1]FCPs with silicon in bridging position (**3**; Figure 1-1).[2] While the initial work in this area was started on strained FCPs (**1**: M = Fe), this field of organometallic chemistry has been extended to many different metallacyclophanes with a wide variety of different metals, π-hydrocarbons and bridging elements such as [n]metallarenophanes (**4**; Figure 1-1), where the sandwich unit is composed of two benzene rings, and [n]troticenophanes (**5**:

M = Ti) or [n]trovacenophanes (**5**: M = V), where the transition metal is sandwiched between η^7-tropylium and η^5-cyclopentadienyl (Cp) ligand.

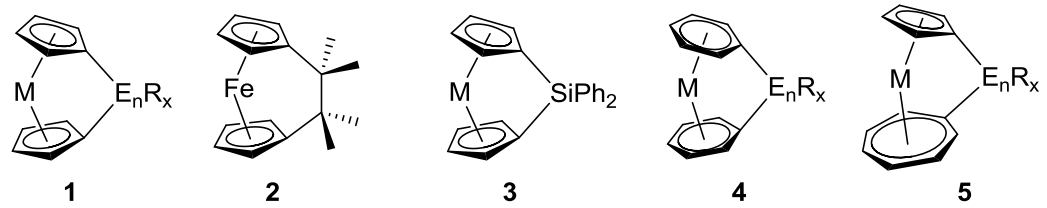

Figure 1-1. Metallacyclophanes.

In ferrocene as a parent metallocene, the two Cp rings are parallel to each other. The introduction of short *ansa*[n] bridges (n = 1, 2) affects the geometry of metallacyclophanes resulting in a ring-tilted structure. As illustrated in Figure 1-2, the tilt angel α is the angle between the planes of two Cp rings, showing the degree of ring tilt. In addition to the angle α, a series of angles can also describe the tilted structures of [n]metallocenophanes: β ($Cp_{centroid}$-C_{ipso}-E angle), δ ($Cp_{centroid}$-M-$Cp'_{centroid}$ angle) and θ (C_{ipso}-E-C'_{ipso} angle) (Figure 1-2).

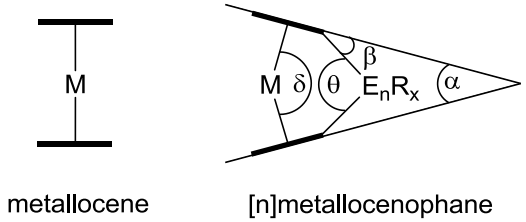

Figure 1-2. Set of angles to illustrate ring-tilt in [n]metallocenophanes.

The tilt angle α of [n]metallacyclophanes decreases with the increase of the number of bridging elements of the same kind; for example, the tilt angle α of trithia[3]ferrocenophane is 4.5°,[3] whereas that of the thia[1]ferrocenophane is 31.0°.[4] The angle α is inversely proportional to the size of bridging elements; the smaller the

bridging-element, the larger the angle is. The size of elements decreases along a row of the periodic table, therefore, α increases in the same direction; for instance, from aluminum (α ≈ 15° for alumina[1]ferrocenophane)[5] to silicon (α ≈ 21° for sila[1]ferrocenophane)[6] to phosphorus (α ≈ 27° for phospha[1]ferrocenophane)[7] to sulfur (α ≈ 31° for thia[1]ferrocenophane).[4] For the same reason, α decreases on descending down a group in the periodic table; for example, α of silicon-bridged [1]FCP (α ≈ 21°)[6] is higher than that of germanium-bridged [1]FCP (α ≈ 19°),[8] which is even higher than that of tin-bridged [1]FCP (α ≈ 14°).[9] The degree of tilting affects the energy of molecular-orbitals, which is reflected by a change of colors in metallacyclophanes bridged by increasingly smaller elements.[4] For instance, a gradual change in color is observed in FCPs bridged by the third period elements form red (λ_{max}: 478 nm for Me_2Si[1]FCP) to intense red (λ_{max}: 498 nm for PhP[1]FCP) to deep purple (λ_{max}: 504 nm for S[1]FCP). This red shift, caused by the progressively increase of tilting, can be rationalized by the gradual decrease of the HOMO-LUMO energy gap.[4]

There are two well-established routes for the synthesis of [n]metallacyclophanes. The most commonly employed strategy involves the salt-metathesis reaction of dilithio-sandwich compounds with element dihalides equipped with an appropriate ligand (Scheme 1-1). One of the vital steps for the preparation of [n]metallacyclophanes is the dilithiation of sandwich compounds, which is accomplished by using butyllithium and an amine base such as *N*,*N*,*N*′,*N*′-tetramethylethylenediamine (tmeda) and *N*,*N*,*N*′,*N*′,*N*″-pentamethyldiethylenetriamine (pmeda).[10] For the preparation of most of [1]metallacyclophanes, including compounds bridged by main-group elements from group 13 (B, Al, Ga), group 14 (Si, Ge, Sn), group 15 (P, As), group 16 (S, Se) and group

4 (Ti, Zr, Hf), the dilithiation of a sandwich compound is the commonly used method. The less preferred approach for the synthesis of [n]metallocenophanes, commonly referred to as the "flytrap" route, involves an appropriately bridged dianionic linker with an iron(II) dihalide (Scheme 1-1). The first metallacyclophane, the dicarba[2]ferrocenophane **2** (Figure 1-1) was synthesized by employing the "flytrap" route,[1] whereas the preparation of first [1]metallacyclophane, the silicon-bridged [1]FCP **3** (Figure 1-1), was achieved by the salt-metathesis reaction of dilithioferrocene·tmeda and diphenylsilicon dichloride.[2]

Scheme 1-1. Commonly employed synthetic routes for [n]metallocenophanes.

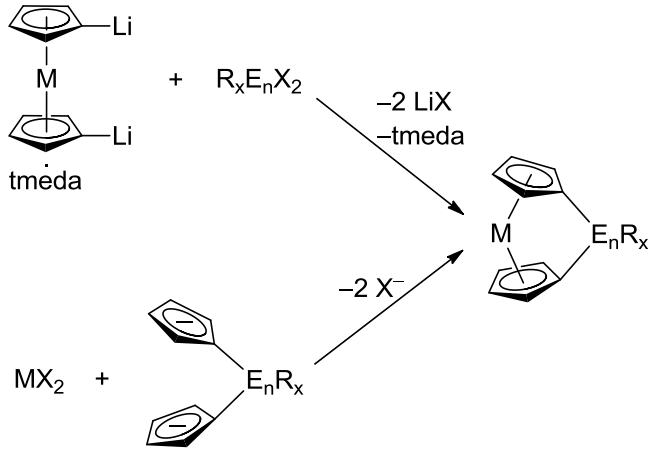

The deviation from the coplanar ring orientation in metallocenes into a tilted ring structure in [n]metallocenophanes introduces ring-strain, which can be released by ring-opening polymerization (ROP) resulting in poly(metallocene)s. In practice, high-molecular-weight metallopolymers cannot be accessed by the conventional polycondensation route. On the other hand, the chain-growth process of ROP is a very effective route to synthesize high-molecular-weight metallopolymers. Especially, [1]metallocenophanes with the large tilt angles are highly strained and are very

susceptible to release the strain by ROP. Calculations using density functional theory indicate that the tilt angle α plays the key role in determining the propensity toward ROP for FCPs.[11] In these studies, it was found that the energy required to tilt the Cp rings is similar to the experimentally determined ΔH^{ROP} value. The most important aspect is that the ROP of [1]metallocenophanes opens the door to readily produce metallopolymers with functionality determined by the presence of metals and spacers. In principle, metallopolymers can be fabricated into films, shapes and fibers by conventional polymer technology.

The first report on ROP of [1]metallocenophanes was published by Manners et al. who synthesized high-molecular-weight poly(ferrocenylsilane)s by the thermal ROP of silicon-bridged [1]FCPs.[12] To date, poly(ferrocenylsilane)s are an important class of metallopolymers and found applications in material science such as precursors to ceramics,[13] tunable components of photonic crystals displays[14] and redox-tunable capsules.[15] ROP within various templates affords nanostructure materials. Some ROP methods can be performed as a living polymerization, which gives access to block copolymers. Block copolymers in block-selective solvent allows the formation of nanoscopic aggregates of different morphologies such as cylinders, vesicles and spherical micelles, which shows considerable potentials for applications in nanotechnology.[16]

A comprehensive overview of all published metallacyclophanes is beyond the scope of this thesis and the reader is referred to recent reviews detailing the synthesis, characterization and ROP of metallacyclophanes with a wide variety of different metals, π-hydrocarbons and bridging elements.[17] Because of the importance for the thesis on hand, the following sections will offer an overview on the synthesis and characterization

of metallocenophanes with group 13 and 14 elements as bridges (Chapter 1.1) and their ROP to yield poly(metallocene)s (Chapter1.2). Moreover, a brief summary of [1.1]FCPs, bis(ferrocenyl) species and ferrocene-containing macrocycles (Chapter 1.3) will be provided, so that the reader has the proper background knowledge to judge the importance of other parts described in this thesis.

1.1 [1]Metallocenophanes

As mentioned before, Osborne et al. started the journey of [1]metallacyclophanes by synthesizing silicon-bridged [1]FCPs in 1975.[2] Since then, the family of [1]metallacyclophanes has grown enormously in last four decades. The most intensively studied [1]metallacyclophanes are [1]metallocenophanes, which contain a wide range of transition metals sandwiched between two Cp or substituted Cp rings. Following is a brief summary of [1]metallacyclophanes with group 13 or 14 in bridging positions.

As illustrated in Figure 1-3, all group 4 metals titanium, zirconium and hafnium have been introduced in [1]metallocenophanes, species which are commonomly called *ansa*-titanocenes, *ansa*-zirconocenes and *ansa*-halfnocenes, respectively. Theoretical studies on metallocenophanes suggested that species containing transition metals with less than two d electrons are unlikely to possess significant strain.[11] Therefore, *ansa*-metallocenes are expected to be unstrained. As shown in Figure 1-3, an extensive number of those *ansa*-complexes with group 14 elements (C, Si, Ge) as bridges (**6**) are described in literature.[18] Silicon-bridged *ansa*-titanocenes, *ansa*-zirconocenes and *ansa*-halfnocenes with substituted Cp rings (**7** and **8**; Figure 1-3) are also plentiful in literature.[18] Group-13-bridged *ansa*-metallocenes with Ti, Zr and Hf are very rare compared to their group-14-bridged analogues. In 1997, Shapiro et al. synthesized the first example of an *ansa*-zirconocene with a three-coordinated boron (**9**; Figure 1-3).[19] Two years later, boron-bridged *ansa*-titanocenes (**10**; Figure 1-3) was reported by Braunschweig et al.[20] Later, our group synthesized the first aluminum- and gallium-bridged *ansa*-zirconocenes (**11**; Figure 1-3) employing the sterically bulky Pytsi ligand.[21] In *ansa*-titanocenes, *ansa*-zirconocenes and *ansa*-halfnocenes, the Cp rings are inherently tilted. The fact that the bridging elements do not introduce much strain into the system, is realized by a low

increase of tilt angles in *ansa*-zirconocene (**11** with E = Al: α = 57.2°, $Me_2Si(C_5H_4)_2ZrCl_2$: α = 60.1°) as compared to the unbridged zirconocene dichloride (α = 53.5°). The attempted thermal and transition-metal-catalyzed (Pt(0)) ROP of [1]zirconocenophanes were unsuccessful and there is no literature evidence that suggests how significant the amount of strain these compounds possess. However, those *ansa*-complexes especially of titanium and zirconium have already proven to be a very efficient Ziegler-Natta-type catalyst for the olefin polymerization.

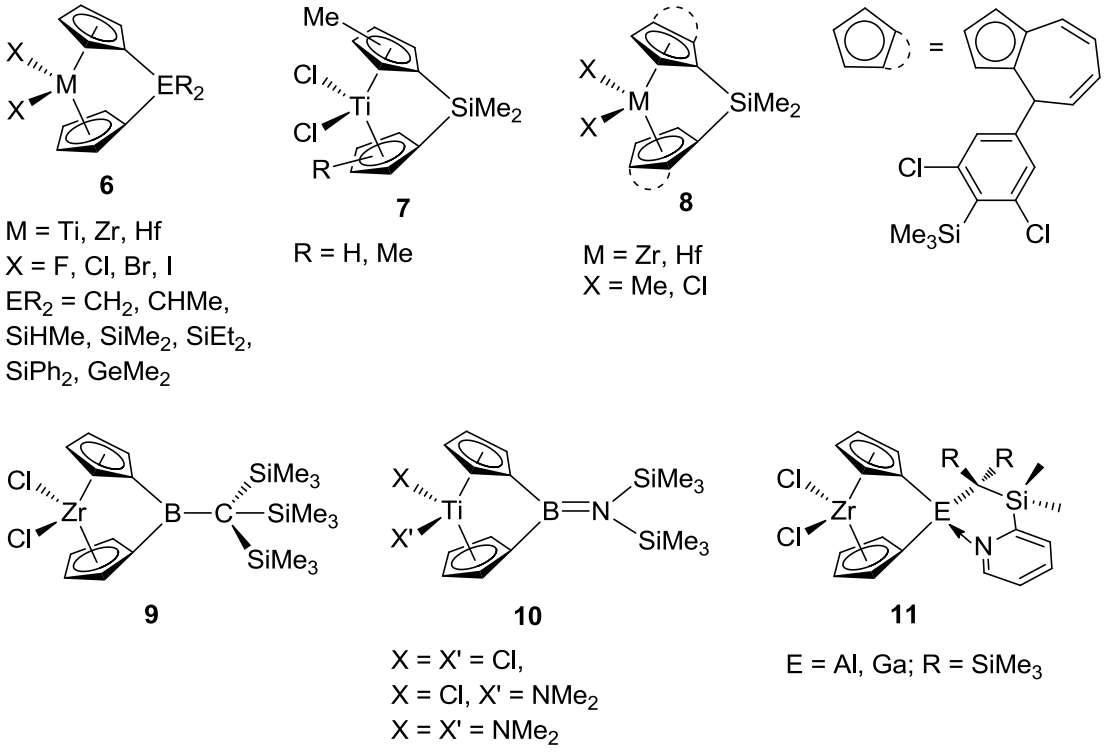

Figure 1-3. *Ansa*-Titanocenes, *ansa*-zirconocenes and *ansa*-halfnocenes with group 13 and 14 elements as bridges.

Ansa-metallocenes of group 5, 6 and 7 transition metals Nb[22] (group 5); Cr, Mo, W (group 6)[23] and Re (group 7)[24] are also known in the literature, however, containing only group 14 elements (C, Si) as bridges (**12**, **13**, **14**, **15**; Figure 1-4). Some of those [1]metallocenophanes possess high tilt angles, for instance the tilt angle α falls in the

range of 55-65° for [1]metallocenophanes of W. There is no evidence of a successful ROP of those species. However, Green et al. reported that **14b** was converted to insoluble polymeric material upon storing under N_2 for several months.[23d] No report describes how significant the amount of strain these *ansa*-complexes possess.

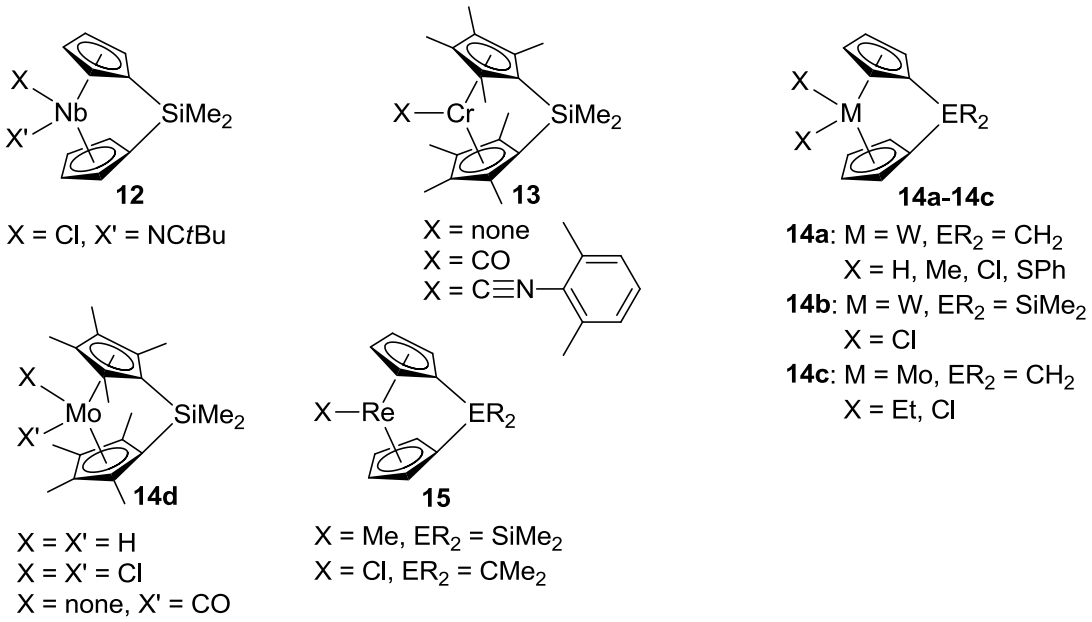

Figure 1-4. [1]Metallocenophanes of group 5, 6 and 7.

Though there is no report describing [1]metallocenophanes of group 9 and 10 transition metals, [1]metallocenophanes of group 8 metals (Fe, Ru) are abundant. Because of the direct relevance to this thesis, [1]ferrocenophanes and [1]ruthenocenophanes with group 13 and 14 elements as bridges will be discussed in details in the following subchapters.

1.1.1 Group-14-bridged [1]Ferrocenophanes

There is no example of carbon-bridged [1]FCP reported in literature. Scientists believe that carba[1]ferrocenephanes would be too strained to exist.

Though some researches on strained [1]metallacyclophanes had been carried out in seventies and eighties, the area was relatively unexplored until 1992 when Manners et al. synthesized high-molecular-weight polymers by ROP of sila[1]ferrocenophanes. The successful use of sila[1]ferrocenophanes as monomers for ROP has stimulated an intensive research in this field, which resulted in a vast range of sila[1]ferrocenophanes. Numerous silicon-bridged [1]FCPs (**16**) have been synthesized by employing the salt-metathesis route, which involves the reaction of dilithioferrocene and silicon dichlorides equipped with two organic ligands (Scheme 1-2).[2,6,10a,25]

Scheme 1-2. Synthesis of sila[1]ferrocenophanes.

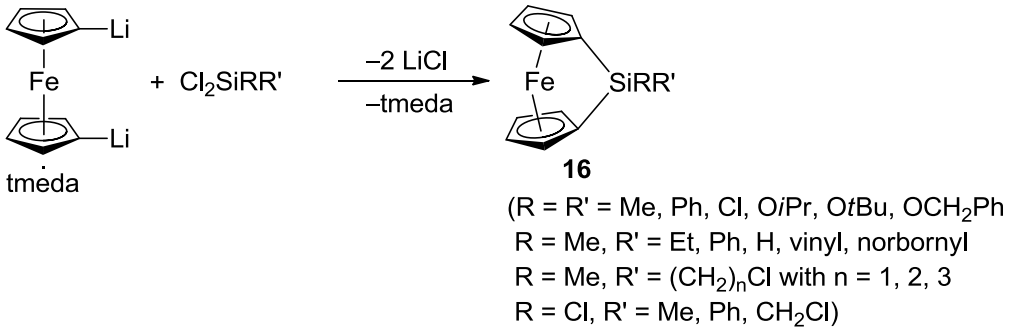

Scheme 1-3. Substitution reaction on dichlorosila[1]ferrocenophane.

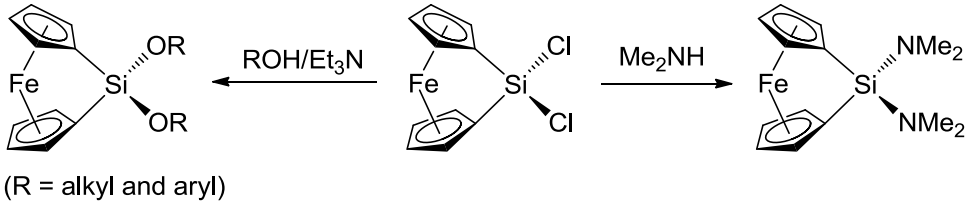

The $SiCl_2$-bridged [1]FCP serves as a precursor for other silicon-bridged [1]FCP. As illustrated in Scheme 1-3, chlorides can be replaced by amines, alcohols and phenols to give access to amino-, alkoxy-, and aryloxy-substituted sila[1]ferrocenophanes, respectively.[25b,25f] All these four-coordinated silicon-bridged [1]FCPs are structurally very similar with tilt angles in the range of 19-21°.

Manners et al. reported a [1]FCP (**17a**) with a hypercoordinated silicon atom, which was synthesized by the chloride substitution reaction of an unsymmetrically substituted sila[1]ferrocenophane by employing a lithium reagent at low temperature (-78 °C) (Scheme 1-4a).[26a] Hatanaka et al. synthesized another sila[1]ferrocenophane (**17b**) with a similar hypercoordinated silicon atom from a different unsymmetrically substituted silicon-bridged [1]FCP, employing a similar synthetic strategy (Scheme 1-4b).[26b] In the hypercoordinated silicon-bridged [1]FCPs, the five-coordinated silicon adopts a distorted trigonal bipyramidal geometry with elongated and, thus, weaker Si-Cp bonds.

Scheme 1-4. Synthesis of the hypercoordinated silicon-bridged [1]FCPs.

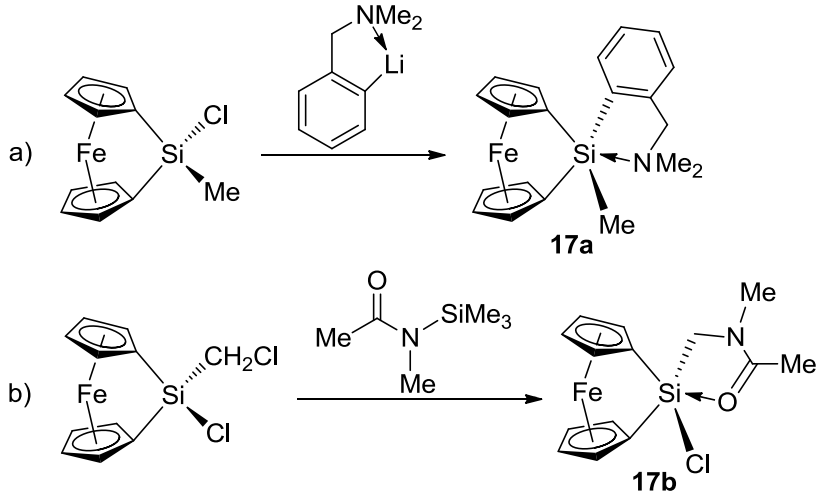

In 1980, Osborne et al. described the first spirocyclic [1]FCP (**18a**), where the silicon atom serves the role of the *ansa*-bridge for both ferrocenophane moieties (Figure 1-5).[25a] In the late nineties, Manners et al. reported another spirocyclic [1]FCP (**18b**) with silicon as a bridging element (Figure 1-5).[27] In **18a**, the silicon atom is sterically protected by four surrounding Cp rings, which might be the reason for its unusually stability against air and moisture. However, a considerable moisture sensitivity of **18b** arises from the fact that the silicon center lacks steric protection.

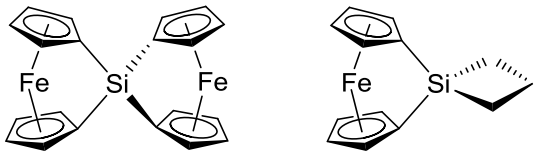

18a **18b**

Figure 1-5. Spirocyclic silicon-bridged [1]FCPs.

Various sila[1]ferrocenophanes with substituted Cp rings have been reported in literature (**19**-**25**; Figure 1-6).[28] The air and moisture stability of these sila[1]ferrocenophanes increases with the introduction of sterically bulky substituents on the Cp rings such as in **24** and **25**. The electron-donating alkyl substituents in these silicon-bridged [1]FCPs make the Cp rings more electron rich and, thus, the Fe-Cp bond strength increases. In compound **24**, the trimethylsilyl groups are stacked on top of each other and the steric repulsion of the bulky groups result in a highly tilted structure with unusually large tilt angle of 26.3°. However, the bulky *t*Bu groups in compound **25** lie between each other avoiding steric repulsion, which is reflected in a normal tilt angle of 20.3°.

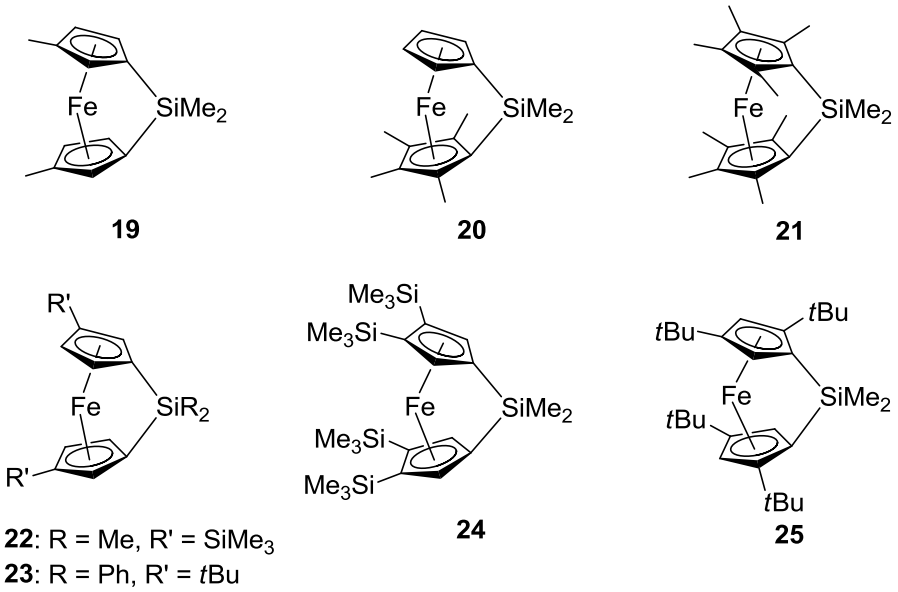

19 **20** **21**

22: R = Me, R' = $SiMe_3$
23: R = Ph, R' = *t*Bu

24 **25**

Figure 1-6. Sila[1]ferrocenophanes with substituted Cp rings.

Similar to the silicon-bridged [1]FCPs, various germa[1]ferrocenophanes have been reported.[8,25a,29] The germanium-bridged [1]FCPs have been synthesized by employing the salt-metathesis route (Scheme 1-5a). The spirocyclic [1]FCP **27** with germanium as a bridging element has been synthesized in a very similar way (Scheme 1-5b).[27] Germanium is larger in size than silicon and, thus, germa[1]ferrocenophanes have smaller tilt angles (α = 16-18°) compared to sila[1]ferrocenophanes (α = 19-21°).

Scheme 1-5. Synthesis of germa[1]ferrocenophanes.

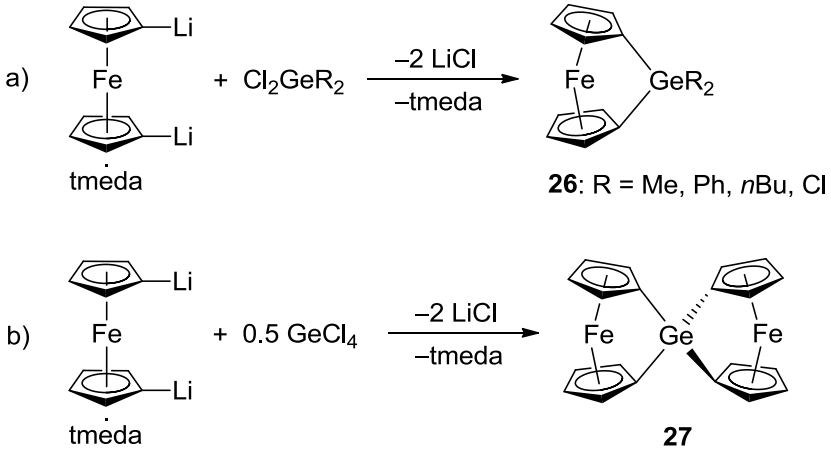

Scheme 1-6. Salt-metathesis reaction of dilithoferrocene and tin dichlorides.

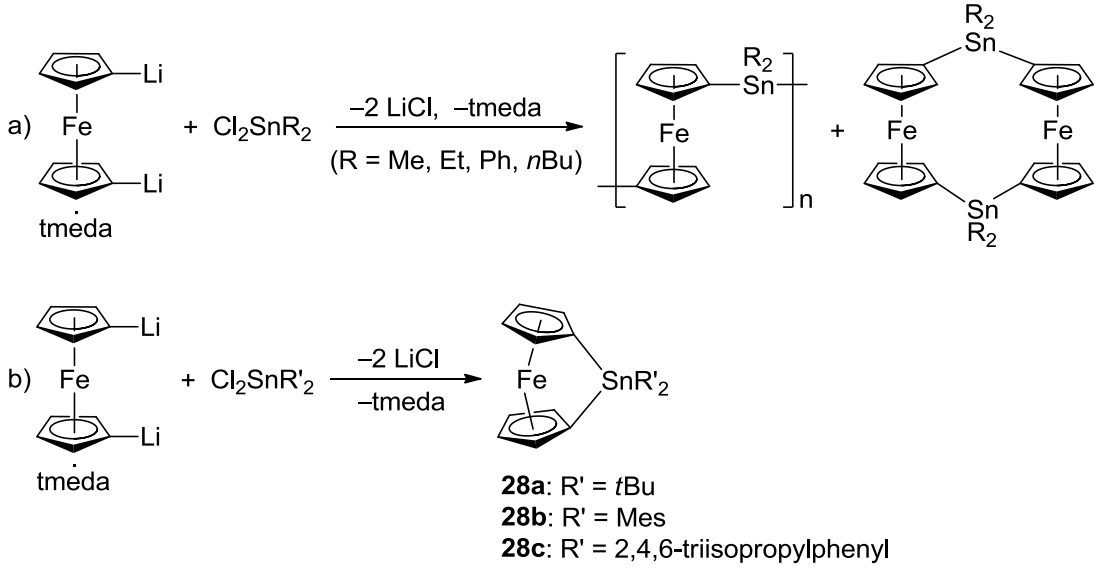

Although the salt-metathesis route was successfully used for the preparation of sila and germa[1]ferrocenophanes with a wide variety of ligands on the group 14 elements, the salt-metathesis reaction of dilithioferrocene and R_2SnCl_2 (R = Me, Et, Ph, *n*Bu) resulted in oligomers and cyclic dimers (Scheme 1-6a).[25a,30] However, the first tin-bridged [1]FCPs (**28a**, **28b**) were synthesized by Manners et al. by utilizing sterically demanding substituents (*t*Bu, Mes) on tin (Scheme 1-6b).[9,31a] Few years later, Pannell et al. reported the stanna[1]ferrocenophane **28c** with bulky 2,4,6-triisopropylphenyl groups on tin (Scheme 1-6b).[31b] To date, these three compounds are the only stanna[1]ferrocenophanes known in literature.

Scheme 1-7. Reactivity of tin-bridged [1]FCPs.

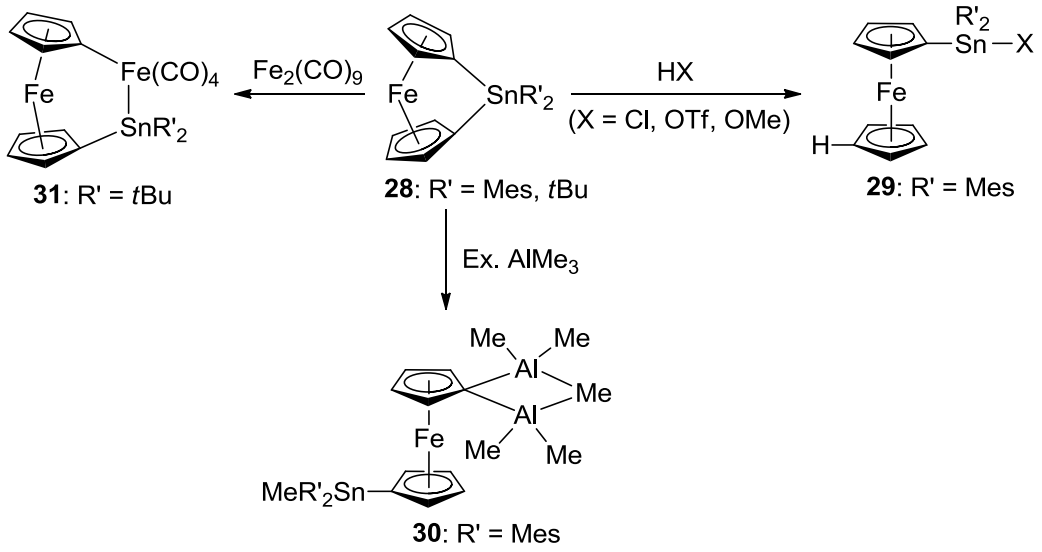

The tin-bridged [1]FCPs displayed similar reativities as shown by sila[1]ferrocenophanes, such as the reaction of **28b** with the protic species like HCl, HOTf, and MeOH resulted in the respective ring-opened species **29** (Scheme 1-7). The influence of the Lewis acid $AlMe_3$ on stanna[1]ferrocenophanes was also explored (Scheme 1-7). Unlike silicon-bridged [1]FCPs, the tin-bridged species **28a** displayed

reactivity toward a metal carbonyl with the insertion of a metal carbonyl fragment into the Sn-Cp bond (Scheme 1-7).

1.1.2 Group 13-bridged [1]Ferrocenophanes

In 1997, Braunschweig and Manners et al. reported the first examples of boron-bridged [1]FCPs, a major accomplishment, which still remain the only examples of [1]FCPs with a bridging element from the second period.[32a] The synthesis of bora[1]ferrocenophanes was accomplished by reacting dilithioferrocene with aminodichloroboranes with sterically bulky substituents on the nitrogen atom (Scheme 1-8a). It seemed that the bulky amines on boron were necessary for the synthesis of bora[1]ferrocenophanes as aminodichloroboranes with the less bulky amines such as NMe_2, N(Ph)Me and N(Me)*n*Bu resulted in insoluble products when treated with dilithioferrocene. In 2000, another report was published describing the synthesis of a similar bora[1]ferrocenophane (**31c**) with B=N*i*Pr_2 as bridge (Scheme 1-8a).[32b]

Scheme 1-8. Synthesis of the boron-bridged [1]FCPs.

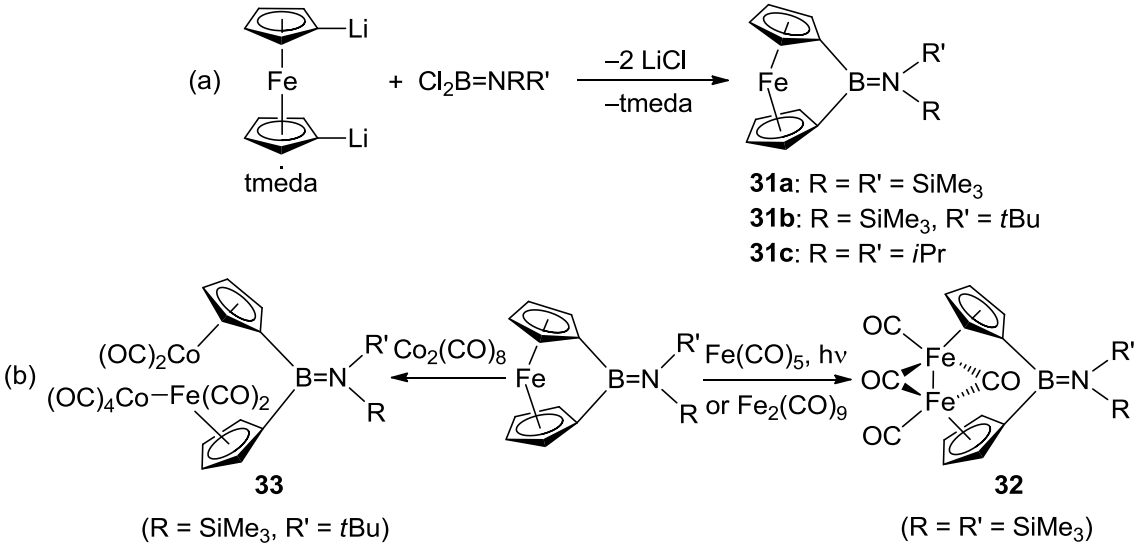

Till today, boron is the smallest element known in bridging positions of [1]FCPs. Therefore, it is understandable that the incorporation of boron into the bridged structure resulted in the extremely strained [1]FCP, which is reflected by the large tilt angle of approx. 32°. The highly tilted Cp rings are reflected in the ^{13}C NMR spectra of boron-bridged [1]FCPs with a significantly high downfield shift of the *ipso*-carbon [$(Me_3Si)_2N$=B[1]FCP: δ = 45.0, (Me_3Si)*t*BuN=B[1]FCP: δ = 45.2, $(i\text{Pr})_2$N=B[1]FCP: δ = 44.2] with respect to the parent ferrocene (δ = 68.2). The high tilt is also reflected in UV-visible spectra with a considerable red shifts of λ_{max} [$(Me_3Si)_2$N=B[1]FCP: λ_{max} = 479 nm, (Me_3Si)*t*BuN=B[1]FCP: λ_{max} = 489 nm, $(i\text{Pr})_2$N=B[1]FCP: λ_{max} = 498 nm] with respect to ferrocene (λ_{max} = 440 nm). The reactivity of these boron-bridged [1]FCPs was explored with metal carbonyls. As illustrated in Scheme 1-8b, the photochemical reaction of $(i\text{Pr})_2$N=B[1]FCP (**31c**) with $Fe(CO)_5$ at low temperature resulted in the insertion of an iron carbonyl fragment into the Fe-Cp bond. The reaction of $Fe_2(CO)_9$ with **31c** in a 2:1 ratio also yielded the very same species (**32**; Scheme 1-8b). The reaction of $Co_2(CO)_8$ with (Me_3Si)*t*BuN=B[1]FCP (**31b**) in a 1:1 ratio yielded the interesting trimetallic species **33**, which contained a $CpCo(CO)_2$ and a $Cp(CO)_2$Fe-$Co(CO)_4$ fragment linked by a boron bridge (Scheme 1-8b). The breakage of a Fe-Cp bond followed by the insertion of metal carbonyl fragments is unusual in ferrocenophane chemistry.

Our group reported the synthesis of all aluminum- and gallium-bridged [1]FCPs, which was achieved by the salt-metathesis reaction of dilithioferrocene and heavier group 13 element dihalides equipped with the appropriate ligands (Scheme 1-9).[5,33] In 2005, the first heavier group-13-bridged [1]FCP, an aluminum species (**35a**), was synthesized. The synthesis was achieved by employing the bulky *trisyl* derived ligand Pytsi, which

provided the steric shielding through two bulky trimethylsilyl groups next to aluminum and the intramolecular stabilization through the pyridine donor. Following by this report, the synthesis of the first gallium-bridged [1]FCP was accomplished by the reaction of (Pytsi)$GaCl_2$ and dilithioferrocene. One year later, the second pair of [1]FCPs with aluminum and gallium as bridging elements were synthesized by employing the similarly bulky, intramolecularly coordinating ligand Me_2Ntsi. In Me_2Ntsi, the pyridine donor is replaced by a dimethylamine group. The presence of strain in those aluminum- and gallium-bridged [1]FCPs with tilted Cp rings was reflected in their ^{13}C NMR spectra by the upfield shift of *ipso*-carbons [(Pytsi)Al[1]FCP: δ = 52.9, (Pytsi)Ga[1]FCP: δ = 47.2, (Me_2Ntsi)Al[1]FCP: δ = 53.0, (Me_2Ntsi)Ga[1]FCP: δ = 47.3] with respect to the parent ferrocene (δ = 68.2). The tilt angle α of those heavier group-13-bridged [1]FCPs falls in the range of 14-16° [(Pytsi)Al[1]FCP: α = 14.9°, (Pytsi)Ga[1]FCP: α = 15.7°, (Me_2Ntsi)Al[1]FCP: α = 14.3°, (Me_2Ntsi)Ga[1]FCP: α = 15.8°].

Scheme 1-9. Synthesis of aluminum- and gallium-bridged [1]FCPs.

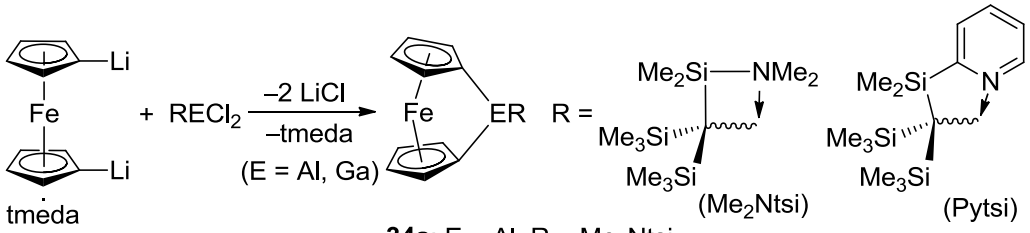

34a: E = Al, R = Me_2Ntsi
34b: E = Ga, R = Me_2Ntsi
35a: E = Al, R = Pytsi
35b: E = Ga, R = Pytsi

To date, indium-bridged [1]FCPs are not reported in the literature.

1.1.3 [1]Ruthenocenophanes

As illustrated before, the family of [1]FCPs has grown significantly with the incorporation of a variety of bridging elements such as group 13 (B, Al, Ga), group 14 (Si, Ge, Sn), group 15 (P, As) and group 16 (S, Se) elements. Contrary to the vast knowledge about [1]FCPs, surprisingly little is known about their 4d counterpart, the [1]ruthenocenophane (RCP). In contrast to the abundant silicon-bridged [1]FCPs prepared by reacting dialkylsilicon dichlorides with dilithioferrocene (Scheme 1-2), the reaction of silicon dichlorides with dilithioruthenocene resulted in oligomeric species.[34] The [2]ruthenocenophane with a CH_2CH_2 bridge exhibited a significantly higher ring tilt than its iron analogue, as a result of the larger size of the ruthenium atom, which forces the Cp rings to be further apart.[35] Therefore, it was concluded that the introduction of the larger bridging elements such as tin or zirconium might lead to less strained and, therefore, more stable [1]RCPs. Finally in 2004, the first examples of [1]RCPs with $SnMes_2$ (**36**) and $Zr(C_5H_4tBu)_2$ (**37**) as the bridging moieties were published by Manners et al. These [1]RCPs **36** and **37** were synthesized by reacting the respective tin and zirconium dichlorides with dilithioruthenocene at low temperature (Scheme 1-10).[36] The identity of those [1]RCPs were confirmed by the NMR spectroscopy, mass spectrometry and single-crystal X-ray analysis. For Sn-bridged [1]RCP **36**, three independent molecules were found in the asymmetric unit with the tilt angles of 20.2, 20.8 and 20.9°. These angles are significantly higher than that of analogous [1]FCP **28b**, which also exhibited three independent molecules in the asymmetric unit (α = 14.5, 15.3 and 15.7°). Similarly, the molecular structure of the Zr-bridged [1]RCP **37** exhibited a higher ring tilt of 10.4° than the corresponding iron compound (α = 6.0°).

Scheme 1-10. Synthesis of the first examples of [1]RCPs bridged by tin and zirconium.

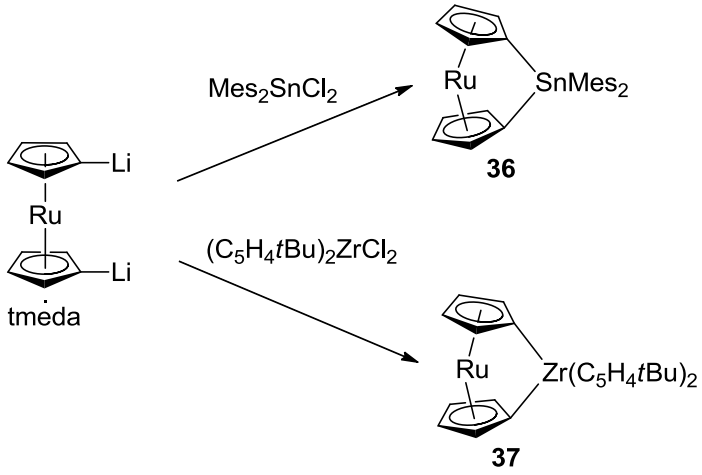

Scheme 1-11. Synthesis of aluminum- and gallium-bridged [1]RCPs.

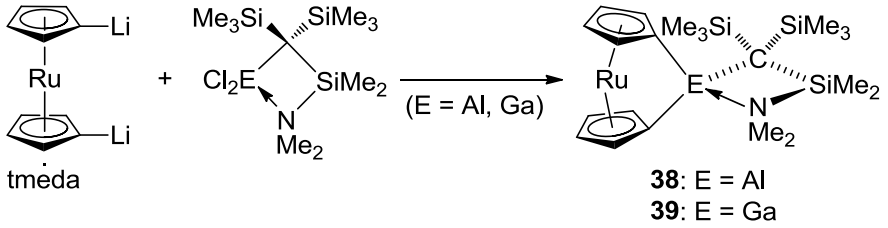

Followed by the synthesis of tin- and zirconium-bridged [1]RCPs, our group reported the successful synthesis of [1]RCPs with aluminum (**38**) and gallium (**39**) as bridging elements, employing the *trisyl*-derived ligand Me_2Ntsi (Scheme 1-11).[37] Expectedly, the aluminum- and gallium-bridged [1]RCPs [(Me_2Ntsi)Al[1]RCP: α = 20.31°, (Me_2Ntsi)Ga[1]RCP: α = 20.91°] are more strained than their iron counterparts [(Me_2Ntsi)Al[1]FCP: α = 14.33°, (Me_2Ntsi)Ga[1]FCP: α = 15.83°]. To best of my knowledge, these four species are only known [1]RCPs in literature, leaving ample room for the synthesis of new [1]RCPs.

1.2 Poly(metallocene)s by Ring-Opening Polymerization

Natural polymers such as amber, natural rubber and cellulose have been used by humankind for centuries. In the last century, a wide variety of synthetic organic polymers such as polyethylene, polypropylene, polystyrene, synthetic rubber, neoprene, nylon, polyvinyl chloride and polyvinyl butyral has been developed in chemical laboratories and manufactured on a gigantic scale by industries. Metallopolymer, a polymer containing metals in the repeating unit either as part of backbone or as pendant, is a newer addition to the family of polymers. However, DuPont started exploring the area of metal-containing polymer in 1955 with the synthesis of polyvinylferrocene by the radical polymerization,[38] the field of metallopolymers is relatively unexplored. Metallopolymers represent an extremely fascinating area of research both from academic and industrial point of view. Transition-metal-containing metallopolymers, exhibiting excellent electronic and optical properties, have potential applications for advanced electronic data storage devices, chemosensors, biosensors and photovoltaic devices in future technologies. Even though, polyvinylferrocene with ferrocene units as pendants of polymer chains was synthesized in mid-fifties, metallopolymers that contain metallocene as a backbone of the polymer is even a younger member of the class of these synthetic polymers. In 1982, Seyferth and Garrou et al. synthesized the high-molecular-weight poly(ferrocenylphenylphosphine) $\mathbf{40_n}$ (M_w = 8.9-161 kDa) by reacting dichlorophenylphosphine with dilithioferrocene in different organic solvents (Scheme 1-12a).[39] It could be assumed that the reaction of dichlorophenylphosphine and dilithioferrocene generated phospha[1]ferrocenophane (**40**) as a reactive intermediate which ring-open polymerized to yield poly(ferrocenylphenylphosphine). No suggestion was proposed about the probable *in situ* formation of species **40** and its subsequent

anionic ROP, initiated by dilithioferrocene. Surprisingly, Seyferth et al. isolated only oligomers when the phospha[1]ferrocenophane **40** was treated with PhLi as an anionic initiator (Scheme 1-12b).

Scheme 1-12. Synthesis of poly(ferrocenylphenylphosphine).

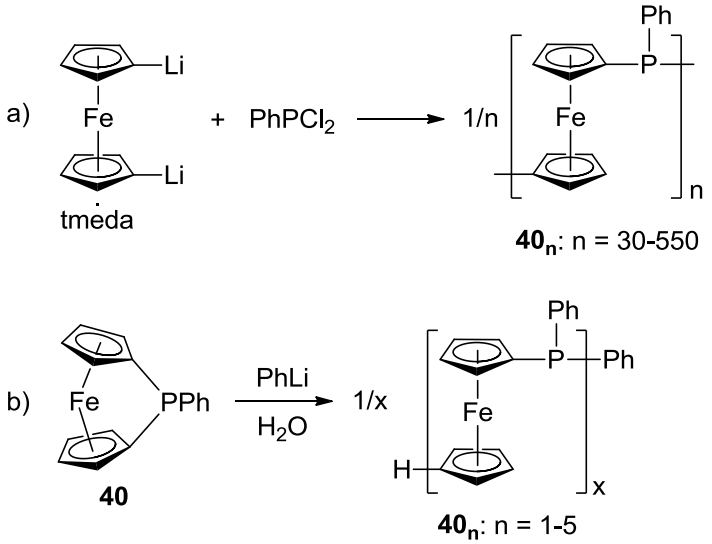

The anionic ROP of the phosphorus-bridged [1]FCP **40** apparently failed to produce high-molecular-weight polymer. Likely due to this unsuccessful ROP, investigation in this field ceased for about 10 years until Rauchfuss and Brand et al. synthesized the high-molecular-weight poly(ferrocenylylpersulfide) $\mathbf{41_n}$ from trithia[3]ferrocenophane (**41**) by the atom-abstraction-based ROP pathway (Scheme 1-13).[3]

Scheme 1-13. Synthesis of poly(ferrocenylpersulfide).

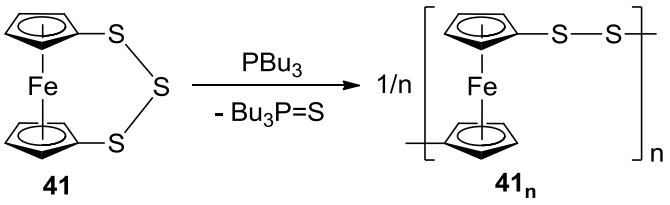

A few months later, this field of the ROP of [n]metallocenophanes gained momentum, when the high-molecular-weight poly(ferrocenylsilane)s **16$_n$** was synthesized by thermal ROP of sila[1]ferrocenophanes (**16**) (Scheme 1-14). As already mentioned before, this report was published by Manners et al. and a new era of organometallic polymers was started.[12]

Scheme 1-14. Synthesis of poly(ferrocenylsilane)s by thermal ROP of sila[1]ferrocenophanes.

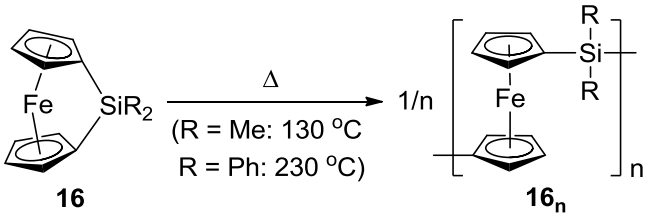

Scheme 1-15. Synthesis of oligo(ferrocenylsilane)s by polycondensation route.

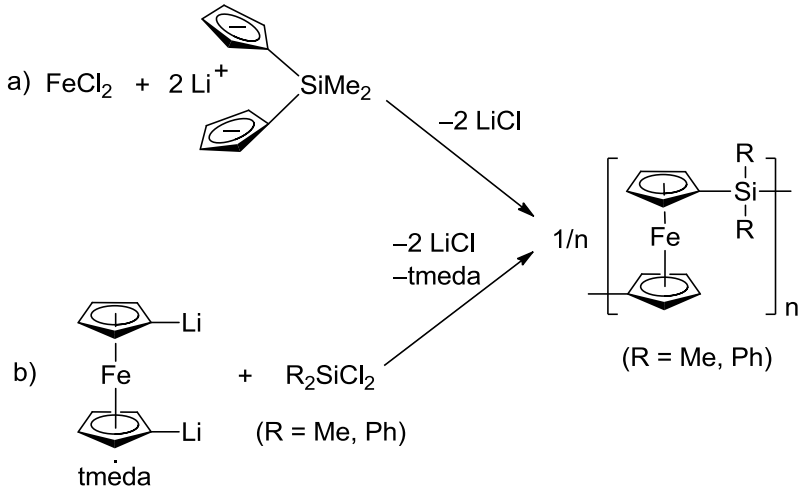

In the 1960s, mainly polycondensation routes were employed for the synthesis of poly(metallocene)s with different bridging elements.[40] In 1962, poly(ferrocenyldimethylsilane) was prepared by the polycondensation reaction of iron dichloride and anionic dicyclopentadienyl bridged by dimethylsilicon (Scheme 1-15a).[40a] In 1969, poly(ferrocenylsilane)s were synthesized by employing a slightly different

polycondensation route, which involved the reaction between dilithioferrocene and dialkylsilicon dichlorides (Scheme 1-15b).[40b] However, both polycondensation pathways yielded low-molecular-weight poly(ferrocenylsilane)s. As mentioned before, the polycondensation of dilithioferrocene and different dialkyltin dichlorides also yielded low-molecular-weight oligomers (Scheme 1-6a).

As expected, the polycondesation route failed to produce high-molecular-weight poly(metallocene)s. In the case of polycondesation reaction, many species with varying chain lengths are present in the reaction mixture at the same time and the species with different chain lengths can react randomly among themselves, often resulting in polymers with the broad molecular weight distributions. The high-molecular-weight polymers can be achieved by the polycondensation reactions only if two requirements are satisfied: 1) starting monomers with the high purity level must be used and 2) the stoichiometry between the starting monomers must be precise. The failure to achieve high-molecular-weight poly(metallocene)s by polycondesations is attributed to the common difficulties of reaching highly pure monomers, as well as maintaining precise stoichiometry. For example, dilithioferrocene·tmeda adduct always contains ferrocene as a major impurity and the actual ratio of tmeda varies from 2/3 to 2.[28a] Therefore, it was not surprising that low-molecular-weight poly(ferrocenylsilane)s and poly(ferrocenylstannane)s were obtained by polycondensation reactions, when dilithioferrocene·tmeda adduct was one of the starting monomer. However, the chain-growth process by ROP of [n] metallocenophanes is a very effective route to synthesize high-molecular-weight metallopolymers. ROP is also successfully employed for the synthesis of a wide variety of inorganic polymers such as polysilanes,[41] polysiloxanes[42] and polyphosphazenes.[43]

[n]Metallocenophanes with highly tilted Cp rings are very strained and are susceptible to release the strain by undergoing ROP.

Different ROP methodologies, which are very effective routes for the synthesis of poly(metallocene)s with different bridging elements, will be discussed in the following section.

1.2.1 ROP Methodologies

Since 1992, various ROP methodologies have been developed. The most successful and commonly employed methods to achieve high-molecular-weight poly(metallocene)s are thermal, anionic, photocontrolled and transition-metal-catalyzed ROP. Following is the brief discussion about those ROP pathways.

Thermal ROP: Manners et al. were the first to introduce thermal ROP in the metallocenophane chemistry.[12] The successful thermal ROP of sila[1]ferrocenophanes to high-molecular-weight ($M_w \approx 10^5$) poly(ferrocenylsilane)s is considered as a milestone in the history of poly(metallocene)s (Scheme 1-14). The thermal ROP of strained [n]metallocenophanes is generally performed at elevated temperature either in solution or in bulk (melt). The most commonly adopted technique is to heat the bulk [n]metallocenophane sealed in a pyrex glass tube above its melting point. Though high-molecular-weight poly(metallocene)s are achieved by thermal ROP, the resulted polymers often possess broad distribution of molecular weights. However, most of known [1]FCPs have been successfully used as monomers for thermal ROP, there is a potential chance of decomposition at high temperature.

Little is known about the mechanism of thermal ROP or more precisely, the nature of the propagating species. It is believed that the mechanism of thermal ROP involves a

radical pathway. In order to get insight into the mechanism, Manners et al. performed the thermal ROP of a silicon-bridged [1]FCP with the unsymmetrically-methylated Cp rings **20** (Scheme 1-16).[44] The result was not very informative as the ring-opening proceeded through a nonselective cleavage of Si-Cp^{H} and Si-Cp^{Me} bonds. More research is required to gain insight into the mechanism of the thermal ROP of strained [n]metallocenophanes.

Scheme 1-16. Thermal ROP of sila[1]ferrocenophane with the unsymmetrically-substituted Cp rings.

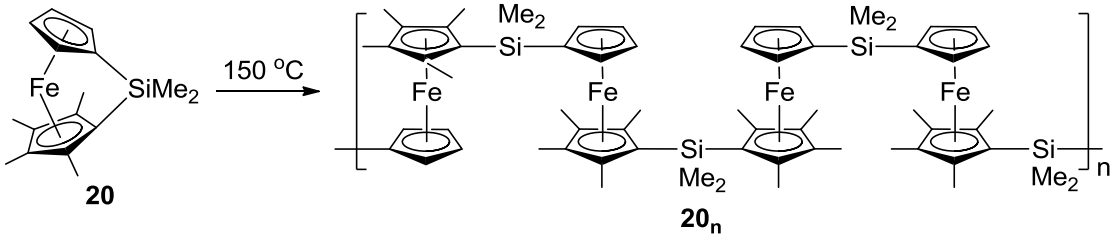

20 **20_n**

Anionic ROP: As mentioned earlier, Seyferth et al. reported the first example of an anionic ROP of the phosphorus-bridged [1]FCP **40** with the isolation of oligomers in 1980s (Scheme 1-12b), when **40** was treated with phenyl lithium as an anionic initiator (Scheme 1-12b).[39] However, the first example of a successful living carbanionic ROP was reported in 1994 by Manners et al., when poly(ferrocenylsilane) with a predictable molecular weight and a narrow distribution of molecular weights was synthesized by reacting sila[1]ferrocenophane with the anionic initiator ferrocenyl lithium.[45] Many other anionic initiators such as MeLi, *n*BuLi and *t*BuLi have been successfully used for anionic ROP of [n]metallocenophanes. The mechanism involves the breakage of the bond between the bridging element and the *ipso*-carbon of a Cp ring.[46] The anionic ROP has been used to prepare high-molecular-weight poly(metallocene)s with a high degree of compositional homogeneity [polydispersity index (PDI) ≈ 1]. By changing the ratios of monomers and anionic initiators, it is possible to achieve polymers with a predictable

molecular weight. Since the thermal ROP is unable to produce materials with a narrow molecular weight distribution, living anionic ROP has great importance. Unlike the thermal ROP, anionic ROP occurs under relatively mild conditions. However, anionic ROP is restricted to monomers with functionalities, which are inert toward carbanions. As illustrated in Scheme 1-17, the living anionic ROP provided the tool to obtain block

Scheme 1-17. Synthesis of block copolymers through the living anionic ROP.

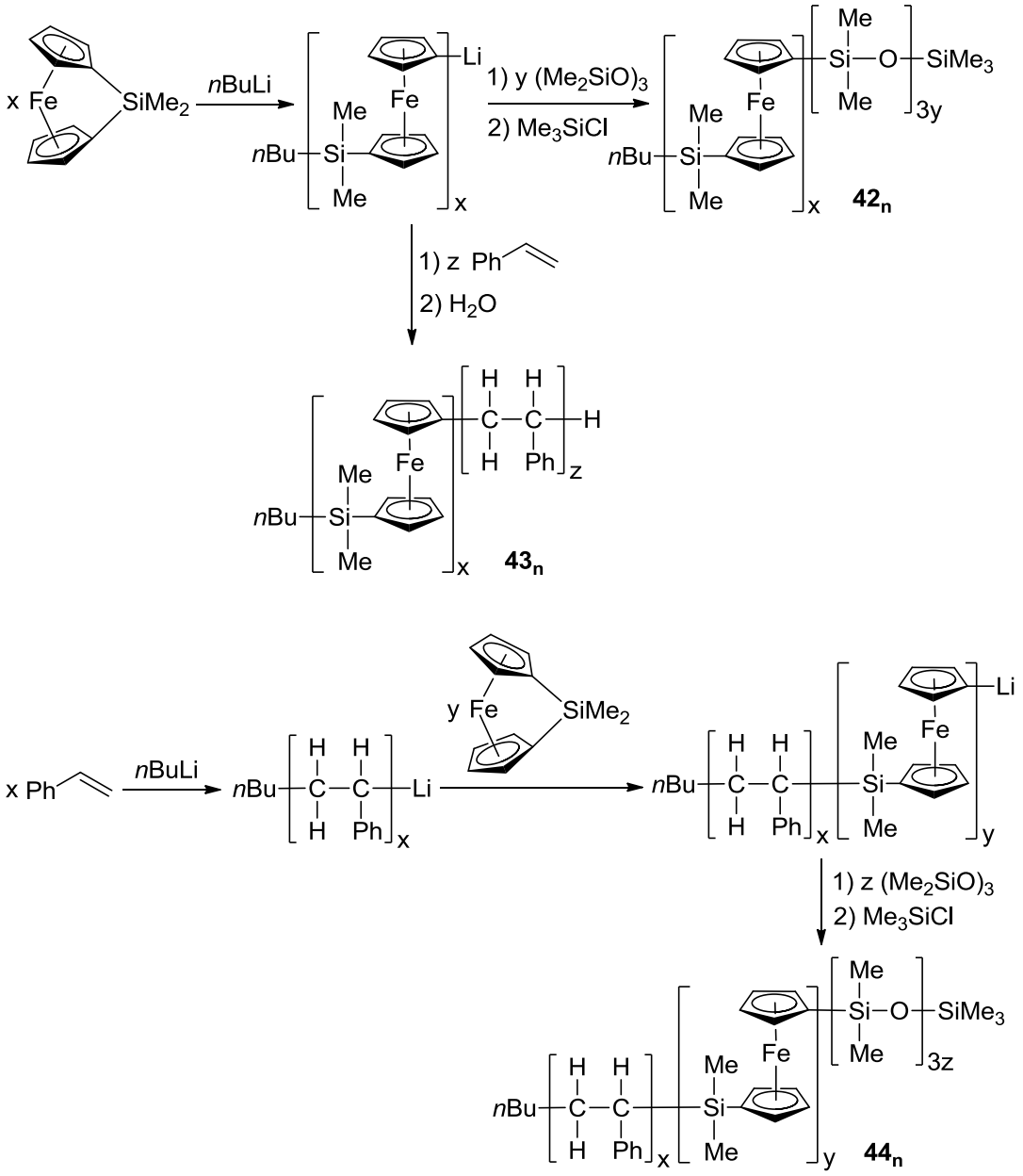

copolymers such as **42$_n$**, **43$_n$** and **44$_n$** with well-defined structures.[46b] However, the vital drawback is that anionic ROP demands high purity level of monomers to avoid early, and thus, undesired chain termination.

Photocontrolled ROP: In 2000, Miyoshi et al. described the synthesis of high-molecular-weight ($M_w \approx 10^4$) poly(ferrocenylphosphine)s, when the phosphorus-bridged species X(Ph)P[1]FCP [organometallic fragment X = $W(CO)_5$, $Mn(C_5H_5)(CO)_2$, $Mn(C_5H_4)(CO)_2$] was irradiated with UV light in a donor solvent such as thf or acetonitrile.[47] This was the first report of a photocontrolled ROP and the only report described the ROP of metallized [1]FCP. The same research group studied the mechanism of photocontrolled ROP.[48] When the phospha[1]ferrocenophane **45** was treated with an excess of $P(OMe)_3$ under UV-radiation, an intermediate (**46**) formed. In **46** one Cp ring is coordinated to the iron center in a η^5-mode, whereas the coordination mode of the other Cp has changed from η^5 to η^1 (Scheme 1-18). Upon heating, the intermediate **46** yielded poly(ferrocenylphosphine) (**45$_n$**; Scheme 1-19). The reaction of **45** with the stronger donor PMe_3 under UV-radiation resulted in a species (**47**) with one Cp completely dissociated from the iron center (Scheme 1-18). Based on these results, Miyoshi et al. proposed the mechanism illustrated in Scheme 1-19.

Scheme 1-18. Reactivity of phospha[1]ferrocenophane with bases under UV-radiation.

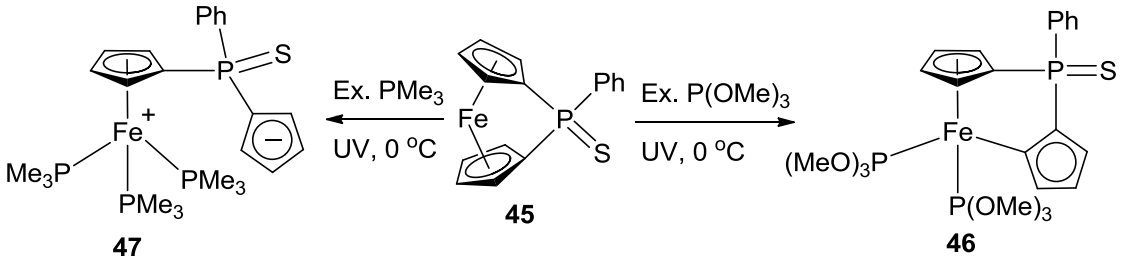

47 **45** **46**

Scheme 1-19. Proposed mechanism for the photocontrolled ROP of phospha[1]ferrocenophane.

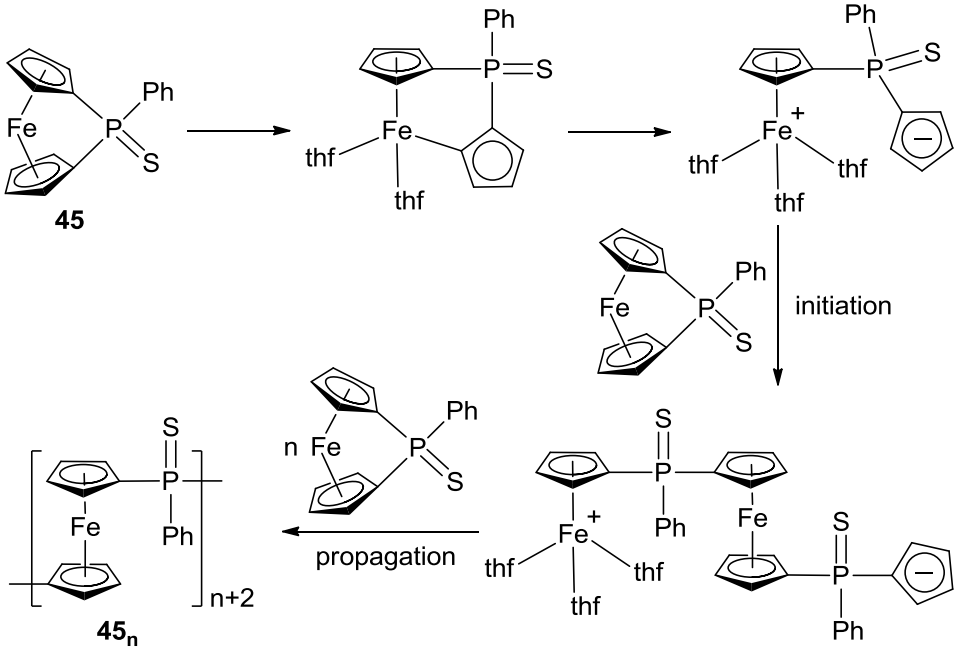

Manners et al. reported the first living anionic photocontrolled ROP of sila[1]ferrocenophane in 2006.[49] Poly(ferrocenylsilane) with an extremely narrow molecular weight distribution (PDI < 1.1) was synthesized when dimethylsila[1]ferrocenophane was treated with an anionic initiator such as $(C_5H_5)Na$ or $(C_5H_4Me)Na$ in presence of UV-irradiation (Scheme 1-20). The UV-radiation weakens

Scheme 1-20. Photocontrolled ROP of sila[1]ferrocenophane and mechanism.

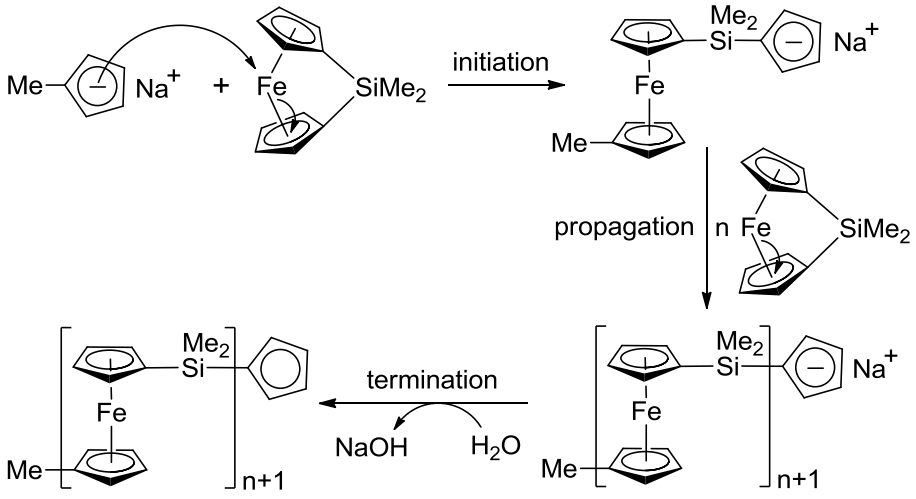

the Fe-Cp bond in [1]FCP, which facilitates the attack of the anionic initiator at the iron center, and thus, the mechanism of photocontrolled ROP involves initial breakage of Fe-Cp bond (Scheme 1-20).

Transition-metal-catalyzed ROP: In 1995, Tanaka et al. was the first to describe transition-metal-catalyzed ROP of [1]FCPs.[50] The treatment of dimethylsila[1]ferrocenophane with 2 mol% of [$Pt(cod)_2$] (cod = 1,5-cyclooctadiene) resulted in high-molecular-weight ($M_w \approx 10^6$) polymers with a broad molecular weight distribution (PDI = 2.8) within 3 h. More soluble catalysts such as [$Pt_2(dba)_3$] and [$Pd(dba)_2$] (dba = dibenzylideneacetone) resulted in faster polymerizations, but a lower molecular weight polymer ($M_w \approx 10^4$). Extremely fast polymerization (within seconds) with a bimodal molecular weight distribution ($M_w \approx 10^4$ and 10^6) was observed for the catalyst [$Pt(cod)_2Cl_2$]. However, palladium- and platinum-phosphine complexes such as [$M(PPh_3)_4$] and [$M(PPh_3)_2Cl_2$] (M = Pd, Pt) did not stimulate the ROP of dimethylsila[1]ferrocenophane, even at ambient temperature. Similar reactivities were observed for germanium-bridged [1]FCPs, when treated with transition-metal catalysts. The copolymerization of silicon- and germanium-bridged [1]FCPs was also achived by employing 2 mol% [$Pt(cod)_2$]. In 1995, Manners et al. also reported the transition-metal-catalyzed ROP of silicon-bridged [1]FCPs by using catalytic amount of [$PtCl_2$], [$PdCl_2$], [$Pd(cod)Cl_2$] and [$Rh(cyclooctene)_2(\mu\text{-}Cl)]_2$.[51] Transition-metal-catalyzed ROP was believed to proceed through a homogeneous pathway[52] till 2001, when Manners et al. proposed a heterogeneous route for the polymerization of sila[1]ferrocenophane.[53] The catalyst [$Pt(cod)_2$] reacts with the sila[1]ferrocenophane to yield a platinasila[2]ferrocenophane (**48**) by oxidative addition of the transition-metal-fragment,

which was believed to be the active precatalyst for the homogeneous transition-metal-catalyzed pathway (Scheme 1-21). However, an intensive study suggested that this precatalyst, the [2]FCP **48**, did not incorporate into the growing chain. It was proposed that the reductive elimination of the transition metal from the [2]FCP **48**, followed by the elimination of the attached ligand, cod, resulted in platinum colloids, which acted as the active species. The suggestion of metal colloids as the active species was further supported by the retardation of ROP by using mercury, a well-established inhibitor for heterogeneous reactions. However, the homogeneous pathway for transition-metal-catalyzed ROP cannot be ruled out completely, as the effect of inhibitors for the homogeneous reactions were not investigated.

Scheme 1-21. Proposed mechanism for the transition-metal-catalyzed ROP.

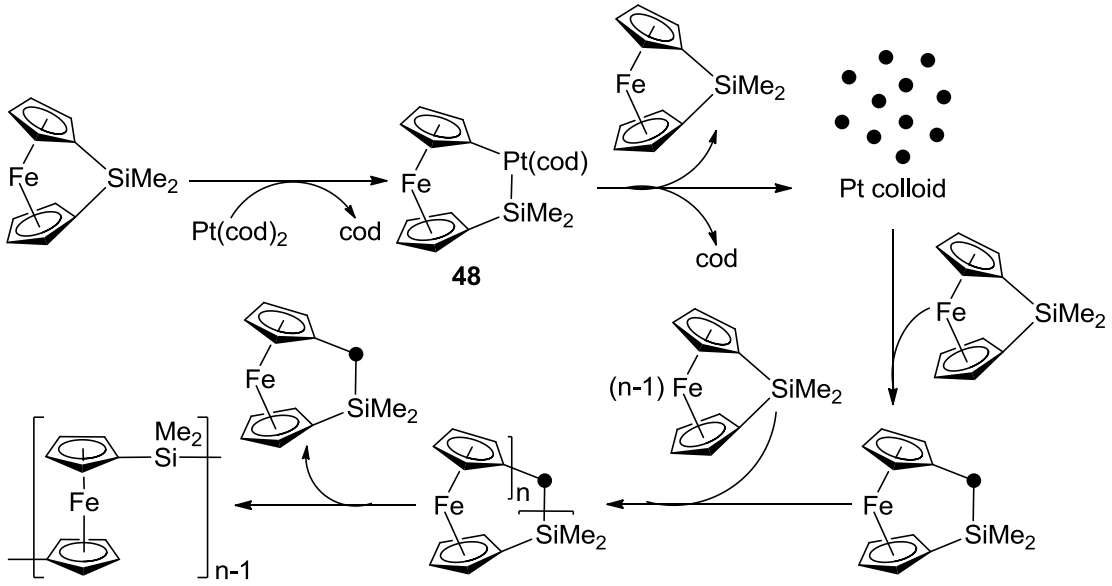

In contrary to the thermal ROP, transition-metal-catalyzed ROP operates under mild reaction conditions. This convenient approach worked successfully for the polymerization of [1]FCPs with a wide variety of bridging elements and displayed a significant tolerance towards various functionalities. However, this method did not work

for the ROP of phosphorus-bridged [1]FCPs. In contrast to the anionic ROP, transition-metal-catalyzed ROP does not require high purity level of monomers.

1.2.2 Poly(ferrocene)s with Group 14 Elements as Bridges

Currently, carbon-bridged [1]FCPs are not known in literature. However, there are few examples of poly(ferrocene)s that contain carbon as bridging element, which were derived from carbon-bridged [n]FCPs (n>1). The hydrocarbon-bridged [2]FCPs such as **49**[54] and **50**[55], which possess high tilt angles (**49**: α = 21.6°; **50**: α = 23.0°), are prone to ROP (Figure 1-7). The doubly hydrocarbon-bridged [2_2]FCP **52** has a more tilted structure (α = 28.8°) than its single hydrocarbon-bridged counterpart **49** (Figure 1-7).[56] The unsaturated-carbon-bridged [2]FCP **53** is equally strained (α = 22.6°) (Figure 1-7).[57] Unsaturated-hydrocarbon-bridged [3]FCPs (**54** and **55**; Figure 1-7) contain slightly tilted Cp rings with a tilt angle of approx. 12°,[58] whereas the Cp rings of [4]FCPs with an olefinic bridge (**56**, **57** and **58**; Figure 1-7) are almost parallel to each other with no significant ring-strain.[59]

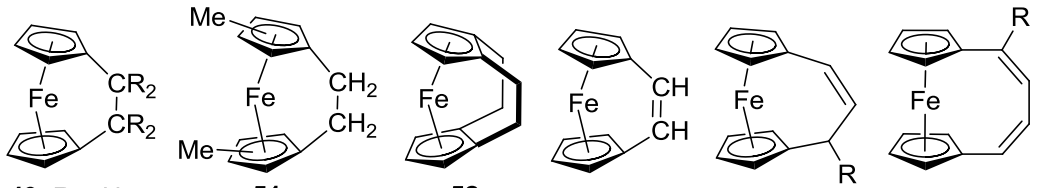

Figure 1-7. Carbon-bridged [n]FCPs (n > 1).

Despite of the high ring-strain, the ROP of carbon-bridged [2]FCPs was not very successful.[55] They are inert towards transition-metal-catalyzed ROP [Rh(I), Pt(0), and Pt(II) were tested]. Thermal ROP of the dicarba[2]ferrocenophanes **49** and **51** resulted in

low-molecular-weight poly(ferrocenylethylene) ($M_w \approx 10^3$). Photocontrolled ROP of dicarba[2]ferrocenophanes in the presence of a phosphine base was equally unsuccessful.[55] However, the olefin-bridged [n]FCPs (n = 2, 3 and 4) are appropriate candidates for the ring-opening metathesis polymerization (ROMP). The [2]FCP **53** polymerized in presence of a molybdenum-catalyst to yield an insoluble polymer.[57] The ROMP of the [3]FCP **54** by using a molybdenum-catalyst also yielded an insoluble polymer.[58] However, the ROMP of the [4]FCP **57** in presence of a tungsten-catalyst resulted in a high-molecular-weight ($M_w \approx 10^5$) polymer that was soluble in common organic solvents (Scheme 1-22).[59b] The polymer was stable under ambient condition. By changing the ratio of catalyst and monomer, it was possible to prepare polymers with a wide range of molecular weights ($M_w \approx 1x10^5$ to $3x10^5$) and polydispersities (PDI = 1.6-2.3). It was observed that both molecular weight and polydispersity increased as the ratio of catalyst and monomer increased. Similarly, **56** and **58** were also polymerized by using tungsten-catalysts and yielded similarly high-molecular-weight polymers ($M_w \approx 10^4$-10^5) (Scheme 1-22).

Scheme 1-22. ROMP of olefin-bridged [4]FCPs.

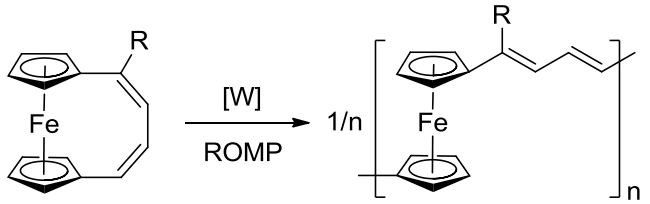

56: R = Ph
57: R = *t*Bu
58: R = Mes

56_n: R = Ph
57_n: R = *t*Bu
58_n: R = Mes

Sila[1]ferrocenophanes have a moderate ring-strain with a considerably tilted structures. The enthalpy of ring-opening of silicon-bridged [1]FCPs, found by DSC

analysis, is significantly high (60-80 kJ/mol). All of the four most common ROP methodologies (thermal,[12] anionic,[45] photocontrolled[49] and transition-metal-catalyzed[51] ROP) have been successfully employed to prepare poly(ferrocenylsilane)s from many different silicon-bridged [1]FCPs. As mentioned before, poly(ferrocenylsilane)s are the most intensively studied metallopolymers, which have found a wide range of potential applications in material science. The spirocyclic sila[1]ferrocenophane **18b** has been ring-open polymerized at high temperature to yield the cross-linked poly(ferrocenylsilane) **18b$_n$** with three possible microenvironments (Scheme 1-23).[13]

Scheme 1-23. Synthesis of the cross-linked poly(ferrocenylsilane).

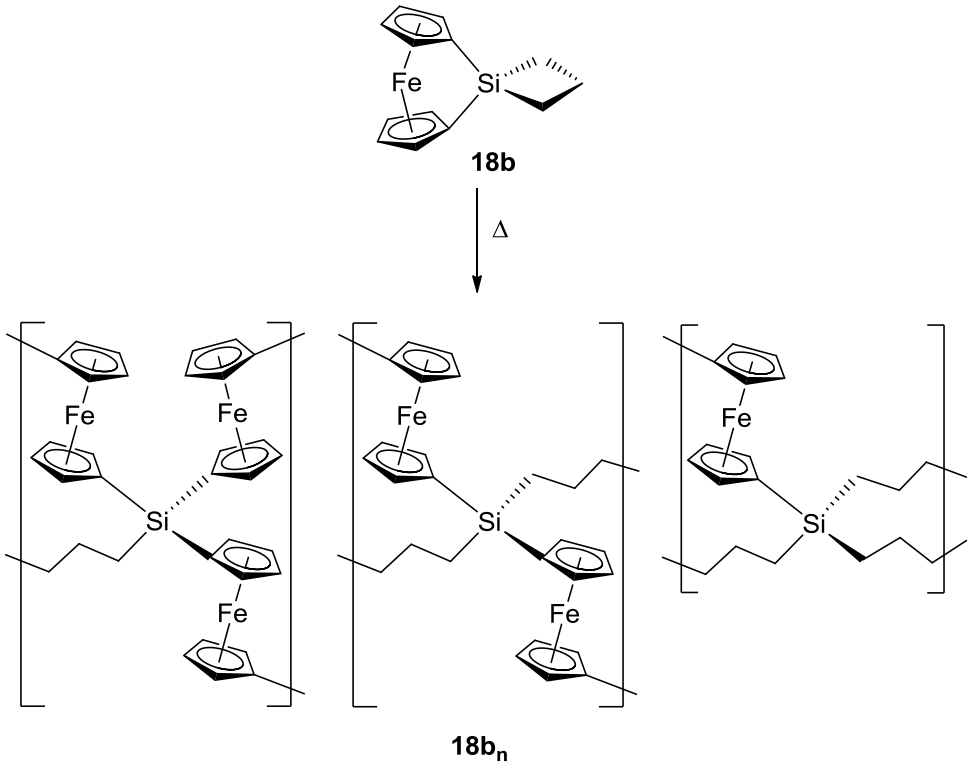

Cross-linked polymers increase the ceramic yield by reducing the amount of volatile decomposition products. Upon pyrolysis, the polymer **18b$_n$** resulted in a shape-retaining ceramic material with more than 90% ceramic yield. Moreover, polymer **18b$_n$** has been

successfully employed in a reflective display technology based on the electrical actuation of photonic crystals.[14]

Scheme 1-24. Synthesis of the water soluble ionic poly(ferrocenylsilane)s.

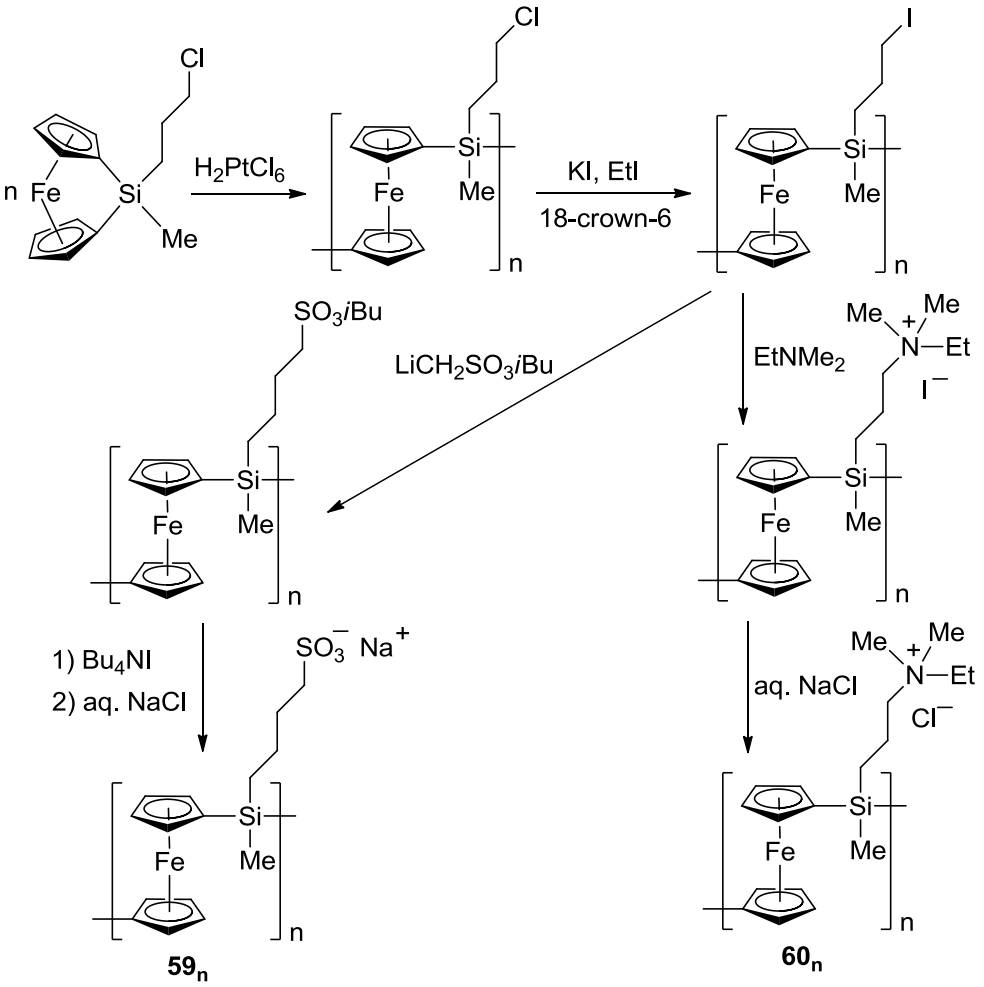

The neutral poly(ferrocenylsilane)s are insoluble in water. However, an ionic poly(ferrocenylsilane) is water soluble, and thus, these polymers are of great interest as they can be processed in aqueous media to develop multilayer films by employing the electrostatic self-assembly. As illustrated in Scheme 1-24, the starting material for ionic poly(ferrocenylsilane)s, poly(ferrocenyl[3-iodopropyl)methylsilane] was readily obtained by transition-metal-catalyzed ROP of (3-chloropropyl)methylsila[1]ferrocenophane

followed by a halide exchange.[60] The functionalization of poly[ferrocenyl(3-iodopropyl)methylsilane] was readily performed by the nucleophilic substitution of iodide using different nucleophiles. The water soluble poly(ferrocenylsilane)-based capsules were fabricated by electrostatic layer-by-layer self-assembly of anionic (**59$_n$**) and cationic poly(ferrocenylsilane)s (**60$_n$**) on colloidal templates followed by the removal of templates.[15] The redox-controlled permeability of these water soluble capsules promises a high hope for potential application in drug delivery.

Scheme 1-25. Transition-metal-catalyzed ROP of digerma[2]ferrocenophane.

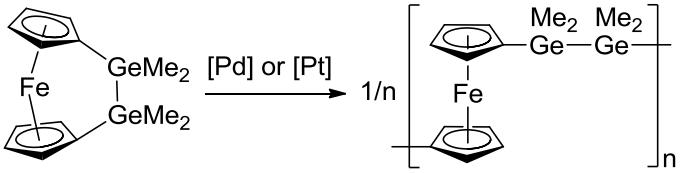

61 **61$_n$**

Germanium-bridged [1]FCPs are also considerably strained with fairly tilted Cp rings ($\alpha \approx 18°$). Thermal,[29a] anionic,[61] and transition-metal-catalyzed[62] ROP have been successfully employed to synthesize different poly(ferrocenylgermane)s from respective germa[1]ferrocenophanes. The poly(ferrocenylgermane)-based block copolymers such as polyisoprene-block-poly(ferrocenylgermane) have been synthesized by living anionic polymerization technique.[61] The epitaxial crystallization driven living copolymerization of micelles, that contain poly(ferrocenylsilane) and poly(ferrocenylgermane) core, in block selective solvents allowed the formation of micelles with triblock and pentablock core.[16] Even though the Cp rings in digerma[2]FCPs are very poorly tilted ($\alpha \approx 4°$), they were used as monomers for ROP. The digerma[2]ferrocenophane **61** underwent ROP in the presence of catalytic amount of Pd(0), Pd(II), and Pt(II) to yield a high-molecular-

weight ($M_w \approx 10^4$-10^5) poly(ferrocenylgermane) (**61$_n$**; Scheme 1-25).[63] Thermal and anonic ROP of **61** could not be achieved using various conditions.

The polycondesation reaction of dilithioferrocene and R_2SnCl_2 (R = Me, Et, Ph, *n*Bu) resulted in low-molecular-weight ($M_w \approx 10^3$) poly(ferrocenylstannane)s.[25a,30] However, the salt-metathesis reaction of dilithioferrocene and tin dichlorides equipped with bulky alkyl or aryl groups resulted in strained stanna[1]ferrocenophanes, which were potential candidates for ROP to yield poly(ferrocenylstannane)s.[9,31a] The DSC analysis of tin-bridged [1]FCPs **28a** and **28b** (Scheme 1-5) showed a ring-opening exotherm at 150-180 °C without any melt endotherm. The thermal ROP of **28a** and **28b** yielded high-molecular-weight ($M_w \approx 10^5$) poly(ferrocenylstannane)s (**28a$_n$**, **28b$_n$**) with PDIs in the range of 1.6-1.9 (Scheme 1-26). Surprisingly, the stanna[1]ferrocenophanes **28a** and **28b** are not stable in solution. They displayed spontaneous ROP in solution and yielded very high-molecular-weight polymers ($M_w \approx 10^6$), with relatively narrow molecular weight distributions (PDI = 1.3-1.6); small amounts of the cyclic dimers were found as well.

Scheme 1-26. ROP of stanna[1]ferrocenophanes.

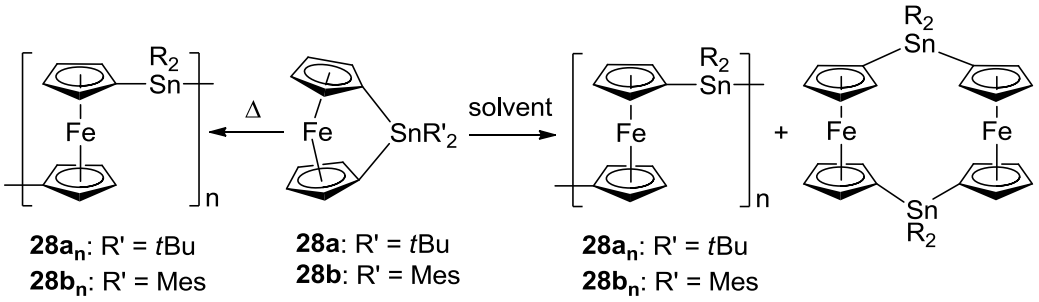

The transition-metal-catalyzed ROP of **28a** and **28b** failed. It appeared that Karstedt's catalyst [Pt(0)], which was a very successful catalyst for ROP of silicon- and germanium-bridged [1]FCPs, inhibited the ROP of **28a** and **28b** in solution. The insertion product,

platinastanna[2]ferrocenophane (**62**) was isolated when **28a** was treated with stoichiometric amount of [Pt(cod)$_2$] (Scheme 1-27). A very slow (5 days) ROP of **28a** was observed when a catalytic amount of **62** was treated with a solution of **28a**.

Scheme 1-27. Reaction of tin-bridged [1]FCP with Pt(cod)$_2$.

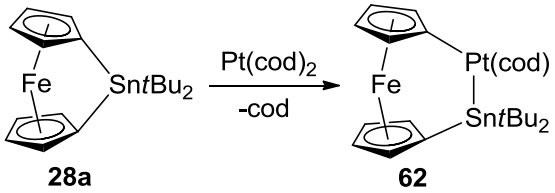

28a **62**

1.2.3 Poly(ferrocene)s with Group 13 Elements as Bridges

The boron-bridged [1]FCPs exhibited the highest known tilt angle ($\alpha \approx 32°$), and thus, offered a high potential value as monomers for the synthesis of poly(ferrocenylborane) through ROP.[32] Similar to silicon-bridged [1]FCPs, $(Me_3Si)_2N$=B[1]FCP (**31a**) displayed a ROP exotherm at 190 °C with a melt endotherm at 115 °C in the DSC thermogram. (Me_3Si)*t*BuN=B[1]FCP (**31b**) showed a melt endotherm at 150 °C overlapping with the ROP exotherm at only slightly higher temperature. Similarly, the thermogram of *i*Pr$_2$N=B[1]FCP (**31c**) showed a melt endotherm at ca. 185 °C overlapping with a ROP exotherm. The ring-opening enthalpy of $(Me_3Si)_2N$=B[1]FCP (ΔH_{ROP} = 95 kJmol^{-1}) was greater than that of silicon-bridged [1]FCPs (ΔH_{ROP} = 70-80 kJmol^{-1}) which readily ring-open polymerized under various conditions. Therefore, DSC experiments presented a high hope for the thermal ROP of boron-bridged [1]FCPs. However, the thermal ROP of $(Me_3Si)_2N$=B[1]FCP (**31a**), performed at 180 °C, yielded mostly insoluble polymer (**31a$_n$**) (Scheme 1-28). Cyclic dimers were identified in the ^{1}H NMR spectrum of the soluble fraction. The solid state ^{13}C NMR spectrum of the insoluble polymer showed

characteristic peaks, for example, at 77.6 and 74.1 ppm corresponding to Cp protons and at 5.1 ppm corresponding to $SiMe_3$ groups. The pyrolysis mass spectrum of the polymer showed molecular ion peaks for oligo(ferrocenylborane) with only 1, 2 and 3 repeating units. Completely insoluble material was obtained, when (Me_3Si)*t*BuN=B[1]FCP (**31b**) was heated to 200 °C (Scheme 1-28). However, the thermal ROP of *i*Pr_2N=B[1]FCP (**31c**) at 200 °C resulted in polymer (**31c$_n$**), which was almost completely soluble in organic solvents such as toluene, thf, CH_2Cl_2 and $CHCl_3$ (Scheme 1-28). In addition, the dimeric and trimeric ferrocenylboranes with cyclic structure were identified by mass spectrometry. The cyclic dimer and trimer were separated from the bulk polymer, which were then characterized by multinuclear NMR spectroscopy. The molecular weight of **31c$_n$** could not be determined, as GPC was not applicable because of a high moisture sensitivity of the polymer. The dynamic light scattering (DLS) experiment in toluene did not display any detectable signal, hinting at low-molecular-weight polymers.

Scheme 1-28. Thermal ROP of boron-bridged [1]FCPs.

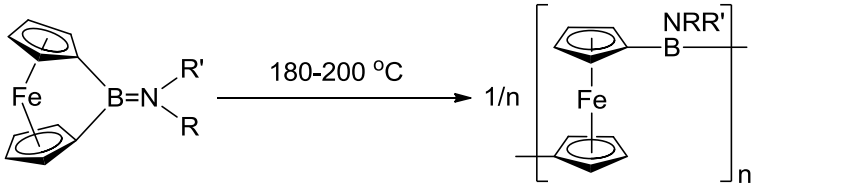

31a: R = R' = $SiMe_3$
31b: R = $SiMe_3$, R' = *t*Bu
31c: R = R' = *i*Pr

31a$_n$: R = R' = $SiMe_3$
31b$_n$: R = $SiMe_3$, R' = *t*Bu
31c$_n$: R = R' = *i*Pr

In summary, the thermal ROP of bora[1]ferrocenophanes produced mostly insoluble polymers; only oligomers with 1, 2 and 3 repeating units were well characterized. However, Jäkle, Holthausen and Wagner et al. employed a very different strategy to synthesize poly(ferrocenylborane)s.[64] The coupling reaction of ($C_5H_4BBr_2$)$_2$Fe and three

equivalent of triethylsilane cleanly produced the poly(ferrocene) **63a$_n$** with boron bridges. The polymer **63a$_n$** was highly sensitive to air and moisture and insoluble in common organic solvents (Scheme 1-29).

Scheme 1-29. Synthesis of poly(ferrocenylbromoborane).

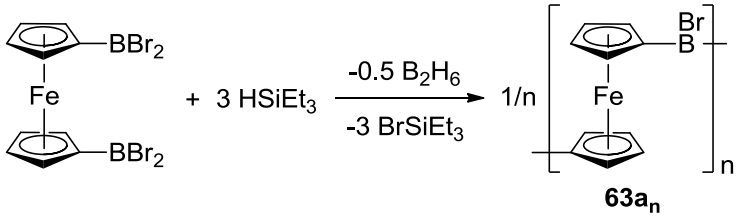

63a$_n$

To improve the solubility and air stability of the poly(ferrocenylborane) **63a$_n$**, the bromine on boron atoms was replaced with mesityl group by treating **63a$_n$** with CuMes (Scheme 1-30). The mesityl-substituted polymer **63b$_n$** was fairly soluble in organic solvents and moderately stable in air. The polymer was characterized by ^{1}H NMR spectroscopy, DSC, thermogravimetric analysis (TGA), GPC and MALDI TOF mass spectrometry. The GPC analysis showed a monomodal weight distribution with M_w of 7.5 kDa. The highest molecular ion peak corresponding to 21 ferrocene moieties was found in the MALDI TOF mass spectrum.

Scheme 1-30. Synthesis of the mesityl-substituted poly(ferrocenylborane).

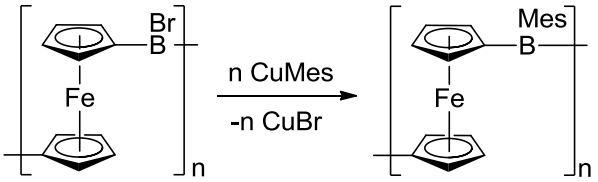

63b$_n$

The tilt angle α of all four heavier group 13 element-bridged [1]FCPs (**34a**, **34b**, **35a**, **35b**; Scheme 1-9) were found in the range of 14-16°, which indicates that they are moderately strained with respect to the well-studied silicon-bridged [1]FCPs with tilt

angle of 19-21°.[37] Both aluminum- and gallium-bridged [1]FCPs equipped with Me_2Ntsi ligands (**34a**, **34b**) showed a melt endotherm (alumina[1]ferrocenophane: 177 °C, galla[1]ferrocenophane: 183 °C) and a ROP exotherm (alumina[1]ferrocenophane: 212 °C, galla[1]ferrocenophane: 220 °C) in DSC experiments. DSC thermograms displayed only ROP exotherms (alumina[1]ferrocenophane: 180 °C, galla[1]ferrocenophane: 173 °C) for heavier group-13-bridged [1]FCPs equipped with the Pytsi ligand (**35a**, **35b**). However, the thermal ROP of **34a** and **34b** at 220 °C resulted in a complete conversion of monomers into oligomers with M_w of ca. 1.5 kDa (DLS analysis). Surprisingly, the species (Me_2Ntsi)E[1]FCP (E = Al, Ga) was found to be resistant to an anionic initiator as no indication of ring-opening was detected, when both [1]FCPs **34a** and **34b** were treated with one equivalent of MeLi, *n*BuLi and *t*BuLi in organic solvent at r.t. and even at elevated temperature. The ^{1}H NMR spectra from the reaction mixture of (Pytsi)E[1]FCP (E = Al, Ga) and *n*BuLi displayed the signal of unreacted [1]FCP as well as a new product, which was identified as the new [1]FCP **64** (Scheme 1-31). The photocontrolled ROP in the presence of the anionic initiator NaCp was equally fruitless.

Scheme 1-31. Reaction of (Pytsi)Al[1]FCP with anionic initiator.

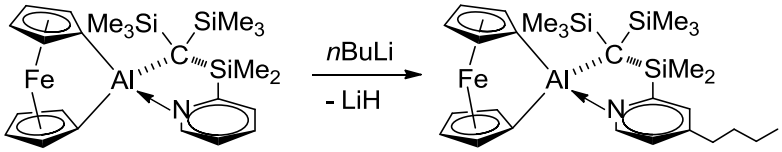

64

However, the transition-metal-catalyzed ROPs of heavier group 13 element-bridged [1]FCPs were successful with the most promising result obtained for (Pytsi)Ga[1]FCP (**35b**). The treatment of a solution of (Pytsi)Ga[1]FCP with 2 mol% Pd(0) catalyst resulted in a polymeric material with M_w of 21.1 kDa as determined by GPC. In

summary, various ROP methodologies were unsucessful for aluminum- and gallium-bridged [1]FCPs with the exception of transition-metal-catalyzed ROP. It was concluded that the sterically bulky Me_2Ntsi or Pytsi ligand either blocked the group 13 element from the nucleophilic attack or protected the E-Cp bond (E = Al, Ga) from the oxidative insertion of a ring-opening initiator.

1.2.4. Poly(ruthenocene)s

Reports describing the synthesis of poly(ruthenocene)s through ROP of [n]RCPs are extremely rare in literature. Shortly after the first report on ROP of [1]FCPs, Manners et al. reported the successful synthesis of poly(ruthenocene)s with carbon bridges by thermal ROP of the dicarba[2]ruthenocenophanes **65** and **66** (Scheme 1-32).[35] Expectedly, disila[2]ferrocenophanes ($\alpha \approx 4°$) are poorly strained if compared to sila[1]ferrocenophanes (α = 19-21°), and thus, resistant to ROP.[65] However, [2]FCPs with smaller carbon as bridging element are slightly more strained (α = 21-23°) than that of sila[1]ferrocenophanes and found to undergo ROP at high temperature. As expected from the larger size of ruthenium as compared to iron, dicarba[2]ruthenocenophanes possess even higher tilt angles (α = 29-30°), which suggested that dicarba[2]ruthenocenophanes are excellent candidates for ROP. The [2]RCP **65** with a CH_2CH_2-bridge underwent thermal ROP at 220 °C, which resulted in an insoluble poly(ruthenocenylethylene) (**65_n**) (Scheme 1-32). To improve the solubility of the poly(ruthenocene) **65_n**, a similar dicarba[2]ruthenocenophane, **66** with one methyl group on each Cp ring was subjected to ROP at 220 °C (Scheme 1-32). This resulted in a soluble, white fibrous poly(ruthenocenylethylene), **66_n**, which was characterized by NMR

spectroscopy and GPC analysis. The GPC exhibited a bimodal molecular weight distribution with M_w of 43.1 and 12.7 kDa.

Scheme 1-32. Thermal ROP of dicarba[2]ruthenocenophanes to yield poly(ruthenocenylethylene)s.

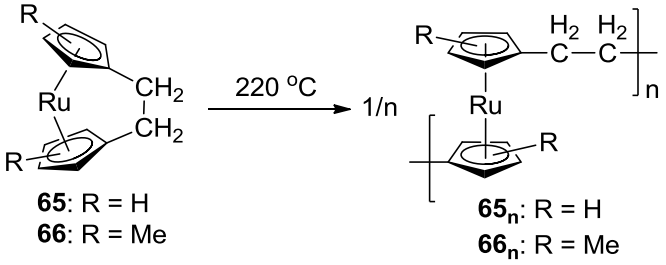

65: R = H
66: R = Me

65$_n$: R = H
66$_n$: R = Me

Manners et al. also studied the ROP behavior of zirconium and tin-bridged [1]RCPs.[36] DSC experiment of the zirconium-bridged [1]RCP **37** did not exhibit any ROP exotherm up to 200 °C; only a melt endotherm was detected at 188°C. Still, **37** (Scheme 1-10) was heated at 200 °C in a sealed tube for four days, but it did not polymerized and only the starting [1]RCP was recovered. The anionic ROP of the **37** with MeLi as an anionic initiator was also fruitless. The unsuccessful ROP of **37** was not surprising considering the low tilt angle of only 10.4°. However, the higher tilt angle (14-16°) of tin-bridged [1]RCP, **36** suggested that it might be prone to ROP. The DSC experiment displayed a ROP exotherm at 181°C with no melt endotherm. The tin-bridged [1]ferrocenophane **36** was heated at 200 °C for 4.5 h to produce a poly(ruthenocenylstannane) (**36$_n$**) with a moderate yield of 45% after purification (Scheme 1-33). GPC analysis of the polymer revealed a very high-molecular-weight polymer (M_w = 615 kDa) with a broad molecular weight distribution (PDI = 2.28). The ^{1}H NMR spectrum displayed broad peaks for Cp protons as well as for mesityl groups, which was expected for a polymer with such a broad molecular weight distribution. The ^{13}C NMR spectrum of **36$_n$** displayed a

downfield shift of the *ipso*-carbon at 76.9 ppm compared to the chemical shift of the *ipso*-carbon of Sn[1]RCP at δ = 31.8. The ceramic yield of the poly(ruthenocene) $\mathbf{36_n}$ was found to be 32% at 900 °C.

Scheme 1-33. Synthesis of poly(ruthenocenylstannane) by thermal ROP.

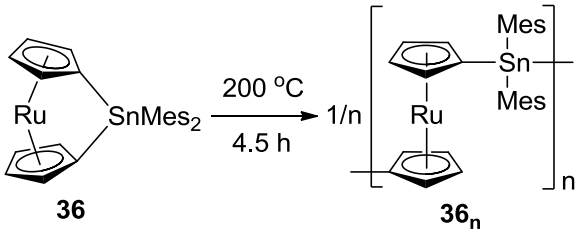

36 **$\mathbf{36_n}$**

As stated before, our group reported the first heavier group-13-bridged [1]RCPs **38** and **39** (Scheme 1-11) in 2007.[37] The high tilt angles of those (Al[1]RCP: α = 20.3°, Ga[1]RCP: α = 20.9°), which are very similar to that of Me_2Si-bridged [1]FCP ($\alpha \approx 21°$), suggested their potential use as monomer for ROP. DSC experiments of the aluminum-bridged [1]RCP **38** exhibited a ROP exotherm at 216 °C with no melt endotherm; however, the gallium-bridged [1]RCP **39** displayed a featureless spectrum with no exotherm and endotherm. The recovered material of Ga[1]RCP after the DSC experiment was poorly soluble in organic solvents and the soluble fraction showed signals of ruthenocene and hydrolyzed ligand in the NMR spectrum, indicating that decomposition of starting [1]RCP had occured. Both aluminum- and gallium-bridged [1]RCPs, **38** and **39**, were subjected to thermal, anionic, photocontrolled, and transition-metal-catalyzed ROP. The thermal ROP of **38** and **39** was unsuccessful. Half an equivalent of anionic initiator *n*BuLi was treated with **38**; however, no sign of ring-opening was observed at r.t. or at elevated temperature. Species **38** was also subjected to one equivalent of anionic initiator NaCp under UV irradiation, but no indiacation of ring-opening was detected.

Transition-metal-catalyzed ROP was equally unproductive for those heavier group-13-bridged [1]RCPs. The unsuccessful ROP of **38** and **39** could not be explained, however it left sufficient interest for future work.

1.3 Bis(ferrocenyl) Species, [1.1]Ferrocenophanes and Ferrocene-containing Macrocycles

In bis(ferrocenyl) species, two ferrocenyl moieties are bridged by an element (Figure 1-8). Bis(ferrocenyl) compounds can be envisioned as the smallest structural unit of a respective poly(ferrocene). [1.1]FCPs are cyclic compounds, which can be considered as a formal dimer of the respective [1]FCP. [1.1]FCPs exist as both *syn* and *anti* conformations (Figure 1-8). They belong to an old class of compounds, that was described for the first time in 1956.[66] [1.1]Ferrocenophanes devoid of ring-strain and there is no report of a successful ROP of [1.1]FCPs.[67] Numerous [1.1]FCPs are known with a wide range of bridging-elements. However, ferrocene-containing macrocycles, consisting of three or more ferrocene moieties, are rare in literature (Figure 1-8). All

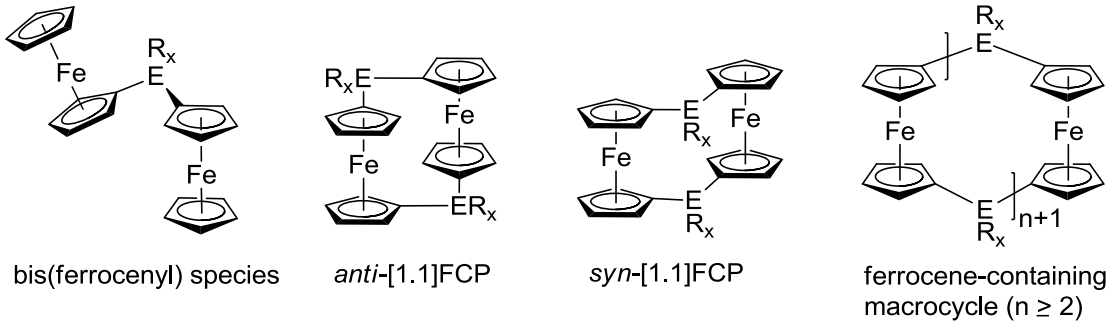

Figure 1-8. Bis(ferrocenyl) species, [1.1]FCP and ferrocene-containing macrocycle.

these compounds, bis(ferrocenyl) species, [1.1]FCPs and ferrocene-containing macrocycles, contain two or more iron redox centers and the electronic communication among the iron centers have been intensively studied by different techniques of electrochemistry. A comprehensive overview of all reported bis(ferrocenyl) species, [1.1]FCPs and ferrocene-containing macrocycles is beyond the scope of this thesis as they are known with varieties of bridging elements. Because of the importance for the thesis on hand, the following chapters will offer an overview on group 13 and 14

element-bridged bis(ferrocenyl) species (Chapter 1.3.1), [1.1]FCPs (Chapter 1.3.2), ferrocene-containing macrocycles (Chapter 1.3.3) and their interesting electrochemical behaviors (Chapter1.3.4).

1.3.1 Bis(ferrocenyl) Species with Group 14 and 13 Elements as Bridges

A vast number of carbon-bridged bis(ferrocenyl) species are reported in literature. Bis(ferrocenyl)methane and substituted methanes are known since the early 1960s.[68] The

Scheme 1-34. Synthesis of bis(ferrocenyl) species with carbon as a bridging element.

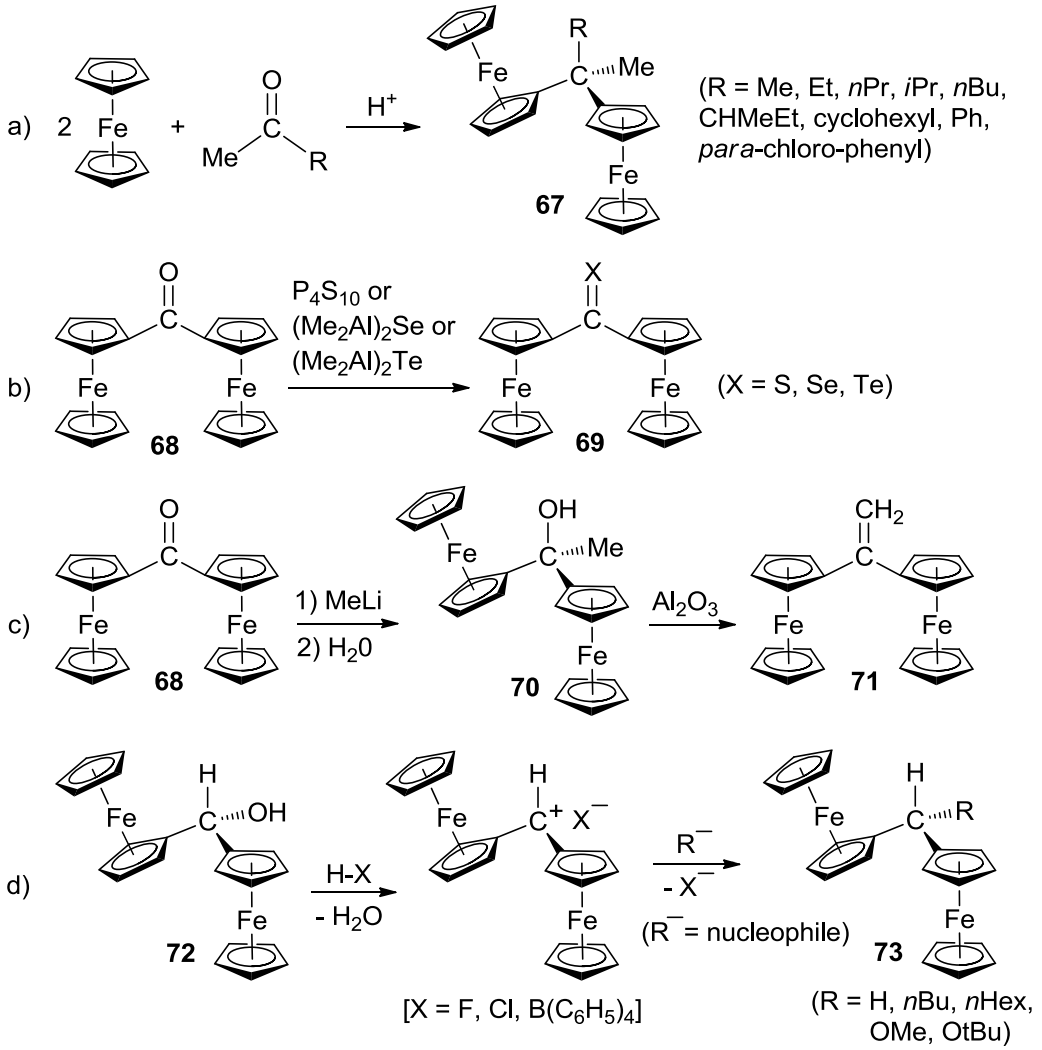

condensation reaction of ferrocene and a ketone in the presence of a catalytic amount of concentrated sulfuric acid resulted in various bis(ferrocenyl) species (**67**) with carbon bridges (Scheme 1-34a).[69] Chalcogeno ketones of the type $Fc_2C=X$ (**69**), where X is S, Se and Te and Fc is $(C_5H_5)Fe(C_5H_4)$, have been synthesized by reacting the bis(ferrocenyl) ketone **68** with P_4S_{10}, bis(dimethylaluminum) selenide and bis(dimethylaluminum) telluride, respectively (Scheme 1-34b).[70] Bis(ferrocenyl)ethylene (**71**) was synthesized by reducing bis(ferrocenyl) ketone (**68**), followed by the reaction with Al_2O_3 (Scheme 1-34c).[71] As illustrated in Scheme 1-34d, a varieties of substituted bis(ferrocenyl)methane (**73**) were synthesized from the bis(ferrocenyl) alcohol **72**.[72]

Silicon- and tin-bridged bis(ferrocenyl) compounds are also old classes of ferrocene derivatives. Starting in the 1960s, the major synthetic route employed for the preparation of silicon-bridged bis(ferrocenyl) species (**74**, **75**) has been the salt-metathesis reaction of lithioferrocene and silicon dichlorides (Scheme 1-35a).[73] However, a different method was used to synthesize bis(ferrocenyl)silanediol (**74**: R = R′ = OH) (Scheme 1-35b). The treatment of spirocyclic sila[1]ferrocenophane **18a** with HCl resulted in bis(ferrocenyl)dichlorosilane, which was hydrolyzed to prepare bis(ferrocenyl)silanediol.[74] The dimethylsilicon-bridged bis(ferrocenyl) species (**74**: R = R′ = Me) was also isolated as a component from a mixture of poly(ferrocenyldimethylsilane)s, which was synthesized by anionic ROP of dimethylsila[1]ferrocenophane initiated by lithioferrocene or dilithioferrocene.[75] Similar to silicon-bridged bis(ferrocenyl) species, analogous tin compounds have been synthesized by the salt-metathesis reactions of lithioferrocene and tin dichlorides.[73a] As illustrated in Scheme 1-35c, some of the tin-bridged bis(ferrocenyl) compounds (**76**) were

Scheme 1-35. Synthesis of bis(ferrocenyl) species with silicon, germanium and tin as bridging elements.

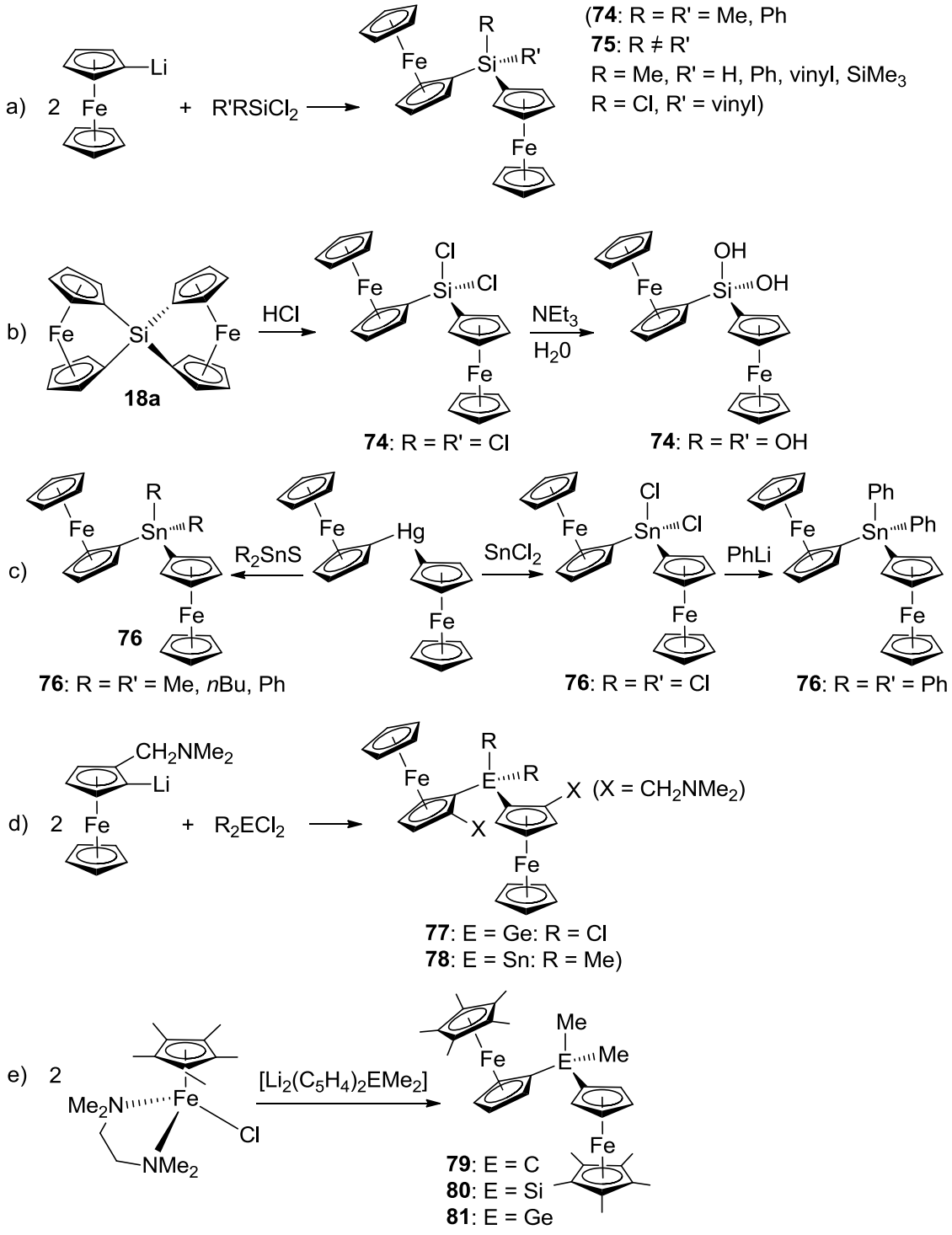

prepared differently as compared to the analogous silicon-bridged species.[76] However, the synthesis of germanium-bridged bis(ferrocenyl) species by the salt-metathesis

reaction of lithioferrocene and germanium dichlorides was proposed in mid-sixties;[73a] the first species, bis(ferrocenyl)diphenylgermane was synthesized in 1980 by Osborne et al.[25a] The reaction of dilithioferrocene and diphenylgermanium dichloride and subsequent treatment with water resulted in a mixture of oligomers, from which bis(ferrocenyl)diphenylgermane was isolated by column chromatography. As shown in Scheme 1-35d, germanium (**77**) and tin-bridged bis(ferrocenyl) species (**78**) with the substituted Cp rings were synthesized by the salt-metathesis route.[77] The "flytrap" route was also utilized to synthesize group-14-bridged bis(ferrocenyl) species (**79**, **80**, **81**) containing substituted Cp rings (Scheme 1-35e).[78]

Scheme 1-36. Synthesis of boron-bridged bis(ferrocenyl) species.

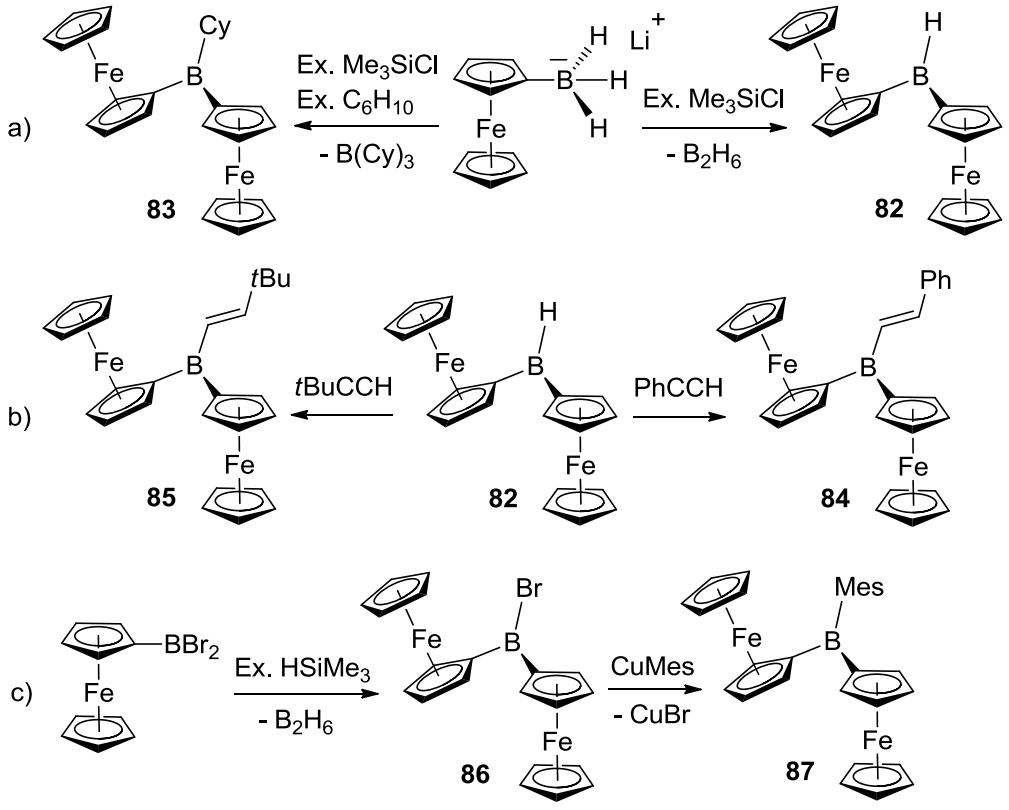

Bis(ferrocenyl) species with group 13 elements as bridges are relatively scarce. In recent years, Wagner and Jäkle et al. published three reports describing six boron-bridged bis(ferrocenyl) species. The treatment of ferrocenylborohydride with excess of Me_3SiCl yielded bis(ferrocenyl)borane **82** (Scheme 1-36a). However, the reaction of ferrocenylborohydride with an excess of a mixture of Me_3SiCl and cyclohexene resulted in bis(ferrocenyl)cyclohexylborane **83** (Scheme 1-36a).[79] Bis(ferrocenyl)borane **82** is a rare example of monomeric organylborane. Hydroboration of PhCCH and *t*BuCCH by **82** resulted in the two different bis(ferrocenyl)vinylboranes **84** and **85** (Scheme 1-36b).[79b] The reaction of dibromoferrocenylborane, $FcBBr_2$, with an excess of $HSiEt_3$ yielded bis(ferrocenyl)bromoborane **86** (Scheme 1-36c).[80] The bromine in **86** was readily replaced by a mesityl group, which gave the bis(ferrocenyl) species **87**.

Scheme 1-37. Synthesis of aluminum-bridged bis(ferrocenyl) species.

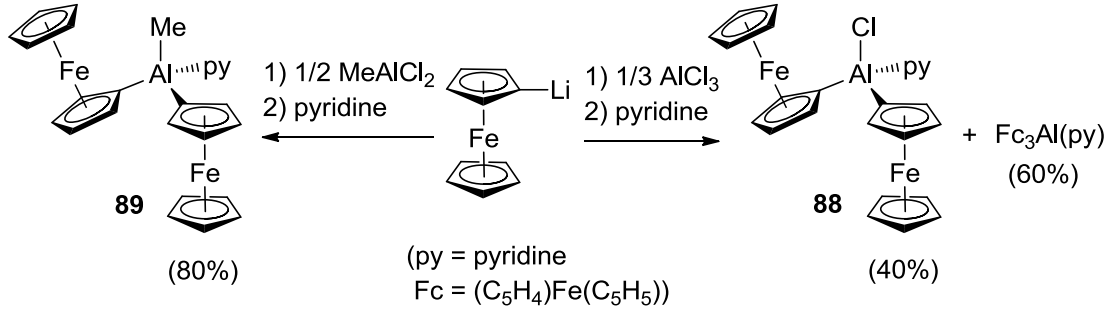

Only one report was published that described the synthesis of two bis(ferrocenyl) species with aluminum as bridging element.[81] The synthesis of aluminum-bridged bis(ferrocenyl) species (**88**, **89**; Scheme 1-37) followed the salt-metathesis route which involved the reaction of lithioferrocene and aluminum chlorides in the presence of a base. The aluminum-bridged bis(ferrocenyl) compounds **88** and **89** were obtained as a mixture

with other compounds and could not be isolated in pure form. Till today, there is no report of gallium- or indium-bridged bis(ferrocenyl) species.

1.3.2 [1.1]Ferrocenophanes Bridged by Group 14 and 13 Elements

The first [1.1]FCP was a dicarba[1.1]ferrocenophane (**90**: R = H; Scheme 1-38) reported by Nesmeyanov and Kritskaya et al. in 1956.[66] Since then, numerous dicarba[1.1]ferrocenophanes with CH_2, CHMe, CMe_2, CO as symmetric bridges and in combination of CH_2 and CO as unsymmetric bridges have been synthesized.[82] In 1973, Paul et al. solved the first molecular structure of a dicarba[1.1]ferrocenophane, which was a CHMe-bridged [1.1]FCP. Surprising, it was found to be a *syn* isomer, which is not a favoured conformation because of the steric crowding around bridging carbon atoms.[82c] The possible existence of the more favoured *anti* conformation of carbon-bridged [1.1]FCP was debated till 1993, when the structure of the *anti* conformation of CHMe-bridged [1.1]FCP was published.[82e] The *syn* conformer of the methylene-bridged [1.1]ferrocenophane catalyzed the formation of H_2 upon protonation in acidic aqueous solution.[82f] An intensive study of dicarba[1.1]ferrocenophanes was performed by Mueller-Westerhoff et al., who describe the synthesis of various carbon-bridged [1.1]FCPs (**90**) by employing different "flytrap" approaches (route A and B; Scheme 1-38).[82e] Mueller-Westerhoff et al. also synthesized the dicarba[1.1]ferrocenophnaes **90** by reducing the carbonyl-bridged [1.1]FCP **91** (route C; Scheme 1-38).[82e] Species **91** was synthesized in very poor yield by double Friedel-Crafts reaction of chlorocarbonylferrocene with itself (route D; Scheme 1-38).[82b]

Scheme 1-38. Synthesis of dicarba[1.1]ferrocenophanes.

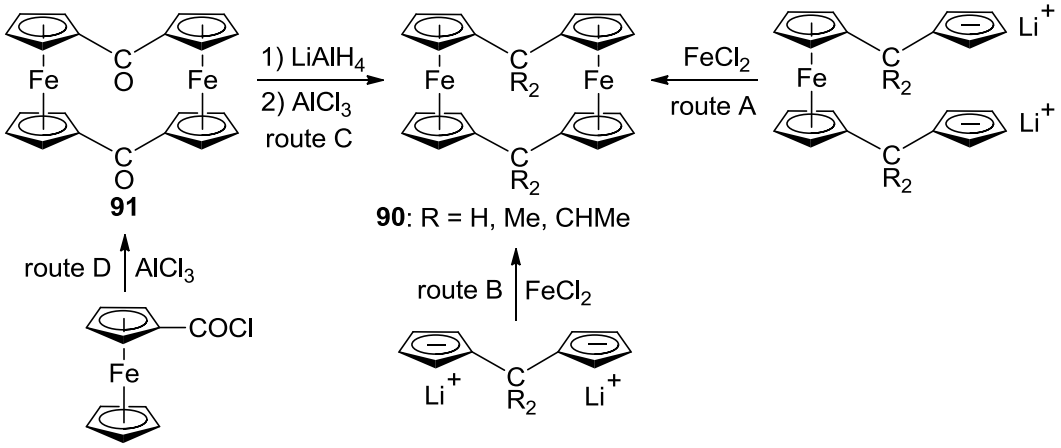

The first disila[1.1]ferrocenophane, a $SiMe_2$-bridged species (**92**) was reported independently by two groups in 1995. Both groups synthesized Me_2Si[1.1]FCP (**92**) by employing slightly different "flytrap" methods (Scheme 1-39).[83] Manners et al. also isolated **92** as a minor component from a mixture of poly(ferrocenyldimethylsilane)s, which was prepared either by transition-metal catalyzed ROP[51] or Lewis base induced

Scheme 1-39. Synthesis of Me_2Si-bridged [1.1]FCP.

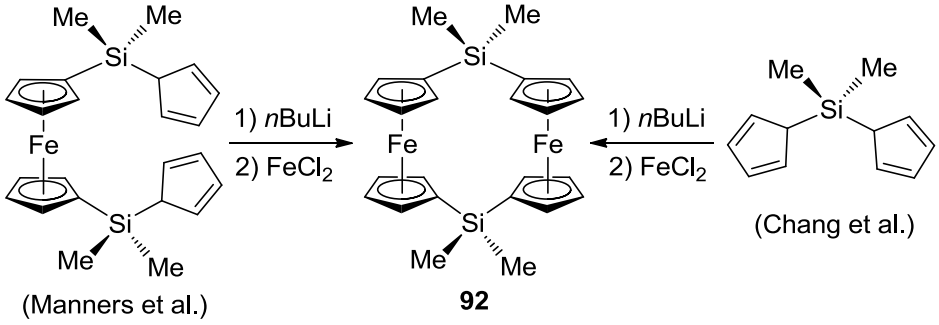

photocontrolled ROP[84] of Me_2Si[1]FCP. However, Tanaka et al. was able to synthesize **92** selectively from Me_2Si[1]FCP by using $Pd(PCy_3)_2Cl_2$ as a catalyst.[85] A similar species, Cl_2Si[1.1]FCP (**93;** Figure 1-9) was isolated by Cerveau et al. from a mixture of poly(ferrocenyldichlorosilane)s, which was synthesized by thermal ROP of Cl_2Si[1]FCP.[86] Another [1.1]FCP with (PhCC)(Me)Si-bridges (**94**; Figure 1-9) was

isolated as a byproduct from the Pt-catalyzed ROP of (PhCC)(Me)Si-bridged [1]FCP.[87] Similarly, the first penta-coordinated silicon-bridged [1.1]FCP (**95**; Figure 1-9) was isolated as a byproduct from the Pt-catalyzed ROP of the respective sila[1]ferrocenophane.[88]

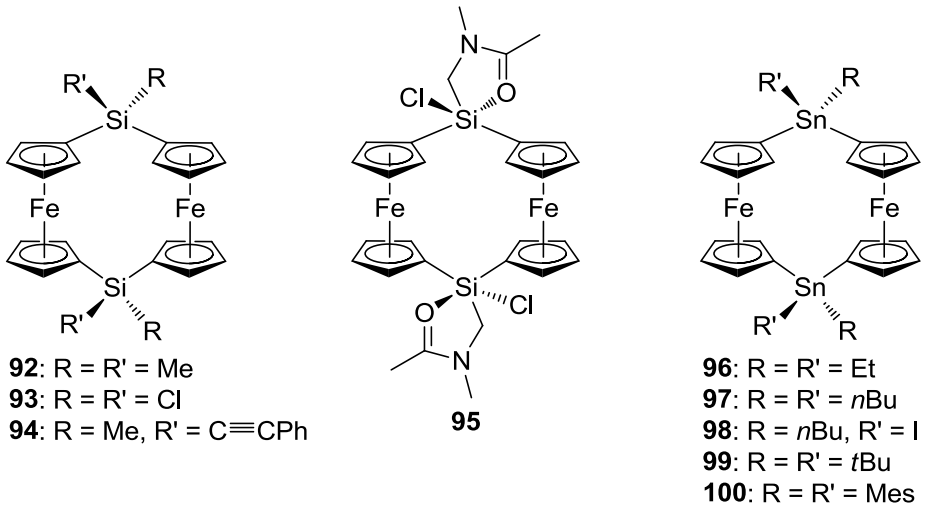

Figure 1-9. Silicon- and tin-bridged [1.1]FCPs.

Although, there are numerous carbon- and silicon-bridged [1.1]FCPs known in literature, surprisingly, there is no report of germanium-bridged [1.1]FCP. However, few examples of tin-bridged [1.1]FCPs are described in literature (Figure 1-9). In the early eighties, Seyferth et al. reported two tin-bridged [1.1]FCPs, one with Et_2Sn-bridge (**96**) and one with $n Bu_2Sn$-bridge (**97**).[30a] Species **96** and **97** were isolated from the reaction mixture of dilithioferrocene and respective dialkyltin dichlorides. The oxidation of **97** by iodine in CH_2Cl_2 resulted in a mixture of product, from which a new [1.1]FCP with (*n*Bu)ISn-bridges (**98**) was isolated by column chromatography.[89] Later in 1998, Manners et al. reported the isolation of two other tin-bridged [1.1]FCPs **99** and **100**, which were formed as a byproduct from the spontaneous ROP of the respective stanna[1]ferrocenophanes in solution.[9,31a]

Most of the carbon-bridged [1.1]FCPs adopt a *syn* conformation, whereas all known heavier group-14-bridged (Si, Sn) [1.1]FCPs exist as *anti* isomers. In general, group-14-bridged [1.1]FCPs are fluxional in solution and displayed *syn*-to-*syn* as well as *anti*-to-*anti* isomerization (Scheme 1-40). The degenerate isomerization (*syn*-to-*syn*) was described for the first time for dicarba[1.1]ferrocenophanes.[82e] Because of this fluxional behavior in solution, most of the group-14-bridged [1.1]FCPs displayed two signals for all Cp protons in their ^{1}H NMR spectra, one for α- and one for β-protons. However, the more rigid, *anti* conformer of Me_2C-bridged [1.1]FCP exhibited four signals for all Cp protons in the ^{1}H NMR spectrum.

Scheme 1-40. Degenerate *syn*-to-*syn* and *anti*-to-*anti* isomerization in group-14-bridged [1.1]FCPs.

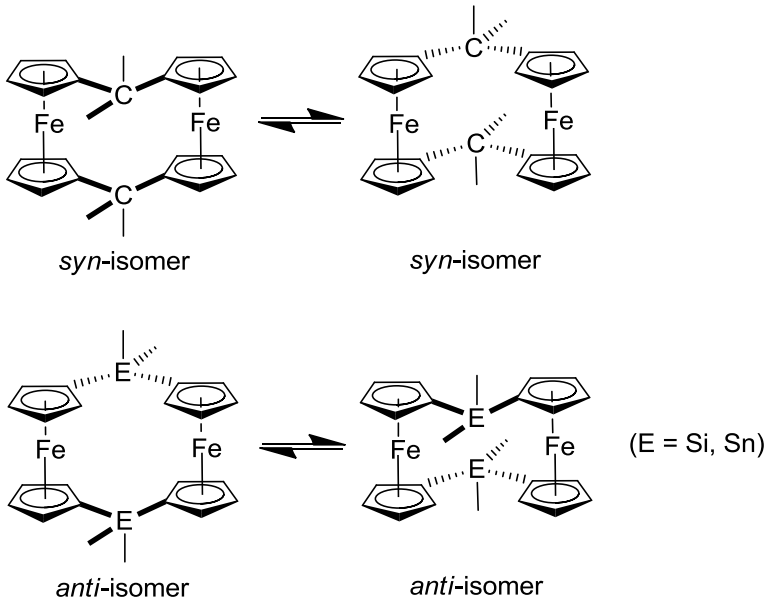

There are only few examples of group-13-bridged [1.1]FCPs. As illustrated in Scheme 1-41a, the reaction of dilithioferrocene with bis(dimethylboryl)ferrocene yielded an anionic diborata[1.1]ferrocenophane, **101**, which is a highly efficient lithium scavenger.[90] The molecular structure of the anionic diborata[1.1]ferrocenophane was determined by

single-crystal X-ray analysis and found to be a *syn* conformer. A different group made an unsuccessful attempt to synthesize the cationic diborata[1.1]ferrocenophane **103** from the neutral dibora[1.1]ferrocenophane **102** by treating it with bipyridine (Scheme 1-40b). However, no information about the synthesis and characterization of the neutral BrB-bridged [1.1]FCP **102** was provided.[91]

Scheme 1-41. (a) Synthesis of anionic diborata[1.1]ferrocenophane and (b) unsuccessful attempt to prepare cationic diborata[1.1]ferrocenophane.

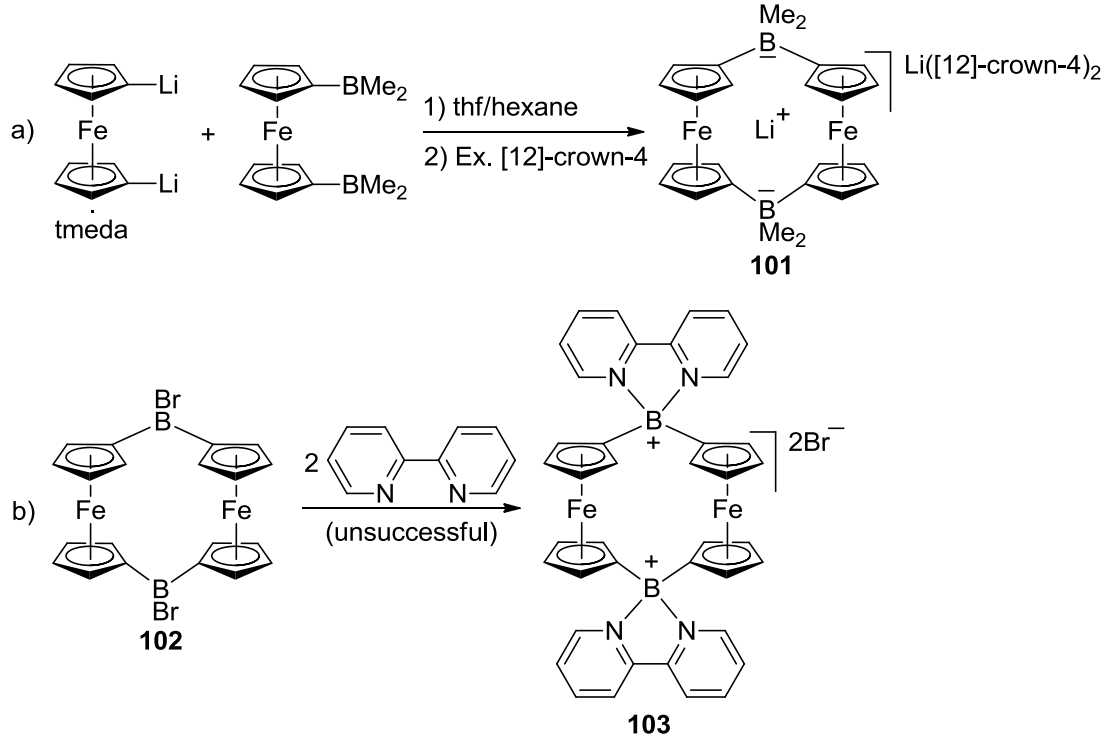

In 2005, the first aluminum-bridged [1.1]FCP (**104**; Figure 1-10) was isolated in very low yield by our group from the reaction of (Pytsi)$AlCl_2$ and dilithioferrocene in hexane.[92] However, the same reaction in toluene yielded the alumina[1]ferrocenophane **35a** (Scheme 1-9).[5] As illustrated in section 1.1.2, the salt-metathesis reaction of dilithioferrocene and aluminum and gallium dichlorides decorated with bulky ligands (Me_2Ntsi and Pytsi) resulted in strained [1]FCPs (**34a**, **34b**, **35a**, **35b**).[5,33] Two different

groups indepently reported a very different outcome of the salt-metathesis reaction of dilithioferrocene and element dichlorides, when slim ligand, Ar′ (Ar′: 2-(Me_2NCH_2)-C_6H_4; Figure 1-10) was employed.[93] Both of the dichlorides, (Ar′)$AlCl_2$ and (Ar′)$GaCl_2$ resulted in unstrained [1.1]FCPs (**105** and **106**; Figure 1-10), when treated with dilithioferrocene. However already in 2001, the first gallium-bridged [1.1]FCP (**107**; Figure 1-10) was synthesized by the salt-metathesis reaction of dilithioferrocene and lithium trichloroalkylgallate, Li[$Cl_3GaCH(SiMe_3)_2$].[94] In 2001 Jutzi et al. described the

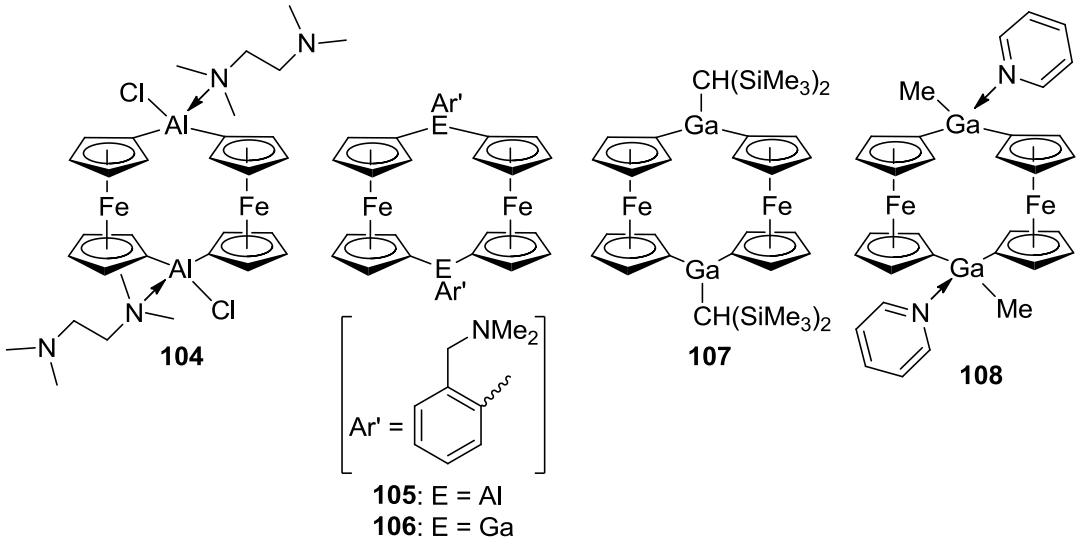

Figure 1-10. Aluminum- and gallium-bridged [1.1]FCPs.

isolation of a different gallium-bridged [1.1]FCP (**108**; Figure 1-10) as a byproduct, when 1,1'-bis(dimethylgallyl)ferrocene was heated in presence of pyridine.[95] Two years later, Jutzi et al. synthesized the donor-free gallium-bridged [1.1]FCP **109** from a solution of 1,1'-bis(dimethylgallyl)ferrocene in $CHCl_3$ (Scheme 1-42).[96] Crystals of the diethylether adduct of **109** were obtained, when a solution of bis(dimethylgallyl)ferrocene in Et_2O was cooled down to 6 °C. However at r.t., the ether-adduct decomposed to **109** and diethyl ether. The ether molecules in the adduct could be easily replaced by pyridine

donors (Scheme 1-42). Recently, a new aluminum-bridged [1.1]FCP, **110**, which is analogous to **108**, was synthesized by heating of a toluene solution of two ferrocene-derivatives (Scheme 1-43).[97]

Scheme 1-42. Synthesis and reactivity of gallium-bridged [1.1]FCPs.

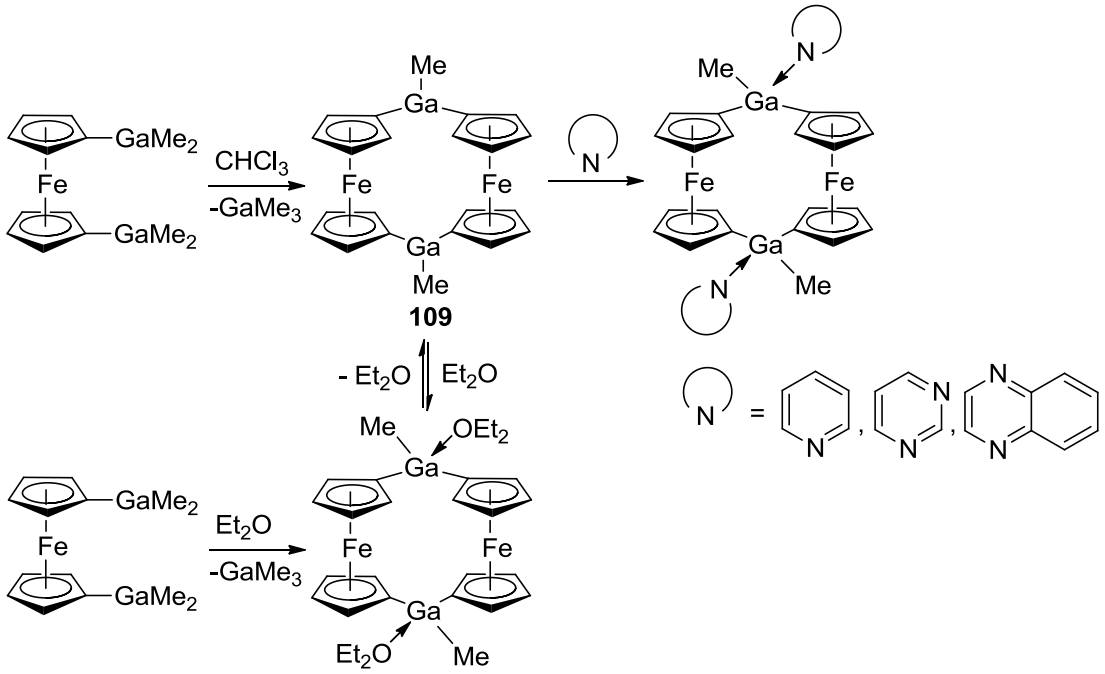

Scheme 1-43. Synthesis of aluminum-bridged [1.1]FCP.

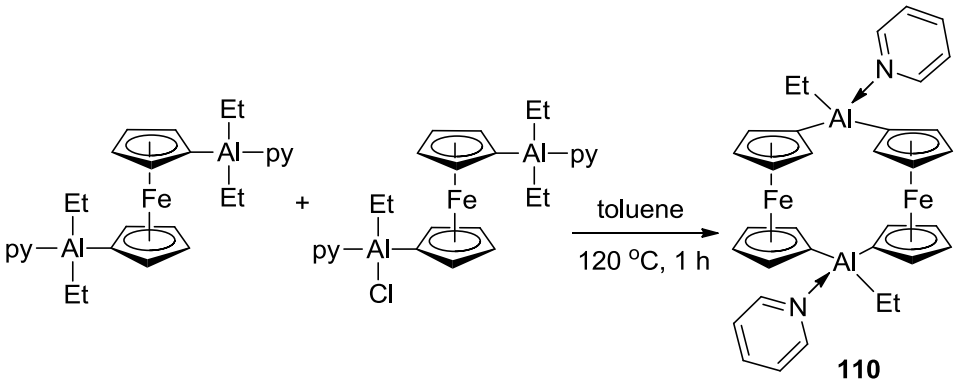

Indium-bridged [1.1]FCPs were reported only by our group (Figure 1-11). Indium dichlorides, equipped with either bulky ligand Me_2Ntsi or the slim Ar′ ligand, reacted with dilithioferrocene to yield respective diinda[1.1]ferrocenophanes, **111** and **112**.[93,98]

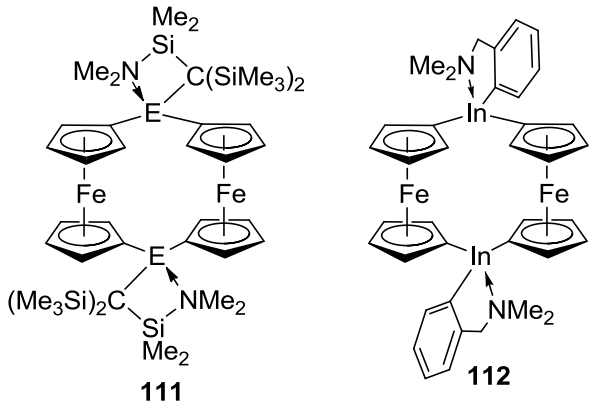

Figure 1-11. Indium-bridged [1.1]FCPs.

All heavier group-13-bridged [1.1]FCPs adopt *anti* conformation (Scheme 1-44). Gallium-bridged [1.1]FCPs, **107** (Figure 1-10) and **109** (Scheme 1-42) displayed fluxional behavior in solution.[94,96] In the respective ^{1}H NMR spectrs, they showed one signal for all α-protons and one signal for all β-protons. Species **108** (Figure 1-10) also displayed fluxional behavior. However, the analogous aluminum-bridged species, **110** (Scheme 1-43) appeared to be nonfluxional in solution as it exhibited four Cp signals in the ^{1}H NMR spectrum.[97] This difference in behavior, exhibited by aluminum- (**110**) and gallium-bridged (**108**) species, was attributed to the fact that the coordinative N(py)–Al bond in **110** is stronger than the N(py)–Ga bond in **108**.[97] In solution, degenerate *anti*-to-*anti* isomerization (Scheme 1-44) was not observed for the aluminum- and gallium-bridged [1.1]FCPs **105** and **106** (Figure 1-10), respectively, with more rigid environment around group 13 elements. In the ^{1}H NMR spectrum of diinda[1.1]ferrocenophane **111** with ligand Me_2Ntsi, two Cp signals were found for all 16 Cp protons.[98] The appeanrance of the two Cp signals was rationalized by fast, degenerate *anti*-to-*anti* isomerization (Scheme 1-44). In contrast, dynamic behavior of inda[1.1]ferrocenophane **112** with Ar′ ligands was not revealed by one dymentional NMR spectroscopy.[98] However, NOE

experiments clearly revealed the exchange of Cp protons, a clear indication of *anti*-to-*anti* isomerization.

Scheme 1-44. *Anti*-to-*anti* isomerization in heavier group-13-bridged [1.1]FCPs.

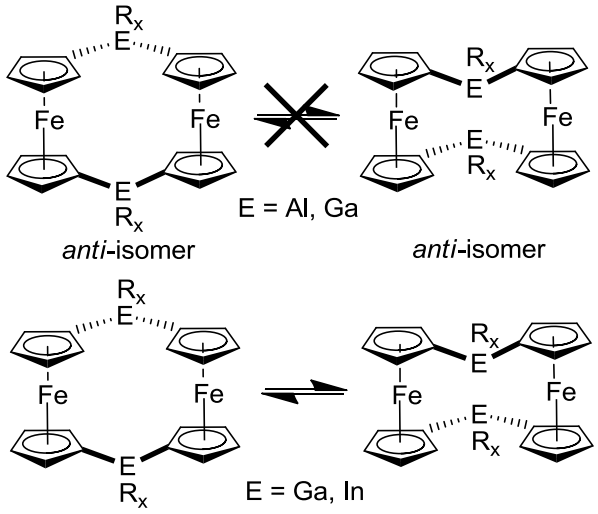

1.3.3 Ferrocene-Containing Macrocycles

Ferrocene-containing macrocycles are rare; there are only few examples reported in literature. In 1969, the first examples of macrocyclic ferrocenophanes, the methylene-bridged cyclic trimer (**113$_3$**), tetramer (**113$_4$**) and pentamer (**113$_5$**) were reported by Katz et al. (Scheme 1-45a).[99] They were characterized by NMR spectroscopy. The molecular structure of the CH_2-bridged [1^3]FCP **113$_3$** analyzed by single-crystal X-ray analysis was published in the following year.[100] These methylene-bridged ferrocenophanes **113$_3$**, **113$_4$** and **113$_5$** were isolated in low yields by column chromatography from a polymeric mixture obtained by the polycondesation reaction of $Li_2[(C_5H_4)_2CH_2]$ and $FeCl_2$ (Scheme 1-45a). However, Mueller-Westerhoff et al. synthesized methylene-bridged [1^4]FCP (**113$_4$**) in high yields by rapid mixing of a dilute solution of anionic dicyclopentadienyl linker with a dilute solution of $FeCl_2$ (Scheme 1-45b).[101] An analogous CH_2-bridged

[1[4]]metallocenophane with two alternative ferrocene and ruthenocene moieties was also reported by Mueller-Westerhoff et al.[82e] In the late nineties, Köhler et al. reported MALDI-TOF mass spectra of a doubly silicon-bridged cyclic poly(ferrocenylsilane)

Scheme 1-45. Synthesis of ferrocene-containing macrocycles.

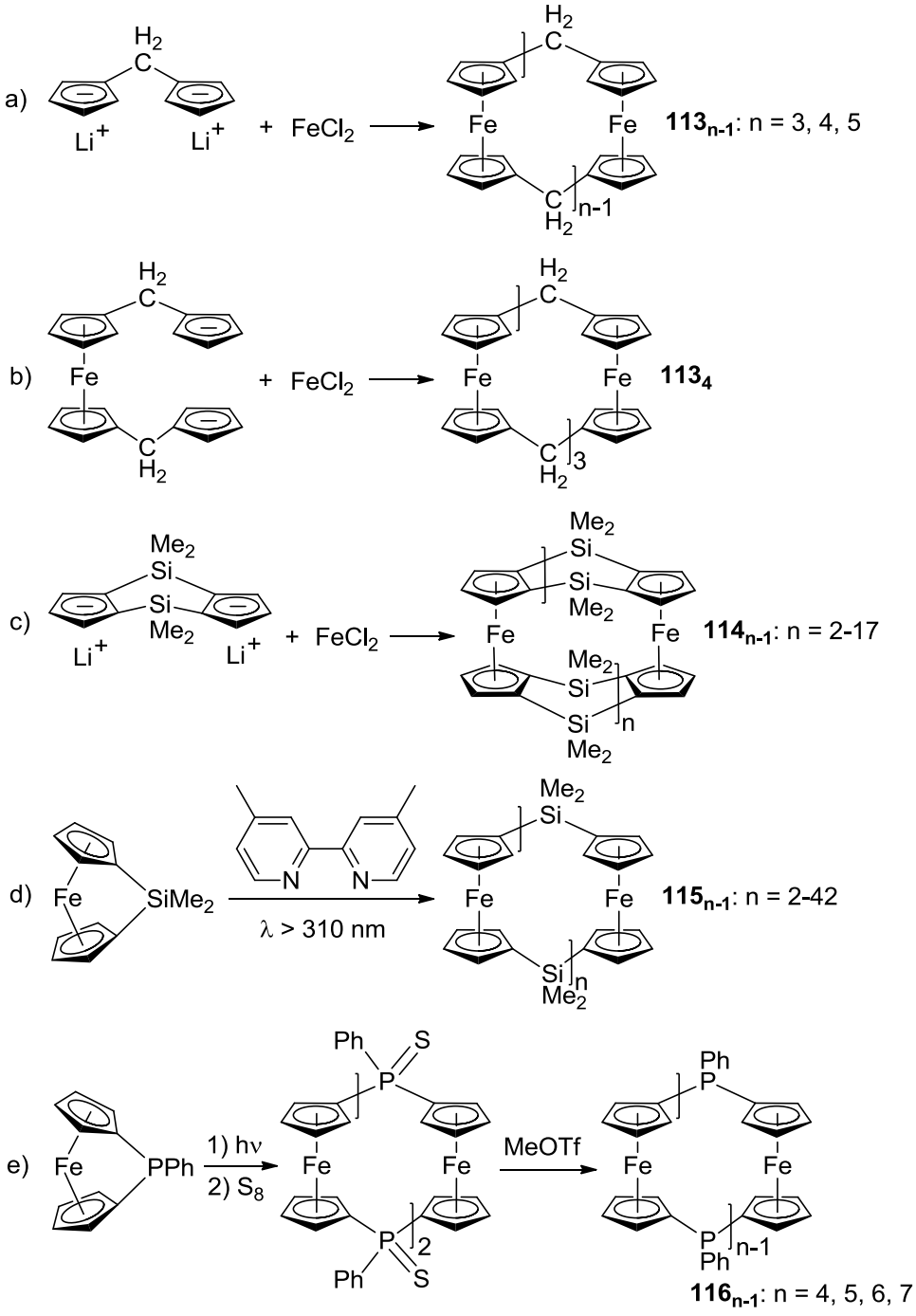

114_{n-1} with up to 17 ferrocene moieties (Scheme 1-45c). The polymer **114_{n-1}** was synthesized by reacting $Li_2[(C_5H_3)_2(SiMe_2)_2]$ and $FeCl_2$ (Scheme 1-45c).[102] They isolated the macrocycle with seven doubly silicon-bridged ferrocenophane (**114_7**), which is the largest isolated ferrocene-containing macrocycle till today. The molecular structure of **114_7** was also determined by single-crystal X-ray analysis. Recently, Manners et al. reported the cyclic, Me_2Si-bridged poly(ferrocene)s **115_{n-1}**, which were synthesized by base-catalyzed photocontrolled ROP of dimethylsila[1]ferrocenophane (Scheme 1-45d).[84] The MALDI-TOF mass analysis of **115_{n-1}** revealed the presence of macrocycles with more than 40 ferrocene units. Molecular structures of the tetramer **115_4**, pentamer **115_5**, hexamer **115_6**, and heptamer **115_7** were determined by single-crystal X-ray analysis. Mizuta et al. obtained a mixture of linear and cyclic poly(ferrocenylphosphane)s (**116_{n-1}**) by photocontrolled ROP of phospha[1]ferrocenophane and the PhP-bridged [1^3]FCP **116_3** was isolated and structurally characterized by single-crystal X-ray analysis (Scheme 1-45e).[103] Phosphorus-bridged cyclic tetramer (**116_4**), pentamer (**116_5**), and hexamer (**116_6**) were detected by MALDI TOF mass analysis, but could not be isolated in pure form.

1.3.4 Electrochemistry

There are two or more ferrocene moieties present in bis(ferrocenyl) species, [1.1]FCPs and ferrocene-containing macrocycles. The electronic communication between iron redox centers have been studied since 1970s. Possibly there are two types of iron-iron interaction in bridged-ferrocenes: 1) direct interaction through space and 2) interaction propagated through bonds.[104] Bis(ferrocenyl) species bridged by group 14 and 13 elements displayed stepwise oxidations of two iron centers: one iron gets oxidized at some potential, the positive charge is felt by the second iron, which gets oxidized at a

higher potential (Scheme 1-46). In 1973, Hendrickson et al. studied the electrochemistry of various bis(ferrocenyl) species bridged by -CH_2-, -CH_2CH_2-, -$(CH_3)_2CC(CH_3)_2$- and -$CH{=}CHC_6H_4CH{=}CH$-. The CH_2-bridged species (**73**: R = H; Scheme 1-34d) exhibited two reversible oxidation waves with half wave potential, $\Delta E^{0\prime}$ ($\Delta E^{0\prime}$ = separation between two oxidation potentials) of 170 mV, while other three bis(ferrocenyl) species with -CH_2CH_2-, -$(CH_3)_2CC(CH_3)_2$- and -$CH{=}CHC_6H_4CH{=}CH$-bridges showed only one reversible redox wave in differential pulse voltammogram (using CH_3CN as solvent and $[Et_4N][ClO_4]$ as supporting electrolyte).[104] The iron-iron distances increase with the number of bridging C-atoms. Thus, the observation of two redox waves for the CH_2-bridged bis(ferrocenyl) species is consistent with the closest iron-iron distance, where the positive charge on one iron is felt by the other iron. Very recently, Han et al. performed the cyclic voltammetry of bis(ferrocenyl) compounds bridged by CMe_2, CMeEt, CMe(*n*Bu) and CMePh (**67**; Scheme 1-34a) in CH_2Cl_2 using $[n\text{Bu}_4N][PF_6]$ as supporting electrolyte.[69] All these compounds displayed two reversivle redox waves with $\Delta E^{0\prime}$ in the close range of 195-223 mV. Manners et al. also observed two reversible redox waves with $\Delta E^{0\prime}$ of 150 mV for the $SiMe_2$-bridged bis(ferrocenyl) species **74** (Scheme 1-35a), when electrochemistry was performed in a 1:1 mixture of CH_2Cl_2 and CH_3CN using $[n\text{Bu}_4N][PF_6]$ as the supporting electrolyte.[46] In bis(ferrocenyl) compounds, the iron-iron distance also increases with the increase of the size of bridging element, and therefore, $\Delta E^{0\prime}$ should decrease from smaller bridging element to larger bridging elements. The cyclic voltammetry (solvent: thf, supporting electrolyte: $[n\text{Bu}_4N][PF_6]$) of CMe_2 (**79**; Scheme 1-35e), $SiMe_2$ (**80**; Scheme 1-35e), and $GeMe_2$-bridged (**81**; Scheme 1-35e) bis(ferrocenyl) compounds displayed two reversible redox waves.[78] The half wave

potential decreased in the order CMe_2 (113 mV)>$SiMe_2$ (93 mV)>$GeMe_2$ (74 mV), which was consistent with the increasing iron-iron separation. Therefore, a through-space interaction was proposed for these bis(ferrocenyl) species. Boron is even smaller than that of carbon, and thus, it was not surprising that the MesB-bridged bis(ferrocenyl) species **87** (Scheme 1-36c) displayed two reversible redox waves with a large separation of 422 mV in CH_2Cl_2 using [nBu$_4$N][B(C_6F_5)$_4$] as supporting electrolyte. The high $\Delta E^{0\prime}$ displayed by [(C_5H_5)Fe(C_5H_4)]BMes indicated a very strong electronic communication between two close iron redox centers, which are significantly close to each other.

Scheme 1-46. Stepwise redox process for bis(ferrocenyl) compounds.

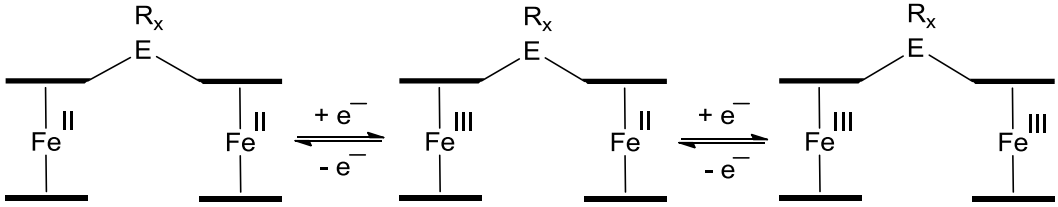

Similar to bis(ferrocenyl) species, [1.1]FCP also possess two iron redox centers and generally exhibits two reversible redox waves. The $\Delta E^{0\prime}$ for Me_2Si- (**92**; Figure 1-9) and nBu$_2$Sn-bridged (**97**; Figure 1-9) [1.1]FCPs are 250 mV and 200 mV, respectively. This result is consistent with the iron-iron separation of 5.17 Å for Me_2Si[1.1]FCP and 5.50 Å for nBu$_2$Sn[1.1]FCP.[83a,89] However, CH_2-bridged [1.1]FCP (**90**: R = H; Scheme 1-38) displayed a lower $\Delta E^{0\prime}$ of 200 mV as compared to silicon-bridged [1.1]FCPs, which is contradictory to the shorter iron-iron separation of 4.82 Å.[105] Manners et al proposed that more efficient through-bond communication was responsible for the larger $\Delta E^{0\prime}$ observed for Me_2Si- and nBu$_2$Sn-bridged [1.1]FCPs as compared to the smaller $\Delta E^{0\prime}$ of H_2C-bridged species. The cyclic voltammetry of borata[1.1]FCP (**101**; Scheme 1-41a) displayed a complex behavior. At first the species was irreversibly oxidized at -0.58 V

(vs. ferrocene/ferrocenium). Two partially reversible waves emerged at even higher negative potentials, when the sweep was continued into the cathodic regime.[90] The authors suggested that the strange electrochemical behavior was a result of some unknown chemical processes. The cyclic voltammetry of the gallium [1.1]FCP **106** (Figure 1-10) exhibited two reversible redox waves, each corresponded to one electron.[93] The analogous indium species **112** (Figure 1-11) showed two major and two minor redox waves. It was suggested that the set of two redox waves was probably due to the presence of two isomers of **112** that can be differentiated by cyclic voltammetry in solution. This stepwise oxidation of two iron centers, which is characteristic for most [1.1]FCPs, displayed by Ga and In-bridged [1.1]FCPs was classified as class II behavior, according to Robin-Day classification. However, the aluminum-bridged [1.1]FCP **105** (Figure 1-10) showed an unprecedented behavior with a fully reversible redox wave corresponding to two-electron event.[93] The lack of electronic communication between the iron centers in alumina[1.1]ferrocenophane was categorized as a class I behavior. However, the cyclic voltammetry of diinda[1.1]ferrocenophane **111** (Figure 1-11) exhibited an irreversible oxidation wave.[98] This unprecedented result was probably due to the degradation of **111** under the condition of the electrochemical measurement.

The ferrocene-containing macrocycles contains more than two iron redox centers often displayed complex electrochemical behaviors. An intensive electrochemical study was conducted for the Me_2Si-bridged [1.1]FCP **92** (Figure 1-9) and the larger cyclic species **115_3**, **115_4**, **115_5**, **115_6**, and **115_7** (Scheme 1-45d) in a 1:1 mixture of CH_2Cl_2 and C_6H_5CN. The data was interpreted with the proposed redox events as illustrated in Scheme 1-47.[84b] As expected, the cylic dimer **92** showed two reversible redox waves

($\Delta E^{0\prime}$ = 240 mV), which suggests stepwise oxidation of two iron centers. The cyclic tetramer **115_4** displayed two broad redox waves indicating two sets of two overlapping one-electron redox processes. The cyclic hexamer **115_6** showed two even broader redox waves. This behavior was explained by the oxidation of three alternative iron centers

Scheme 1-47. Illustraion of proposed redox events for cyclic oligo(ferrocenylsilane)s (O represents a ferrocene unit and — represents an element bridge).

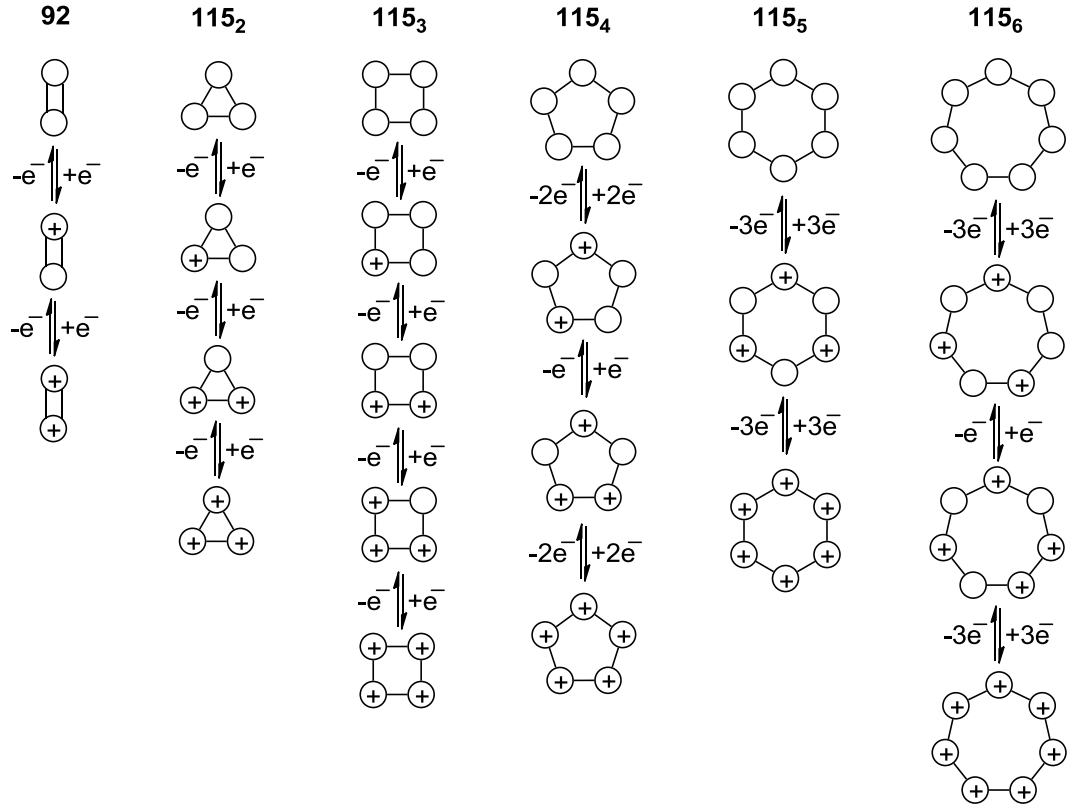

followed by the oxidation of three intervening irons. Cyclic oligo(ferrocenyldimethylsilanes) with odd number of ferrocene moieties (**115_3**, **115_5**, and **115_7**) displayed three redox waves. For the cyclic trimer **115_3**, the intensity ratio of three redox waves was 1:1:1 indicating stepwise oxidation of three iron centers. The cyclic pentamer **115_5** showed three redox waves with 2:1:2 intensity ratios and the three redox waves correspond to two, one and two electrons, respectively. Similarly, a relative

intensity ratio of 3:1:3 for three partially overlapped redox waves was observed for the cyclic heptamer **115_7**. The three redox waves corresponded to three, one and three electrons, respectively. However, the doubly Me_2Si-bridged cyclic heptamer **114_7** (Scheme 1-45c) exhibited three nicely resolved redox waves with 3:1:3 intensity ratios.[102]

1.4 Research Objectives

Part 1. The primary objective of my Ph.D. work was to synthesize strained [1]metallocenophanes with heavier group 13 elements as bridges, which would be reactive enough to yield poly(metallocene)s through ROP. As mentioned earlier, transition-metal-containing metallopolymers with excellent electronic and optical properties have potential applications in future technology and, thus, it is important to synthesize new metallopolymers. A wide variety of poly(metallocene)s with group 14, 15 and 16 elements as bridges have been synthesized by ROP of respective [n]metallocenophanes. However, poly(metallocene)s with group 13 elements as bridges are very rare. In spite of the high strain possessed by bora[1]ferrocenophanes, the attempted ROPs were not very successful (Scheme 1-28). Before this Ph.D. work was undertaken, our group had reported the first heavier group-13-bridged (Al, Ga) [1]metallocenophanes, which were obtained by reacting dilithiometallocenes with element dihalides equipped with appropriate ligands. For example, Jörg A. Schachner, a former member in our group, synthesized aluminum- and gallium-bridged [1]FCPs and [1]RCPs by employing the sterically bulky ligands Me_2Ntsi and Pytsi (Scheme 1-9). However, the attempted ROP of those strained [1]metallocenophanes were either unsuccessful or sluggish. The reasons for the unsuccessful ROPs were not clearly understood. It seemed that the bulky ligands hindered the attack of the ring-opening initiators (Scheme 1-31). Jörg A. Schachner isolated heavier group-13-bridged (Al, Ga, In) [1.1]FCPs, when the slimmer Ar′ ligand was employed. Those [1.1]FCPs were devoid of ring-strain and could not be utilized as monomers for ROP to yield metallopolymers. Therefore, the crucial strategy of this Ph.D. thesis was to design and synthesize suitable ligands for heavier group 13 elements, which could give access to new reactive

[1]metallocenophanes in the respective salt-metathesis reactions. Obviously, the ultimate goal of my research was to explore the reactivity of those strained [1]metallocenophanes for the synthesis of heavier group-13-bridged poly(metallocene)s. ROP of [1]metallocenophanes under controlled reaction conditions is of key importance to obtained metallopolymers with well-defined properties such as molecular weight and molecular structure, which are important features for further use in technology. An ultimate goal of my Ph.D. work was the synthesis of poly(metallocene)s by ROP of heavier group-13-bridged [1]metallocenophanes under controlled reaction conditions.

Chapter 2 describes my research of using the sterically bulky ligand Mamx for the synthesis of the new strained [1]FCPs and [1]RCPs with aluminum, gallium and indium as bridging elements. The ROP behaviors of those reactive [1]metallocenophanes are discussed as well. Chapter 2 contains three subchapters, which are the verbatim copies of a published communication as well as a published article, and a manuscript which is under preparation for submission. Moreover, selective materials from supporting information are included. At the beginning of each subchapter, there is a short summary of the work, a preface describing the contribution made by each author, and a section addressing how each contribution is related to the research objectives.

Part 2. The other vital objective of my research was to study the electronic communication between metal centers in metallocene-derivatives that contain two or more redox centers. As discussed before, the metal-metal interaction in bis(ferrocenyl) species with group 14 elements (C, Si, Ge, Sn) has been studied intensively. However, a few boron-bridged bis(ferrocenyl) compounds and their electrochemistry were reported. There was no examples of a well-characterized bis(ferrocenyl) species with heavier group

13 elements in bridging possition. Therefore, a primary goal of this research was to synthesize heavier group-13-bridged (Al, Ga) bis(ferrocenyl) species and study the electronic communication between the two iron redox centers. The heavier group-13-bridged (Al, Ga, In) [1.1]FCPs and their electrochemistry were described by our group before my Ph.D. work was started. As the unprecedented electrochemical behavior exhibited by aluminum- and indium-bridged [1.1]FCPs was not accounted for, another goal of my Ph.D. work was to reinvestigate and shed some light on the electrochemistry of [1.1]FCPs with heavier group 13 elements. Even though numerous [1.1]FCPs with a wide range of bridging elements are known, not a single example of an unsymmetrically bridged [1.1]FCP, a compound with two different bridging elements, was known. Therefore, a synthetic strategy to get access to such species was explored. The research toward unsymmetrically bridged [1.1]FCPs led to discoveries that triggered new investigations. The reaction of dilithiated ferrocene-derivatives, where two lithioferrocene moieties are connected by a silicon-bridge, with element dichlorides resulted in a series of linear and macrocyclic poly(ferrocene)s. On the same line of thought, an old reaction of dilithioferrocene and tin dichlorides was reinvestigated.

Chapter 3 describes the outcome of the research carried out to synthesize bis(ferrocenyl) species and [1.1]FCPs with heavier group 13 element bridges, and unsymmetrically bridged [1.1]FCPs equipped with two different bridging elements. This chapter also describes the metal-metal interaction of redox centers in bis(ferrocenyl) species, [1.1]FCPs and ferrocene-containing macrocycles. Chapter 3 contains four subchapters which are the verbatim copies of a published article, a published

communication, a submitted manuscript, and a manuscript, which is under preparation for submission.

1.5 References

(1) Rinehart, K. L.; Frerichs, Jr. A. K.; Kittle, P. A.; Westman, L. F.; Gustafson, D. H.; Pruett, R. L.; McMahon, J. E. *J. Am. Chem. Soc.* **1960**, *82*, 4111-4112.

(2) Osborne, A. G.; Whiteley, R. H. *J. Organomet. Chem.* **1975**, *101*, C27-C28.

(3) Brandt, P. F.; Rauchfuss, T. B. *J. Am. Chem. Soc.* **1992**, *114*, 1926-1927.

(4) Rulkens, R.; Gates, D. P.; Balaishis, D.; Pudelski, J. K.; McIntosh, D. F.; Lough, A. J.; Manners, I. *J. Am. Chem. Soc.* **1997**, *119*, 10976-10986.

(5) Schachner, J. A.; Lund, C. L.; Quail, J. W.; Müller, J. *Organometallics* **2005**, *24*, 785-787.

(6) Fischer, A. B.; Kinney, J. B.; Staley, R. H.; Wrighton, M. S. *J. Am. Chem. Soc.* **1979**, *101*, 6501-6506.

(7) (a) Seyferth, D.; Withers, Jr. H. P. *J. Organomet. Chem.* **1980**, *185*, C1-C5. (b) Stoeckli-Evans, H.; Osborne, A. G.; Whiteley, R. H. *J. Organomet. Chem.* **1980**, *194*, 91-101.

(8) Foucher, D. A.; Manners, I. *Macromol. Chem. Rapid Commun.* **1993**, *14*, 63-66.

(9) Jäkle, F.; Rulkens, R.; Zech, G.; Foucher, D. A.; Lough, A. J.; Manners, I. *Chem.−Eur. J.* **1998**, *4*, 2117-2128.

(10) (a) Wrighton, M. S.; Palazzotto, M. C.; Bocarsly, A. B.; Bolts, J. M.; Fischer, A. B.; Nadjo, L. *J. Am. Chem. Soc.* **1978**, *100*, 7264-7271. (b) Butler, I. R.; Cullen, W. R.; Ni, J.; Rettig, S. J. *Organometallics* **1985**, *4*, 2196-2201. (c) Vogel, U.; Lough, A. J.; Manners, I. *Angew. Chem., Int. Ed.* **2004**, *43*, 3321-3325. (d) Herberhold, M.; Hoffmann, T.; Weinberger, S.; Wrackmeyer, B. *Z. Naturforsch. B* **1997**, *52*, 1037-1042.

(11) Green, J. C.; *Chem. Soc. Rev.* **1998**, *27*, 263-272.

(12) Foucher, D. A.; Tang, B.-Z.; Manners, I. *J. Am. Chem. Soc.* **1992**, *114*, 6246-6248.

(13) MacLachlan, M. J.; Ginzburg, M.; Coombs, N.; Coyle, T. W.; Raju, N. P.; Greedan, J. E.; Ozin, G. A.; Manners, I. *Science* **2000**, *287*, 1460-1463.

(14) Arsenault, A. C.; Puzzo, D. P.; Manners, I.; Ozin, G. A. *Nature Photonics* **2007**, *1*, 468-472.

(15) Ma, Y. J.; Dong, W. F.; Hempenius, M. A.; Möhwald, H.; Vancso, G. J. *Nature Mater.* **2006**, *5*, 724-729.

(16) Gädt, T.; Ieong, N. S.; Cambridge, G.; Winnik, M. A.; Manners, I. *Nature Mater.* **2009**, *8*, 144-150.

(17) (a) Herbert, D. E.; Mayer, U. F. J.; Manners, I. *Angew. Chem., Int. Ed.* **2007**, *46*, 5060-5081. (b) Bellas, V.; Rehahn, M. *Angew. Chem., Int. Ed.* **2007**, *46*, 5082-5104.

(18) Prashar, S.; Antiñolo, A.; Otero, A. *Coord. Chem. Rev.* **2006**, *250*, 133–154.

(19) Stelck, D. S.; Shapiro, P. J.; Basickes, N.; Rheingold, A. L. *Organometallics* **1997**, *16*, 4546-4550.

(20) Braunschweig, H.; von Koblinski, C.; Wang, R. *Eur. J. Inorg. Chem.* **1999**, 69-73.

(21) Lund, C. L.; Hanson, S. S.; Schatte, G.; Quail, J. W.; Müller, J. *Organometallics* **2010**, *29*, 6038-6044.

(22) Antinolo, A.; Otero, A.; Prashar, S.; Rodriguez, A. M. *Organometallics* **1998**, *17*, 5454-5459.

(23) (a) Schaper, F.; Wrobel, O.; Schwoerer, R.; Brintzinger, H.-H. *Organometallics* **2004**, *23*, 3552-3555. (b) Labella, L.; Chernega A.; Green, M. L. H.; *J. Chem. Soc. Dalton Trans.* **1995**, 395-402. (c) Chernega, A.; Cook, J.; Green, M. L. H.; Labella, L.; Simpson, S. J.; Souter J.; Stephens, A. H. H. *J. Chem. Soc. Dalton Trans.* **1997**, 3225-

3243. (d) Conway, S. L. J.; Dijkstra, T.; Doerrer, L. H.; Green, J. C.; Green, M. L. H.; Stephens, A. H. H. *J. Chem. Soc. Dalton Trans.* **1998**, 2689-2695.

(24) (a) Heinekey, D. M.; Radzewich, C. E. *Organometallics* **1999**, *18*, 3070-3074. (b) Conway, S. L. J.; Doerrer, L. H.; Green, J. C.; Green, M. L. H.; Scottow, A.; Stephens, A. H. H.; *J. Chem. Soc. Dalton Trans.* **2000**, 329-333.

(25) (a) Osborne, A. G.; Whiteley, R. H.; Meads, R. E. *J. Organomet. Chem.* **1980**, *193*, 345-357. (b) Calleja, G.; Carré, F.; Cerveau, G.; Corriu, R. J. P.; *C. R. Acad. Sci. Ser. IIc* **1998**, *1*, 285-291. (d) Foucher, D.; Ziembinski, R.; Petersen, R.; Pudelski, J.; Edwards, M.; Ni, Y. Massey, J. Jaeger, C. R.; Vancso, G. J.; Manners, I. *Macromolecules* **1994**, *27*, 3992-3999. (e) Zechel, D. L.; Hultszch, K. C.; Rulkens, R.; Balaishis, D.; Ni, Y.; Pudelski, J. K.; Lough, A. J.; Manners, I.; Foucher, D. A. *Organometallics* **1996**, *15*, 1972-1978. (f) Nguyen, P.; Lough, A. J.; Manners, I. *Macromol. Rapid Commun.* **1997**, *18*, 953-959.

(26) (a) Jäkle, F.; Vejzovic, E.; Power-Billard, K. N.; MacLachlan, M. J.; Lough, A. J.; Manners, I. *Organometallics* **2000**, *19*, 2826-2828. (b) Hatanaka, Y.; Okada, S.; Minami, T.; Goto, M.; Shimada, K. *Organometallics* **2005**, *24*, 1053-1055.

(27) MacLachlan, M. J.; Lough, A. J.; Geiger, W. E.; Manners, I. *Organometallics* **1998**, *17*, 1873-1883.

(28) (a) Masson, G.; Beyer, P.; Cyr, P.W.; Lough, A. J.; Manners, I. *Macromolecules* **2006**, *39*, 3720-3730. (b) Peckham, T. J.; Foucher, D. A.; Lough, A. J.; Manners, I. *Can. J. Chem.* **1995**, *73*, 2069-2078. (c) Pudelski, J. K.; Foucher, D. A.; Honeyman, C. H.; Lough, A. J.; Manners, I.; Barlow, S.; O'Hare, D. *Organometallics* **1995**, *14*, 2470-2479.

(d) Schultz, M.; Sofield, C. D.; Walter, M. D.; Andersen, R. A. *New J. Chem.* **2005**, *29*, 919-927.

(29) (a) Foucher, D. A.; Edwards, M.; Burrow, R. A.; Lough, A. J.; Manners, I. *Organometallics* **1994**, *13*, 4959-4966. (b) Kapoor, R. N.; Crawford, G. M.; Mahmoud, J.; Dementiev, V. V.; Nguyen, M. T.; Diaz, A. F.; Pannell, K. H. *Organometallics* **1995**, *14*, 4944-4947.

(30) (a) Seyferth, D.; Withers, H. P. *Organometallics* **1982**, *1*, 1275-1282. (b) Clearfield, A.; Simmons, C. J.; Withers, H. P.; Seyferth, D. *Inorg. Chim. Acta* **1983**, *75*, 139-144.

(31) (a) Rulkens, R.; Lough, A. J.; Manners, I. *Angew. Chem., Int. Ed.* **1996**, *35*, 1805-1807. (b) Sharma, H. K.; Cervantes-Lee, F.; Mahmoud, J. S.; Pannell, K. H. *Organometallics* **1999**, *18*, 399-403.

(32) (a) Braunschweig, H.; Dirk, R.; Müller, M.; Nguyen, P.; Resendes, R.; Gates, D. P.; Manners, I. *Angew. Chem., Int. Ed.* **1997**, *36*, 2338-2340. (b) Berenbaum, A.; Braunschweig, H.; Dirk, R.; Englert, U.; Green, J. C.; Jäkle, F.; Lough, A. J.; Manners, I. *J. Am. Chem. Soc.* **2000**, *122*, 5765-5774.

(33) (a) Schachner, J. A.; Lund, C. L.; Quail, J. W.; Müller, J. *Organometallics* **2005**, *24*, 4483-4488. (b) Lund, C. L.; Schachner, J. A.; Quail, J. W.; Müller, J. *Organometallics* **2006**, *25*, 5817-5823.

(34) (a) Vogel, U.; Nelson, J. M.; Manners, I. unpublished results. (b) Bagh, B.; Müller, J. unpublished results.

(35) Nelson, J. M.; Lough, A. J.; Manners, I. *Angew. Chem., Int. Ed.* **1994**, *33*, 989-991.

(36) Vogel, U.; Lough, A. J.; Manners, I. *Angew. Chem., Int. Ed.* **2004**, *43*, 3321-3325.

(37) Schachner, J. A.; Tockner, S.; Lund, C. L.; Quail, J. W.; Rehahn, M.; Müller, J. *Organometallics* **2007**, *26*, 4658-4662.

(38) Arimoto, F. S.; Haven, A. C. *J. Am. Chem. Soc.* **1955**, *77*, 6295-6297.

(39) Withers, H. P.; Seyferth, D.; Fellmann, J. D.; Garrou, P. E.; Martin, S. *Organometallics* **1982**, *1*, 1283-1288.

(40) (a) Rosenberg, H.; Rausch, M. D. US 3060215, **1962**. (b) Rosenberg H. (US Air Force), US 3426053, **1969**.

(41) (a) Cypryk, M.; Gupta, Y.; Matyjaszewski, K. *J. Am. Chem. Soc.* **1991**, *113*, 1046-1047. (b) Fossum, E.; Matyjaszewski, K. *Macromolecules* **1995**, *28*, 1618-1625.

(42) Rózga-Wijas, K.; Chojnowski, J.; Zundel. T.; Boileau, S. *Macromolecules* **1996**, *29*, 2711-2720.

(43) Manners, I.; Riding, G. H.; Dodge, J. A.; Allcock, H. R. *J. Am. Chem. Soc.* **1989**, *111*, 3067-3069.

(44) Pudelski, J. K.; Manners, I. *J. Am. Chem. Soc.* **1995**, *117*, 7265-7266.

(45) Rulkens, R.; Lough, A. J.; Manners, I. *J. Am. Chem. Soc.* **1994**, *116*, 797-798.

(46) (a) Rulkens, R.; Lough, A. J.; Manners, I.; Lovelace, S. R.; Grant, C. Geiger, W. E. *J. Am. Chem. Soc.* **1996**, *118*, 12683-12695. (b) Ni, Y.; Rulkens, R.; Manners, I. *J. Am. Chem. Soc.* **1996**, *118*, 4102-4114.

(47) Mizuta, T.; Onishi, M.; Miyoshi, K. *Organometallics* **2000**, *19*, 5005-5009.

(48) Mizuta, T.; Imamura, Y.; Miyoshi, K.; Yorimitsu, H.; Oshima, K. *Organometallics* **2005**, *24*, 990-996.

(49) Tanabe, M.; Manners, I. *J. Am. Chem. Soc.* **2004**, *126*, 11434-11435.

(50) Reddy, N. P.; Yamashita, H.; Tanaka, M. *J. Chem. Soc. Chem. Commun.* **1995**, 2263-2264.

(51) Ni, Y.; Rulkens, R.; Pudelski, J. K.; Manners, I. *Macromol. Rapid Commun.* **1995**, *16*, 637-641.

(52) Sheridan, J. B.; Temple, K.; Lough, A. J.; Manners, I. *J. Chem. Soc. Dalton Trans.* **1997**, 711-713.

(53) Temple, K.; Jäkle, F.; Sheridan, J. B.; Manners, I. *J. Am. Chem. Soc.* **2001**, *123*, 1355-1364.

(54) Rinehart, Jr., K. L.; Frerichs, A. K.; Kittle, P. A.; Westman, L. F.; Gustafson, D. H.; Pruett, R. L.; McMahon, J. E. *J. Am. Chem. Soc.* **1960**, *82*, 4111-4112.

(55) (a) Lentzner, H. L.; Watts, W. E. *Tetrahedron* **1971**, *27*, 4343-4351. (b) Nelson, J. M.; Rengel, H.; Manners, I. *J. Am. Chem. Soc.* **1993**, *115*, 7035-7036.

(56) Hafner, K.; Mink, C.; Lindner, H. J. *Angew. Chem., Int. Ed.* **1994**, *33*, 1479-1480.

(57) Buretea, M. A.; Tilley, T. D. *Organometallics* **1997**, *16*, 1507-1510.

(58) Arisandy, C.; Cowley, A. R.; Barlow, S. *J. Organomet. Chem.* **2004**, *689*, 775-780.

(59) (a) Heo, R. W.; Somoza, F. B.; Lee, T. R. *J. Am. Chem. Soc.* **1998**, *120*, 1621-1622. (b) Heo, R. W.; Park, J. S.; Lee, T. R. *Macromolecules* **2005**, *38*, 2564-2573.

(60) Hempenius, M. A.; Brito, F. F.; Vancso, J. G. *Macromolecules* **2003**, *36*, 6683-6688.

(61) Ieong, N. S.; Manners, I. *Macromol. Chem. Phys.* **2009**, *210*, 1080-1086.

(62) Peckham, T. J.; Massey, J. A.; Edwards, M.; Manners, I. *Macromolecules* **1996**, *29*, 2396-2403.

(63) Mochida, K.; Shibayama, N.; Goto, M. *Chem. Lett.* **1998**, 339-340.

(64) Heilmann, J. B.; Scheibitz, M.; Qin, Y.; Sundararaman, A.; Jäkle, F.; Kretz, T.; Bolte, M.; Lerner, H.-W.; Holthausen, M. C.; Wagner, M. *Angew. Chem., Int. Ed.* **2006**, *45*, 920 -925.

(65) Nelson, J. M.; Lough, A. J.; Manners, I. *Organometallics* **1994**, *13*, 3703-3710.

(66) Nesmeyanov, A. N.; Kritskaya, I. I. *Bull. Acad. Sci. USSR, Div. Chem. Sci. (Eng. Transl.)* **1956**, 243-244.

(67) Zechel, D. L.; Foucher, D. A.; Pudelski, J. K.; Yap, G. P. A.; Rheingold, A. L.; Manners, I. *J. Chem. Soc., Dalton Trans.* **1995**, 1893-1899.

(68) (a) Schlogl, K.; Mohar, A. *Monatsh. Chem.* **1961**, *92*, 219-235. (b) Schloegl, K.; Pelousek, H.; Mohar, A. *Monatsh. Chem.* **1961**, *92*, 533-541. (c) Pauson, P. L.; Watts, W. E. *J. Chem. Soc.* **1962**, 3880-3886.

(69) Xie, R.-J.; Han, L.-M.; Suo, Q.-L.; Hong, H.-L.; Luo, M.-H. *J. Coord. Chem.* **2010**, *63*, 1700-1710.

(70) Schottenberger, H.; Buchmeiser, M.; Polin, J.; Schwarzhans, K. E. *Z. Naturforsch, B: Chem. Sci.* **1993**, *48*, 1524-1532.

(71) Klimova, E. I.; García, M. M.; Klimova, T.; Stivalet, J. M.; Ortega, S. H.; Ramírez, L. H. *J. Organomet. Chem.* **2002**, *659*, 56-63.

(72) Bildstein, B.; Denifl, P.; Wurst, K. *J. Organomet. Chem.* **1995**, *496*, 175-186.

(73) (a) Rosenberg, H.; Ohio, D. Diferrocenyl Dericatives of Group IV-A elements. U.S. Patent 3,426,053, February 4, 1969. (b) Bocarsly, A. B.; Walton, E. G.; Bradeley, M. G.; Wrighton, M. S. *J. Electroanal. Chem. Interfacial Electrochem.* **1979**, *100*, 283-306. (c) Liu, Y.-P.; Li, Z.-Q.; Tan Y.-X.; Zhang, Z.-J. *Acta Crystallogr., Sect. E* **2011**, *E67*, m635.

(d) Losada, J.; García-Armada, P.; Robles, V.; Martínez, A. M.; Casado, C. M.; Alonso, B. *New J. Chem.* **2011**, *35*, 2187–2195.

(74) (a) MacLachlan, M. J.; Zheng, J.; Lough, A. J.; Manners, I. *Organometallics* **1999**, *18*, 1337-1345. (b) Thieme, K.; Bourke, S. C.; Zheng, J.; MacLachlan, M. J.; Zamanian, F.; Lough, A. J.; Manners, I. Can. J. Chem. **2002**, *80*, 1469-1480.

(75) Rulkens, R.; Lough, A. J.; Manners, I.; Lovelace, S. R.; Grant, C.; Geiger, W. E. *J. Am. Chem. Soc.* **1996**, *118*, 12683-12695.

(76) (a) Kabouche, Z.; Nguyen, H. D. *J. Organomet. Chem.* **1989**, *375*, 191-195. (b) Nesmeyanov, A. N.; Tolstaya, T. P.; Korol'kov, V. V. *Dokl. Akad. Nauk* **1973**, *209*, 1113-1116.

(77) Fischer, A.; Jacob, K.; Edelmann, F. T. *Z. Anorg. Allg. Chem.* **2003**, *629*, 963-967.

(78. Jones, S. C.; Barlow, S.; O'Hare, D. *Chem.−Eur. J.* **2005**, *11*, 4473-4481.

(79) (a) Scheibitz, M.; Bats, J. W.; Bolte, M.; Lerner, H.-W.; Wagner, M. *Organometallics* **2004**, *23*, 940-942. (b) Scheibitz, M.; Li, H.; Schnorr, J.; Perucha, A. S.; Bolte, M.; Lerner, H.-W.; Jäkle, F.; Wagner, M. *J. Am. Chem. Soc.* **2009**, *131*, 16319-16329.

(80) Heilmann, J. B.; Scheibitz, M.; Qin, Y.; Sundararaman, A.; Jäkle, F.; Kretz, T.; Bolte, M.; Lerner, H.-W.; Holthausen, M. C.; Wagner, M. *Angew. Chem., Int. Ed. Engl.* **2006**, *45*, 920 -925.

(81) Wrackmeyer, B.; Klimkina, E. V.; Ackermann, T.; Milius, W. *Inorg. Chim. Acta* **2009**, *362*, 3941-3948.

(82) (a) Nesmeyanov, N. A.; Reutov, O. A. *Dokl. Akud. Nauk* **1958**, *120*, 1267-1269. (b) Lau, H.; Hart, H. *J. Org. Chem.* **1959**, *24*, 280-281. (c) McKechnie, J. S.; Maier, C. A.;

Bersted, B.; Paul, I. C. *J. Chem. Soc., Perkin Trans. 2* **1973**, 138-143. (d) Cassens, A.; Eilbracht, P.; Nazzal, A.; Prössdorf, W.; Mueller-Westerhoff, U. T. *J. Am. Chem. Soc.* **1981**, *103*, 6367-6372. (e) Mueller-Westerhoff, U. T. *Angew. Chem., Int. Ed.* **1986**, *25*, 702-717. (f) Löewendahl, M.; Davidsson, Ö.; Ahlberg, P.; Håkansson, M. *Organometallics* **1993**, *12*, 2417-2419. (g) Håkansson, M.; Löewendahl, M.; Davidsson, Ö.; Ahlberg, P. *Organometallics* **1993**, *12*, 2841-2844. (h) Löewendahl, J.-M.; Håkansson, M. *Organometallics* **1995**, *14*, 4736-4741. (i) Watanabe, M.; Sato, M.; Nagasawa, A.; Motoyama, I.; Takayama, T. *Bull. Chem. Soc. Jpn.* **1998**, *71*, 2127-2136.

(83) (a) Zechel, D. A.; Foucher, D. A.; Pudelski, J. K.; Yap, G. P. A.; Rheingold, A. L.; Manners, I. *J. Chem. Soc. Dalton Trans.* **1995**, 1893-1899. (b) Park, J.; Seo, Y.; Cho, S.; Whang, D.; Kim, K.; Chang, T. *J. Organomet. Chem.* **1995**, *489*, 23-25.

(84) (a) Chan, W. Y.; Lough, A. J.; Manners, I. *Angew. Chem., Int. Ed. Engl.* **2007**, *46*, 9069-9072. (b) Herbert, D. E.; Gilroy, J. B.; Chan, W. Y.; Chabanne, L.; Staubitz, A.; Lough, A. J.; Manners, I. *J. Am. Chem. Soc.* **2009**, *131*, 14958-14968.

(85) Reddy, N. P.; Choi, N.; Shimada, S.; Tanaka, M. *Chem. Lett.* **1996**, 649-650.

(86) Calleja, G.; Carré, F.; Cerveau, G.; Labbé, P.; Coche-Guérente, L. *Organometallics* **2001**, *20*, 4211-4215.

(87) Berenbaum, A.; Lough, A. J.; Manners, I. *Organometallics* **2002**, *21*, 4415-4424.

(88) Bao, M.; Hatanaka, Y.; Shimada, S. *Chem. Lett.* **2004**, *33*, 520-521.

(89) Dong, T. Y.; Hwang, M. Y.; Wen, Y. S.; Hwang, W. S. *J. Organomet. Chem.* **1990**, *391*, 377-85.

(90) Scheibitz, M.; Winter, R. F.; Bolte, M.; Lerner, H.-W.; Wagner, M. *Angew. Chem., Int. Ed. Engl.* **2003**, *42*, 924-927.

(91) Heilmann, J.; Lerner, H.-W.; Bolte, M. *Acta. Crystallogr., Sect. E* **2006**, *E62*, m1477-m1478.

(92) Schachner, J. A.; Lund, C. L.; Quail, J. W.; Müller, J. *Acta. Crystallogr., Sect. E* **2005**, *E61*, m682-m684.

(93) (a) Braunschweig, H.; Burschka, C.; Clentsmith, G. K. B.; Kupfer, T.; Radacki, K. Inorg. Chem. 2005, 44, 4906-4908. (b) Schachner, J. A.; Orlowski, G. A.; Quail, J. W.; Kraatz, H.-B.; Müller, J. *Inorg. Chem.* **2006**, *45*, 454-459.

(94) Uhl, W.; Hahn, I.; Jantschak, A.; Spies, T. *J. Organomet. Chem.* **2001**, *637-639*, 300-303.

(95) Jutzi, P.; Lenze, N.; Neumann, B.; Stammler, H.-G. *Angew. Chem., Int. Ed. Engl.* **2001**, *40*, 1423-1427.

(96) Althoff, A.; Jutzi, P.; Lenze, N.; Neumann, B.; Stammler, A.; Stammler, H.-G. *Organometallics* **2003**, *22*, 2766-2774.

(97) Wrackmeyer, B.; Klimkina, E. V.; Milius, W. *Eur. J. Inorg. Chem.* **2009**, 3155–3162.

(98) Schachner, J. A.; Lund, C. L.; Burgess, I. J.; Quail, J. W.; Schatte, G.; Müller, J. *Organometallics* **2008**, *27*, 4703-4710.

(99) Katz, T. J.; Acton, N.; Martin, G. *J. Am. Chem. Soc.* **1969**, *91*, 2804-2805.

(100) Lippard, S. J.; Martin, G. *J. Am. Chem. Soc.* **1970**, *92*, 7291-7296.

(101) Mueller-Westerhoff, U. T.; Swiegers, G. F. *Chem. Lett.* **1994**, 67-68.

(102) Grossmann, B.; Heinze, J.; Herdtweck, E.; Köhler, F. H.; Nöth, H.; Schwenk, H.; Spiegler, M.; Wachter, W.; Weber, B. *Angew. Chem., Int. Ed. Engl.* **1997**, *36*, 387-389.

(103) (a) Mizuta, T.; Onishi, M.; Miyoshi, K. *Organometallics* **2000**, *19*, 5005-5009. (b) Mizuta, T.; Aotani, T.; Imamura, Y.; Kubo, K.; Miyoshi, K. *Organometallics* **2008**, *27*, 2457-2463.

(104) Morrison, Jr., W. H.; Krogsrud, S.; Hendrickson, D. N. *Inorg. Chem.* **1973**, *12*, 1998-2004.

(105) Diaz, A. F.; Müller-Westerhoff, U. T.; Nazzal, A.; Tanner, M. *J. Organornet. Chem* **1982**, *236*, C45-C48.

CHAPTER 2
HEAVIER GROUP-13-BRIDGED [1]METALLOCENOPHANES AND POLY(METALLOCENE)S BY RING-OPENING POLYMERIZATION OF [1]METALLOCENOPHANES

This part presents the synthesis of heavier group-13-bridged [1]metallocenophanes followed by the ring-opening polymerization (ROP) of reactive [1]metallocenophanes to yield poly(metallocene)s. This includes the results of two published papers and one manuscript, which is under preparation.

Contribution 1: Ring-Opening Polymerization of a Galla[1]ferrocenophane: A Gallium-Bridged Poly(ferrocene) with Observable Tacticity

2.1.1 Description

The following chapter is a verbatim copy of a communication that was published in *Journal of the American Chemical Society*[1] in January 2010[2] and describes the synthesis and characterization of a poly(ferrocenylgallane) (**7$_n$**). The salt metathesis reaction of a gallium dichloride complex (**6**), decorated with the sterically bulky Mamx ligand, with dilithioferrocene resulted in a galla[1]ferrocenophane (**7**) as a reactive intermediate, which ring-opened to yield a poly(ferrocenylgallane). The polymer was characterized by elemental analysis, GPC, DLS, WAXS, DSC, TGA, CV, UV/Vis, ^{1}H- and ^{13}C NMR spectroscopy. NMR spectra of this first well-characterized poly(ferrocenylgallane) exhibited some peaks with a rich fine structure caused by the tacticity of the polymer.

[1] Reprinted with permission from Journal of the American Chemical Society. Copyright (2010) American Chemical Society

Pentads were resolved for the signal of *ortho-t*Bu group, which acts as a fine sensor toward the tacticity of the polymer.

2.1.2 Author Contribution

I synthesized the starting (Mamx)$GaCl_2$ (**6**) and performed its reaction with dilithioferrocene to synthesized poly(ferrocenylgallane) (**7_n**). The co-authors on this paper are Joe B. Gilroy and Anne Staubitz, who helped to characterize the polymer by NMR, GPC, DLS, WAXS, DSC, TGA and CV.

I prepared parts of the first version of the manuscript, which was edited by my supervisor Jens Müller.

2.1.3 Relation of Contribution 1 with Research Objectives

As mentioned in the introduction, the key strategy to reach the research goal, the preparation and isolation of strained [1]metallocenophanes, was to design and synthesize suitable ligand framework for heavier group 13 element dihalides, which can be utilized in the salt-metathesis reaction with dilithiometallocenes to synthesisze reactive [1]metallocenophanes. As the heavier group 13 element dichlorides equipped with the slim Ar′ ligand yielded [1.1]FCPs in the salt-metathesis reaction, the initial strategy was to increase the steric bulk around group 13 element by introducing bulky substituents at the Ar′-framework. To achieve this, the known Mamx ligand was choosen as it was expected that the *ortho-t*Bu would provide required steric protection around group 13 elements. As the first step, I synthesized the complex (Mamx)$GaCl_2$, **6**. Thereafter, the

[2] Bagh, B.; Gilroy, J. B.; Staubitz, A.; Müller, J. *J. Am. Chem. Soc.* **2010**, *132*, 1794-1795.

dichloride **6,** decorated with the sterically bulky Mamx ligand, was utilized in the salt-metathesis reaction to prepare strained [1]metallocenophane. In fact, the reaction of **6** with dilithioferrocene yielded the desired [1]FCP **7** with gallium as a bridging element. The galla[1]ferrocenophane **7** was clearly identified as the major product in the reaction mixture, but could not be isolated as a pure compound as it spontaneously ring-open polymerized in solution to yield the poly(ferrocenylgallane) $\mathbf{7_n}$. In summary, I could not reach the ultimate goal of my research, because the isolation of galla[1]ferrocenophane **7** was not possible and, thus, this strained species could not be utilized as a monomer under controlled conditions.

2.1.4 Reprint of Contribution 1

Ring-Opening Polymerization of a Galla[1]ferrocenophane: A Gallium-Bridged Poly(ferrocene) with Observable Tacticity

Bidraha Bagh,[‡] Joe B. Gilroy,[§] Anne Staubitz,[§] Jens Müller[‡]*

[‡]Department of Chemistry, University of Saskatchewan, 110 Science Place, Saskatoon, Saskatchewan S7N 5C9, Canada and [§]School of Chemistry, University of Bristol, Bristol BS8 1TS, United Kingdom.

Received December 17, 2009

Since Manners *et al.* reported that thermal ring-opening polymerization (ROP) of dimethylsila[1]ferrocenophane **1** yields high-molecular-weight poly(ferrocenyldimethylsilane) **2**,[1a] the tools box for ROP of strained sandwich compounds has been developed significantly.[1] To date, in addition to thermal ROP, transition-metal-catalyzed, anionic, and photo-controlled ROP of metallacyclophanes are

described in the literature.[1c] The latter two methods are of particular interest as they can be performed as living polymerizations, which give access to block copolymers.

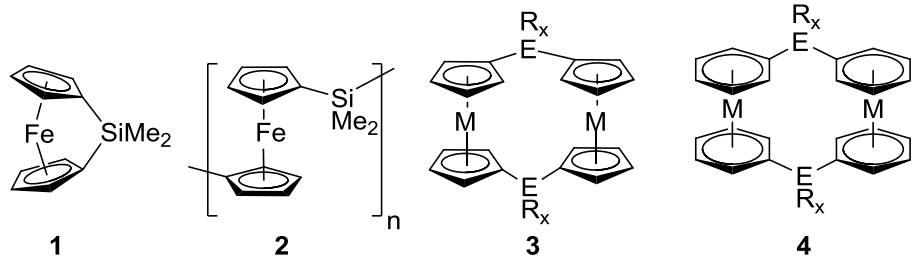

1 **2** **3** **4**

Poly(ferrocenylsilane)s are functional materials applicable as plasma-etch resists for nanopatterning,[2] precursors to ceramics,[3] tunable component of photonic crystals displays (photonic ink),[4] redox-tunable surfaces,[5] and polyelectrolyte capsules with redox-dependable permeability.[6] Block copolymers in block-selective solvents allow control of different micelle morphologies, and poly(ferrocenyldimethylsilane) containing block copolymers, which form cylindrical micelles with semicrystalline cores,[7] show significant promise for future applications in nanotechnology.[8]

Despite these recent advances, the number of well-defined metallopolymers is still quite restricted. Recently, we synthesized strained sandwich compounds with aluminum or gallium in bridging positions with the aim of developing new polymeric materials through ROP.[9] In this paper, we describe the first, well-characterized poly(ferrocene) with gallium in bridging positions.[10] In depth NMR spectroscopy studies reveal that this air-stable organometallic polymer shows a surprising sensitivity towards the stereochemistry of the polymer backbone.

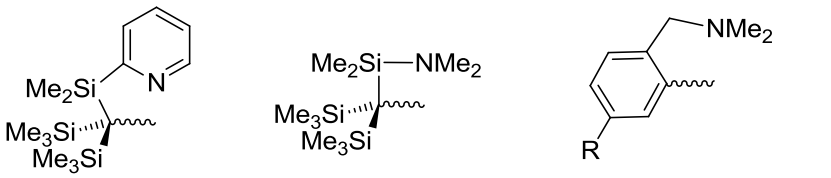

Pytsi **Me$_2$Ntsi** R = H (**Ar'**), *t*Bu (**p-*t*BuAr'**)

All known strained aluminum- or gallium-bridged [1]metallacyclophanes[9] were equipped with the bulky, intramolecularly coordinating, *trisyl*-based ligands **Pytsi** or **Me$_2$Ntsi**. However, ROP attempts with these [1]ferrocenophanes and [1]ruthenocenophanes either failed or resulted in sluggish polymerizations.[9e] On the other hand, employing the "one-armed phenyl" ligand **Ar′** or **p-*t*BuAr′** gave [1.1]metallacyclophanes as the only isolatable products [**3** (M = Fe) and **4 (**M = Cr, Mo)].[11] Obviously, the bulkiness of the group-13 bound ligand has a major effect on the outcome of reactions between a dilithiated sandwich species and a aluminum or gallium dihalide. Within this paper, we report on results obtained using a new "one-armed phenyl" ligand designed to incorporate steric bulk.

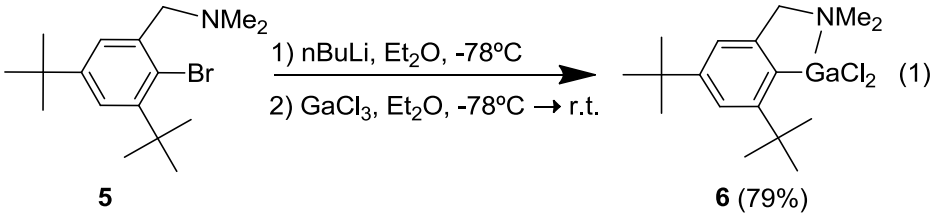

Scheme 2-1-1. Synthesis of intermediate **7** and polymer **7$_n$**

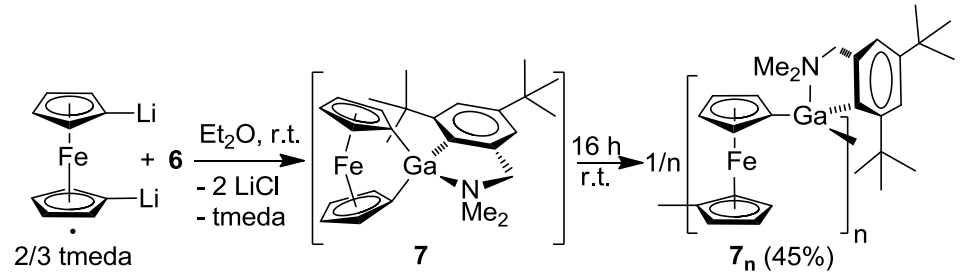

Starting from commercially available 3,5-di-*tert*-butyl-toluene, the known amine **5**[12] was prepared in three steps (eq. 1), from which the gallium dichloride **6** was obtained as an analytically pure solid (see Supp. Inf. for details). Species **6** reacted readily with

dilithioferrocene to form the targeted galla[1]ferrocenophane **7** as an intermediate (Scheme 2-1-1).

Attempts to isolate this new strained sandwich compound **7** gave an orange powder, which was characterized as the poly(ferrocenylgallane) $\mathbf{7_n}$. The formation of species **7** was confirmed by ^{1}H NMR spectroscopy studies. If the Et_2O from an aliquot of the reaction mixture, taken after ca. 15 min, was quickly replaced by C_6D_6, intermediate **7** was observed by ^{1}H NMR spectroscopy with resonances in the typical Cp range at δ 4.69 (4 β-H), 4.56 (2 α-H), and 4.01 (2 α-H). This pattern and the chemical shifts match very well with other gallium-bridged [1]ferrocenophanes we have characterized previously [bridging moiety Ga(Pytsi)[9b]: δ 4.65 (2 β-H), 4.61 (2 β-H), 4.45 (2 α-H), 4.08 (2 α-H); or Ga(Me_2Ntsi)[9c]: δ 4.54 (4 β-H), 4.24 (2 α-H), 3.90 (2 α-H)].

Polymer $\mathbf{7_n}$ was purified by precipitation into MeOH (45% isolated yield) and characterized by elemental analysis, GPC, DLS, WAXS, DSC, TGA, CV, UV/Vis, ^{1}H- and ^{13}C NMR spectroscopy (Supp. Infor.). Material $\mathbf{7_n}$ is an amorphous polymer with a glass transition at 205 ºC. The polymer is thermally robust as it retained 98% of its mass at 340 ºC; further heating to 600 ºC gave a non-magnetic char with a low yield of 14% (TGA). Electrochemical studies (cyclic voltammetry) revealed two poorly resolved oxidation waves and one broad reduction wave. The midpoint between the main redox waves was found at -0.047 V versus the couple $FeCp_2$ / $FeCp_2^+$. GPC analysis showed a broad peak corresponding to an M_w of 48 kDa (DP_w = 96, PDI = 3.3) with respect to polystyrene. Dynamic light scattering of $\mathbf{7_n}$ resulted in a hydrodynamic radius of 2.99 ± 0.36 nm. Assuming that $\mathbf{7_n}$ can be described as a random coil, with CH_2Cl_2 being a good solvent, this R_h value gives a radius of gyration of 6.13 ± 0.74 nm (R_g / R_h = 2.05),[13]

which translates into a M_w of 36 kDa (DP_w = 72) with respect to poly(ferrocenyldimethylsilane).[14]

^{1}H NMR spectrum of $\mathbf{7_n}$ showed broad peaks relative to those of the monomer **7**, with some peaks exhibiting a rich fine structure. For example, the *t*Bu group *para* to gallium appears as a singlet (δ 1.32), whereas the *t*Bu group *ortho* to gallium is split into 10 signals (centered at δ 1.53). This *ortho*-*t*Bu group is oriented towards the polymer backbone and acts as a fine sensor for the tacticity of $\mathbf{7_n}$. As shown in Figure 2-1-1, the 10 peaks can be sorted into three groups with 3, 4, and 3 singlets, respectively (see A, B, and C in Fig. 1). Every Ga atom in polymer $\mathbf{7_n}$ is a stereogenic centre and neighboring Ga atoms could have either the same or a different chirality, leading to *racemo* or *meso* diads. For three repeat units, three different arrangements are possible, which are illustrated in Figure 2-1-1. The splitting of the signal of the *ortho*-*t*Bu group into the three groups A, B and C is due to a triad sensitivity. The approx. intensity ratios between those three groups are 1 : 2 : 1, indicating that $\mathbf{7_n}$ is a polymer with a statistical distribution of stereogenic centers; hence, signal B can be assigned to heterotactic triads *mr* and *rm*. The fine structure in A, B and C can be explained by a further sensitivity towards pentads.

An extension from three to five repeat units results in 16 possible pentads, from which 10 are distinguishable.[15] In case of a polymer with a statistical distribution of stereogenic centers, isotactic and syndiotactic triads both result in four pentads from which three are distinguishable giving a distribution ratio of 1 : 2 : 1 (A and C in Fig. 1). In contrast, the heterotactic triad results in eight pentads with four being distinguishable giving a distribution ratio of 2 : 2 : 2: 2 (B in Fig. 1). Expectedly, the signal pattern of the ferrocene units is more complex than that of the *ortho*-*t*Bu group. The Cp protons could

show a diad or tetrad sensitivity, with the latter being the pendant to the pentad sensitivity of the *t*Bu group. A diad sensitivity in form of two sets of four Cp signals in an approx. 1 : 1 intensity ratio can be clearly seen in ^{1}H NMR spectra of **7$_n$**. Some of the individual peaks show an additional fine structure, but a full resolution into tetrads was not observed. The ^{13}C{^{1}H} NMR spectrum of **7$_n$** is similarly complex as the proton spectrum. For example, while the tertiary carbon atom of the *para*-*t*Bu group gives one resonance only, that of the *ortho*-*t*Bu group gives three signals (triad resolution).

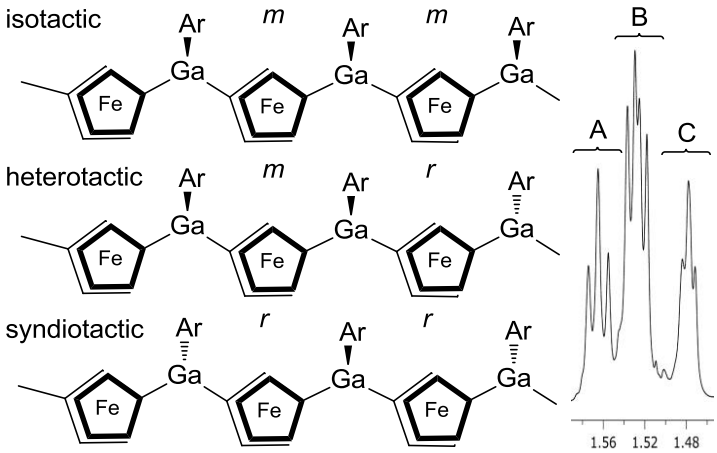

Figure 2-1-1. Illustration of different triads in **7$_n$** (the NMe_2 group at the aryl ligand is omitted for clarity). ^{1}H NMR signal of the *ortho*-*t*Bu group of **7$_n$** exhibiting pentad resolution (intensity ratio A : B : C ≈ 1 : 2 : 1).

In summary, all attempts to synthesize the strained [1]ferrocenophane **7** resulted in the isolation of the air-stable poly(ferrocenylgallane) **7$_n$**. However, ^{1}H NMR spectroscopy revealed that the targeted monomer is first formed and one can assume that a spontaneous ROP results in **7$_n$**. This behavior is reminiscent of the chemistry of stanna[1]ferrocenophanes.[1b,16] Interestingly, one of the two *t*Bu groups of the ligand points towards the polymer backbone and serves as a very sensitive probe of the polymer stereochemistry.[17] Polymer **7$_n$** is thermally robust, and can be purified and handled under

ambient conditions, making it an ideal candidate for incorporation into polymer based materials offering an alternative to existing poly(ferrocene)s. Future work will focus on the isolation of monomers such as **7**, towards the realization of well-defined poly(ferrocenylgallane)s via living ROP methodologies.

ACKNOWLEDGEMENTS

Dedicated to Prof. Peter Paetzold (RWTH Aachen) on the occasion of his 75th birthday. We thank Prof. Ian Manners (University of Bristol) for sabbatical support and helpful discussions and NSERC of Canada (J.B.G. for a PDF; J.M. for a DG) and EPSRC of the United Kingdom (A.S.) for support.

Supporting Information. Experimental section for **5**, **6**, and $\mathbf{7_n}$; spectra and diagrams for $\mathbf{7_n}$ (NMR, GPC, DLS, WAXS, DSC, TGA, CV). This material is available free of charge via the internet at http://pubs.acs.org.

REFERENCES

(1) (a) Foucher, D. A.; Tang, B.-Z.; Manners, I. *J. Am. Chem. Soc.* **1992**, *114*, 6246-6248. (b) Herbert, D. E.; Mayer, U. F. J.; Manners, I. *Angew. Chem. Int. Ed.* **2007**, *46*, 5060-5081. (c) Bellas, V.; Rehahn, M. *Angew. Chem. Int. Ed.* **2007**, *46*, 5082-5104.

(2) (a) Korczagin, I.; Lammertink, R. G. H.; Hempenius, M. A.; Golze, S.; Vancso, G. J. In *Ordered Polymeric Nanostructures at Surfaces; Springer:* 2006; Vol. 200, p 91-117. (b) Lu, J.; Chamberlin, D.; Rider, D. A.; Liu, M. Z.; Manners, I.; Russell, T. P. *Nanotechnology* **2006**, *17*, 5792-5797. (c) Chuang, V. P.; Gwyther, J.; Mickiewicz, R. A.; Manners, I.; Ross, C. A. *Nano Letters* **2009**, *9*, 4364-4369.

(3) (a) MacLachlan, M. J.; Ginzburg, M.; Coombs, N.; Coyle, T. W.; Raju, N. P.; Greedan, J. E.; Ozin, G. A.; Manners, I. *Science* **2000**, *287*, 1460-1463. (b) Lastella, S.; Mallick, G.; Woo, R.; Karna, S. P.; Rider, D. A.; Manners, I.; Jung, Y. J.; Ryu, C. Y.; Ajayan, P. M. *J. Appl. Phys.* **2006**, 99.

(4) (a) Arsenault, A. C.; Puzzo, D. P.; Manners, I.; Ozin, G. A. *Nature Photonics* **2007**, *1*, 468-472. (b) Puzzo, D. P.; Arsenault, A. C.; Manners, I.; Ozin, G. A. *Angew. Chem. Int. Ed.* **2009**, *48*, 943-947.

(5) Peter, M.; Lammertink, R. G. H.; Hempenius, M. A.; Vancso, G. J. *Langmuir* **2005**, *21*, 5115-5123.

(6) Ma, Y. J.; Dong, W. F.; Hempenius, M. A.; Möhwald, H.; Vancso, G. J. *Nature Mater.* **2006**, *5*, 724-729.

(7) (a) Wang, X. S.; Guerin, G.; Wang, H.; Wang, Y. S.; Manners, I.; Winnik, M. A. *Science* **2007**, *317*, 644-647. (b) Gädt, T.; Ieong, N. S.; Cambridge, G.; Winnik, M. A.; Manners, I. *Nature Mater.* **2009**, *8*, 144-150.

(8) Rowan, S. J. *Nature Mater.* **2009**, *8*, 89-91.

(9) (a) Schachner, J. A.; Lund, C. L.; Quail, J. W.; Müller, J. *Organometallics* **2005**, *24*, 785-787. (b) Schachner, J. A.; Lund, C. L.; Quail, J. W.; Müller, J. *Organometallics* **2005**, *24*, 4483-4488. (c) Lund, C. L.; Schachner, J. A.; Quail, J. W.; Müller, J. *Organometallics* **2006**, *25*, 5817-5823. (d) Lund, C. L.; Schachner, J. A.; Quail, J. W.; Müller, J. *J. Am. Chem. Soc.* **2007**, *129*, 9313-9320. (e) Schachner, J. A.; Tockner, S.; Lund, C. L.; Quail, J. W.; Rehahn, M.; Müller, J. *Organometallics* **2007**, *26*, 4658-4662.

(10) For recent advances in boron-bridged poly(ferrocene)s see (a) Scheibitz, M.; Li, H. Y.; Schnorr, J.; Perucha, A. S.; Bolte, M.; Lerner, H. W.; Jäkle, F.; Wagner, M. *J. Am.*

Chem. Soc. **2009**, *131*, 16319-16329. (b) Heilmann, J. B.; Scheibitz, M.; Qin, Y.; Sundararaman, A.; Jäkle, F.; Kretz, T.; Bolte, M.; Lerner, H. W.; Holthausen, M. C.; Wagner, M. *Angew. Chem. Int. Ed.* **2006**, *45*, 920-925. (c) Heilmann, J. B.; Qin, Y.; Jäkle, F.; Lerner, H. W.; Wagner, M. *Inorg. Chim. Acta* **2006**, *359*, 4802-4806.

(11) (a) Braunschweig, H.; Burschka, C.; Clentsmith, G. K. B.; Kupfer, T.; Radacki, K. *Inorg. Chem.* **2005**, *44*, 4906-4908. (b) Schachner, J. A.; Orlowski, G. A.; Quail, J. W.; Kraatz, H.-B.; Müller, J. *Inorg. Chem.* **2006**, *45*, 454-459. (c) Lund, C. L.; Schachner, J. A.; Burgess, I. J.; Quail, J. W.; Schatte, G.; Müller, J. *Inorg. Chem.* **2008**, *47*, 5992–6000.

(12) Yoshifuji, M.; Kamijo, K.; Toyota, K. *Tetrahedron Lett.* **1994**, *35*, 3971-3974.

(13) Burchard, W. *AdV. Polym. Sci.* **1999**, *143*, 113–194.

(14) Massey, J. A.; Kulbaba, K.; Winnik, M. A.; Manners, I. J. *Polym. Sci., Part B: Polym. Phys.* **2000**, *38*, 3032-3041.

(15) The splitting of triads into 16 pentads can be illustrated as follows (indistinguishable pentads shown in parenthesis): isotactic triad: mmmm, (mmmr, rmmm), rmmr; heterotactic triad: (mmrm, mrmm), (mmrr, rrmm), (rmrm, mrmr), (rmrr, rrmr); syndiotactic triad: mrrm, (mrrr, rrrm), rrrr.

(16) Rulkens, R.; Lough, A. J.; Manners, I. *Angew. Chem. Int. Ed.* **1996**, *35*, 1805-1807.

(17) Poly(ferrocenylmethylphenylsilane) showing a triad resolution is described in Rasburn, J.; Foucher, D. A.; Reynolds, W. F.; Manners, I.; Vancso, G. J. *Chem. Commun.* **1998**, 843-844.

2.1.5 Selective Materials from Supporting Information of Contribution 1

EXPERIMENTAL SECTION

Syntheses. Manipulations were done using standard Schlenk and glovebox techniques (O_2 level < 0.1 ppm; N_2 as inert gas), unless noted differently. Solvents were dried using an MBraun Solvent Purification System and stored under nitrogen over 4 Å molecular sieves. Compounds $(LiC_5H_4)_2Fe \cdot 2/3$ tmeda,[1] 2-CH_3-4,6-*t*$Bu_2C_6H_2Br$,[2] and 2-($BrCH_2$)-4,6-*t*$Bu_2C_6H_2Br$[3] were synthesized as described in the literature. Compound **5** is a known species,[4] but was synthesized in a different way compare to the literature (see below).

Standard Analyses. Mass spectra were measured on a VG 70SE and were reported in the form M (%I) [F], where M is the mass observed, %I is the intensity of the peak relative to the most intense peak in the spectrum, and F is the molecular ion or fragment; only partial data are reported. Elemental analyses were carried out at the Saskatchewan Structural Sciences Center at the University of Saskatchewan (Perkin Elmer 2400 CHN Elemental Analyzer; compounds **6**) and by Laboratory for Microanalysis at the University of Bristol (Model 3000 Euro EA Elemental Analyzer; compound $\mathbf{7_n}$) using V_2O_5 to promote combustion. UV/Vis spectra were recorded with a Varian Cary 50 UV-visible spectrometer using thf as a solvent. For NMR measurements, C_6D_6 was prepared through freeze-pump-thaw procedures and stored under nitrogen over 4 Å molecular sieves, and CD_2Cl_2 was dried over CaH_2 and filtered before use. ^1H and ^{13}C NMR spectra were recorded at 25 ºC on a Bruker 500 MHz Avance spectrometer (^1H: 500.2 MHz, ^{13}C: 125.8 MHz; compounds **5** and **6**) and on a Varian 500 spectrometer (^1H: 499.9 MHz, ^{13}C: 125.7 MHz; compound $\mathbf{7_n}$). ^1H NMR chemical shifts were referenced to the residual protons of the deuterated solvent (C_6D_6: δ 7.15; CD_2Cl_2: 5.32); ^{13}C chemical shifts were

referenced to δ 128.00 (C_6D_6) or 54.00 (CD_2Cl_2). Assignments for **6** and $\mathbf{7_n}$ were supported by 2D NMR experiments (**6**: HMBC, HMQC; $\mathbf{7_n}$: COSY, TOCSY, HMBC, HMQC, and NOESY).

Electrochemistry. Electrochemical studies were carried out using an EG&G model 273A potentiostat linked to a PC using EG&G model 270 Research Electrochemistry software in conjunction with a three-electrode cell. The working electrode was a glassy carbon disc (3.0 mm diameter) and the auxiliary electrode a platinum wire. The reference electrode was a saturated calomel electrode separated from the test solution by a fine porosity frit and an agar bridge saturated with KCl. CVs were conducted in dichloromethane, each with 0.1 M nBu_4NPF_6 as supporting electrolyte, at scan rates of 200 mV/s. The concentration of analyte for polymers was approximately 2 mM in monomer unit. Voltammograms were referenced vs. the $Fe(\eta^5\text{-}C_5H_5)_2/[Fe(\eta^5\text{-}C_5H_5)_2]^+$ redox couple using $Fe(\eta^5\text{-}C_5Me_5)_2$ as an internal standard. The $Fe(\eta^5\text{-}C_5Me_5)_2/[Fe(\eta^5\text{-}C_5Me_5)_2]^+$ redox couple was determined to be -540 mV relative to the $Fe(\eta^5\text{-}C_5H_5)_2/[Fe(\eta^5\text{-}C_5H_5)_2]^+$ redox couple in an independent experiment conducted under identical conditions.

WAXS Measurements. Wide-angle X-ray diffraction experiments were performed with Cu-Kα radiation (λ = 1.5418 Å) on a Bruker D8 Advance powder diffractometer fitted with a 0.6 mm fixed divergence slit, knife-edge collimator and a LynxEye area detector. Data were collected between 2θ = 5-50° in θ\2θ mode with a step width of 0.0025°.

Thermal Studies. TGA was run on a TGA Q500 apparatus at a heating rate of 10 °C/min. The samples were studied in non-hermetic aluminum pans. DSC analyses were

performed on a TA Instruments Q100 coupled to a RCS90 refrigerated cooling system at a heating rate of 10 °C/min. The samples, sealed in hermetic aluminum pans, were tared using a XT220A Precisa microbalance. TGA and DSC data were analyzed with TA Instruments Universal Analysis 2000 software.

GPC Analyses. Chromatograms were recorded on a Viscotek VE2001 (ViscoGel HHR 5000/2500), using a flow rate of 1 mL min^{-1} in thf with 0.1 w/w % $n$$Bu_4NBr$ (column temperature of 30 ºC), calibrated for polystyrene standards. The samples were filtered through 0.2 μm syringe PTFE filters (Pall Acrodisc) before they were analyzed at concentrations of approximately 4 mg mL^{-1}.

DLS Analyses. Dynamic light scattering experiments were performed using a nano series Malvern zetasizer instrument equipped with a 633 nm red laser. Samples were filtered through 0.2 μm syringe PTFE filters (Millex or Whatman) before they were analyzed in 1 cm glass cuvettes at concentrations of 0.5 mg mL^{-1}, 1.0 mg mL^{-1}, and 2.0 mg mL^{-1} in CH_2Cl_2 at 25 °C. Similar studies in thf did not result in significantly different hydrodynamic radii. The refractive index of the polymer $\mathbf{7_n}$ was assumed to be 1.5.

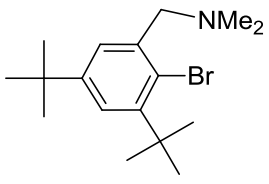

5

Synthesis of 2-(Me_2NCH_2)-4,6-$tBu_2C_6H_2Br$ (5).[4] Condensed dimethylamine (30 mL, 0.45 mol) was added dropwise to a cold (0 ºC) solution of 2-($BrCH_2$)-4,6-$t$$Bu_2C_6H_2Br$ (40.1 g, 111 mmol) in hexane (200 mL). The reaction mixture was stirred at r.t. for 3 h resulting in a clear and colorless solution with white precipitate. The precipitate was filtered off and all volatiles were removed from the filtrate under high vacuum, resulting in product **5** as a colorless oil (31.3 g, 87%). ^1H NMR (C_6D_6): δ

1.28 (s, 9H, *t*Bu), 1.59 (s, 9H, *t*Bu), 2.16 (s, 6H, NMe_2), 3.60 (s, 2H, CH_2), 7.52 (d, 1H, CH), 7.66 (d, 1H, CH).

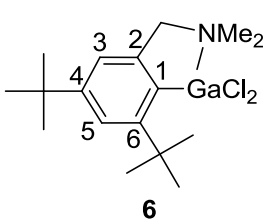

6

Synthesis of [2-(Me_2NCH_2)-4,6-$tBu_2C_6H_2$]$GaCl_2$ (6). *n*BuLi (2.8 M in hexane, 6.00 mL, 16.8 mmol) was added dropwise to a cold (-78 ºC) solution of **5** (5.03 g, 15.4 mmol) in Et_2O (30 mL). The reaction mixture was stirred at -78 ºC for 45 min and a cold (0 ºC) solution of $GaCl_3$ (2.70 g, 15.3 mmol) in Et_2O (30 mL) was added dropwise. The resulting mixture was warmed up to r.t. and stirred for 16 h, yielding a pale yellow solution with white precipitate. After the solid was filtered off, the pale yellow solution was concentrated to approx. 20 mL. Needle shaped colorless crystals were obtained at -22 ºC as pure product **6** (4.65 g, 79%). ^{1}H NMR (C_6D_6): δ 1.31 (s, 9H, *t*Bu-4), 1.55 (s, 9H, *t*Bu-6), 1.95 (s, 6H, NMe_2), 3.04 (s, 2H, CH_2), 6.74 (s, 1H, CH-3), 7.59 (s, 1H, CH-5). ^{13}C NMR (C_6D_6): δ 31.47 [C($\underline{C}H_3)_3$-4], 32.60 [C($\underline{C}H_3)_3$-6], 34.91 [$\underline{C}(CH_3)_3$-4], 36.99 [$\underline{C}(CH_3)_3$-6], 45.40 (NMe_2), 65.08 (CH_2), 120.07 (C-3), 123.34 (C-5), 132.9 (br., C-1), 141.05 (C-2), 152.69 (C-4) 158.66 (C-6). MS (70 eV, EI+): *m/z* (rel intens) 387 (15) [M^+], 372 (14) [M^+ - Me], 350 (19) [M^+ - Cl], 345 (29), 334 (63) [M^+ - Me - HCl], 327 (13), 246 (43) [M^+ - $GaCl_2$], 203 (65) [MH^+ - $GaCl_2$ - NMe_2], 187 (15) [$C_{14}H_{19}^+$], 148 (16) [$C_{11}H_{16}^+$], 133 (28) [$C_{10}H_{13}^+$], 58 (100) [$C_4H_{10}^+$], 57 (47) [$C_4H_9^+$]. Anal. Calcd for $C_{17}H_{28}Cl_2GaN$ (387.04): C, 52.75; H, 7.29; N, 3.62. Found: C, 52.70; H, 7.84; N, 3.40.

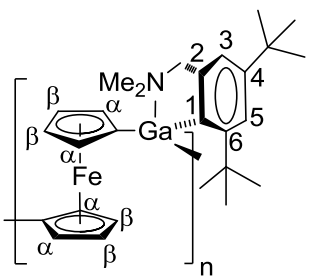

7_n

Synthesis of poly(ferrocenylgallane) 7_n. A solution of **6** (1.16 g, 3.00 mmol) in Et_2O (75 mL) was added dropwise to a slurry of $(LiC_5H_4)_2Fe \cdot 2/3$ tmeda (0.835 g, 3.03 mmol) in Et_2O (30 mL) at r.t. and the resulting reaction mixture was stirred for

16 h. All volatiles were removed under vacuum, resulting in a red solid (2.04 g). The following work-up was done without inert-gas protection using ACS or laboratory grade solvents as received. The crude product was extracted with CH_2Cl_2 (100 mL). After removal of the solvent under vacuum, a red solid (1.37 g) remained, which was washed with hexanes (3 x 75 mL), leaving an orange solid behind (0.832 g). For further purification, the orange solid was dissolved in thf (40 mL) and added dropwise to MeOH (240 mL) with vigorous stirring, resulting in an orange precipitate and a pale yellow solution. The precipitate was filtered off and dried under vacuum to give analytically pure **7$_n$** (0.679 g, 45 %). T_g = 205 ºC. UV/Vis: λ_{max} = 455 nm, ε = 0.27 $(mg/mL)^{-1}$ cm^{-1}. Note: Two different diads can be seen in the Cp range of the proton spectrum. As we have no evidence which set of peaks belongs to the *meso* and which to the *racemo* diad, they are assigned to diad x and diad y. ^{1}H NMR (CD_2Cl_2): δ 1.32 (s, 9 H, *t*Bu-4), 1.471, 1.477, 1.483, 1.517, 1.525, 1.529, 1.536, 1.555, 1.565, 1.574 (10 s, 9 H, *t*Bu-6; for assignments see discussion in the main text), 2.087 (br. s with shoulders at 2.095 and 2.115; 6 H, NMe_2), 3.53 (br. s, 2 H, CH_2), 3.95 (br. s with shoulder at 3.94, CH-α of Cp, diad x), 4.00 (br. s, CH-α of Cp, diad y), 4.19 (br. s, CH-α of Cp, diad y), 4.22 (br. s, CH-α of Cp, diad x), 4.41 (br. s, CH-β of Cp, diad x), 4.45 (br. s, CH-β of Cp, diad y), 4.54 (shoulder, CH-β of Cp, diad x), 6.88 (br. s, 1 H, CH-3), 7.39, 7.41 (2 br. s with shoulders at 7.40 and 7.42, 1 H, CH-5). ^{13}C{^{1}H} NMR (CD_2Cl_2): δ 31.87 [C(<u>C</u>H_3)$_3$-4], 33.60, 33.65, 34.88 [C(<u>C</u>H_3)$_3$-6], 34.98 [<u>C</u>$(CH_3)_3$-4], 37.21, 37.26, 37.31 [<u>C</u>$(CH_3)_3$-6], 46.39 (NMe_2), 67.69 (CH_2), 71.03 (CH-β of Cp), 75.40, 75.46, 75.58, 75.71 (CH-α of Cp), 76.58, 76.64, 76.71 (C-*ipso* of Cp), 119.89 (C-3), 122.06 (C-5), 143.16, 143.24, 143.38 (C-1), 143.93,

143.99, 144.04 (C-2), 149.76 (C-4) 159.05 (C-6). Anal. Calcd for $C_{27}H_{36}FeGaN$ (500.149): C, 64.48; H, 7.25; N, 2.80. Found C, 65.51; H, 7.23; N, 3.15.

REFERENCES

(1) Butler, I. R.; Cullen, W. R.; Ni, J.; Rettig, S. J. *Organometallics* **1985**, *4*, 2196-2201.

(2) Baudler, M.; Simon, J. *Chem. Ber.* **1988**, *121*, 281-285.

(3) Yoshifuji, M.; Kamijo, K.; Toyota, K. *Bull. Chem. Soc. Jpn.* **1993**, *66*, 3440-3443.

(4) Yoshifuji, M.; Kamijo, K.; Toyota, K. *Tetrahedron Lett.* **1994**, *35*, 3971-3974.

Contribution 2: Understanding the Reactivity of Strained Sandwich Compounds with Aluminum or Gallium in Bridging Positions: Experiments and DFT Calculations.

2.2.1 Description

The following chapter is a verbatim copy of an article that was published in *Journal of the American Chemical Society*[1] in April 2012[2] and describes the synthesis, characterization and reactivity study of a series of reactive strained sandwich compounds bridged by heavier group 13 elements. Salt metathesis reaction of aluminum- (**1a**) and gallium dichlorides (**1b**), equipped with the bulky Mamx ligand, with $(C_5H_4Li)_2M{\cdot}$tmeda (M = Fe, Ru) yielded poly(metallocene)s bridged by aluminum and gallium through ROP of reactive [1]metallocenophanes (MCPs). The gallium[1]ruthenocenophane (RCP) **3b** was isolated in pure form and treated with a Pt^0-catalyst to yield poly(ruthenocenylgallane). Other reactive [1]MCPs could not be isolated and were characterized by ^{1}H NMR spectroscopy from crude reaction mixtures. The polymers were characterized by ^{1}H and ^{13}C NMR spectroscopy as well as by dynamic light scattering (DLS) experiments, which resulted in M_w in the range of 8-106 kD. In order to get some structural information of polymers, aluminum- (**4a**) and gallium-bridged bis(ferrocenyl) species (**4b**) were synthesized and structurally characterized.

DFT calculation was performed to shed some light on the unexpected high reactivity of these new [1]metallocenophanes. In particular, the role of the *ortho*-*t*Bu group on the high reactivity of strained sandwich species was investigated and an unprecedented effect

[1] Reprinted with permission from Journal of the American Chemical Society. Copyright (2012) American Chemical Society

of the *ortho-t*Bu group on high reactivity of [1]metallocenophane was uncovered by DFT calculation.

2.2.2 Author Contribution

The co-authors on this paper are Gabriele Schatte, who performed the structure determinations by single-crystal X-ray analysis and Jennifer C. Green, who performed DFT calculations. I synthesized the starting heavier group 13 dichlorides equipped with the Mamx ligand and performed their reaction with dilithio sandwich compounds to yield metallopolymers which were characterized by multinuclear NMR spectroscopy and DLS. I characterized the transient [1]MCP by ^{1}H NMR spectroscopy. The transition-metal catalyzed ROP of isolated Ga[1]RCP was performed by me. I also synthesized the bis(ferrocenyl) compounds with Al- and Ga-bridges.

I prepared parts of the first version of the manuscript, which was edited by my supervisor Jens Müller.

2.2.3 Relation of Contribution 2 with Research Objectives

The primary results discussed in Contribution 1, provided a foundation to begin exploring the chemistry of heavier group 13 element dichlorides equipped with the bulky Mamx ligand. Analogous to (Mamx)$GaCl_2$ (**1b**), the aluminum dichloride **1a** with Mamx ligand was synthesized by using similar synthetic route. With the aim of preparing new strained [1]metallocenophanes, both aluminum and gallium dichlorides, **1a** and **1b** were reacted with dilithioferrocene and dilithioruthenocene. In fact, all these reactions yielded reactive [1]metallocenophanes ([1]FCPs and [1]RCPs), which ring-open polymerized to give respective poly(metallocene)s. Only galla[1]ruthenocenophane (**3b**) was isolated and

[2] Bagh, B.; Schatte, G.; Green, J. C.; Müller, J. *J. Am. Chem. Soc.* **2012**, *134*, 7924-7936.

polymerized by usisng transition-metal catalyst [Pt(0)]. The results described in Contribution 2 has proved that suitable ligand framework, such as Mamx, is absolutely necessary for the synthesis of reactive [1]metallocenophanes. Moreover, DFT calculation was implemented to understand the influence of the novel Mamx ligand towards the high reactivity of those [1]metallocenophanes. Therefore, the results presented in Contribution 2 indicate that the goal of my research is achived to a good extend because Contribution 2 provided a detailed description of synthesizing heavier group-13-bridged [1]metallocenophanes and respective metallopolymers.

2.2.4 Reprint of Contribution 2

Understanding the Reactivity of Strained Sandwich Compounds with Aluminum or Gallium in Bridging Positions: Experiments and DFT Calculations

Bidraha Bagh,[†] Gabriele Schatte,[‡] Jennifer C. Green,[§] and Jens Müller[*,†]

[†]Department of Chemistry and [‡]Saskatchewan Structural Sciences Centre, University of Saskatchewan, 110 Science Place, Saskatoon, Saskatchewan S7N 5C9, Canada;

[§]Department of Chemistry, Inorganic Chemistry Laboratory, University of Oxford, Oxford OX1 3QR, United Kingdom

Received February 27, 2012

ABSTRACT: The aluminum- and gallium dichlorides (Mamx)ECl_2 **1a** (E = Al; 82%) and **1b** (E = Ga; 79%) (Mamx = 2,4-di-*tert*-butyl-6-[(dimethylamino)methyl]phenyl) reacted with dilithioferrocene or dilithioruthenocene to give [1]ferrocenophanes (**2a**, **2b**) and [1]ruthenocenophanes (**3a**, **3b**), respectively. The galla[1]ruthenocenophane **3b** could be isolated from the reaction mixtures through precipitations into hexanes (50%), while

2a, **2b**, and **3a** underwent ring-opening polymerization under the reaction conditions of their formation reaction to give metallopolymers (M_w (DLS) between 8.07 and 106 kDa). Monomer **3b** was polymerized using Karstedt's catalyst resulting in an M_w of 28.6(±4.9) kDa. In order to get an indication of the structure of polymers, bis(ferrocenyl) compounds (Mamx)EFc_2 (E = Al (**4a**), 51%; E = Ga (**4b**), 49%) were prepared and characterized by single crystal X-ray analysis. DFT calculations shed some light on the unexpected high reactivity of these new strained sandwich species. Optimized geometries of known aluminum and gallium-bridged [1]ferrocenophanes (Al(Pytsi) (**6a**), Ga(Pytsi) (**6b**); Pytsi = [dimethyl(2-pyridyl)silyl]bis(trimethylsilyl)methyl) and [1]ruthenocenophanes (Al(Me_2Ntsi) (**7a**), Ga(Me_2Ntsi) (**7b**); Me_2Ntsi = [(dimethylamino)dimethylsilyl]bis(trimethylsilyl)methyl) matched very well with experimental molecular structures. Geometries of species **2a**, **2b**, **3a**, and **3b** were optimized (BP86/TZ2P).and the structural influence of the *t*Bu group of the Mamx ligand in *ortho*-position was evaluated by optimizing molecular structures of the four unknown species where the *ortho*-*t*Bu group was replaced by a H atom (**2a^{H}**, **2b^{H}**, **3a^{H}**, **3b^{H}**). The most pronounced structural effect was seen as a change of the orientation of the bridging moiety with respect to the sandwich unit. As the *t*Bu group was removed, the aromatic ligand moved towards the freed-up space. The energetics (ΔE, ΔH^{298K}, and ΔG^{298K}) accompanied by the structural changes were evaluated by a hydrogenolysis reaction of strained species resulting in Cp_2M (M = Fe, Ru) and respective aluminum and gallium dihydrides. This non-isodesmic reaction showed that [1]metallocenophanes equipped with the *ortho*-*t*Bu group were on average 5.5 kcal/mol higher strained (ΔH^{298K}) than species where the *t*Bu group was lacking. The investigation of the isodesmic reaction

between strained species and Cp_2M yielding bis(metallocenyl) compounds revealed that the *ortho-t*Bu group sterically interacts with one of the metallocenyl units. The bis(metallocenyl) compounds are model compounds for the respective metallopolymers and one can conclude that even though the *ortho-t*Bu group imposes additional strain on the starting metallocenophanes, this effect cancels out in ROPs because the *ortho-t*Bu group imposes a similar strain on the resulting polymers. The uncovered steric repulsion between the *ortho-t*Bu group and the sandwich moieties probably causes the *ortho-t*Bu to act as an unusually sensitive NMR probe of the tacticity of the polymers.

INTRODUCTION

In 1992, Manners *et al.* discovered that ring-opening polymerization (ROP) of sila[1]ferrocenophanes gives access to high-molecular-weight polymers.[1] Since this benchmark discovery, the synthesis of many new strained sandwich compounds has been reported.[2] In addition, different ROP methodologies were developed for the conversion of strained sandwich compounds into new metallopolymers,[3] a growing class of functional materials with high promise for applications in various areas.[3-4] Anionic-ROP of dimethylsila[1]ferrocenophane can be performed as a living polymerization, giving access to the important class of block copolymers.[5] These copolymers, with a poly(ferrocenylsilane) core (**PFS**; Chart 2-2-1), can form "living" micelles in block selective solvents; addition of further unimers results in larger micelles of uniform lengths. This new process was termed "crystallization-driven living self-assembly" and allows for controlled fabrication of uniform nanomaterials.[6]

Chart 2-2-1. Poly(ferrocenyldimethylsilane), [1]Ferrocenophanes, and [1.1]Ferrocenophanes.

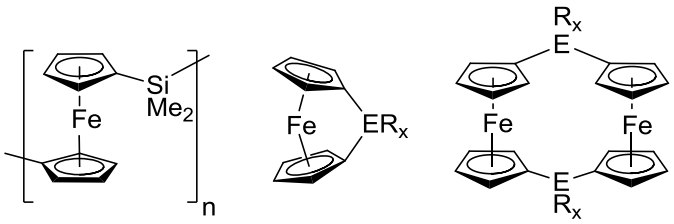

PFS **[1]FCP** **[1.1]FCP**

Chart 2-2-2.

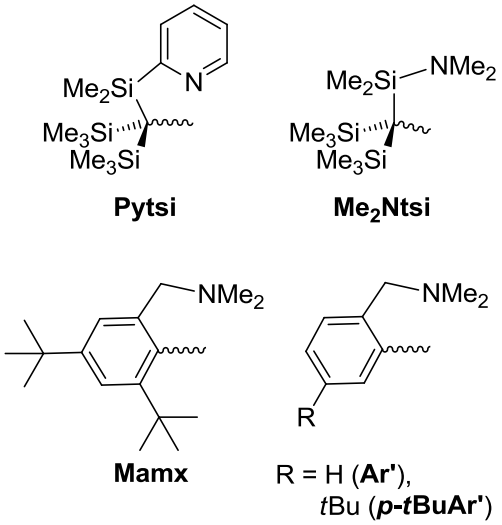

Pytsi **Me$_2$Ntsi**

Mamx R = H (**Ar'**), *t*Bu (***p*-*t*BuAr'**)

Compared to vast knowledge about PFS-based materials, that of respective group-13-containing polymers is still scarce. The most advanced class of group-13-containing polymers is that of boron[7] and ferrocene-based materials had been prepared by either ROP of bora[1]ferrocenophanes[8] or, more recently, through unusual redistribution/polycondensation reactions starting from 1,1′-bis(boryl)ferrocenes.[9] In order to develop poly(ferrocenyl) compounds of the heavier group 13 elements by ROP, we synthesized aluminum- and gallium-bridged sandwich compounds. After the preparation of the first aluminum- and gallium-bridged [1]ferrocenophanes (Chart 2-2-1) in 2005,[10a,10b] [1]vanadarenophanes,[10c] [1]chromarenophanes,[10] [1]molybdarenophanes,[11]

and [1]ruthenocenophanes[12] could be synthesized. All these [1]metallacyclophanes were obtained by common salt metathesis reactions starting from dilithio-sandwich compounds and bulky dichlorides (Pytsi)ECl_2 or (Me_2Ntsi)ECl_2 (E = Al, Ga; Chart 2-2-2).

Unfortunately, attempts to polymerize by ring-opening aluminum- and gallium-bridged [1]ferrocenophanes and [1]ruthenocenophanes either failed or resulted in sluggish reactions[12] and it seemed that the bulkiness of the *trisyl*-type ligands Pytsi or Me_2Ntsi was hindering the ROP of those species. The bulkiness of the stabilizing ligand cannot easily be reduced: employing the less sterically encumbered ligands Ar′ or *p*-*t*BuAr′ (Chart 2-2-2) resulted in [1.1]metallacyclophanes[13] instead of the targeted [1]metallacyclophanes in respective salt metathesis reactions. Structural data of metallacyclophanes revealed that the bridging ER_x unit in [1.1]metallacyclophanes has less space available than in [1]metallacyclophanes.[14] On that basis, we speculated that, first, unstrained [1.1]metallacyclophanes are thermodynamically preferred when starting compounds are equipped with the slim ligands Ar′ or *p*-*t*BuAr′ (Chart 2-2-2) and that, secondly, strained [1]metallacyclophanes are obtained exclusively when the bulkiness of ligands hinders or even blocks the formation of [1.1]metallacyclophanes. Therefore, we intended to use a ligand with just the right bulkiness to allow the formation of [1]metallacyclophanes but, at the same time, would not block their polymerizability. Our plan was to increase the bulkiness of the 2-[(dimethylamino)methyl]phenyl ligand (Ar' in Chart 2-2-2) such that the formation of [1.1]ferrocenophanes, the outcome of salt metathesis reaction of (Ar')ECl_2 (E = Al, Ga) with dilithioferrocene,[13a,13b] would be impossible. From the known molecular structures of (Ar')E-bridged [1.1]ferrocenophanes[13a,13b] it was evident that a *t*Bu group in the *ortho* position on the

phenyl ring of the Ar' ligand could not be accommodated. A ligand with these steric requirements was already known in form of the Mamx[15] ligand (Chart 2-2-2), which was introduced by Yoshifuji et al.[16] and had been used to stabilize phosphorus compounds.[17] Jutzi et al. employed the Mamx ligand to stabilize germanium species.[18]

In a recent short communication, we reported on the salt metathesis reaction of (Mamx)$GaCl_2$ with dilithioferrocene, which resulted in the formation of the targeted [1]ferrocenophane **2b** (Scheme 2-2-1).[19] Unexpectedly, this strained sandwich compound (**2b**) withstood all attempts at isolation and underwent ROP from reaction mixtures to give the poly(ferrocenylgallane) $\mathbf{2b_n}$ (Scheme 2-2-1). The *ortho*-*t*Bu group[20] acts as a very sensitive probe of the stereochemistry of the polymer backbone and pentads were resolved in proton NMR spectra.[19] The splitting pattern of the *ortho*-*t*Bu group clearly revealed that polymer $\mathbf{2b_n}$ has a random tacticity. Here we report on the completed study of the reaction between (Mamx)ECl_2 (E = Al, Ga) and dilithioferrocene and dilithioruthenocene. New [1]ferrocenophanes and [1]ruthenocenophanes and their respective metallopolymers are described. Using DFT calculations, we uncovered that the *ortho*-*t*Bu group significantly increases the strain in [1]metallocenophanes, an unprecedented effect in metallocenophane chemistry.

RESULTS AND DISCUSSION

Synthesis of [1]Ferrocenophanes and [1]Ruthenocenophanes. The aluminum- and gallium dichlorides **1a** and **1b**[19], respectively, are accessible in good yields starting from the bromide of the Mamx ligand following common methodologies (Scheme 2-2-1). As expected, NMR spectra of **1a** and **1b** are consistent with both species being C_s symmetric

on the NMR time scale. That nitrogen is indeed coordinated to the group 13 element could be confirmed by a single crystal analysis of the gallium species **1b** (Figure 2-2-1 and Table 2-2-1), which showed a Ga-N bond length of 2.066(2) Å. As expected, the molecular structure of **1b** did not reveal any surprises and is very similar to the known compounds 2-(Me_2NCH_2)$C_6H_4GaCl_2$ and 2-(Me_2NCHMe)$C_6H_4GaCl_2$, which exhibit Ga-N bond lengths of 2.071(2)[21] and 2.049(3)[22] Å, respectively.

Scheme 2-2-1.

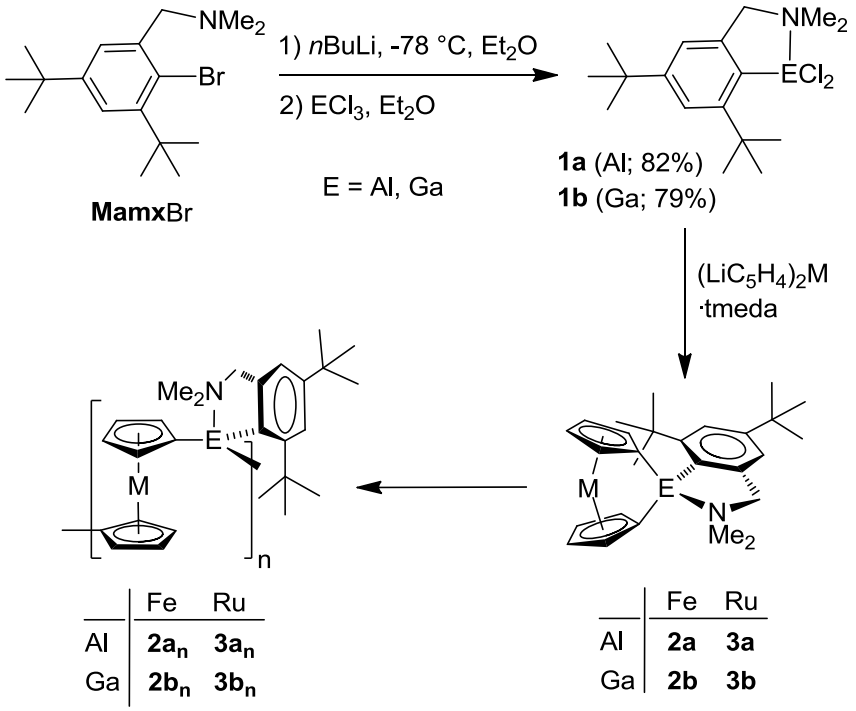

Table 2-2-1. Crystal and Structural Refinement Data for Compounds **1b**, **4a**, and **4b**.

	1b·C_7H_8	**4a·½C_6H_6**	**4b**
empirical formula	$C_{24}H_{36}Cl_2GaN$	$C_{40}H_{49}AlFe_2N$	$C_{37}H_{46}Fe_2GaN$
fw	479.19	682.50	686.17
cryst. size / mm^3	0.23 × 0.18 × 0.15	0.14 × 0.08 × 0.05	0.21 × 0.20 × 0.13

cryst. system, space group	*monoclinic*, $P2_1/c$	*monoclinic*, $P2_1/c$	*triclinic*, $P\bar{1}$
Z	4	4	2
a / Å	10.7202(5)	14.7365(3)	10.3706(3)
b / Å	17.6730(6)	10.9109(2)	11.7881(3)
c / Å	14.0352(5)	21.9806(5)	14.3895(3)
α / °	90	90	109.0902(7)
β / °	109.9730(10)	101.4210(10)	102.3199(8)
γ / °	90	90	97.1448(6)
volume / Å^3	2499.15(15)	3464.24(12)	1587.77(7)
ρ_{calc} / mg m^{-3}	1.273	1.309	1.435
temperature / K	173(2)	173(2)	173(2)
$\mu_{calc.}$/ mm^{-1}	3.525	7.161	8.404
θ range / °	4.18 to 66.64	3.06 to 69.76	3.38 to 60.00
reflns collected / unique	15167 / 4183	20971 / 6574	20043 / 4683
absorption correction	multi-scan [SADABS]	multi-scan [SADABS]	multi-scan [SADABS]
data / restraints / params	4183/ 15 / 262	6374 / 0 / 405	4683 / 0 / 378
goodness-of-fit	1.055	1.031	1.046
R_1 [I > 2 σ(I)][a]	0.0424	0.0660	0.0767
wR_2 (all data)[a]	0.1182	0.1799	0.1961
largest diff. peak and hole, $\Delta\rho_{elect}$ / e Å^{-3}	0.725 and -0.555	1.458 and -0.409	1.450 and -1.248

[a] $R_1 = [\Sigma||F_o|-|F_c||]/[\Sigma|F_o|]$ for $[F_o^2 > 2\sigma(F_o^2)]$, $wR_2 = \{[\Sigma w(F_o^2-F_c^2)^2]/[\Sigma w(F_o^2)^2]\}^{1/2}$ [all data].

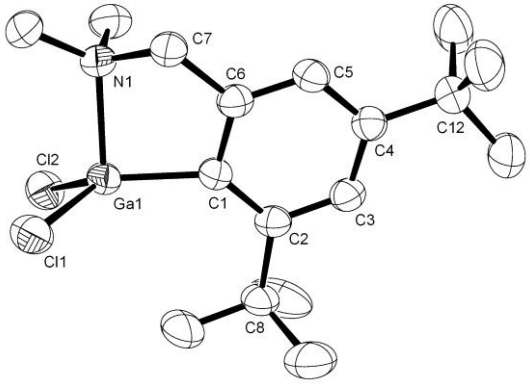

Figure 2-2-1. Molecular structure of **1b** with thermal ellipsoids at the 50% probability level. Hydrogen atoms are omitted for clarity. Selected atom-atom distances [Å] and bond angles [º] for **1b**: Ga1–C1 = 1.956(2), Ga1–Cl1 = 2.1955(7), Ga1–Cl2 = 2.1878(7), Ga1–N1 = 2.066(2), C1–Ga1–Cl1 = 118.70(7), C1–Ga1–Cl2 = 125.94(7), C1–Ga1–N1 = 89.26(9), Cl1–Ga1–Cl2 = 108.51(3), N1–Ga1–Cl1 = 103.59(6), N1–Ga1–Cl2 = 104.40(7), Ga1–C1–C2 = 134.12(18), Ga1–C1–C6 = 106.88(17).

The dichlorides **1a** and **1b** were employed to prepare new aluminum- and gallium-bridged [1]ferrocenophanes (**2a**, **2b**[19]) and [1]ruthenocenophanes (**3a**, **3b**), starting from respective dilithio sandwich compounds (Scheme 2-2-1). Recently, we have shown that attempts to isolate the ferrocenophane **2b** resulted in isolation of the polymer $\mathbf{2b_n}$ (Scheme 2-2-1).[19] The respective aluminum compound **2a** shows a similar behavior and its isolation also gave polymers ($\mathbf{2a_n}$). Proton NMR spectra taken from aliquots of reaction mixtures after 15 to 30 min clearly showed the presence of the strained [1]ferrocenophanes **2a** or **2b**, in particular by patterns and chemical shifts of the Cp protons, which are characteristic for alumina- or galla[1]ferrocenophanes with donor-stabilizing ligands (C_s point-group symmetries).[10,12] This is illustrated in Figure 2-2-2, where the Cp range of the proton NMR spectrum of the aluminum compound **2a** is depicted. The two signals for the four H atoms in α-position to the bridging element are shifted upfield with respect to those of the four H atoms in β-potions [**2a**: δ 4.72 (2 β-H),

4.70 (2 β-H), 4.23 (2 α-H), 3.85 (2 α-H); **2b**: δ 4.69 (4 β-H), 4.56 (2 α-H), 4.01 (2 α-H)] (Figure 2-2-2 and S7 for **2a**; ref. 19 for **2b**). In addition, the difference between the two signals of the α-protons is significantly larger than that of the β-protons.[23] Obviously, the influence of the disturbing bridging unit on α- compared to β-protons is distance dependent. Two chemically equivalent α-protons on one side of the [1]ferrocenophane are in the neighborhood of the amine donor group, while the other pair of equivalent α-protons are on the opposite side of the sandwich (Figure 2-2-2). Because the β-protons are further away from the bridging moiety, they are not so sensitive toward the two different sides of the stabilizing ligand. In addition to the Cp protons, all expected signals were found for the [1]ferrocenophanes **2a** and **2b** (Figure S7 for **2a**; ref. 19 for **2b**).

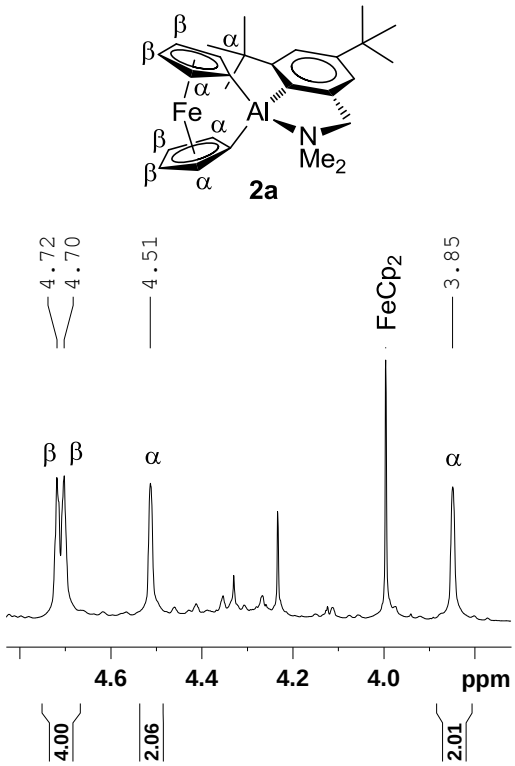

Figure 2-2-2. Cp range of the ^{1}H NMR spectrum of **2a** measured from an aliquot of the reaction mixture after ca. 30 min (C_6D_6).

Judging by ^{1}H NMR spectra of reaction mixtures, the targeted species **2a** and **2b**, respectively, are the main products (e.g. Figure 2-2-2 and S7; ref. 19 for **2b**). However, numerous attempts to isolate **2a** or **2b** through crystallization or precipitation into hexane failed (see Experimental Section). Instead of the monomers **2a** and **2b**, the respective polymers $\mathbf{2a_n}$ and $\mathbf{2b_n}$ were isolated and further purified through precipitations into hexane and methanol, respectively, with isolated yields of 37% for $\mathbf{2a_n}$ and 45%[19] for $\mathbf{2b_n}$ (Scheme 2-2-1).

As shown in Scheme 2-2-1, the [1]ruthenocenophanes **3a** and **3b** were prepared using similar methods as were used for the [1]ferrocenophanes **2a** and **2b**. The aluminum-bridged [1]ruthenocenophane **3a** showed a reactivity similar to that of the [1]ferrocenophanes **2a** and **2b**; however, the gallium-bridged [1]ruthenocenophane **3b** showed a lower reactivity and was isolated as a light yellow powder (50%) from filtered reaction mixtures through precipitation into hexanes. Applying the same procedure to the aluminum species **3a** mainly gave polymers. Proton NMR spectra taken from the mother liquor after the precipitation into hexanes did not reveal significant amounts of the monomer **3a** showing that nearly all of the strained [1]ruthenocenophane **3a** polymerized to $\mathbf{3a_n}$ under these conditions. However, the reactivities of **3a** and **3b** are not vastly different. If reaction mixtures of the gallium species **3b** are left for 6 h, only its polymer $\mathbf{3b_n}$ could be isolated.

Attempts to grow crystals of **3b** for structural analysis failed (see Experimental Section). However, ^{1}H NMR spectroscopy unequivocally revealed that strained [1]ruthenocenophanes **3a** and **3b** indeed formed in salt metathesis reactions of dichlorides and dilithioruthenocene (Scheme 2-2-1). Their Cp protons give similar patterns as those

of the [1]ferrocenophanes. For example, the two signals of the α-protons show the characteristic splitting that is significantly larger than that of the *β*-protons [**3a**: *δ* 5.34 (2 *β*-H), 5.30 (2 *β*-H), 4.65 (2 *α*-H), 4.02 (2 *α*-H); **3b**: *δ* 5.36 (2 *β*-H), 5.34 (2 *β*-H), 4.59 (2 *α*-H) 4.05 (2 *α*-H)] (Figure S10 and S13).

Metallopolymers. All four strained [1]metallocenophanes **2a**, **2b**, **3a**, and **3b** undergo ring-opening polymerizations (ROPs) at ambient temperature under the conditions of the salt metathesis reaction (Scheme 2-2-1). In addition, as we could isolate the monomer **3b**, ROPs using Karstedt's catalyst at ambient temperatures were performed (toluene, 5 mol% catalyst). All polymers were characterized by ^{1}H and ^{13}C NMR spectroscopy as well as by Dynamic Light Scattering (DLS). Table 2-2-2 summarizes the results of the DLS analysis.

Table 2-2-2. DLS Analysis of Metallopolymers[a]

	R_h [nm]	M_w [kDa]	DP_w
2a$_n$ [c]	5.38(±0.05)	106(±2)	232(±4)
2b$_n$ [b,c]	2.99(±0.36)	36.0(±8.4)	72(±17)
3a$_n$ [c]	1.33(±0.11)	8.07(±1.3)	16(±3)
3b$_n$ [c]	1.50(±0.14)	10.1(±1.8)	19(±3)
3b$_n$ [d]	2.64(±0.19)	28.6(±4.9)	52(±7)

[a] See also Tables 2-2-S1 to 2-2-S5. [b] Data taken from ref. 19. [c] Polymer from uncontrolled ROP. [d] Polymer from transition-metal-catalyzed ROP.

Assuming that the measured polymers were random coils in a good solvent, the radii of gyration can be calculated from the measured hydrodynamic radii (R_g / R_h = 2.05).[24] For poly(ferrocenyldimethylsilane) R_g and the absolute M_w are known,[25] which we employed to calculate the molecular weights shown in Table 2-2-2 (see Experimental

Section for details). The molecular weights of aluminum- and gallium-containing polymers vary between 8.07 and 106 kDa (Table 2-2-2). For the uncontrolled ROP, poly(ferrocenyl) species $\mathbf{2a_n}$ and $\mathbf{2b_n}$ show significantly higher M_w values compared to their ruthenium analogues $\mathbf{3a_n}$ and $\mathbf{3b_n}$. The molecular weight of the polymer $\mathbf{3b_n}$ could be improved by using Karstedt's catalyst resulting in M_w values that were nearly three times as large compared to those of polymers obtained from the spontaneous, uncontrolled ROP (Table 2-2-2). For the gallium-containing polymer $\mathbf{2b_n}$, molecular weights were also determined with gel permeation chromatography (GPC) with polystyrene as a standard, resulting in 48 kDa for the sample that gave 36 kDa with respect to PFS as a standard by DLS analysis.[19]

Metallopolymers $\mathbf{2a_n}$, $\mathbf{2b_n}$, $\mathbf{3a_n}$, and $\mathbf{3b_n}$ are formed by ROP of the respective [1]metallocenophanes under the conditions of the metathesis formation reactions. So far, the mechanism of these ROPs is unknown, but it seems likely that some dilithioferrocene in reaction mixtures of the salt metathesis reaction acts as an anionic initiator (Scheme 2-2-1). Therefore, we wanted to test if addition of $ClSiMe_3$ to the reaction mixture influences the outcome of the ROP and we investigated the reaction of the gallium dichloride **1b** with dilithioferrocene. Two parallel reactions were started in two different reaction vessels under the same reaction conditions and, after 15 min, excess Me_3SiCl was added to one reaction mixture. Both reactions were run for an additional 16 h followed by the work up as described for the synthesis of poly(ferrocenylgallane) $\mathbf{2b_n}$ (Experimental Section). The polymers that resulted from the two reactions were identical with respect to ^1H NMR spectroscopy. The DLS analysis of the polymers gave similar hydrodynamic radii; R_h for the polymer of the reaction without Me_3SiCl was 3.31 nm and

that with Me_3SiCl was 2.54 nm. The reaction in the presence of Me_3SiCl was done two additional times and gave identical polymers with respect to ^1H NMR spectroscopy. Comparison of polymers (with and without the addition of $ClSiMe_3$) did not reveal the presence of any Me_3Si end groups.

Bis(ferrocenyl) Species. In order to get an indication of the structure of polymers, the bis(ferrocenyl) compounds **4a** and **4b** have been prepared as they can be envisioned as small cutouts of the polymers $\mathbf{2a_n}$ and $\mathbf{2b_n}$, respectively. As illustrated in Scheme 2-2-2, both species were obtained by salt metathesis reactions starting from **1a** and **1b**, respectively, and isolated in moderate yields of 51% (**4a**) and 49% (**4b**). Both species have been characterized by NMR spectroscopy, mass spectrometry, elemental analysis, and single crystal X-ray analysis (Table 2-2-1, Figure 2-2-3 and 2-2-4).

Scheme 2-2-2.

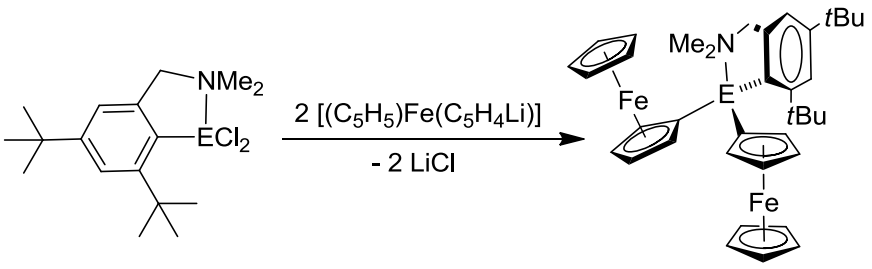

1a (Al)
1b (Ga)

4a (Al: 51%)
4b (Ga: 49%)

Whereas the aluminum species **4a** (Figure 2-2-3) exhibits two ferrocenyl moieties oriented in approximately opposite directions, they are approximately parallel to each other in the gallium species **4b** (Figure 2-2-4). Both compounds show highly distorted tetrahedral coordination geometries around the group 13 element that are best described as trigonal-base pyramids with C1, C20, and C30 at the base and N1 at the tip. This description is justified as the sums over the three C-E-C (E = Al, Ga) angles with 352

(**4a**) and 359º (**4b**), respectively, are very close to 360º, indicating that the group-13 elements are only slightly lifted out of the plane of the base (**4a**: 0.322(5) Å; **4b**: 0.135(2) Å). The C-E bond lengths are very similar in both compounds and, as expected, respective bonds are slightly longer in the case of gallium. The Ga-N donor bond in **4b** of 2.153(3) Å is significantly longer than the Al-N bond of 2.038(3) Å in **4a**. Similar differences are known from comparable species and are a testament to the higher Lewis acidity toward N-donors of aluminum compared to respective gallium compounds.[26]

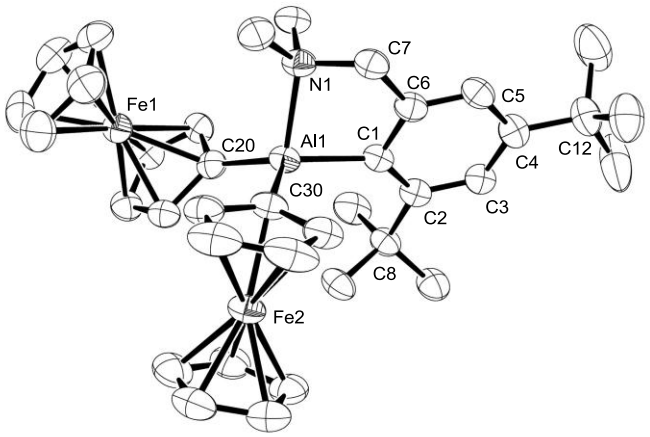

Figure 2-2-3. Molecular structure of **4a** with thermal ellipsoids at the 50% probability level. Hydrogen atoms and the solvent molecule C_6H_6 are omitted for clarity. Selected atom-atom distances [Å] and bond angles [º] for **4a**: Al1–C1 = 2.012(3), Al1–C20 = 1.966(4), Al1–C30 = 1.969(3), Al1–N1 = 2.038(3), Fe1-Al1 = 3.7250(11), Fe2-Al1 = 3.7746(10), C1–Al1–C20 = 124.08(14), C1–Al1–C30 = 114.03(14), C1–Al1–N1 = 86.87(12), C20–Al1–C30 = 114.06(14), N1–Al1–C20 = 111.05(13), N1–Al1–C30 = 99.85(13), Al1–C1–C2 = 137.8(2), Al1–C1–C6 = 106.0(2).

In ^{1}H and ^{13}C NMR spectra, compounds **4a** and **4b** each show similar signal patterns. For example, in the typical Cp range of ^{1}H NMR spectra, the presence of five peaks in a 5:1:1:1:1 intensity ratio shows the equivalency of both ferrocenyl moieties; i.e., **4a** and **4b** are C_s symmetric on the NMR time scale (500 MHz; C_6D_6 solutions). Two different conformers of the homologues **4a** and **4b** were found in the solid state (Figure 2-2-3 and

2-2-4), which probably indicates that the barrier of rotation of the ferrocenyl moieties is low. Therefore, the finding of C_s symmetric species in solution is expected.

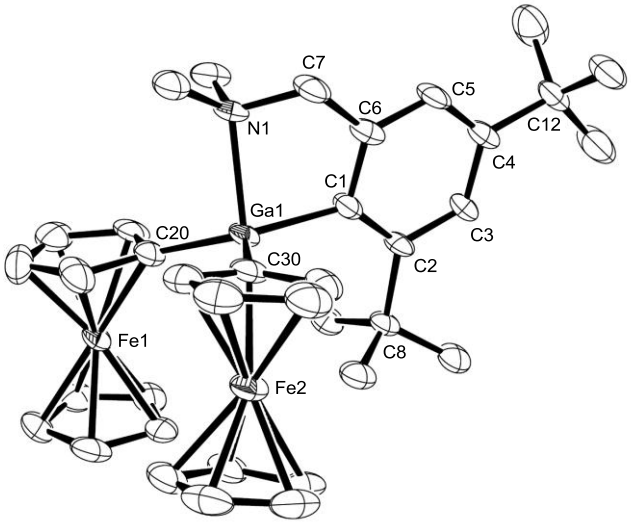

Figure 2-2-4. Molecular structure of **4b** with thermal ellipsoids at the 50% probability level. Hydrogen atoms are omitted for clarity. Selected atom-atom distances [Å] and bond angles [º] for **4b**: Ga1–C1 = 2.011(4), Ga1–C20 = 1.971(4), Ga1–C30 = 1.984(4), Ga1–N1 = 2.153(3), Fe1-Ga1 = 3.8107(7), Fe2-Ga1 = 3.7569(8), C1–Ga1–C20 = 129.04(17), C1–Ga1–C30 = 111.99(17), C1–Ga1–N1 = 84.11(15), C20–Ga1–C30 = 117.57(18), N1–Ga1–C20 = 98.27(15), N1–Ga1–C30 = 99.75(15);, Ga1–C1–C2 = 133.7(3), Ga1–C1–C6 = 108.6(3).

DFT Calculations. The distortion in [1]metallacyclophanes is commonly described by a set of angles (Figure 2-2-5). The most discussed angle to illustrate the distortion in a [1]metallacyclophane is the angle between the two least square planes defined by the carbon atoms of the Cp rings (tilt angle α). Despite the large number of [1]ferrocenophanes only four [1]ruthenocenophanes are known to date [ER_x: $Zr(C_5H_4tBu)_2$,[27] $SnMes^*_2$,[27] $Al(Me_2Ntsi)$,[12] $Ga(Me_2Ntsi)$[12]]. Comparing respective [1]ferrocenophanes with [1]ruthenocenophanes shows that the α angle increases from iron to ruthenium in the range of 4.4–6.0° (Zr,[27,28] Sn,[27,29], Al,[10,12] Ga,[10,12]). One expects that an increase of the tilt of both Cp moieties is accompanied by an increase in strain,

which is expected to result in species of higher reactivity.[2a,30] On that basis, it is very surprising that the galla[1]ruthenocenophane **3b** is isolable, whereas its iron counterpart **2b** is not. Furthermore, tilt angles α for alumina- and galla[1]ferrocenophanes **2a** and **2b**, respectively, should be similar to those of other aluminum- and gallium-bridged [1]ferrocenophanes, which were found in the range of 15–16°.[10,31] Tilt angles in that range are not expected to impose enough strain that alone can explain the high reactivity observed for **2a** and **2b**. We set out to further our understanding of these surprising experimental results with DFT calculations. In particular, we were interested in evaluating if different reactivities can be traced back to differences in ground-state geometries; e.g., if the Mamx ligand introduces different amounts of strain on [1]ferrocenophanes than on [1]ruthenocenophanes. Secondly, we wanted to find out if the *ortho*-*t*Bu has an influence on the structures and the reactivity of the strained sandwich compounds. This intention originated in the observation that the *ortho*-*t*Bu in the metallopolymers $\mathbf{2a_n}$ and $\mathbf{2b_n}$ is a very sensitive probe of the tacticity; e.g., for $\mathbf{2b_n}$ pentads of the polymer could be resolved by ^{1}H NMR spectroscopy.[19] This unusually high sensitivity could be caused by an intimate contact between this group and ferrocene repeating moieties.

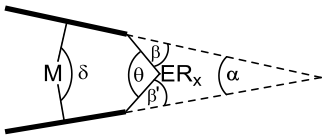

Figure 2-2-5. Common angles to describe distortions in [1]metallacyclophanes.

In a first set of calculations, geometries of known aluminum and gallium-bridged [1]ferrocenophanes (**6a**, **6b**) and [1]ruthenocenophanes (**7a**, **7b**) were optimized and compared to molecular structures known from single crystal X-ray analyses (Chart 2-2-3

and Table 2-2-3). Geometry optimizations were done on a BP86/TZ2P level using the ADF suite of programs.[32] This method has been shown to reproduce structures of metallocenophanes successfully.[8b,33] Calculated and experimentally determined angles to describe distortions in [1]metallacyclophanes are compiled in Table 2-2-3 showing good to excellent agreement. For example, the tilt angles α calculated for the two [1]ferrocenophanes **6a** and **6b** agree with measured values within three estimated standard deviations, if one considers molecule **6b** with the higher α angle of 16.40(20)°

Chart 2-2-3. Overview of [1]Ferrocenophanes and [1]Ruthenocenophanes.

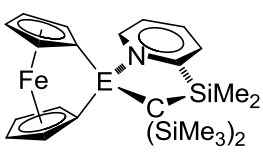

6a (Al)
6b (Ga)

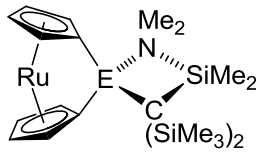

7a (Al)
7b (Ga)

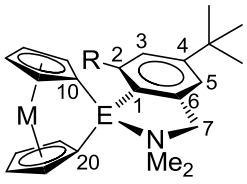

	R = *t*Bu		R = H	
	Fe	Ru	Fe	Ru
Al	**2a**	**3a**	**2a^H**	**3a^H**
Ga	**2b**	**3b**	**2b^H**	**3b^H**

(Table 2-2-3). For the aluminum-bridged [1]ruthenocenophane **7a**, the calculated α angle is 0.92° below, while for the gallium species **7b** it is 1.81° above the measured value. For the [1]ferrocenophane **6b** two independent molecules had been found in the asymmetric unit with tilt angles α of 15.44(21) and 16.40(20)°, respectively.[31] This example illustrates that the deviation of ±1° can be caused by packing effects in the solid state. In addition, for known aluminum- and gallium-bridged [1]metallacyclophanes, aluminum species always exhibit smaller tilt angles than their gallium counterparts. For example,

for [1]chromarenophanes the difference is 1.4° [Al: 11.81(9)°; Ga: 13.24(13)°],[10c] whereas for [1]molybdarenophanes, equipped with the same bridging moiety E(Me_2Ntsi) (Chart 2-2-2), the difference amounts to 3.0° [Al: 18.28(17)°; Ga: 21.24(10)°].[11] The measured difference of only 0.6° for [1]ruthenocenophanes **7a** and **7b** is surprisingly small [Al: 20.31(19)°; Ga: 20.91(19)°][12]. Based on the difference of 3.0° found for [1]molybdarenophanes, the calculated difference of 3.3° for **7a** and **7b** matches with the expectation better than the experimentally determined difference of only 0.6°.

Table 2-2-3. Comparison of Calculated and Measured Angles [°] of the Known [1]Ferrocenophanes **6a,b** and [1]Ruthenocenophanes **7a,b**[a]

	α		β/β′		θ		δ	
	calc.	exp. [a]	calc.	exp. [a]	calc.	exp. [a]	calc.	exp. [a]
6a	14.02	14.9(3)	39.96/40.05	39.6(4)/40.5(4)[b]	94.22	94.7(2)	169.02	167.9(3)
6b[c]	16.17	15.44(21)[c] 16.40(20)	37.38/37.52	38.3(3)/39.0(2)[c] 38.5(3)/37.6(2)	90.95	92.68(13)[c] 92.22(13)	166.91	166.96(17)[c] 166.31(16)
7a	19.39	20.31(19)	41.48/41.21	39.9(4)/40.6(4)	102.63	101.3(2)	166.26	165.2(2)
7b	22.72	20.91(19)	37.63/38.01	38.6(2)/38.6(3)	98.30	98.42(13)	163.33	163.71(15)

[a] See Figure 2-2-5 and Chart 2-2-3. [b] Experimental data taken from references 23a (**6a**), 32 (**6b**) and 12 (**7a**,**b**). [c] Published value of 43.1° has been recalculated. [d] Two independent molecules were found in the asymmetric unit of **6b**.[31]

In a second series of calculations, geometries of the known [1]ferrocenophanes, **2a** and **2b**, and [1]ruthenocenophanes, **3a** and **3b**, were optimized on the same level of theory that was successfully applied to **6a**,**b** and **7a**,**b**. As mentioned before, we intended to find out if the *ortho*-*t*Bu group has an influence on the structure and, potentially, on the reactivity of strained sandwich compounds. In order to evaluate the structural influence of the *ortho*-*t*Bu group, molecular structures of the four unknown species $\mathbf{2a^H}$, $\mathbf{2b^H}$, $\mathbf{3a^H}$, and $\mathbf{3b^H}$ (Chart 2-2-3), where this group was replaced by a H atom, were calculated as

well. Table 2-2-4 compiles all calculated structural parameters commonly used to describe [1]metallocenophanes (Figure 2-2-5). The tilt angle α varies between 12.36 and 15.80° for [1]ferrocenophanes, and between 18.29° and 22.90° for [1]ruthenocenophanes. Comparing respective aluminum and gallium compounds, the gallium species show α angles that are larger by 2.58 and 2.92° for ferrocenophanes and by 3.53 and 3.79° for ruthenocenophanes. The tilt angle α is not very sensitive toward the *ortho*-*t*Bu group. If this group is absent, the angle α decreases only by 0.86 and 0.52° for ferrocenophanes and by 1.08 and 0.82° for ruthenocenophanes.

Table 2-2-4. Calculated Angles [°] for [1]Ferrocenophanes and [1]Ruthenocenophanes[a]

	M/E/R	α	β/β′	θ	δ
2a	Fe/Al/*t*Bu	13.22	40.61/40.89	95.13	169.73
2a^{H}	Fe/Al/H	12.36	43.06/43.33	97.45	170.16
2b	Fe/Ga/*t*Bu	15.80	38.06/37.78	91.59	167.30
2b^{H}	Fe/Ga/H	15.28	39.57/39.30	93.28	167.49
3a	Ru/Al/*t*Bu	19.37	41.90/41.46	102.80	166.44
3a^{H}	Ru/Al/H	18.29	44.80/44.47	105.41	166.90
3b	Ru/Ga/*t*Bu	22.90	37.49/37.90	98.06	163.23
3b^{H}	Ru/Ga/H	22.08	39.88/40.21	100.47	163.66

[a] See Figure 2-2-5 and Chart 2-2-3.

Table 2-2-5 compiles bond lengths around aluminum and gallium, respectively, of all calculated species (see Chart 2-2-3 for numbering of atoms). Data in Table 2-2-5 reveals that all bonds around the bridging element are slightly lengthened in species equipped with the *ortho*-*t*Bu group. The average overall difference for all four types of bonds (E-N,

E-C1, E-C10, E-C20) is just 0.017 Å, with the smallest average difference found for E-N bonds (0.006 Å) and the largest found for E-C1 (0.033 Å). Even though the absolute values are small, they hint at a tension caused by the presence of the *t*Bu in *ortho* position. However, the most pronounced structural effect can be seen as a change of the orientation of the bridging moiety with respect to the sandwich unit. The M-E-C1 angle decreases between 8.08 (**2b** to **2b^{H}**) and 12.73° (**3a** to **3a^{H}**) (see Table 2-2-5) while at the same time the tilt of the aromatic ring relative to the sandwich moiety changes the torsion angle M–E–C1–C2 in the range of 5.26 and 6.98° (Table 2-2-5 and Chart 2-2-3). It appears that as the *t*Bu group gets removed, the aromatic ligand moves towards the freed-up space. This main structural change is also illustrated in Figure 2-2-6 with the galla[1]ruthenocenophanes **3b** and **3b^{H}** as examples. The species without the *ortho*-*t*Bu group (**3b^{H}**) shows a significant larger distance between C1 and the plane Ru-C10-C20 (double headed arrow in Figure 2-2-6). All other respective distances are listed in Table 2-2-5.

Table 2-2-5. Calculated Bond Lengths [Å] and Angles [°] for [1]Ferrocenophanes and [1]Ruthenocenophanes[a]

	M/E/R	E–N	E–C1	E–C10	E–C20	M–E–C1	M–E–C1–C2	pl^{M,C10,C20}–C1 [a]
2a	Fe/Al/*t*Bu	2.078	2.014	2.015	2.005	153.31	-27.62	1.042
2a^{H}	Fe/Al/H	2.071	1.980	1.997	1.990	141.88	-22.36	1.603
2b	Fe/Ga/*t*Bu	2.193	2.013	2.025	2.036	157.24	-25.66	0.906
2b^{H}	Fe/Ga/H	2.184	1.981	2.012	2.019	149.16	-19.95	1.291
3a	Ru/Al/*t*Bu	2.070	2.011	2.033	2.044	151.26	-30.42	1.174
3a^{H}	Ru/Al/H	2.065	1.979	2.021	2.029	138.53	-23.44	1.770
3b	Ru/Ga/*t*Bu	2.181	2.013	2.049	2.062	155.60	-28.01	1.003
3b^{H}	Ru/Ga/H	2.177	1.980	2.035	2.043	144.88	-21.33	1.518

[a] See Chart 2-2-3. [b] distance of C1 from the plane defined by M, C10, and C20 (see Figure 2-2-6).

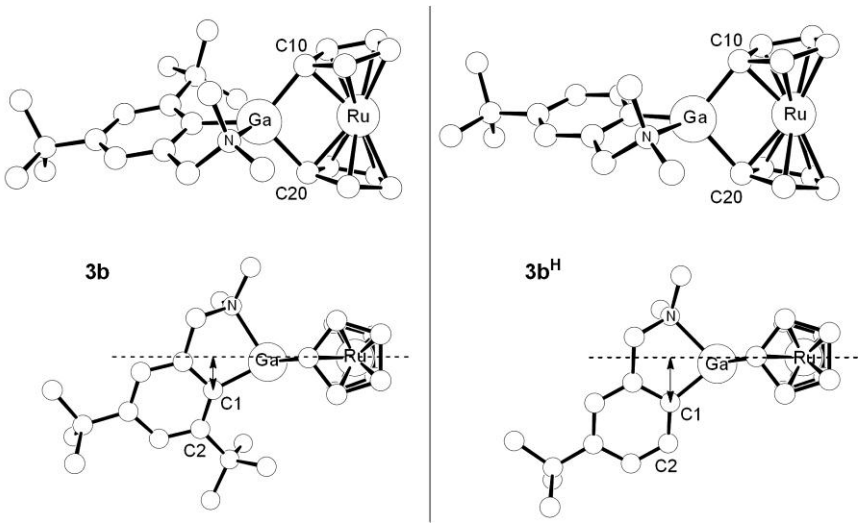

Figure 2-2-6. Optimized geometries of the galla[1]ruthenocenophanes **3b** and **3b^{H}**. Hydrogen atoms are omitted for clarity. The double-headed arrow illustrates the distance of C1 of 1.003 (**3b**) and 1.518 Å (**3b^{H}**) from the plane Ru-C10-C20 (dotted line) (see Table 2-2-3 and 2-2-4).

Thermochemistry. We intended to evaluate the effect of the *ortho-t*Bu group on the reactivity of strained species. So far, only structural effects of the *ortho-t*Bu group have been described showing that the removal of the *t*Bu group results in a relaxation of the remaining ligand toward the opened-up space. We wanted to quantify the energy change associated with these structural changes and, consequently, the amount of strain in species with and without the *t*Bu group needed to be calculated. Intrinsic strain of a compound can be best described by the enthalpy of a reaction where the strained species is transformed into an unstrained species. As shown in Scheme 2-2-3, the hydrogenation reaction (eq. 1) was chosen as the chemically simplest possibility to release the strain. Table 2-2-6 provides an overview of the calculated thermodynamic values. The hydrogenation reaction (eq. 1) is not isodesmic and, therefore, calculated enthalpies are not equal to the intrinsic strain of respective metallocenophanes. The calculated thermodynamic values are a mix of the release of strain of the sandwich species and the

loss and gain of energy associated with bond breakage and formation. However, if one compares the hydrogenation of a *t*Bu containing species (e. g. **2a**) with that of the respective metallocenophane where the *t*Bu group is lacking (e. g. **2a^{H}**), then the difference in the calculated thermodynamic values (ΔΔE, ΔΔH, and ΔΔG) provide a measure of the effect of the *ortho-t*Bu group. From the listed ΔΔE, ΔΔH , and ΔΔG values in Table 2-2-7 one can see that all species with the *ortho-t*Bu group (**2a**, **2b**, **3a**, and **3b**) are more strained than their slimmer counterparts (**2a^{H}**, **2b^{H}**, **3a^{H}**, and **3b^{H}**).

Scheme 2-2-3. Hydrogenation Reaction to Evaluate Strain in [1]Metallacyclophanes

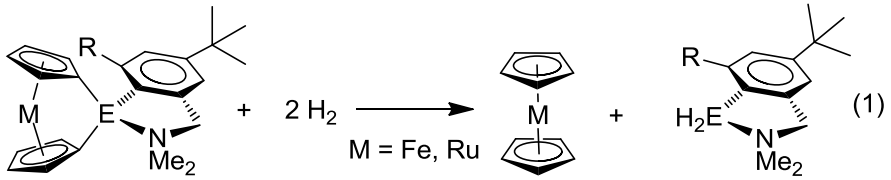

E \ R	*t*Bu	H
Al	**8a**	**8a^{H}**
Ga	**8b**	**8b^{H}**

Table 2-2-6. Thermodynamic Data [kcal/mol] of the Hydrogenolysis Reaction (eq 1 in Scheme 2-2-3).

	M/E/R	ΔE	ΔH ^{298K}	ΔG ^{298K}
2a	Fe/Al/*t*Bu	-29.31	-18.97	-13.47
2a^{H}	Fe/Al/H	-25.83	-12.64	-9.922
2b	Fe/Ga/*t*Bu	-40.41	-28.54	-24.54
2b^{H}	Fe/Ga/H	-37.59	-23.74	-21.13
3a	Ru/Al/*t*Bu	-32.31	-22.45	-15.67
3a^{H}	Ru/Al/H	-28.63	-16.52	-10.56
3b	Ru/Ga/*t*Bu	-44.87	-33.38	-28.02
3b^{H}	Ru/Ga/H	-41.83	-28.35	-24.15

Table 2-2-7. Effect of the *ortho-t*Bu Group on the Hydrogenolysis Reaction (eq. 1 in Scheme 2-2-3)[a]

M/E	ΔΔE	$\Delta\Delta H^{298K}$	$\Delta\Delta G^{298K}$
Fe/Al	-3.48	-6.33	-3.55
Fe/Ga	-2.82	-4.80	-3.41
Ru/Al	-3.68	-5.94	-5.10
Ru/Ga	-3.86	-5.03	-3.86

[a] Values in kcal/mol. Negative values indicate that species with R = *t*Bu result in a larger release of energy.

The calculated increases of enthalpies are between -4.80 and -6.33 kcal/mol (Table 2-2-7) which raises the question of whether these increases are significant. The best experimental measurement of the strain present in a metallocenophane is the enthalpy of the thermal ROP. The text book example of a strained sandwich compound, dimethylsila[1]ferrocenophane, was found to release ca 19 kcal/mol (ΔH^{ROP}).[34] With respect to this value, the average increase of strain caused by the *ortho-t*Bu group of 5.5 kcal/mol is indeed substantial.

As mentioned above, the hydrogenation reaction has the disadvantage that the absolute values of calculated thermodynamic data are meaningless. Therefore, an isodesmic reaction was sought and reaction 2 was investigated (Scheme 2-2-4). Reaction 2 results in bis(metallocenyl) species of type **4** or **5**, which can be envisioned as model compounds for the respective polymers obtained by ROP of strained [1]metallocenophanes. Hence, the calculated heat of eq. 2 should be a very good approximation of the exothermy of a ROP.

Scheme 2-2-4. Isodesmic Reactions to Evaluate Strain in [1]Metallacyclophanes.

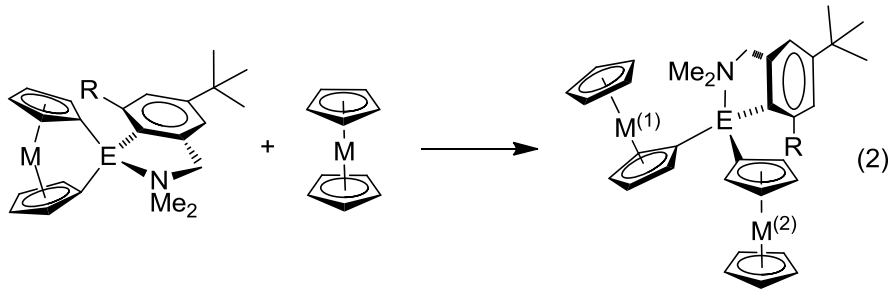

	R = *t*Bu		R = H	
	Fe	Ru	Fe	Ru
Al	**4a**	**5a**	**4a^{H}**	**5a^{H}**
Ga	**4b**	**5b**	**4b^{H}**	**5b^{H}**

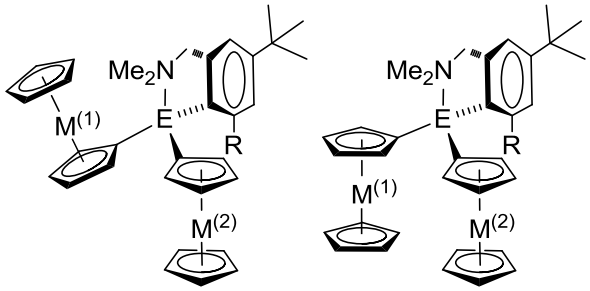

conformer I conformer II

Figure 2-2-7. Conformers I and II of bis(metallocenyl) species **4a**, **4b**, **5a**, **5b**, **4a^{H}**, **4b^{H}**, **5a^{H}**, and **5b^{H}** (see Tables S14 – S29 for Cartesian coordinates of all 16 optimized geometries).

As discussed above, the bis(ferrocenyl) compounds **4a** and **4b** crystallized with different orientations of the ferrocenyl moieties (Figure 2-2-3 and 2-2-4). These two different conformers, I and II, are illustrated in Figure 2-2-7. Two series of geometry calculations have been performed: one with starting geometries like that of **4a** (conformer I) and one with starting geometries like that of **4b** (conformer II). In both series convergence was obtained, but the size and floppiness of the bis(metallocenyl) compounds precluded reliable frequency calculations. Except for the two ferrocenophanes **4a^{H}** and **4b^{H}**, conformer I is energetically preferred over conformer II (ΔE = 1.63 (**4a**), 0.56 (**4b**), 2.80 (**5a**), 3.07 (**5b**), 1.69 (**5a^{H}**), and 0.54 (**5b^{H}**) kcal/mol). For

the aluminum compound **4a^{H}**, both conformers are of equal energy (ΔE = -0.08 kcal/mol), whereas in the case of the gallium analogue **4b^{H}**, conformer II is slightly more stable (ΔE = -0.61 kcal/mol).

Table 2-2-8. Comparison of Thermodynamic Data [kcal/mol] of the Isodesmic Reaction (eq. 2 in Scheme 2-2-4).

	M/E/R	ΔE		M/E/R	ΔE	ΔΔE[a]
2a	Fe/Al/*t*Bu	-16.73	**2a^{H}**	Fe/Al/H	-17.74	1.01
2b	Fe/Ga/*t*Bu	-19.94	**2b^{H}**	Fe/Ga/H	-21.27	1.33
3a	Ru/Al/*t*Bu	-22.13	**3a^{H}**	Ru/Al/H	-22.32	0.19
3b	Ru/Ga/*t*Bu	-26.74	**3b^{H}**	Ru/Ga/H	-26.74	0.00

[a] positive values indicate that species with R = H result in a larger release of energy.

Because the size and floppiness of the bis(metallocenyl) compounds precluded reliable frequency calculations, only ΔE values could be determined for the isodesmic reaction 2 (Table 2-2-8). As indicated in Scheme 2-2-4, only conformer I was taken into account. All eight reactions are exothermic with ΔE values varying for ferrocenophanes between -16.73 and -21.27 kcal/mol and for ruthenocenes between -22.13 and -26.74 kcal/mol. Surprisingly, species with the *ortho*-*t*Bu group seemed to be either slightly less than (**2a** and **2b**) or similarly strained (**3a** and **3b**) as their slimmer counterparts **2a^{H}**, **2b^{H}**, **3a^{H}**, and **3b^{H}** (see ΔΔE values in Table 2-2-8). These unexpected results contrast the results of the hydrogenation reaction (eq. 1) discussed above.

Table 2-2-9. Calculated Structural Parameters [Å and °] of Conformer I of Bis(metallocenyl) Species of Type **4** and **5** (Scheme 2-2-4).[a]

	E-M(1)	E-M(2)	E-N	E-C_{ipso}(1)	E-C_{ipso}(2)	E-$C_{arom.}$	E-C_{ipso}-centr(1)	E-C_{ipso}-centr(2)	τ [b]
4a	3.792 [3.7250(11)]	3.791 [3.7746(10)]	2.109 [2.038(3)]	1.985 [1.966(4)]	1.981 [1.969(3)]	2.022 [2.012(3)]	171.26 [174.55]	171.65 [170.89]	171.65 [170.89]
4a^{H}	3.740	3.542	2.126	1.978	1.972	1.995	173.40	174.08[a]	185.92
4b	3.803	3.775	2.247	1.989	1.986	2.029	170.95	172.52	172.52
4b^{H}	3.757	3.590	2.275	1.979	1.970	1.998	172.71	177.02[a]	182.98
5a	3.892	3.881	2.106	1.988	1.985	2.016	171.99	172.87	172.87
5a^{H}	3.883	3.673	2.120	1.982	1.976	1.993	172.44	176.27[a]	183.73
5b	3.892	3.863	2.235	1.989	1.985	2.024	171.68	173.37	173.37
5b^{H}	3.897	3.700	2.255	1.981	1.974	1.995	171.14	178.39[a]	181.61

[a] Measured values of **4a** are given in square brackets. [b] sandwich unit is tilted toward the element E and not away from the element like in **4a**, **4b**, **5a**, and **5b** as shown in Figure 2-2-9 (see text for discussion). [c] angle τ is defined as in Figure 2-2-9 (see text for discussion).

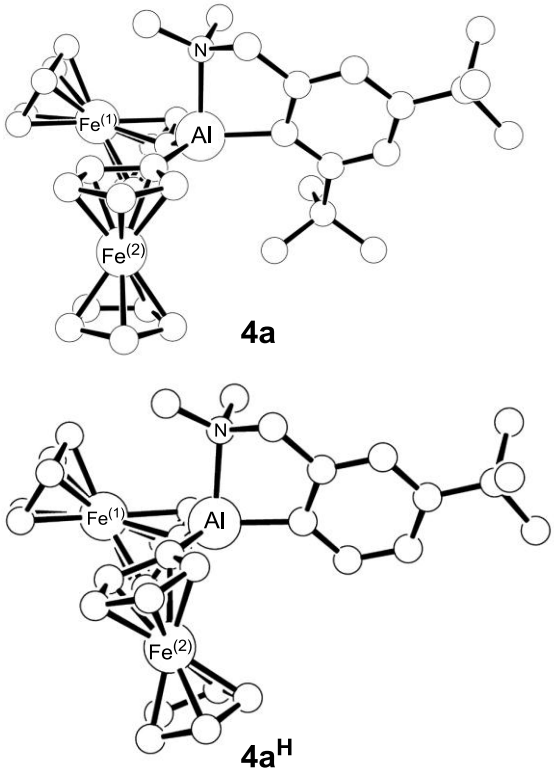

Figure 2-2-8. Optimized geometries of **4b** and **4b^{H}**. Hydrogen atoms are omitted for clarity.

A close inspection of the structures of conformer I of bis(metallocenyl) species **4** and **5** uncovers that the species with the *ortho-t*Bu group are structurally distorted compared to those without the *ortho-t*Bu group. Table 2-2-9 provides an overview of selected structural parameters of products of type **4** and **5**; Figure 2-2-8 shows the calculated geometries of the two aluminum species **4a** and **4a^{H}**. The comparison of measured and calculated structural parameters for **4a** (Table 2-2-9) illustrates the excellent match of theory and experiment. Only the Al-N bond cannot be reproduced well. The most striking effect of the *ortho-t*Bu on the structures of the bis(metallocenyl) compounds **4** and **5** can be best illustrated by a comparison of E-M distances (E = Al or Ga; M = Fe or Ru; Figure 2-2-8 and Table 2-2-9). For example, by changing from species **4a** to species **4a^{H}** one Al-Fe distance is shortened by only 0.052 Å (E---Fe(1)), whereas the other Al-Fe distance decreases strongly by 0.249 Å from 3.791 to 3.542 Å (E---Fe(2); Figure 2-2-8). This structural difference can also be seen by a comparison of angles between E, the *ipso*-C^{Cp} atom, and the centroid of that Cp ring (E-C_{ipso}-centr(1) and E-C_{ipso}-centr(2) in Table 2-2-9). For the *t*Bu-containing species the centroid-M(2)-centroid axis of the metallocenyl unit is tilted away from the element E, whereas for the slimmer species the respective axis is tilted in the opposite direction, toward the element E. This difference in the direction of the tilting is illustrated with angle τ which is defined in Figure 2-2-9 as the centroid(2)-E-C_{ipso} angle. Starting from centroid(2), τ is smaller than 180^{o} for the *ortho-t*Bu containing compounds and larger than 180^{o} for the less bulkier species **2a^{H}**, **2b^{H}**, **3a^{H}**, and **3b^{H}** (Figure 2-2-9). The differences for angle τ for respective pairs range from 8.24^{o} (**5b** / **5b^{H}**) to 14.27^{o} (**4a** / **4a^{H}**) (see Table 2-2-9 and Figure 2-2-9). These

differences show the space requirements of the *ortho*-*t*Bu group: the *t*Bu group points toward the metallocenyl unit M(2) and forces it to be bent away ($\tau < 180^{o}$). Removal of the *t*Bu group let the metallocenyl unit M(2) relax, which goes hand-in-hand with the decrease of E-M(2) distances as discussed above (Figure 2-2-8 and 2-2-9; Table 2-2-9). The degree of bending is less pronounced for ruthenium compounds than for iron species, with differences of respective E----M(2) distances of 0.249 (Al) and 0.185 (Ga) for ferrocene species and 0.208 (Al) and 0.163 (Ga) for ruthenocene compounds (Table 2-2-9). Presumably, the larger spacing between the two Cp rings in ruthenocenes reduces the steric congestion compared to that in ferrocenes.

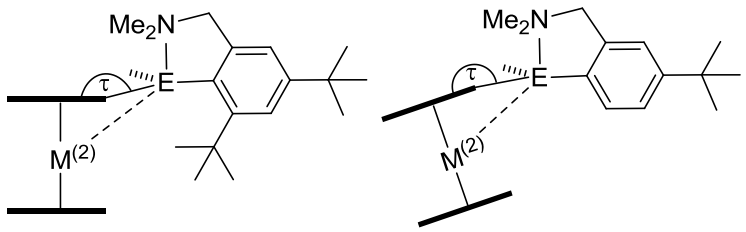

4a, **4b**, **5a**, **5b** **4a^{H}**, **4b^{H}**, **5a^{H}**, **5b^{H}**

Figure 2-2-9. Illustration of the effect of the *ortho*-*t*Bu group on the tilting direction of the metallocenyl moiety of $M^{(2)}$ (angle τ) and the associated change in E---$M^{(2)}$ distances (see Scheme 2-2-4 and Table 2-2-9 and text for discussion).

The structural differences caused by the *ortho*-*t*Bu group in species of type **4** and **5** clearly show that molecules equipped with the *ortho*-*t*Bu group are strained compared to their less bulky counterparts **4a^{H}**, **4b^{H}**, **5a^{H}**, and **5b^{H}**. Hence, the isodesmic reaction 2 (Scheme 2-2-4) does not provide a good measurement of the effect of the *ortho*-*t*Bu group on the strain in metallocenophanes.

SUMMARY AND CONCLUSION

Common salt metathesis reactions between dilithio sandwich species and aluminum or gallium dichlorides (Mamx)ECl_2 (**1a**, **1b**) resulted in the two [1]ferrocenophanes **2a** and **2b**[19] and the two new [1]ruthenocenophanes **3a** and **3b**. In contrast to the large number of known [1]ferrocenophanes, their ruthenium counterparts are rare and **3a** and **3b** being only the fifth and the sixth species of this type known to date. Surprisingly, only the gallium-bridged ruthenocenophane **3b** was isolable, whereas the other three strained sandwich compounds polymerized under the reaction conditions of their formation reactions. However, the isolable **3b** is similarly reactive as the other strained species and polymerizes if left in solution. Polymer $\mathbf{3b_n}$ can be obtained with a significantly increased molecular weight through Pt^0-catalyzed ROP employing Karstedt's catalyst. Overall, polymers $\mathbf{2a_n}$, $\mathbf{2b_n}$,[19] $\mathbf{3a_n}$, and $\mathbf{3b_n}$ were prepared with molecular weights between 8.07 and 106 kDa (Table 2-2-2). DFT calculations have been performed to shed some light on the unexpected high reactivity of these new strained sandwich species. In particular, the role of the *t*Bu group in the *ortho* position at the bulky Mamx ligand was investigated (Scheme 2-2-1) by comparing species equipped with the Mamx ligand (**2a**, **2b**, **3a**, and **3b**) with those where the *ortho*-*t*Bu group had been eliminated ($\mathbf{2a^H}$, $\mathbf{2b^H}$, $\mathbf{3a^H}$, and $\mathbf{3b^H}$). These investigations uncovered that the average increase in strain caused by the *ortho*-*t*Bu group is 5.5 kcal/mol ($\Delta\Delta H^{298K}$; Table 2-2-7). This is a significant increase of strain, if compared to measured enthalpy of polymerization of dimethylsila[1]ferrocenophane (ΔH^{ROP} = 19 kcal/mol).[34] Structurally, the effect of the *ortho*-*t*Bu group can mainly be seen in a tilting of the Mamx ligand toward the side, while tilt angles α do not change significantly (Figure 2-2-6). To the best of our knowledge, such an unusual effect has

never been observed in strained sandwich compounds before. This unusual effect of a *t*Bu group was deduced from a hydrogenolysis of the strained sandwich compounds, which had the disadvantage of being a non-isodesmic reaction (Scheme 2-2-3). The isodesmic reaction of aluminum- or gallium-bridged [1]metallocenophanes with ferrocene or ruthenocene (Scheme 2-2-4) could not be used to extract the strain present in [1]ferrocenophanes (**2a**, **2b**) or [1]ruthenocenophanes (**3a**, **3b**). The *ortho-t*Bu group in the resulting bis(metallocenyl) species **4a**, **4b**, **5a**, and **5b** sterically interacts with one of the metallocenyl units (Figure 2-2-9). The resulting structural distortion was confirmed by comparing the calculated and measured molecular structures of the aluminum compound **4a** (Figure 2-2-3 and Table 2-2-9). Bis(metallocenyl) species of type **4** and **5** can be envisioned as the smallest representative cutout of metallopolymers and the isodesmic reaction 2 (Scheme 2-2-4) provides important information about the ROP of [1]metallocenophanes **2a**, **2b**, **3a**, and **3b**. Even though the *ortho-t*Bu group imposes additional strain on the starting metallocenophanes, this effect cancels out in ROPs because the *ortho-t*Bu group imposes a similar strain on the resulting polymers.

We reported that the proton NMR signal of the *ortho-t*Bu group of polymer $\mathbf{2b_n}$ is split into 10 singlets,[19] revealing a random tacticity of the polymer. It was a surprise that the *ortho-t*Bu group was so sensitive toward the tacticity of the polymer and its signal could be resolved into the different pentads. Our new finding that the *ortho-t*Bu group in bis(metallocenyl) species sterically interacts with the sandwich moieties clearly reveals that similar interactions must be present in respective metallopolymers. We speculate that this steric repulsion causing the *ortho-t*Bu to act as such an unusually sensitive probe of the tacticity.

The initial intention of the DFT calculations was to improve our understanding of the high reactivity of aluminum- and gallium-bridged [1]metallocenophanes. We were puzzled that only one [1]ruthenocenophane (**3b**) was isolable, whereas compounds **2a**, **2b**, and **3a** were not isolable. However, theory did not reveal any unexpected differences between the geometries of [1]ferrocenophanes and [1]ruthenocenophanes. We could not find any clear evidence for the unexpected high reactivity of the prepared strained sandwich compounds and, hence, we can only conclude that kinetics governs the reactivity of these species. Unfortunately, the mechanism of the ROP of the aluminum- and gallium-bridged compounds is still unknown. It seems likely that small amounts of dilithioferrocene in reaction mixtures of the salt metathesis reaction act as an anionic initiator for ROP (Scheme 2-2-1), but several attempts to trap anions by addition of excess of Me_3SiCl did not result in a measurable effect on the polymerization reaction.

EXPERIMENTAL SECTION

General Procedures. All syntheses were carried out using standard Schlenk and glovebox techniques (O_2 level < 0.1 ppm, H_2O level < 2 ppm), unless noted differently. Toluene, Et_2O, thf, hexane, and CH_2Cl_2 were dried using a MBraun Solvent Purification System and stored under nitrogen over 3 Å molecular sieves. Degassed C_6H_6 and MeOH were dried over 3 Å molecular sieves under N_2. All solvents for NMR spectroscopy were degassed prior to use and stored under N_2 over 3 Å molecular sieves. ^1H and ^{13}C NMR spectra were recorded on a Bruker 500 MHz Avance NMR spectrometer at 25 ºC in C_6D_6 and CD_2Cl_2, respectively (^1H at 500.28 MHz; ^{13}C at 125.80 MHz). ^1H chemical shifts were referenced to the residual protons of the deuterated solvents (δ 7.15 for C_6D_6 and

5.32 for CD_2Cl_2); ^{13}C chemical shifts were referenced to the C_6D_6 signal at δ 128.00 and the CD_2Cl_2 signal at δ 54.00. Carbon atoms directly bound to group 13 elements in **1a**, **3b**, and **4a** were not detected in respective ^{13}C NMR spectra. UV-Visible spectra were measured on a Varian Cary 50 UV-Visible spectrophotometer. Mass spectra were measured on a VG 70SE and are reported in the form m/z (rel intens) [M^+] where 'm/z' is the mass observed, 'rel intens' is intensity of the peak relative to the most intense peak and 'M^+' is the molecular ion or fragment; only characteristic mass peaks are reported. For isotopic pattern, only the mass peak of the isotopoloque or isotope with the highest natural abundance is listed. Elemental analyses were performed on a Perkin Elmer 2400 CHN Elemental Analyzer using V_2O_5 to promote complete combustion.

Dynamic light scattering. Dynamic light scattering experiments were performed using a nano series Malvern zetasizer instrument equipped with a 633 nm red laser. Samples were filtered through 0.2 μm syringe PTFE filters before they were analyzed in 1 cm glass cuvettes at concentrations of 4.0 mg/mL, 3.0 mg/mL, 2.0 mg/mL and 1.0 mg/mL in CH_2Cl_2 at 25 °C. The refractive index of the polymers was assumed to be 1.5. For each polymer, three samples were prepared at each concentration. Every sample was measured three times. Few measured D_h values stand out as being either far too small or far too large and were not included in the analysis. For poly(ferrocenyldimethylsilane) (PFS) the absolute molecular weights (M_w) in the range of 10 to 100 kDa and their radii of gyration (R_g) are known in literature.[25] Assuming that the polymers $\mathbf{2a_n}$, $\mathbf{3a_n}$, and $\mathbf{3b_n}$ are random coils in good solvents, measured R_h values were converted into R_g values using the factor $R_g / R_h = 2.05$[24] and the published relation between log(R_g) and log(M_w) for PFS[26] was used to calculate M_w for $\mathbf{2a_n}$, $\mathbf{3a_n}$, and $\mathbf{3b_n}$ (see SI for more details).

Chemicals. $AlCl_3$ (98%), $FeCp_2$ (98%), *n*BuLi (2.8 M in hexanes), platinum(0)-1,3-divinyl-1,1,3,3-tetramethyldisiloxane (Karstedt's catalyst; 2 wt% in xylene), and C_6D_6 (99.6 atom % D) were purchased from Sigma Aldrich; $AlCl_3$ was sublimed prior to use. $GaCl_3$ (Alfa Aesar; 99.999%) and tetramethylethylenediamine (Alfa Aesar; 99%) were purchased from VWR. $RuCl_3 \cdot xH_2O$ (99%) was purchased from Precious Metals Online. CD_2Cl_2 (99.9 atom % D) was purchased from Cambridge Isotope Laboratories. The compounds $(LiC_5H_4)CpFe$,[35] $(LiC_5H_4)_2Fe \cdot 2/3tmeda$,[36] $RuCp_2$,[37] $(LiC_5H_4)_2Ru \cdot tmeda$,[27] 6-$(Me_2NCH_2)$-2,4-*t*$Bu_2C_6H_2Br$ (MamxBr)[19] and $(Mamx)GaCl_2$ (**1b**)[19] were synthesized according to literature procedures.

Synthesis of {2,4-di-*tert*-butyl-6-[(dimethylamino)methyl]phenyl}-dichloroalumane (1a). *n*BuLi (2.8 M in hexanes, 7.90 mL, 22.1 mmol) was added dropwise to a cold (-78 ºC) solution of MamxBr (6.53 g, 20.0 mmol) in Et_2O (30 mL). The reaction mixture was stirred at -78 ºC for 45 min and a cold (0 ºC) solution of $AlCl_3$ (2.66 g, 20.0 mmol) in Et_2O (30 mL) was added dropwise. The resulting mixture was warmed up to r.t. and stirred for 16 h, resulting in a pale yellow solution with a colorless precipitate. After the solid was filtered off, the pale yellow solution was concentrated to approx. 20 mL, and analytically pure product **1a** was obtained as needle-shaped, colorless crystals -22 ºC (5.65 g, 82%). ^{1}H NMR (C_6D_6): δ 1.33 (s, 9H, *t*Bu-4), 1.59 (s, 9H, *t*Bu-2), 1.92 (s, 6H, NMe_2), 3.13 (s, 2H, CH_2), 6.74 (s, 1H, CH-5), 7.58 (s, 1H, CH-3). ^{13}C NMR (C_6D_6): δ 31.60 [C($\underline{C}H_3)_3$-4], 32.84 [C($\underline{C}H_3)_3$-2], 34.87 [$\underline{C}(CH_3)_3$-4], 37.31 [$\underline{C}(CH_3)_3$-2], 45.57 (NMe_2), 65.66 (CH_2), 119.22 (C-5), 122.37 (C-3), 142.75 (C-6), 152.28 (C-4) 160.68 (C-2). MS (70 eV, EI+): *m/z* (rel intens) 343 (14) [M^+], 328 (21) [M^+ - Me], 301 (48) [$C_{14}H_{22}AlCl_2N^+$], 292 (14) [$C_{16}H_{24}AlClN^+$], 247 (88) [$C_{17}H_{29}N^+$], 246 (57)

[$C_{17}H_{28}N^+$], 203 (55) [$C_{15}H_{23}^+$], 190 (24) [$C_{14}H_{22}^+$], 189 (18) [$C_{14}H_{21}^+$], 187 (30) [$C_{14}H_{19}^+$], 148 (61) [$C_{11}H_{16}^+$], 147 (15) [$C_{11}H_{15}^+$], 146 (12) [$C_{11}H_{14}^+$], 133 (100) [$C_{10}H_{13}^+$], 131 (16) [$C_{10}H_{11}^+$], 91 (13) [$C_7H_7^+$], 58 (75) [$C_4H_{10}^+$], 57 (25) [$C_4H_9^+$]. Anal. Calcd for $C_{17}H_{28}Cl_2AlN$ (344.30): C, 59.30; H, 7.84; N, 4.07. Found: C, 59.39; H, 7.55; N, 4.07.

Identification of {2,4-di-*tert*-butyl-6-[(dimethylamino)methyl]phenyl}alumina[1]-ferrocenophane (2a). Product **2a** is an intermediate in the preparation of polymer $\mathbf{2a_n}$ (see below) and can be identified via ^{1}H NMR spectroscopy. All attempts to isolate pure **2a** resulted in the isolation of polymer $\mathbf{2a_n}$. ^{1}H NMR (C_6D_6; taken from an aliquot of the reaction mixture after 30 mins): δ 1.42 (s, 9H, *t*Bu-4), 1.71 (s, 9H, *t*Bu-2), 2.09 (s, 6H, NMe_2), 3.41 (s, 2H, CH_2), 3.85 (pst, 2H, CH-α of Cp), 4.23 (pst, 2H, CH-α of Cp), 4.70 (pst, 2H, CH-β of Cp), 4.72 (pst, 2H, CH-β of Cp), 6.87 (s, 1H, CH-5), 7.64 (s, 1H, CH-3).

Attempted isolations of [1]metallocenophanes 2a, **2b**, and **3a.** As soon as the [1]metallocenophane was detected by ^{1}H NMR spectroscopy (approx. 15-20 min after mixing the solution/slurry of the respective group 13 element dichloride and the dilithiometallocene), quick filtration was performed to remove LiCl. Following are the descriptions of our attempts to isolate [1]metallocenophanes from the respective filtrate: (1) The filtrated was kept at -80 °C for several (7-30) days without any precipitate or crystals forming. The solution was warmed up to r.t. and ^{1}H NMR measurement from the solution revealed the presence of the [1]metallocenophane as well as respective polymeric product. (2) In many attempts, the filtrate was concentrated to variable degrees (approx. 2/3, 1/2, 1/3, 1/4) under reduced pressure. Different attempts were made to

isolate [1]metallocenophane from these concentrated solutions: (a) A concentrated solution was kept at -22 °C or -80 °C for several (3-14) days, resulting in precipitates that were isolated and found to be polymeric product (^{1}H NMR spectroscopy). (b) A concentrated solution was added to well stirred hexane (approx. 3-4 times the volume of the concentrated solution) with the formation of precipitate which was isolated as polymeric material. (c) An open vial containing the concentrated solution was placed in a larger vial filled with hexane and the larger vial was closed to allow diffusion of one solvent into other. The set up was left at r.t. or at -30 °C for several (3-14) days which gave precipitates that were again identified as polymers.

Synthesis of poly(ferrocenylalumane) $2a_n$. A solution of **1a** (0.797 g, 2.31 mmol) in Et_2O (65 mL) was added dropwise to a slurry of $(LiC_5H_4)_2Fe{\cdot}2/3$tmeda (0.639 g, 2.32 mmol) in Et_2O (40 mL) at r.t. The resulting reaction mixture was stirred for 4 h and then left unstirred for 16 h, resulting in a red gelatinous material. All volatiles were removed under vacuum, yielding a red paste. The crude product was extracted with benzene (50 mL) and the benzene solution was concentrated to approx. 10 mL. The concentrated benzene solution was added dropwise to hexane (60 mL) with vigorous stirring, yielding an orange precipitate with a red solution. The precipitate (0.438 g) was filtered off and dried under vacuum. For further purification, the orange solid was dissolved in benzene (15 mL) and added dropwise to MeOH (60 mL) with vigorous stirring, resulting in an orange precipitate and a pale yellow solution. The precipitate was filtered off and dried under vacuum to give **$2a_n$** (0.391 g, 37%). UV/Vis: λ_{max} = 475 nm, ε = 0.29 mL (mg cm)$^{-1}$. ^{1}H NMR (C_6D_6): δ 1.40 (br. s, 9 H, *t*Bu-4), 1.86 (br. s with shoulders at 1.77, 9 H, *t*Bu-2), 1.97 (br. s, 6 H, NMe_2), 3.39 (br. s with shoulder at 3.43, 2 H, CH_2), 4.26, 4.33,

4.42 (3 br. s, 4H, CH-α of Cp), 4.76 (br. s, 4H, CH-β of Cp), 6.90 (br. s, 1 H, CH-3), 7.64 (br. s, 1 H, CH-5). ^{13}C NMR (C_6D_6): δ 31.90 [C($\underline{C}H_3$)$_3$-4], 33.79 [C($\underline{C}H_3$)$_3$-2], 34.71 [$\underline{C}$(CH$_3$)$_3$-4], 37.37 [$\underline{C}$(CH$_3$)$_3$-2], 45.73 (NMe$_2$), 67.21 (CH$_2$), 71.55, 72.87, 76.47, 76.60, 76.78 (C_5H_4), 118.91 (C-5), 121.67 (C-3), 142.41 (C-1), 144.49 (C-6), 149.77 (C-4), 160.75 (C-2).

Identification of {2,4-di-*tert*-butyl-6-[(dimethylamino)methyl]phenyl}alumina[1]-ruthenocenophane (3a). Product **3a** is an intermediate in the preparation of polymer **3a$_n$** (see below) and can be identified via ^{1}H NMR spectroscopy. All attempts to isolate pure **3a** resulted in the isolation of polymer **3a$_n$**. ^{1}H NMR (C_6D_6; taken from an aliquot of the reaction mixture after 30 mins): δ 1.40 (s, 9H, *t*Bu-4), 1.60 (s, 9H, *t*Bu-2), 1.97 (s, 6H, NMe$_2$), 3.42 (s, 2H, CH$_2$), 4.02 (pst, 2H, CH-α), 4.65 (pst, 2H, CH-α), 5.30 (pst, 2H, CH-β), 5.34 (pst, 2H, CH-β), 6.86 (s, 1H, CH-5), 7.61 (s, 1H, CH-3).

Synthesis of poly(ruthenocenylalumane) 3a$_n$. A solution of **1a** (0.575 g, 1.67 mmol) in toluene (20 mL) was added dropwise to a slurry of (LiC_5H_4)$_2$Ru·tmeda (0.600 g, 1.67 mmol) in toluene (15 mL) at r.t. The resulting reaction mixture was stirred for 4 h and then left unstirred for 16 h, resulting in a yellow solution with a colorless precipitate. The solid was filtered off and the yellow solution was concentrated to approx. 8 mL. The concentrated toluene solution was added dropwise to hexane (30 mL) with vigorous stirring, yielding in a pale yellow precipitate with a yellow solution. The precipitate (0.416 g) was filtered off and dried under vacuum. For further purification, the pale yellow solid was dissolved in 1:1 mixture of toluene/Et$_2$O (10 mL) and added dropwise to MeOH (30 mL) with vigorous stirring, resulting in an off-white precipitate and a pale yellow solution. The precipitate was filtered off and dried under vacuum to give **3a^n**

(0.361 g, 43%). UV/Vis: λ_{max} = 341nm, ε = 0.29 mL (mg cm)$^{-1}$. ^{1}H NMR (CD_2Cl_2): δ 1.32 (br. s, 18 H, *t*Bu-2 and *t*Bu-4), 2.37 (br. s with shoulders at 2.36, 2.38 and 2.41, 6 H, NMe_2), 3.66 (br. s with shoulder at 3.68, 2 H, CH_2), 4.35, 4.37, 4.41, 4.43, 4.48, 4.49, 4.59, 4.60 (3 br. s with shoulders, 8H, CH-α and CH-β of Cp), 6.92 (br. s with shoulder at 6.93, 1 H, CH-5), 7.38 (br. s, 1 H, CH-3). ^{13}C NMR (CD_2Cl_2): δ 31.81,[C($\underline{C}H_3)_3$-4], 33.54 [C($\underline{C}H_3)_3$-2], 34.99 [$\underline{C}(CH_3)_3$-4], 37.26 [$\underline{C}(CH_3)_3$-2], 46.36 (NMe_2), 67.85 (CH_2), 70.47, 70.59, 70.95, 71.79, 72.06, 73.35, 77.58, 77.78, 77.96, 79.52 (C_5H_4), 119.79 (C-5), 122.01 (C-3), 142.25, 142.52, 142.91 (C-1), 143.34 (C-6), 149.40 (C-4), 158.65 (C-2).

Synthesis of {2,4-di-*tert*-butyl-6-[(dimethylamino)methyl]phenyl}galla[1]-ruthenocenophane (3b). A solution of **1b** (1.51 g, 3.90 mmol) in toluene (35 mL) was added dropwise to a slurry of $(LiC_5H_4)_2Ru{\cdot}$tmeda (1.42 g, 3.95 mmol) in toluene (20 mL). The reaction mixture was stirred at r.t. for 2 h, resulting in a yellow solution with a colorless precipitate. After the solid was filtered off, the yellow solution was concentrated to approx. 15 mL, yielding a cloudy mixture which was added dropwise to hexane (35 mL) with vigorous stirring, yielding a yellow solution with a pale yellow precipitate. The reaction flask was kept at -30 °C for 16 h to complete the precipitation. The precipitate was filtered off and dried under vacuum to give product **3b** (1.06 g, 50%). Attempt to crystallize **3b**: A saturated solution of **3b** was prepared in different organic solvents (Et_2O, thf, toluene, and benzene). Following are the attempts to crystallize **3b** from the saturated solutions: (1) The solutions were kept for several (7-14) days at low temperature (-22 °C for Et_2O, thf and toluene solutions and 6 °C for benzene solution). (2) An open vial containing the saturated solution was placed in a larger vial filled with hexane and the larger vial was closed to allow diffusion of one solvent into other. The set

up was left at r.t. or at lower temperatures (6 or -30 °C) for several (7-14) days. Crystals were never obtained; however, these attempts gave precipitates that were identified as polymers by ^{1}H NMR spectroscopy.

^{1}H NMR (C_6D_6): δ 1.39 (s, 9H, *t*Bu-4), 1.55 (s, 9H, *t*Bu-2), 1.95 (s, 6H, NMe_2), 3.30 (s, 2H, CH_2), 4.05 (pst, 2H, CH-α of Cp), 4.59 (pst, 2H, CH-α of Cp), 5.34 (pst, 2H, CH-β of Cp), 5.36 (pst, 2H, CH-β of Cp), 6.89 (s, 1H, CH-5), 7.62 (s, 1H, CH-3). ^{13}C NMR (C_6D_6): δ 31.67 [C($\underline{C}H_3)_3$-4], 32.92 [C($\underline{C}H_3)_3$-2], 34.81 [$\underline{C}(CH_3)_3$-4], 36.49 [$\underline{C}(CH_3)_3$-2], 46.55 (NMe_2), 67.65 (CH_2), 76.32, 78.41, 78.81, 79.34 (C_5H_4), 119.46 (C-5), 121.26 (C-3), 142.16 (C-6), 150.46 (C-4) 158.38 (C-2). Anal. Calcd for $C_{27}H_{36}GaNRu$ (545.37): C, 59.46; H, 6.65; N, 2.57. Found: C, 58.59; H, 6.95; N, 2.45.

Synthesis of poly(ruthenocenylgallane) $3b_n$ through transition-metal-catalyzed ROP. Platinum(0)-1,3-divinyl-1,1,3,3-tetramethyldisiloxane (2 wt% Pt in xylene, 0.557 mL, 0.025 mmol) was added dropwise to a solution of **3b** (0.275 g, 0.504 mmol) in toluene (5 mL) at r.t. The reaction mixture was stirred at r.t. for 16 h, yielding a brown solution which was concentrated to ca. 2 mL. The concentrated solution was added to hexane (30 mL) with vigorous stirring, yielding a brown solution with pale yellow precipitate which was filtered off and dried under vacuum. For further purification, the pale yellow solid was dissolved in toluene (3 mL) and added dropwise to MeOH (30 mL) with vigorous stirring, resulting in an off-white precipitate and a pale yellow solution. The precipitate was filtered off and dried under vacuum to give **$3b_n$** (0.141 g, 56%). UV/Vis: λ_{max} = 347 nm, ε = 0.32 mL (mg cm)$^{-1}$. ^{1}H NMR (C_6D_6): δ 1.37 (br. s, 9 H, *t*Bu-4), 1.58 (br. s with shoulders at 1.56,1.63, 1.65 and 1.67, 9 H, *t*Bu-2), 2.10 (br. s with shoulders at 2.05, 2.08, 2.18 and 2.19, 6 H, NMe_2), 3.42 (br. s with shoulder at 3.30, 2 H,

CH_2), 4.65 (br. s with shoulders at 4.56, 4.60 and 4.73, 4H, CH-α of Cp), 4.93 (br. s with shoulders at 4.90 and 5.01, 4H, CH-β of Cp), 6.98 (br. s with shoulder at 6.95, 1 H, CH-5), 7.62 (br. s, 1 H, CH-3). ^{13}C NMR (C_6D_6): δ 31.44 [C($\underline{C}H_3)_3$-4], 33.28 [C($\underline{C}H_3)_3$-2], 34.38 [$\underline{C}(CH_3)_3$-4], 36.89 [$\underline{C}(CH_3)_3$-2], 45.23, 45.27 (NMe_2), 67.09 (CH_2), 70.06, 70.28, 70.56, 70.65, 71.61, 71.85, 71.95, 72.80, 73.15, 77.47, 78.86, 79.11 (C_5H_4), 118.98 (C-5), 121.70 (C-3), 142.50 (C-1), 143.30 (C-6), 149.16 (C-4), 158.93 (C-2).

Synthesis of poly(ruthenocenylgallane) $3b_n$ through uncontrolled ROP. A solution of **1b** (3.75 g, 9.69 mmol) in toluene (55 mL) was added dropwise to a slurry of $(LiC_5H_4)_2Ru{\cdot}$tmeda (3.51 g, 9.77 mmol) in toluene (30 mL) at r.t. The resulting reaction mixture was stirred for 16 h, resulting in a yellow solution with white precipitate. The solid was filtered off and the yellow solution was concentrated to ca. 20 mL. The concentrated solution was added dropwise to hexane (100 mL) with vigorous stirring, yielding a pale yellow precipitate with a yellow solution. The precipitate (0.438 g) was filtered off and dried under vacuum. For further purification, the pale yellow solid was dissolved in toluene (25 mL) and added dropwise to MeOH (100 mL) with vigorous stirring, resulting in an off-white precipitate and a pale yellow solution. The precipitate was filtered off and dried under vacuum to give product **$3b_n$** (2.53 g, 52%).

Synthesis of {2,4-di-*tert*-butyl-6-[(dimethylamino)methyl]phenyl}bisferrocenylalumane (4a). A solution of **1a** (0.690 g, 2.00 mmol) in Et_2O (40 mL) was added dropwise to a slurry of $(LiC_5H_4)CpFe$ (0.967 g, 5.04 mmol) in Et_2O (30 mL) at r.t. The reaction mixture was stirred for 16 h, resulting in a red solution with an orange precipitate. After the solid was filtered off, all volatiles were removed under vacuum, yielding a red paste as the crude product which was washed with hexanes (3 x 50 mL),

resulting in an orange solid. The solid was dissolved in Et_2O (30 mL), the Et_2O solution was concentrated to approx. to 10 mL and added to hexane (50 mL) with vigorous stirring. The resulting orange precipitate was filtered off and dried under vacuum, yielding **4a** as an orange powder (0.657 g, 51%). ^{1}H NMR (C_6D_6): δ 1.38 (s, 9H, *t*Bu-4), 1.71 (s, 9H, *t*Bu-2), 1.83 (s, 6H, NMe_2), 3.28 (s, 2H, CH_2), 4.11, 4.27, 4.35, 4.41 (pst, 8H, C_5H_4), 4.23 (s, 10H, C_5H_5), 6.89 (s, 1H, CH-5), 7.66 (s, 1H, CH-3). ^{13}C NMR (C_6D_6): δ 31.69 [C($\underline{C}H_3)_3$-4], 33.66 [C($\underline{C}H_3)_3$-2], 34.72 [$\underline{C}(CH_3)_3$-4], 37.29 [$\underline{C}(CH_3)_3$-2], 45.55 (NMe_2), 67.07 (CH_2), 68.34 (C_5H_5), 70.83, 70.90, 76.52, 76.91 (C_5H_4), 118.86 (C-5), 121.62 (C-3), 144.29 (C-6), 150.15 (C-4) 160.78 (C-2). MS (70 eV, EI+): m/z (rel intens) 643 (100) [M^+], 458 (12) [M^+ - $C_{10}H_9Fe$], 186 (17) [$C_{10}H_{10}Fe^+$]. Anal. Calcd for $C_{37}H_{46}AlFe_2N$ (643.44): C, 69.07; H, 7.21; N, 2.18. Found: C, 69.84; H, 7.05; N, 2.01.

Synthesis of {2,4-di-*tert*-butyl-6-[(dimethylamino)methyl]phenyl}bisferrocenyl-gallane (4b). A solution of **1b** (1.06 g, 2.02 mmol) in Et_2O (30 mL) was added dropwise to a slurry of (LiC_5H_4)CpFe (0.967 g, 5.53 mmol) in Et_2O (30 mL) at r.t. The reaction mixture was stirred for 16 h, resulting in a red solution with an orange precipitate. After the solid was filtered off, all volatiles were removed under vacuum, yielding a red paste as the crude product which was dissolved in thf (10 mL). Pure product **4b** (0.685 g, 49%) was obtained in form of red-orange crystals from this thf solution at -22 ºC. ^{1}H NMR (C_6D_6): δ 1.37 (s, 9H, *t*Bu-4), 1.71 (s, 9H, *t*Bu-2), 1.73 (s, 6H, NMe_2), 3.20 (s, 2H, CH_2), 4.06, 4.30, 4.31, 4.39 (pst, 8H, C_5H_4), 4.27 (s, 10H, C_5H_5), 6.93 (s, 1H, CH-5), 7.69 (s, 1H, CH-3). ^{13}C NMR (C_6D_6): δ 31.70 [C($\underline{C}H_3)_3$-4], 33.49 [C($\underline{C}H_3)_3$-2], 34.68 [$\underline{C}(CH_3)_3$-4], 37.04 [$\underline{C}(CH_3)_3$-2], 45.39 (NMe_2), 66.95 (CH_2), 68.45 (C_5H_5), 70.27, 70.33, 75.40, 75.78, 76.76 (C_5H_4), 119.45 (C-5), 122.00 (C-3), 142.42 (C-1), 143.65 (C-6), 149.67 (C-

4) 159.02 (C-2). MS (70 eV, EI+): m/z (rel intens) 685 (14) [M^+], 535 (100) [$C_{30}H_{36}FeGaN^+$], 186 (96) [$C_{10}H_{10}Fe^+$]. Anal. Calcd for $C_{37}H_{46}GaFe_2N$ (686.18): C, 64.76; H, 6.76; N, 2.04. Found: C, 64.48; H, 6.76; N, 1.98.

Crystal Structure Determination. Single crystals of **1b, 4a**·½C_6H_6 and **4b** were coated with Paratone-N oil, mounted using a Micromount™ (*MiTeGen* - Microtechnologies for Structural Genomics), and frozen in the cold stream of the Oxford cryojet attached to the diffractometer. Crystal data were collected at -100°C on a Bruker-AXS Proteum R Smart 6000 3-Circle diffractometer using monochromated Cu K_α radiation (λ = 1.54184 Å). An initial orientation matrix and cell was determined from ω-scans, and the X-ray data were measured using φ and ω scans.[38] Data reduction was performed using *SAINT* included in the *APEX2* software package.[39] A multiscan absorption correction was applied (*SADABS*).[39]

Structures were solved by direct methods (*SIR-2004*)[40] and refined by full-matrix least-squares methods on F^2 with *SHELX-97*.[39] Unless otherwise stated, the non-hydrogen atoms were refined anisotropically; hydrogen atoms were included at geometrically idealized positions but not refined. The isotropic thermal parameters of the hydrogen atoms were fixed at 1.2 times that of the preceding carbon atom. For the structure **4b** diffraction data from two crystals with similar size were combined in order to obtain enough data for solving the structure. It appeared that the crystals decomposed over time upon exposure to X-ray radiation.

Computational Details. Theoretical calculations were carried out using the Amsterdam Density Functional package (version ADF2010.02).[32] The Slater-type orbital (STO) basis sets were of triple-ζ quality augmented with a two polarization functions

(ADF basis TZ2P). Core electrons were frozen (C, N 1s; Al, Si, Fe 2p; Ru 3d) in our model of the electronic configuration for each atom. Relativistic effects were included by virtue of the zero order regular approximation (ZORA).[41] The local density approximation (LDA) by Vosko, Wilk and Nusair (VWN)[42] was used together with the exchange correlation corrections of Becke[43] and Perdew[44] (BP86).[43,44] Tight optimization conditions were used for the monomer series of compounds **2**, **3**, **6**, **7**, **8**, MCp_2 and H_2. Frequency calculations were used to confirm minima and provide thermodynamic information. Some compounds showed small imaginary frequencies corresponding to barrierless rotation of cyclopentadienyl rings or *t*Bu groups. The large size and number of conformers of the bis(metallocenyl) species of type **4** and **5** necessitated TZP basis sets and more relaxed optimization conditions for these molecules. The resulting optimized structures were then subjected to single point calculations with TZ2P basis sets to obtain consistent values for the reaction 2 (Scheme 2-2-4).

ASSOCIATED CONTENT

Supporting Information

Crystallographic data for **1b**, **4a**, and **4b** in CIF file format; DLS data for $\mathbf{2a_n}$, $\mathbf{3a_n}$, and $\mathbf{3b_n}$ (Tables S1 – S5; Figures S1 – S4); NMR spectra of **1a**, **2a**, $\mathbf{2a_n}$, **3a**, $\mathbf{3a_n}$, **3b**, $\mathbf{3b_n}$, **4a**, and **4b** (Figures S5 – S22); Cartesian coordinates for all calculated species (Tables S6 – S39). This material is available free of charge via the internet at http://pubs.acs.org.

Notes

The authors declare no competing financial interest.

ACKNOWLEDGMENTS

We thank the Natural Sciences and Engineering Research Council of Canada (NSERC Discovery Grant, JM) for support. We thank the Canada Foundation for Innovation (CFI) and the government of Saskatchewan for funding of the X-ray and NMR facilities in the Saskatchewan Structural Sciences Centre (SSSC). We thank Prof. Ildiko Badea (University of Saskatchewan, College of Pharmacy and Nutrition) for making the DLS instrument available for our studies.

REFERENCES

(1) Foucher, D. A.; Tang, B.-Z.; Manners, I. *J. Am. Chem. Soc.* **1992**, *114*, 6246-6248.

(2) (a) Herbert, D. E.; Mayer, U. F. J.; Manners, I. *Angew. Chem., Int. Ed.* **2007**, *46*, 5060-5081; (b) Tamm, M. *Chem. Commun.* **2008**, 3089-3100; (c) Braunschweig, H.; Kupfer, T. *Acc. Chem. Res.* **2010**, *43*, 455-465.

(3) Bellas, V.; Rehahn, M. *Angew. Chem., Int. Ed.* **2007**, *46*, 5082-5104.

(4) Selected Reviews: (a) Manners, I. *Science* **2001**, *294*, 1664-1666; (b) Manners, I. *Synthetic Metal-Containing Polymers*; Wiley-VCH: Weinheim, 2004; (c) Marin, V.; Holder, E.; Hoogenboom, R.; Schubert, U. S. *Chem. Soc. Rev.* **2007**, *36*, 618-635; (d) Whittell, G. R.; Manners, I. *Adv. Mater.* **2007**, *19*, 3439-3468; (e) Williams, K. A.; Boydston, A. J.; Bielawski, C. W. *Chem. Soc. Rev.* **2007**, *36*, 729-744; (f) Eloi, J. C.; Chabanne, L.; Whittell, G. R.; Manners, I. *Mater. Today* **2008**, *11*, 28-36; (g) Hempenius, M. A.; Cirmi, C.; Lo Savio, F.; Song, J.; Vancso, G. J. *Macromol. Rapid Comm.* **2010**, *31*, 772-783; (h) Wong, W. Y.; Harvey, P. D. *Macromol. Rapid Comm.* **2010**, *31*, 671-713; (i) Krüger, R. A.; Baumgartner, T. *J. Chem. Soc., Dalton Trans.* **2010**, *39*, 5759-

5767; (j) Manners, I. *J. Organomet. Chem.* **2011**, *696*, 1146-1149; (k) Whittell, G. R.; Hager, M. D.; Schubert, U. S.; Manners, I. *Nat. Mater.* **2011**, *10*, 176-188.

(5) (a) Rulkens, R.; Ni, Y. Z.; Manners, I. *J. Am. Chem. Soc.* **1994**, *116*, 12121-12122; (b) Ni, Y. Z.; Rulkens, R.; Manners, I. *J. Am. Chem. Soc.* **1996**, *118*, 4102-4114.

(6) (a) Wang, X. S.; Guerin, G.; Wang, H.; Wang, Y. S.; Manners, I.; Winnik, M. A. *Science* **2007**, *317*, 644-647; (b) Gädt, T.; Ieong, N. S.; Cambridge, G.; Winnik, M. A.; Manners, I. *Nat. Mater.* **2009**, *8*, 144-150; (c) Gilroy, J. B.; Gädt, T.; Whittell, G. R.; Chabanne, L.; Mitchels, J. M.; Richardson, R. M.; Winnik, M. A.; Manners, I. *Nature Chemistry* **2010**, *2*, 566-570; (d) Presa Soto, A.; Gilroy, J. B.; Winnik, M. A.; Manners, I. *Angew. Chem., Int. Ed.* **2010**, *49*, 8220-8223; (e) Gädt, T.; Schacher, F. H.; McGrath, N.; Winnik, M. A.; Manners, I. *Macromolecules* **2011**, *44*, 3777-3786; (f) Gilroy, J. B.; Patra, S. K.; Mitchels, J. M.; Winnik, M. A.; Manners, I. *Angew. Chem., Int. Ed.* **2011**, *50*, 5851-5855; (g) He, F.; Gädt, T.; Manners, I.; Winnik, M. A. *J. Am. Chem. Soc.* **2011**, *133*, 9095-9103; (h) Patra, S. K.; Ahmed, R.; Whittell, G. R.; Lunn, D. J.; Dunphy, E. L.; Winnik, M. A.; Manners, I. *J. Am. Chem. Soc.* **2011**, *133*, 8842–8845.

(7) (a) Cheng, F.; Jäkle, F. *Polym. Chem.* **2011**, *2*, 2122-2132; (b) Jäkle, F. *Chem. Rev.* **2010**, *110*, 3985-4022.

(8) (a) Braunschweig, H.; Dirk, R.; Müller, M.; Nguyen, P.; Resendes, R.; Gates, D. P.; Manners, I. *Angew. Chem., Int. Ed.* **1997**, *36*, 2338-2340; (b) Berenbaum, A.; Braunschweig, H.; Dirk, R.; Englert, U.; Green, J. C.; Jäkle, F.; Lough, A. J.; Manners, I. *J. Am. Chem. Soc.* **2000**, *122*, 5765-5774.

(9) (a) Heilmann, J. B.; Qin, Y.; Jäkle, F.; Lerner, H. W.; Wagner, M. *Inorg. Chim. Acta* **2006**, *359*, 4802-4806; (b) Heilmann, J. B.; Scheibitz, M.; Qin, Y.; Sundararaman, A.;

Jäkle, F.; Kretz, T.; Bolte, M.; Lerner, H. W.; Holthausen, M. C.; Wagner, M. *Angew. Chem., Int. Ed.* **2006**, *45*, 920-925; (c) Scheibitz, M.; Li, H. Y.; Schnorr, J.; Perucha, A. S.; Bolte, M.; Lerner, H. W.; Jäkle, F.; Wagner, M. *J. Am. Chem. Soc.* **2009**, *131*, 16319-16329.

(10) Lund, C. L.; Schachner, J. A.; Quail, J. W.; Müller, J. *Organometallics* **2006**, *25*, 5817-5823.

(11) Lund, C. L.; Schachner, J. A.; Quail, J. W.; Müller, J. *J. Am. Chem. Soc.* **2007**, *129*, 9313-9320.

(12) Schachner, J. A.; Tockner, S.; Lund, C. L.; Quail, J. W.; Rehahn, M.; Müller, J. *Organometallics* **2007**, *26*, 4658-4662.

(13) (a) Braunschweig, H.; Burschka, C.; Clentsmith, G. K. B.; Kupfer, T.; Radacki, K. *Inorg. Chem.* **2005**, *44*, 4906-4908; (b) Schachner, J. A.; Orlowski, G. A.; Quail, J. W.; Kraatz, H.-B.; Müller, J. *Inorg. Chem.* **2006**, *45*, 454-459; (c) Lund, C. L.; Schachner, J. A.; Burgess, I. J.; Quail, J. W.; Schatte, G.; Müller, J. *Inorg. Chem.* **2008**, *47*, 5992–6000.

(14) Schachner, J. A.; Lund, C. L.; Burgess, I. J.; Quail, J. W.; Schatte, G.; Müller, J. *Organometallics* **2008**, *27*, 4703-4710.

(15) Mamx stands for methylaminomethyl-*m*-xylyl; see ref. 16.

(16) Yoshifuji, M.; Kamijo, K.; Toyota, K. *Tetrahedron Lett.* **1994**, *35*, 3971-3974.

(17) (a) Yoshifuji, M.; Sangu, S.; Kamijo, K.; Toyota, K. *Chem. Ber.* **1996**, *129*, 1049-1055; (b) Kamijo, K.; Otoguro, A.; Toyota, K.; Yoshifuji, M. *Bull. Chem. Soc. Jpn.* **1999**, *72*, 1335-1342; (c) Kamijo, K.; Toyota, K.; Yoshifuji, M. *Chem. Lett.* **1999**, 567-568; (d) Kawasaki, S.; Fujita, T.; Toyota, K.; Yoshifuji, M. *Bull. Chem. Soc. Jpn.* **2005**, *78*, 1082-1090.

(18) (a) Schmidt, H.; Keitemeyer, S.; Neumann, B.; Stammler, H.-G.; Schoeller, W. W.; Jutzi, P. *Organometallics* **1998**, *17*, 2149-2151; (b) Jutzi, P.; Keitemeyer, S.; Neumann, B.; Stammler, H.-G. *Organometallics* **1999**, *18*, 4778-4784.

(19) Bagh, B.; Gilroy, J. B.; Staubitz, A.; Müller, J. *J. Am. Chem. Soc.* **2010**, *132*, 1794-1795.

(20) *ortho* refers to the position of the *t*Bu group with respect to gallium.

(21) Isom, H. S.; Cowley, A. H.; Decken, A.; Sissingh, F.; Corbelin, S.; Lagow, R. J. *Organometallics* **1995**, *14*, 2400-2406.

(22) Schumann, H.; Wassermann, B. C.; Schutte, S.; Heymer, B.; Nickel, S.; Seuss, T. D.; Wernik, S.; Demtschuk, J.; Girgsdies, F.; Weimann, R. *Z. Anorg. Allg. Chem.* **2000**, *626*, 2081-2095.

(23) Sometimes the difference between peaks for β-protons in ^{1}H NMR spectra is not measurable; see for example **2b**.

(24) Burchard, W. In *Branched Polymers II* 1999; Vol. 143, p 113-194.

(25) Massey, J. A.; Kulbaba, K.; Winnik, M. A.; Manners, I. *J. Polym. Sci., Part B: Polym. Phys.* **2000**, *38*, 3032-3041.

(26) See donor bond lengths in [1.1]ferrocenophanes[13a,13b] (Al-N = 2.0748(14); Ga-N = 2.178(3) Å; bridging moieties Ar'E), [1.1]chromarenophanes[13c] (Al-N = 2.089(4); Ga-N = 2.192(2) Å; bridging units (*p*-*t*BuAr')E), or [1.1]molybdarenophanes[13c] (Al-N = 2.096(3); Ga-N = 2.207(3) Å; bridging units (*p*-*t*BuAr')E).

(27) Vogel, U.; Lough, A. J.; Manners, I. *Angew. Chem., Int. Ed.* **2004**, *43*, 3321-3325.

(28) Broussier, R.; Darold, A.; Gautheron, B.; Dromzee, Y.; Jeannin, Y. *Inorg. Chem.* **1990**, *29*, 1817-1822.

(29) Jäkle, F.; Rulkens, R.; Zech, G.; Foucher, D. A.; Lough, A. J.; Manners, I. *Chem.-Eur. J.* **1998**, *4*, 2117-2128.

(30) Green, J. C. *Chem. Soc. Rev.* **1998**, *27*, 263-271.

(31) Schachner, J. A.; Quail, J. W.; Müller, J. *Acta Crystallogr.* **2008**, *E64*, m517.

(32) (a) Baerends, E. J.; Ellis, D. E.; Ros, P. *Chem. Phys.* **1973**, *2*, 41-51; (b) Versluis, L.; Ziegler, T. *J. Chem. Phys.* **1988**, *88*, 322-328; (c) Velde, G. T.; Baerends, E. J. *J. Comput. Phys.* **1992**, *99*, 84-98; (d) Fonseca Guerra, C. F.; Snijders, J. G.; te Velde, G.; Baerends, E. J. *Theor. Chem. Acc.* **1998**, *99*, 391-403.

(33) (a) Matas, I.; Whittell, G. R.; Partridge, B. M.; Holland, J. P.; Haddow, M. F.; Green, J. C.; Manners, I. *J. Am. Chem. Soc.* **2010**, *132*, 13279-13289; (b) Masson, G.; Herbert, D. E.; Whittell, G. R.; Holland, J. P.; Lough, A. J.; Green, J. C.; Manners, I. *Angew. Chem., Int. Ed.* **2009**, *48*, 4961-4964; (c) Barlow, S.; Drewitt, M. J.; Dijkstra, T.; Green, J. C.; O'Hare, D.; Whittingham, C.; Wynn, H. H.; Gates, D. P.; Manners, I.; Nelson, J. M.; Pudelski, J. K. *Organometallics* **1998**, *17*, 2113-2120.

(34) ca 80 kJ/mol were measured by DSC in the range of 120-170 °C; see ref 1.

(35) Bildstein, B.; Malaun, M.; Kopacka, H.; Wurst, K.; Mitterbock, M.; Ongania, K.-H.; Opromolla, G.; Zanello, P. *Organometallics* **1999**, *18*, 4325-4336.

(36) Butler, I. R.; Cullen, W. R.; Ni, J.; Rettig, S. J. *Organometallics* **1985**, *4*, 2196-2201.

(37) Liu, D.; Xie, F.; Zhang, W. *J. Org. Chem.* **2007**, *72*, 6992-6997.

(38) Bruker; Bruker AXS Inc.: Madison, Wisconsin, 2009.

(39) Sheldrick, G. M. *Acta Crystallogr., Sec A* **2008**, *64*, 112-122.

(40) Burla, M. C.; Caliandro, R.; Camalli, M.; Carrozzini, B.; Cascarano, G. L.; De Caro, L.; Giacovazzo, C.; Polidori, G.; Spagna, R. *J. Appl. Crystallogr.* **2005**, *38*, 381-388.

(41) (a) Snijders, J. G.; Baerends, E. J.; Ros, P. *Mol. Phys.* **1979**, *38*, 1909-1929; (b) Ziegler, T.; Tschinke, V.; Baerends, E. J.; Snijders, J. G.; Ravenek, W. *J. Phys. Chem.* **1989**, *93*, 3050-3056; (c) van Lenthe, E.; Baerends, E. J.; Snijders, J. G. *J. Chem. Phys.* **1993**, *99*, 4597-4610.

(42) Vosko, S. H.; Wilk, L.; Nusair, M. *Can. J. Phys.* **1980**, *58*, 1200-1211.

(43) Becke, A. D. *Phys. Rev. A* **1988**, *38*, 3098-3100.

(44) Perdew, J. P. *Phys. Rev. B* **1986**, *33*, 8822-8824.

2.2.5 Selective Materials from Supporting Information of Contribution 2

DLS Analyses. Dynamic light scattering experiments were performed using a nano series Malvern zetasizer instrument equipped with a 633 nm red laser. Samples were filtered through 0.2 μm syringe PTFE filters (Millex) before they were analyzed in 1 cm glass cuvettes at concentrations of 4.0, 3.0, 2.0 and 1.0 mg/mL in CH_2Cl_2 at 25 °C. The refractive index of the polymers was assumed to be 1.5. For each polymer, three samples were prepared at each concentration. Every sample was measured three times. Few measured R_h values stand out as being either far too small or far too large and were not included in the analysis (see dashes in tables).

Table 2-2-S1. DLS Data of Poly(ferrocenylalumane) **2a$_n$**.

concentration	4.0 mg/mL			3.0 mg/mL			2.0 mg/mL			1.0 mg/mL		
	1	2	3	1	2	3	1	2	3	1	2	3
R_h (nm)	5.465	5.360	5.375	5.555	5.270	5.330	5.565	5.330	5.105	5.855	5.370	5.340
	5.330	5.160	5.065	5.400	5.265	5.265	5.705	5.275	5.490	5.500	5.360	5.320
	5.300	5.465	5.375	5.400	5.540	5.255	5.415	5.650	5.440	5.470	5.350	5.040
average (nm)	5.32			5.37			5.44			5.40		
SD (nm)	0.13			0.11			0.19			0.22		
overall average (nm)	5.38											
overall SD (nm)	0.05											

Table 2-2-S2. DLS Data of Poly(ruthenocenylalumane) **3a$_n$**.

concentration	4.0 mg/mL			3.0 mg/mL			2.0 mg/mL			1.0 mg/mL		
	1	2	3	1	2	3	1	2	3	1	2	3
R_h (nm)	1.413	1.331	1.083	1.336	1.083	1.319	1.492	1.460	1.018	1.543	---	1.246
	1.341	1.318	1.035	2.210	1.035	1.025	1.487	1.120	1.999	1.318	1.218	1.367
	1.418	1.372	1.166	1.504	1.166	1.042	1.522	1.407	1.321	1.104	1.216	1.482
average (nm)	1.28			1.30			1.43			1.31		
SD (nm)	0.14			0.38			0.28			0.15		
overall average (nm)	1.33											
overall SD (nm)	0.11											

Table 2-2-S3. DLS Data of Poly(ruthenocenylgallane) **3b$_n$** through Uncontrolled ROP.

concentration	4.0 mg/mL			3.0 mg/mL			2.0 mg/mL			1.0 mg/mL		
	1	2	3	1	2	3	1	2	3	1	2	3
R_h (nm)	1.982	2.232	1.689	1.621	1.442	1.252	1.315	1.514	1.769	1.417	1.402	1.489
	1.080	1.354	1.466	1.622	1.889	1.371	1.419	1.163	1.32	1.888	1.184	1.469
	1.724	1.908	1.942	1.391	1.520	1.173	---	1.383	1.203	---	1.390	1.336
average (nm)	1.71			1.48			1.39			1.45		
SD (nm)	0.36			0.22			0.19			0.20		
overall average (nm)	1.50											
overall SD (nm)	0.14											

Table 2-2-S4. DLS Data of Poly(ruthenocenylgallane) **3b$_n$** through Transition-Metal-Catalyzed ROP.

concentration	4.0 mg/mL			3.0 mg/mL			2.0 mg/mL			1.0 mg/mL		
	1	2	3	1	2	3	1	2	3	1	2	3
R_h (nm)	2.524	2.131	2.186	2.964	---	2.514	3.332	2.056	3.095	3.207	3.040	2.441
	2.479	2.479	2.266	2.216	2.490	2.269	2.451	2.714	2.640	3.273	2.636	2.725
	2.884	2.384	2.206	2.620	3.092	---	2.897	2.971	2.973	3.100	2.106	2.540
average (nm)	2.39			2.60			2.79			2.79		
SD (nm)	0.22			0.24			0.25			0.47		
overall average (nm)	2.64											
overall SD (nm)	0.19											

Table 2-2-S5. Calculations of M_w for Polymers **2a$_n$**, **3a$_n$**, and **3b$_n$**.

polymer	R_h (nm)	SD_h (nm)	R_g (nm)	SD_g (nm)	R_g+SD_g (nm)	log(R_g)	log(R_g+SD_g)	log(M_{w1})	log(R_g)	M_{w1} (Da)	log(M_{w2})	log(R_g+SD_g)	M_{w2} (Da)	SD (Da)
PFS40 [a]			2.98					3.98408	0.47	9640				
PFS100 [a]			5.26					4.43616	0.72	27300				

PFS150 [a]			6.88					4.63144	0.84	42800				
PFS200 [a]			10.1					4.96614	1.00	92500				
$2a_n$	5.38	0.05	11.0	0.10	11.1	1.04	1.05	5.02581	1.04	106123	5.03303	1.05	107902	1779
$2b_n$ [b]	2.99	0.36	6.13	0.74	6.87	0.79	0.84	4.55632	0.79	36001	4.64741	0.84	44402	8401
$3a_n$	1.33	0.11	2.72	0.23	2.95	0.43	0.47	3.90689	0.43	8070	3.97177	0.47	9371	1301
$3b_n$ [c]	1.50	0.14	3.08	0.29	3.37	0.49	0.53	4.00623	0.49	10144	4.07815	0.53	11972	1828
$3b_n$ [d]	2.64	0.19	5.41	0.39	5.80	0.73	0.76	4.45646	0.73	28606	4.51209	0.76	32515	3909

Contribution 3: Effect of Bulkiness of Ligands on the Synthesis of Inda[1]Ferrocenophanes and Poly(ferrocenylindane)s.

2.3.1 Description

The following chapter is a verbatim copy of a manuscript that is under preparation[1] and describes the synthesis of the first two examples of inda[1]ferrocenophanes (**7_1** and **9_1**). The first indium-bridged [1]FCP **7_1** was synthesized by the salt metathesis reaction of dilithioferrocene and the indium dichloride **6**, equipped with the bulky Mamx ligand. The salt metathesis reaction yielded an indium-bridged [1]FCP (**7_1**), an indium-bridged [1.1]FCP (**7_2**) and oligomers (**7_n**). (Mamx)$InCl_2$ **6** was also reacted with 1,1′-dilithio-2,2′-di(*iso*-propyl)ferrocene resulting in a new In[1]FCP, **9_1** selectively. However, the new In[1]FCP **9_1** could not be isolated as it ring-open polymerized in solution to yield the first poly(ferrocenylindane).

2.3.2 Author Contribution

One of the starting materials, 1,1′-dibromo-2,2′-di(*iso*-propyl)ferrocene, was synthesized by Saeid Sadeh. All the other reactions, including isolation and purification of products, were performed by me.

2.3.3 Relation of Contribution 3 with Research Objectives

As discussed in Contribution 1 and 2, the Mamx ligand provided a suitable steric demand to access strained [1]metallocenophanes. As there is no example of an indium-bridged [1]FCP known in literature, the synthesis of a inda[1]ferrocenophane would

[1] Bagh, B.; Sadeh, S.; Müller, J. manuscript under preparation, **2012**.

enrich the metallocenophane chemistry. Therefore, I first synthesized the indium dichloride **6**, equipped with the Mamx ligand, to be used in the salt-metathesis reactions. As the reaction of **6** with dilithioferrocene produced an indium-bridged [1]FCP (**7_1**), a [1.1]FCP (**7_2**) and a poly(ferrocene) (**7_n**), there was a need to find a way to yield inda[1]ferrocenophane selectively. In fact, inda[1]ferrocenophane **9_1** was formed selectively in the reaction of **6** with the dilithioferrocene **8**, equipped with two bulky *i*Pr groups adjacent to lithium. Species **9_1** yielded poly(ferrocenylindane) (**9_n**) by spontaneous ring-opening in solution. Even though Contribution 3 satisfied the goal of synthesizing indium-bridged [1]FCPs (**7_1**, **9_1**) and poly(ferrocene)s (**7_n**, **9_n**), more research is needed to performed ROP of inda[1]ferrocenophane under controlled reaction conditions.

2.3.4 Manuscript of Contribution 3

Effect of Bulkiness of Ligands on the Synthesis of Inda[1]ferrocenophanes and Poly(ferrocenylindane)s

Bidraha Bagh, Saeid Sadeh, Jens Müller*

Department of Chemistry, University of Saskatchewan, 110 Science Place, Saskatoon, Saskatchewan S7N 5C9, Canada

ABSTRACT: Indium-bridged [1]FCP (**7_1**), [1.1]FCP (**7_2**) and poly(ferrocene) (**7_n**) have been isolated in moderate yields (**7_1**: 19, **7_2**: 23, **7_n**: 32%) from a reaction mixture of (Mamx)$InCl_2$ **6** and dilithioferrocene. **7_n** was found to be a low-molecular-weight polymer (DLS: M_w = 4.8 ± 0.08 kDa). The reaction of **6** with dilithioferrocene **8**, equipped with two *i*Pr groups *ortho* to lithium atoms, yielded selectively inda[1]ferrocenophane **9_1** as an reactive intermediate. Species **9_1** could not be isolated as

it spontaneously ring-open polymerized to give poly(ferrocenylindane) $\mathbf{9_n}$. $\mathbf{9_n}$ was found to be a high-molecular-weight polymer by DLS (M_w = 27.9 ± 0.4 kDa).

Since Manners et al. reported the first ring-opening polymerization (ROP) of silicon-bridged [1]ferrocenophanes (**1**: M = Fe; ER_x = $SiMe_2$, $SiPh_2$; Figure 2-3-1) in 1992,[1] [1]ferrocenophanes have been developed as precursors for the synthesis of metallopolymers (**2**; Figure 2-3-1). The related [1.1]ferrocenophanes (**3**: M = Fe; Figure 2-3-1) are considered as a cyclic dimer of respective [1]ferrocenophanes and exist as both *syn* and *anti* isomers. In addition to the large number of [1.1]ferrocenophanes with a variety of different bridging elements, unsymmetrically bridged [1.1]ferrocenophanes (**4**: $ER_x \neq E'R'_y$; Figure 2-3-1) with two different bridging elements in the same molecule have been reported recently.[2] In contrast to [1]ferrocenophanes, [1.1]ferrocenophanes are devoid of ring-strain and cannot be polymerized.[3]

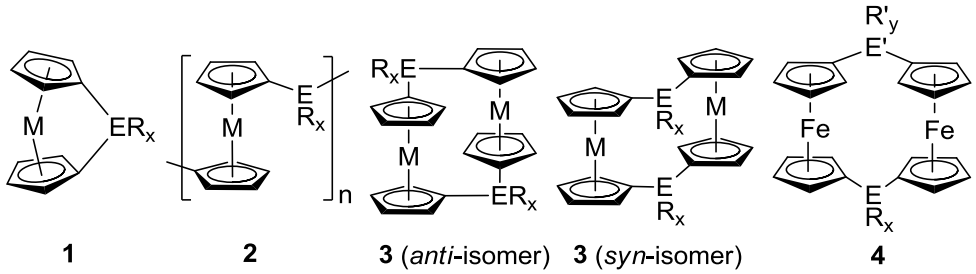

Figure 2-3-1. [1]Metallocenophane (**1**), poly(metallocene) (**2**) and [1.1]metallocenophanes (**3**, **4**).

Poly(ferrocenylsilane)s are an important class of metallopolymers and found applications in material science such as tunable component of photonic crystals displays,[4] precursors to ceramic materials,[5] capsules with redox-tunable permeability.[6] Living polymerization sila[1]ferrocenophanes gives access to block copolymers.[7] Block

copolymers in block-selective solvent allows the formation of nanoparticles with different morphologies,[8] which promises applications in future nanotechnology.

In spite of the tremendous development during the last two decades, the availability of metallopolymers is still very limited. In particular, poly(metallocene)s with group 13 elements in bridging possitions are very rare, as compared to the large number of respective group-14-containing polymers. The ROP of bora[1]ferrocenophanes (**1**: M = Fe; E = B; Figure 2-3-1) yielded mostly insoluble oligomers.[9] More recently, low-molecular-weight poly(ferrocenylborane) ($M_w \approx 7.5$ kDa by GPC) was synthesized by an unusual polycondensation of 1,1'-bis(boryl)ferrocenes.[10] Our group synthesized several [1]metallocenophanes (**1**; Figure 2-3-1) with aluminum and gallium as bridging elements.[11] Very recently, we reported the synthesis of high-molecular-weight poly(ferrocenylalumane) (M_w = 106 kDa by DLS) and poly(ferrocenylgallane) (M_w = 48 kDa by GPC), which were obtained by an uncontrolled ROP of respective strained sandwich compounds.[12] Relatively low-molecular-weight poly(ruthenocene) ($M_w \approx$ 8-29 kDa by DLS) with aluminum- and gallium-bridges were reported as well.[12b] To best of our knowledge, there are no examples of indium-bridged [1]metallocene and poly(metallocene).

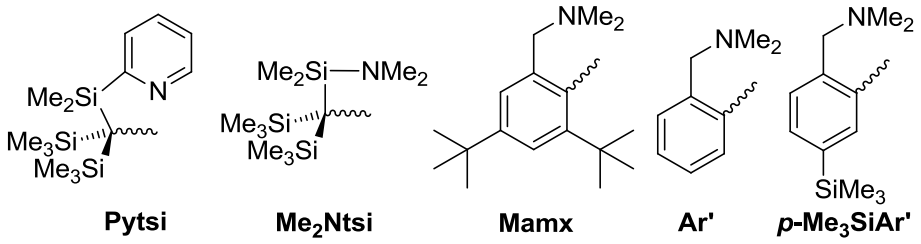

Figure 2-3-2. Different ligands utilized for the synthesis of heavier group 13 element-bridged [1]- and [1.1]metallocenophanes.

Bulky, intramolecularly coordinating ligands **Pytsi** and **Me_2Ntsi** (Figure 2-3-2) were utilized for the synthesis of aluminum- and gallium-bridged [1]ferrocenophanes[11a,11b,11c] and [1]ruthenocenophanes[11d] (**1**: M = Ru; Figure 2-3-1) before. However, the attempted ROP of those [1]metallocenophanes either failed or resulted in sluggish polymerization.[11d] On the other hand, employing the bulky **Mamx** ligand (Figure 2-3-2) gave aluminum- and gallium-bridged [1]metallocenophanes, which were highly reactive.[12] Even though the galla[1]ruthenocenophane was isolated in pure form, other analogous strained sandwich compounds polymerized under the conditions of their formation reactions.[12b] In contrast to the bulky ligands, slim ligands **Ar′** and ***p*-$SiMe_3$Ar′** (Figure 2-3-2) gave [1.1]ferrocenophanes with aluminum and gallium as bridging elements.[13] Obviously, the type of ligand attached to aluminum or gallium plays a key role for the outcome of the salt-metathesis reaction, as well as for the reactivity of strained sandwich compounds. However, the influence of ligands was not realized in case of indium as both bulky **Me_2Ntsi**[14] and slim **Ar′**[13b] ligands gave inda[1.1]ferrocenophanes. Within this report, we present the influence of **Mamx** ligand on the synthesis of indium-bridged ferrocenophanes. The first examples of inda[1]ferrocenophanes and respective poly(ferrocenylindane)s, as well as an indium-bridged [1.1]ferrocenophane, are described.

As illustrated in Scheme 2-3-1, lithiation of (Mamx)Br (**5**) followed by the reaction with $InCl_3$ resulted in (Mamx)$InCl_2$ (**6**) as an analytical pure solid in moderate yield of 44%. As shown by NMR spectroscopy, **6** is C_s symmetric on NMR time scale. The signal for the *ipso*-C was not observed in the ^{13}C NMR spectrum of **6**.

Scheme 2-3-1. Synthesis of (Mamx)$InCl_2$.

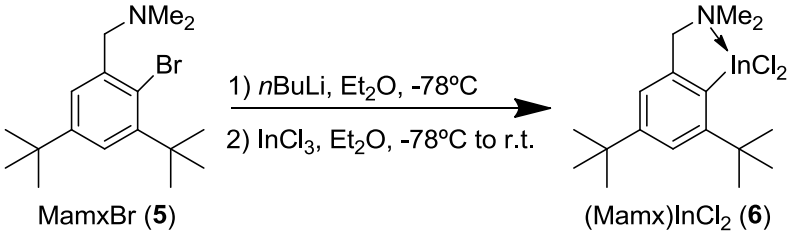

The indium dichloride **6** was reacted with dilithioferrocene, resulting in a mixture of products as shown by ^{1}H NMR spectroscopy (Scheme 2-3-2). From the mixture, indium-bridged [1]ferrocenophane (**7$_1$**), [1.1]ferrocenophane (**7$_2$**), and poly(ferrocene) (**7$_n$**) were isolated by utilizing different solubilities of those species in different solvents (see Supporting Information for details).

Scheme 2-3-2. Reaction of **6** with dilithioferrocene.

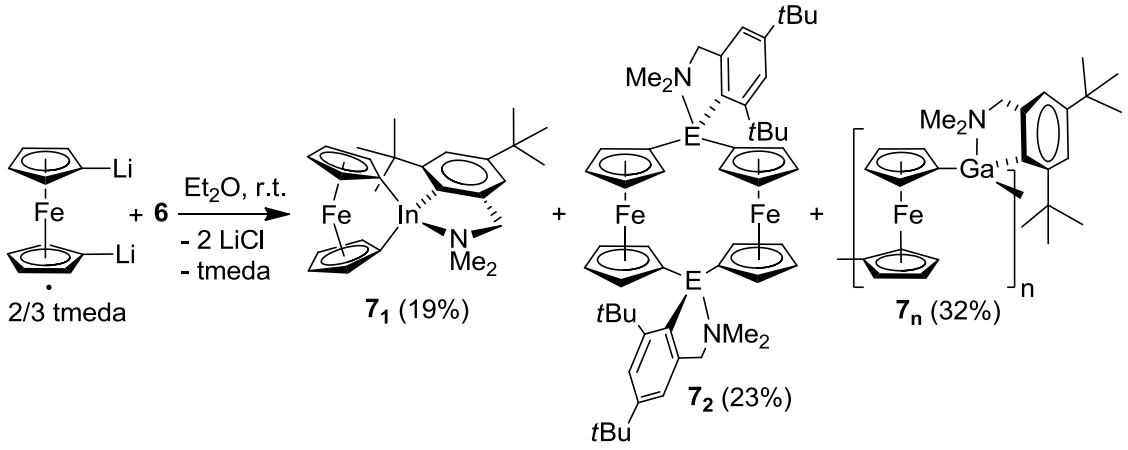

Species **7$_1$** and **7$_2$** were characterized by ^{1}H and ^{13}C NMR spectroscopy, mass spectrometry and elemental analysis. In the mass spectra, both **7$_1$** and **7$_2$** displayed respective molecular ion peaks. Species **7$_1$** is C_s symmetric on NMR time scale. Beside other characteristic signals, **7$_1$** displayed four signals in the typical Cp range at δ 4.22 (2 α-H), 4.39 (2 α-H), 4.41 (2 β-H) and 4.46 (2 β-H). This pattern of two β-protons (separation: 0.05 ppm) close together and two α-protons (separation: 0.17 ppm) further

apart is typical for previously characterized heavier group 13 element-bridged [1]ferrocenophane with C_s symmetry [bridging moiety Ga(Pytsi): δ 4.08 (2 α-H), 4.45 (2 α-H), 4.61 (2 β-H) and 4.65 (2 β-H);[11b] Ga(Mamx): δ 4.01 (2 α-H), 4.56 (2 α-H) and 4.69 (4 β-H);[12a] Al(Pytsi): δ 3.91 (2 α-H), 4.31 (2 α-H), 4.64 (2 β-H) and 4.68 (2 β-H);[11a] Al(Mamx): δ 3.85 (2 α-H), 4.51 (2 α-H), 4.70 (2 β-H) and 4.72 (2 β-H)[12b]]. Consistent with the ^{1}H NMR spectrum, the ^{13}C NMR spectrum of **7_1** showed characteristic signals. However, signals for *ipso*-C atoms of Cp and benzene rings were not observed. Unfortunately, all attempted crystallizations of **7_1** were unsuccessful (see Supporting Information).

The NMR spectroscopy showed signal patters for compound **7_2** that could be interpreted as being caused by C_{2h} symmetric species in solution. For example the ^{1}H NMR spectrum of **7_2** displayed three signals in the characteristic range of Cp protons [δ 3.91 (2 H), 4.26 (4 H), 4.40 (2 H)]. As reported before, Cp protons of heavier group 13 elements-bridged [1.1]ferrocenophanes displayed a distinctive signature: the two signals of the β-protons exhibit a small splitting and appear in the middle between the two signals of the α-protons, which show a significantly larger splitting [bridging moiety In(Me_2Ntsi) (*anti* isomer): 4.36 (2 α-H), 4.43 (2 β-H), 4.45 (2 β-H) and 4.57 (2 α-H);[14] In(Ar′): δ 4.04 (2 α-H), 4.45 (2 β-H), 4.53 (2 β-H) and 4.97 (2 α-H);[13b] Ga(Ar′): δ 3.99 (2 α-H), 4.37 (2 β-H), 4.48 (2 β-H) and 5.07 (2 α-H);[13b] Al(Ar′): δ 3.97 (2 α-H), 4.42 (2 β-H), 4.52 (2 β-H) and 5.17 (2 α-H)[13a]]. Species **7_2** exhibited a very similar pattern; however, two β-protons overlapped. Similar to the species **7_1**, resonances of *ipso*-C atoms were not observed in ^{13}C NMR spectrum of **7_2**.

All reported aluminum-, gallium- and indium-bridged [1.1]ferrocenophanes exist as *anti* isomers in solid state.[13,14] Similarly, species **7_2** is expected to be an *anti* isomer. As revealed by ^{1}H NMR spectroscopy, indium-bridged [1.1]ferrocenophane with **Me_2Ntsi** ligand displayed fluxional behavior in solution.[14] Two signals were observed for all 16 Cp protons at r.t. As shown in Scheme 2-3-3, the fast, degenerate *anti*-to-*anti* isomerization (4 Cp signals are expected for each *anti* isomer with C_{2h} symmetric) results in a structure that appears on time average to be flat (D_{2h} symmetry), which should show two Cp signals. In contrast, a dynamic behavior of inda[1.1]ferrocenophane with **Ar′** ligands was not revealed by one dymensional NMR spectroscopy.[14] However, EXSY experiments revealed the exchange of Cp protons, a clear indication of *anti*-to-*anti*

Scheme 2-3-3. *Anti*-to-*anti* isomerization in indium-bridged [1.1]ferrocenophane (H' and H" are swapping positions).

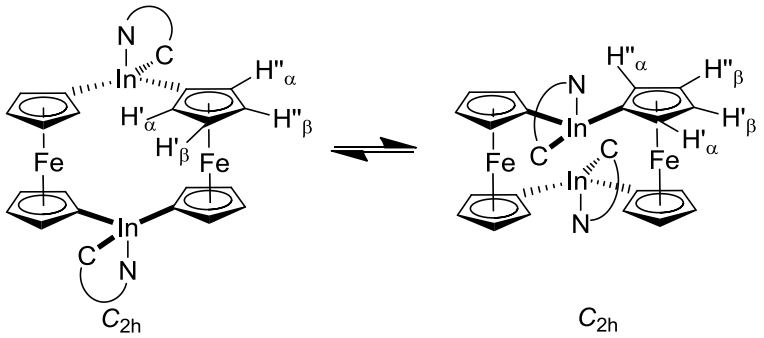

isomerization. Species **7_2** did not display any fluxional behavior in the temperature range of 50 to −50 °C; NOESY and EXSY experiments did not show any indication of exchange of Cp protons. The *anti*-to-*anti* isomerization in inda[1.1]ferrocenophane must involve the breakage of In–N coordinate bonds, rotation of ligands around In–C^{ipso} bonds, and reformation of In–N bonds on the opposite side. It is quite feasible that the bulkiness

of the **Mamx** ligands, in particular the presence of the *ortho-t*Bu group, restricts the rotation around In–C^{ipso} bonds and, hence, prevents an *anti*-to-*anti* isomerization in $\mathbf{7_2}$.

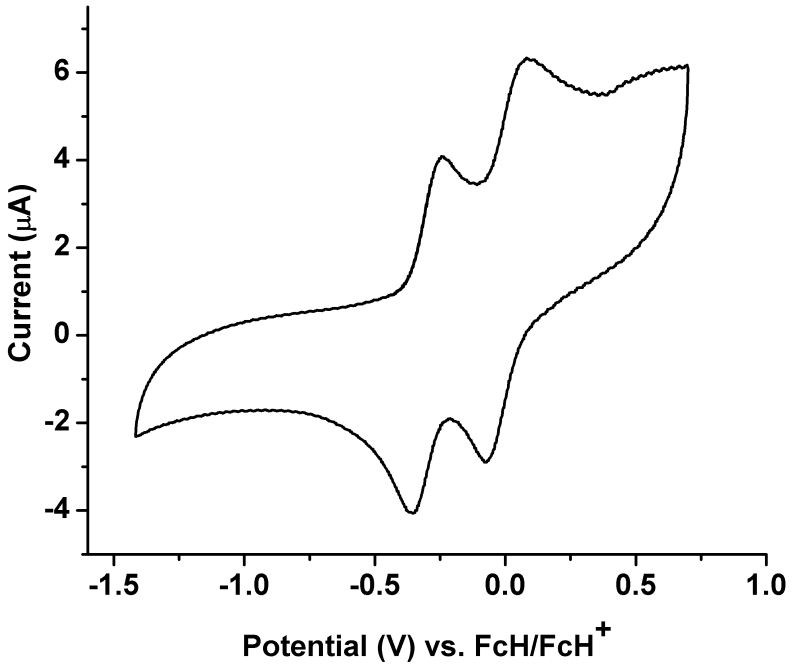

Figure 2-3-3. Cyclic voltammogram of $\mathbf{7_2}$ (1 mM) in CH_2Cl_2 (0.1 M [nBu$_4$N][PF_6]; scan rate = 50 mV/s; $E_1°' = -0.300$ and $E_2°' = 0.005$ V).

Two reversible redox waves were observed in the cyclic voltammogram of $\mathbf{7_2}$ (Figure 2-3-3). The sequential oxidations of two iron centers in $\mathbf{7_2}$ is typical for [1.1]ferrocenophanes. In the cyclic voltammogram of previously reported (Ar′)In-bridged [1.1]ferrocenophane, two major redox waves and two poorly resolved minor redox waves was observed.[13b] The presence of two set of redox waves was possibly due to the presence of two isomers. In fact, the presence of two isomers was confirmed by low temperature (−80 °C) ^{1}H NMR spectroscopy. It was speculated that two major redox waves belonged to the *anti* conformer, the geometry found in the crystal lattice. The stepwise oxidation of two redox centers in each isomer of (Ar′)In-bridged [1.1]ferrocenophane was similar to that found in $\mathbf{7_2}$. In contrast, (Me_2Ntsi)In-bridged

[1.1]ferrocenophane displayed complicated redox behavior, which is likely due to degradation of the [1.1]ferrocenophane under the conditions of electrochemical measurement.[14] Species **7₂** displayed a moderate separation between two redox waves ($\Delta E^{\circ\prime} = E_2^{\circ\prime} - E_1^{\circ\prime}$ = 295 mV), which is similar to other heavier group-13-bridged [1.1]ferrocenophane [bridging moiety Ga(Ar′): 300 mV;[13b] In(Ar′): 270 (separation between two major redox waves);[13b] Al(*p*-SiMe$_3$Ar′): 332 mV;[13c] Ga(*p*-SiMe$_3$Ar′): 301mV[13c]].

Broad multiple peaks were observed in the ^{1}H NMR spectrum of **7$_n$**, which suggested that **7$_n$** consists of a mixture of low-molecular-weight polymers. The oligomeric nature of **7$_n$** was established by dynamic-light scattering (DLS) analysis.‡[15] The average molecular weight (M_w) was found to be 4.8 ± 0.08 kDa (ca. 10 repeating units). Presumably, **7$_n$** formed as a polycondensation product of the reaction between **6** and dilithioferrocene.

As discussed above, the utilization of the bulky **Mamx** ligand gave the first inda[1]ferrocenophane **7₁**, but it formed in a mixture with the indium-bridged [1.1]ferrocenophane **7₂** and the poly(ferrocene) **7$_n$**. We intended to obtain an indium-bridged [1]ferrocenophane selectively by using steric congestion as a directional force. Structural evidence for aluminum- and gallium-bridged [1]ferrocenophanes, poly(ferrocene)s, and [1.1]ferrocenophanes suggests that the space available for the bridging moiety decreases in that order; the bulkiest ligands can be best accommodated in the strained [1]ferrocenophanes. Recently, we developed a synthesis of the bulky dithioferrocene species **8** [1,1'-dilithio-2,2'-di(isopropyl)ferrocene] and used it for the preparation of aluminum- and gallium-bridged [1]ferrocenophanes (Scheme 2-3-4).[16] The reactions shown in Scheme 2-3-4 proceed nearly quantitatively, with no indication of the

formation of [1.1]ferrocenophanes; in contrast, dilithioferrocene resulted in [1.1]ferrocenophanes.[13a,13b] This demonstrates that two *i*Pr groups in proximity to the bridging moiety effectively blocks the formation of unwanted [1.1]ferrocenophanes (Scheme 2-3-4). Consequently, we explored the reactivity of **6** with the dilithioferrocene **8**.

Scheme 2-3-4. Reaction of Ar′ECl_2 with dilithioferrocene 8.

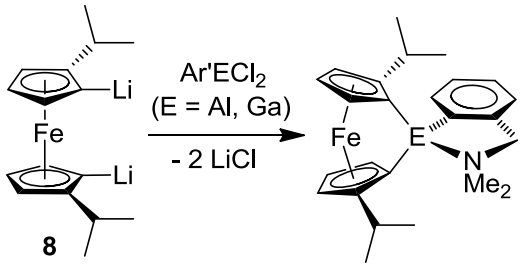

As illustrated in Scheme 2-3-5, dilithioferrocene **8**, which was prepared *in situ* from 1,1'-dibromo-2,2'-di(iso-propyl)ferrocene, reacted readily with the dichloride **6** to give the targeted inda[1]ferrocenophane $\mathbf{9_1}$. Reaction control by proton NMR spectroscopy revealed that species $\mathbf{9_1}$ formed selectively. The ^{1}H NMR spectrum of $\mathbf{9_1}$ showed all characteristic signals, which suggested a C_1 symmetric molecule in solution. As for example, species $\mathbf{9_1}$ displayed six signals in the range of 3.68-4.74 ppm for all six Cp protons, four doublets for the four CH_3 moieties of the two *i*Pr groups, two singlets for the NMe_2 group and two doublets for CH_2 protons (see Supporting Information). However, all attempts to isolate $\mathbf{9_1}$ failed (see Supporting Information) and a poly(ferrocenylindane), $\mathbf{9_n}$ was isolated as the final product. The spontaneous ROP of $\mathbf{9_1}$ under the condition of its formation reaction resulted in the polymer $\mathbf{9_n}$, which was found to be a high-molecular-weight polymer by DLS analysis (M_w = 27.9 ± 0.4 kDa, repeating unit ≈ 48).

Scheme 2-3-5. Synthesis of intermediate $\mathbf{9_1}$ and polymer $\mathbf{9_n}$.

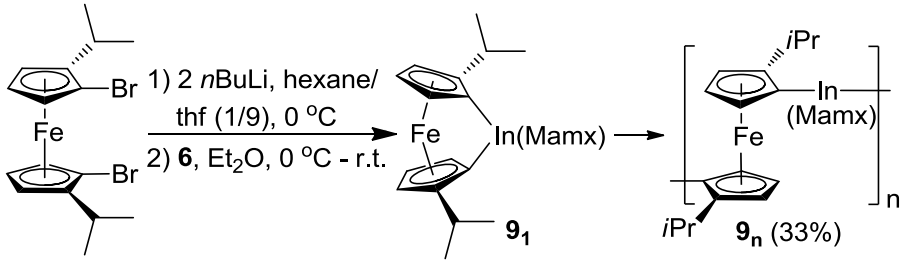

In summary, the bulky, intramolecularly coordinating ligand **Mamx** was successfully utilized for the synthesis of the first indium-bridged [1]ferrocenophanes. Our results demonstrate that the steric bulk around the bridging element is of crucial importance for the outcome of the salt-metathesis reaction of dilithio sandwich compounds and element dihalides. The formation of indium-bridged [1]ferrocenophane ($\mathbf{7_1}$), [1.1]ferrocenophane ($\mathbf{7_2}$), and oligomers ($\mathbf{7_n}$) during the reaction of indium dichloride **6** and dilithioferrocenophane indicates that the steric bulk around indium should be increased in order to obtain inda[1]ferrocenophane selectively. The formation of inda[1]ferrocenophane $\mathbf{9_1}$ as a single intermediate in the reaction of **6** and **8** suggests that the steric requirements for the selective formation of [1]ferrocenophane can be satisfied by introducing bulky groups into the ferrocene moiety. However, it is a surprise that an inda[1]ferrocenophane with an expected low tilt angle still is highly reactive. This hints at the unusual properties of the Mamx ligand. This primary report also describes the isolation of the high-molecular-weight poly(ferrocenylindane) $\mathbf{9_n}$, which is the newest addition in the class of poly(ferrocene)s. The future work will focus on the isolation of the monomer $\mathbf{9_1}$ such that a well-defined poly(ferrocenyl)indane can be synthesized by living ROP methodologies.

ASSOCIATED CONTENT

Supporting Information. Experimental section for **6**, $\mathbf{7_1}$, $\mathbf{7_2}$, $\mathbf{7_n}$ and $\mathbf{9_n}$; identification of $\mathbf{9_1}$; NMR spectra of **6**, $\mathbf{7_1}$, $\mathbf{7_2}$, $\mathbf{7_n}$, $\mathbf{9_1}$ and $\mathbf{9_n}$ (Figure S3-S14); DLS data of $\mathbf{7_n}$ and $\mathbf{9_n}$ (Table 2-3-S1to 2-3-S2; Figure S1-S2).

Notes

‡ Assuming that polymers $\mathbf{7_n}$ and $\mathbf{9_n}$ can be described as random coils, with thf being a good solvent, hydrodynamic radii R_h ($\mathbf{7_n}$: 1.003 ± 0.086 nm; $\mathbf{9_n}$: 2.340 ± 0.262 nm) gave radii of gyration (R_g) ($\mathbf{7_n}$: 2.508 ± 0.176 nm; $\mathbf{9_n}$: 4.797 ± 0.537 nm) by using the equation R_g/R_h = 2.05 (see Ref 15a). Thereafter, R_g was translated into an M_w with respect to poly(ferrocenyldimethylsilane)s (see Ref 15b).

ACKNOWLEDGMENTS

We thank the Natural Sciences and Engineering Research Council of Canada (NSERC Discovery Grant, J.M.) for support. We thank Prof. Ildiko Badea (University of Saskatchewan, College of Pharmacy and Nutrition) and Prof. Ian Burgess (University of Saskatchewan, Department of Chemistry) for making instruments available for our studies.

REFERENCES

(1) Foucher, D. A.; Tang, B.-Z.; Manners, I. *J. Am. Chem. Soc.* **1992**, *114*, 6246-6248.

(2) (a) Bagh, B.; Breit, N. C.; Dey, S.; Gilroy, J. B.; Schatte, G.; Harms, K.; Müller, J. *Chem.–Eur. J.* **2012**, *18*, 9722-9733. (b) Bagh, B.; Breit, N. C.; Gilroy, J. B.; Schatte, G.; Müller, J. Chem. Commun. **2012**, *48*, 7823-7825.

(3) Zechel, D. A.; Foucher, D. A.; Pudelski, J. K.; Yap, G. P. A.; Rheingold, A. L.; Manners, I. *J. Chem. Soc. Dalton Trans.* **1995**, 1893-1899.

(4) (a) Arsenault, A. C.; Puzzo, D. P.; Manners, I.; Ozin, G. A. *Nature Photonics* **2007**, *1*, 468-472. (b) Puzzo, D. P.; Arsenault, A. C.; Manners, I.; Ozin, G. A. *Angew. Chem. Int. Ed.* **2009**, *48*, 943-947.

(5) (a) MacLachlan, M. J.; Ginzburg, M.; Coombs, N.; Coyle, T. W.; Raju, N. P.; Greedan, J. E.; Ozin, G. A.; Manners, I. *Science* **2000**, *287*, 1460-1463. (b) Lastella, S.; Mallick, G.; Woo, R.; Karna, S. P.; Rider, D. A.; Manners, I.; Jung, Y. J.; Ryu, C. Y.; Ajayan, P. M. *J. Appl. Phys.* **2006**, *99*.

(6) Ma, Y. J.; Dong, W. F.; Hempenius, M. A.; Möhwald, H.; Vancso, G. J. *Nature Mater.* **2006**, *5*, 724-729.

(7) Ni, Y.; Rulkens, R.; Manners, I. *J. Am. Chem. Soc.* **1996**, *118*, 4102-4114.

(8) (a) Wang, X. S.; Guerin, G.; Wang, H.; Wang, Y. S.; Manners, I.; Winnik, M. A. *Science* **2007**, *317*, 644-647. (b) Gädt, T.; Ieong, N. S.; Cambridge, G.; Winnik, M. A.; Manners, I. *Nature Mater.* **2009**, *8*, 144-150.

(9) (a) Braunschweig, H.; Dirk, R.; Müller, M.; Nguyen, P.; Resendes, R.; Gates, D. P.; Manners, I. *Angew. Chem., Int. Ed.* **1997**, *36*, 2338-2340. (b) Berenbaum, A.; Braunschweig, H.; Dirk, R.; Englert, U.; Green, J. C.; Jäkle, F.; Lough, A. J.; Manners, I. *J. Am. Chem. Soc.* **2000**, *122*, 5765-5774.

(10) Heilmann, J. B.; Scheibitz, M.; Qin, Y.; Sundararaman, A.; Jäkle, F.; Kretz, T.; Bolte, M.; Lerner, H.-W.; Holthausen, M. C.; Wagner, M. *Angew. Chem., Int. Ed.* **2006**, *45*, 920 -925.

(11) (a) Schachner, J. A.; Lund, C. L.; Quail, J. W.; Müller, J. *Organometallics* **2005**, *24*, 785-787. (b) Schachner, J. A.; Lund, C. L.; Quail, J. W.; Müller, J. *Organometallics* **2005**, *24*, 4483-4488. (c) Lund, C. L.; Schachner, J. A.; Quail, J. W.; Müller, J. *Organometallics* **2006**, *25*, 5817-5823. (d) Schachner, J. A.; Tockner, S.; Lund, C. L.; Quail, J. W.; Rehahn, M.; Müller, J. *Organometallics* **2007**, *26*, 4658-4662.

(12) (a) Bagh, B.; Gilroy, J. B.; Staubitz, A.; Müller, J. *J. Am. Chem. Soc.* **2010**, *132*, 1794-1795. (b) Bagh, B.; Schatte, G.; Green, J. C.; Müller, J. *J. Am. Chem. Soc.*, 2012, **134**, 7924−7936.

(13) (a) Braunschweig, H.; Burschka, C.; Clentsmith, G. K. B.; Kupfer, T.; Radacki, K. *Inorg. Chem.* **2005**, *44*, 4906-4908. (b) Schachner, J. A.; Orlowski, G. A.; Quail, J. W.; Kraatz, H.-B.; Müller, J. *Inorg. Chem.* **2006**, *45*, 454-459. (c) Bagh, B.; Breit, N. C.; Harms, K.; Schatte, G.; Burgess, I. J.; Braunschweig, H.; Müller, J. **2012**, unpublished result.

(14) Schachner, J. A.; Lund, C. L.; Burgess, I. J.; Schatte, G.; Quail, J. W.; Müller, J. *Organometallics* **2008**, *27*, 4703-4710.

(15) (a) Burchard, W. In *Branched Polymers II* 1999; Vol. 143, p 113-194. (b) Massey, J. A.; Kulbaba, K.; Winnik, M. A.; Manners, I. *J. Polym. Sci. Part B: Polym. Phys.* **2000**, *38*, 3032-3041.

(16) Sadeh, S.; Schatte, G.; Müller, J. **2012**, unpublished result.

2.3.5 Selective Materials from Supporting Information of Contribution 3

EXPERIMENTAL SECTION

General information. Syntheses were carried out using standard Schlenk and glovebox techniques (N_2 as inert gas). Solvents were dried using a MBraun Solvent

Purification System and stored under nitrogen over 3 Å molecular sieves. All solvents for NMR spectroscopy were degassed prior to use and stored under nitrogen over 3 Å molecular sieves. ^{1}H and ^{13}C NMR spectra were recorded on a Bruker 500 MHz Avance NMR spectrometer at 25 ºC in C_6D_6 and $CDCl_3$, respectively. ^{1}H chemical shifts were referenced to the residual protons of the deuterated solvents (δ 7.15 for C_6D_6 and 7.26 for $CDCl_3$); ^{13}C chemical shifts were referenced to the C_6D_6 signal at δ 128.00 and the $CDCl_3$ signal at δ 77.00. Mass spectra were measured on a VG 70SE and were reported in the form *m/z* (%) [M^+] where "*m/z*" is the mass observed, the intensities are reported relative to the most intense peak, and "M^+" is the molecular ion or fragment; only characteristic mass peaks are listed. For isotopic pattern, only the mass peak of the isotopoloque or isotope with the highest natural abundance is listed. Elemental analyses were performed on a PerkinElmer 2400 CHN Elemental Analyzer using V_2O_5 to promote complete combustion.

Ferrocene (98%) and *n*BuLi (2.5 M in hexanes) were purchased from Sigma Aldrich. C_6D_6 (99.6 atom % D) and CDCl3 (99.8 atom % D) was purchased from Cambridge Isotope Laboratories, Inc. 2-(Me_2NCH_2)-4,6-*t*$Bu_2C_6H_2Br$[1] and 1,1'-dilithio-2,2'-di(isopropyl)ferrocene[2] were synthesized following literature.

Electrochemistry. A computer controlled system, consisting of a HEKA potentiostat PG590 (HEKA, Mahone Bay, NS, Canada) was used for the cyclic voltammetry experiments. Data was collected using a multifunction DAQ card (PCI 6251 M Series, National Instruments Austin, Texas) and in-house software written in the LabVIEW environment. Glassy carbon (BAS, 3 mm) was used as the working electrode. The quasi-reference electrode (QRE) was a silver wire and all measurements were made against the

QRE. A loop of gold wire was used as the auxiliary electrode. Before each measurement, 1 mM solution of **7_2** was freshly prepared in dry CH_2Cl_2 with 0.1 M $[Bu_4N][PF_6]$ as the supporting electrolyte. The electrolyte was dried overnight under high vacuum at 100 °C. The scan rate for the CVs reported was 50 mV/s. The measurements were conducted inside a glovebox and taken at ambient temperature (25 °C).

DLS Analyses. Dynamic light scattering experiments were performed using a nano series Malvern zetasizer instrument equipped with a 633 nm red laser. Samples were filtered through 0.2 μm syringe PTFE filters (Millex) before they were analyzed in 1 cm glass cuvettes at concentrations of 5.0 and 2.5 mg/mL in thf at 25 °C. The refractive index of the polymers was assumed to be 1.5. For each polymer, two samples were prepared at each concentration. Every sample was measured three times.

Synthesis of (Mamx)$InCl_2$ (6). *n*BuLi (2.5 M in hexanes, 2.40 mL, 6.00 mmol) was added dropwise to a cold (-78 ºC) solution of (Mamx)Br (1.80 g, 5.51 mmol) in Et_2O (20 mL). The reaction mixture was stirred at -78 ºC for 1 h, resulting in a pale yellow solution. The pale yellow solution was added dropwise to a cold (0 ºC) solution of $InCl_3$ (2.66 g, 20.0 mmol) in Et_2O (20 mL). The resulting mixture was warmed up to r.t. and stirred for 16 h, resulting in a pale green solution with a white precipitate. After the solid was filtered off, the pale green solution was concentrated to approx. 20 mL, and analytically pure product (Mamx)$InCl_2$ was obtained as colorless crystals at -80 ºC (1.04 g, 44%). ^{1}H NMR (C_6D_6): δ 1.30 (s, 9H, *t*Bu), 1.39 (s, 9H, *t*Bu), 1.90 (s, 6H, NMe_2), 2.89 (s, 2H, CH_2), 6.74 (s, 1H, C_6H_2), 7.57 (s, 1H, C_6H_2). ^{13}C NMR (C_6D_6): δ 31.46 [C($\underline{C}H_3)_3$], 32.47 [C($\underline{C}H_3)_3$], 34.88 [$\underline{C}(CH_3)_3$], 35.84 [$\underline{C}(CH_3)_3$], 45.28 (NMe_2), 65.61 (CH_2), 121.79, 123.73, 141.35, 152.62, 158.54 (C_6H_4). MS (70 eV): *m/z* (rel intens) 431

(9) [M^+], 396 (21) [M^+ - Cl], 245 (100) [$C_{17}H_{27}N^+$], 203 (78) [$C_{15}H_{23}^+$], 58 (39) [$C_4H_{10}^+$]. HRMS (EI; m/z): calcd for $C_{17}H_{28}Cl_2InN$, 431.0638; found, 431.0624. Anal. Calcd for $C_{17}H_{28}Cl_2InN$ (432.13): C, 47.25; H, 6.53; N, 3.24. Found: C, 47.33; H, 6.57; N, 3.19.

Synthesis of indium-bridged [1]FCP 7_1, [1.1]FCP 7_2 and poly(ferrocene) 7_n. A solution of (Mamx)$InCl_2$ (0.935 g, 2.16 mmol) in Et_2O (45 mL) was added dropwise to a slurry of $(LiC_5H_4)_2Fe{\cdot}$tmeda (0.681 g, 2.17 mmol) in Et_2O (20 mL). The reaction mixture was stirred at r.t. for 5 h, resulting in a red solution with a white precipitate. After the solid was filtered off, the red solution was kept at -78 °C for 48 h, which resulted in an orange precipitate and a red solution. The precipitate was filtered off, washed with hexane (3 x 10 mL), and dried under vacuum to give $\mathbf{7_2}$ (0.273 g, 23%). All volatiles were removed from the mother liquor (red solution), which yielded a red paste. The red paste was dissolve in toluene (5 mL) and added dropwise to hexane while stirring vigorously. An orange-red precipitate and an orange solution were obtained. The precipitate was filtered off, washed with cold (-20 °C) hexane (3 x 10 mL), and dried under vacuum to give $\mathbf{7_1}$ (0.219 g, 19%). All volatiles were removed from the mother liquor (orange solution), which yielded an orange paste. The paste was dissolve in toluene (5 mL) and added dropwise to MeOH (30 mL) while stirring vigorously. An orange precipitate and a pale orange solution were obtained. The precipitate was filtered off, washed with MeOH (3 x 15 mL), and dried under vacuum to give $\mathbf{7_n}$ (0.378 g, 32%).

Inda[1]ferrocenophane 7_1. ^{1}H NMR ($CDCl_3$): δ 1.21 (s, 9H, *t*Bu), 1.35 (s, 9H, *t*Bu), 2.45 (s, 6H, NMe_2), 3.55 (s, 2H, CH_2), 4.01 (pst, 2H, CH-α Cp), 4.04 (pst, 2H, CH-α Cp), 4.18 (pst, 2H, CH-β Cp), 4.19 (pst, 2H, CH-β of Cp), 6.80 (s, 1H, C_6H_2), 7.62 (s, 1H, C_6H_2). ^{1}H NMR (C_6D_6): δ 1.40 (s, 9H, *t*Bu), 1.60 (s, 9H, *t*Bu), 2.16 (s, 6H, NMe_2),

3.33 (s, 2H, CH_2), 4.22 (pst, 2H, CH-α Cp), 4.39 (pst, 2H, CH-α Cp), 4.41 (pst, 2H, CH-β of Cp), 4.46 (pst, 2H, CH-β of Cp), 7.00 (s, 1H, C_6H_2), 7.67 (s, 1H, C_6H_2). ^{13}C NMR (C_6D_6): δ 31.80 [C($\underline{C}H_3)_3$], 33.16 [C($\underline{C}H_3)_3$], 34.72 [$\underline{C}(CH_3)_3$], 36.93 [$\underline{C}(CH_3)_3$], 46.24 (NMe_2), 68.84 (CH_2), 70.13, 70.53, 75.54, 76.96 (Cp), 120.49, 121.87, 143.94, 149.17, 159.50 (C_6H_4). MS (70 eV): *m/z* (rel intens) 545 (13) [M^+], 515 (31) [M^+ - NMe_2], 432 (25) [M^+ - *t*Bu], 301 (18) [$C_{18}H_{17}FeN^+$], 184 (62) [$C_{10}H_8Fe$], 121 (100) [$C_5H_5Fe^+$]. HRMS (EI; m/z): calcd for $C_{27}H_{36}FeInN$, 545.1236; found, 545.1249. Anal. Calcd for $C_{27}H_{36}FeInN$ (545.24): C, 58.48; H, 6.65; N, 2.57. Found: C, 58.58; H, 6.58; N, 2.46.

Diinda[1.1]ferrocenophane 7_2. ^{1}H NMR ($CDCl_3$): δ 1.35 (s, 18H, *t*Bu), 1.74 (s, 18H, *t*Bu), 1.95 (s, 12H, NMe_2), 3.45 (s, 4H, CH_2), 3.91 (pst, 4H, CH-α Cp), 4.26 (pst, 8H, CH-β Cp), 4.40 (pst, 4H, CH-α Cp), 6.90 (s, 2H, C_6H_2), 7.50 (s, 2H, C_6H_2). Note: Due to the poor solubility of **7_2** in organic solvents, the ^{13}C NMR spectrum had a high noise level. ^{13}C NMR ($CDCl_3$): δ 31.56 [C($\underline{C}H_3)_3$], 33.06 [C($\underline{C}H_3)_3$], 34.62 [$\underline{C}(CH_3)_3$], 36.29 [$\underline{C}(CH_3)_3$], 45.30 (NMe_2), 67.42 (CH_2), 69.34, 69.38, 75.13, 76.84 (Cp), 126.49, 120.55 (C_6H_4). MS (70 eV): *m/z* (rel intens) 1090 (9) [M^+], 731 (17) [M^+ - In(Mamx)], 626 (20) [$C_{24}H_{24}FeIn_2N_2^+$], 581 (100) [$C_{23}H_{19}FeIn_2^+$], 546 (36) [$C_{27}H_{37}FeInN^+$], 425 (17) [$C_{22}H_{32}InN^+$], 247 (34) [$C_9H_{10}InN^+$], 186 (87) [$C_{10}H_{10}Fe^+$]. HRMS (EI; m/z): calcd for $C_{54}H_{72}Fe_2In_2N_2$, 1090.2472; found, 1090.2481. Anal. Calcd for $C_{54}H_{72}Fe_2In_2N_2$ (1090.49): C, 58.48; H, 6.65; N, 2.57. Found: C, 58.00; H, 6.44; N, 2.43.

Poly(ferrocenylindane) 7_n. ^{1}H NMR (C_6D_6): δ 1.24-1.38 (m, 9 H, *t*Bu), 1.48-1.66 (m, 9 H, *t*Bu), 2.15-2.77 (m, 6 H, NMe_2), 3.40-3.69 (m, 2 H, CH_2), 3.84-4.62 (m, 8H, Cp), 6.86-7.04 (m, 1 H, C_6H_2), 7.38-7.55 (m, 1 H, C_6H_2).

Synthesis of poly(ferrocenylindane) $\mathbf{9_n}$. *n*BuLi (2.5 M in hexanes, 0.85 mL, 2.13 mmol) was added dropwise to a cold (0 ºC) solution of 1,1'-dibromo-2,2'-di(*iso*-propyl)ferrocene (0.432 g, 1.01 mmol) in a mixture of thf (1 mL) and hexane (9 mL). The reaction mixture was stirred at 0 ºC for 30 min, resulting in a red solution. A solution of (Mamx)$InCl_2$ **6** (0.438 g, 1.01 mmol) in Et_2O (20 mL) was added dropwise to the red solution. The resulting reaction mixture was warmed up to r.t. and stirred for 30 min, resulting in a red solution with a white precipitate. All volatiles were removed under vacuum, yielding a red solid. Et_2O (25 mL) was added to the red solid and the mixture was stirred for 30 mins, yielding a red solution with white precipitate. The solid was filtered off and the filtrate was stirred for 3 h, resulting in an orange-red solution with orange gelatinous material. All volatiles were removed under vacuum, yielding an orange-red paste, which was dissolved in toluene (5 mL). The toluene solution was added dropwise to hexane (20 mL) with vigorous stirring, yielding an orange precipitate with a red solution. The precipitate (0.438 g) was filtered off, washed with hexane (3x5 mL) and dried under vacuum to give the poly(ferrocenylindane) $\mathbf{9_n}$ (0.211 g, 33%). ^{1}H NMR (C_6D_6): δ 1.24-1.38 (m, 9 H, *t*Bu), 1.48-1.66 (m, 9 H, *t*Bu), 2.15-2.77 (m, 6 H, NMe_2), 3.40-3.69 (m, 2 H, CH_2), 3.84-4.62 (m, 8H, Cp), 6.86-7.04 (m, 1 H, C_6H_2), 7.38-7.55 (m, 1 H, C_6H_2).

Identification of the inda[1]ferrocenophane $\mathbf{9_1}$. Inda[1]ferrocenophane ($\mathbf{9_1}$) is an intermediate in the preparation of the poly(ferrocenylindane) $\mathbf{9_n}$ and can be identified via ^{1}H NMR spectroscopy. All attempts to isolate pure the inda[1]ferrocenophane $\mathbf{9_1}$ were unsuccessful. ^{1}H NMR (C_6D_6; taken from an aliquot of the reaction mixture after 30 min): δ 1.16 (d, 3H, CH_3 of *i*Pr), 1.19 (d, 3H, CH_3 of *i*Pr), 1.39 (s, 9H, *t*Bu), 1.50 (d, 3H,

CH_3 of *i*Pr), 1.53 (d, 3H, CH_3 of *i*Pr), 1.65 (s, 9H, *t*Bu), 1.91 (s, 3H, CH_3 of NMe_2), 2.30 (s, 3H, CH_3 of NMe_2), 2.38 (m, 1H, CH of *i*Pr), 2.65 (d, 1H, CH of CH_2), 2.38 (m, 1H, CH of *i*Pr), 3.94 (d, 1H, CH of CH_2), 3.68, 4.11, 4.47, 4.50, 4.67, 4.73 (m, 6H, Cp), 6.94 (s, 1H, C_6H_2), 7.72 (s, 1H, C_6H_2).

Table 2-4-S1. DLS Data of Poly(ferrocenylindane) $\mathbf{7_n}$.

Concentration (mg/mL)	5		2.5	
	1	2	1	2
D_h (nm)	1.962	2.112	1.925	1.766
	2.118	1.945	1.851	2.035
	1.757	2.228	2.065	2.308
R_h (nm)	0.981	1.056	0.963	0.883
	1.059	0.973	0.926	1.018
	0.879	1.114	1.033	1.154
Average (nm)	1.010		0.996	
SD (nm)	0.084		0.096	
Overall Average (nm)	1.003			
Overall SD (nm)	0.086			

Table 2-4-S2. DLS Data of Poly(ferrocenylindane) $\mathbf{9_n}$.

Concentration (mg/mL)	5		2.5	
	1	2	1	2
D_h (nm)	4.408	4.654	4.93	5.066
	4.667	3.128	4.905	5.049
	4.724	4.986	4.830	4.816
R_h (nm)	2.204	2.327	2.465	2.533
	2.334	1.564	2.453	2.525
	2.362	2.493	2.415	2.408
Average (nm)	2.214		2.466	
SD (nm)	0.331		0.053	

Overall Average (nm)	2.340
Overall SD (nm)	0.262

REFERENCES

(1) Bagh, B.; Gilroy, J. B.; Staubitz, A.; Müller, J. *J. Am. Chem. Soc.* **2010**, *132*, 1794-1795.

(2) Sadeh, S.; Schatte, G.; Müller, J. **2012**, unpublished result.

CHAPTER 3
HEAVIER GROUP 13 AND 14 ELEMENTS-BRIDGED [1.1]FERROCENOPHANES, BIS(FERROCENYL) SPECIES AND POLY(FERROCENE)S WITH LINEAR AND CYCLIC STRUCTURES

This part presents the synthesis of new [1.1]ferrocenophanes and bis(ferrocenyl) species bridged by aluminum, gallium and silicon, their electrochemical behavior as well as the synthesis and electrochemistry of unsymmetrically bridged [1.1]ferrocenophanes with Si-Sn and Si-Ga as bridging pairs. In addition, poly(ferrocene)s with linear structures and macrocyclic species will be discussed. This will included the results of two published articles, one manuscript which is submitted for publication, and one manuscript which is under preparation.

Contribution 1: [1.1]Ferrocenophanes and Bis(ferrocenyl) Species with Aluminum and Gallium as Bridging Elements: Synthesis, Characterization, and Electrochemical Studies.

3.1.1. Description

The following chapter is a verbatim copy of a manuscript which has been submitted to be published in *Inorganic Chemistry*[1] and describes the synthesis, characterization and electrochemical studies of a series of bis(ferrocenyl) species and [1.1]FCPs with aluminum, gallium and silicon as bridging elements. Aluminum and gallium dichloride complexes with new slim ligands (*p*-$SiMe_3Ar'$ and Mpysm) were synthesized and utilized for the salt metathesis reaction to yield new [1.1]FCPs. Two pairs of aluminum and gallium-bridged bis(ferrocenyl) species, where two ferrocenyl moieties are bridged by

[1] Bagh, B.; Breit, N. C.; Harms, K.; Schatte, G.; Burgess, I. J.; Braunschweig, H.; Müller, J. *Inorg. Chem.* **2012** , *51*, 11155-11167.

only one bridging element, were synthesized by the reaction of lithioferrocene and respective element dichlorides. Similar reaction of lithioferrocene and dialkylsilicon dichloride yielded silicon-bridged bis(ferrocenyl) compounds. Bis(ferrocenyl) species and [1.1]FCPs contain two iron redox centers and the electronic communication between the iron centers was investigated by cyclic voltammetry.

3.1.2. Author Contributions

The co-authors on this paper are Nora C. Breit, who performed the synthesis and characterizion of a pair of aluminum and gallium-bridged bis(ferrocenyl) compounds, Gabriele Schatte and Klaus Harms, who performed the structure determinations by single crystal X-ray analysis and Ian Burgess, who helped us performing the electrochemical studies with his expertise. Holger Braunschweig had a minor contribution to the manuscript by sublying us with two cyclic voltammograms of the known [1.1]FCP **1a**. I prepared the first version of the manuscript, which was edited by my supervisor Jens Müller.

3.1.3. Relation of Contribution 4 with Research Objectives

As mentioned in Part 2 of the research objectives, a main goal of my research was to study the electronic communication between the redox centers of [1.1]FCPs and bis(ferrocenyl) species with heavier group 13 elements in bridging possitions. Therefore, two [1.1]FCPs with (*p*-$SiMe_3Ar'$)Al (**4a**) and (*p*-$SiMe_3Ar'$)Ga (**4b**) as bridging moieties were synthesized. Four bis(ferrocenyl) species with aluminum (**5a**, **6a**) and gallium (**5b**, **6b**) equipped with two different ligands (*p*-$SiMe_3Ar'$, Mpysm) were synthesized as well. Moreover, two silicon-bridged bis(ferrocenyl) species ($\mathbf{7^{Me}}$, $\mathbf{7^{Et}}$) were also prepared. The

redox behaviors of those species were studied. The unprecedented electrochemical behavior exihibited by the (Ar′)Al-bridged [1.1]FCP **1a** was a second motivation for the synthesis and electrochemical study of new [1.1]FCPs with heavier group-13-bridges. In contrast to the published electrochemistry of **1a**, the current measurements displayed two main redox waves in the cyclic voltammograms of **1a** and **4a**. The gallium-species **4b** showed two symmetric oxidation and reduction waves. The electrochemical behaviors of the new bis(ferrocenyl) species (**5a**, **5b**, **6a**, **6b**, $\mathbf{7^{Me}}$, $\mathbf{7^{Et}}$) along with two previously reported aluminum- (**8a**) and gallium-bridged bis(ferrocenyl) species (**8b**) were studies as well. The electrochemical measurements provided important informations about metal-metal interactions in [1.1]FCPs and bis(ferrocenyl) species.

3.1.4. Manuscript of Contribution 1

[1.1]Ferrocenophanes and Bis(ferrocenyl) Species with Aluminum and Gallium as Bridging Elements: Synthesis, Characterization, and Electrochemical Studies

Bidraha Bagh,[‡] Nora C. Breit,[‡] Klaus Harms,[¥] Gabriele Schatte,[§] Ian J. Burgess,[‡] Holger Braunschweig,[¢] and Jens Müller*[,‡]

[‡]Department of Chemistry and [§]Saskatchewan Structural Sciences Centre, University of Saskatchewan, 110 Science Place, Saskatoon, Saskatchewan S7N 5C9, Canada; [¥]Fachbereich Chemie der Philipps-Universität Marburg, Hans-Meerwein-Strasse, 35032 Marburg, Germany; [¢]Institut für Anorganische Chemie, Julius-Maximilians-Universität Würzburg, Am Hubland, 97074, Würzburg, Germany

ABSTRACT: Salt-metathesis reactions between dilithioferrocene and intramolecularly coordinated aluminum and gallium species $RECl_2$ [R = 5-Me_3Si-2-

(Me_2NCH_2)C_6H_3; E = Al (**2a**), Ga (**2b**); and R = (2-C_5H_4N)Me_2SiCH_2; E = Al (**3a**), Ga (**3b**)] gave respective [1.1]ferrocenophanes ([1.1]FCPs). Those obtained from **2a** and **2b**, respectively, were isolated as analytically pure compounds and fully characterized including single-crystal X-ray structure determinations [**4a** (Al): 43%; **4b** (Ga): 47%]. Bis(ferrocenyl) compounds of the type $REFc_2$ [R = 5-Me_3Si-2-(Me_2NCH_2)C_6H_3; E = Al (**5a**), Ga (**5b**); and R = (2-C_5H_4N)Me_2SiCH_2; E = Al (**6a**), Ga (**6b**)] and R_2SiFc_2 [R = Me ($\mathbf{7^{Me}}$); Et ($\mathbf{7^{Et}}$)] were prepared, starting from respective element dichlorides and lithioferrocene (LiFc). Molecular structures of **6a**, $\mathbf{7^{Me}}$, and $\mathbf{7^{Et}}$ were solved by single-crystal X-ray analyses. One of the two Fc moieties of **6a** was bent toward the open coordination site of the aluminum atom. The measured dip angles α* of the two independent molecules in the asymmetric unit were 11.9(5) and 13.3(5)°, respectively. The redox behavior of [1.1]FCPs **4** and bis(ferrocenyl) species **5**, **6**, **7**, and (Mamx)EFc_2 [Mamx = 2,4-*t*Bu_2-6-(Me_2NCH_2)C_6H_2; E = Al (**8a**), Ga (**8b**)] were investigated with cyclic voltammetry (CV). While all gallium and silicon compounds gave meaningful and interpretable data, all aluminum compounds were problematic with the exception of **8a**. Aluminum species, compared to respective gallium species, are more sensitive and, presumably, fluoride ions or residual water from the electrolyte and solvent are causing degradation. The splitting between the formal potentials for bis(ferrocenyl) species was significantly smaller (**5b**, **6b**, and **8b**: $\Delta E^{o\prime}$ = 0.138 – 0.159 V) than that of the [1.1]FCP **4b** ($\Delta E^{o\prime}$ = 0.309 V). These results were explained by assuming an electrostatic interaction between the two iron centers; differences between bis(ferrocenyl) species and [1.1]FCPs are likely due to a more effective solvation of Fe-containing moieties in the more flexible bis(ferrocenyl) species.

INTRODUCTION

[n]Ferrocenophanes ([n]FCPs; Chart 3-1-1) with one or two-atom bridges (n = 1, 2) with significantly tilted Cp rings (α angles above ca. 14°) often show a propensity toward ring-opening polymerization (ROP) resulting in poly(ferrocene)s.[1] This area of chemistry began with the synthesis a [2]FCP equipped with a C_2Me_4 bridge, which was the first strained sandwich compound published in 1960.[2] After the first [1]FCPs (ER_x = $SiMe_2$, $SiPh_2$; Chart 3-1-1) had been described in 1975,[3] it took more than 15 years before this area of polymer chemistry started to blossom with the discovery that silicon-bridged [1]FCPs yield high-molecular-weight polymers through thermal ROP.[4] To date, silicon-bridged [1]FCPs form the most prominent class of strained sandwich compounds and serve as excellent precursors for metallopolymers.[1,5]

Chart 3-1-1.

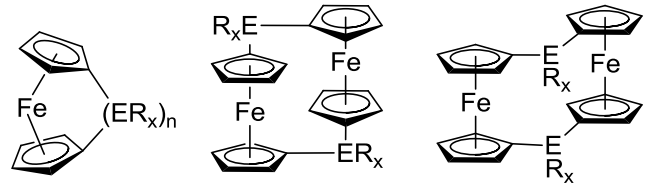

[n]FCP *anti*-[1.1]FCP *syn*-[1.1]FCP

[1.1]Ferrocenophanes ([1.1]FCPs; Chart 3-1-1) are unstrained dimers of [1]FCPs and had been investigated as early as 1956.[6] Today, the large class of [1.1]FCPs consists of examples with a variety of bridging moieties ER_x (Chart 3-1-1; E = B,[7] Al,[8] Ga,[8b,9] In,[8b,10] Si,[11] Sn,[12] Pb,[13] P,[14] As,[15] S,[16] Zn,[17] and Hg[18]). Recently, we developed a methodology for the preparation of unsymmetric [1.1]FCPs, compounds with two different single-atom bridges, and realized the element combinations of Si/Sn and Si/Ga, respectively.[19] In addition, cyclic species with 4 ferrocenediyl units [fc = $(C_5H_4)_2Fe$] were isolated, while,

in some cases, macrocycles with up to 20 fc units were detected by MALDI-TOF mass spectrometry.[19] Macrocyclic ferrocenophanes with multiple fc moieties are known, but significantly rarer compared to the large class of [1.1]FCPs.[11f,14b,20] To the best of our knowledge, the largest isolated FCPs contained seven ferrocene moieties,[20e,20i,20l] while [1^n]FCPs[21] with n > 40 are the largest macrocycles of this type described in literature (detected by MALDI-TOF mass spectrometry).[20l]

Despite the impressive progress made during the last two decades to use strained sandwich compounds for new metallopolymers, there is still a need to develop new monomers, in particular, species that can be polymerized in a living fashion. Since 2004, we prepared aluminum- and gallium-bridged sandwich compounds and explored their polymerizability.[22] Our first generation of these species had been equipped with bulky, intramolecularly coordinating ligand at the group 13 elements (e.g., Pytsi; Chart 3-1-2). However, attempts to polymerize [1]FCPs or their ruthenium counterparts ([1]RCPs) either failed or resulted in sluggish polymerizations,[22d] indicating that the bulkiness of the stabilizing ligands was hindering the ROP. We discovered that the use of the related, but slimmer 2-[(dimethylamino)methyl]phenyl ligand (Ar′ in Chart 3-1-2) in respective salt-metathesis reactions of dilithioferrocene and aluminum or gallium dichlorides Ar'ECl_2 resulted in [1.1]FCPs (**1a** and **1b**; Chart 3-1-3) instead of the strained [1]FCPs.[8a,8b] The use of (Mamx)ECl_2 species (E = Al, Ga; Chart 3-1-2), equipped with a ligand of intermediate bulkiness, led to [1]FCPs and [1]RCPs, which were surprisingly reactive and ROP occurred already in reaction mixtures.[22a,22c] The bulkiness of the stabilizing ligand at the group 13 element plays a key role for the accessibility of strained sandwich compounds as well as for their polymerizability.

Within this report, we describe new aluminum and gallium dichlorides, (Mpysm)ECl_2 and (*p*-$SiMe_3$Ar')ECl_2 (Chart 3-1-2), and their utilization in salt metathesis reactions with dilithioferrocene (Li_2fc) and lithioferrocene (LiFc). We intended to compare Fe-Fe interactions in [1.1]FCPs with those in the related bis(ferrocenyl) compounds (Mpysm)EFc_2 and (*p*-$SiMe_3$Ar')EFc_2. For this study, we equipped the Ar' ligand with a $SiMe_3$ group in *para* position (*p*-$SiMe_3$Ar'; Chart 3-1-2) to access [1.1]FCPs, like the known species **1a** and **1b** (Chart 3-1-3), but with an improved solubility in organic solvents. Such a tactics had been successfully applied for [1.1]metallacyclophanes through the use of the *t*BuAr' ligand (Chart 3-1-2).[23] The Mpysm ligand[24] was applied because of its relation to the Pytsi ligand (Chart 3-1-2).

Chart 3-1-2. Intramolecularly Coordinating Ligands.

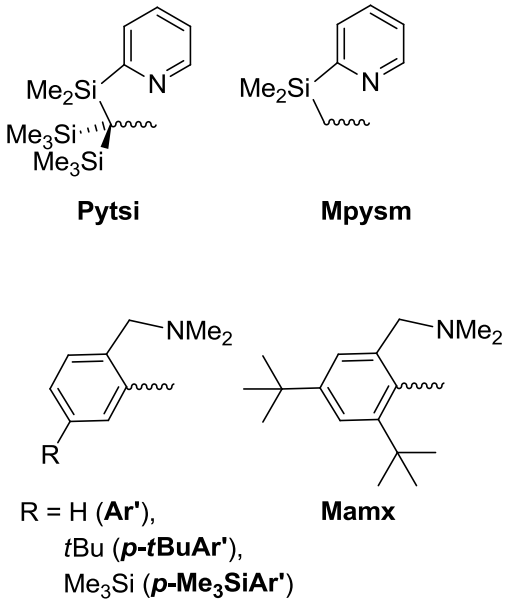

Chart 3-1-3. Known [1.1]FCPs **1a** and **1b**.

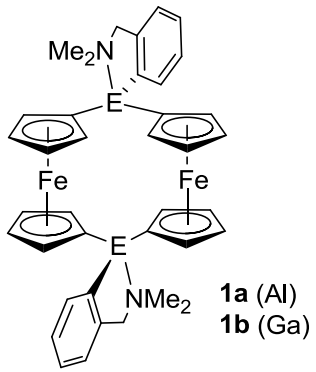

RESULTS AND DISCUSSION

Synthesis of aluminum- and gallium dichlorides. Scheme 3-1-1 illustrates the preparation of new intramolecularly coordinated aluminum- and gallium dichlorides, which were isolated in yields between 47 and 73%.[25] As expected, NMR spectra of all four species show signal pattern consistent with C_s symmetric molecules.

Scheme 3-1-1.

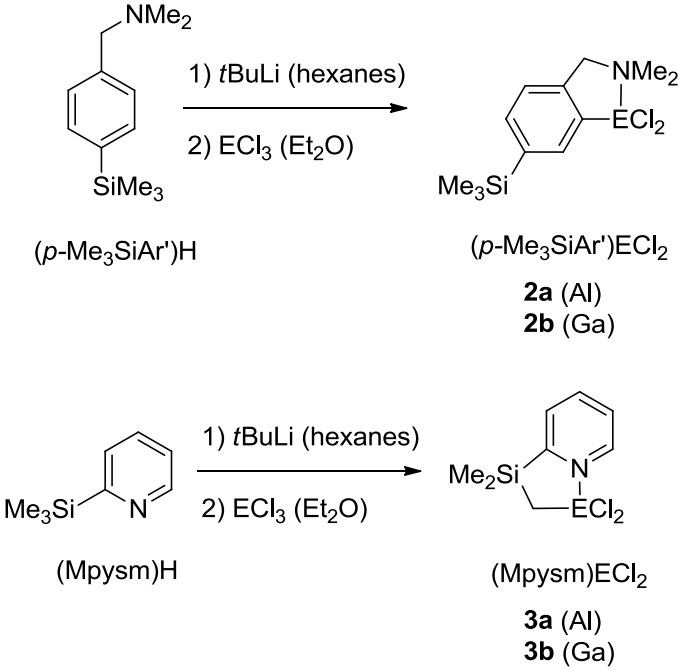

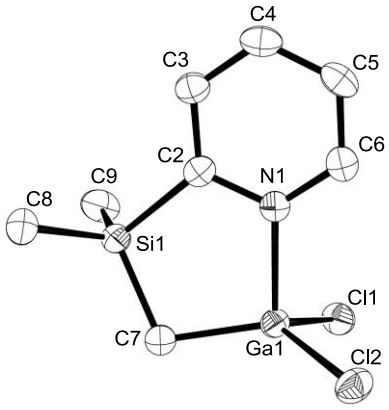

Figure 3-1-1. Molecular structure of **3b** with thermal ellipsoids at the 50% probability level. Hydrogen atoms are omitted for clarity. Selected atom-atom distances [Å] and bond angles [º] for **3b**: Ga1-N1 = 2.0126(16), Ga1-C7 = 1.949(2), Ga1-Cl1 = 2.2024(5), Ga1-Cl2 = 2.1927(6), C7-Ga1-Cl1 = 118.10(7), C7-Ga1-Cl2 = 121.94(7), C7-Ga1-N1 = 98.79(7), N1-Ga1-Cl1 = 103.42(5), N1-Ga1-Cl2 = 102.16(5), Cl1-Ga1-Cl2 = 108.54(2).

We were interested to compare the structures of the halides equipped with the Mpysm ligand with those of the respective (Pytsi)ECl_2 species. Therefore, the molecular structure of **3b** was determined by single-crystals X-ray analysis (Figure 3-1-1, Table 3-1-1).

The molecular structure of **3b** is very similar to that of the related dihalide (Pytsi)$GaCl_2$.[22g] The geometry at gallium is distorted tetrahedral in both species and the bite angles are nearly identical (C7-Ga1-N1 = 98.79(7) (**3b**), 98.03(9)° [(Pytsi)$GaCl_2$]). The Ga-N bond lengths of 2.0126(16) Å (**3b**) is within three esd's identical to that in (Pytsi)$GaCl_2$ [Ga-N = 2.004(2) Å]. The other three covalent bonds around the Ga atom in **3b** are only slightly different, with the largest difference of 0.04 Å found for the Ga-C bonds [**3b**: 1.949(2) Å; (Pytsi)$GaCl_2$: 1.988(2) Å]. For a better comparison of the geometries of both species, the coordination could be described as trigonal pyramidal with C7, Cl1, and Cl2 at the base and N1 at the tip of the pyramid. The pyramid of **3b** is more acute compared with that of (Pytsi)$GaCl_2$, which can be illustrated with the sum of the three angles C7-Ga1-Cl2, C7-Ga1-Cl1, Cl1-Ga1-Cl2. Whereas this sum for **3b** of

335.4° is close to the expected value for a tetrahedral coordination, that in (Pytsi)$GaCl_2$[22g] of 350.0° is closer to the expected value of a trigonal-planar coordination at the base. This difference is probably due to the steric requirements of the two $SiMe_3$ groups in (Pytsi)$GaCl_2$ which results in a widening of the two C-Ga-Cl angles [121.49(8) and 124.77(8)°] compared with those in **3b** [103.42(5) and 102.16(5)°].

Table 3-1-1. Crystal and Structural Refinement Data for Compounds **3b**, **4a**, and **4b**.

	3b	**4a**·2thf	**4b**·2thf
empirical formula	$C_8H_{12}Cl_2GaNSi$	$C_{52}H_{72}Al_2Fe_2N_2O_2Si_2$	$C_{52}H_{72}Ga_2Fe_2N_2O_2Si_2$
fw	290.90	978.96	1064.44
cryst. size / mm^3	0.31 × 0.20 × 0.08	0.09 × 0.06 × 0.06	0.10 × 0.09 × 0.07
cryst. system, space group	monoclinic, *C*2/*c*	monoclinic, $P2_1/c$	monoclinic, $P2_1/c$
Z	8	2	2
a / Å	24.8987 (15)	11.1745(3)	11.1015(3)
b / Å	8.4418 (3)	19.2904(5)	19.3907(6)
c / Å	11.9599 (7)	12.1908(4)	12.2577(4)
α / °	90	90	90
β / °	104.633(5)	106.1100(17)	106.5540(10)
γ / °	90	90	90
volume / $Å^3$	2432.3(2)	2524.66(13)	2529.30(13)
ρ_{calc} / mg m^{-3}	1.589	1.288	1.398
temperature / K	100	173(2)	173(2)
$\mu_{calc.}$/ mm^{-1}	2.76	5.708	6.484
θ range / °	1.69 – 26.69	4.12 – 66.63	4.15 – 66.90
reflns collected / unique	15220 / 2577	17246 / 4373	17093 / 4369
absorption correction	multiscan	multiscan	multiscan
data / restraints /	2577 / 0 / 120	4373 / 178 / 331	4369 / 178 / 331

params			
goodness-of-fit	0.917	1.015	1.039
R_1 [I > 2 σ(I)][a]	0.0218	0.0410	0.0418
wR_2 (all data)[a]	0.0501	0.1156	0.1197
largest diff. peak and hole, $\Delta\rho_{elect}$ / e Å^{-3}	0.47, -0.22	0.443, -0.261	0.814, -0.734

[a] $R_1 = [\Sigma||F_o|-|F_c||]/[\Sigma|F_o|]$ for $[F_o^2 > 2\sigma(F_o^2)]$, $wR_2 = \{[\Sigma w(F_o^2-F_c^2)^2]/[\Sigma w(F_o^2)^2]\}^{1/2}$ [all data].

Synthesis of Aluminum- and Gallium-bridged [1.1]Ferrocenophanes. With the heavier group-13-element dichlorides in hand, the reactivity toward dilithioferrocene was explored. Following standard procedures, the two [1.1]ferrocenophanes **4a** and **4b**, equipped with the *p*-$SiMe_3$Ar′ ligand (Chart 3-1-2), were synthesized and isolated in moderate yields (**4a**: 43%; **4b**: 47%; Scheme 3-1-2).

Scheme 3-1-2.

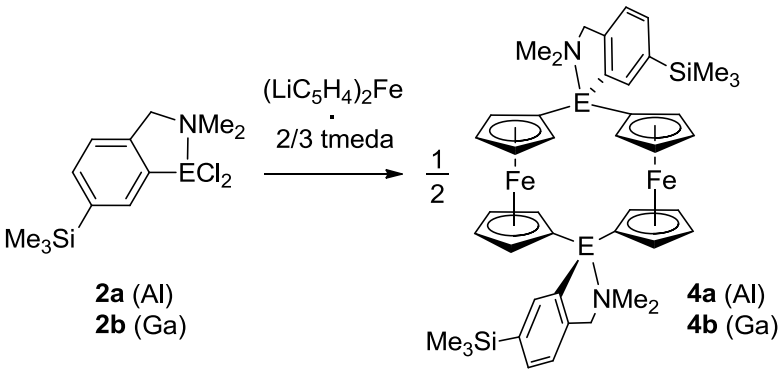

Both species gave single crystals of suitable quality for structural determinations from thf solution at -22 °C (Figure 3-1-2, Table 3-1-1). Species **4a** and **4b** are isostructural to each other and to the known [1.1]FCPs (**1a** and **1b**; Chart 3-1-3), where the $SiMe_3$ group is absent (space group $P2_1/c$). As expected, both species crystallize as *anti* isomers (Chart 3-1-1) and their bond lengths and angles are unremarkable and very similar to those of

the known species **1a** and **1b** (Chart 3-1-3).[8a,8b] For example, the Fe···Fe distances of the aluminum [5.3946(8) (**4a**); 5.443 Å (**1a**)[8a]] and gallium species [5.4277(8) (**4b**); 5.462 Å (**1b**)[8b]] are all in the narrow range of 5.395 – 5.462 Å.

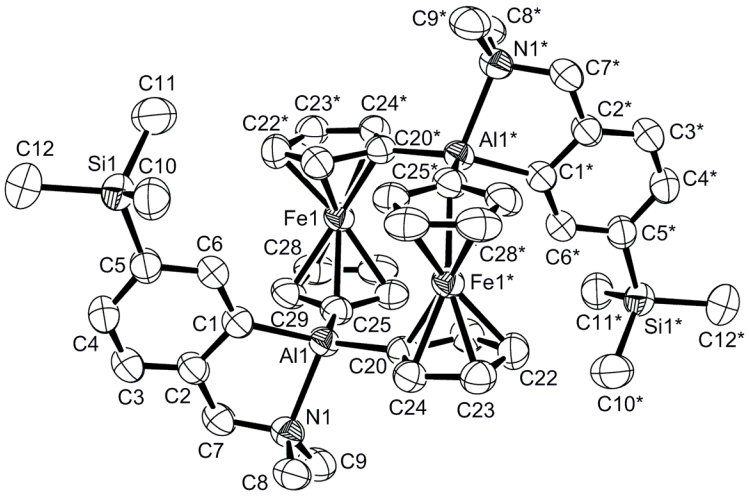

Figure 3-1-2. Molecular structure of **4a** with thermal ellipsoids at the 50% probability level. Hydrogen atoms are omitted for clarity. For a thermal ellipsoid plot of **4b** see Figure S1. Selected atom-atom distances [Å] and bond angles [º] for **4a**: Al1-N1 = 2.071(2), Al1-C1 = 1.985(3), Al1-C20 = 1.964(3), Al1-C25 = 1.972(3), Fe1···Fe1* = 5.3946(8), C1-Al1-C20 = 122.84(11), C1-Al1-C25 = 114.47(12), C1-Al1-N1 = 84.96(10), N1-Al1-C20 = 107.62(10), N1-Al1-C25 = 102.67(10), C20-Al1-C25 = 116.21(11). Selected atom-atom distances [Å] and bond angles [º] for **4b**: Ga1-N1 = 2.173(2), Ga1-C1 = 1.976(3), Ga1 = C20 = 1.968(3), Ga1-C25 = 1.963(3), Fe1···Fe1* = 5.4277(8), C1-Ga1-C20 = 114.60(12), C1-Ga1-C25 = 123.15(11), C1-Ga1-N1 = 83.35(10), N1-Ga1-C20 = 101.47(10), N1-Ga1-C25 = 106.25(10), C20-Ga1-C25 = 117.65(12). Symmetry transformation used to generate equivalent atoms (*): -x + 1, -y, -z.

NMR data of **4a** and **4b** are very similar to that of the known species **1a** and **1b**.[8a,8b] The most indicative area in ^{1}H NMR spectra is the Cp range, where both species (**4a**, **4b**) show only four signals, which can be explained by the presence of time-averaged C_{2h} symmetrical species.[26] This means that both species have similar structures in solution as in the solid state (C_i point group symmetry), if one takes into account that the five-membered rings of the coordinated *p*-SiMe$_3$Ar' will invert fast in soltuion.[27]

The motivation to use the *p*-$SiMe_3$Ar′ ligand instead of the Ar′ ligand was to increase the solubility of the targeted [1.1]FCPs. Such a tactic had worked for [1.1]chromarenophanes before;[23] however, compounds **4a** and **4b** turned out to be sparingly soluble in common organic solvents. A ^{13}C NMR spectrum of **4b** employing $CDCl_3$ could be measured. In contrast, the instability of the aluminum species **4a** in $CDCl_3$ and its poor solubility in other deuterated solvents prevented its ^{13}C NMR analysis.

Similar to the reaction shown in Scheme 3-1-2, the reactivity of the two halides **3a** and **3b** (Scheme 3-1-1) toward Li_2fc was explored. ^1H NMR analysis of crude products revealed the presence of the targeted [1.1]FCPs by typical signal patterns in the Cp region [(Mpysm)Al-bridged [1.1]FCP: δ 4.17, 4.49, 4.69 and 5.31 (C_6D_6); (Mpysm)Ga-bridged [1.1]FCP: δ 4.18, 4.41, 4.64 and 5.17 (C_6D_6)]. In addition to these sharp peaks, reaction mixtures always exhibited broad signals indicating the presence of oligomeric ferrocenylalumanes and gallanes, respectively.[22b] Despite of our best efforts, we were not able to isolate the [1.1]FCPs from these mixtures.

Synthesis of Bis(ferrocenyl) Species with Aluminum, Gallium, and Silicon as Bridging Elements. One of the motivations to prepare [1.1]FCPs was to investigate the interaction between both redox-active iron atoms. In [1.1]FCPs the relative orientation of ferrocene moieties is fixed. In order to address the question if the degree of interaction between two ferrocene moieties depends on their orientation, related compounds exhibiting a higher flexibility were targeted. Therefore, bis(ferrocenyl) species of aluminum and gallium were prepared (Scheme 3-1-3), which were equipped with the same intramolecularly coordinating ligands employed for the

Scheme 3-1-3. Synthesis of bis(ferrocenyl) species.

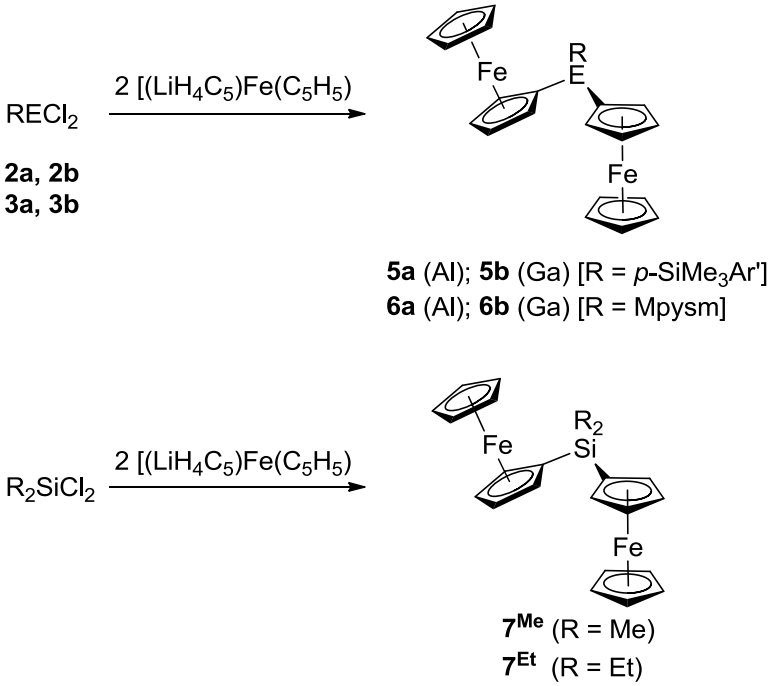

synthesis of [1.1]FCPs. Furthermore, we wanted to find out if the type of bridging element had a significant influence on the metal-metal interaction and prepared bis(ferrocenyl)silanes (**7**$^{\mathbf{Me}}$, **7**$^{\mathbf{Et}}$; Scheme 3-1-3). Whereas the isolated yields for the group-13-containing species were only low to moderate (21 – 47%), those of the silanes were expectedly better (**7**$^{\mathbf{Me}}$: 70%; **7**$^{\mathbf{Et}}$: 72%). The synthesis of the silane **7**$^{\mathbf{Me}}$ had been described in a patent before,[28] where LiFc was prepared *in situ* from ClHgFc and *n*BuLi; we prepared LiFc from FcH and *t*BuLi in thf as described in the literature.[29] Furthermore, Manners *et al.* found small amounts of species **7**$^{\mathbf{Me}}$ in mixtures of oligomers of various chain lengths obtained by anionic ROP of dimethylsila[1]ferrocenophane.[30]

Table 3-1-2. Crystal and Structural Refinement Data for Compounds **6a**, **7**$^{\mathbf{Me}}$, and **7**$^{\mathbf{Et}}$.

	6a	**7**$^{\mathbf{Me}}$	**7**$^{\mathbf{Et}}$
empirical formula	$C_{28}H_{30}AlFe_2Nsi$	$C_{22}H_{24}Fe_2Si$	$C_{24}H_{28}Fe_2Si$
fw	547.30	428.20	456.25
cryst. size / mm^3	0.21 × 0.21 × 0.01	0.32 × 0.14 × 0.06	0.30 × 0.24 × 0.06

cryst. system, space group	triclinic, $P\bar{1}$	monoclinic, $P2_1/n$	triclinic, $P\bar{1}$
Z	4	4	2
a / Å	10.6268(9)	8.0197(3)	7.4304(4)
b / Å	12.8724(10)	22.8843(6)	10.6917(5)
c / Å	18.6478(17)	10.1397(4)	13.0227(6)
α / °	88.174(7)	90	80.412(4)
β / °	82.917(7)	90.662(3)	81.259(4)
γ / °	87.039(7)	90	86.783(4)
volume / Å^3	2527.2(4)	1860.77(11)	1007.77(9)
ρ_{calc} / mg m^{-3}	1.438	1.529	1.504
temperature / K	100	100	100
$\mu_{calc.}$/ mm^{-1}	1.25	1.63	1.51
θ range / °	1.6 – 25.0	1.8 – 25.0	1.6 – 25.0
reflns collected / unique	13945 / 6615	17039 / 3277	10498 / 3546
absorption correction	multiscan	multiscan	multiscan
data / restraints / params	6615 / 94 / 599	3277 / 0 / 228	3546 / 0 /246
goodness-of-fit	0.581	1.036	0.880
R_1 [I > 2 σ(I)][a]	0.0421	0.0202	0.0255
wR_2 (all data)[a]	0.0886	0.0495	0.0576
largest diff. peak and hole, $\Delta\rho_{elect}$ / e Å^{-3}	0.28, −0.23	0.33, −0.24	0.41, −0.35

[a] $R_1 = [\Sigma||F_o|-|F_c||]/[\Sigma|F_o|]$ for $[F_o^2 > 2\sigma(F_o^2)]$, $wR_2 = \{[\Sigma w(F_o^2-F_c^2)^2]/[\Sigma w(F_o^2)^2]\}^{1/2}$ [all data].

All bis(ferrocenyl) species have been characterized by NMR spectroscopy, mass spectrometry, and elemental analysis. Furthermore, the molecular structures of the aluminum species **6a** and the two silanes **7^{Me}** and **7^{Et}** were solved by single-crystal X-ray analyses (Figure 3-1-3 and 3-1-4; Table 3-1-2).[31] All four aluminum- and gallium-containing bis(ferrocenyl) compounds (**5a**, **5b**, **6a**, **6b**) show pattern in ^{1}H and ^{13}C NMR spectra consistent with time-averaged C_s symmetrical molecules. Recently, we

characterized species (Mamx)EFc_2 [E = Al (**8a),** Ga (**8b**)] to better understand the structure and properties of respective poly(ferrocene)s equipped with the same bridging units.[22a] Similar to the species of type **5** and **6**, compounds **8a** and **8b** exhibit a plane of symmetry in solution, which can be explained with fast rotations of both Fc moieties. Expectedly, the Fc groups in the two silanes $\mathbf{7^{Me}}$ and $\mathbf{7^{Et}}$ also rotate fast, so that signal patterns in NMR spectra can be interpreted by assuming C_{2v} symmetrical species on time average. As mentioned before, species $\mathbf{7^{Me}}$ was isolated before and our NMR data matches those reported.[30]

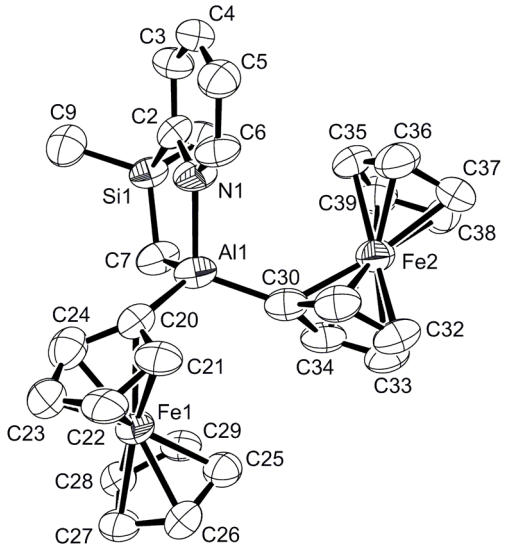

Figure 3-1-3. Molecular structure of **6a** with thermal ellipsoids at the 50% probability level. Hydrogen atoms are omitted for clarity. Selected atom-atom distances [Å] and bond angles [º] for **6a** (values in braces refer to the second independent molecule that is not shown): Al1-N1 = 2.000(7) {2.034(7)}, Al1-C7 = 1.977(8) {1.980(7)}, Al1-C20 = 1.962(9) {1.962(9)}, Al1-C30 = 1.930(9) {1.950(8)}, Al1···Fe1 = 3.416(3) {3.403(3)}, Al1···Fe2 = 3.667(3) {3.680(3)}, Fe1···Fe2 = 6.045(2) {6.125(2)}, C7-Al1-C20 = 115.3(4) {114.8(3)}, C7-Al1-C30 = 117.1(3) {118.4(3)}, C7-Al1-N1 = 96.1(3) {94.8(3)}, N1-Al1-C20 = 106.8(3) {106.4(3)}, N1-Al1-C30 = 108.1(3) {108.4(3)}, C20-Al1-C30 = 111.5(3) {111.7(3)}, Al1- C20-$Centr^{C20\text{-}C24}$ = 166.7(5) {168.1(5)}, Al1-C30-$Centr^{C30\text{-}C34}$ = 177.2(6) {176.3(6)}.

Figure 3-1-3 depicts the molecular structure of one of the two crystallographically independent molecules of **6a**. The covalent bonds around the aluminum have a similar length as those of the aluminum-bridged [1.1]FCP **4a** (Figure 3-1-2). The most interesting aspect of the molecular structure of **6a** is the different degree of bending the two Fc moieties toward aluminum. Such a bending has been described for boryl-substituted ferrocenes ($FcBX_2$) and was expressed with a dip angle α* (Figure 3-1-5).[32,33] In species **6a**, the Fc moiety (Fe2) close to the pyridyl group exhibits dip angles α* of only 2.8(6) and 3.7(6)º, respectively, whereas the other Fc moiety (Fe1) exhibits dip angles α* of 13.3(5) and 11.9(5)º, respectively (Figure 3-1-3). For borylferrocenes, α* decreases with decreasing Lewis acidity of the boryl group. Within this series, Br_2BFc showed the largest experimentally determined α* angles of 17.7 and 18.9º for two crystallographically independent molecules.[32,34] The dip angles of 11.9(5) and 13.3(5)º found for **6a** are comparable to those determined for Me_2BFc (α* = 13.0º) and (HO)MeBFc (α* = 10.3, 10.8, and 12.9º).[32] Recently, the silicon cation *t*BuMeSiFc^+ was characterized crystallographically, showing an extreme dip angle of 44.8°[35], which is significantly larger than that of the well-known species Ph_2CFc^+ (α* = 20.7°).[36] For the known systems, it has been shown that the bending is caused by a direct bonding interaction between the Lewis-acid atom and iron.[32,37] For the strongly bent silicon moiety in *t*BuMeSiFc^+, a 3c-2e bond between silicon, iron, and one of the carbon atoms of the unsubstituted Cp ring was discussed.[35]

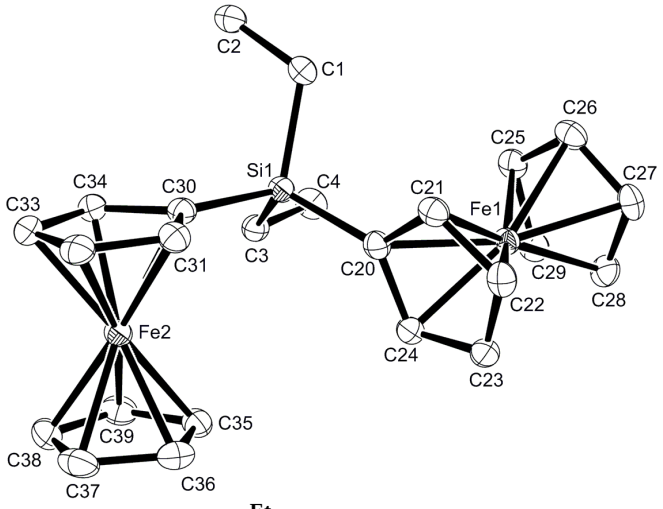

Figure 3-1-4. Molecular structure of $\mathbf{7^{Et}}$ with thermal ellipsoids at the 50% probability level. Hydrogen atoms are omitted for clarity. For a thermal ellipsoid plot of $\mathbf{7^{Me}}$ see Figure S2. Selected atom-atom distances [Å] and bond angles [º] for $\mathbf{7^{Et}}$ (respective values of $\mathbf{7^{Me}}$ given in braces): Si1-C1 = 1.880(2) {1.8677(17)}, Si1-C3 = 1.876(2) {1.8646(17)}, Si1-C20 = 1.861(2) {1.8580(16)}, Si1-C30 = 1.866(2) {1.8681(16)}, Si1···Fe1 = 3.5765(7) {3.4804(5)}, Si1···Fe2 = 3.5162(7) {3.5412(5)}, Fe1···Fe2 = 6.1409(6) {6.3150(4)}, C1-Si1-C3 = 111.23(10) {109.23(8)}, C1-Si1-C20 = 108.51(10) {109.10(8)}, C1-Si1-C30 = 108.49(9) {108.49(7)}, C3-Si1-C20 = 114.47(10) {112.17(7)}, C3-Si1-C30 = 106.47(9) {111.91(7)}, C20-Si1-C30 = 107.44(9) {105.81(7)}. Si1-C20-Centr$^{C20\text{-}C24}$ = 176.31(15) {177.78(12)}, Si1-C30-Centr$^{C30\text{-}C34}$ = 178.57(17) {177.88(12)}.

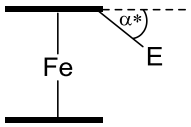

Figure 3-1-5. Definition of the dip angle $\alpha^* = 180 - \alpha(Cp^{centr}–C^{ipso}–E)$.[32]

As expected, molecular structures of both bis(ferrocenyl)silanes $\mathbf{7^{Me}}$ and $\mathbf{7^{Et}}$ are very similar (Figure 3-1-4). Silicon atoms like those in $\mathbf{7^{Me}}$ and $\mathbf{7^{Et}}$ should not exhibit any significant Lewis acidity and bending toward the Fc moieties is not expected, an expectation that is confirmed by measured α* angles of only 2.12(12) and 2.22(12)º for $\mathbf{7^{Me}}$, and 1.43(17) and -3.69(15)º for $\mathbf{7^{Et}}$.

Electrochemistry. The redox behavior of the [1.1]FCPs **4** and the bis(ferrocenyl) species **5**, **6**, **7**, and **8** were investigated with cyclic voltammetry (CV) using CH_2Cl_2 and thf, respectively, as solvents (Table 3-1-3).[38] While all gallium and silicon compounds gave meaningful and interpretable data (Table 3-1-3), all aluminum compounds were problematic with the exception of **8a**. The CVs for [1.1]FCPs should provide two, distinct redox couples, whose formal potential separation is dictated by the extent to which the presence of a charge on one ferrocene perturbs the redox potential of the neighboring centre. Furthermore, assuming that 1) the diffusion coefficients for the three redox forms (neutral molecule, monovalent cation and the divalent cation) of the [1.1]FCPs are not significantly different, 2) each redox couple has a transfer coefficient close to 0.5, and 3) each redox event corresponds to a single-electron transfer reaction, then it is expected that each individual redox event should provide identical peak currents when isolated from all other current contributions.[39] The gallium-bridged species **4b** shows precisely this behavior with two redox events ($\Delta E^{o\prime}$ = 0.309 V) and corrected peak heights that are essentially identical in magnitude. A cursory inspection of the CV for the aluminum compound **4a** (Figure 3-1-6a) seems comparable as two main redox events are clearly evident. However, a more detailed inspection reveals the presence of two small, additional, reduction waves (ca. -0.4 V and -0.6 V). The peak current of the second oxidation wave is also seen to be much larger than that of the first oxidation wave. Cumulatively, these features indicate poorer electrochemical stability of the aluminum compound and/or the presence of electroactive impurities in the samples. Nevertheless, if one interprets the four main peaks in the CV of **4a** as being caused by the ferrocene moieties of **4a**, then the splitting between the two formal potentials $\Delta E^{o\prime}$ amounts to 0.332

V. This splitting is similar to that of the gallium compound **4b** ($\Delta E^{o\prime}$ = 0.309 V), but its voltammetry needs to be taken with some caution for the reasons described above. As mentioned in the introduction, the known aluminum [1.1]FCP **1a**, in contrast to its gallium counterpart **1b** (Chart 3-1-3), showed significantly different CVs (CH_2Cl_2 / [*n*Bu_4N][PF_6]).[8b] While the gallium species **1b** displayed the expected *two* one-electron redox events ($\Delta E^{o\prime}$ = 0.30 V) the aluminum species **1a** displayed only *one* two-electron redox event.[8b] The published formal potential for the aluminum species at 0.36 V with respect to Ag/AgCl is where that of ferrocene is expected,[8b] indicating that a complete removal of the bridging moieties had taken place.[39] A reinvestigation of the CV of species **1a** in CH_2Cl_2 with [*n*Bu_4N][PF_6] has shown that, in contrast to the published results, it displays two main redox event. However, as in the case of compound **4a**, the recorded CV peak heights were unequal. Using the electrolyte [*n*Bu_4N][$B(C_6F_6)_4$] with a weakly coordinating anion again gave a highly asymmetrical CV, now with an expected larger splitting between the main redox events (see Figures S42 and S43).[40,41] The second pair of redox waves is right were the FcH/FcH^+ appears and it is very likely that at least some of the increased current is due to the presence of ferrocene. Aluminum species, compared to respective gallium species, are much more sensitive and we speculate that small amounts of fluoride ions or residual water from the electrolyte and solvent are causing degradation. In 2008, similar observations were made for the related [1.1]chromarenophanes and [1.1]molybdarenophanes: only the gallium-bridged species gave reproducible results, while measurements of the aluminum species showed the presence of significant amounts of the parent bis(benzene) complexes.[23]

Table 3-1-3. Measured Formal Potentials versus FcH/FcH^+ [V] of [1.1]FCPs and Bis(ferrocenyl) Species (0.1 M nBu$_4$N[PF_6]; Scan Rate of 50 mV/s).

	$E^{o\prime}$	$E^{o\prime}$	$\Delta E^{o\prime}$	Fe···Fe / Å[a]
4b (CH_2Cl_2)	-0.049	0.260	0.309	5.4277(8)[b]
4b (thf)	-0.091	0.127	0.218	
5b (CH_2Cl_2)	-0.002	0.136	0.138	---
5b (thf)		0.224	0	
6b (CH_2Cl_2)	0.117	0.256	0.139	---
6b (thf)		0.066	0	
$\mathbf{7^{Me}/7^{Et}}$ (CH_2Cl_2)	0.071/0.128	0.257/0.332	0.186/0.204	6.3150(4)/6.1409(6)[b]
$\mathbf{7^{Me}/7^{Et}}$ (thf)		0.176/0.191	0/0	
8a (CH_2Cl_2)	-0.032	0.135	0.167	5.6833(7)[c]
8a (thf)		0.079	0	
8b (CH_2Cl_2)	0.044	0.201	0.157	5.5944(9)[c]
8b (thf)		0.200	0	

[a] values from single-crystal X-ray structure determinations; see text for discussion. [b] this work. [c] taken from ref. 22a.

As shown in Table 3-1-3, the measured $\Delta E^{o\prime}$ values for the bis(ferrocenyl) species were found in the range 0.138 – 0.167 V and are significantly smaller compared to those of the [1.1]FCPs **4a** and **4b**. The largest splitting was found for the aluminum compound **8a** ($\Delta E^{o\prime}$ = 0.167 V), which was the only aluminum species in this study that gave an expected CV (Figure 3-1-7). The CV of the respective gallium compound **8b** looks very similar with a slightly smaller $\Delta E^{o\prime}$ value of 0.157 V (Figure 3-1-7).

Geiger et al. systematically investigated the medium effect on the splitting $\Delta E^{o\prime}$ and has shown that for electrochemically generated cations, solvents of low polarity and low donor number (DN)[42] cause the largest values of $\Delta E^{o\prime}$.[40,41] To test if the solvent effect[43] also holds true for the compounds described here, CH_2Cl_2 and thf solutions were

investigated for all species. Furthermore, as aluminum species can be sensitive toward chlorinated solvents, we wanted to find out if thf improves the appearance of CVs; however, this was not the case. As expected, all $\Delta E^{o\prime}$ values were significantly reduced by changing from CH_2Cl_2 (DN = 0) to thf (DN = 20) (Table 3-1-3).[40,41] Whereas the [1.1]FCP **4b** still showed resolved waves, all other species listed in Table 3-1-3 displayed only one redox wave. The $\Delta E^{o\prime}$ value of the [1.1]FCP **4b** diminished from 0.309 V (CH_2Cl_2) to 0.218 V (thf). As the splitting between formal potentials of the bis(ferrocenyl) species is already small in CH_2Cl_2, it is not surprising that it is absent in thf solutions.[44]

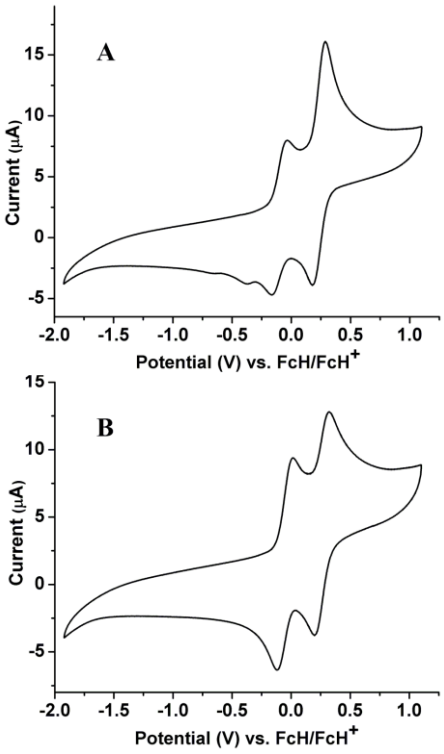

Figure 3-1-6. Cyclic voltammograms of **4a** (A) and **4b** (B) (CH_2Cl_2; 0.1 M [nBu$_4$N][PF$_6$]; scan rate = 50 mV/s).

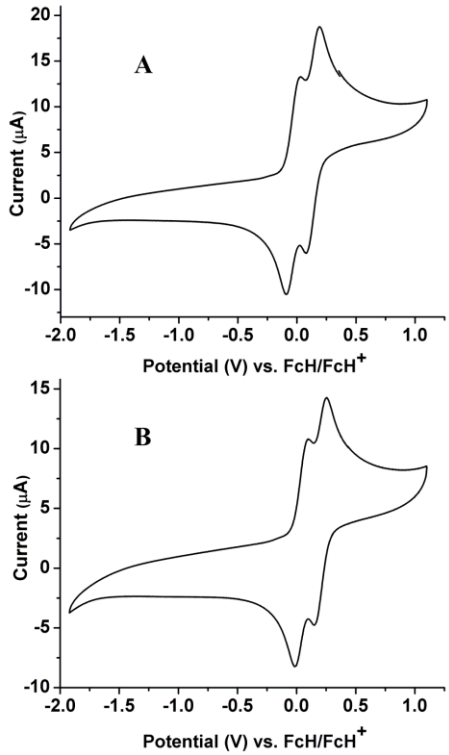

Figure 3-1-7. Cyclic voltammograms of **8a** (A) and **8b** (B) (CH_2Cl_2; 0.1 M [nBu$_4$N][PF_6]; scan rate = 50 mV/s).

As mentioned above, the only aluminum species that exhibited expected two, one-electron oxidations in the CV was compound **8a** (Figure 3-1-7). The overall shape of its CV is very similar to that of the gallium compound **8b** (Figure 3-1-7). While the aluminum compound **8a** gets oxidized at lower potentials compared to its gallium analogue **8b**, their $\Delta E^{o\prime}$ values are very similar (**8a**: 0.167 V; **8b**: 0.157 V; Table 3-1-3). Aluminum is significantly less electronegative compared to gallium, resulting in an increase of the electron density on the ferrocenyl moieties, explaining the increased ease by which **8a** gets oxidized compared to **8b** [Allred-Rochow electronegativities:[45] 1.47 (Al), 1.82 (Ga)].

Why is compound **8a** the only electrochemically well-behaved aluminum species in our study? All the aluminum and gallium compounds were equipped with intramolecularly coordinating ligands (Chart 3-1-2). The Mamx ligand stands out as the only ligand used that carries a bulky group in the vicinity of the group 13 element. This *t*Bu group in *ortho* position of the Mamx ligand is directed toward the fifth coordination site on the group 13 element and, hence, provides steric protection. For example, in contrast to the bis(ferrocenyl) species **6a** (Figure 3-1-3), the ferrocenyl units of species **8a** and **8b** are not bent *toward* the group 13 element, but *away* from it (e.g., **8a**: $\alpha^* = 9.11°$).[22a] One can assume that the fifth coordination site of the group 13 elements is of key importance for any substitution reaction, including hydrolysis, as a Lewis acid-base adduct will likely form first. We speculate that this extra protection provided by the *ortho*-*t*Bu group of the Mamx ligand efficiently suppresses any unwanted reactions during the electrochemical measurement.

Chart 3-1-4. Two Conformers of (Mamx)EFc_2 [E = Al (**8a**), Ga (**8b**)][22a]

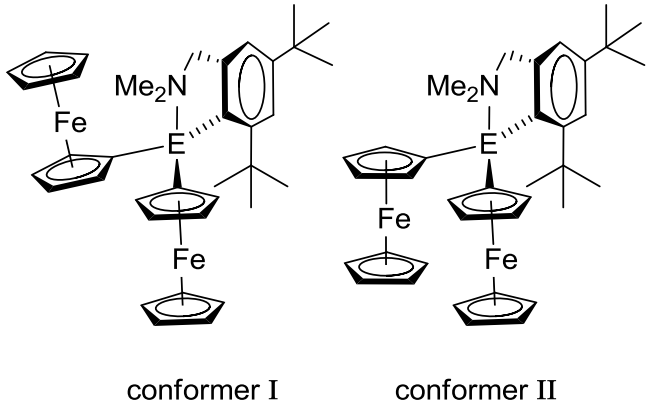

conformer I conformer II

Recently, a comprehensive study on the electronic coupling in bis(ferrocene) species of the type $(Cp^*FeC_5H_4)ER_2$ with bridging moieties ER_2 of CMe_2, $SiMe_2$, and $GeMe_2$ was undertaken.[46] From the analysis of the intervalence charge-transfer band of the mixed-valence monocations $(Cp^*FeC_5H_4)ER_2^+$ is was revealed that the coupling decreases in the order of C > Si > Ge. The $\Delta E^{o\prime}$ values (thf / $[n\text{Bu}_4\text{N}][PF_6]$), determined by square-wave voltammetry, showed the same trend with [0.113 (C), 0.093 (Si), and 0.073 (Ge) V], which is consistent with Fe···Fe distances. The authors concluded that an electrostatic through-space and not a through-bond mechanism was operative.[46] As mentioned before, species $\mathbf{7^{Me}}$ is a known species[28,30] and was investigated with electrochemical methods before.[47,30] The published $\Delta E^{o\prime}$ value of 0.15 V were determined using a 1:1 solvent mixture of CH_2Cl_2 and MeCN and $[n\text{Bu}_4\text{N}][PF_6]$ as the electrolyte.[30] Our value for $\mathbf{7^{Me}}$ in CH_2Cl_2 is with 0.186 V (Table 3-1-3) expectedly higher. We also determined the CV of $\mathbf{7^{Me}}$ in MeCN (Figure S35) and found a splitting value $\Delta E^{o\prime}$ of 0.15 V, identical to the published value of 0.15 V in CH_2Cl_2/MeCN. The $\Delta E^{o\prime}$ values of $\mathbf{7^{Me}}$ and $\mathbf{7^{Et}}$ are with 0.186 and 0.204 V (Table 3-1-3), respectively, similar and slightly larger than those measured for the gallium species **5b**, **6b**, and **8b** ($\Delta E^{o\prime}$ = 0.138 – 0.159 V) and of the aluminum species **8a** ($\Delta E^{o\prime}$ = 0.167 V). Table 3-1-3 also lists the Fe···Fe distances known from single-crystal X-ray analysis. For the silicon species, exhibiting the largest $\Delta E^{o\prime}$ values, the Fe···Fe distances are significantly larger ($\mathbf{7^{Me}}$: 6.3150(4) Å; $\mathbf{7^{Et}}$: 6.1409(6) Å) than those found for the Mamx-containing aluminum and gallium species [**8a**: 5.6833(7) Å; **8b**: 5.5944(9) Å]. The only other bis(ferrocenyl) species for which the molecular structure could be determined in the solid state was the aluminum compound **6a** (Figure 3-1-3) and Fe···Fe distances of 6.045(2) and 6.125(2) Å for two independent

molecules were found. The covalent radii of Al and Ga are nearly identical and one can assume that the Fe···Fe distance in **6b** is very similar to those determined for **6a**. The gallium compound **6b** showed with 0.139 V one of the smallest $\Delta E^{o\prime}$ values (Table 3-1-3). Of course, the Fe···Fe distances discussed so far are not necessarily identical to those present in solution. As evident from NMR spectra of all bis(ferrocenyl) species, both Fc units rotate fast and one could imagine that Fe···Fe distances vary depending on the relative orientation of the two Fc moieties. For the Mamx-containing species two different conformers were found in the solid state (Chart 3-1-4). While the aluminum species **8a** showed the Fc moieties pointing in opposite directions (conformer I) those of the gallium species **8b** were approximately parallel to each other (conformer II).[22a] However, the Fe···Fe distances in both species were very similar [**8a**: 5.6833(7) Å; **8b**: 5.5944(9) Å], which indicates that rotations of Fc moieties do not alter the Fe···Fe distances significantly. Overall, there is no obvious correlation between the Fe···Fe distances and $\Delta E^{o\prime}$ values of the bis(ferrocenyl) species equipped with different bridging moieties (Table 3-1-3).

The $\Delta E^{o\prime}$ values of the [1.1]FCP **4b** and the bis(ferrocenyl) compound **5b**, both equipped with the same bridging moiety, are significantly different (**4b**: 0.309 V; **5b**: 0.138 V). While the Fe···Fe distance in **4b** could be determined that of species **5b** is unknown. However, the Fe···Fe distance of the closely related compound **8b** was found to be 5.5944(9) Å (Table 3-1-3),[22a] which is very similar to 5.4277(8) Å measured for the [1.1]FCP **4b** (Figure 3-1-2; Table 3-1-3). Obviously, the huge difference in $\Delta E^{o\prime}$ values cannot be rationalized on the basis of Fe···Fe distances. As pointed out earlier, the relative orientations of the two fc units of [1.1]FCPs (e.g. **4b**) are fixed, while the Fc

moieties of bis(ferrocenyl) compounds (e.g. **5b**) can freely rotate. We speculate that the flexibility in bis(ferrocenyl) compounds allows for an effective solvation of both Fc moieties, resulting in an effective screening of positive charges. In contrast, the solvation of [1.1]FCPs will be less effective as a solvent penetration between both fc moieties will be hindered; hence, the electrostatic interaction between the two iron centers in the monocations will be stronger than in bis(ferrocenyl) compounds, giving larger $\Delta E^{o\prime}$ values. In addition, in conformer I of bis(ferrocenyl) compounds (Chart 3-1-4) one Cp moiety is in between the two Fe atoms, a scenario that is not possible for [1.1]FCPs. It is feasible that this extra electron density provided by the Cp ligand also contributes to the screening of charges.

SUMMARY AND CONCLUSION

The two new [1.1]FCPs **4a** (Al) and **4b** (Ga) could be prepared and crystallized as *anti* isomers. As expected, their structures are very similar to the known [1.1]FCPs (**1a**, **1b**; Chart 3-1-3). Ferrocenyl-substituted aluminum and gallium compounds are rare.[48] The new bis(ferrocenyl) compounds of aluminum (**5a**, **6a**) and gallium (**5b**, **6b**) equipped with two different ligands capable of intramolecular donation were prepared. Only the aluminum compound **6a** gave crystals of sufficient quality that allowed a structure determination by X-ray crystallography (Figure 3-1-3). One of the two Fc units in species **6a** is significantly bent toward the open coordination site of aluminum [dip angle α* = 13.3(5) and 11.9(5)º]. Such an effect is well-known for boron compounds and other species with Lewis-acidic moieties in this *pseudo* benzylic position, but had never been observed for aluminum compounds. The bending of a Fc unit in **6a** illustrates that the aluminum atom still possess Lewis-acidity despite being four-fold coordinated.

The bis(ferrocenyl) species **5a**, **5b**, **6a**, and **6b** were prepared so that Fe-Fe interactions could be investigated and compared with those in the related [1.1]FCPs **4a** and **4b**. The series of CV measurements also included the recently published bis(ferrocenyl) compounds (Mamx)EFc_2 [**8a** (Al), **8b** (Ga)] and the known aluminum-bridged [1.1]FCP **1a** (Chart 3-1-3). In order to include bis(ferrocenyl) species with saturated bridging moieties, the silanes R_2SiFc_2 [R = Me (**7^{Me}**), Et (**7^{Et}**)] were prepared and their CVs were determined. While all gallium and silicon compounds gave meaningful and interpretable data (Table 3-1-3), all aluminum compounds were problematic with the exception of **8a** (Chart 3-1-4, Figure 3-1-7). The fact that **8a** was the only well-behaved aluminum species is probably due to the steric protection of the Lewis-acid aluminum atom by the bulky Mamx ligand, which suppresses unwanted degradation reactions. The degree of splitting between formal potentials of bis(ferrocenyl) compounds **5b**, **6b**, **7^{Me}**, **7^{Et}**, **8a**, and **8b** varied between 0.138 – 0.204 V ($\Delta E^{o\prime}$ in CH_2Cl_2; Table 3-1-3).

Recently, it had been shown that for group-14-bridged bis(ferrocenyl) compounds a through-space coupling is operative and, hence, through-bond coupling is relatively unimportant.[46] In this study, a qualitative correlation between $\Delta E^{o\prime}$ values and Fe···Fe distances was found: the larger the distances, the smaller the $\Delta E^{o\prime}$ values. Our $\Delta E^{o\prime}$ values measured for the two silanes **7^{Me}** and **7^{Et}** seem to support such a correlation, if Fe···Fe distances found in the solid state are indicative of Fe···Fe distances in solution: species **7^{Et}** with the *smaller* Fe···Fe distance gave the *stronger* interaction (Table 3-1-3). Structural evidence suggests that Fe···Fe distances in bis(ferrocenyl) aluminum and gallium species are *shorter* than in the silicon compounds **7^{Me}** and **7^{Et}**, but their $\Delta E^{o\prime}$ values are *smaller*. Geiger et al. performed a comprehensive study of solvent and

electrolyte effects on $\Delta E^{o\prime}$ values by keeping the analyte constant.[40,41] For electrochemically produced cations, $\Delta E^{o\prime}$ can be maximized by applying solvents of low polarity and low donor number and a weakly ion-pairing electrolyte anion. We investigated a series of different species under the same conditions, where all the electrochemically produced cations were different. Therefore, for all cations the overall effects of ion pairing and solvation must be different. All the seemingly similar bis(ferrocenyl) compounds are, with respect to all the factors that govern the splitting between formal potentials, too different and a correlation of $\Delta E^{o\prime}$ with Fe···Fe distances cannot be expected.

The splitting between formal potentials in [1.1]FCPs is significantly larger than in related (ferrocenyl) compounds, even though the Fe···Fe distances are similar [e.g, $\Delta E^{o\prime}$ = 0.309 (**4b**), 0.138 (**5b**) V]. It might be that the flexibility in bis(ferrocenyl) compounds allows for an effective solvation of both Fc moieties, resulting in an effective screening of positive charges leading to a small $\Delta E^{o\prime}$. However, in the absence of additional data, the latter statement remains speculative.

EXPERIMENTAL SECTION

Syntheses. All syntheses were carried out using standard Schlenk and glovebox techniques. Solvents were dried using an MBraun Solvent Purification System and stored under nitrogen over 3 Å molecular sieves. All solvents for NMR spectroscopy were degassed prior to use and stored under nitrogen over 3 Å molecular sieves. ^{1}H and ^{13}C NMR spectra were recorded on a 500 MHz Bruker Avance NMR spectrometer at 25 ºC

in C_6D_6 and $CDCl_3$, respectively. ^1H chemical shifts were referenced to the residual protons of the deuterated solvents (δ 7.15 for C_6D_6 and 7.26 for $CDCl_3$); ^{13}C chemical shifts were referenced to the C_6D_6 signal at δ 128.00 and $CDCl_3$ signal at δ 77.00. Mass spectra were measured on a VG 70SE and were reported in the form *m/z* (rel intens) [M^+] where '*m/z*' is the mass observed, 'rel intens' is intensity of the peak relative to the most intense peak and 'M^+' is the molecular ion or fragment; only characteristic mass peaks are reported. Elemental analyses were performed on a Perkin Elmer 2400 CHN Elemental Analyzer using V_2O_5 to promote complete combustion.

Note that small amounts of ferrocene ($FeCp_2$) were present in the isolated products **4a**, **4b**, **5a**, **5b**, **6a**, and **6b**; complete removal of this impurity was not successful. The three aluminum species show larger amounts of ferrocene impurities compared to their gallium counterparts (see NMR spectra in the Supporting Information). Elemental analysis gave carbon values for all **4a**, **5a**, and **6a** below their calculated amounts. The difficulties to obtain analytically pure aluminum species reflect their higher sensitivity toward hydrolysis compared to respective gallium compounds.

Reagents. The compounds $(LiC_5H_4)Fe(C_5H_5)$ (LiFc),[29] $(LiC_5H_4)_2Fe{\cdot}2/3tmeda$[49], 2-(trimethylsilyl)pyridine,[50] and **2b**[19a] were synthesized according to literature procedures. The known species 1-bromo-4-[(dimethylamino)methyl]benzene[51] and 1-[(dimethylamino)methyl]-4-trimethylsilylbenzene[52] were synthesized according to the published procedures with small alterations (see Supporting Information). $AlCl_3$ (98%), ferrocene (98%), *n*BuLi (2.8 M in hexanes), *t*BuLi (1.7 M in pentane), Me_3SiCl (98%) and C_6D_6 (99.6 atom % D) were purchased from Sigma Aldrich; $AlCl_3$ was sublimed prior to use. $GaCl_3$ (Alfa Aesar; 99.999%), 2-bromopyridine (Alfa Aesar; 99%) and 1-

bromo-4-(bromomethyl)benzene (Alfa Aesar; 99%) were purchased from VWR. N,N,N',N'-tetramethylethylenediamine (Acros Organics; 99%) was purchased from Fisher Scientific.

Electrochemical measurements. A computer controlled system, consisting of a HEKA potentiostat PG590 (HEKA, Mahone Bay, NS, Canada) was used for the cyclic voltammetry experiments. Data was collected using a multifunction DAQ card (PCI 6251 M Series, National Instruments Austin, Texas) and in-house software written in the LabVIEW environment. Glassy carbon (BAS, 3 mm) was used as the working electrode. The quasi-reference electrode (QRE) was a silver wire and all measurements were made against the QRE. A coiled gold wire was used as the auxiliary electrode. Before each measurement, 1 mM solutions of samples were freshly prepared in dry organic solvent with 0.1 M [*n*Bu_4N][PF_6] as the supporting electrolyte. The electrolyte was dried overnight under high vacuum at 100 °C before. The scan rate for the CVs reported was 50 mV/s. The measurements were conducted inside a glovebox and taken at ambient temperature.

Synthesis of dichloro{2-[(dimethylamino)methyl]-5-(trimethylsilyl)phenyl-κ^2*C,N*}alumane (2a). *t*BuLi (1.7 M in pentane), 9.8 mL, 17 mmol) was added dropwise to a cold (0 °C) solution of 1-[(dimethylamino)methyl]-4-trimethylsilylbenzene (3.55 g, 15.1 mmol) in hexane (40 mL). The reaction mixture was warmed up to r.t. and stirred for 16 h, yielding a pale yellow solution with a white precipitate. The solid lithium salt was filtered off and dried under high vacuum (2.24 g, 10.5 mmol). Et_2O (30 mL) was added to the white solid, resulting a slurry which was cooled down to -78 °C. The cold slurry was added dropwise to a cold (-78 °C) solution of $AlCl_3$ (1.39 g, 10.4 mmol) in

Et_2O (40 mL). The reaction mixture was warmed up to r.t. and stirred for 16 h, resulting in a pale yellow solution with a white precipitate. The solid was filtered off and all volatiles were removed under high vacuum. Sublimation (110 °C, high vacuum) yielded analytically pure product **2a** as a colorless crystalline solid (2.33 g, 73%). ^{1}H NMR (C_6D_6): δ 0.26 (s, 9H, $SiMe_3$), 1.90 (s, 6H, NMe_2), 2.97 (s, 2H, CH_2), 6.75 (d, 1H, C_6H_3), 7.45 (d, 1H, C_6H_3), 7.91 (s, 1H, C_6H_3). ^{13}C NMR (C_6D_6): δ -1.09 ($SiMe_3$), 45.35 (CH_2), 64.72 (NMe_2), 125.06, 134.86, 140.64, 141.097 (C_6H_3). MS (70 eV, EI): m/z (rel intens) 303 (15) [M^+], 288 (100) [M^+ - Me], 272 (16) [$C_{10}H_{13}AlCl_2NSi^+$], 245 (18) [$C_9H_{12}AlCl_2Si^+$]. HRMS (EI; m/z): calcd for $C_{12}H_{20}AlCl_2NSi$, 305.0528; found, 305.0521. Anal. Calcd for $C_{12}H_{20}AlCl_2NSi$ (304.27): C, 47.37; H, 6.63; N, 4.60. Found: C, 47.39; H, 6.55; N, 4.61.

Synthesis of dichloro{[dimethyl(2-pyridyl)silyl]methyl-*κ*^{2}*C,N*}alumane (3a). *t*BuLi (1.7 M in pentane, 11.8 mL, 20.1 mmol) was added dropwise to a solution of 2-(trimethylsilyl)pyridine (2.89 g, 19.1 mmol) in Et_2O (30 mL) at -78°C. After 40 min of stirring at -78°C, a suspension of $AlCl_3$ (2.44 g, 18.3 mmol) in Et_2O (30 mL) was added slowly at -78°C. It was stirred for 16 h at r.t. and then the solvent was removed under vacuum. The product was dissolved in toluene (35 mL) and the precipitate was filtered off and washed with toluene (10 x 5 mL). All volatile were removed at high vacuum at 90 °C and crystallization from toluene (5 mL) yielded colorless crystals of **3a** (2.60 g, 47%). ^{1}H NMR (C_6D_6): δ -0.32 (s, 2H, CH_2), 0.02 (s, 6H, $SiMe_2$), 6.27 (m, 1H, Ar-H), 6.70 (m, 2H, Ar-H), 8.28 (m, 1H, Ar-H). ^{13}C NMR (C_6D_6): δ -0.60 (CH_2), 1.36 ($SiMe_2$), 124.92, 130.29, 139.35, 146.91, 171.05 (C_5H_4N). MS (70 eV, EI): m/z (rel intens) 247 (7) [M^+], 232 (100) [M^+ - Me], 212 (11) [M^+ - Cl], 151 (11) [MH^+ - $AlCl_2$], 150 (15) [M^+ - $AlCl_2$],

106 (14) [$C_5H_4NSi^+$]. HRMS (EI; m/z): calcd for $C_8H_{12}Cl_2AlNSi$, 248.9902; found, 248.9901. Anal. Calcd for $C_8H_{12}AlCl_2NSi$ (248.16): C, 38.72; H, 4.87; N, 5.64. Found: C, 39.66; H, 5.32, N, 5.51.

Synthesis of dichloro{[dimethyl(2-pyridyl)silyl]methyl-κ^2*C,N*}gallium (3b). *t*BuLi (1.7 M in pentane, 8.60 mL, 14.6 mmol) was added dropwise to a solution of 2-(trimethylsilyl)pyridine in Et_2O (25 mL) at -78 °C. After 40 min at -78 °C the solution was slowly added to a solution of $GaCl_3$ (2.38 g, 13.5 mmol) in Et_2O (35 mL) at -78 °C. After the reaction mixture was stirred for 16 h at r.t., all volatiles were removed under vacuum. The crude product was dissolved in toluene (40 mL) and the precipitate was filtered off and washed with toluene (4 x 10 mL). Sublimation (120 °C; high vacuum) gave **3b** as a colorless crystalline product (2.00 g, 50%) that contained only very minor impurities. Analytically pure product (1.36 g, 35%) was obtained by crystallization from toluene (4 mL). Crystals suitable for single-crystal X-ray analysis were obtained from toluene solution at -25 ºC. ^{1}H NMR (C_6D_6): δ -0.07 (s, 2H, CH_2), -0.02 (s, 6H, $SiMe_2$), 6.42 (m, 1H, Ar-H), 6.77 (d, 1H, Ar-H), 6.82 (m, 1H, Ar-H), 8.41 (d, 1H, Ar-H). ^{13}C NMR (C_6D_6): δ -6.83 (CH_2), -1.11 ($SiMe_3$), 125.50, 130.28, 139.24, 146.80, 167.22 (C_5H_4N). MS (70 eV, EI): m/z (rel intens) 291 (7) [M^+], 276 (100) [M^+ - Me], 256 (54) [M^+ - Cl], 170 (11) [$(NC_5H_4)SiMeCH_2Cl^+$], 149 (14) [$C_8H_7NSi^+$], 120 (16) [$C_6H_6NSi^+$], 106 (12) [$C_5H_4NSi^+$], 92 (11) [$C_5H_4Si^+$], 91 (15) [$C_5H_3Si^+$], 69 (14) [Ga]. HRMS (EI; m/z): calcd for $C_8H_{12}Cl_2GaNSi$, 290.9363; found, 290.9350. Anal. Calcd for $C_8H_{12}Cl_2GaNSi$ (290.90): C, 33.03; H, 4.16; N, 4.81. Found: C, 33.82; H, 4.33; N, 4.61.

Synthesis of bis({2-[(dimethylamino)methyl]-5-(trimethylsilyl)phenyl-κ^2*C,N*}alumina)[1.1]ferrocenophane (4a). A solution of **2a** (0.710 g, 2.33 mmol) in

Et_2O (30 mL) was added dropwise to a slurry of $(LiC_5H_4)_2Fe{\cdot}2/3$tmeda (0.701 g, 2.55 mmol) in Et_2O (20 mL). The reaction mixture was stirred at r.t. for 16 h, resulting in a red solution with white precipitate. After the solid was filtered off, all volatiles were removed from the filtrate under vacuum. The resulting deep orange, sticky crude product was washed with hexane (3 x 50 mL), yielding the pure product **4a** as an orange solid (0.420 g, 43%). Crystals suitable for single-crystal X-ray analysis were obtained from thf solution at -22 ºC. Note: **4b** is poorly solubility in organic solvents, expect for chloroform. However, it slowly reacts with the solvent preventing its ^{13}C NMR analysis. ^1H NMR (500 MHz): δ 0.43 (s, 18H, $SiMe_3$), 1.74 (s, 12H, NMe_2), 3.33 (s, 4H, CH_2), 4.01, 4.46, 4.60, 5.30 (pst, 8H, C_5H_4), 7.04 (d, 2H, C_6H_3), 7.64 (d, 2H, C_6H_3), 8.90 (s, 2H, C_6H_3). MS (70 eV, EI): m/z (rel intens) 834 (12) [M^+], 206 (32) [$C_{12}H_{20}NSi^+$], 207 (45) [$C_{12}H_{21}NSi^+$], 186 (100) [$C_{10}H_{10}Fe^+$], 163 (11) [$C_{10}H_{15}Si^+$], 135 (14) [$C_9H_{13}N^+$], 134 (14) [$C_9H_{12}N^+$], 121 (29) ($C_5H_5Fe^+$]. HRMS (EI; m/z): calcd for $C_{44}H_{56}Fe_2Al_2N_2Si_2$, 834.2380; found, 834.2367. Anal. Calcd for $C_{44}H_{56}Al_2Fe_2N_2Si_2$ (834.75): C, 63.31; H, 6.76; N, 3.36. Found: C, 61.19; H, 7.00; N, 3.22.

Synthesis of bis({2-[(dimethylamino)methyl]-5-(trimethylsilyl)phenyl-*κ*^{2}*C,N*}galla)[1.1]ferrocenophane (4b). A solution of **2b** (1.12 g, 3.23 mmol) in Et_2O (40 mL) was added dropwise to a slurry of $(LiC_5H_4)_2Fe{\cdot}2/3$tmeda (0.998 g, 3.62 mmol) in Et_2O (30 mL). The reaction mixture was stirred at r.t. for 16 h, yielding a red solution with a white precipitate. After the solid was filtered off, all volatiles were removed from the filtrate under vacuum. The resulting deep orange, sticky crude product was washed with *n*-hexane (3 × 50 mL), yielding the pure product as an orange solid (0.701 g, 47%). Crystals suitable for single-crystal X-ray analysis were obtained from thf solution at -22

ºC. ^{1}H NMR ($CDCl_3$): δ 0.40 (s, 18H, $SiMe_3$), 2.14 (s, 12H, NMe_2), 3.72 (s, 4H, CH_2), 3.86, 4.26, 4.32, 4.74 (pst, 8H, C_5H_4), 7.15 (d, 2H, C_6H_3), 7.50 (d, 2H, C_6H_3), 8.34 (s, 2H, C_6H_3). ^{1}H NMR (C_6D_6): δ 0.43 (s, 18H, $SiMe_3$), 1.84 (s, 12H, NMe_2), 3.28 (s, 4H, CH_2), 4.03, 4.40, 4.58, 5.22 (pst, 8H, C_5H_4), 7.07 (d, 2H, C_6H_3), 7.60 (d, 2H, C_6H_3), 8.80 (s, 2H, C_6H_3). ^{13}C NMR ($CDCl_3$): δ -0.72 ($SiMe_3$), 46.22 (NMe_2), 66.61 (CH_2), 70.02, 70.19, 70.52, 74.31, 74.81 (C_5H_4), 123.93, 131.97, 138.05, 142.00, 145.09, 149.54 (C_6H_3). MS (70 eV, EI): m/z (rel intens) 920 (100) [M^+], 460 (19) [$C_{22}H_{29}FeGaNSi^+$], 69 (12) [Ga^+]. HRMS (EI; m/z): calcd for $C_{44}H_{56}Fe_2Ga_2N_2Si_2$, 920.1184; found, 920.1170. Anal. Calcd for $C_{44}H_{56}Fe_2Ga_2N_2Si_2$ (920.24): C, 57.43; H, 6.13; N, 3.04. Found: C, 56.94; H, 6.31; N, 2.91.

Synthesis of {2-[(dimethylamino)methyl]-5-(trimethylsilyl)phenyl-*κ*^{2}*C,N*}bis(ferrocenyl)alumane (5a). A solution of **2a** (0.610 g, 2.00 mmol) in benzene (40 mL) was added dropwise to a slurry of LiFc (0.968 g, 5.04 mmol) in benzene (25 mL) at r.t. and stirred for 16 h, after which a red solution with an orange precipitate was obtained. After the solid was filtered off, all volatiles were removed under vacuum, yielding a red paste as the crude product. The product was extracted with cyclohexane (40 mL), the cyclohexane solution was concentrated to a volume of approx. 10 mL and kept at 6 °C for 16 h, resulting in orange crystals. The crystals were washed with hexane (2 × 5 mL) and dried under vacuum, yielding pure **5a** as an orange powder (0.568 g, 47 %). ^{1}H NMR (C_6D_6): δ 0.35 (s, 9H, $SiMe_3$), 1.90 (s, 6H, NMe_2), 3.35 (s, 2H, CH_2), 4.02, 4.41, 4.45, 4.48 (pst, 8H, C_5H_4), 4.33 (s, 10H, C_5H_5), 7.01 (d, 1H, C_6H_3), 7.59 (d, 1H, C_6H_3), 8.50 (s, 1H, C_6H_3). ^{13}C NMR (C_6D_6): δ -0.73 ($SiMe_3$), 45.87 (NMe_2), 67.28 (CH_2), 68.12 (C_5H_5), 71.54, 71.65, 76.35, 77.21 (C_5H_4), 123.69, 132.87, 138.19, 142.96,

145.09 (C_6H_3). MS (70 eV, EI): m/z (rel intens) 603 (100) [M^+], 301 (10) [$C_{17}H_{14}AlFe^+$], 186 (27) [$C_{10}H_{10}Fe^+$], 120 (10) [$C_5H_5Fe^+$]. HRMS (EI; m/z): calcd for $C_{32}H_{38}Fe_2AlNSi$, 603.1288; found, 603.1291. Anal. Calcd for $C_{32}H_{38}AlFe_2NSi$ (603.41): C, 63.70; H, 6.35; N, 2.32. Found: C, 60.02; H, 6.35; N, 2.11.

Synthesis of {2-[(dimethylamino)methyl]-5-(trimethylsilyl)phenyl-*κ*^{2}*C,N*}bis(ferrocenyl)gallane (5b). A solution of **2b** (0.495 g, 1.43 mmol) in benzene (30 mL) was added dropwise to a slurry of LiFc (0.678 g, 3.53 mmol) in benzene (10 mL) at r.t. The resulting reaction mixture was stirred for 16 h, resulting in a red solution with an orange precipitate. After the solid was filtered off, all volatiles were removed under vacuum, yielding a red paste as the crude product. The product was extracted with cyclohexane (30 mL), the cyclohexane solution was concentrated to a volume of approx. 10 mL and kept at 6 °C for 16 h, resulting in orange crystals. The crystals were washed with hexane (2 × 5 mL) and dried under vacuum, yielding the product as an orange powder (0.568 g, 41 %). ^{1}H NMR (C_6D_6): δ 0.35 (s, 9H, $SiMe_3$), 1.82 (s, 6H, NMe_2), 3.27 (s, 2H, CH_2), 4.01, 4.37, 4.44, 4.47 (pst, 8H, C_5H_4), 4.36 (s, 10H, C_5H_5), 7.04 (d, 1H, C_6H_3), 7.57 (d, 1H, C_6H_3), 8.46 (s, 1H, C_6H_3). ^{13}C NMR (C_6D_6): δ 0.68 ($SiMe_3$), 46.02 (NMe_2), 67.01 (CH_2), 68.18 (C_5H_5), 70.96, 71.08, 72.19, 75.50, 76.06 (C_5H_4), 124.24, 132.55, 138.59, 141.88, 144.54, 150.22 (C_6H_3). MS (70 eV, EI): m/z (rel intens) 645 (75) [M^+], 460 (33) [$C_{22}H_{29}FeGaNSi^+$], 186 (100) [$C_{10}H_{10}Fe^+$]. HRMS (EI; m/z): calcd for $C_{32}H_{38}Fe_2GaNSi$, 645.0728; found, 645.0740. Anal. Calcd for $C_{32}H_{38}Fe_2GaNSi$ (646.15): C, 59.48; H, 5.93; N, 2.17. Found: C, 59.92; H, 6.11; N, 2.11.

Synthesis of {[dimethyl(2-pyridyl)silyl]methyl-κ^2C,N}bis(ferrocenyl)alumane (6a). A solution of **3a** (0.49 g, 2.0 mmol) in benzene (20 mL) was added to a suspension of LiFc (0.95 g, 5.0 mmol) in benzene (30 mL). After 16 h, the precipitate was filtered off and all volatiles were removed under vacuum. The product was extracted with hexane (105 mL) and crystallized at -25 °C (0.22 g, 21%). Crystals suitable for single-crystal X-ray analysis were obtained from Et_2O solution at -25 ºC. ^{1}H NMR (C_6D_6): δ -0.15 (s, 4H, CH_2), 0.37 (s, 12H, $SiMe_2$), 4.11 (m, 2H, C_5H_4), 4.15 (s, 10H, C_5H_5), 4.43 (m, 2H, C_5H_4), 4.47 (m, 4H, C_5H_4), 6.28 (m, 1H, Ar-H), 6.74 (m, 1H, Ar-H), 6.96 (m, 1H, Ar-H), 8.28 (m, 1H, Ar-H). ^{13}C NMR (C_6D_6): δ 0.72 ($SiMe_2$), 67.93 (C_5H_5), 71.18, 71.41, 75.92, 77.04 (C_5H_4), 123.87, 129.95, 137.85, 147.43, 172.22 (C_5H_4N). MS (70 eV, EI): m/z (rel intens) 547 (15) [M^+], 187 (13) [$C_{10}H_{11}Fe^+$], 186 (100) [$C_{10}H_{10}Fe^+$], 150 (11) [$C_8H_{12}NSi^+$], 136 (24) [$C_7H_{10}NSi^+$], 121 (30) [$C_7H_6NSi^+$]. HRMS (EI; m/z): calcd for $C_{28}H_{30}Fe_2GaNSi$, 547.0662; found, 547.0665. Anal. Calcd for $C_{28}H_{30}AlFe_2NSi$ (547.30): C, 61.45; H, 5.52; N, 2.56. Found: C, 59.90; H, 6.56; N, 2.26.

Synthesis of {[dimethyl(2-pyridyl)silyl]methyl-κ^2C,N}bis(ferrocenyl)gallane (6b). Species **3b** (0.61 g, 2.1 mmol) and LiFc (1.00 g, 5.21 mmol) were stirred for two days in a mixture of hexane (100 mL) and Et_2O (30 mL). After the removal of a part of the solvent (ca. 30 mL) in vacuum, the precipitate was filtered off and washed with hexane (3 × 10 mL). The volume of the solution was reduced in vacuum. Upon cooling to -25 °C a small amount of an orange colored material deposited on the walls of the flask. The mother liquor was syringed off, cooling at -78 °C resulted in an orange colored precipitate, which was separated and washed with hexane (15 and 10 mL) at -78 °C. All volatiles were removed in vacuum at ambient temperature to leave product **6b** behind

(0.41 g, 33%). ^{1}H NMR (C_6D_6): δ 0.05 (s, 2H, CH_2), 0.38 (s, 6H, $SiMe_2$), 4.10 (m, 2H, C_5H_4), 4.17 (s, 10H, C_5H_5), 4.37 (m, 2H, C_5H_4), 4.44 (m, 2H, C_5H_4), 4.50 (m, 2H, C_5H_4), 6.29 (m, 1H, Ar-H), 6.76 (m, 1H, Ar-H), 6.97 (m, 1H, Ar-H), 8.18 (m, 1H, Ar-H). ^{13}C NMR (C_6D_6) δ -9.99 (CH_2), 0.58 ($SiMe_2$), 68.03 (C_5H_5), 70.58, 70.79, 75.00, 75.88, 76.12 (C_5H_4), 123.96, 129.58, 136.98, 147.55, 170.07 (C_5H_4N). MS (70 eV, EI): m/z (rel intens) 589 (100) [M^+], 404 (75) [M^+ - $C_{10}H_9Fe$], 69 (12) [Ga^+]. HRMS (EI; m/z): calcd for $C_{28}H_{30}Fe_2AlNSi$, 589.0102; found, 589.0119. Anal. Calcd for $C_{28}H_{30}Fe_2GaNSi$ (590.04): C, 57.00; H, 5.12; N, 2.37. Found: C, 56.65; H, 5.05; N, 2.44.

Synthesis of bis(ferrocenyl)dimethylsilane (7^{Me}). A solution of Me_2SiCl_2 (0.515 g, 3.99 mmol) in hexane (40 mL) was added dropwise via tubing to a slurry of LiFc (1.93 g, 10.1 mmol) in a mixture of hexane (15 mL) and Et_2O (10 mL) at r.t. The resulting reaction mixture was stirred for 16 h, yielding a red solution with orange precipitate. After the solid was filtered off, the red solution was concentrated to approx. 10 mL and kept at -22 °C for 16 h. Red crystals were obtained as pure product (1.19 g, 70%). ^{1}H NMR (C_6D_6): δ 0.50 (s, 6H, CH_3), 4.02 (s, 10H, C_5H_5), 4.08, 4.19 (pst, 8H, C_5H_4). ^{13}C NMR (C_6D_6): δ -0.60 (CH_3), 68.58 (C_5H_5), 71.10, 71.62, 73.45 (C_5H_4). MS (70 eV, EI): m/z (rel intens) 428 (100) [M^+], 363 (32) [M^+ - C_5H_5], 242 (9) [M^+ - $C_{10}H_{10}Fe$], 186 (8) [$C_{10}H_{10}Fe^+$]. HRMS (EI; m/z): calcd for $C_{22}H_{24}Fe_2Si$, 428.0346; found, 428.0361. Anal. Calcd for $C_{22}H_{24}Fe_2Si$ (428.20): C, 61.71; H, 5.65. Found: C, 61.53; H, 5.53.

Synthesis of diethylbis(ferrocenyl)silane (7^{Et}). A solution of Et_2SiCl_2 (0.631 g, 4.02 mmol) in hexane (40 mL) was added dropwise via tubing to a slurry of LiFc (1.93 g, 10.1 mmol) in a mixture of hexane (15 mL) and Et_2O (10 mL) at r.t. The resulting reaction mixture was stirred for 16 h, yielding a red solution with orange precipitate. After the

solid was filtered off, the red solution was concentrated to approx. 10 mL and kept at -22 °C for 16 h. Red crystals (1.31 g, 72%) were obtained pure product. ^{1}H NMR (C_6D_6): δ 0.99 (q, 4H, CH_2), 1.18 (t, 6H, CH_3), 4.02 (s, 10H, C_5H_5), 4.11, 4.21 (pst, 8H, C_5H_4). ^{13}C NMR (C_6D_6): δ 6.53 (CH_2), 8.44 (CH_3), 68.68 (C_5H_5), 69.75, 70.92, 73.87 (C_5H_4). MS (70 eV, EI): m/z (rel intens) 456 (100) [M^+], 427 (38) [M^+ - Et], 333 (9) [$C_{15}H_{13}Fe_2Si^+$], 213 (30) [$C_{10}H_9FeSi^+$]. HRMS (EI; m/z): calcd for $C_{24}H_{28}Fe_2Si$, 456.0659; found, 456.0664. Anal. Calcd for $C_{24}H_{28}Fe_2Si$ (456.25): C, 63.18; H, 6.19. Found: C, 63.12; H, 6.19.

Single-crystal X-ray analysis of 3b, 6a, 7^{Me}, and 7^{Et}. Data was collected with an STOE IPDS-2 or IPDS-2T diffractometer with graphite-monochromated Mo K_α radiation (λ = 0.71073 Å) using an oil-coated schock-cooled crystal at 100 K. Absorption effects were corrected semi-empirical using multi-scanned reflections (*PLATON*).[53] Cell constants were refined using many thousands of observed reflections of the data collections.[54] The structures were solved by direct methods by using the programs SIR2008[55] (**6a**, **3b**), SIR92[56] (**7^{Me}**), or SIR97[57] (**7^{Et}**), and refined by full matrix least squares procedures on F^2 using SHELXL-97[58]. The non-hydrogen atoms have been refined anisotropically, hydrogen atoms were included at calculated positions and refined using the 'riding model' with isotropic temperature factors at 1.2 times (for CH_3 groups 1.5 times) that of the preceding carbon atom. CH_3 groups were allowed to rotate about the bond to their next atom to fit the electron density.

Compound **6a** happened to be a non-merohedral twin with twin law [-1 0 0 0 1 0 0 0 -1]. Only the undistorted data of one twin domain have been used for the refinement (completeness of the data set 74 %). Because of this twinning and the small size of the

crystal the overall intensity of the data was low. During the refinement of **6a** restraints were included for the anisotropic temperature factors.

Single-crystal X-ray analysis of 4a and 4b. Single crystals of **4a**·2thf and **4b**·2thf were coated with Paratone-N oil, mounted using a Micromount™ (*MiTeGen* - Microtechnologies for Structural Genomics), and frozen in the cold stream of the Oxford cryojet attached to the diffractometer. Crystal data were collected at 173 K on a Bruker-AXS Proteum R Smart 6000 diffractometer using monochromated Cu K_α radiation (λ = 1.54184 Å). An initial orientation matrix and cell was determined from ω-scans, and the X-ray data were measured using φ and ω scans.[59] Data reduction was performed using *SAINT*[60] *i*ncluded in the *APEX2* software package.[59] A multi-scan absorption correction was applied (*SADABS*).[58] Structures were solved by direct methods (*SIR-2004*)[61] and refined by full-matrix least-squares methods on F^2 with *SHELX-97*.[58] Unless otherwise stated, the non-hydrogen atoms were refined anisotropically; hydrogen atoms were included at geometrically idealized positions but not refined. The isotropic thermal parameters of the hydrogen atoms were fixed at 1.2 times that of the preceding carbon atom.

All thermal ellipsoid plots were prepared using ORTEP-3 for Windows.[62]

ACKNOWLEDGMENTS

We thank the Natural Sciences and Engineering Research Council (NSERC) of Canada for a Discovery Grant (J.M.). We thank the Canada Foundation for Innovation (CFI) and the government of Saskatchewan for funding of the NMR and XRD facilities in the Saskatchewan Structural Sciences Centre (SSSC). We thank Dr. C. L. Lund

(LANXESS, London, ON) and Dr. P. P. Jana (Lund University, Lund, Sweden) for contributions.

SUPPORTING INFORMATION

Crystallographic data for **3b**, **4a**, **4b**, **6a**, $\mathbf{7^{Me}}$, and $\mathbf{7^{Et}}$ in CIF file format; NMR spectra of **2a**, **3a**, **3b**, **4a**, **4b**, **5a**, **5b**, **6a**, **6b**, $\mathbf{7^{Me}}$ and $\mathbf{7^{Et}}$; cyclic voltammograms of **4a**, **4b**, **5a**, **5b**, **6a**, **6b**, $\mathbf{7^{Me}}$, $\mathbf{7^{Et}}$, **8a** and **8b**. This material is available free of charge via the internet at http://pubs.acs.org. Crystallographic data has been deposited with the Cambridge Crystallographic Data Centre under CCDC 895302 (**3b**), 895306 (**4a**), 895307 (**4b**), 895303 (**6a**), 895304 ($\mathbf{7^{Me}}$), and 895305 ($\mathbf{7^{Et}}$). Copies of this information may be obtained free of charge from The Director, CCDC, 12 Union Road, Cambridge CB2 1EZ, U.K. (fax, +44-1223-336033; e-mail, deposit@ccdc.cam.ac.uk; web, http://www.ccdc.cam.ac.uk).

REFERENCES

(1) (a) Bellas, V.; Rehahn, M. *Angew. Chem., Int. Ed.* **2007**, *46*, 5082-5104. (b) Herbert, D. E.; Mayer, U. F. J.; Manners, I. *Angew. Chem., Int. Ed.* **2007**, *46*, 5060-5081.

(2) Rinehart, K. L.; Frerichs, A. K.; Kittle, P. A.; Westman, L. F.; Gustafson, D. H.; Pruett, R. L.; McMahon, J. E. *J. Am. Chem. Soc.* **1960**, *82*, 4111-4112.

(3) Osborne, A. G.; Whiteley, R. H. *J. Organomet. Chem.* **1975**, *101*, C27-C28.

(4) Foucher, D. A.; Tang, B.-Z.; Manners, I. *J. Am. Chem. Soc.* **1992**, *114*, 6246-6248.

(5) Selected recent examples: (a) Korczagin, I.; Hempenius, M. A.; Fokkink, R. G.; Stuart, M. A. C.; Al-Hussein, M.; Bomans, P. H. H.; Frederik, P. M.; Vancso, G. J. *Macromolecules* **2006**, *39*, 2306-2315. (b) Wang, X. S.; Guerin, G.; Wang, H.; Wang, Y.

S.; Manners, I.; Winnik, M. A. *Science* **2007**, *317*, 644-647. (c) Gädt, T.; Ieong, N. S.; Cambridge, G.; Winnik, M. A.; Manners, I. *Nat. Mater.* **2009**, *8*, 144-150. (d) Gilroy, J. B.; Gädt, T.; Whittell, G. R.; Chabanne, L.; Mitchels, J. M.; Richardson, R. M.; Winnik, M. A.; Manners, I. *Nat. Chem.* **2010**, *2*, 566-570. (e) Presa Soto, A.; Gilroy, J. B.; Winnik, M. A.; Manners, I. *Angew. Chem., Int. Ed.* **2010**, *49*, 8220-8223. (f) Gädt, T.; Schacher, F. H.; McGrath, N.; Winnik, M. A.; Manners, I. *Macromolecules* **2011**, *44*, 3777-3786. (g) Gilroy, J. B.; Patra, S. K.; Mitchels, J. M.; Winnik, M. A.; Manners, I. *Angew. Chem., Int. Ed.* **2011**, *50*, 5851-5855. (h) He, F.; Gädt, T.; Manners, I.; Winnik, M. A. *J. Am. Chem. Soc.* **2011**, *133*, 9095-9103. (i) Patra, S. K.; Ahmed, R.; Whittell, G. R.; Lunn, D. J.; Dunphy, E. L.; Winnik, M. A.; Manners, I. *J. Am. Chem. Soc.* **2011**, *133*, 8842–8845. (j) Yusoff, S. F. M.; Hsiao, M. S.; Schacher, F. H.; Winnik, M. A.; Manners, I. *Macromolecules* **2012**, *45*, 3883-3891.

(6) Nesmeyanov, A. N.; Kritskaya, I. I. *Bull. Acad. Sci. USSR, Div. Chem. Sci. (Eng. Transl.)* **1956**, 243-244.

(7) Scheibitz, M.; Winter, R. F.; Bolte, M.; Lerner, H.-W.; Wagner, M. *Angew. Chem., Int. Ed.* **2003**, *42*, 924-927.

(8) (a) Braunschweig, H.; Burschka, C.; Clentsmith, G. K. B.; Kupfer, T.; Radacki, K. *Inorg. Chem.* **2005**, *44*, 4906-4908. (b) Schachner, J. A.; Orlowski, G. A.; Quail, J. W.; Kraatz, H.-B.; Müller, J. *Inorg. Chem.* **2006**, *45*, 454-459. (c) Schachner, J. A.; Lund, C. L.; Quail, J. W.; Müller, J. *Acta Crystallogr.* **2005**, *E61*, m682-m684.

(9) (a) Uhl, W.; Hahn, I.; Jantschak, A.; Spies, T. *J. Organomet. Chem.* **2001**, *637*, 300-303. (b) Jutzi, P.; Lenze, N.; Neumann, B.; Stammler, H. G. *Angew. Chem., Int. Ed.* **2001**, *40*, 1423-1427. (c) Althoff, A.; Jutzi, P.; Lenze, N.; Neumann, B.; Stammler, A.;

Stammler, H.-G. *Organometallics* **2002**, *21*, 3018-3022. (d) Althoff, A.; Jutzi, P.; Lenze, N.; Neumann, B.; Stammler, A.; Stammler, H. G. *Organometallics* **2003**, *22*, 2766-2774.

(10) Schachner, J. A.; Lund, C. L.; Burgess, I. J.; Quail, J. W.; Schatte, G.; Müller, J. *Organometallics* **2008**, *27*, 4703-4710.

(11) (a) Herberhold, M.; Bärtl, T. *Z. Naturforsch. B* **1995**, *50*, 1692-1698. (b) Park, J. W.; Seo, Y. S.; Cho, S. S.; Whang, D. M.; Kim, K. M.; Chang, T. Y. *J. Organomet. Chem.* **1995**, *489*, 23-25. (c) Zechel, D. L.; Foucher, D. A.; Pudelski, J. K.; Yap, G. P. A.; Rheingold, A. L.; Manners, I. *J. Chem. Soc., Dalton Trans.* **1995**, 1893-1899. (d) Ni, Y. Z.; Rulkens, R.; Pudelski, J. K.; Manners, I. *Macromol. Rapid Commun.* **1995**, *16*, 637-641. (e) Reddy, N. P.; Choi, N.; Shimada, S.; Tanaka, M. *Chem. Lett.* **1996**, 649-650. (f) MacLachlan, M. J.; Zheng, J.; Thieme, K.; Lough, A. J.; Manners, I.; Mordas, C.; LeSuer, R.; Geiger, W. E.; Liable-Sands, L. M.; Rheingold, A. L. *Polyhedron* **2000**, *19*, 275-289. (g) Calleja, G.; Carré, F.; Cerveau, G. *Organometallics* **2001**, *20*, 4211-4215. (h) Berenbaum, A.; Lough, A. J.; Manners, I. *Organometallics* **2002**, *21*, 4415-4424. (i) Bao, M.; Hatanaka, Y.; Shimada, S. *Chem. Lett.* **2004**, *33*, 520-521.

(12) (a) Seyferth, D.; Withers, H. P. *Organometallics* **1982**, *1*, 1275-1282. (b) Dong, T. Y.; Hwang, M. Y.; Wen, Y. S.; Hwang, W. S. *J. Organomet. Chem.* **1990**, *391*, 377-385. (c) Jäkle, F.; Rulkens, R.; Zech, G.; Foucher, D. A.; Lough, A. J.; Manners, I. *Chem.–Eur. J.* **1998**, *4*, 2117-2128. (d) Jäkle, F.; Rulkens, R.; Zech, G.; Massey, J.; Manners, I. *J. Am. Chem. Soc.* **2000**, *122*, 4231-4232. (e) Baumgartner, T.; Jäkle, F.; Rulkens, R.; Zech, G.; Lough, A. J.; Manners, I. *J. Am. Chem. Soc.* **2002**, *124*, 10062-10070.

(13) Utri, G.; Schwarzhans, K. E.; Allmaier, G. M. *Z. Naturforsch. B* **1990**, *45*, 755-762.

(14) (a) Brunner, H.; Klankermayer, J.; Zabel, M. *J. Organomet. Chem.* **2000**, *601*, 211-219. (b) Mizuta, T.; Onishi, M.; Miyoshi, K. *Organometallics* **2000**, *19*, 5005-5009. (c) Mizuta, T.; Imamura, Y.; Miyoshi, K. *Organometallics* **2005**, *24*, 990-996.

(15) Spang, C.; Edelmann, F. T.; Noltemeyer, M.; Roesky, H. W. *Chem. Ber.* **1989**, *122*, 1247-1254.

(16) Ieong, N. S.; Chan, W. Y.; Lough, A. J.; Haddow, M. R.; Manners, I. *Chem.–Eur. J.* **2008**, *14*, 1253-1263.

(17) Perucha, A. S.; Heilmann-Brohl, J.; Bolte, M.; Lerner, H. W.; Wagner, M. *Organometallics* **2008**, *27*, 6170-6177.

(18) (a) Lemenovskii, D. A.; Urazowski, I. F.; Baukova, T. V.; Arkhipov, I. L.; Stukan, R. A.; Perevalova, E. G. *J. Organomet. Chem.* **1984**, *264*, 283-288. (b) Kuz'mina, I. G.; Struchkov, Y. T.; Lemenovsky, D. A.; Urazowsky, I. F. *J. Organomet. Chem.* **1984**, *277*, 147-151.

(19) (a) Bagh, B.; Breit, N. C.; Gilroy, J. B.; Schatte, G.; Müller, J. *Chem. Commun.* **2012**, *48*, 7823-7825. (b) Bagh, B.; Breit, N. C.; Dey, S.; Gilroy, J. B.; Schatte, G.; Harms, K.; Müller, J. *Chem.–Eur. J.* **2012**, *18*, 9722–9733.

(20) For example: (a) Katz, T. J.; Acton, N.; Martin, G. *J. Am. Chem. Soc.* **1969**, *91*, 2804-2805. (b) Lippard, S. J.; Martin, G. *J. Am. Chem. Soc.* **1970**, *92*, 7291-7296. (c) Mueller-Westerhoff, U. T. *Angew. Chem., Int. Ed.* **1986**, *25*, 702-717. (d) Barlow, S.; Ohare, D. *Organometallics* **1996**, *15*, 3885-3890. (e) Grossmann, B.; Heinze, J.; Herdtweck, E.; Köhler, F. H.; Nöth, H.; Schwenk, H.; Spiegler, M.; Wachter, W.; Weber, B. *Angew. Chem., Int. Ed.* **1997**, *36*, 387-389. (f) Temple, K.; Lough, A. J.; Sheridan, J. B.; Manners, I. *J. Chem. Soc., Dalton Trans.* **1998**, 2799-2805. (g) Haberhauer, G.;

Rominger, F.; Gleiter, R. *Angew. Chem., Int. Ed.* **1998**, *37*, 3376-3377. (h) Mueller-Westerhoff, U. T.; Swiegers, G. F. *Chem. Lett.* **1994**, 67-68. (i) Köhler, F. H.; Schell, A.; Weber, B. *Chem.-Eur. J.* **2002**, *8*, 5219-5227. (j) Schaller, R. J.; Gleiter, R.; Hofmann, J.; Rominger, F. *Angew. Chem., Int. Ed.* **2002**, *41*, 1181-1183. (k) Mizuta, T.; Aotani, T.; Imamura, Y.; Kubo, K.; Miyoshi, K. *Organometallics* **2008**, *27*, 2457-2463. (l) Herbert, D. E.; Gilroy, J. B.; Chan, W. Y.; Chabanne, L.; Staubitz, A.; Lough, A. J.; Manners, I. *J. Am. Chem. Soc.* **2009**, *131*, 14958-14968.

(21) For ferrocenophanes with more than two fc units a different nomenclature is commonly used; e.g. a FCP with 4 fc units and single-atom bridges is usually referred to as a [1^4]FCP instead of a [1.1.1.1]FCP (see reference 20a).

(22) (a) Bagh, B.; Schatte, G.; Green, J. C.; Müller, J. *J. Am. Chem. Soc.* **2012**, *134*, 7924−7936. (b) Breit, N. C.; Ancelet, T.; Quail, J. W.; Schatte, G.; Müller, J. *Organometallics* **2011**, *30*, 6150-6158. (c) Bagh, B.; Gilroy, J. B.; Staubitz, A.; Müller, J. *J. Am. Chem. Soc.* **2010**, *132*, 1794-1795. (d) Schachner, J. A.; Tockner, S.; Lund, C. L.; Quail, J. W.; Rehahn, M.; Müller, J. *Organometallics* **2007**, *26*, 4658-4662. (e) Lund, C. L.; Schachner, J. A.; Quail, J. W.; Müller, J. *J. Am. Chem. Soc.* **2007**, *129*, 9313-9320. (f) Lund, C. L.; Schachner, J. A.; Quail, J. W.; Müller, J. *Organometallics* **2006**, *25*, 5817-5823. (g) Schachner, J. A.; Lund, C. L.; Quail, J. W.; Müller, J. *Organometallics* **2005**, *24*, 4483-4488. (h) Schachner, J. A.; Lund, C. L.; Quail, J. W.; Müller, J. *Organometallics* **2005**, *24*, 785-787.

(23) Lund, C. L.; Schachner, J. A.; Burgess, I. J.; Quail, J. W.; Schatte, G.; Müller, J. *Inorg. Chem.* **2008**, *47*, 5992–6000.

(24) Mpysm stands for [dimethyl(2-pyridyl)silyl]methyl.

(25) Synthesis of **2b**, which was applied for the preparation the first silagalla[1.1]ferrocenophane, is described in reference 19a.

(26) All 16 H atoms at the C_5H_4 groups of **4a** or **4b** can only be in special positions (not on a symmetry element), hence, the finding of 4 signals shows a point-group symmetry with the group order of h = 4 (number of detected signals: 16/h = 4).

(27) Measured chemical shifts of the four [1.1]FCPs are very similar: δ 4.01, 4.46, 4.60, 5.30 (**4a**) and 4.03, 4.40, 4.58, 5.22 (**4b**) compared with δ 4.10, 4.55, 4.64, 5.30 (**1a**) and 3.99, 4.37, 4.48, 5.07 (**1b**); see references 8a and 8b.

(28) Rosenberg, H.; Office, U. S. P., Ed. 1969.

(29) Bildstein, B.; Malaun, M.; Kopacka, H.; Wurst, K.; Mitterbock, M.; Ongania, K.-H.; Opromolla, G.; Zanello, P. *Organometallics* **1999**, *18*, 4325-4336.

(30) Rulkens, R.; Lough, A. J.; Manners, I.; Lovelace, S. R.; Grant, C.; Geiger, W. E. *J. Am. Chem. Soc.* **1996**, *118*, 12683-12695.

(31) The molecular structure of $\mathbf{7^{Me}}$ is mentioned in reference Andrianov, V. I. *Kristallografiya* **1987**, *32*, 1258-1260 (*Sov. Phys. Crystallogr.* **1987**, *32*, 742-744). However, besides cell constancies, structural data was not published.

(32) Scheibitz, M.; Bolte, M.; Bats, J. W.; Lerner, H. W.; Nowik, I.; Herber, R. H.; Krapp, A.; Lein, M.; Holthausen, M. C.; Wagner, M. *Chem.–Eur. J.* **2005**, *11*, 584-603.

(33) The dip angle α* is similarly defined as the angle β in metallacyclophanes.

(34) Appel, A.; Jäkle, F.; Priermeier, T.; Schmid, R.; Wagner, M. *Organometallics* **1996**, *15*, 1188-1194.

(35) (a) Muther, K.; Fröhlich, R.; Muck-Lichtenfeld, C.; Grimme, S.; Oestreich, M. *J. Am. Chem. Soc.* **2011**, *133*, 12442-12444. (b) Schmidt, R. K.; Muther, K.; Muck-Lichtenfeld, C.; Grimme, S.; Oestreich, M. *J. Am. Chem. Soc.* **2012**, *134*, 4421-4428.

(36) Behrens, U. *J. Organomet. Chem.* **1979**, *182*, 89-98.

(37) Gleiter, R.; Bleiholder, C.; Rominger, F. *Organometallics* **2007**, *26*, 4850-4859, and cited references.

(38) Silicon species $\mathbf{7^{Me}}$ and $\mathbf{7^{Et}}$ were also investigated using MeCN as a solvent (see Supporting Information).

(39) Bard, A. J.; Faulkner, L. R. *Electrochemical Methods*; 2 ed.; John Wiley & Sons, Inc.: New York, 2001.

(40) Barrière, F.; Camire, N.; Geiger, W. E.; Mueller-Westerhoff, U. T.; Sanders, R. *J. Am. Chem. Soc.* **2002**, *124*, 7262-7263.

(41) Barrière, F.; Geiger, W. E. *J. Am. Chem. Soc.* **2006**, *128*, 3980-3989.

(42) (a) Gutmann, V. *Electrochim. Acta* **1976**, *21*, 661-670. (b) Linert, W.; Fukuda, Y.; Camard, A. *Coord. Chem. Rev.* **2001**, *218*, 113-152.

(43) Additonal references on solvent effects on $\Delta E^{o\prime}$ values: (a) Neyhart, G. A.; Hupp, J. T.; Curtis, J. C.; Timpson, C. J.; Meyer, T. J. *J. Am. Chem. Soc.* **1996**, *118*, 3724-3729. (b) Glöckle, M.; Kaim, W. *Angew. Chem., Int. Ed.* **1999**, *38*, 3072-3074.

(44) Some CVs of bis(ferrocenyl) species using thf as a solvent exhibit weak shoulders on the main waves indicative of overlap of waves (see Supporting Information).

(45) Holleman-Wiberg *Inorganic Chemistry*; 1. English ed.; Academic Press: San Diego, London, 2001.

(46) Jones, S. C.; Barlow, S.; O'Hare, D. *Chem.–Eur. J.* **2005**, *11*, 4473-4481.

(47) Bocarsly, A. B.; Walton, E. G.; Bradley, M. G.; Wrighton, M. S. *J. Electroanal. Chem.* **1979**, *100*, 283-306.

(48) (a) Atwood, J. L.; Bailey, B. L.; Kindberg, B. L.; Cook, W. J. *Aust. J. Chem.* **1973**, *26*, 2297-2298. (b) Atwood, J. L.; Shoemaker, A. L. *Chem. Commun.* **1976**, 536-537. (c) Rogers, R. D.; Cook, W. J.; Atwood, J. L. *Inorg. Chem.* **1979**, *18*, 279-282. (d) Robinson, G. H.; Bott, S. G.; Atwood, J. L. *J. Coord. Chem.* **1987**, *16*, 219-224. (e) Lee, B.; Pennington, W. T.; Laske, J. A.; Robinson, G. H. *Organometallics* **1990**, *9*, 2864-2865. (f) Wrackmeyer, B.; Klimkina, E. V.; Ackermann, T.; Milius, W. *Inorg. Chem. Commun.* **2007**, *10*, 743-747. (g) Wrackmeyer, B.; Klimkina, E. V.; Milius, W. *Eur. J. Inorg. Chem.* **2009**, 3155-3162. (h) Wrackmeyer, B.; Klimkina, E. V.; Ackermann, T.; Milius, W. *Inorg. Chim. Acta* **2009**, *362*, 3941-3948.

(49) Butler, I. R.; Cullen, W. R.; Ni, J.; Rettig, S. J. *Organometallics* **1985**, *4*, 2196-2201.

(50) Cook, I. B. *Aust. J. Chem.* **1989**, *42*, 1493-1518.

(51) (a) Sindelar, K.; Holubek, J.; Svatek, E.; Matousova, O.; Metysova, J.; Protiva, M. *J. Heterocycl. Chem.* **1989**, *26*, 1325-1330. (b) Nielsen, S. F.; Larsen, M.; Boesen, T.; Schonning, K.; Kromann, H. *J. Med. Chem.* **2005**, *48*, 2667-2677. (c) Wang, Z.; Masson, G.; Peiris, F. C.; Ozin, G. A.; Manners, I. *Chem.–Eur. J.* **2007**, *13*, 9372-9383.

(52) (a) Steenwinkel, P.; James, S. L.; Grove, D. M.; Veldman, N.; Spek, A. L.; van Koten, G. *Chem.– Eur. J.* **1996**, *2*, 1440-1445. (b) Kleij, A. W.; Gebbink, R.; Lutz, M.; Spek, A. L.; van Koten, G. *J. Organomet. Chem.* **2001**, *621*, 190-196.

(53) (a) Blessing, R. H. *Acta Crystallogr., Sec A* **1995**, *51*, 33-38. (b) Spek, A. L. *Acta Crystallogr., Sect. D: Biol. Crystallogr.* **2009**, *65*, 148-155.

(54) *X-AREA and X-RED*; Stoe & Cie GmbH, Darmstadt, Germany: 2009.

(55) Burla, M. C.; Caliandro, R.; Camalli, M.; Carrozzini, B.; Cascarano, G. L.; De Caro, L.; Giacovazzo, C.; Polidori, G.; Siliqi, D.; Spagna, R. *J. Appl. Crystallogr.* **2007**, *40*, 609-613.

(56) Altomare, A.; Cascarano, G.; Giacovazzo, C.; Guagliardi, A. *J. Appl. Crystallogr.* **1993**, *26*, 343-350.

(57) Altomare, A.; Burla, M. C.; Camalli, M.; Cascarano, G.; Giacovazzo, C.; Guagliardi, A.; Moliterni, A. G. G.; Polidori, G.; Spagna, R. *J. Appl. Crystallogr.* **1999**, *32*, 115-119.

(58) Sheldrick, G. M. *Acta Crystallogr., Sec A* **2008**, *64*, 112-122.

(59) Bruker *APEX2*; Bruker AXS Inc.: 2009.

(60) Bruker *SAINT and SADABS*; Bruker AXS Inc.: 2009.

(61) Burla, M. C.; Caliandro, R.; Camalli, M.; Carrozzini, B.; Cascarano, G. L.; De Caro, L.; Giacovazzo, C.; Polidori, G.; Spagna, R. *J. Appl. Crystallogr.* **2005**, *38*, 381-388.

(62) Farrugia, L. J. *J. Appl. Crystallogr.* **1997**, *30*, 565.

3.1.5. Selective Materials from Supporting Information of Contribution 1

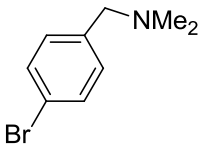

Synthesis of 1-bromo-4-[(dimethylamino)methyl]benzene. Dimethylamine (30 mL, 0.40 mol) was added dropwise to a cold (0 °C) suspension of 1-bromo-4-(bromomethyl)benzene (25.25 g, 101.0 mmol) in hexane (50 mL). The reaction mixture was warmed up to r.t. and stirred for 16 h. The solid was filtered off and all volatiles were removed from the filtrate under vacuum. Flask-to-flask condensation (50 °C, high vacuum) gave the pure product as a colorless oil (21.09 g, 98%). ^{1}H NMR (C_6D_6): δ 1.98 (s, 6H, CH_3), 3.02 (s, 2H, CH_2), 6.94 (d, 2H, C_6H_4), 7.26 (d, 2H, C_6H_4).

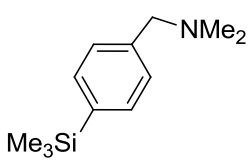

Synthesis of 1-[(dimethylamino)methyl]-4-trimethylsilyl-benzene. *t*BuLi (1.6 M in hexane, 69 mL, 110.4 mmol) was added dropwise to a cold (-78 °C) solution of 1-bromo-4-[(dimethylamino)methyl]benzene (10.70 g, 49.98 mmol) in thf (75 mL). The reaction mixture was stirred for 15 min at -78 °C, followed by the dropwise addition of chlorotrimethylsilane (19 mL, 150.0 mmol). The resultant reaction mixture was warmed up to r.t. and after stirring for 16 h a pale yellow solution with white precipitate was obtained. The solid was filtered off and all volatiles were removed under vacuum. Flask-to-flask condensation (65 °C, high vacuum) gave the pure product as a colorless oil (9.85 g, 95%). ^{1}H NMR (C_6D_6): δ 0.22 (s, 9H, $SiMe_3$), 2.10 (s, 6H, NMe_2), 3.30 (s, 2H, CH_2), 7.40 (d, 2H, C_6H_4), 7.49 (d, 2H, C_6H_4).

Contribution 2: Cyclic and Linear Poly(ferrocene)s with Silicon and Tin as Alternating Bridges.

3.2.1. Description

The following chapter is a verbatim copy of an article that is published in *Chemistry - A European Journal*[1] in April , 2012[2] and describes the synthesis and characterization of a series of poly(ferrocene)s with silicon and tin as alternating bridges. Dimethylsilicon- (**5**$^{\mathbf{Me}}$) and diethylsilicon-bridged (**5**$^{\mathbf{Et}}$) bis(bromoferrocenyl) compounds were synthesized by the salt metathesis reaction of lithioferrocene and respective dialkylsilicon dichlorides. The reaction of dilithiated species of above mentioned bis(bromoferrocenyl) compounds (**5**$^{\mathbf{Me}}$, **5**$^{\mathbf{Et}}$) with R'_2SnCl_2 (R' = Me, *n*Bu, *t*Bu) resulted in a mixture of oligomers where the ferrocene moieties were bridged by alternating silicon and tin atoms. The oligomers were characterized by ^{1}H, ^{13}C, ^{29}Si and ^{119}Sn NMR spectroscopy. MALDI-TOF mass analysis of those oligomers revealed the presence of a series of linear and cyclic species with up to 20 ferrocene moieties. The molecular weights of the oligomers were determined by gel permeation chromatography (GPC) and dynamic light scattering (DLS). GPC analysis revealed average molecular weights of 2110 to 6330 Da with respect to polystyrene as a standard. DLS analysis yielded very similar results. Some compounds, such as cyclic dimers and cyclic tetramers, were isolated in pure form either by column chromatography or by crystallization from mixtures of oligomers. The cyclic dimers were the first example of unsymmetrically bridged [1.1]FCPs. The cyclic

[1] Reprinted with permission from Chemistry – European Journal. Copyright (2012) John Wiley and Sons.

tetramers with silicon and tin as alternating bridges were among the rare examples of macrocyclic FCPs. The cyclic tetramers were structurally characterized by single-crystal X-ray analysis.

3.2.2. Author Contributions

I developed the idea and the methodology to prepare species with different bridges. I was the leading researcher of this project and my co-authors N. C. Breit and S. Dey performed chemistry following my suggestions. I analyzed and interpreted the results obtained. The co-authors on this paper are Subhayan Dey, who synthesized the starting bis(bromo-ferrocenyl) species, Nora C. Breit, who worked with the bis(bromoferrocenyl) diethylsiliane, Gabriele Schatte and Klaus Harms, who performed the structure determinations by single-crystal X-ray analysis and Joe B. Gilroy, who carried out GPC and MALDI-TOF mass analysis. I prepared the first version of the manuscript, which was edited by my supervisor Jens Müller.

3.2.3. Relation of Contribution 2 with Research Objectives

To enrich the chemistry of [1.1]FCPs, a new synthetic strategy was developed to prepare unsymmetrically bridged [1.1]FCPs that contained two different bridging elements in the same molecule. Even though this synthetic method resulted in a mixture of linear and cyclic poly(ferrocene)s (**$6^{Me}SnMe_2$**, **$6^{Et}SnMe_2$**, **$6^{Me}Sn\mathit{n}Bu_2$**, **$6^{Et}Sn\mathit{n}Bu_2$**, **$6^{Me}Sn\mathit{t}Bu_2$** **$6^{Et}Sn\mathit{t}Bu_2$**) with alternating silicon- and tin-bridges, two silastanna[1.1]ferrocenophanes [***c*-($6^{Me}SnMe_2$)$_1$**, ***c*-($6^{Et}SnMe_2$)$_1$**] were isolated from the

[2] Bagh, B.; Breit, N. C.; Dey, S.; Gilroy, J. B.; Schatte, G.; Harms, K.; Müller, J. *Chem.−Eur. J.* **2012**, *18*, 9722-9733.

oligomeric mixtures. The poly(ferrocene)s with different elements as alternative bridges represents a new class of poly(metallocene)s. Large macrocylic poly(ferrocene)s of the size as those found in our investigations with up to 20 ferrocene units are indeed rare in literature. Therefore, Contribution 5 provided a new methodology that not only produced unsymmetrically bridged [1.1]FCP, but also a new type of metallopolymers.

3.2.4. Reprint of Contribution 2

Cyclic and Linear Poly(ferrocene)s with Silicon and Tin as Alternating Bridges

Bidraha Bagh,[a] Nora C. Breit,[a] Subhayan Dey,[a] Joe B. Gilroy,[b] Gabriele Schatte,[c] Klaus Harms,[d] and Jens Müller*[a]

[a]Department of Chemistry, University of Saskatchewan, 110 Science Place, Saskatoon, Saskatchewan S7N 5C9 (Canada); [b]School of Chemistry, University of Bristol, Bristol BS8 1TS (UK); [c]Saskatchewan Structural Sciences Centre, University of Saskatchewan, 110 Science Place, Saskatoon, Saskatchewan S7N 5C9 (Canada); [d]Fachbereich Chemie, Philipps-Universität Marburg, Hans-Meerwein-Strasse, 35032 Marburg, (Germany)

Received March 20, 2012

ABSTRACT: The synthesis and characterization of ferrocene-based oligomers that contained two different elements (Si and Sn) as alternating bridges is described for the first time. The salt-metathesis reaction of $R_2Si[(C_5H_4)Fe(C_5H_4Li)]_2$ (R = Me, Et) with R'_2SnCl_2 (R′ = Me, *n*Bu, *t*Bu) afforded a mixture of oligomers (**6^{Me}SnMe$_2$**, **6^{Et}SnMe$_2$**, **6^{Me}Sn*n*Bu$_2$**, **6^{Et}Sn*n*Bu$_2$**, **6^{Me}Sn*t*Bu$_2$**, and **6^{Et}Sn*t*Bu$_2$**). These oligomers were characterized by ^{1}H, ^{13}C, ^{29}Si, and ^{119}Sn NMR spectroscopy and mass spectrometry. MS (MALDI-

TOF) studies of **6^{Et}SnMe$_2$** revealed the presence of linear (***l***) and cyclic (***c***) species that contained up to 20 ferrocene moieties. The molecular weights of the polymers were determined by gel permeation chromatography (GPC) and by dynamic light scattering (DLS). GPC analysis revealed average molecular weights of 2100 to 6300 Da with respect to polystyrene as a standard. DLS analysis yielded very similar results. Some compounds, ***c*-(6^{Me}SnMe$_2$)$_1$**, ***c*-(6^{Me}Sn*t*Bu$_2$)$_2$**, ***c*-(6^{Et}SnMe$_2$)$_1$**, ***c*-(6^{Et}Sn*t*Bu$_2$)$_2$**, ***l*-(6^{Me}Sn*n*Bu$_2$)$_2$**, and ***l*-(6^{Me}Sn*n*Bu$_2$)$_3$**, which contained up to six ferrocene moieties, were isolated in pure form either by column chromatography or by crystallization. The Si- and Sn-bridged macrocycles that contained four ferrocene units (***c*-(6^{Me}Sn*t*Bu$_2$)$_2$** and ***c*-(6^{Et}Sn*t*Bu$_2$)$_2$**) were structurally characterized by single-crystal X-ray analysis.

KEYWORDS: ferrocene · macrocycles · metallocenes · silicon · tin

INTRODUCTION

Since the discovery that the thermal ring-opening polymerization (ROP) of sila[1]ferrocenophanes **1a** and **1b** results in high-molecular-weight polymers,[1] the field of metallopolymers has been extended to various transition metals and bridging elements.[2] Poly(ferrocenylsilane)s, in particular compound **2a**, are one of the most-studied metallopolymers and have been used in various applications, for example, as precursors to ceramics,[3] tunable component of photonic crystals displays,[4] and redox-tunable capsules.[5] The living anionic ROP of sila[1]ferrocenophanes allows excellent control over molecular weights of the block copolymers, which have recently been shown to self-assemble into block-selective solvents to give nanoscopic aggregates of different morphologies.[6]

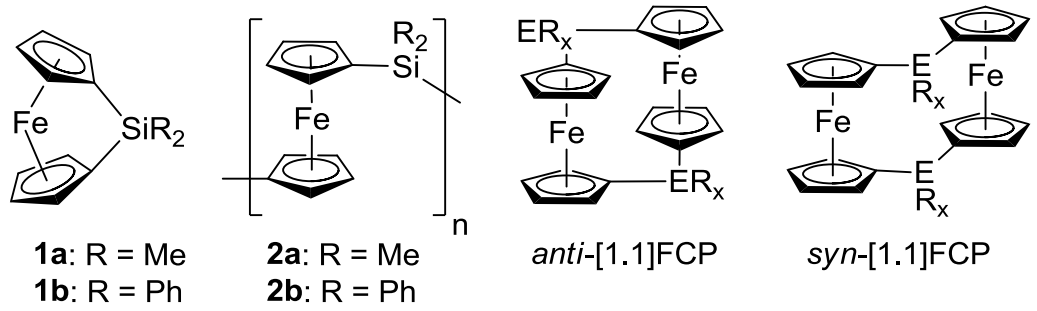

Figure 3-2-1. [1]Ferrocenophanes (**1a**, **1b**), poly(ferrocenylsilane)s (**2a**, **2b**), and [1.1]ferrocenophanes.

Half a century ago, Nesmeyanov and Kritskaya first reported the synthesis of [1.1]ferrocenophanes ([1.1]FCPs; Figure 3-2-1);[7] these ferrocene derivatives were bridged by carbon atoms and were later confirmed as *syn* isomers.[8] The first *anti* isomer of a dicarba[1.1]ferrocenophane was structurally characterized a few decades later.[9] Since the synthesis of the first [1.1]FCPs in 1956,[7] this family of compounds has grown significantly with the incorporation of B,[10] Al,[11] Ga,[11b, 12] In,[11b, 13] Si,[14] Sn,[15] Pb,[16] P,[17] As,[18] S,[19] Zn,[20] and Hg[21] atoms as heteroatom bridges. In addition to these [1.1]FCPs, other [1.1]metallacyclophanes has been synthesized such as [1.1]ruthenocenophanes,[14a, 22] [1.1]chromarenophanes,[23] [1.1]molybdarenophanes,[23] and mixed [1.1]metallacyclophanes,[22] that contained Fe/Ru or Fe/Co metal combinations. In contrast to [1]metallacyclophanes, their formal dimers lack ring strain and no report of successful ROP of [1.1]metallacyclophanes has been published to date. However, [1.1]FCPs have attracted considerable interest following the report that the *syn* conformer of the methylene-bridged [1.1]ferrocenophane catalyzed the formation of H_2 upon protonation in acidic aqueous solution.[22]

In contrast to numerous reported [1.1]FCPs that contained a variety of different elements at the bridging positions, species that exhibit two different bridging elements in

the same molecule have not been reported. To enrich the chemistry of [1.1]metallacyclophanes, we were interested in developing a synthetic method that allows the formation of [1.1]ferrocenophanes with two different bridging elements. Herein, we describe the first silastanna[1.1]ferrocenophanes and other cyclic species that contain to 20 ferrocene moieties with alternating silicon and tin atoms at the bridging positions.

RESULTS AND DISCUSSION

Scheme 3-2-1 shows our synthetic approach toward asymmetrically bridged [1.1]FCPs, which starts with a dilithiation of the dibromide **5**, followed by addition of a respective element dichloride ($R'_yE'Cl_2$). Within this approach, the scope of the first bridging element (E, Scheme 3-2-1) is limited because the bridge must withstand the conditions of the attempted lithiation. Therefore, we decided to synthesize the starting material with silicon as the bridging element between the two ferrocene moieties; thus, we prepared $\mathbf{5^{Me}}$ (R = Me) and $\mathbf{5^{Et}}$ (R = Et) from 1,1'-bromolithioferrocene and respective dichlorodialkylsilanes (Scheme 3-2-2). Besides the required chemical inertness toward lithiation, silicon was selected because of the large amount of data that was available on silicon-bridged FCPs and poly(ferrocenylsilane)s.[2c, 24] Most of these compounds are air-stable, which simplifies their purification. Both dibromides were purified by column chromatography on Al_2O_3 ($\mathbf{5^{Me}}$: 55%; $\mathbf{5^{Et}}$: 69%) and characterized by ^1H and ^{13}C NMR spectroscopy and MS. As expected, the NMR data is consistent with both species adopting time-averaged C_{2v} symmetry.

Scheme 3-2-1. Proposed synthetic route to unsymmetrically bridged [1.1]FCPs.

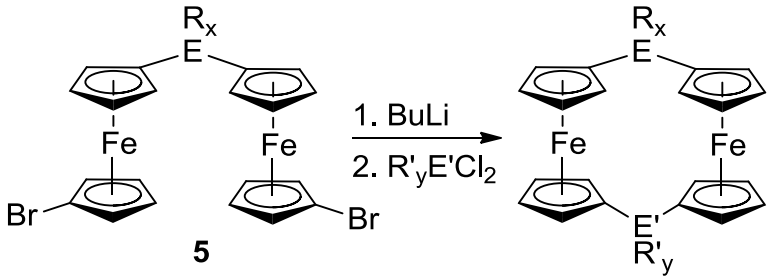

Scheme 3-2-2. Synthesis of $\mathbf{5^{Me}}$ and $\mathbf{5^{Et}}$.

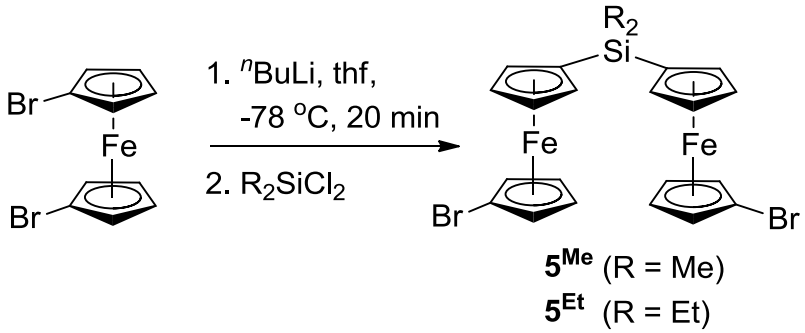

We chose tin as the second bridging element because many tin-dihalide compounds are readily available, tin can serve as an excellent NMR probe, and, similar to silicon, tin should afford air-stable products. As depicted in Scheme 3-2-3, dibromides $\mathbf{5^{Me}}$ and $\mathbf{5^{Et}}$ were lithiated with *t*BuLi in *n*-hexane/thf,[25] followed by the addition of R'_2SnCl_2 (R′ = Me, *n*Bu, *t*Bu). These salt-metathesis reactions gave red solids or gummy materials in approximately 65-85% yield. For $\mathbf{6^{Me}Sn}\boldsymbol{t}\mathbf{Bu_2}$ and $\mathbf{6^{Et}SnMe_2}$, pure compounds were obtained by crystallizations in low yields (7% and 3%, respectively). Column chromatography resulted in the isolation of four additional species but crystals could only be obtained from one fraction of mixture $\mathbf{6^{Et}Sn}\boldsymbol{t}\mathbf{Bu_2}$. MS studies of these three crystalline samples suggested that one species was a [1.1]FCP (***c*-($\mathbf{6^{Et}SnMe_2}$)$_1$**), whereas the other two samples were [1.1.1.1]FCPs (***c*-($\mathbf{6^{Me}Sn}\boldsymbol{t}\mathbf{Bu_2}$)$_2$** and ***c*-($\mathbf{6^{Et}Sn}\boldsymbol{t}\mathbf{Bu_2}$)$_2$**).[26] Attempted structural characterization of all three species by single-crystal X-ray analysis was not successful for the [1.1]FCP ***c*-($\mathbf{6^{Et}SnMe_2}$)$_1$**. Crystals that were grown under different

conditions were always twinned (see Experimental Section). Figure 3-2-2 and Figure 3-2-3 show ORTEPs of macrocyclic species ***c*-(6^{Me}Sn*t*Bu$_2$)$_2$** and ***c*-(6^{Et}Sn*t*Bu$_2$)$_2$** (Table 3-2-1).

Scheme 3-2-3. Targeted [1.1]FCPs ***c*-(6^{R}SnR'$_2$)$_1$** as one component of the reaction mixtures **6^{R}SnR'$_2$**.

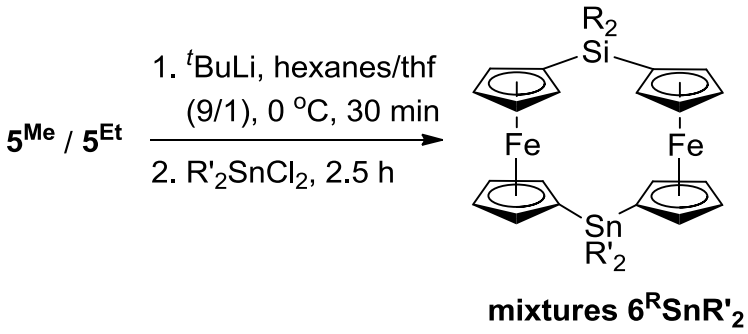

The most striking difference between the two macrocycles is their overall shape. Whilst $SiMe_2$-bridged species ***c*-(6^{Me}Sn*t*Bu$_2$)$_2$** (Figure 3-2-2) is oval, its $SiEt_2$-bridged counterpart (***c*-(6^{Et}Sn*t*Bu$_2$)$_2$**, Figure 3-2-3) is square. This difference can be illustrated by the Fe···Fe distances: the four iron atoms in ***c*-(6^{Me}Sn*t*Bu$_2$)$_2$** form a rectangle with a short site of 5.440(4) Å (Fe1···Fe2) and a long site of 6.948(4) Å (Fe1···Fe2*), whereas the iron atoms in ***c*-(6^{Et}Sn*t*Bu$_2$)$_2$** form a square with Fe···Fe distances in the narrow range of 5.5652(4) to 5.9956(5) Å. Converting one ring conformer into the other conformer would require rotations around Si-Cp and Sn-Cp bonds, as well as around Fe-Cp bonds. For the 1,1'-disubstituted ferrocene repeating units, one expects that the most preferred conformation is that in which both substituents are on opposite sides. However, this "hinge" in the macrocycle will be very flexible and different conformations should be of similar energy as long as steric interactions between the two substituents are avoided. Inspections of the other "hinges" in the macrocycles, that is, the silicon and tin atoms,

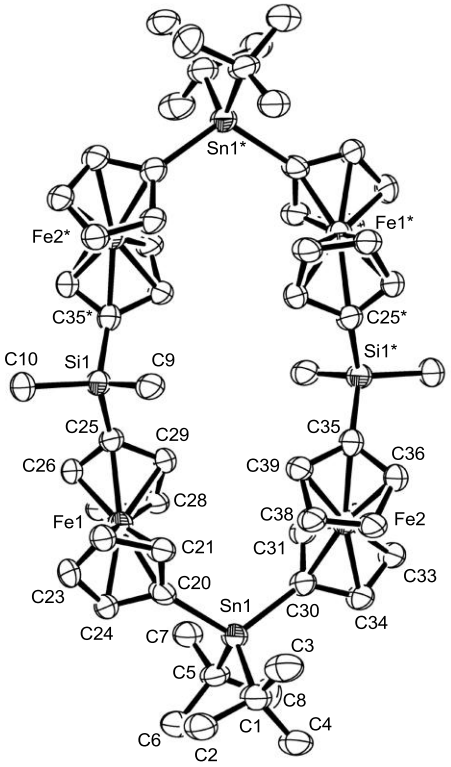

Figure 3-2-2. Molecular structure of ***c*-(6^{Me}Sn*t*Bu$_2$)$_2$**; thermal ellipsoids are set at the 50% probability level. Hydrogen atoms are omitted for clarity. Selected distances [Å] and bond angles [º]: Si1-C9 = 1.812(12), Si1-C10 = 1.873(9), Si1-C25 = 1.876(11), Si1-C35* = 1.860(11), Sn1-C1 = 2.170(12), Sn1-C5 = 2.175(12), Sn1-C20 = 2.151(9), Sn1-C30 = 2.130(9), Fe1···Fe2 = 5.440(4), Fe1···Fe2* = 6.948(4), Fe1···Fe1* = 8.815(5), C9-Si1-C10 = 113.3(5), C9-Si1-C25 = 109.8(5), C9-Si1-C35* = 109.3(5), C10-Si1-C25 = 108.7(5), C10-Si1-C35* = 108.8(5), C25-Si1-C35* = 106.7(5), C1-Sn1-C5 = 112.0(4), C1-Sn1-C20 = 105.0(4), C1-Sn1-C30 = 111.0(4), C5-Sn1-C20 = 109.5(4), C5-Sn1-C30 = 105.9(4), C20-Sn1-C30 = 113.7(4). Symmetry transformation used to generate equivalent atoms (*): –x, –y + 1, –z.

reveals the presence of only two different conformations, as shown in Figure 3-2-4a, which shows Newman projections along the E-Cp bonds (E = Si, Sn). One conformation shows the Cp^{centr}–Fe–Cp^{centr} axis of one ferrocenediyl (fc) moiety staggered with respect to the two R groups at Si or Sn (*trans* conformation) and the second conformation shows the Cp^{centr}–Fe–Cp^{centr} axis staggered with respect to the one R and the fc group (*gauche* conformation; fc = $(H_4C_5)_2Fe$). Because each bridging element has two E-Cp bonds, three

conformers are feasible, namely, *trans,gauche-*, *gauche,gauche-*, *and trans,trans-*conformers. Compound ***c*-(6^{Me}Sn*t*Bu$_2$)$_2$** (Figure 3-2-2) shows *gauche,gauche*-conformations at tin atom and *trans,trans*-conformations at the silicon center, whereas ***c*-(6^{Et}Sn*t*Bu$_2$)$_2$** (Figure 3-2-3) shows *gauche,gauche*-conformations for both types of bridging elements.[27]

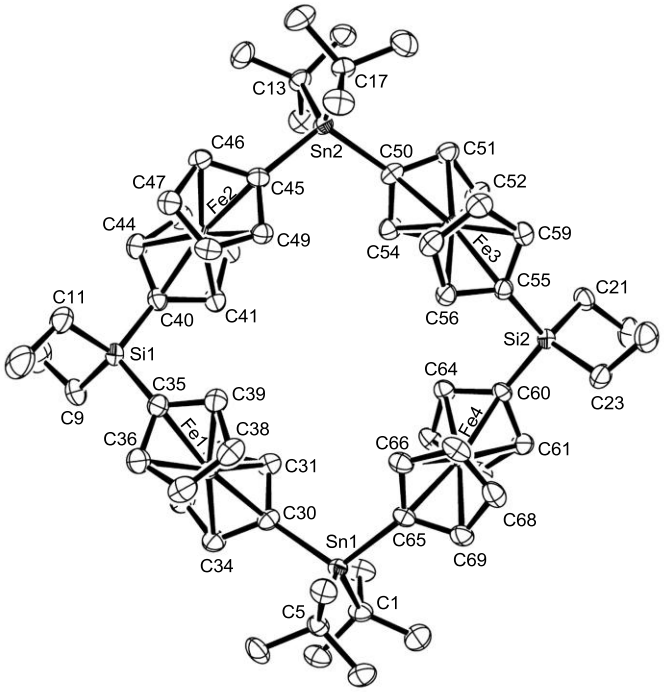

Figure 3-2-3. Molecular structure of *c*-(6^{Et}Sn*t*Bu$_2$)$_2$; thermal ellipsoids are set at the 50% probability level. Hydrogen atoms are omitted for clarity. Selected atom-atom distances [Å] and bond angles [º]: Si1-C9 = 1.878(3), Si1-C11 = 1.877(3), Si1-C35 = 1.861(2), Si1-C40 = 1.857(3), Si2-C21 = 1.878(2), Si2-C23 = 1.880(2), Si2-C55 = 1.861(2), Si2-C60 = 1.859(2), Sn1-C1 = 2.185(2), Sn1-C5 = 2.187(2), Sn1-C30 = 2.129(2), Sn1-C65 = 2.132(2), Sn2-C13 = 2.195(2), Sn2-C17 = 2.193(2), Sn2-C45 = 2.127(2), Sn2-C50 = 2.135(2), Fe1···Fe2 = 5.5979(5), Fe1···Fe4 = 5.9956(5), Fe2···Fe3 = 5.9813(5), Fe3···Fe4 = 5.5652(4), Fe1···Fe3 = 8.2023(5), Fe2···Fe4 = 8.1558(5), C30-Sn1-C65 = 112.57(9), C35-Si1-C40 = 112.23(11), C45-Sn2-C50 = 111.17(9), C55-Si2-C60 = 111.47(10).

Table 3-2-1. Crystal and Structural Refinement Data for Compounds ***c*-(6^{Et}SnMe$_2$)$_2$** and ***c*-(6^{Et}Sn*t*Bu$_2$)$_2$**.

	***c*-(6^{Me}Sn*t*Bu$_2$)$_2$·C$_7$H$_8$**	***c*-(6^{Et}Sn*t*Bu$_2$)$_2$**

CCDC No.[a]	871839	871838
Fw	1410.33	1374.30
crystal size [mm^3]	0.24×0.07×0.06	0.25×0.20×0.18
crystal System	monoclinic	triclinic
Z	2	2
a [Å]	20.486(11)	14.6681(2)
b [Å]	14.217(5)	14.7976(3)
c [Å]	10.770(3)	16.0618(3)
α [°]	90	66.5243(8)
β [°]	95.98(3)	89.3170(10)
γ [°]	90	77.2124(9)
V [$Å^3$]	3120(2)	3107.03(10)
ρ_{calcd} [mg m^{-3}]	1.501	1.469
T [K]	100(2)	173(2)
μ_{calcd} [mm^{-1}]	1.771	1.776
θ range [°]	1.75 to 25.50	3.01 to 30.01
reflns collected/unique	23198 / 5795	32741 / 14495
absorption correction	integration	multi-scan [SCALEPACK]
data/restraints/parameters	5795/334/366	17452/0/665
GOF	0.883	1.047
R_1 [$I > 2\sigma(I)$][b]	0.0683	0.0354
wR_2 (all data)[b]	0.1687	0.0794
$\Delta\rho_{elect}$ [e $Å^{-3}$],	1.971 and -1.416	0.429 and -0.761

[a] These CCDC numbers contain the supplementary crystallographic data for this paper. These data can be obtained free of charge from the Cambridge Crystallographic Data Centre via www.ccdc.cam.ac.uk/data_request/cif. [b] $R_1 = [\Sigma||F_o|-|F_c||]/[\Sigma|F_o|]$ for $[F_o^2 > 2\square(F_o^2)]$, $wR_2 = \{[\Sigma w(F_o^2-F_c^2)^2]/[\Sigma w(F_o^2)^2]\}^{1/2}$ (all data).

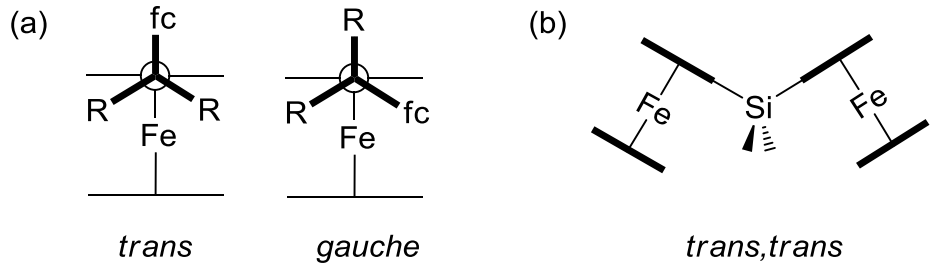

Figure 3-2-4. Illustration of possible conformations at bridging atoms in ferrocenophanes: a) Newman projection along Si-Cp or Sn-Cp bonds; *trans* and *gauche* refer to the orientation of the Cp^{cent}–Fe–Cp^{cent} axis of one sandwich moiety with respect to the second ferrocendiyl moiety (fc = $(H_4C_5)_2Fe$). b) *trans,trans*-Conformation of a fc_2SiMe_2 moiety. [27]

The isolation of linear oligomeric ferrocenyldimethylsilanes of the general formula $Fc[SiMe_2\text{-}fc\text{-}]_{n\text{-}1}H$ [Fc = $CpFe(C_5H_4)$] that contained up to nine sandwich moieties (n = 2 – 9) had been isolated and the molecular structures of the trimer and pentamer were solved by crystallography.[28] In these two oligomers, the central -fc-$SiMe_2$-fc- building blocks show *trans,trans*-conformations, whereas the Fc end groups are *gauche*. Cyclic oligomers of the type $[\text{-fc-}SiMe_2\text{-}]_n$ that contained up to seven fc moieties were recently described and molecular structures of the tetramer, pentamer, hexamer, and heptamer were solved by single-crystal X-ray analysis.[29] The tetramer has a similar molecular structure as ***c*-(6^{Et}Sn*t*Bu$_2$)$_2$** (Figure 3-2-3).

As mentioned above, column chromatography was used to isolate individual compounds from the six reaction mixtures. However, only two cyclic species, [1.1]FCP ***c*-(6^{Me}SnMe$_2$)$_1$** and the [1.1.1.1]FCP ***c*-(6^{Et}Sn*t*Bu$_2$)$_2$** (Figure 3-2-3), and two linear species that contained four or six ferrocenediyl moieties, ***l*-(6^{Me}Sn*n*Bu$_2$)$_2$** and ***l*-(6^{Me}Sn*n*Bu$_2$)$_3$**, could be separated as pure or fairly pure compounds (Figure 3-2-5; see Experimental Section).

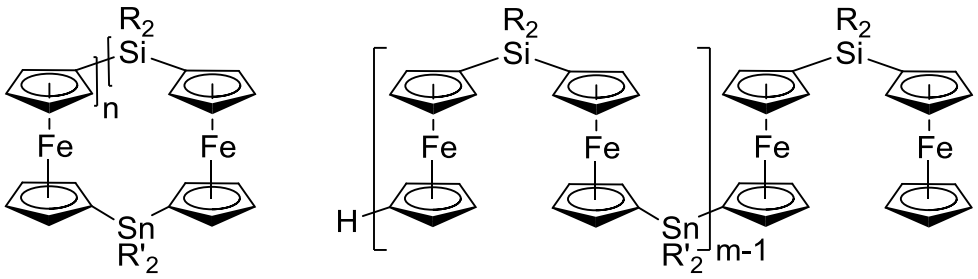

Figure 3-2-5. Cyclic and linear oligomers that contain 2n or 2m ferrocene units.

NMR characterization of isolated cyclic and linear species: The two [1.1]FCPs, ***c*-(6^{Me}SnMe$_2$)$_1$** and ***c*-(6^{Et}SnMe$_2$)$_1$**, and the two [1.1.1.1]FCPs, ***c*-(6^{Me}Sn*t*Bu$_2$)$_2$** (Figure 3-2-2) and ***c*-(6^{Et}Sn*t*Bu$_2$)$_2$** (Figure 3-2-3), each display only four equally intense signals in the Cp region of their ^{1}H NMR spectra (see the Supporting Information, Figures S29, S31, S32, S34 and S35). These results show that, in solution, each species exhibits only one type of Si-bound Cp rings and one type of Sn-bound Cp rings; each type of Cp ring results in two signals, one for the α protons and one for the β protons. The four Cp-signals of ***c*-(6^{Me}Sn*t*Bu$_2$)$_2$** and ***c*-(6^{Et}Sn*t*Bu$_2$)$_2$** are well-separated from each other (see the Supporting Information, Figures S31, S34 and S35), whereas the four Cp-resonances of ***c*-(6^{Me}SnMe$_2$)$_1$** and ***c*-(6^{Et}SnMe$_2$)$_1$** cover a much smaller range of chemical shifts (see the Supporting Information, Figures S29 and S32).

[1.1]FCPs are known to be fluxional in solution and their carbon-bridged species have been called "molecular acrobats".[22,30] Disila[1.1]ferrocenophanes are known to crystallize as *anti* isomers,[14] and we assume that our mixed-bridged [1.1]FCPs ***c*-(6^{Me}SnMe$_2$)$_1$** and ***c*-(6^{Et}SnMe$_2$)$_1$** are *anti* isomers too. As shown for ***c*-(6^{Me}SnMe$_2$)$_1$** (Scheme 3-2-4), these

cyclic species show a degenerate isomerization from one *anti* isomer to another *anti* isomer.[31] This degenerate isomerization is a ring inversion, whereby α or β protons that are positioned inside the macrocycle swap positions with α or β protons outside the macrocycle (Scheme 3-2-4). This fast degenerate isomerization from one *anti* conformer (C_s symmetry) to another *anti* conformer (C_s symmetry) results in a time-averaged C_{2v} point-group symmetry. Through the same dynamic process, the two chemically nonequivalent R groups at silicon center and the two R′ groups at the tin center become equivalent so that, for example, species ***c*-(6^{Me}SnMe$_2$)$_1$** shows two methyl-group signals instead of four.

Scheme 3-2-4. Degenerate isomerization of [1.1]FCPs, as illustrate with species ***c*-(6^{Me}SnMe$_2$)$_1$**.

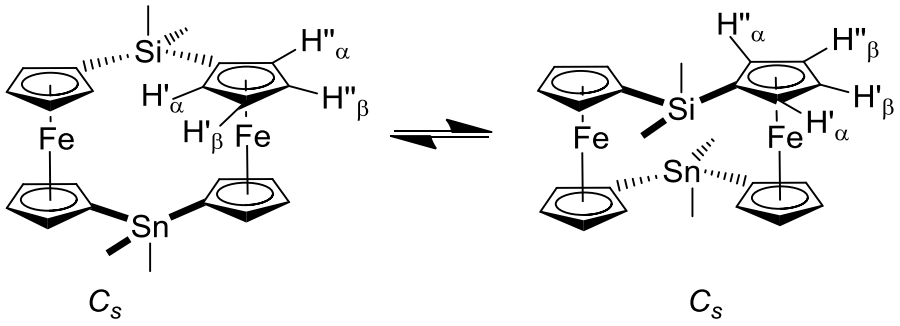

A fast ring-inversion also occurs for the [1.1.1.1]FCPs, thereby resulting in a *pseudo* mirror plane (σ_h) that makes inner and outer H atoms, such as the H′′$_\alpha$ and H′$_\alpha$ or H′′$_\beta$ and H′$_\beta$ protons (Scheme 3-2-4), equivalent. In general, compound ***c*-(6^{Me}Sn*t*Bu$_2$)$_2$** is C_{2h} symmetric in the solid state (Figure 3-2-2) and a fast degenerate isomerization results in time-averaged D_{2h} symmetry. Similarly, compound ***c*-(6^{Et}Sn*t*Bu$_2$)$_2$** is approximately D_2 symmetric in the solid state (Figure 3-2-3), thereby also giving a time-averaged D_{2h} symmetry in solution. Of course, these arguments are based on the assumption that the molecular structures of ***c*-(6^{Me}Sn*t*Bu$_2$)$_2$** and ***c*-(6^{Et}Sn*t*Bu$_2$)$_2$** in the solid state also

represent the most stable structures in solution.[32] This assumption is consistent with what has been found for similar species before. For example, the cyclic tetramer [fc-$SiMe_2$]$_4$ (see above) shows just one *pseudo* triplet for all α-protons and one for all β-protons, which can only be explained by a fast ring-inversion (time-averaged D_{4h} symmetry).[29] The first macrocycle that contained four ferrocene moieties was reported by Katz et al., who prepared methylene-bridged species of the type [fc-CH_2]$_n$ (n = 2 – 5).[33] For the tetramer only one ^{1}H chemical shift was found, which might either be due to the low resolution of the NMR spectrometer or to coincidental equivalency of α- and β-protons.[33]

Comparing the ^{1}H NMR spectra of the isolated species with those of the six reaction mixtures (Scheme 3-2-3), it was evident that the major fraction of the isolated products were not the targeted [1.1]FCPs nor any of the isolated compounds. ^{1}H NMR spectra of all six product mixtures displayed broad peaks for the Cp-protons and their respective alkyl groups on either silicon or tin atoms. The broadness of these peaks suggested the presence of polymers but their NMR spectra could not easily be assigned. To obtain some information regarding the nature of these mixtures, all six mixtures were investigated by MALDI-TOF analysis as a non-fragmentary analytical technique.

MALDI-TOF mass spectrometry: Samples for MALDI-TOF analysis were prepared as 1:10 mixtures of a solution of the sample (1 mg mL^{-1} in thf) with a solution of dithranol (10 mg mL^{-1} in thf). The mass spectra of the four samples that contained either methyl or ethyl groups at silicon (**6^{Me}SnMe$_2$**, **6^{Et}SnMe$_2$**, **6^{Me}Sn*n*Bu$_2$**, and **6^{Et}Sn*n*Bu$_2$**) were similar and revealed the presence of various linear and cyclic oligomers. In contrast, MALDI-TOF mass spectra of samples from the salt-metathesis with *t*Bu_2SnCl_2

(**6^{Me}Sn*t*Bu$_2$** and **6^{Et}Sn*t*Bu$_2$**) showed only the molecular ion peak of the respective [1.1]FCP, as well as some additional peaks. Both samples showed the loss of a *t*Bu group

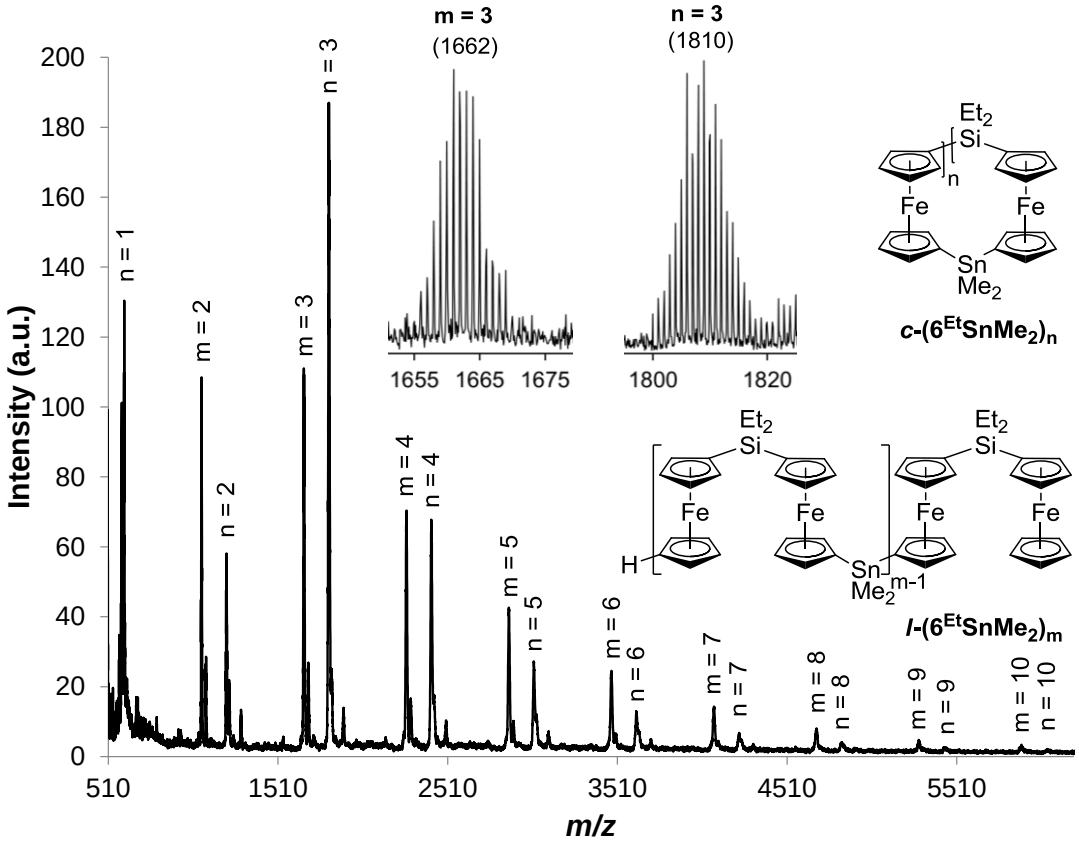

Figure 3-2-6. MS (MALDI-TOF, linear mode) of the mixture **6^{Et}SnMe$_2$**; insets show the isotopic pattern of selected species that were obtained by using the high-resolution reflector mode.

by the presence of a lower mass peak at [1.1]FCP$^+$–57, thus indicating that fragmentation is occurring (see Figure S42 and S43). The results for mixture **6^{Et}SnMe$_2$** are shown in Figure 3-2-6; the MALDI-TOF spectrum reveals the presence of linear ***l*-(6^{Et}SnMe$_2$)$_m$** and cyclic species ***c*-(6^{Et}SnMe$_2$)$_n$** that contain up to 20 ferrocene moieties (Figure 3-2-6: ***l*-6^{Et}(SnMe$_2$)$_m$**: m = 2 – 10; ***c*-6^{Et}(SnMe$_2$)$_n$**: n = 1 – 10). Similarly,mixture **6^{Me}SnMe$_2$** consists of linear and cyclic species that contain up to 16 ferrocene moieties (***l*-(6^{Me}SnMe$_2$)$_m$**: m = 2 –8; ***c*-(6^{Me}SnMe$_2$)$_n$**: n = 1 – 8; see the Supporting Information,

Figure S39), whereas for the dibutyltin-containing compounds the series of detected species was less pronounced (***l*-(6^{Me}Sn*n*Bu$_2$)$_m$**: m = 2 – 7; ***c*-(6^{Me}Sn*n*Bu$_2$)$_n$**: n = 1 – 7, ***l*-(6^{Et}Sn*n*Bu$_2$)$_m$**: m = 2 – 5; ***c*-(6^{Et}Sn*n*Bu$_2$)$_n$**: n = 1 – 5; see the Supporting Information, Figure S40 and S41).

In contrast to the large number of known [1.1]ferrocenophanes, the number of cyclic oligomers that contain more than two ferrocenediyl units is very limited. For example, cyclic oligomers that contain seven doubly silicon-bridged ferrocenyl units[34] were the largest isolated macrocycles of this kind till 2009, when Manners and co-workers reported on MALDI-TOF MS of silicon-bridged cyclic polymers that contained more than 40 ferrocenediyl units.[29] These macrocycles were obtained as mixtures from photocontrolled ROP of dimethylsila[1]ferrocenophane (**1a**; Figure 3-2-1). In contrast to these cyclic poly(ferrocenylsilane)s, our mixtures, such as **6^{Me}SnMe$_2$** and **6^{Et}SnMe$_2$**, consist of smaller cycles and exhibit Si and Sn atoms in alternating bridging positions. Such a structural motif would be very difficult to obtain through copolymerization of the respective sila and stanna[1]ferrocenophanes by a chain-growth-polymerization pathway, in particular because tin-bridged species with SnMe$_2$ or Sn*n*Bu$_2$ units are unknown, let alone the required perfect control over the copolymerization reaction.[35]

NMR characterization. The six mixtures of linear and cyclic species were characterized by ^{1}H, ^{13}C, ^{29}Si, and ^{119}Sn NMR spectroscopy. The ^{1}H NMR spectra of all the samples showed broad resonances in the alkyl range δ = 0-2 ppm (see the Supporting Information, Figures S5 to S28). All of the alkyl protons on both silicon and tin atoms appeared as separate, broad peaks in their respective ^{1}H NMR spectra with the exception of **6^{Me}SnMe$_2$**, where the signals from methyl protons on silicon and tin atoms

overlapped. However, a more-complex signal pattern was found in the Cp region (δ = 4.00-4.40) with either four major peaks of similar intensity (Figure 3-2-7c) or three major

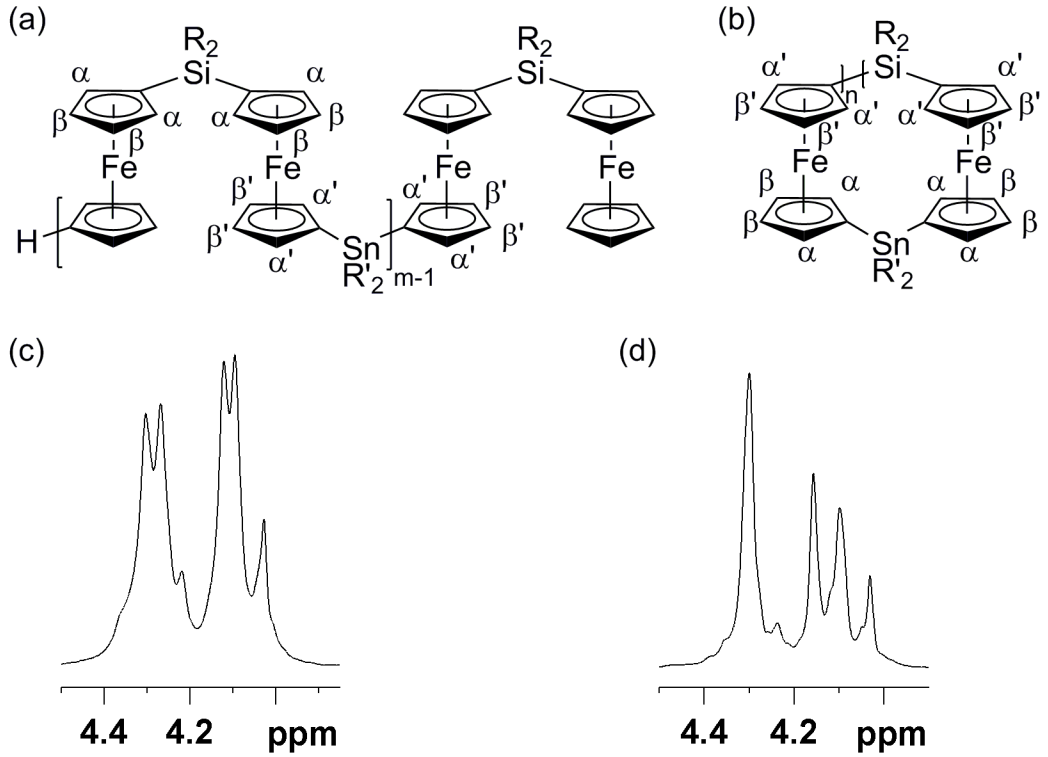

Figure 3-2-7. Different types of Cp protons in a) linear polymers and b) cyclic polymers. Cp region of the ^{1}H NMR spectra of c) **6^{Me}SnMe$_2$** and d) **6^{Et}SnMe$_2$**.

peaks in an approximate ratio of 1:1:2 (Figure 3-2-7d). In the latter case, the more-intense peak is caused by an overlap of two peaks of the same intensity. Moreover, in all proton NMR spectra another signal with lower intensity was detected between δ = 4.00-4.10 ppm (Figure 3-2-7c and Figure 3-2-7d). For linear and cyclic oligomers, one expects four signals: one peak for α protons and one peak for β protons of silicon-bound Cp rings and, similarly, two peaks for the tin-bound Cp rings (α' and β' protons). By using previously reported NMR data of poly(ferrocenylsilane)[1,36] and poly(ferrocenylstannane),[15c,37] peaks in the Cp range of the six mixtures could be assigned to silicon- and tin-bound Cp rings.

For example, the two peaks at δ = 4.09 and 4.27 for **6^{Me}SnMe$_2$** and those at δ = 4.10 and 4.30 for **6^{Et}SnMe$_2$** result from Si-Cp rings (poly(ferrocenyldimethylsilane): δ = 4.10, 4.25 ppm;[1, 36] poly(ferrocenyldiethylsilane): δ = 4.10, 4.30 ppm[36]), whereas those at δ = 4.12 and 4.30 ppm (**6^{Me}SnMe$_2$**) and δ = 4.16 and 4.30 ppm (**6^{Et}SnMe$_2$**) are due to the Sn-Cp moieties (poly(ferrocenyldimethylstannane): δ = 4.07, 4.29 ppm)[37]. The less-intense signal at the upfield end of the Cp range between δ = 4.00 and 4.10 is caused by Cp end-groups. Our measured values match very well with those reported for Cp end-groups in poly- and oligo(ferrocenylsilane).[38]

NMR data of all six mixtures are consistent with the interpretation of the ^{1}H NMR data discussed above (also see the Supporting Information). Again, resonances of the Cp moieties are the most-informative ones and Figure 3-2-8 shows two representative ^{13}C NMR spectra. For oligomers or polymers, six carbon resonances are expected: three for silicon-bound Cp rings and three for tin-bound Cp rings. Furthermore, linear species will show one additional signal for Cp end-groups (Figure 3-2-8). As shown for sample **6^{Me}SnMe$_2$** (Figure 3-2-8c), all of the expected signals were observed. Our assignments are based on published chemical shifts of α-, β-, and C^{ipso} atoms of poly(ferrocenylsilane)[1,36] and poly(ferrocenylstannane).[15c] For example, the reported chemical shifts of poly(ferrocenyldimethylsilane)[1,36] (δ = 73.6 (β), 71.9 (C^{ipso}), and 71.8 ppm (α)) match very well with those found for samples **6^{Me}SnMe$_2$**, **6^{Me}Sn*n*Bu$_2$**, and **6^{Me}Sn*t*Bu$_2$** (**6^{Me}SnMe$_2$**: δ = 73.5, 71.8, 71.7 ppm; **6^{Me}Sn*n*Bu$_2$**: δ = 73.6, 71.8, 71.6 ppm; **6^{Me}Sn*t*Bu$_2$**: δ = 73.6, 71.7, 71.4 ppm). Consequently, the other set of three signals of each sample must be due to the tin-bound Cp rings (**6^{Me}SnMe$_2$**: δ = 74.7, 71.4, 69.3 ppm; **6^{Me}Sn*n*Bu$_2$**: δ = 74.9, 71.5, 69.3 ppm; **6^{Me}Sn*t*Bu$_2$**: δ = 74.9, 72.1, 70.7 ppm). Similarly,

the three samples that contain $SiEt_2$-bridging units (**6^{Et}SnMe$_2$**, **6^{Et}Sn*n*Bu$_2$**, and **6^{Et}Sn*t*Bu$_2$**) each display two resonances for the α-C and α'-C, two for the β-C and β'-C

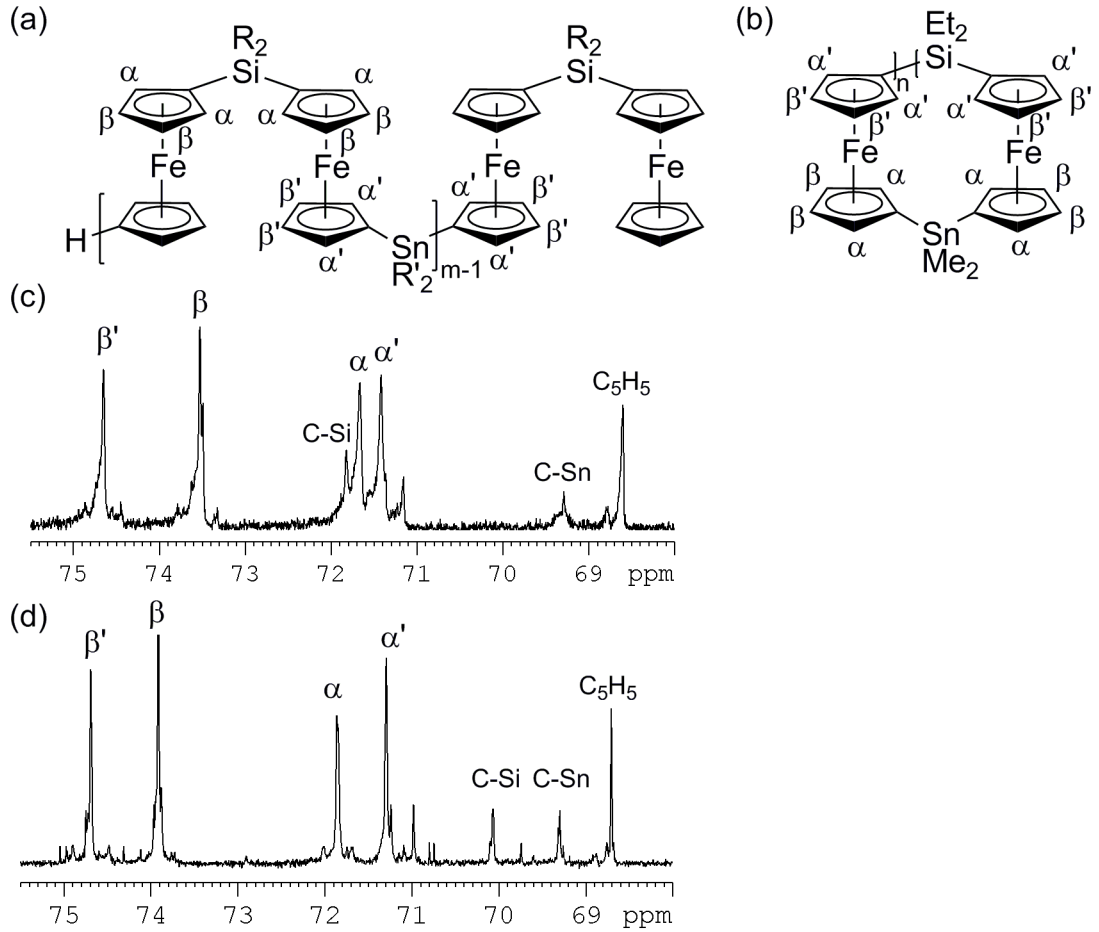

Figure 3-2-8. Different types of Cp carbons atoms in a) linear polymers and b) cyclic polymers. Cp region of the ^{13}C NMR spectra of c) **6^{Me}SnMe$_2$** and d) **6^{Et}SnMe$_2$**.

and two for C^{ipso} atoms (C-Si and C-Sn) (Figure 3-2-8d). The reported chemical shifts of poly(ferrocenyldiethylsilane)[36] of (δ = 74.4, 72.3, and 70.4 ppm) match very well with those found for samples **6^{Et}SnMe$_2$**, **6^{Et}Sn*n*Bu$_2$**, and **6^{Et}Sn*t*Bu$_2$** (**6^{Et}SnMe$_2$**: δ = 74.0, 71.9, 70.1 ppm; **6^{Et}Sn*n*Bu$_2$**: δ 74.0, 71.8, 70.0 ppm; **6^{Et}Sn*t*Bu$_2$**: δ 74.0, 71.6, 69.9 ppm).[39] Again, the remaining set of three signals of each sample must be resonances from the tin-bound Cp ring (**6^{Et}SnMe$_2$**: δ = 74.7, 71.3, 69.3 ppm; **6^{Et}Sn*n*Bu$_2$**: δ = 74.9, 71.4, 69.2

ppm; **6^{Et}Sn*t*Bu$_2$**: δ = 74.9, 72.0, 70.7 ppm); these assignments are consistent with those made for the $SiMe_2$-bridged mixtures (see above). Furthermore, our assignment made for the two Sn*t*Bu$_2$-containing mixtures (**6^{Me}Sn*t*Bu$_2$** and **6^{Et}Sn*t*Bu$_2$**) are similar to those reported for poly(ferrocenyldi-*tert*-butylstannane);[15c] differences are probably due to the use of different NMR solvents (δ = 74.5, 71.1, 70.6 ppm (C^{ipso}) in $CDCl_3$; **6^{Me}Sn*t*Bu$_2$**: δ = 74.9, 72.1, 70.7 ppm; **6^{Et}Sn*t*Bu$_2$**: δ = 74.9, 72.0, 70.9 ppm in C_6D_6). All six samples showed a sharp signal at δ = 68.6 or 68.7 ppm, which is caused by Cp end-groups and is consistent with the reported Cp signal of oligo(ferrocenylsilane) at δ = 68.6 ppm.[28c]

In the ^{29}Si NMR spectra, resonances for the Me_2Si-bridged samples appeared in the range of δ = −6 to −7 ppm, whereas those of the Et_2Si-bridged samples appeared in the range of δ = −2 to −3. These chemical shifts match well with the chemical shifts of reported poly(ferrocenyldimethylsilane) (δ = −6.4)[1,36] and poly(ferrocenyldiethylsilane) (δ = −2.7),[36] respectively. For each of the samples, two ^{29}Si NMR signals were detected, as shown for mixtures **6^{Me}SnMe$_2$** and **6^{Et}Sn*t*Bu$_2$** in Figure 3-2-9 (**6^{Me}SnMe$_2$**: δ = −6.9, −6.8 ppm; **6^{Me}Sn*n*Bu$_2$**: δ = −6.9, −6.7 ppm; **6^{Me}Sn*t*Bu$_2$**: δ = −6.8, −6.7 ppm; **6^{Et}SnMe$_2$:** δ = −3.0, −2.9 ppm; **6^{Et}Sn*n*Bu$_2$**: δ = −3.0, −2.9 ppm; **6^{Et}Sn*t*Bu$_2$**: δ = −3.0, −2.9 ppm). Assuming that ^{29}Si nuclei are insensitive to the ring size, one expects just one signal for a mixture of cyclic species. However, linear oligomers should give rise to two different resonances: one for internal-Si atoms (Figure 3-2-9, indicated by "o") and one for terminal-Si atoms (Figure 3-2-9, indicated by "*"). This result has been reported before: cyclic oligo(ferrocenyldimethylsilane) with 2-7 repeating units gave just one resonance at δ = −6.2, −6.3 or −6.4 ppm,[29] whereas linear oligo(ferrocenyldimethylsilane)s with Cp end-groups or $C_5H_4(SiMe_3)$ end-groups showed two resonances in the range δ = −6.4 to

−6.8 ppm.[28c] Therefore, we assigned the less-intense ^{29}Si NMR signal to terminal Si atoms and the more-intense peak to internal Si atoms (Figure 3-2-9).

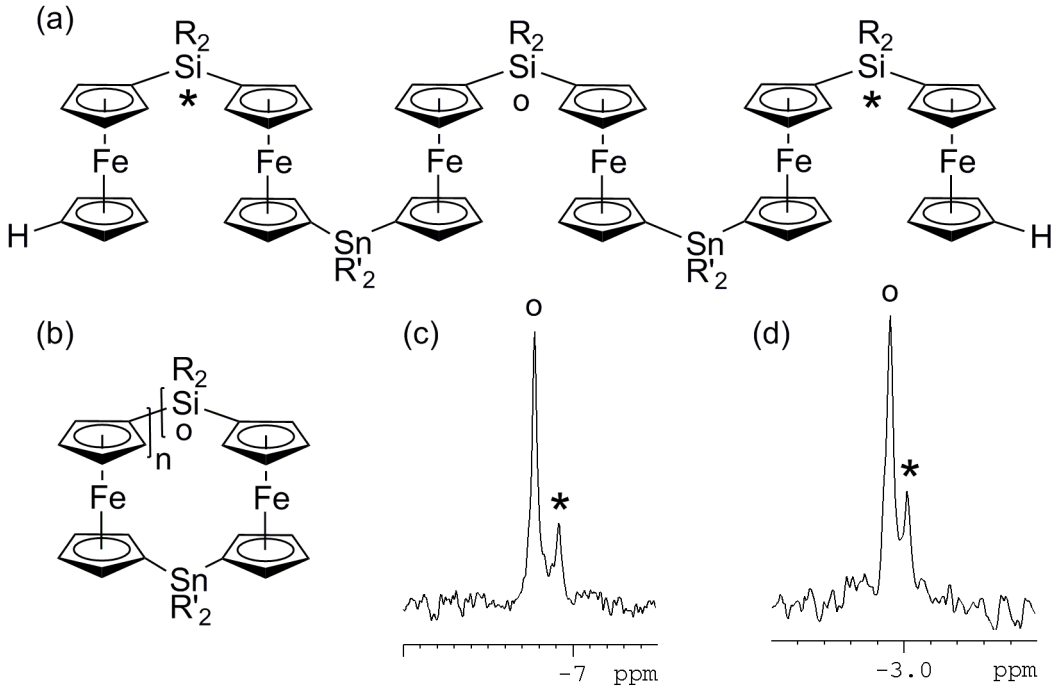

Figure 3-2-9. Terminal and internal Si atoms in a) linear species ***l*-(6^{R}SnR'$_2$)$_3$** and b) cyclic species ***c*-(6^{R}SnR'$_2$)$_n$**. ^{29}Si NMR spectra of c) **6^{Me}SnMe$_2$** and d) **6^{Et}SnMe$_2$**.

The ^{119}Sn NMR spectrum of each of the six mixtures exhibits one intense resonance and 2-4 weaker signals. The signals appeared in the range δ = −23 to −7 ppm for the Me_2Sn-bridged species (**6^{Me}SnMe$_2$**: δ = −16.8, −16.1, −15.3, −10.1, −7.4 ppm; **6^{Et}SnMe$_2$**: δ = −23.0, −15.8, −10.1, −7.5) and in the range δ = −32 to −26 ppm for the *n*Bu_2Sn-bridged species (**6^{Me}Sn*n*Bu$_2$**: δ = −29.0, −28.4, −27.0; **6^{Et}Sn*n*Bu$_2$**: δ = −31.8, −30.4, −28.5, −26.6 ppm). Most signals for *t*Bu_2Sn-bridged species **6^{Me}Sn*t*Bu$_2$** and **6^{Et}Sn*t*Bu$_2$** concentrated in the range of δ = −49 to −34 ppm (**6^{Me}Sn*t*Bu$_2$**: δ = −48.9, −48.2, −38.3, −34.6 ppm; **6^{Et}Sn*n*Bu$_2$**: δ = −48.7, −43.1, −38.2, −34.4 ppm); however, a weak signal appeared further downfield at δ = 75.0 ppm (**6^{Me}Sn*t*Bu$_2$**) and δ = 75.2

(**6^{Et}Sn*t*Bu$_2$**). The chemical shifts of the weak signals are very similar to that reported for FcSn*t*Bu$_2$Cl (δ = 72.3),[40] which indicates the presence of small amounts of Sn*t*Bu$_2$Cl end groups. The known ^{119}Sn chemical shifts for poly(ferrocenyldi-*tert*-butylstannane) (δ = −45.2 ppm)[15c] and for di-*tert*-butylstanna[1.1]ferrocenophane (δ= −33.3 ppm)[15c] show that both samples **6^{Me}Sn*t*Bu$_2$** and **6^{Et}Sn*t*Bu$_2$** contain linear and cyclic species. This is in contrast to the ^{29}Si NMR spectroscopic studies (see above), in which the linear and cyclic species could not be differentiated. However, ^{119}Sn chemical shifts of organotin compounds cover a range of 5200 ppm with two extremes at δ = 2960 ppm for (2,6-Mes$_2$C$_6$H$_3$)Sn(*t*Bu$_3$Ge)[41] and at δ = −2247 ppm for (η^5-Me$_5$C$_5$)Sn[BF$_4$].[42] With such a sensitive nucleus, it is feasible that different linear and cyclic species give different ^{119}Sn resonances; however, assignment of all of the measured peaks was not possible.

Molecular weight determinations: As shown by NMR spectroscopy and MALDI-TOF MS, each of the six samples (**6^{Me}SnR′$_2$** and **6^{Et}SnR′$_2$**) is a mixture of cyclic and linear species. Therefore, gel-permeation chromatography (GPC) was used to determine their average molecular weights by using polystyrene as a standard. As shown in Table 3-2-2, molecular weights M_w were found in the range of 2100-6300 Da. From the six samples, only the two *n*Bu$_2$Sn-bridged samples stand out with relatively broad molecular weight distributions (PDIs = 2.52 and 2.26); the reason for this difference is currently unknown. We employed dynamic light scattering (DLS) to estimate the M_w values, which gave comparable results to those from GPC (for details, see Supporting Information).

Table 3-2-2. Determinations of Molecular Weight [Da] by GPC.[a]

polymers	M_n	M_w	PDI	DP_w[b]
6^{Me}SnMe$_2$	2000	2900	1.45	5

$6^{Me}Sn^{n}Bu_2$	2500	6300	2.52	10
$6^{Me}Sn^{t}Bu_2$	1800	2500	1.39	4
$6^{Et}SnMe_2$	1800	2600	1.44	4
$6^{Et}Sn^{n}Bu_2$	2300	5200	2.26	8
$6^{Et}Sn^{t}Bu_2$	1600	2100	1.31	3

[a] From solutions in thf against polystyrene as a standard. [b] The Molecular weights of the [1.1]FCPs were taken as idealized repeating units to calculate the degree of polymerization DP_w) from the M_w values.

CONCLUSION

The two bis(1'-bromoferrocenyl)dialkylsilanes, **5^{Me}** and **5^{Et}**, were prepared using standard methods. These new species were lithiated with *t*BuLi (0 °C; *n*-hexane/thf, 9 : 1),[25] followed by addition of R'_2SnCl_2 (R' = Me, *n*Bu, *t*Bu; Scheme 3-2-3) to give six different mixtures of oligomers from which cyclic (***c*-($6^{Me}SnMe_2$)$_1$**, ***c*-($6^{Me}Sn$*t*Bu_2)$_2$**, ***c*-($6^{Et}SnMe_2$)$_1$**, ***c*-($6^{Et}Sn$*t*Bu_2)$_2$**) and linear species (***l*-($6^{Me}Sn$*n*Bu_2)$_2$**, ***l*-($6^{Me}Sn$*n*Bu_2)$_3$**) with up to six ferrocene moieties could be isolated. Single-crystal X-ray analysis of the two [1.1.1.1]FCPs, ***c*-($6^{Me}Sn$*t*Bu_2)$_2$** and ***c*-($6^{Et}Sn$*t*Bu_2)$_2$**, revealed different ring conformations: whilst the $SiMe_2$-bridged species shows an oval shape in the solid state, the $SiEt_2$-bridged species exhibits square-shaped macrocycles. This difference is probably a consequence of the unique conformation at fc-$SiMe_2$-fc moieties in which both ferrocenediyl units (fc) are in *trans* positions (Figure 3-2-4), a conformation that has not been reported previously for fc-$SiEt_2$-fc moieties. However, in solution, all cyclic species undergo fast ring inversions; e.g., the two [1.1.1.1]FCPs both show the highest possible symmetry for such macrocycles (D_{2h} symmetries). Initially, we intended to develop synthetic methods to prepare [1.1]FCPs with mixed bridging elements; however, finding cyclic species with two fc units, as well as with four fc units, was not a surprise. Still, the extended array of

cyclic species that contain up to 20 fc moieties for some samples, as uncovered by MALDI-TOF MS measurements, was unexpected. To date, to the best of our knowledge, only photocontrolled ROP of dimethylsila[1]ferrocenophane (**1a**; Figure 3-2-1) has resulted in larger macrocycles[29] (>40 fc units).[43] In contrast to these known cyclic poly(ferrocenylsilane)s, our compound mixtures exhibit silicon and tin atoms at alternating bridging positions, a structural motif that would be difficult to realize through a chain-growth-polymerization pathway of strained sandwich compounds.

The linear species that were formed from the salt-metathesis reactions between lithiated $\mathbf{5}^{\mathbf{Me}}$ or $\mathbf{5}^{\mathbf{Et}}$ and R'_2SnCl_2 (R′ = Me, *n*Bu; Scheme 3-2-3) could only be identified with Cp rings as the end-groups. These end-groups are possibly the result of chain terminations through hydrolysis of lithiated chain-ends. To our surprise, NMR spectroscopy only suggested the presence of Sn*t*Bu$_2$Cl end-groups in the metathesis reaction with Sn*t*Bu$_2$Cl$_2$. In all other cases, we did not obtain any evidence for such end-groups. We can only speculate that R′ = Me or *n*Bu chain-ends are too short-lived and either cyclization or further reaction with lithiated Cp moieties occurs. It seems that the steric hindrance in case of *t*Bu-equipped species lowers the reactivity of the Sn*t*Bu$_2$Cl end-groups so that some survive the reaction conditions.

EXPERIMENTAL SECTION

General information: Syntheses were carried out partly carried out by using standard Schlenk techniques and partly in air. Dry solvents were used for the reactions and solvents that were used for workup and purifications were used as received. Solvents were dried using a MBraun Solvent Purification System and stored under a nitrogen

atmosphere over 3 Å molecular sieves. All solvents for NMR spectroscopy were used as received. Ferrocene, *n*BuLi, *t*BuLi, nBu$_2$SnCl$_2$, and tBu$_2$SnCl$_2$ were purchased from Sigma Aldrich, and Me_2SiCl_2, Et_2SiCl_2, and Me_2SnCl_2 were purchased from Alfa Aesar and used as received. Silica gel 60 (EMD, Geduran®, particle size 0.040-0.063 mm) and Al_2O_3 (Alpha Aesar, activated, neutral, Brockmann grade I, 58 Å) were used for column chromatography. 1,1′-Dibromoferrocene[44] and poly(ferrocenyldiethylsilane) [39,45] were synthesized according to literature procedures. ^{1}H, ^{13}C, ^{29}Si and ^{119}Sn NMR spectra were recorded on a Bruker 500 MHz Avance NMR spectrometer at 25 ºC in C_6D_6, $CDCl_3$ and [D_8]toluene, respectively. ^{29}Si NMR chemical shifts were referenced to tetramethylsilane and ^{119}Sn NMR values were referenced to tributyltin chloride (δ 152.0 in $CDCl_3$). ^{1}H chemical shifts were referenced to the residual protons of the deuterated solvents (δ 7.15 for C_6D_6, 7.26 for $CDCl_3$ and 2.08 for [D_8]toluene); ^{13}C chemical shifts were referenced to the C_6D_6 signal at δ 128.00, the $CDCl_3$ signal at δ 77.00, and the [D_8]toluene signals at δ 20.43. Assignments of the relative chemical shifts of α-C atoms (upfield) with respect to β-C atoms (downfield) in ^{13}C NMR spectra are based on assignments reported reviously.[36] Mass spectra (70 eV) were measured on a VG 70SE and the data reported in the form *m/z* (%) $[M]^+$ where *m/z* is the mass observed. The intensities are reported relative to the most intense peak and $[M]^+$ is the molecular ion or a fragment, only characteristic mass peaks are listed. For isotopic pattern, only the mass peak of the isotopoloque or of the isotope with the highest natural abundance is listed. Elemental analyses were performed on a PerkinElmer 2400 CHN Elemental Analyzer by using V_2O_5 to promote complete combustion.

MALDI-TOF Mass Spectrometry: MALDI-TOF mass spectra were collected on a 4700 Proteomics Analyzer (Applied Biosystems) that was equipped with a Nd:Yag laser and operated at 335 nm. Positive-ion mass spectra were obtained in reflector- or linear mode over the range *m/*z 500-5000. Each spectrum was an accumulation of 12500 laser shots over 100 points on the sample (125 shots/point). The laser intensity was varied for each sample. Solutions of the analytes (1 mg mL^{-1} in thf) and dithranol (10 mg mL^{-1} in thf) were prepared and then mixed in a 1:10 ratio. The resulting solutions were drop-cast by using a micropipette into sample wells and allowed to evaporate for 1 h prior to analysis.

Gel Permeation Chromatography (GPC): The molecular weights of polymers and the polydispersity indices (PDI = M_w / M_n) of all of the samples were obtained by using a Viscotek VE 2001 Gel Permeation Chromatograph that was equipped with an automatic sampler, a pump, an injector, an in-line degasser, a column oven (30 °C), styrene/divinylbenzene columns with pore sizes of 500 and 100,000 Å, and a VE 3580 refractometer. Tetrahydrofuran that was stabilized with 0.025% butylated hydroxytoluene (Fisher) was used as the eluent at a flow rate of 1.0 mL min^{-1}. These samples were dissolved in the eluent (2 mg mL^{-1}) and filtered (Acrodisc, PTFE membrane, 0.45 μm) before analysis. Calibration of the refractive index detector was performed by using polystyrene standards (Viscotek).

Synthesis of bis(1'-bromoferrocenyl)dimethylsilane (5^{Me}): According to a literature procedure[46] *n*BuLi (2.5 M in hexane, 8.20 mL, 20.5 mmol) was added dropwise into a cold (−78 °C) solution of 1,1′-dibromoferrocene (6.87 g, 20.0 mmol) in thf (50 mL). The reaction mixture was stirred for 20 min at −78 °C, followed by the addition of Me_2SiCl_2

(1.24 g, 9.60 mmol). The reaction mixture was warmed to RT and stirred for 16 h, thereby resulting in a red solution. The following work-up was done in air, by using ACS grade solvents. All of the volatiles compounds were removed from the red solution, thereby yielding a red paste that was extracted with *n*-hexane (50 mL). All of the volatile compounds were removed from the *n*-hexane solution under high vacuum, thereby resulting in a red oil (5.14 g) as the crude product. Column chromatography on alumina (*n*-hexane) afforded compound $\mathbf{5^{Me}}$ as an orange solid (3.10 g, 55%). Note: $\mathbf{5^{Me}}$ could not be obtained as an analytically pure compound and contained small amounts of Fc_2SiMe_2 (see the Supporting Information, Figure S1 and S2). ^{1}H NMR ($CDCl_3$): δ = 0.55 (s, 6H; $SiMe_2$), 4.01, 4.14, 4.35, 4.42 (pst, 16H; C_5H_4); ^{13}C NMR ($CDCl_3$): δ = -0.9 (CH_3), 67.4, 70.3, 74.0, 75.6 (C_5H_4), 73.0, 77.7 (C^{ipso} of C_5H_4); MS (70 eV): *m/z* (%): 586 (100) [M^+], 506 (27) [M^+–Br], 291 (29) [$C_{10}H_8BrFeSi^+$], 241 (24) [$C_{12}H_{14}FeSi^+$], 169 (14) [$C_{11}H_9Si^+$], 121 (38) [$C_7H_9Si^+$]; HRMS (70 eV): *m/z* calcd for $C_{22}H_{22}Br_2Fe_2Si$: 585.8552 [M^+]; found: 585.8535; elemental analysis calcd (%) for $C_{22}H_{22}Br_2Fe_2Si$: C 45.09, H 3.78; found: C 46.44, H, 3.91.

Synthesis of bis(1'-bromoferrocenyl)diethylsilane ($\mathbf{5^{Et}}$). As described for the synthesis of compound $\mathbf{5^{Me}}$, the reaction of *n*BuLi (2.5 M in *n*-hexane, 10.6 mL, 26.5 mmol), 1,1'-dibromoferrocene (8.96 g, 26.1 mmol) and Et_2SiCl_2 (1.84 g, 11.7 mmol) in thf (70 mL) afforded a red oil (6.66 g), which gave compound $\mathbf{5^{Et}}$ as an orange solid (4.93 g, 69%) after column chromatography on alumina (*n*-hexane). Note: compound $\mathbf{5^{Et}}$ could not be obtained as an analytically pure compound and contained small amounts of Fc_2SiEt_2 (see the Supporting Information, Figure S3 and S4). ^{1}H NMR ($CDCl_3$): δ = 1.05 (q, 4H; CH_2), 1.15 (t, 6H; CH_3), 3.97, 4.17, 4.33, 4.42 (pst, 16H; C_5H_4); ^{13}C NMR

($CDCl_3$): δ = 6.0 (CH_2), 8.1 (CH_3), 67.6, 70.4, 74.1, 75.9 (C_5H_4), 71.1, 77.7 (C^{ipso} of C_5H_4); MS (70 eV): *m/z* (%): 614 (100) [M^+], 534 (14) [$C_{24}H_{27}BrFe_2Si^+$], 504 (11) [$C_{22}H_{21}BrFe_2Si^+$], 305 (35) [$C_{11}H_{10}BrFeSi^+$], 277 (24) [$C_{15}H_{13}FeSi^+$], 213 (21) [$C_{10}H_9FeSi^+$], 93 (17) [$C_5H_5Si^+$]; HRMS (70 eV): *m/z* calcd for $C_{24}H_{26}Br_2Fe_2Si$: 613.8849 [M^+]; found: 613.8859; elemental analysis calcd (%) for $C_{24}H_{26}Br_2Fe_2Si$ (614.047): C 46.94, H 4.27; found: C 47.10, H 4.18.

General procedure for the syntheses of the six mixtures ($6^{Me}SnMe_2$, $6^{Me}Sn$*n*Bu_2, $6^{Me}Sn$*t*Bu_2, $6^{Et}SnMe_2$, $6^{Et}Sn$*n*Bu_2, and $6^{Et}Sn$*t*Bu_2): *t*BuLi (1.7 M in pentane) was added dropwise to a cold solution (0 °C) of $\mathbf{5^{Me}}$ or $\mathbf{5^{Et}}$ in a mixture of dry thf/*n*-hexane (1:9) under a N_2-atmosphere. After the addition of *t*BuLi, the reaction mixture was stirred for 20 min at 0 °C, followed by the addition of a solution of R'_2SnCl_2 (R' = Me, *n*Bu, *t*Bu) in thf. The reaction mixture was warmed to r.t. and stirred for an additional 2.5 h, thereby resulting in a red solution. The following work-up was done in air by using ACS grade solvents: All of the volatile compounds were removed under vacuum, thereby resulting in a red paste, which was extracted with toluene. The toluene solution was concentrated to one third of its original volume and added dropwise to *n*-hexane (3-4 times the volume of the toluene solution) while stirring vigorously to afford a red solution with an off-white precipitate. The solid was filtered off and all of the volatile compounds were removed from the red solution under vacuum, thus yielding a red paste, which was redissolved in toluene. The toluene solution was added dropwise to MeOH (3-4 times the volume of the toluene solution) while stirring vigorously to afford a gummy red precipitate within an orange solution. The solid was filtered off, dried under high vacuum, and redissolved in toluene. A second precipitation into MeOH resulted in a gummy red precipitate and a

pale yellow solution. The solid was filtered off and dried under high vacuum at 65 °C for 16 h, yielding either a red solid or gummy materials.

Synthesis of $6^{Me}SnMe_2$: As described in the general procedure, the reaction of a solution of compound $\mathbf{5^{Me}}$ (1.08 g, 1.84 mmol) in thf/*n*-hexane (4mL/36mL), *t*BuLi (4.50 mL, 7.65 mmol), and Me_2SnCl_2 (0.405 g, 1.84 mmol) in thf (25 mL) afforded $\mathbf{6^{Me}SnMe_2}$ as a red solid (0.904 g, ca. 85%). ^{1}H NMR (C_6D_6): δ = 0.4-0.7 (br m, 12H; $SiMe_2$ and $SnMe_2$), 3.9-4.5 (br m, 16H; Cp); ^{13}C NMR (C_6D_6): δ = −8.5 ($SnMe_2$), −0.5 ($SiMe_2$), 68.6 (C_5H_5), 73.5 (β), 71.8 (C^{ipso}), 71.7 (α, Si-bound C_5H_4), 74.7 (β'), 71.4 (α'), 69.3 (C^{ipso}, Sn-bound C_5H_4), 71.2; ^{29}Si NMR: δ = −6.9, −6.8 ($SiMe_2$); ^{119}Sn NMR: δ = −7.4, −10.1, −15.3, −16.1, −16.8 ($SnMe_2$).

Synthesis of $6^{Me}Sn$*n*Bu_2. As described in the general procedure, the reaction of a solution of compound $\mathbf{5^{Me}}$ (1.20 g, 2.05 mmol) in thf/*n*-hexane (4mL/36mL), *t*BuLi (5.00 mL, 8.50 mmol), and *n*Bu_2SnCl_2 (0.621 g, 2.04 mmol) affordd $\mathbf{6^{Me}Sn}$*n*$\mathbf{Bu_2}$ as a red solid (0.906 g, ca. 81%). ^{1}H NMR (C_6D_6): δ = 0.4-0.7 (br m, 6H; $SiMe_2$), 0.9-1.1 (br m, 6H; CH_3 of Sn*n*Bu_2), 1.2-1.4 (br m, 6H; CH_2 of Sn*n*Bu_2), 1.4-1.6 (br m, 6H; CH_2 of Sn*n*Bu_2), 1.7-2.0 (br m, 6H; CH_2 of Sn*n*Bu_2), 3.9-4.5 (br m, 16H; Cp); ^{13}C NMR: δ = −0.5 ($SiMe_2$), −11.8, −14.2, −27.8, −29.7 (Sn*n*Bu_2), 68.6 (C_5H_5), 73.6 (β), 71.8 (C^{ipso}), 71.6 (α, Si-bound C_5H_4), 74.9 (β'), 71.5 (α'), 69.3 (C^{ipso}, Sn-bound C_5H_4), 71.2; ^{29}Si NMR: δ = −6.9, −6.7; ^{119}Sn NMR: δ = −29.0, −28.4, −27.0 (Sn*n*Bu_2).

Synthesis of $6^{Me}Sn$*t*Bu_2. As described in the general procedure, the reaction of a solution of compound $\mathbf{5^{Me}}$ (1.17 g, 2.00 mmol) in thf/*n*-hexane (4mL/36mL), *t*BuLi (4.90 mL, 8.33 mmol), and *t*Bu_2SnCl_2 (0.609 g, 2.00 mmol) in thf (25 mL) afforded $\mathbf{6^{Me}Sn}$*t*$\mathbf{Bu_2}$ as a red solid (0.905 g, ca. 83%). ^{1}H NMR (C_6D_6): δ = 0.4-0.7 (br m, 6H; $SiMe_2$), 1.2-1.6

(br m, 18H; Sn*t*Bu$_2$), 3.9-4.5 (br m, 16H; Cp); ^{13}C NMR: δ = −0.6 (SiMe$_2$), 29.0 (C of Sn*t*Bu$_2$), 32.0 (CH$_3$ of Sn*t*Bu$_2$), 68.6 (C$_5$H$_5$), 73.6 (β), 71.7 (C^{ipso}), 71.4 (α, Si-bound C$_5$H$_4$), 74.9 (β'), 72.1 (α'), 70.7 (C^{ipso}, Sn-bound C$_5$H$_4$), 71.2; ^{29}Si NMR: δ = −6.8, −6.7; ^{119}Sn NMR: δ = −34.6, −38.3, −48.2, −48.9, (Sn*t*Bu$_2$), 75.0 (Sn*t*Bu$_2$Cl end-groups; see text).

Synthesis of 6^{Et}SnMe$_2$. As described in the general procedure, the reaction of a solution of compound **5^{Et}** (1.29 g, 2.10 mmol) in thf/*n*-hexane (4mL/36mL), *t*BuLi (5.10 mL, 8.67 mmol), and Me$_2$SnCl$_2$ (0.463 g, 2.11 mmol) in thf (25 mL) afforded **6^{Et}SnMe$_2$** as a red solid (0.706 g, ca. 61%). ^{1}H NMR (C$_6$D$_6$): δ = 0.4-0.6 (br m, 6H; SnMe$_2$), 0.9-1.1 (br m, 4H; CH$_2$ of SiEt$_2$), 1.1-1.3 (br m, 6H; CH$_3$ of SiEt$_2$), 3.9-4.5 (br m, 16H; Cp); ^{13}C NMR (C$_6$D$_6$): δ = −8.5 (SnMe$_2$), 6.5 (CH$_2$ of SiEt$_2$), 8.6 (CH$_3$ of SiEt$_2$), 68.7 (C$_5$H$_5$), 74.0 (β), 71.9 (α), 70.1 (C^{ipso}, Si-bound C$_5$H$_4$), 74.7 (β'), 71.3 (α'), 69.3 (C^{ipso}, Sn-bound C$_5$H$_4$), 71.0; ^{29}Si NMR: δ = −2.9, −3.0; ^{119}Sn NMR: δ = −23.0, −15.8, −10.0, −7.5 (SnMe$_2$).

Synthesis of 6^{Et}Sn*n*Bu$_2$. As described in the general procedure, the reaction of a solution of compound **5^{Et}** (1.30 g, 2.11 mmol) in thf/*n*-hexane (4mL/36mL), *t*BuLi (5.10 mL, 8.67 mmol), and *n*Bu$_2$SnCl$_2$ (0.649 g, 2.14 mmol) in thf (25 mL) afforded **6^{Et}Sn*n*Bu$_2$** as a red solid (0.750 g, ca. 56 %). ^{1}H NMR (C$_6$D$_6$): δ = 0.9-1.1 (br m, 6H; CH$_3$ of Sn*n*Bu$_2$), 1.1-1.2 (br m, 4H; CH$_2$ of SiEt$_2$), 1.2-1.3 (br m, 6H; CH$_3$ of SiEt$_2$), 1.3-1.4 (br m, 4H; CH$_2$ of Sn*n*Bu$_2$), 1.4-1.6 (br m, 4H; CH$_2$ of Sn*n*Bu$_2$), 1.7-1.9 (br m, 4H; CH$_2$ of Sn*n*Bu$_2$), 3.9-4.5 (br m, 16H; Cp); ^{13}C NMR (C$_6$D$_6$): δ = 6.5 (CH$_2$ of SiEt$_2$), 8.6 (CH$_3$ of SiEt$_2$), 11.9, 14.0, 27.9, 29.7 (Sn*n*Bu$_2$), 68.7 (C$_5$H$_5$), 74.0 (β), 71.8 (α), 70.0

(C^{ipso}, Si-bound C_5H_4), 74.9 (β'), 71.4 (α'), 69.2 (C^{ipso}, Sn-bound C_5H_4), 71.3; ^{29}Si NMR: $\delta = -2.9, -3.0$; ^{119}Sn NMR: $\delta = -31.8, -30.4, -28.5, -26.6$ (Sn*n*Bu_2).

Synthesis of $\mathbf{6^{Et}Sn}$*t*$\mathbf{Bu_2}$. As described in the general procedure, the reaction of a solution of compound $\mathbf{5^{Et}}$ (1.26 g, 2.05 mmol) in thf/*n*-hexane (4mL/36mL), *t*BuLi (5.00 mL, 8.50 mmol), and *t*Bu_2SnCl_2 (0.622 g, 2.05 mmol) in thf (25 mL) afforded $\mathbf{6^{Et}Sn}$*t*$\mathbf{Bu_2}$ as a red solid (0.848 g, ca. 66%). ^{1}H NMR (C_6D_6): δ = 0.9-1.1 (br m, 4H; CH_2 of $SiEt_2$), 1.1-1.3 (br m, 6H; CH_3 of $SiEt_2$), 1.3-1.5 (br m, 18H; Sn*t*Bu_2), 3.9-4.5 (br m, 16H; Cp); ^{13}C NMR (C_6D_6): δ = 6.5 (CH_2 of $SiEt_2$), 8.6 (CH_3 of $SiEt_2$), 31.6 (C of Sn*t*Bu_2), 31.8 (CH_3 of Sn*t*Bu_2), 68.7 (C_5H_5), 74.0 (β), 71.6 (α), 69.9 (C^{ipso}, Si-bound C_5H_4), 74.9 (β'), 72.0 (α'), 70.7 (C^{ipso}, Sn-bound C_5H_4); plus additional unassigned peaks (see the Supporting Information, Figure S16); ^{29}Si NMR: $\delta = -2.9, -3.0$ ($SiMe_2$); ^{119}Sn NMR: $\delta = -48.7, -43.1, -38.2, -34.4$, (Sn*t*$Bu_2$) 75.2 (Sn*t*$Bu_2$Cl end-groups; see text).

Isolation and characterization of *c*-$\mathbf{(6^{Me}SnMe_2)_1}$, *c*-$\mathbf{(6^{Me}Sn}$*t*$\mathbf{Bu_2)_2}$, *c*-$\mathbf{(6^{Et}SnMe_2)_1}$, *c*-$\mathbf{(6^{Et}Sn}$*t*$\mathbf{Bu_2)_2}$, *l*-$\mathbf{(6^{Me}Sn}$*n*$\mathbf{Bu_2)_2}$, and *l*-$\mathbf{(6^{Me}Sn}$*n*$\mathbf{Bu_2)_3}$: Compound *c*-$\mathbf{(6^{Me}SnMe_2)_1}$ was isolated from the mixture $\mathbf{6^{Me}SnMe_2}$ by column chromatography on silica gel (CH_2Cl_2/*n*-hexane, 1:10) as an orange solid (0.065 g, 6%); the product was eluted as the first orange band. ^{1}H NMR (C_6D_6): δ = 0.52 (s, 6H; $SnMe_2$), 0.56 (s, 6H; $SiMe_2$), 4.11, 4.13, 4.28, 4.32 (pst, 16H; C_5H_4); ^{13}C NMR (C_6D_6): δ = −8.5 ($SnMe_2$), −0.5 ($SiMe_2$), 69.3 (C^{ipso} of Si-C_5H_4 or Sn-C_5H_4), 71.9 (C^{ipso} of Si-C_5H_4 or Sn-C_5H_4), 71.4, 73.5 (α-C and β-C of Si-C_5H_4), 71.7, 74.7 (α-C and β-C of Sn-C_5H_4); MS (70 eV): *m/z* (%): 576 (18) $[M]^+$, 561 (29) $[M–Me]^+$, 426 (43) $[M–SnMe_2]^+$, 411 (16) $[M–SnMe_2–Me]^+$, 363 (24) $[M–C_{10}H_8Fe–2Me]^+$, 335 (28) $[C_{10}H_{11}FeSiSn]^+$, 243 (48) $[M–C_{10}H_8Fe–SnMe_2]^+$, 149 (21) $[C_2H_5Sn]^+$. HRMS (70 eV): *m/z* calcd for $C_{24}H_{28}Fe_2SiSn$: 575.9692 [M^+]; found: 575.9681.

Compund ***c*-($\mathbf{6^{Me}Sn}$*t*$\mathbf{Bu_2)_2}$** was isolated as orange crystals as ***c*-($\mathbf{6^{Me}Sn}$*t*$\mathbf{Bu_2)_2}$·$\mathbf{C_7H_8}$** (0.102 g, 7%) from a solution of the mixture **$\mathbf{6^{Me}Sn}$*t*$\mathbf{Bu_2}$** in toluene at RT. ^{13}C NMR could not be performed because of the poor solubility of ***c*-($\mathbf{6^{Me}Sn}$*t*$\mathbf{Bu_2)_2}$·$\mathbf{C_7H_8}$** in common organic solvents. ^{1}H NMR ($CDCl_3$): δ = 0.60 (s, 12H; $SiMe_2$), 1.25 (s, 36H; Sn*t*Bu_2), 4.12, 4.20, 4.31, 4.38 (pst, 32H; C_5H_4); MS (70 eV): *m/z* (%): 1318 (16) $[M]^+$, 1261 (7) $[M–t\text{Bu}]^+$, 603 (100) $[C_{26}H_{31}Fe_2SiSn]^+$, 540 (100) $[C_{22}H_{22}Fe_2SiSn]^+$; HRMS (70 eV): *m/z* calcd for $C_{60}H_{40}Fe_4Si_2Sn_2$: 1318.1233; found: 1318.1234.

Compound ***c*-($\mathbf{6^{Et}SnMe_2)_1}$** was isolated as orange crystals (0.041 g, 3%) from a solution of the mixture **$\mathbf{6^{Et}SnMe_2}$** in MeOH at RT. Crystals for attempted analysis of the molecular structure by single crystal X-ray analysis were isolated from the solutions in hexane at RT, -22 °C and -80 °C, in acetone at -22 °C, and in Et_2O at -22 °C. ^{1}H NMR (C_6D_6): δ = 0.37 (s, 6H; $SnMe_2$), 0.88-0.92 (q, 4H; CH_2 of $SiEt_2$), 1.01-1.04 (t, 6H; CH_3 of $SiEt_2$), 4.25, 4.26, 4.29, 4.30 (pst, 16H; C_5H_4); ^{13}C NMR (C_6D_6): δ = −7.0 ($SnMe_2$), 8.1 (CH_2), 8.5 (CH_3 of $SiEt_2$), 68.8 (C^{ipso} of Si-C_5H_4 or Sn-C_5H_4), 69.3 (C^{ipso} of Si-C_5H_4 or Sn-C_5H_4), 70.7, 74.3 (α-C and β-C of Si-C_5H_4), 70.8, 75.0 (α-C and β-C of Sn-C_5H_4); MS (70 eV): *m/z* (%): 604 (100) $[M]^+$, 589 (64) $[M–\text{Me}]^+$, 440 (57) $[C_{23}H_{24}Fe_2Si]^+$, 425 (37) $[C_{22}H_{21}Fe_2Si]^+$, 411 (33) $[C_{21}H_{19}Fe_2Si]^+$, 397 (20) $[C_{20}H_{17}Fe_2Si]^+$, 333 (14) $[C_{15}H_{13}Fe_2Si]^+$, 213 (15) $[C_{10}H_9FeSi]^+$, 185 (12) $[C_{10}H_9Fe]^+$, 93 (17) $[C_5H_5Si]^+$; HRMS (70 eV): *m/z* calcd for $C_{26}H_{32}Fe_2SiSn$: 603.9994; found: 604.0016.

Compound ***c*-($\mathbf{6^{Et}Sn}$*t*$\mathbf{Bu_2)_2}$** was isolated from the mixture **$\mathbf{6^{Et}Sn}$*t*$\mathbf{Bu_2}$** by column chromatography on silica gel (CH_2Cl_2/*n*-hexane, 1:20) as an orange solid (0.045 g, 3%). The product was eluted as the fifth orange band. All the other four orange bands were mixture of compounds. Single crystals suitable for X-ray analysis were obtained from a

solution in hexane at RT. ^{1}H NMR (C_6D_6): δ = 1.16 (q, 8H; CH_2), 1.25 (t, 12H; CH_3 of $SiEt_2$), 1.28 (s, 36H; *t*Bu), 4.18, 4.33, 4.42, 4.50 (pst, 32H; C_5H_4); ^{1}H NMR ([D_8]toluene): δ = 1.14 (q, 8H; CH_2), 1.24 (t, 12H; CH_3 of $SiEt_2$), 1.33 (s, 36H; *t*Bu), 4.13, 4.27, 4.37, 4.45 (pst, 32H; C_5H_4); ^{13}C NMR ([D_8]toluene): δ = 6.8 (CH_2 of $SiEt_2$), 8.5 (CH_3 of $SiEt_2$), 28.8 (C of Sn*t*Bu_2), 31.6 (CH_3 of Sn*t*Bu_2), 70.2 (C^{ipso} of Si-C_5H_4 or Sn-C_5H_4), 70.7 (C^{ipso} of Si-C_5H_4 or Sn-C_5H_4), 71.9, 74.5 (α-C and β-C of Si-C_5H_4), 71.6, 75.2 (α-C and β-C of Sn-C_5H_4); MS (70 eV): *m/z* (%): 1374 (23) $[M]^+$, 1317 (5) $[M–t\text{Bu}]^+$, 985 (25) $[C_{41}H_{32}Fe_4Sn_2]^+$, 838 (88) $[C_{43}H_{42}Fe_4Si_2]^+$, 782 (100) $[C_{43}H_{42}Fe_3Si_2]^+$. HRMS (70 eV): *m/z* calcd for $C_{64}H_{88}Fe_4Si_2Sn_2$: 1374.1866; found: 1374.1860.

Compound ***l*-($\mathbf{6^{Me}Sn}n\mathbf{Bu_2})_2$** was isolated from the mixture **$\mathbf{6^{Me}Sn}n\mathbf{Bu_2}$** by column chromatography on silica gel (CH_2Cl_2/*n*-hexane, 1:15) as an orange gummy material (0.063 g). The product was eluted from the column as the third orange band and it contained a minor amount of impurities (see the Supporting Information, Figure S37). The other two orange bands were a mixture of compounds. ^{1}H NMR ($CDCl_3$): δ = 0.49 (s, 12H; $SiMe_2$), 0.96-0.99 (t, 6H; CH_3 of Sn*n*Bu_2), 1.21-1.25 (m, 4H; CH_2 of Sn*n*Bu_2), 1.41-1.48 (m, 4H; CH_2 of Sn*n*Bu_2), 1.66-1.72 (m, 4H; CH_2 of Sn*n*Bu_2), 4.02, 4.04, 4.12, 4.21, 4.28, 4.34 (pst, 24H; C_5H_4), 4.09 (s, 10H; C_5H_5); MS (70 eV): *m/z* (%): 1088 (17) $[M]^+$, 667 (100) $[C_{31}H_{35}Fe_2SiSn]^+$, 612 (20) $[C_{27}H_{29}Fe_2SiSn]^+$, 603 (29) $[C_{30}H_{39}FeSiSn]^+$, 546 (12) $[C_{22}H_{22}Fe_2SiSn]^+$. HRMS (70 eV): *m/z* calcd for $C_{52}H_{64}Fe_4Si_2Sn$: 1088.0972; found: 1088.0962.

Compound ***l*-($\mathbf{6^{Me}Sn}n\mathbf{Bu_2})_3$** was isolated from the mixture **$\mathbf{6^{Me}(Sn}n\mathbf{Bu_2)}$** by column chromatography on silica gel (CH_2Cl_2/*n*-hexane, 1:15) as an orange gummy material (0.071 g). The product was eluted as the fourth orange band and it contained a minor

amount of impurities (see the Supporting Information, Figure S38). The first two orange bands were a mixture of compounds, whereas the third band was ***l*-(6^{Me}Sn*n*Bu$_2$)$_2$**. ^{1}H NMR ($CDCl_3$): δ = 0.51 (s, 6H; $SiMe_2$), 0.52 (s, 12H; $SiMe_2$), 0.99-1.02 (t, 12H; CH_3 of Sn*n*Bu_2), 1.24-1.27 (m, 8H; CH_2 of Sn*n*Bu_2), 1.44-1.50 (m, 8H; CH_2 of Sn*n*Bu_2), 1.69-1.74 (m, 8H; CH_2 of Sn*n*Bu_2), 4.04, 4.05, 4.07, 4.15, 4.24, 4.30, 4.31, 4.37 (pst, 40H; C_5H_4), 4.13 (s, 10H; C_5H_5); MS (70 eV): *m/z* (%): 1746 (2) $[M]^+$, 1560 (20) $[M–C_{10}H_9Fe]^+$, 1504 (3) $[M–C_{10}H_9Fe–SiMe_2]^+$, 1450 (8) $[C_{64}H_{80}Fe_5Si_3Sn_2]^+$, 1430 (3) $[C_{65}H_{77}Fe_5Si_2Sn_2]^+$, 1398 (24) $[C_{64}H_{84}Fe_4Si_3Sn_2]^+$, 1376 (100) $[M–2C_{10}H_9Fe]^+$; HRMS (70 eV): *m/z* calcd for $C_{82}H_{104}Fe_6Si_3Sn_2$: 1746.1635; found: 1746.1642.

Single-crystal X-ray analysis of *c*-(6^{Et}Sn*t*Bu$_2$)$_2$: A transparent orange block-like crystal of ***c*-(6^{Et}Sn*t*Bu$_2$)$_2$** was coated with oil, collected onto the aperture of a mounted Micromount^{TM}(MiTeGen, USA) mounted onto the goniometer head, which was quickly transferred into the cold stream of the Oxford cryo-jet. All measurements were recorded on a Nonius KappaCCD 4-Circle Kappa FR540C diffractometer by using monochromated $Mo_{K\alpha}$ radiation at 173 K. An initial orientation matrix and cell was determined from 10 frames using ϕ scans. Data were measured using ϕ and ω scans.[47] Cell parameters were initially retrieved by using the COLLECT[47] software and then refined with the HKL DENZO and SCALEPACK software[48] by using 16207 observed reflections in the data collection. Data reduction was performed with the HKL DENZO and SCALEPACK software,[48] which corrects for beam inhomogeneity, possible crystal decay, Lorentz and polarization effects. A multiscan absorption correction was applied (SCALEPACK).[48] The structure was solved using direct methods (SIR-2004)[49] and refined by full-matrix least-squares procedures on F^2 with SHELXL97-2.[50] The non-

hydrogen atoms were refined anisotropically. Hydrogen atoms were included at geometrically idealized positions (C-H bond distances 0.95/0.98/0.99 Å) and were not refined. The isotropic thermal parameters of these hydrogen atoms were fixed at 1.2 times that of the preceding carbon atom. Neutral atom-scattering factors for non-hydrogen atoms and anomalous dispersion coefficients are contained in the SHELXTL-NT 6.14 program library.[51]

Single-crystal X-ray analysis of *c*-(6^{Me}Sn*t*Bu$_2$)$_2$·C$_7$H$_8$: Data was collected on an STOE IPDS-2T diffractometer with graphite-monochromated $Mo_{K\alpha}$ radiation (λ = 0.71073 Å) by using an oil-coated schock-cooled crystal at 100 K. Absorption effects were corrected empirically by using indexed faces of the crystal.[52] Cell constants were refined using 11794 observed reflections of the data collection. The structure was solved by direct methods and refined by full matrix least-squares procedures on F^2 using the SHELX-97.[50] The non-hydrogen atoms had been refined anisotropically. Hydrogen atoms were included at their calculated positions and refined by using the riding model with isotropic temperature factors at 1.2 times (for CH_3 groups 1.5 times) that of the preceding carbon atom. CH_3 groups were allowed to rotate about the bond to their next atom to fit the electron density. One molecule toluene per molecule of complex was present in the crystal structure that was disordered by crystallographic inversion symmetry. To fit the electron density, a complete toluene molecule was generated by this symmetry from maxima of the difference Fourier synthesis map and was introduced into the refinement as a rotating rigid group with occupation of 0.5 for all atoms. Both thermal ellipsoid plots were prepared using ORTEP-3 for Windows (Figure 3-2-2 and 3-2-3).[53]

ACKNOWLEDGEMENTS

J.M. thanks the NSERC of Canada for support through a Discovery Grant. J.B.G. is grateful to the EU (Marie Curie Programme) and the NSERC of Canada for postdoctoral fellowships. We thank the Canada Foundation for Innovation (CFI) and the government of Saskatchewan for funding the NMR facilities in the Saskatchewan Structural Sciences Centre (SSSC). We thank Prof. Ian Manners (University of Bristol) for making MALDI-TOF and GPC instruments available for our studies. We thank Prof. Ildiko Badea (University of Saskatchewan, College of Pharmacy and Nutrition) for allowing us to use the DLS instrument. We thank Ken Thoms for performing the MS measurements (EI mode).

REFERENCES

(1) Foucher, D. A.; Tang, B.-Z.; Manners, I. *J. Am. Chem. Soc.* **1992**, *114*, 6246-6248.

(2) (a) Manners, I. *Science* **2001**, *294*, 1664-1666. (b) Manners, I. *Synthetic Metal-Containing Polymers*, Wiley-VCH, Weinheim, **2004**. (c) Bellas, V.; Rehahn, M. *Angew. Chem., Int. Ed.* **2007**, *46*, 5082-5104. (d) Marin, V.; Holder, E.; Hoogenboom, R.; Schubert, U. S. *Chem. Soc. Rev.* **2007**, *36*, 618-635. (e) Whittell, G. R.; Manners, I. *Adv. Mater.* **2007**, *19*, 3439-3468. (f) Williams, K. A.; Boydston, A. J.; Bielawski, C. W. *Chem. Soc. Rev.* **2007**, *36*, 729-744. (g) Eloi, J. C.; Chabanne, L.; Whittell, G. R.; Manners, I. *Mater. Today* **2008**, *11*, 28-36. (h) Hempenius, M. A.; Cirmi, C.; Lo Savio, F.; Song, J.; Vancso, G. J. *Macromol. Rapid Commun.* **2010**, *31*, 772-783. (i) Wong, W. Y.; Harvey, P. D. *Macromol. Rapid Commun.* **2010**, *31*, 671-713. (j) Krüger, R. A.; Baumgartner, T. *Dalton Trans.* **2010**, *39*, 5759-5767. (k) Manners, I. *J. Organomet.*

Chem. **2011**, *696*, 1146-1149. (l) Whittell, G. R.; Hager, M. D.; Schubert, U. S.; Manners, I. *Nat. Mater.* **2011**, *10*, 176-188.

(3) MacLachlan, M. J.; Ginzburg, M.; Coombs, N.; Coyle, T. W.; Raju, N. P.; Greedan, J. E.; Ozin, G. A.; Manners, I. *Science* **2000**, *287*, 1460-1463.

(4) Arsenault, A. C.; Puzzo, D. P.; Manners, I.; Ozin, G. A. *Nat. Photonics* **2007**, *1*, 468-472.

(5) Ma, Y. J.; Dong, W. F.; Hempenius, M. A.; Möhwald, H.; Vancso, G. J. *Nat. Mater.* **2006**, *5*, 724-729.

(6) (a) Gilroy, J. B.; Gädt, T.; Whittell, G. R.; Chabanne, L.; Mitchels, J. M.; Richardson, R. M.; Winnik, M. A.; Manners, I. *Nat. Chem.* **2010**, *2*, 566-570. (b) Gilroy, J. B.; Rupar, P. A.; Whittell, G. R.; Chabanne, L.; Terrill, N. J.; Winnik, M. A.; Manners, I.; Richardson, R. M. *J. Am. Chem. Soc.* **2011**, *133*, 17056-17062. (c) Wang, X. S.; Guerin, G.; Wang, H.; Wang, Y. S.; Manners, I.; Winnik, M. A. *Science* **2007**, *317*, 644-647. (d) He, F.; Gädt, T.; Manners, I.; Winnik, M. A. *J. Am. Chem. Soc.* **2011**, *133*, 9095-9103. (e) Gädt, T.; Ieong, N. S.; Cambridge, G.; Winnik, M. A.; Manners, I. *Nat. Mater.* **2009**, *8*, 144-150. (f) Presa Soto, A.; Gilroy, J. B.; Winnik, M. A.; Manners, I. *Angew. Chem., Int. Ed.* **2010**, *49*, 8220-8223.

(7) Nesmeyanov, A. N.; Kritskaya, I. I. *Bull. Acad. Sci. USSR, Div. Chem. Sci. (Eng. Transl.)* **1956**, 243-244.

(8) (a) McKechnie, J. S.; Bersted, B.; Paul, I. C.; Watts, W. E. *J. Organomet. Chem.* **1967**, *8*, P29-P31. (b) McKechnie, J. S.; Maier, C. A.; Bersted, B.; Paul, I. C. *J. Chem. Soc., Perkin Trans. 2* **1973**, 138-143.

(9) Löwendahl, M.; Davidsson, Ö.; Ahlberg, P.; Håkansson, M. *Organometallics* **1993**, *12*, 2417-2419.

(10) Scheibitz, M.; Winter, R. F.; Bolte, M.; Lerner, H.-W.; Wagner, M. *Angew. Chem., Int. Ed.* **2003**, *42*, 924-927.

(11) (a) Braunschweig, H.; Burschka, C.; Clentsmith, G. K. B.; Kupfer, T.; Radacki, K. *Inorg. Chem.* **2005**, *44*, 4906-4908. (b) Schachner, J. A.; Orlowski, G. A.; Quail, J. W.; Kraatz, H.-B.; Müller, J. *Inorg. Chem.* **2006**, *45*, 454-459. (c) Schachner, J. A.; Lund, C. L.; Quail, J. W.; Müller, J. *Acta Crystallogr.* **2005**, *E61*, m682-m684.

(12) (a) Uhl, W.; Hahn, I.; Jantschak, A.; Spies, T. *J. Organomet. Chem.* **2001**, *637*, 300-303. (b) Jutzi, P.; Lenze, N.; Neumann, B.; Stammler, H. G. *Angew. Chem., Int. Ed.* **2001**, *40*, 1423-1427. (c) Althoff, A.; Jutzi, P.; Lenze, N.; Neumann, B.; Stammler, A.; Stammler, H.-G. *Organometallics* **2002**, *21*, 3018-3022. (d) Althoff, A.; Jutzi, P.; Lenze, N.; Neumann, B.; Stammler, A.; Stammler, H. G. *Organometallics* **2003**, *22*, 2766-2774.

(13) Schachner, J. A.; Lund, C. L.; Burgess, I. J.; Quail, J. W.; Schatte, G.; Müller, J. *Organometallics* **2008**, *27*, 4703-4710.

(14) (a) Herberhold, M.; Bärtl, T.; *Z. Naturforsch. B* **1995**, *50*, 1692-1698. (b) Park, J. W.; Seo, Y. S.; Cho, S. S.; Whang, D. M.; Kim, K. M.; Chang, T. Y. *J. Organomet. Chem.* **1995**, *489*, 23-25. (c) Zechel, D. L.; Foucher, D. A.; Pudelski, J. K.; Yap, G. P. A.; Rheingold, A. L.; Manners, I. *J. Chem. Soc., Dalton Trans.* **1995**, 1893-1899. (d) Ni, Y. Z.; Rulkens, R.; Pudelski, J. K.; Manners, I. *Macromol. Rapid Commun.* **1995**, *16*, 637-641. (e) Reddy, N. P.; Choi, N.; Shimada, S.; Tanaka, M. *Chem. Lett.* **1996**, 649-650. (f) MacLachlan, M. J.; Zheng, J.; Thieme, K.; Lough, A. J.; Manners, I.; Mordas, C.; LeSuer, R.; Geiger, W. E.; Liable-Sands, L. M.; Rheingold, A. L. *Polyhedron* **2000**, *19*,

275-289. (g) Calleja, G.; Carré, F.; Cerveau, G. *Organometallics* **2001**, *20*, 4211-4215. (h) Berenbaum, A.; Lough, A. J.; Manners, I. *Organometallics* **2002**, *21*, 4415-4424. (i) Bao, M.; Hatanaka, Y.; Shimada, S. *Chem. Lett.* **2004**, *33*, 520-521. (j) Sato, M.; Suzuki, M.; Okoshi, M.; Kurasina, M.; Watanabe, M. *J. Organomet. Chem.* **2002**, *648*, 72-80.

(15) (a) Seyferth, D.; Withers, H. P. *Organometallics* **1982**, *1*, 1275-1282. (b) Dong, T. Y.; Hwang, M. Y.; Wen, Y. S.; Hwang, W. S. *J. Organomet. Chem.* **1990**, *391*, 377-385. (c) Jäkle, F.; Rulkens, R.; Zech, G.; Foucher, D. A.; Lough, A. J.; Manners, I. *Chem.-Eur. J.* **1998**, *4*, 2117-2128. (d) Jäkle, F.; Rulkens, R.; Zech, G.; Massey, J.; Manners, I. *J. Am. Chem. Soc.* **2000**, *122*, 4231-4232. (e) Baumgartner, T.; Jäkle, F.; Rulkens, R.; Zech, G.; Lough, A. J.; Manners, I. *J. Am. Chem. Soc.* **2002**, *124*, 10062-10070.

(16) Utri, G.; Schwarzhans, K. E.; Allmaier, G. M. *Z. Naturforsch. B* **1990**, *45*, 755-762.

(17) (a) Brunner, H.; Klankermayer, J.; Zabel, M. *J. Organomet. Chem.* **2000**, *601*, 211-219. (b) Mizuta, T.; Onishi, M.; Miyoshi, K. *Organometallics* **2000**, *19*, 5005-5009. (c) Mizuta, T.; Imamura, Y.; Miyoshi, K. *Organometallics* **2005**, *24*, 990-996.

(18) Spang, C.; Edelmann, F. T.; Noltemeyer, M.; Roesky, H. W. *Chem. Ber.* **1989**, *122*, 1247-1254.

(19) Ieong, N. S.; Chan, W. Y.; Lough, A. J.; Haddow, M. R.; Manners, I. *Chem.-Eur. J.* **2008**, *14*, 1253-1263.

(20) Perucha, A. S.; Heilmann-Brohl, J.; Bolte, M.; Lerner, H. W.; Wagner, M. *Organometallics* **2008**, *27*, 6170-6177.

(21) (a) Lemenovskii, D. A.; Urazowski, I. F.; Baukova, T. V.; Arkhipov, I. L.; Stukan, R. A.; Perevalova, E. G. *J. Organomet. Chem.* **1984**, *264*, 283-288 (b) Kuz'mina, I. G.;

Struchkov, Y. T.; Lemenovsky, D. A.; Urazowsky, I. F. *J. Organomet. Chem.* **1984**, *277*, 147-151.

(22) Mueller-Westerhoff, U. T. *Angew. Chem., Int. Ed.* **1986**, *25*, 702-717.

(23) Lund, C. L.; Schachner, J. A.; Burgess, I. J.; Quail, J. W.; Schatte, G.; Müller, J. *Inorg. Chem.* **2008**, *47*, 5992–6000.

(24) Herbert, D. E.; Mayer, U. F. J.; Manners, I. *Angew. Chem., Int. Ed.* **2007**, *46*, 5060-5081.

(25) Conditions for the lithiation were chosen according to results described for 1-bromo-4-*tert*-butylbenzene: Bailey, W. F.; Luderer, M. R.; Jordan, K. P. *J. Org. Chem.* **2006**, *71*, 2825-2828.

(26) Abbreviations ***c*-(6^{R}SnR'$_2$)$_n$** and ***l*-(6^{R}SnR'$_2$)$_m$** are used to differentiate between cyclic and linear species; see Figure 3-2-5.

(27) Different conformers of linear oligo(ferrocenyldimethylsilanes) of the general formula $CpFe(C_5H_4)[SiMe_2Fe(C_5H_4)_2]_{n-1}H$ with up to 5 ferrocene moieties have been investigated with forcefield calculations and the relative orientations of fc units at Si were defined by angles ϕ and ψ, each defined as a torsion angle Fe–C^{ipso}–Si–C^{ipso}. For example, for the *trans,trans*-conformer (Figure 3-2-4) ϕ and ψ are 180°; see (a) Barlow, S.; Rohl, A. L.; O'Hare, D. *Chem. Commun.* **1996**, 257-260. (b) Barlow, S.; Rohl, A. L.; Shi, S.; Freeman, C. M.; O'Hare, D. *J. Am. Chem. Soc.* **1996**, *118*, 7578-7592.

(28) (a) Lough, A. J.; Manners, I.; Rulkens, R. *Acta Crystallogr., Sec. C* **1994**, *50*, 1667-1669. (b) Pannell, K. H.; Dementiev, V. V.; Li, H.; Cervanteslee, F.; Nguyen, M. T.; Diaz, A. F. *Organometallics* **1994**, *13*, 3644-3650. (c) Rulkens, R.; Lough, A. J.;

Manners, I.; Lovelace, S. R.; Grant, C.; Geiger, W. E. *J. Am. Chem. Soc.* **1996**, *118*, 12683-12695.

(29) Herbert, D. E.; Gilroy, J. B.; Chan, W. Y.; Chabanne, L.; Staubitz, A.; Lough, A. J.; Manners, I. *J. Am. Chem. Soc.* **2009**, *131*, 14958-14968.

(30) (a) Löwendahl, M.; Davidsson, Ö.; Ahlberg, P. *J. Chem. Res., Synop.* **1993**, 40-41. (b) Löwendahl, J.-M.; Håkansson, M. *Organometallics* **1995**, *14*, 4736-4741.

(31) Carbon-bridged [1.1]FCPs usually crystallize as *syn* isomers and degenerate *syn*-to-*syn* isomerization occurs in solution. [1.1]FCPs that contain larger bridging elements usually crystallize as *anti* isomers. For example, an *anti*-to-*anti* isomerization was investigated with VT NMR spectroscopy for a diinda[1.1]ferrocenophane (see reference 13).

(32) In general, both ***c*-(6^{Me}Sn*t*Bu$_2$)$_2$** and ***c*-(6^{Et}Sn*t*Bu$_2$)$_2$** species each contain 16 α-H atoms and 16 β-H atoms, all of which are in special positions (not on a symmetry element) in their ground state structures (C_{2h} or D_2 symmetry). Because these symmetries both have the group order of h = 4, a set of 16 H atoms will give 16/h = 4 signals. Because the ring inversion results in an increase of the group order by a factor of two (D_{2h}; h = 8), a set of 16 H atoms will give 16/h = 2 signals; i.e., two signals for all the α-H atoms and two for all the β-H atoms.

(33) Katz, T. J.; Acton, N.; Martin, G. *J. Am. Chem. Soc.* **1969**, *91*, 2804-2805.

(34) Grossmann, B.; Heinze, J.; Herdtweck, E.; Kohler, F. H.; Noth, H.; Schwenk, H.; Spiegler, M.; Wachter, W.; Weber, B. *Angew. Chem., Int. Ed.* **1997**, *36*, 387-389.

(35) Stanna[1]ferrocenophanes are only know with the bulky substituents *t*Bu, 2,4,6-trimethylphenyl, and 2,4,6-triisopropylphenyl; see references (a) Rulkens, R.; Lough, A.

J.; Manners, I. *Angew. Chem., Int. Ed.* **1996**, *35*, 1805-1807. (b) Sharma, H. K.; Cervantes-Lee, F.; Mahmoud, J. S.; Pannell, K. H. *Organometallics* **1999**, *18*, 399-403.

(36) Foucher, D. A.; Ziembinski, R.; Tang, B. Z.; Macdonald, P. M.; Massey, J.; Jaeger, C. R.; Vancso, G. J.; Manners, I. *Macromolecules* **1993**, *26*, 2878-2884.

(37) Osborne, A. G.; Whiteley, R. H.; Meads, R. E. *J. Organomet. Chem.* **1980**, *193*, 345-357.

(38) Signals in ^{1}H NMR spectra at δ = 4.04 ppm and between δ = 4.07-4.09 ppm were assigned to Cp end-groups in poly(ferrocenyldiethylsilane) and oligo(ferrocenyldimethylsilane); see references 28c, 45.

(39) In reference 36, the resonance at δ = 72.3 ppm was assigned to the C^{ipso} atom of poly(ferrocenyldiethylsilane). By using ^{13}C-APT measurements, we found that signals at δ = 70.1 (**6^{Et}SnMe$_2$**), 70.0 (**6^{Et}Sn*n*Bu$_2$**) and 69.9 ppm (**6^{Et}Sn*t*Bu$_2$**) are due to C^{ipso} atoms. To explore this discrepancy in the assignments of the C^{ipso} atoms further, a ^{13}C DEPT NMR spectrum of poly(ferrocenyldiethylsilane) was remeasured, thereby revealing that its C^{ipso} atom resonates at δ = 70.4 ppm and confirming that the assignment of δ = 74.4 (Cp), 72.3 (Cp C-Si), 70.4 ppm (Cp) in the original report (reference 36) should have been δ = 74.4 (Cp), 72.3 (Cp), 70.4 (Cp C-Si).

(40) Kumar, M.; Cervantes-Lee, F.; Pannell, K. H.; Shao, J. *Organometallics* **2008**, *27*, 4739-4748.

(41) Setaka, W.; Sakamoto, K.; Kira, M.; Power, P. P. *Organometallics* **2001**, *20*, 4460-4462.

(42) Jutzi, P.; Kohl, F.; Hofmann, P.; Kruger, C.; Tsay, Y. H. *Chem. Ber.* **1980**, *113*, 757-769.

(43) For related macrocyclic sandwich compounds, see (a) Köhler, F. H.; Schell, A.; Weber, B. *Chem.-Eur. J.* **2002**, *8*, 5219-5227. (b) Schaller, R. J.; Gleiter, R., Hofmann, J.; Rominger, F. *Angew. Chem., Int. Ed.* **2002**, *41*, 1181-1183. (c) Altmann, R.; Gausset, O.; Horn, D.; Jurkschat, K.; Schurmann, M.; Fontani, M.; Zanello, P. *Organometallics* **2000**, *19*, 430-443.

(44) Shafir, A.; Power, M. P.; Whitener, G. D.; Arnold, J. *Organometallics* **2000**, *19*, 3978-3982.

(45) Gädt, T.; Schacher, F. H.; McGrath, N.; Winnik, M. A.; Manners, I. *Macromolecules* **2011**, *44*, 3777-3786.

(46) Dong, T. Y.; Lai, L. L. *J. Organomet. Chem.* **1996**, *509*, 131-134.

(47) Nonius, B. V. Nonius BV, Delft, The Netherlands, Delft, The Netherlands, **1998**.

(48) Otwinowski, Z.; Minor, W. in *Macromolecular Crystallography, Part A, Vol. 276* (Eds.: Carter, C. W.; Sweet, R. M.), Academic Press, London, **1997**, pp. 307-326.

(49) Burla, M. C.; Caliandro, R.; Camalli, M.; Carrozzini, B.; Cascarano, G. L.; De Caro, L.; Giacovazzo, C.; Polidori, G.; Spagna, R. *J. Appl. Crystallogr.* **2005**, *38*, 381-388.

(50) Sheldrick, G. M. *Acta Crystallogr., Sec A* **2008**, *64*, 112-122.

(51) Bruker, Bruker AXS, Inc., Madison, WI, **2000-2003**.

(52) Stoe & Cie GmbH, Darmstadt, Germany, **2009**.

(53) Farrugia, L. J. *J. Appl. Crystallogr.* **1997**, *30*, 565.

3.2.5. Selective Materials from Supporting Informations

DLS Analyses. Dynamic light scattering experiments were performed using a nano series Malvern zetasizer instrument equipped with a 633 nm red laser. Samples were filtered through 0.2 μm syringe PTFE filters before they were analyzed in 1 cm glass

cuvettes at concentrations of 5 mg mL^{-1} and 2.5 mg mL^{-1} in thf at 25 °C. The refractive index of the copolymers was assumed to be 1.5. Four sample solutions of two different concentrations in thf for each polymer were analyzed by DLS. The analysis resulted in hydrodynamic radii (R_h) which were converted to radii of gyration (R_g) (R_g/R_h = 2.05), assuming that the polymers had a random coil structure in a good solvent.[1] The R_h values were converted into weight average molecular weight (M_w) with respect to poly(ferrocenylsilane)s.[2] Results are summarized in Table 3-2-S7.

REFERENCES

(1) Burchard, W. In *Branched Polymers II* **1999**; Vol. *143*, p 113-194.

(2) Massey, J. A.; Kulbaba, K.; Winnik, M. A.; Manners, I. *J. Polym. Sci., Part B: Polym. Phys.* **2000**, *38*, 3032-3041.

Table 3-2-S1. DLS Data of **$6^{Me}SnMe_2$**.

concentration	5.0 mg/mL		2.5 mg/mL	
	1	2	1	2
R_h / nm	0.817	0.730	0.790	0.764
	0.782	0.790	0.842	0.830
	0.731	0.741	0.777	0.817
average / nm	0.765		0.803	
SD / nm	0.036		0.031	
overall average / nm	0.784			
overall SD / nm	0.038			

Table 3-2-S2. DLS Data of **$6^{Et}SnMe_2$**.

concentration	5.0 mg/mL		2.5 mg/mL	
	1	2	1	2
R_h / nm	0.867	0.875	0.812	0.989
	1.085	1.107	0.827	0.896
	1.030	1.106	0.887	0.779
average / nm	1.012		0.865	

SD / nm	0.113	0.075
overall average / nm	0.939	
overall SD / nm	0.119	

Table 3-2-S3. DLS Data of **6^{Me}Sn*n*Bu$_2$**.

concentration	5.0 mg/mL		2.5 mg/mL	
	1	2	1	2
R_h / nm	1.229	1.194	1.125	1.183
	1.051	1.379	1.198	1.309
	1.194	1.329	1.636	1.173
average nm	1.229		1.271	
SD nm	0.115		0.189	
overall average / nm	1.250			
overall SD / nm	0.151			

Table 3-2-S4. DLS Data of **6^{Et}Sn*n*Bu$_2$**.

concentration	5.0 mg/mL		2.5 mg/mL	
	1	2	1	2
R_h / nm	1.031	1.154	1.380	1.323
	1.308	1.201	1.046	1.130
	1.197	1.082	1.246	1.319
Average / nm	1.162		1.235	
SD / nm	0.098		0.128	
overall average / nm	1.199			
overall SD / nm	0.116			

Table 3-2-S5. DLS Data of **6^{Me}Sn*t*Bu$_2$**.

concentration	5.0 mg/mL		2.5 mg/mL	
	1	2	1	2
R_h / nm	1.141	1.049	0.993	1.244
	1.233	0.927	0.973	0.894
	1.167	0.968	0.786	0.865
average / nm	1.081		0.959	
SD / nm	0.120		0.158	
overall average / nm	1.020			
overall SD / nm	0.148			

Table 3-2-S6. DLS Data of $\mathbf{6^{Et}Sn}t\mathbf{Bu_2}$.

concentration	5.0 mg/mL		2.5 mg/mL	
	1	2	1	2
	0.711	0.529	0.663	0.501
R_h / nm	0.591	0.598	0.500	0.562
	0.572	0.599	0.535	0.600
average / nm	0.600		0.560	
SD / nm	0.060		0.063	
overall average / nm	0.580			
overall SD / nm	0.062			

Contribution 3: Poly(ferrocene)s with Gallium and Silicon as Alternating Bridges.

3.3.1. Description

The following chapter is a verbatim copy of an article that is published in *Chemical Communications*[1] in June, 2012[2] and describes the synthesis and characterization of a pair of unsymmetrically bridged [1.1]FCPs and poly(ferrocene)s with silicon and gallium as alternatively bridges. The gallium dichloride complexes (Ar′)$GaCl_2$ (**4**) and (p-$SiMe_3$Ar′)$GaCl_2$ (**5**) were reacted with bis(lithioferrocenyl)dimethysilane to synthesize unsymmetrically briged [1.1]FCPs with silicon and gallium as bridging elements. The salt metathesis reactions resulted in red pastes, from which the silagalla[1.1]FCPs (**6a** and **6b**) were extracted by hexane and crystallized from hexane solution with an isolated yield of 41% and 29%. Both silagalla[1.1]FCPs **6a** and **6b** were characterized by NMR spectroscopy, single-crystal X-ray analysis and cyclic voltammetry. ^{1}H NMR spectra from the respective hexane insoluble fraction suggested oligomeric products, which were characterized by GPC analysis. The MALDI-TOF mass analysis revealed the actual nature of oligomers showing mixtures of four series of different species; macrocyclic FCPs (with up to 10 ferrocene moieties) and three different types of linear species (with up to 16 ferrocene moieties) were found. In the cyclic and linear oligomers, the ferrocene moieties were bridged by alternating group 13 and group 14 elements.

---

[1] Reprinted with permission from Chemical Communications. Copyright (2012) Royal Society of Chemistry.

[2] Bagh, B.; Breit, N. C.; Gilroy, J. B.; Schatte, G.; Müller, J. *Chem.Commun.* **2012**, *48*, 7823-7825.

3.3.2. Author Contributions

This project was led by me. The co-authors on this paper are Nora C. Breit, who worked with the (Ar′)$GaCl_2$, Gabriele Schatte, who performed structure determinations by single-crystal X-ray analysis and Joe B. Gilroy, who carried out GPC and MALDI-TOF mass analysis. I have prepared the first version of the manuscript which was edited by my supervisor Jens Müller.

3.3.3. Relation of Contribution 3 with Research Objectives

The methodology discussed in Contribution 5, provided a prospect to synthesize new unsymmetrically bridged [1.1]FCPs with varieties of different bridging elements. However, that particular method reprents its challenge as only two silastanna[1.1]ferrocenophanes were isolated in very poor yields. Therefore, it was crucial to select a ligand framework, which could improve the yields of unsymmetrically bridged [1.1]FCPs. Contribution 6 presents the synthesis of two silagalla[1.1]ferrocenophanes (**6a** and **6b**) and poly(ferrocene)s (**6a**$_x$ and **6b**$_x$) with silicon and gallium as alternating bridges. Compounds **6a** and **6b** were synthesized by reacting dilithiated-**1**^{Me} with (Ar′)$GaCl_2$ and (*p*-$SiMe_3$Ar′)$GaCl_2$, respectively. In fact, the yields of **6a** (29%) and **6b** (41%) were significantly better as compared to silastanna[1.1]ferrocenophanes (**2**$_1$, 3 and 7%). Cyclic voltammetry of **6a** and **6b** were performed to study their redox behavior and, hence, Contribution 6 added valuable information to the general theme of metal-metal interaction in such species. Moreover, the poly(ferrocene)s with a series of linear and cyclic structure provided an extra, interesting flavor.

3.3.4. Reprint of Contribution 3

Ferrocenophanes with Gallium and Silicon as Alternating Bridges

Bidraha Bagh,[a] Nora C. Breit,[a] Joe B. Gilroy,[b] Gabriele Schatte,[c] and Jens Müller[a]*

[a] Department of Chemistry, University of Saskatchewan, 110 Science Place, Saskatoon, Saskatchewan S7N 5C9, Canada; [b] School of Chemistry, University of Bristol, Bristol BS8 1TS, UK; [c] Saskatchewan Structural Sciences Centre, University of Saskatchewan, 110 Science Place, Saskatoon, Saskatchewan S7N 5C9, Canada

Received April 25, 2012

ABSTRACT: [1.1]Ferrocenophanes with gallium and silicon in bridging positions have been prepared in yields of 29 and 41%, respectively. From the same reactions, polymer-containing fractions were isolated (31% in each case) and shown to be comprised of linear and cyclic species with up to 16 ferrocene units (MALDI-TOF analysis).

During the last two decades, [1]ferrocenophanes ([1]FCPs; Scheme 3-3-1) were developed as a class of precursors for the preparation of well-defined metallopolymers.[1] The most researched strained sandwich compounds are silicon-bridged [1]FCPs, which were also the first reported [1]FCPs.[2] The related [1.1]FCPs (Scheme 3-3-1) are an even older class of compounds, which were described as early as 1956.[3] During the 1980s, carbon-bridged [1.1]FCPs were intensively investigated as it was found that the *syn* conformer of the CH_2-bridged species catalyzed the formation of dihydrogen in aqueous acidic solutions.[4] To date, the family of [1.1]FCPs has a significant number of members with heteroatom-bridged species known for B, Al, Ga, In, Si, Sn, Pb, P, As, S, Zn, and Hg.[5]

Scheme 3-3-1. [1]Ferrocenophanes and [1.1]ferrocenophanes.

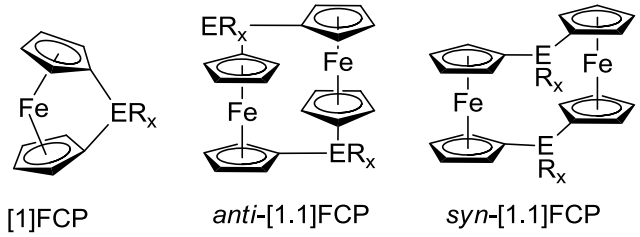

Recently, we developed a synthetic methodology that allowed the preparation of the first [1.1]FCPs bridged by different elements.[5] The first silastanna[1.1]ferrocenophanes were synthesized (Scheme 3-3-2), but could only be obtained in low yields [$\mathbf{2_1}$ (R = Et, R' = Me): 3%; $\mathbf{2_1}$ (R = R' = Me): 7%]. Furthermore, [1.1.1.1]FCPs ($\mathbf{2_2}$) with alternating silicon and tin in bridging positions were isolated and MALDI-TOF mass analysis showed the presence of cyclic ($\mathbf{2_n}$) and linear polymers ($\mathbf{3_m}$) with up to 20 ferrocene units.[5] Cyclic poly(ferrocenes) of this size are very rare and only photocontrolled ring-opening polymerization (ROP) of the Me_2Si-bridged [1]FCP (Scheme 3-3-1) has yielded larger macrocycles (with more than 40 repeating units) to date.[6]

Scheme 3-3-2. Linear and cyclic poly(ferrocenes) with alternating bridges.[5]

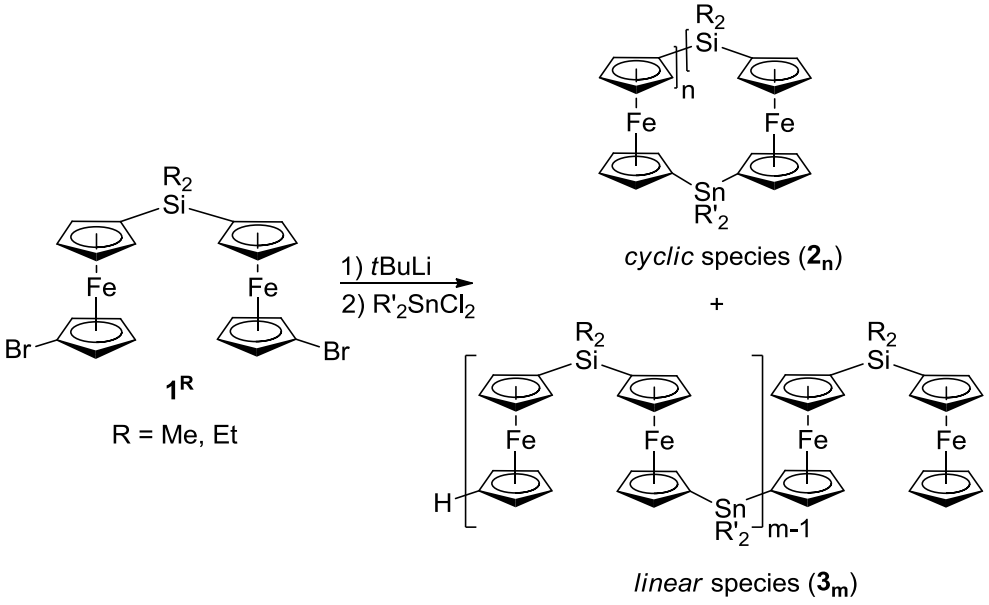

Metal-containing polymers have shown utility as precursors to functional ceramic materials. For example, cross-linked poly(ferrocenylsilane)-based materials yielded shape-retaining ceramics with tunable magnetic properties.[7] Similarly, pyrolysis of short cylindrical micelles with a cross-linked polyisoprene shell and a poly(ferrocenylsilane) core resulted in nanoscale magnetic ceramics.[8] More recently, low-molecular-weight ferrocene-platinum-containing polymers were employed to pattern surfaces with FePt alloy nanoparticles for ultrahigh-density magnetic data storage applications.[9] In each case, the predetermined composition of the metal-containing polymers employed played an important role in the properties of the resulting ceramics. Although recent results in this area have been impressive, there remains a need for synthetic methods that allow for variation in the composition of pre-ceramic metal-containing polymers. For example, pyrolysis of metal-containing polymers containing gallium and iron may lead to magnetostrictive ceramic materials that undergo changes in shape or dimensions during magnetization.[10]

Within this report we present a novel synthetic method towards asymmetrically bridged [1.1]FCPs containing silicon and gallium bridging moieties, which also yield linear and cyclic polymers of similar composition. These results complement our efforts to develop gallium- and aluminum-containing metallopolymers through ROP methodologies.[11]

As illustrated in Scheme 3-3-3, lithiation of the Me_2Si-bridged dibromide $\mathbf{1^{Me}}$ followed by the addition of gallium dichlorides (**4** or **5**), equipped with non-encumbered ligands, gave the targeted silagalla[1.1]ferrocenephanes **6a** and **6b**.‡ [12] The isolated yields of 29 (**6a**) and 41% (**6b**) are significantly higher than those of their silicon-tin

counterparts $\mathbf{2_1}$ (Scheme 3-3-2; 3 and 7%).[5] Single crystal X-ray analysis revealed that compounds **6a** and **6b** exist as *anti* isomers in the solid state (Figure 3-3-1 and Scheme 3-3-1). This is expected as their symmetrically bridged cousins, the disila[1.1]ferrocenophane

Scheme 3-3-3. Synthesis of silagalla[1.1]ferrocenophanes **6a** and **6b**.

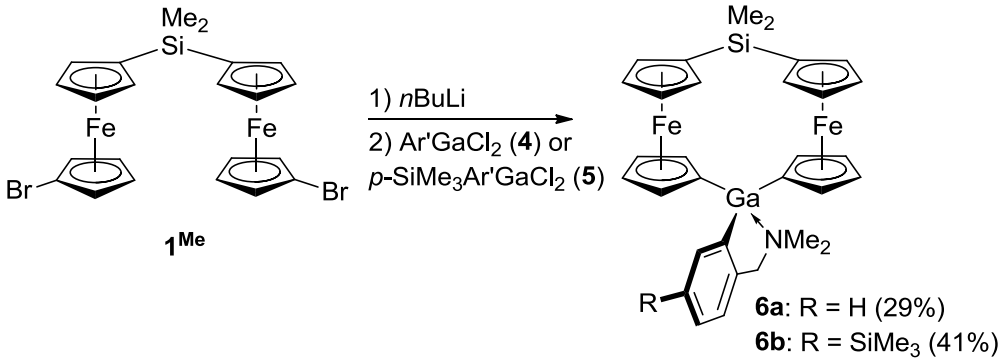

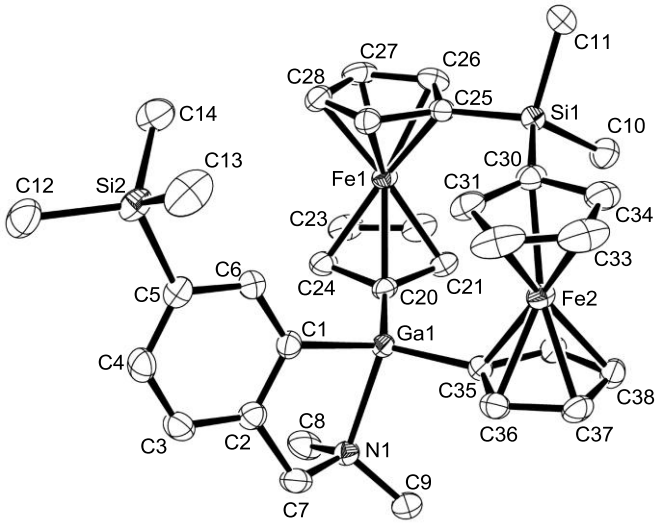

Figure 3-3-1. Molecular structure of **6b** with thermal ellipsoids at the 50% probability level. Hydrogen atoms are omitted for clarity. Selected atom-atom distances [Å] for **6b** (see ESI for **6a**): Ga1-N1 2.1626(16); Ga1-C1 1.973(2); Ga1-C20 1.958(2); Ga1-C35 1.9566(19); Fe1···Fe2 5.3147(4).

(ER_x = $SiMe_2$)[13] and the digalla[1.1]ferrocenophane (ER_x = GaAr'),[14] exhibit the same conformation. The bond lengths around the two bridging elements are very similar to

those of the symmetrically bridged species.[13-14] Species **6b** is asymmetrically bridged by a short Si linkage (C25···C30 3.120(3) Å) and a slightly longer Ga linkage (C20···C35 3.347(3) Å). The Cp rings of each ferrocenediyl unit deviate from coplanarity: tilt angles between least square planes of the C atoms of the Cp rings are 5.07(12) (Fe1) and 4.35(12)º (Fe2). The molecular structure of **6a** in the solid state is very similar to that of **6b** (see ESI).

Species **6a** and **6b** both show similar pattern in their NMR spectra. For example, the ^{1}H NMR spectra show 8 signals of equal intensity for all 16 Cp protons revealing the presence of a two-fold symmetry element. This is consistent with the molecular structures found in the solid state, if one considers that inversion of the envelope conformation of the chelating five-membered rings (Ga1-C1-C2-C7-N1) occurs fast in solution, resulting in time-averaged C_s-symmetrical species. The known dimethylsila[1.1]ferrocenophane[13] is a fluxional molecule in solution, exhibiting fast *anti*-to-*anti* isomerization (Scheme 3-3-4).

Scheme 3-3-4. *Anti*-to-*anti* Isomerization of the known Me_2Si-bridged [1.1]FCP, resulting in swapping of positions of related H′ and H″ atoms.

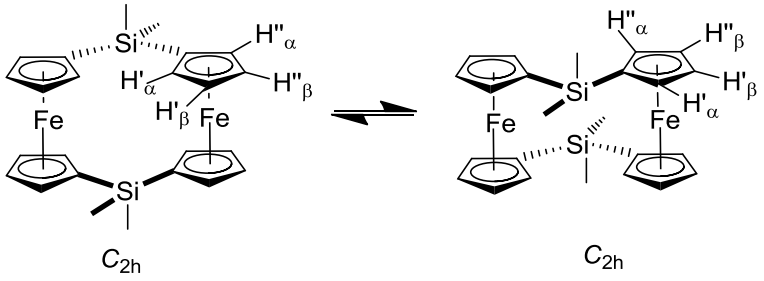

This degenerate isomerization of two C_{2h} symmetrical species creates a *pseudo*-mirror plane (σ_h) resulting in D_{2h} symmetrical molecules on time-average and 2 instead of the expected 4 signals for all Cp protons are observed. Such a fluxional behavior is

characteristic of [1.1]FCPs and usually observed for *syn* as well as for *anti* isomers. This dynamic behavior was first described for the carbon-bridged species, which have been coined "molecular acrobats".[4, 15] However, the known Ar′E-bridged [1.1]FCPs (E = Al, Ga, In) do not exhibit higher symmetries on time-average in proton NMR spectra (500 MHz). For the indium-bridged species an *anti*-to-*anti* isomerization still occurs at ambient temperature, which was shown by exchange proton NMR spectroscopy (EXSY).[16] For group-13-bridged [1.1]FCPs equipped with intramolecularly coordinating ligands, the *anti*-to-*anti* isomerization must involve a breakage of the E-N donor bond, rotation of the ligand about the E-C^{ipso} bond, and reformation of the E-N donor bond which is accompanied by an inversion at the group 13 element. Such a dynamic process is faster for indium compared with aluminum or gallium species, as indium forms the weakest donor bond with nitrogen within the series. Against this background, we measured ^{1}H NMR spectra of **6a** and **6b** in [D_8]toluene in the temperature range of r.t. to 80 ºC (500 MHz), but could not find any indication of fluxional behavior. Thus, we conclude that the gallium-containing moiety does not allow for a fast isomerization, even though the Me_2Si linkage is very flexible.

Cyclic voltammetry of **6a** and **6b** at r.t. revealed the presence of two well-resolved oxidation waves, showing an expected sequential oxidation of the two iron centers (Figure 3-3-2). The separation of these waves, $\Delta E^{o\prime}$, provides a measure of the interaction between the two iron-redox centers.[17] Species **6a** and **6b** are hybrids of the symmetrically bridged disila[1.1]ferrocenophane (ER_x = $SiMe_2$) and digalla[1.1]ferrocenophane (ER_x = GaAr′) and it is not surprising that their $\Delta E^{o\prime}$ of 0.27 V falls between that of 0.25 V (ER_x = $SiMe_2$)[13b] and 0.30 V (ER_x = GaAr′).[14]

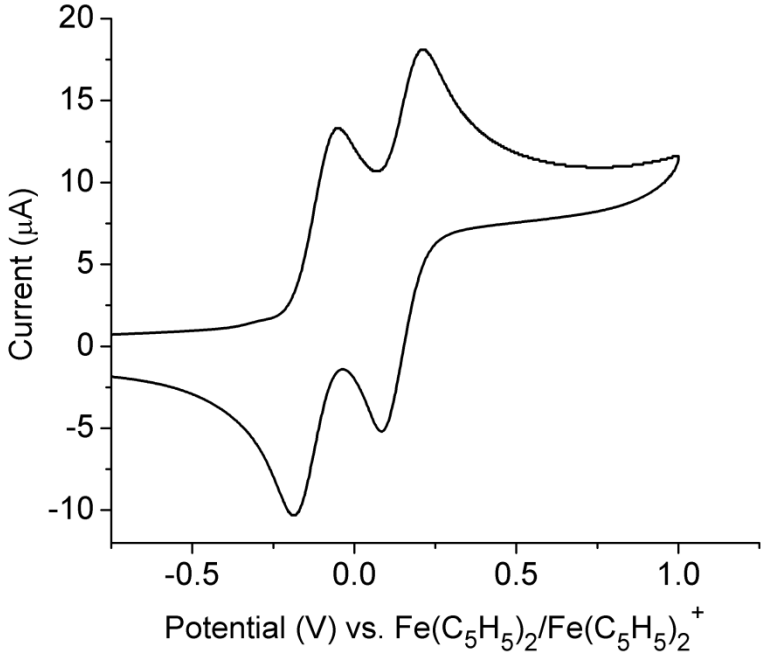

Figure 3-3-2. Cyclic voltammogram of **6a** (1 mM) in CH_2Cl_2 (0.1 M NBu_4PF_6; scan rate = 50 mV/s). The measured $E°'$ for the two reversible redox waves is -0.121 and 0.149 V, respectively.

Proton NMR spectra of reaction mixtures from which the [1.1]FCPs **6a** and **6b** were extracted into hexane (29 and 41%; Scheme 3-3-3) showed broad peaks indicating the formation of oligomers or polymers. The hexane insoluble fractions were purified by precipitation from toluene solutions into hexane, resulting in isolated yields of 31% in both cases. GPC analysis of these fractions, $\mathbf{6a_x}$ and $\mathbf{6b_x}$, showed broad molecular weight distributions and average molecular weights M_w of 3.08 kD ($\mathbf{6a_x}$) and 7.05 kD ($\mathbf{6b_x}$). A clearer picture of the character of these mixtures could be uncovered by MALDI-TOF mass analysis, which showed cyclic and linear polymers. Figure 3-3-3 depicts the mass spectrum for mixture $\mathbf{6a_x}$ with four different series of species. Cyclic ferrocenophanes ($\mathbf{6a_n}$) with up to 12 ferrocenediyl moieties (n = 6) were detected. Furthermore, three

series of linear species were found: one series with only Cp end groups (**7a$_m$**; m = 1 – 8), one with one GaAr′Cl end group (**8a$_m$**; m = 1 – 7), and one with one GaAr′Br end group (**9a$_m$**; m = 1 – 7). Similar series of species were detected for the mixture **6b$_x$**, showing compounds with up to 14 ferrocenediyl moieties; however, only the series of cyclic species was less pronounced than for **6a$_x$** (see ESI).

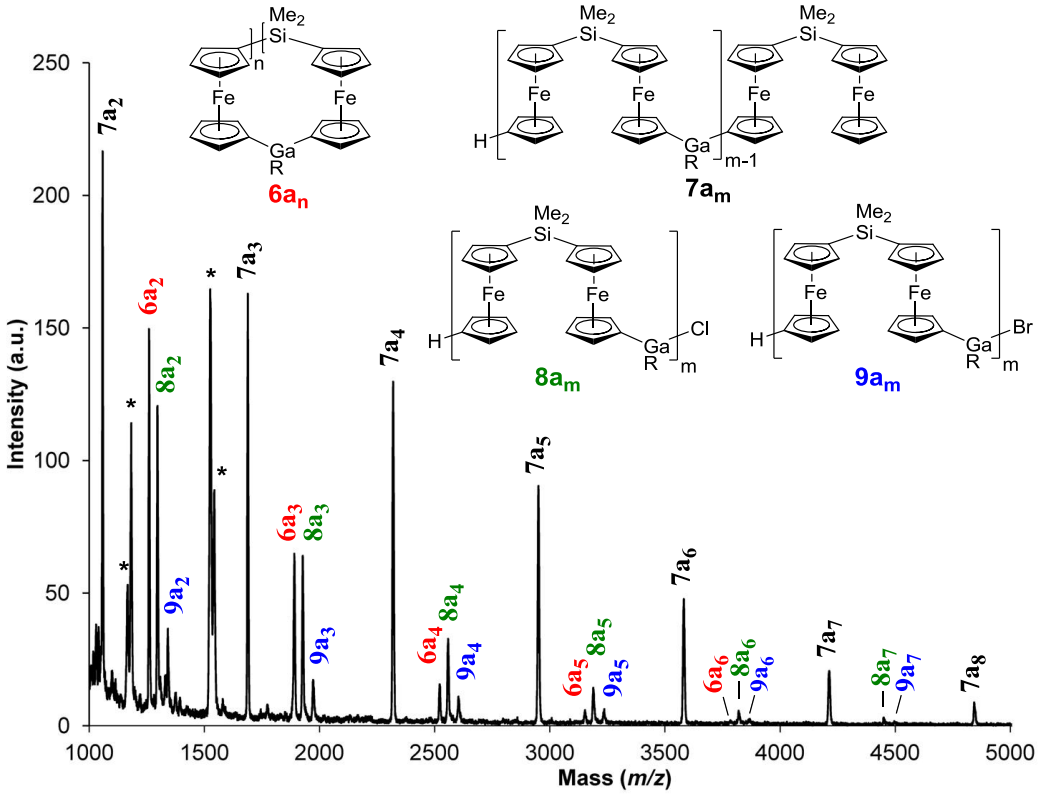

Figure 3-3-3. MALDI-TOF mass spectrum of **6a$_x$** (* indicates unassigned peaks).

The presence of bromide-containing end groups (Fig. 3; series **9a$_m$**) was unexpected. These species must have formed from the respective chlorides (series **8a$_m$**) through a Cl/Br exchange reaction. Recently, we discovered that such a Cl/Br exchange happened during the course of the synthesis of the intramolecularly stabilized gallium compound MxGaCl$_2$.[18] A similar exchange was reported in the literature for the Mes*GaCl$_2$, where the authors speculated that unreacted starting compound Mes*Br was the direct source of

bromide.[19] In the course of the synthesis of $MxGaCl_2$, we found some indication that LiBr reacted with $MxGaCl_2$ to give MxGaClBr and $MxGaBr_2$. Therefore, we speculate that in the reaction mixtures (Scheme 3-3-3) LiBr formed and acted as the reagent for the Cl/Br exchange. In analogy to the well-known reaction of *t*BuLi and *t*BuBr, some fraction of species with lithiated Cp groups might have reacted with the formed *n*BuBr to give LiBr, butene and protonated Cp end groups. Alternatively, substitution could occur to give LiBr and butylated Cp; however, butyl-containing compounds were not detected.

The new methodology described here has allowed for the synthesis of the first examples of poly(ferrocene)s with alternating silicon and gallium in bridging positions. Such species would be very difficult to obtain through ROP of respective sila- and galla[1]ferrocenophanes: the required gallium species are unknown and, in addition, a perfect control over the copolymerization would be needed. The discovered Cl/Br exchange shows that unwanted side reactions occurred, which probably lead to chain growth termination. Future activities will be concentrated on further optimizations of the metallation of $\mathbf{1^{Me}}$ so that chain growth termination can be suppressed, as well as the evaluation of the polymers described as precursors to magnetostrictive ceramic materials.

AKNOWLEDGEMENTS

We acknowledge the NSERC of Canada for support (DG for J.M.; PDF for J.B.G.), the EU for a Marie Curie PDF (J.B.G.), Dr. C. L. Lund (LANXESS, London, ON) and S. Dey (U of Saskatchewan) for contributions, and Prof. I. Burgess (U of Saskatchewan) and Prof. I. Manners (U of Bristol) for making instruments available for our studies.

ASSOCIATED CONTENT

Notes

‡ To improve solubilities of [1.1]FCPs, the Ar′ ligand (2-$Me_2NCH_2C_6H_4$) was equipped with a *p*-$SiMe_3$ group. This tactics had been applied successfully to [1.1]metallarenophanes by introducing a *p*-*t*Bu group (see ref. 12). However, the solubilities of **6a** and **6b** are very similar.

REFERENCES

(1) (a) Foucher, D. A.; Tang B.-Z.; Manners, I. *J. Am. Chem. Soc.* **1992**, *114*, 6246-6248. (b) Herbert, D. E.; Mayer, U. F. J.; Manners, I. *Angew. Chem., Int. Ed.* **2007**, *46*, 5060-5081. (c) Bellas, V.; Rehahn, M. *Angew. Chem., Int. Ed.* **2007**, *46*, 5082-5104.

(2) Osborne, A. G.; Whiteley, R. H. *J. Organomet. Chem.* **1975**, *101*, C27-C28.

(3) Nesmeyanov, A. N.; Kritskaya, I. I. *Bull. Acad. Sci. USSR, Div. Chem. Sci. (Eng. Transl.)* **1956**, 243-244.

(4) Mueller-Westerhoff, U. T. *Angew. Chem., Int. Ed.* **1986**, *25*, 702-717.

(5) Bagh, B.; Breit, N. C.; Dey, S.; Gilroy, J. B.; Schatte, G.; Harms K.; Müller, J. *Chem.–Eur. J.* **2012**, in press (DOI: 10.1002/chem.201200953).

(6) Herbert, D. E.; Gilroy, J. B.; Chan, W. Y.; Chabanne, L.; Staubitz, A.; Lough, A. J.; Manners, I. *J. Am. Chem. Soc.* **2009**, *131*, 14958-14968.

(7) MacLachlan, M. J.; Ginzburg, M.; Coombs, N.; Coyle, T. W.; Raju, N. P.; Greedan, J. E.; Ozin, G. A.; Manners, I. *Science* **2000**, *287*, 1460-1463.

(8) (a) Wang, X. S.; Arsenault, A.; Ozin, G. A.; Winnik, M. A.; Manners, I. *J. Am. Chem. Soc.* **2003**, *125*, 12686-12687. (b) Wang, X.; Liu, K.; Arsenault, A. C.; Rider, D. A.; Ozin, G. A.; Winnik, M. A.; Manners, I. *J. Am. Chem. Soc.* **2007**, *129*, 5630-5639.

(9) Dong, Q.; Li, G. J.; Ho, C. L.; Faisal, M.; Leung, C. W.; Pong, P. W. T.; Liu, K.; Tang, B. Z.; Manners, I.; Wong, W. Y. *Adv. Mater.* **2012**, *24*, 1034-1040.

(10) Atulasimha, J.; Flatau, A. B. *Smart Mater. Struct.* **2011**, *20*, 043001 (15pp).

(11) (a) Bagh, B.; Schatte, G.; Green, J. C.; Müller, J. *J. Am. Chem. Soc.* **2012**, *134*, 7924-7936. (b) Bagh, B.; Gilroy, J. B.; Staubitz, A.; Müller, J. *J. Am. Chem. Soc.* **2010**, *132*, 1794-1795.

(12) Lund, C. L.; Schachner, J. A.; Burgess, I. J.; Quail, J. W.; Schatte, G.; Müller, J. *Inorg. Chem.* **2008**, *47*, 5992-6000.

(13) (a) Park, J. W.; Seo, Y. S.; Cho, S. S.; Whang, D. M.; Kim, K. M.; Chang, T. Y. *J. Organomet. Chem.* **1995**, *489*, 23-25. (b) Zechel, D. L.; Foucher, D. A.; Pudelski, J. K.; Yap, G. P. A.; Rheingold, A. L.; Manners, I. *J. Chem. Soc., Dalton Trans.* **1995**, 1893-1899.

(14) Schachner, J. A.; Orlowski, G. A.; Quail, J. W.; Kraatz, H.-B.; Müller, J. *Inorg. Chem.* **2006**, *45*, 454-459.

(15) (a) Löwendahl, M.; Davidsson, Ö.; Ahlberg, P. *J. Chem. Res., Synop.* **1993**, 40-41. (b) Löwendahl, J.-M.; Håkansson, M. *Organometallics* **1995**, *14*, 4736-4741.

(16) Schachner, J. A.; Lund, C. L.; Burgess, I. J.; Quail, J. W.; Schatte, G.; Müller, J. *Organometallics* **2008**, *27*, 4703-4710.

(17) $E^{o'} = \frac{1}{2}(E_{pa} + E_{pc})$; see Bard, A. J.; Faulkner, L. R. Electrochemical Methods, 2 ed., John Wiley & Sons, Inc., New York, 2001.

(18) Mx: 2,4-di-*tert*-butyl-6-(dimethylamino)phenyl; see Yoshifuji, M.; Hirano, M.; Toyota, K. *Tetrahedron Lett.* **1993**, *34*, 1043-1046.

(19) Schulz, S.; Pusch, S.; Pohl, E.; Dielkus, S.; Herbst-Irmer, R.; Meller, A.; Roesky, H. W. *Inorg. Chem.* **1993**, *32*, 3343-3346.

3.3.5. Selective Materials from Supporting Information of Contribution 3

EXPERIMENTAL SECTION

General Information. Manipulations were done using standard Schlenk and glovebox techniques (N_2 as inert gas), unless noted differently. Solvents were dried using an MBraun Solvent Purification System and stored under nitrogen over 3 Å molecular sieves. All solvents for NMR spectroscopy were degassed prior to use and stored under nitrogen over 3 Å molecular sieves. ^{1}H and ^{13}C NMR spectra were recorded on a Bruker 500 MHz Avance NMR spectrometer at 25 ºC in C_6D_6 and toluene-D_8, respectively (^{1}H at 500.28 MHz; ^{13}C at 125.80 MHz). ^{1}H chemical shifts were referenced to the residual protons of the deuterated solvents (δ 7.15 for C_6D_6 and 2.08 for toluene-D_8); ^{13}C chemical shifts were referenced to the C_6D_6 signal at δ 128.00 and the toluene-D_8 signal at δ 20.43. Mass spectra were measured on a VG 70SE and are reported in the form *m/z* (rel intens) [M^+] where "*m/z*" is the mass observed, 'rel intens' is intensity of the peak relative to the most intense peak and "M^+" is the molecular ion or fragment; only characteristic mass peaks are reported. For isotopic pattern, only the mass peak of the isotopoloque or isotope with the highest natural abundance is listed. Elemental analyses were performed on a Perkin Elmer 2400 CHN Elemental Analyzer using V_2O_5 to promote complete combustion.

Chemicals. Ferrocene (98%), *n*BuLi (2.5 M in hexanes), *t*BuLi (1.7 M in pentane), Me_2SiCl_2 (99%) and C_6D_6 (99.6 atom % D) were purchased from Sigma Aldrich. [D_8]toluene (99.5 atom % D) was purchased from Cambridge Isotope Laboratories, Inc. $GaCl_3$ (Alfa Aesar, 99.999%), 1-bromo-4-(bromomethyl)benzene (Alfa-Aesar, 98%) and $C_2Br_2Cl_4$ (Alfa-Aesar, 98%) were purchased from VWR. $(LiC_5H_4)_2Fe{\cdot}2/3tmeda$,[1] $(BrC_5H_4)_2Fe$,[2] **1**$^{\mathbf{Me}}$,[3] and Ar′$GaCl_2$[4] were synthesized following literature procedures.

Species 1-bromo-4-[(dimethylamino)methyl]benzene[5-7] and 1-[(dimethylamino)-methyl]-4-trimethylsilylbenzene[8-9] are known compounds that were synthesized in a similar way compared to the literature (see details below).

Gel Permeation Chromatography (GPC). Molecular weights and polydispersity indices (PDI = M_w/M_n) of $\mathbf{6a_x}$ and $\mathbf{6b_x}$ were obtained by GPC using a Viscotek VE 2001 Gel Permeation Chromatograph equipped with automatic sampler, pump, injector, in-line degasser, column oven (30 °C), styrene/divinylbenzene columns with pore sizes of 500 Å and 100,000 Å, and VE 3580 refractometer. The solvent thf, stabilized with 0.025% butylated hydroxytoluene (Fisher) and containing 0.1 w/w% *n*Bu_4NBr, was used as the chromatography eluent at a flow rate of 1.0 mL min^{-1}. Samples were dissolved in the eluent (2 mg/mL) and filtered (Whatman, PTFE membrane, 0.2 μm) before analysis. Calibration of the refractive index detector was performed using polystyrene standards purchased from Viscotek.

MALDI-TOF Mass Spectrometry. MALDI-TOF mass spectra were collected on a 4700 Proteomics Analyzer (Applied Biosystems) equipped with a Nd:Yag laser, operating at 335 nm. Positive ion mass spectra were obtained in linear or reflector mode over a range of 500 - 5000 *m/*z. Each spectrum was an accumulation of 12500 laser shots

over 100 points on the sample (125 shots/point). Laser intensity was varied for each sample. Solutions of the analytes (10 mg/mL toluene solution) and benzo[α]pyrene (20 mg/mL toluene solution) were prepared and then mixed in a 1:10 ratio. The resulting solutions were drop-cast by micropipette into sample wells and allowed to evaporate for 3 h in an inert atmosphere glovebox prior to sample analysis.

Electrochemistry. A computer controlled system, consisting of a HEKA potentiostat PG590 (HEKA, Mahone Bay, NS, Canada) was used for the cyclic voltammetry experiments. Data was collected using a multifunction DAQ card (PCI 6251 M Series, National Instruments Austin, Texas) and in-house software written in the LabVIEW environment. Glassy carbon (BAS, 3 mm) was used as the working electrode. The quasi-reference electrode (QRE) was a silver wire and all measurements were made against the QRE. A loop of gold wire was used as the auxiliary electrode. Before each measurement, 1 mM solutions of **6a** and **6b** were freshly prepared in dry CH_2Cl_2 with 0.1 M $[Bu_4N][PF_6]$ as the supporting electrolyte. The electrolyte was dried overnight under high vacuum at 100 °C. The scan rate for the CVs reported was 50 mV/s. The measurements were conducted inside a glovebox and taken at ambient temperature (25 °C).

1-Bromo-4-[(dimethylamino)methyl]benzene. Dimethylamine (ca. 30 mL, 0.40 mol) was added dropwise to a cold (0 °C) suspension of 1-bromo-4-(bromomethyl)benzene (25.25 g, 101.0 mmol) in hexane (50 mL). The reaction mixture was warmed up to r.t. and stirred for 16 h. The solid was filtered off and all volatiles were removed from the filtrate under vacuum. Flask-to-flask condensation (50 °C, high vacuum) gave the pure product as a colorless oil (21.09 g, 98%). ^{1}H NMR (C_6D_6): δ 1.98 (s, 6H, CH_3), 3.02 (s, 2H, CH_2), 6.95 (d, 2H, C_6H_4), 7.26 (d, 2H, C_6H_4).

1-[(Dimethylamino)methyl]-4-trimethylsilylbenzene. *t*BuLi (1.6 M in pentane, 69.0 mL, 110 mmol) was added dropwise to a cold (-78 °C) solution of 1-bromo-4-[(dimethylamino)methyl]benzene (10.70 g, 49.98 mmol) in thf (75 mL). The reaction mixture was stirred for 15 min at -78 °C, followed by the dropwise addition of chlorotrimethylsilane (19.0 mL, 150 mmol). The resultant reaction mixture was warmed up to r.t. and stirred for 16 h, resulting in a pale yellow solution with white precipitate. The solid was filtered off and all volatiles were removed under vacuum. Flask-to-flask condensation (65 °C, high vacuum) gave the pure product as a colorless oil (9.85 g, 95%). ^{1}H NMR (C_6D_6): δ 0.22 (s, 9H, $SiMe_3$), 2.10 (s, 6H, NMe_2), 3.30 (s, 2H, CH_2), 7.40 (d, 2H, C_6H_4), 7.49 (d, 2H, C_6H_4).

Dichloro{2-[(dimethylamino)methyl]-5-(trimethylsilyl)phenyl-κ^{2}C,N}gallane (5). *t*BuLi (1.6 M in pentane, 17.0 mL, 27.2 mmol) was added dropwise to a cold (0 °C) solution of 1-[(dimethylamino)methyl]-4-trimethylsilylbenzene (5.25 g, 25.3 mmol) in hexane (40 mL). The reaction mixture was warmed up to r.t. and stirred for 16 h, yielding a pale yellow solution with a white precipitate. The solid lithium salt was filtered off, washed with hexane (2 x 20 mL) and dried under high vacuum. The cold slurry (-78 °C) of the white solid in Et_2O (15 mL) was added dropwise to a cold (-78 °C) solution of $GaCl_3$ (3.00 g, 17.0 mmol) in Et_2O (20 mL). The reaction mixture was warmed up to r.t. and stirred for 16 h, resulting in a pale yellow solution with a white precipitate. The solid was filtered off and all volatiles were removed from the filtrate under high vacuum, resulting in a pale yellow solid as the crude product. Pure product **5** was obtained by sublimation (120 °C, high vacuum) as a white crystalline solid (3.83 g, 65%). ^{1}H NMR (C_6D_6): δ 0.20 (s, 9H, $SiMe_3$), 1.88 (s, 6H, NMe_2), 3.08 (s, 2H, CH_2), 6.78 (d, 1H, C_6H_3),

7.50 (d, 1H, C_6H_3), 8.08 (s, 1H, C_6H_3). ^{13}C NMR (C_6D_6): δ -1.05 ($SiMe_3$), 45.29 (CH_2), 65.47 (NMe_2), 124.24, 134.47, 139.66, 142.17 (C_6H_3). EIMS (70 eV) *m*/*z*: 347 (16) [M^+], 330 (100) [M^+ - Me], 289 (8) [M^+ - CH_2NMe_2], 206 (18) [M^+ - $GaCl_2$], 58 (38) [$C_3H_8N^+$]. HRMS (EI; *m/z*): calcd for $C_{12}H_{20}GaCl_2NSi$, 346.9989; found, 346.9989. Anal. Calcd for $C_{12}H_{20}GaCl_2NSi$: C, 41.53; H, 5.81; N, 4.04. Found: C, 40.92; H, 6.06; N, 3.80.

General Procedure for the Synthesis of 6a, 6b, $6a_x$ and $6b_x$. *n*BuLi (2.5 M in hexanes) was added dropwise to a cold (-78 °C) solution of $\mathbf{1^{Me}}$ in dry thf (30-35 mL). After the addition of *n*BuLi, the reaction mixture was stirred for 30 min at -78 °C, followed by the addition of a solution of $RGaCl_2$ (R = Ar′ and *p*-$SiMe_3$Ar′) in thf (20-30 mL). The reaction mixture was warmed up to r.t. and stirred for another 3 h, resulting in a red solution. All volatiles were removed in vacuum, resulting in a red paste which was extracted with toluene (35 mL). All volatiles were removed from the toluene solution, yielding a red paste. Hexane (50 mL) was added to the red paste and the mixture was stirred vigorously for 16 h, resulting in a red solution and a red gummy residue. The residue was filtered off and washed with hexane (2 x 5 mL). The combined hexane phase was concentrated to ca. 20 mL and kept at -78 °C for 16 h, resulting in red crystals of pure **6a** or **6b**. The residue was redissolved in toluene (5 mL) and the resulting solution was added dropwise to well-stirred hexane (30 mL), resulting in a red solution with red gummy material sticking to the glass wall. The red solution was syringed off, leaving a gummy material behind, from which all volatiles were removed in high vacuum, yielding a sticky red solid ($\mathbf{6a_x}$ or $\mathbf{6b_x}$).

6a and 6a$_x$. As described in general procedure, **1^{Me}** (1.18 g, 2.01 mmol) in thf (35 mL), *n*BuLi (1.66 mL, 4.15 mmol), and **4** (0.533 g, 1.94 mmol) in thf (30 mL) resulted in **6a** as red crystals (0.355 g, 29%) and **6a$_x$** as a sticky red solid (0.374 g, 31%).

Assignments of ^{1}H NMR signals of **6a** are based on the ^{1}H NMR data of **6b** (see below). ^{1}H NMR of **6a** ([D$_8$]toluene): δ 0.22 (s, 3H, SiMe$_2$), 0.72 (s, 3H, SiMe$_2$), 1.60 (s, 6H, NMe$_2$), 3.15 (s, 2H, CH$_2$), 3.80 (m, 2H, CH-β), 4.14 (m, 2H, CH-α), 4.21 (m, 2H, CH-α, 4.23 (m, 2H, CH-β), 4.25 (m, 2H, CH-β), 4.40 (m, 2H, CH-β), 4.52 (m, 2H, CH-α), 4.82 (m, 2H, CH-α), 6.91 (d, 1H, CH-3), 7.20 (t, 1H, CH-4), 7.33 (t, 1H, CH-5), 8.15 (d, 1H, CH-6). ^{13}C NMR of **6a** ([D$_8$]toluene): δ 0.45, 5.29 (SiMe$_2$), 45.37 (NMe$_2$), 66.25 (CH$_2$), 70.59, 70.72, 70.77, 71.20, 72.55, 72.79, 75.58, 76.85 (α- and β-C), 70.83, 71.03 (*ipso*-C of Cp rings), 127.28, 127.36, 136.71, 144.15, 149.88 (C$_6$H$_3$) [Note: one C$_6$H$_3$ peak is buried under the solvent peak]. EIMS (70 eV) *m/z*: 629 (100) [M$^+$], 428 (24) [C$_{22}$H$_{24}$Fe$_2$Si$^+$], 411 (12) [C$_{21}$H$_{19}$Fe$_2$Si$^+$]. HRMS (EI; *m/z*): calcd for C$_{31}$H$_{34}$Fe$_2$GaNSi, 629.0433; found, 629.0415. Anal. Calcd for C$_{31}$H$_{34}$Fe$_2$GaNSi: C, 59.09; H, 5.44; N, 2.22. Found: C, 59.07; H, 5.27; N, 2.12.

^{1}H NMR of **6a$_x$** (C$_6$D$_6$): δ 0.47-0.77 (multiple peaks, 6H, SiMe$_2$), 1.70-1.85 (multiple peaks with one major broad peak at 1.78, 6H, NMe$_2$), 3.27 (broad peak, 2H, CH$_2$), 3.85-4.86 (multiple peaks, 16H, Cp), 6.72-7.11 (br. peaks, 1H, C$_6$H$_4$), 7.22-7.32 (br. peaks, 1H, C$_6$H$_4$), 7.33-7.44 (br. peaks, 1H, C$_6$H$_4$), 7.94-8.44 (br. peaks, 1H, C$_6$H$_4$). ^{13}C NMR of **6a$_x$** (C$_6$D$_6$): δ -0.45 (br. peak, SiMe$_2$), 45.93 (br. peak, NMe$_2$), 66.92 (br. peak, CH$_2$), 68.30-76.30 (multiple peaks, Cp), 124.50-151.00 (multiple peaks, C$_6$H$_4$).

6b and 6b$_x$. As described in general procedure, **1^{Me}** (1.07 g, 1.82 mmol) in thf (30 mL), *n*BuLi (1.53 mL, 3.83 mmol), and **5** (0.621 g, 1.79 mmol) in thf (20 mL) resulted in

6b as red crystals (0.518 g, 41%) and **6b$_x$** as a sticky red solid (0.389 g, 31%). A series of NOE experiments was performed in order to assign every resonance of the ^{1}H NMR spectrum (C_6D_6) of **6b**: δ 0.35 (s, 3H, $SiMe_2$), 0.40 (s, 9H, $SiMe_3$), 0.79 (s, 3H, $SiMe_2$), 1.63 (s, 6H, NMe_2), 3.18 (s, 2H, CH_2), 3.93 (m, 2H, CH-α), 4.26 (m, 2H, CH-α), 4.28 (m, 2H, CH-β), 4.35 (m, 2H, CH-β), 4.40 (m, 2H, CH-β), 4.48 (m, 2H, CH-β), 4.65 (m, 2H, CH-α), 5.06 (m, 2H, CH-α), 7.03 (d, 1H, CH-3), 7.57 (d, 1H, CH-4), 8.62 (s, 1H, CH-6). ^{13}C NMR of **6b** (C_6D_6) δ 0.64 ($SiMe_3$), -0.60, 5.17 ($SiMe_2$), 45.48 (NMe_2), 66.24 (CH_2), 70.59, 70.82, 70.83, 71.21, 72.54, 72.94, 75.68, 76.94 (α- and β-C), 70.95 (*ipso*-C of Cp), 124.43, 132.74, 138.59, 142.11, 145.28, 149.16 (C_6H_3). Note: One signal for *ipso*-C of Cp was detected in the ^{13}C NMR spectrum in C_6D_6; the other signal for *ipso*-C of Cp overlapped with another Cp signals. The ^{13}C NMR was also measured in [D_8]toluene and signals for two 4*ipso*-C atoms of Cp were observed.] ^{1}H NMR of **6b** ([D_8]toluene): δ 0.27 (s, 3H, $SiMe_2$), 0.39 (s, 9H, $SiMe_3$), 0.75 (s, 3H, $SiMe_2$), 1.64 (s, 6H, NMe_2), 3.20 (s, 2H, CH_2), 3.85 (m, 2H, CH-α), 4.20 (m, 2H, CH-α), 4.24 (m, 2H, CH-β), 4.30 (m, 2H, CH-β), 4.33 (m, 2H, CH-β), 4.44 (m, 2H, CH-β), 4.57 (m, 2H, CH-α), 4.95 (m, 2H, CH-α), 7.00 (d, 1H, CH-3), 7.51 (d, 1H, CH-4), 8.51 (s, 1H, CH-6). ^{13}C NMR of **6b** (C_6D_6): δ -0.63 ($SiMe_3$), 0.59, 5.14 ($SiMe_2$), 45.47 (NMe_2), 66.32 (CH_2), 70.55, 70.75, 70.81, 71.19, 72.51, 72.87, 75.62, 76.94 (α- and β-C), 70.89, 71.15 (*ipso*-C of Cp rings), 124.43, 132.69, 138.42, 142.08, 145.22, 149.09 (C_6H_3). EIMS (70 eV) *m*/*z*: 701 (100) [M^+], 428 (24) [$C_{22}H_{24}Fe_2Si^+$], 411 (12) [$C_{21}H_{19}Fe_2Si^+$]. HRMS (EI; *m/z*): calcd for $C_{34}H_{42}Fe_2GaNSi_2$, 701.0810; found, 701.0810. Anal. Calcd for $C_{34}H_{42}Fe_2GaNSi_2$: C, 58.15; H, 6.03; N, 1.99. Found: C, 58.42; H, 6.07; N, 1.95.

^{1}H NMR of **6b$_x$** (C_6D_6): δ 0.16-0.46 (multiple peaks, 9H, $SiMe_3$), 0.47-0.80 (multiple peaks, 6H, $SiMe_2$), 1.55-2.15 (multiple peaks with one major br. peak at 1.80, 6H, NMe_2), 3.00-3.65 (multiple peaks with one major br. peak at 3.30, 2H, CH_2), 3.85-5.10 (multiple peaks, 16H, Cp), 6.72-7.11 (multiple peaks, 1H, C_6H_3), 7.39-7.67 (multiple peaks, 1H, C_6H_3), 8.30-8.80 (multiple peaks, 1H, C_6H_3). ^{13}C NMR of **6b$_x$** (C_6D_6): δ -1.40-0.00 (multiple peaks, $SiMe_2$ and $SiMe_3$), 45.93 (br. peak, NMe_2), 66.91 (br. peak, CH_2), 68.30-76.30 (multiple peaks, Cp), 124.00-150.00 (multiple peaks, C_6H_3).

Crystal Structure Determination of 6a and 6b. A clear orange plate-like crystal of **6a** ($C_{31}H_{34}Fe_2GaNSi$) having the approximate dimensions of 0.18 × 0.15 × 0.08 mm was coated with oil, collected onto the aperture of a mounted Micromount^{TM}(MiTeGen, USA) mounted onto the goniometer head, which was quickly transferred to the cold stream of the Oxford cryo-jet. The same procedure was applied for mounting a clear yellow needle-like crystal of **6b** ($C_{34}H_{42}Fe_2GaNSi_2$) having the approximate dimensions of 0.18 × 0.08 × 0.05 mm. All measurements were made on a Nonius KappaCCD 4-Circle Kappa FR540C diffractometer using monochromated Mo K_α radiation at -100 °C. An initial orientation matrix and cell was determined from 10 frames using ϕ-scans. Data =was collected using ϕ- and ω-scans.[10] Cell parameters were initially retrieved using the COLLECT[10] software and then refined with the HKL DENZO and SCALEPACK software[11] using 16029 (**6a**) and 17143 (**6b**) observed reflections from the data collection, respectively. Data reduction was performed with the HKL DENZO and SCALEPACK software,[11] which corrects for beam inhomogeneity, possible crystal decay, Lorentz and polarization effects. A multiscan absorption correction was applied (SCALEPACK).[11] The structure was solved using direct methods (SIR-2004)[12] and refined by full-matrix

least-squares method on F^2 with SHELXL97-2.[13] The non-hydrogen atoms were refined anisotropically. Hydrogen atoms were included at geometrically idealized positions (C-H bond distances 0.95/0.98/0.99 Å) and were not refined. The isotropic thermal parameters of these hydrogen atoms were fixed at 1.2 times that of the preceding carbon atom. Neutral atom scattering factors for non-hydrogen atoms and anomalous dispersion coefficients are contained in the SHELXTL-NT 6.14 program library.[14]

Table 3-3-S1. Crystal Data for the Compounds **6a** and **6b**.

Compound reference	**6a**	**6b**
Chemical formula	$C_{31}H_{34}Fe_2GaNSi$	$C_{34}H_{42}Fe_2GaNSi_2$
Formula Mass	630.10	702.29
Crystal system	Monoclinic	Monoclinic
a/Å	27.7463(2)	9.63300(10)
b/Å	11.3739(2)	10.86300(10)
c/Å	17.6834(3)	31.8490(4)
α/°	90.00	90.00
β/°	96.8620(8)	99.9950(6)
γ/°	90.00	90.00
Unit cell volume/Å^3	5540.62(14)	3282.20(6)
Temperature/K	173(2)	173(2)
Space group	$P2_1/c$	$P2_1/c$
No. of formula units per unit cell, *Z*	8	4
Radiation type	MoKα	MoKα
Absorption coefficient, μ/mm^{-1}	2.063	1.784
No. of reflections measured	28035	33427
No. of independent reflections	15486	9546
R_{int}	0.0370	0.0519
Final R_1 values ($I > 2\sigma(I)$)	0.0377	0.0353
Final $wR(F^2)$ values (all data)	0.0844	0.0806
Goodness of fit on F^2	1.016	1.022
CCDC number	878280	878281

Table 3-3-S2. GPC Results of $\mathbf{6a_x}$ and $\mathbf{6b_x}$.

Sample	M_n [kDa]	M_w [kDa]	PDI	DP_w
$\mathbf{6a_x}$	2.11	3.08	1.46	5
$\mathbf{6b_x}$	2.69	7.05	2.62	10

Contribution 4: Reinvestigation of Old Reactions: Reaction of Dialkyltin Dichlorides with Dilithioferrocene.

3.4.1. Description

The following chapter is a copy of a manuscript, which is under preparation to be submitted as an article to *Organometallics*[1] and describes the characterization of a pair of poly(ferrocenylstannane)s synthesized by the polycondesation reaction of dilithioferrocene and dialkyltin dichlorides. In 1980 the reaction of dilithioferrocene with dimethyltin dichloride was reported by Osborne et al. and the isolation of oligo(ferrocenyldimethylstannane) with approx. 13 repeating units was described. Two years later, Seyferth et el. reported a similar reaction of dilithioferrocene with dibutyltin dichloride and obtained oligo(ferrocenyldibutylstannane) as expected; a cyclic dimer, *n*Bu_2Sn-bridged [1.1]FCP was isolated in very poor yield (3%). However, no attempt was made to unravel the nature of the oligomers. We repeated the reaction of R_2SnCl_2 (R = Me, *n*Bu) with dilithioferrocene and obtained oligo(ferrocenyldialkylstannane)s as expected. Those oligomers were subjected to MALDI-TOF mass analysis in order to unravel the identity of those oligomers. Mass spectra of both oligomers revealed the presence of series of cyclic and linear oligomers: cyclic species with up to 12 repeating units and linear species up to 17 repeating units were found. We isolated cyclic dimers, cyclic trimers, a linear dimer, a linear trimer and a linear tetramer from the mixtures of oligomers by column chromatography. Variable temperature NMR experiments of cyclic trimers revealed that these molecuules were fluxional in solution. Line shape analysis

was also performed for those cyclic trimers. The cyclic voltammetry of all those isolated species along with two previously mentioned (Contribution 5) tetrameric FCPs with each ferrocene moiety bridged by alternative silicon and tin revealed interesting electrochemical behavior.

3.4.2. Author Contributions

The co-authors on this paper are Nora C. Breit, who performed the electrochemical analysis of a previously reported cyclic tetramer, Gabriele Schatte, who performed the structure determinations by single-crystal X-ray analysis, Keith Brown, who performed the line shape analysis, Joe B. Gilroy, who carried out the MALDI-TOF mass analysis and Ian J. Burgess, who helped us performing the electrochemical studies with his expertise.

3.4.3. Relation of Contribution 4 with Research Objectives

As illustrated in Contribution 5 and 6, the salt-metathesis reaction of bis(1'-lithioferrocenyl)dialkylsilane with element dichlorides yielded poly(ferrocene)s with linear and cyclic structures. Our successes presented in Contribution 5 and 6 post the question if in the old reactions of dilithioferrocene with R_2SnCl_2 (R = Me, *n*Bu) macrocyclic ferrocene derivatives were also formed. Therefore, I synthesized the known poly(ferrocenyldimethylstannane) $\mathbf{5a_n}$ and poly(ferrocenyldibutylstannane) $\mathbf{5b_n}$ following published procedures to get more insight into the nature of those species. Our investigation revealed that those polymers consist of linear and cyclic poly(ferrocene)s; I

[1] Bagh, B.; Breit, N. C.; Schatte, G.; Brown, K. C.; Burgess, I.; Müller, J.; manuscript under preparation, **2012**.

isolated some species, such as macrocyclic [1.1.1]FCPs (***c*-5a$_3$**, ***c*-5b$_3$**). The redox behavior of isolated linear and cyclic species with two, three and four ferrocene moieties was investigated. The results obtained contribute to knowledge about metal-metal communications in ferrocene-derivatives.

3.4.4. Manuscript of Contribution 4

Reinvestigation of Old Reactions: Reaction of Dialkyltin Dichlorides with Dilithioferrocene

Bidraha Bagh,[‡] Nora C. Breit,[‡] Gabriele Schatte,[§] Keith C. Brown,[‡] Ian J. Burgess,[‡] Joe B. Gilroy,[≠] Jens Müller[‡]*

[‡]Department of Chemistry and [§]Saskatchewan Structural Sciences Centre, University of Saskatchewan, 110 Science Place, Saskatoon, Saskatchewan S7N 5C9, Canada;

[≠]School of Chemistry, University of Bristol, Bristol BS8 1TS, UK.

ABSTRACT: Tin dichlorides Me_2SnCl_2 and nBu_2SnCl_2 were reacted with dilithioferrocene to yield poly(ferrocenylstannane)s **5a$_n$** and **5b$_n$**, respectively. MALDI-TOF mass analysis revealed that **5a$_n$** and **5b$_n$** are comprised of linear species with up to 18 ferrocene moieties and cyclic species with up to 13 ferrocene moieties. Some cyclic species, such as [1.1]FCPs ***c*-5a$_2$** and ***c*-5b$_2$**, [1.1.1]FCPs ***c*-5a$_3$** and ***c*-5b$_3$**, and linear species ***l*-5b$_2$**, ***l*-5b$_3$** and ***l*-5b$_4$** were isolated by column chromatography. Species ***c*-5a$_2$** and ***c*-5a$_3$** were structurally characterized by single-crystal X-ray analysis. The isolated cyclic species ***c*-5a$_2$**, ***c*-5b$_2$**, ***c*-5a$_3$** and ***c*-5b$_3$** displayed dynamic behaviors in solutions as revealed by NMR spectroscopy. The redox behaviors of all isolated species as well as

two previously reported cyclic tetramers with silicon and tin as alternating bridges, **6a** and **6b** were studied by different electrochemical techniques.

INTRODUCTION

Since the discovery of the first [1]ferrocenophane ([1]FCP; Figure 3-4-1) with silicon as the bridging element in 1975,[1] this class of strained sandwich compounds has grown enormously in last four decades. A wide variety of elements, for example B,[2] Al,[3] Ga,[3b] Ge,[4] Sn,[5] P,[6] As,[7] S,[8] and Se[8] has been introduced in the bridging positions of [1]FCPs. Among numerous [1]FCPs, group-14-bridged species are most studied. In 1992, Manners et al. made a milestone discovery of thermal ROP of sila[1]ferrocenophanes (**1**: ER_x = $SiMe_2$, $SiPh_2$; Figure 3-4-1), which resulted in high-molecular-weight poly(ferrocenylsilane)s (**2**: ER_x = $SiMe_2$, $SiPh_2$; Figure 3-4-1).[9] Since then, many different ROP methodologies have been established and, consequently, silicon-bridged [1]FCPs have been developed as an important class of precursors for the synthesis of well-defined metallopolymers. Poly(ferrocenylsilane) has been emerged as a very useful material as it found application in various fields of material science.[10] In contrast to [1]FCPs, the formal dimer [1.1]FCPs (**3**; Figure 3-4-1) lack ring strain. [1.1]FCPs, such as dimethylsila[1.1]ferrocenophane (**3**: ER_x = $SiMe_2$; Figure 3-4-1), cannot be ring-open polymerized to yield polymers.[11] Similar to sila[1]ferrocenophanes, various different ROP methods, such as thermal, anionic and transition-metal-catalyzed ROP, have been successfully employed on germanium-bridged [1]FCPs to prepare poly(ferrocenylgermane)s.[12] However, germanium-bridged [1.1]FCPs are not known in literature. Stanna[1]FCPs (**1**: ER_x = $Sn\textit{t}Bu_2$, $SnMes_2$) were also polymerized under

different conditions and yield high-molecular-weight poly(ferrocenylstannane)s.[5,13] Stanna[1.1]FCPs with tBu$_2$Sn and Mes$_2$Sn as bridging moieties were formed as a byproduct during the polymerization of respective [1]FCPs. Among various ROP techniques, anionic ROP is of great importance as it can be performed as a living polymerization, which gives access to polymers with a narrow distribution of molecular weights[14] as well as block-copolymers.[15] In block-selective solvents, epitaxial crystallization driven living copolymerization of micelles with poly(ferrocenylsilane) and poly(ferrocenylgermane) core allowed the formation of various micelle morphologies.[16]

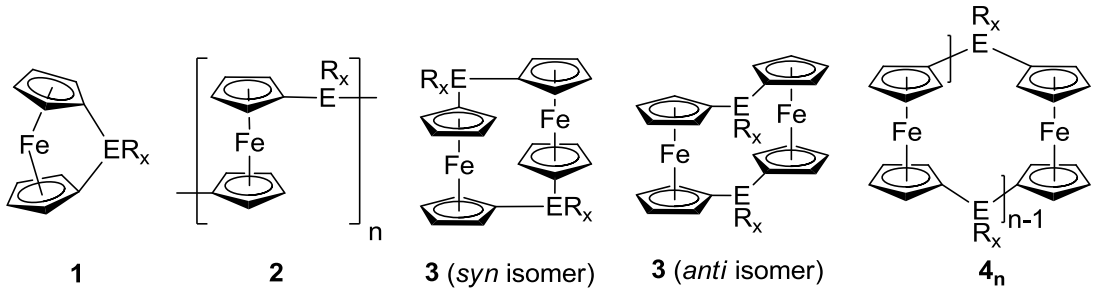

Figure 3-4-1. [1]Ferrocenophane (**1**), poly(ferrocene)s (**2**), [1.1]ferrocenophane (**3**), and ferrocene-containing macrocycle (**4$_n$**).

Recently, we reported a synthetic method that allowed the formation of poly(ferrocene)s that contain two different elements as alternating bridges.[17] As illustrated in Scheme 3-4-1, the salt-metathesis reaction of bis(1'-lithioferrocenyl)dialkylsilane with tin dichlorides resulted in poly(ferrocene)s with various linear and cyclic species.[17a] Linear and cyclic species with up to 20 ferrocene units were identified by MALDI-TOF mass analysis. Similarly, the reaction of bis(1'-lithioferrocenyl)dialkylsilane with gallium dichlorides yielded various linear and cyclic poly(ferrocene)s that contain silicon and gallium as alternating bridges.[17b] Unsymmetrically bridged [1.1]FCPs with a combination of Si/Sn and Si/Ga were isolated

as the smallest cyclic species. These results triggered the reinvestigation of an old reaction of dilithioferrocene with tin dichlorides. In 1980 the reaction of dilithioferrocene with Me_2SnCl_2 was reported by Osborne et al. with the isolation of oligo(ferrocenyldimethylstannane) (molar mass obtained by osmometrically in chloroform: 4.6 kD) containing approx. 13 repeating units.[4] Two years later Seyferth et al. reported a similar reaction of dilithioferrocene with nBu$_2$SnCl$_2$ and obtained oligo(ferrocenyldibutylstannane) as expected.[18] However, they were able to isolate the cyclic dimer dibutyltin[1.1]ferrocenophane (FCP) of low yield (3%). The same reaction was reinvestigated by Manners et al. in 1998 and they reported very similar result with the isolation of dibutyltin[1.1]ferrocenophane from oligo(ferrocenyldibutylstannane) (molar mass obtained by GPC: 6.1 kD).[13] However, no attempt was made to unravel the nature of the oligomers. In this report we reinvestigated those salt metathesis reactions of dilithioferrocene with R_2SnCl_2 (R = Me, nBu) to disclose the nature of those oligomers.

RESULTS AND DISCUSSION

Synthesis and characterization of poly(ferrocenylstannane)s. As described in Scheme 3-4-1, previously reported oligomers, oligo(ferrocenyldimethylstannane) **5a$_n$** and oligo(ferrocenyldibutylstannane) **5b$_n$** were synthesized by reacting dilithioferrocene with

Scheme 3-4-1. Reaction of dialkyl tindichlorides with dilithioferrocene.

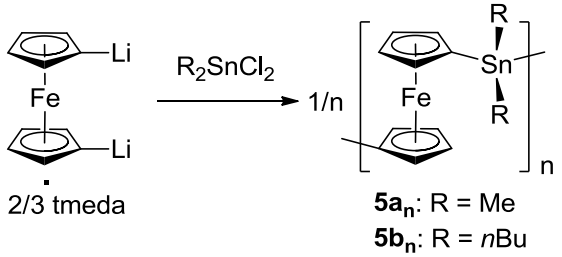

Me_2SnCl_2 and $n$$Bu_2SnCl_2$, respectively. After both reactions were quenched with few drops of water, **5a$_n$** and **5b$_n$** were purified by standard procedures and isolated in good yields of 71 and 73%, respectively.

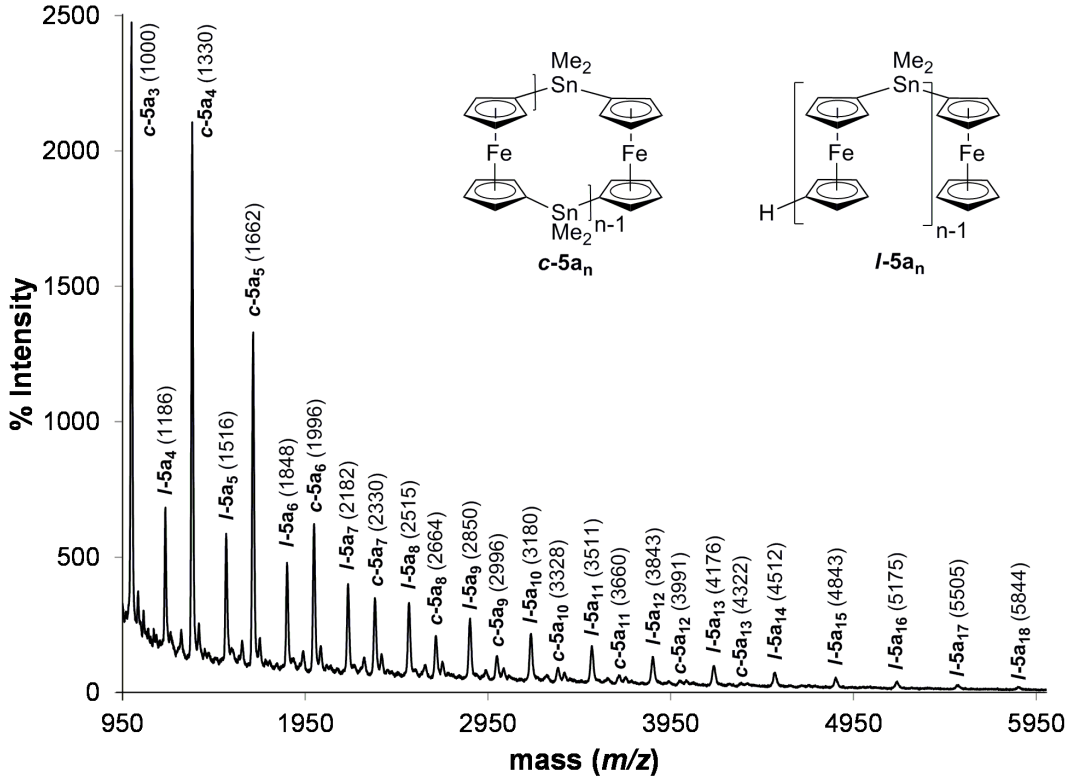

Figure 3-4-2. MALDI-TOF mass spectrum (linear mode) of **5a$_n$**.

With the aim of unraveling the identity of **5a$_n$** and **5b$_n$**, they were subjected to MALDI TOF mass analysis. Samples for MALDI TOF analysis were prepared as 1:10 mixtures of a sample solution (1 mg/mL) with a solution of dithranol (10 mg/mL), both in thf. Mass spectra of **5a$_n$** revealed the presence of various cyclic- (***c*-5a$_n$**) and linear oligomers (***l*-5a$_n$**); cyclic species with up to 13 repeating units and linear species with up to 18 ferrocene moieties were found (Figure 3-4-2). The MALDI-TOF mass spectrum of **5b$_n$** was less pronounced; only molecular ion peaks of smaller cyclic- (***c*-5b$_n$**, n = 2-5) and linear species (***l*-5b$_n$**, n = 2-4) with some additional peaks were found (see Supporting

Information). In addition, two peaks at m/z = 779 and 908 were characterized as [***c*-5b$_2$**$^+$ - *n*Bu] and [***l*-5b$_3$**$^+$ - 2*n*Bu], respectively. This indicates that fragmentation was occurring.

A large number of [1.1]FCPs with group 14 elements (C, Si and Sn) as bridges as well as linear poly(ferrocene)s with C, Si, Ge and Sn as bridging elements are known in literature. However, macrocyclic poly(ferrocene)s (**4$_n$**; Figure 3-4-1) are quite rare. In 1969, Katz et al. reported the first examples of macrocyclic ferrocenophanes with methylene-bridged; the cyclic trimer, tetramer and pentamer were isolated.[19] The cyclic tetramer was structurally characterized. Quin-jin et al. synthesized a cyclic trimer where the ferrocene-moieties are bridged by the π-conjugated linker $C(CH_3)=N–N=C(CH_3)$.[20] Köhler et al. reported the MALDI-TOF mass spectra of cyclic oligo(ferrocene)s with 7-17 doubly silicon-bridged ferrocene units. The macrocycle with seven repeating units was structurally characterized.[21] In 2009, Manners et al. reported on MALDI-TOF mass spectrometry of silicon-bridged cyclic poly(ferrocene)s containing more than 40 ferrocendiyl units as obtained by photocontrolled ROP of dimethylsila[1]ferrocenophane and solid-state structures of cyclic tetramer to heptamer were determined.[22] Very recently, we reported cyclic poly(ferrocene)s that contained silicon and tin as alternating bridging elements.[17a] MALDI-TOF mass analysis showed the presence of macrocycles with up to 20 ferrocene units. Two cyclic tetramers were structurally characterized. We also reported cyclic poly(ferrocene)s with alternating silicon and gallium bridges.[17b] Macrocycles with up to 12 repeating units were identified by MALDI-TOF mass analysis. Besides stanna[1.1]ferrocenophanes, there is no literature evidence of cyclic poly(ferrocene) with tin as bridging element.

Isolation of species *l*-5b$_2$, *l*-5b$_3$, *l*-5b$_4$, *c*-5a$_2$, *c*-5b$_2$, *c*-5a$_3$ and *c*-5b$_3$. The discovery of various cyclic and linear species observed by MALDI-TOF mass analysis encouraged us to separate different species from the mixture of oligomers. Seyferth et al. isolated the cyclic dimer dibutylstanna[1.1]ferrocenophane by column chromatography using dichloromethane/hexanes (1.5/8.5) mixture as eluent and silica gel as stationary phase. Manners et al. achieved the separation of various cyclic oligo(ferrocenyldimethylsilane) using silica gel column with a gradient of 0-70% dichloromethane in hexanes. Similarly, we set out to isolate different species from **5a$_n$** and **5b$_n$** by column chromatography using silica gel as stationary phase and a mixture of dichloromethane/hexanes. At first **5a$_n$** was applied on silica gel column run by a mixture of dichloromethane/hexanes (1.5/8.5) and six yellow to orange bands were separated. Each band was collected and analyzed by ^{1}H NMR spectroscopy. The first band was found to be ferrocene and discarded. The second and third bands were the cyclic dimer ***c*-5a$_2$** and the cyclic trimer ***c*-5a$_3$**, respectively. However, the fourth, fifth and sixth bands contained a mixture of species, of which the cyclic trimer ***c*-5a$_3$** was always a component. Isolation of different components were attempted from the combined fourth, fifth and sixth bands by column chromatography and preparative thin layer chromatography with a gradient of 10-50% of dichloromethane in hexanes. However, the tendency of ***c*-5a$_3$** to crystalize and deposit on stationary phase prevented the isolation of other species. Similarly, five bands were separated from **5b$_n$** using a silica gel column with a mixture of dichloromethane/hexanes (1.5/8.5) as eluent. Those bands were found to be the cyclic dimer (***c*-5b$_2$**) and trimer (***c*-5b$_3$**) and the linear dimer (***l*-5b$_2$**), trimer (***l*-5b$_3$**) and tetramer (***l*-5b$_4$**), respectively. Table 3-4-1 summaries the R_f values in dichloromethane/hexanes (1.5/8.5) and yields of all seven isolated species.

Table 3-4-1. R_f Values and Yields of All Isolated Species.

Species	R_f	Yield
***c*-5a$_2$**	0.364	413 mg (7.1%)
***c*-5a$_3$**	0.206	389 mg (6.7%)
***c*-5b$_2$**	0.756	395 mg (5.4%)
***c*-5b$_3$**	0.649	439 mg (6.0%)
***l*-5b$_2$**	0.410	388 mg
***l*-5b$_3$**	0.286	291 mg
***l*-5b$_4$**	0.196	260 mg

X-ray structures of *c*-5a$_2$, *c*-5a$_3$ and *c*-5b$_3$. X-ray quality crystals of the Me_2Sn-bridged [1.1]FCP ***c*-5a$_2$** and the [1.1.1]FCP ***c*-5a$_3$** were obtained from solutions of a mixture of dichloromethane and hexane (dichloromethane/hexane: 1/3) at -22 °C. Single crystal of nBu$_2$Sn-bridged [1.1.1]FCP ***c*-5b$_3$** was isolated from a solution of acetone at -22 °C. The molecular structures of species ***c*-5a$_2$** and ***c*-5a$_3$** and ***c*-5b$_3$** were determined by single-crystal X-ray analysis. Compound ***c*-5b$_3$** was disordered in the crystal lattice and its molecular structure could not be fully resolved. Figure 3-4-3 and Figure 3-4-4 show ORTEP plots of ***c*-5a$_2$** and ***c*-5a$_3$**, respectively (Table 3-4-2). Similar to previously reported tin-bridged [1.1]FCPs (**3**: ER_x = SnnBu$_2$, SntBu$_2$, $SnMes_2$; Figure 3-4-1), species ***c*-5a$_2$** adopts a chair-like *anti* conformation with an approximate C_{2h} point group symmetry (space group: $P2_1/c$). The Fe···Fe distance in ***c*-5a$_2$** [5.4972(7) Å] is similar to that found in tBu$_2$Sn- [5.474(1) Å][13] and nBu$_2$Sn-bridged [1.1]FCP [5.50 Å],[23] but considerably longer than that of Mes_2Sn-bridged species [5.248(1) Å].[13] All Sn-C^{ipso} bond lengths in ***c*-5a$_2$** falls in a narrow range of 2.129(2)-2.132(3) Å, which is consistent with the other known tin-bridged [1.1]FCPs. The bite-angle at the bridging tin atom [C^{ipso}-Sn-C^{ipso} = 109.84(9)°] is similar to those of the nBu$_2$Sn- [110.0(1)°] and tBu$_2$Sn-bridged species [110.91(13)°], however, considerably smaller than the value found in

Mes_2Sn-bridged [1.1]FCP [117.55(8)]. In ***c*-5a$_2$**, the Cp rings of each ferrocene moieties are not parallel to each other; they are slightly tilted [tilt angle α = -3.25(19)°]. In contrast to stanna[1]ferrocenophanes [bridging moiety *t*Bu_2Sn: α = 14.1(2)°; Mes_2Sn: α = 15.2(2)°], the Cp rings in ***c*-5a$_2$** are significantly less tilted and bent opposite to the bridging tin atoms. However, α in ***c*-5a$_2$** [-3.25(19)°] is similar to those found in known tin-bridged [1.1]FCPs [bridging moiety Mes_2Sn: α = -3.3(2)°, *t*Bu_2Sn: α = -5.0(2)°].

Table 3-4-2. Crystal and Structural Refinement Data for Compounds ***c*-5a$_2$** and ***c*-5a$_3$**.

	***c*-5a$_2$**	***c*-5a$_3$**
empirical formula	$C_{24}H_{28}Fe_2Sn_2$	$C_{36}H_{42}Fe_3Sn_3$
formula weight	665.54	998.32
cryst. size / mm^3	0.15 × 0.15 × 0.08	0.20 × 0.08 × 0.05
cryst. system, space group	monoclinic, $P2_1/c$	monoclinic, $C2/c$
Z	2	4
a / Å	9.4969(2)	16.8047(5)
b / Å	10.8956(3)	18.3228(6)
c / Å	12.1460(3)	13.2797(5)
α / °	90	90
β / °	114.6411(17)°	109.091(2)
γ / °	90	90
volume / $Å^3$	1142.35(5)	3864.0(2)
ρ_{calc} / mg m^{-3}	1.935	1.716
temperature / K	173(2)	173(2)
$\mu_{calc.}$/ mm^{-1}	3.413	3.027
θ range / °	3.69 – 27.48	3.25 – 27.47
reflections collected	4917	8558
absorption correction	multiscan	multiscan
data / restraints / params	2614 / 0 / 130	4416 / 0 / 194
goodness-of-fit	1.100	1.066
R_1 [I > 2 σ(I)][a]	0.0219	0.0295
wR_2 (all data)[a]	0.0511	0.0712
largest diff. peak and hole, $\Delta\rho_{elect}$ / e $Å^{-3}$	0.908, -0.546	0.802, -0.821

[a] $R_1 = [\Sigma||F_o|-|F_c||]/[\Sigma|F_o|]$ for $[F_o^2 > 2\sigma(F_o^2)]$, $wR_2 = \{[\Sigma w(F_o^2-F_c^2)^2]/[\Sigma w(F_o^2)^2]\}^{1/2}$ [all data].

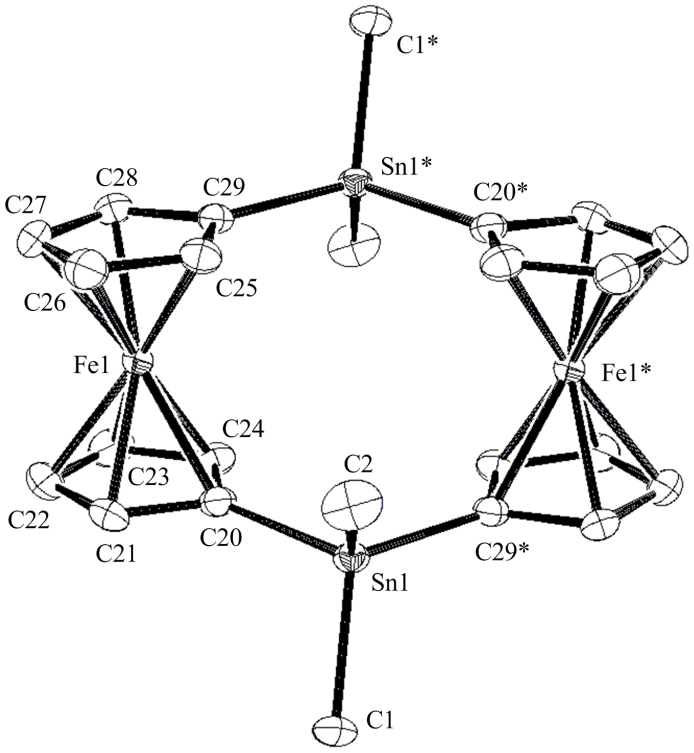

Figure 3-4-3. Molecular structure of ***c*-5a$_2$** with thermal ellipsoids at the 50% probability level. Hydrogen atoms are omitted for clarity. Selected atom-atom distances [Å] and bond angles [º] for ***c*-5a$_2$**: Sn(1)-C(20) 2.132(3); Sn(1)-C(29)* 2.129(2); Sn(1)-C(1) 2.144(2); Sn(1)-C(2) 2.138(3); Fe(1)···Fe(1)* 5.4972(7); C(29)*-Sn(1)-C(20) 109.84(9); C(29)*-Sn(1)-C(2) 111.86(11); C(29)*-Sn(1)-C(1) 111.28(10); C(2)-Sn(1)-C(1) 105.35(12).

The molecular structure of Me_2Sn-bridged [1.1.1]FCP ***c*-5a$_3$** showed that all Sn-C^{ipso} bond lengths falls in a close range of 2.127(3)-2.139(3) Å. Three iron atoms in ***c*-5a$_3$** form an approximate equilateral triangle as revealed by the interatomic Fe···Fe distances [Fe1···Fe2: 5.5213(7) Å, Fe1···Fe1*: 5.5507(8) Å, Fe2···Fe1*: 5.5213(7) Å]. Sn···Sn distances are also very similar to each other [Sn1···Sn2: 7.2270(4) Å, Sn1···Sn1*: 7.2600(5) Å, Sn2···Sn1*: 7.2270(4) Å]. This suggests that the point group symmetry of ***c*-5a$_3$** is approximately D_3. The bite-angles of tin atoms in ***c*-5a$_3$** [110.14(16)°, 112.21(11)°] are similar to that found in ***c*-5a$_2$**. In the molecular structure of species ***c*-5a$_3$**, two Cp rings of each ferrocene moiety are lying above and below the averaged plane

of the molecule; similar structural features were observed in the molecular structure of $C(CH_3)$=N–N=$C(CH_3)$-bridged [1.1.1]FCPs[20] as well as in the calculated structure of Me_2Si-bridged [1.1.1]FCP.[22]

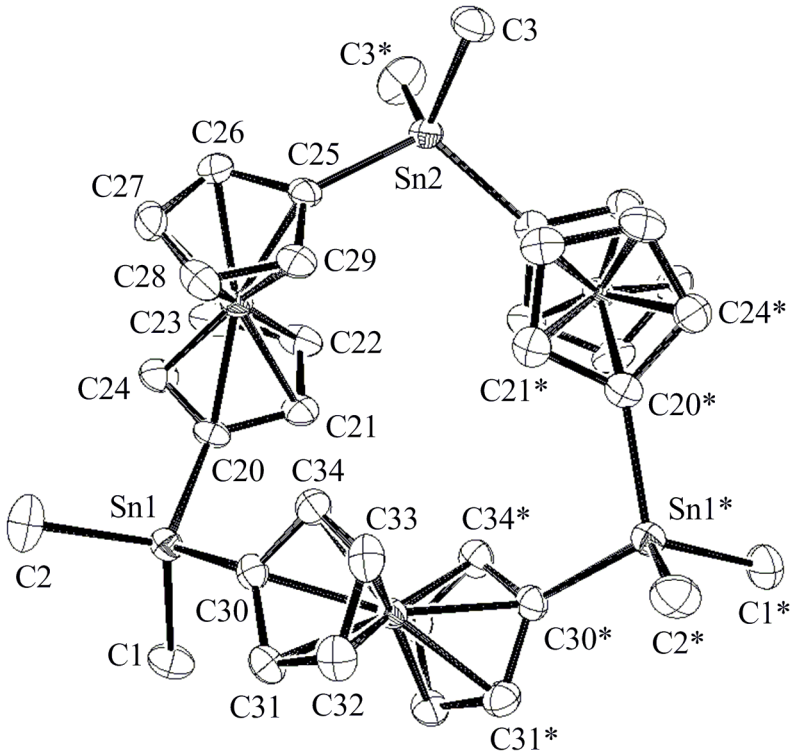

Figure 3-4-4. Molecular structure of ***c*-5a$_3$** with thermal ellipsoids at the 50% probability level. Hydrogen atoms are omitted for clarity. Selected atom-atom distances [Å] and bond angles [º] for ***c*-5a$_3$**: Sn(1)-C(20) 2.127(3); Sn(1)-C(30) 2.139(3); Sn(1)-C(1) 2.147(4); Sn(1)-C(2) 2.144(3); Sn(2)-C(25) 2.128(3); Sn(2)-C(3) 2.137(4); Fe(1)···Fe(2) 5.5213(7); Fe(1)···Fe(1)* 5.5507(8); Sn(1)···Sn(2) 7.2270(4); Sn(1)···Sn(1)* 7.2600(5); C(20)-Sn(1)-C(30) 112.21(11); C(20)-Sn(1)-C(2) 106.51(13); C(30)-Sn(1)-C(2) 109.75(13); C(20)-Sn(1)-C(1) 109.55(14); C(25)-Sn(2)-C(25)* 110.14(16); C(25)-Sn(2)-C(3) 106.27(13).

NMR characterization of isolated species *l*-5b$_2$, *l*-5b$_3$, *l*-5b$_4$, *c*-5a$_2$, *c*-5b$_2$, *c*-5a$_3$ and *c*-5b$_3$. All seven isolated species were characterized by ^{1}H, ^{13}C and ^{119}Sn NMR spectroscopy. The ^{1}H NMR spectra of the cyclic dimers ***c*-5a$_2$** showed a singlet for 4 Me groups and 2 pseudo triplets for 8 Cp protons (Figure 3-4-5a). Species ***c*-5b$_2$** is a known compound and measured NMR data match with published data.[18] Therefore, species ***c***-

5a$_2$ and ***c*-5b$_2$** each displayed one signal or one set of signals for 4 alkyl groups attached to tin atoms and 2 signals for Cp protons. In their solid state structures, species ***c*-5a$_2$** and ***c*-5b$_2$** exhibit C_{2h} point group symmetry with a group order of $h = 4$. If this would be the case in solution, only 4 signals ($16/h = 4$) for all 16 Cp protons are expected. However, [1.1]FCPs, such as sila[1.1]ferrocenophanes, are known to be fluxional in solution.[11]

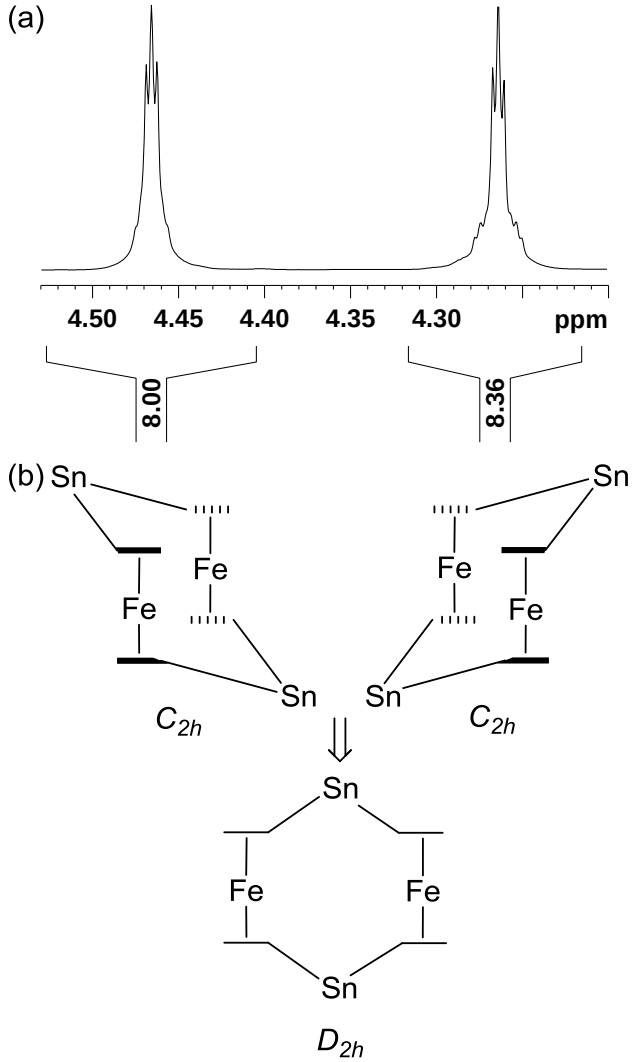

Figure 3-4-5. (a) Cp region of ^{1}H NMR spectrum of ***c*-5a$_2$**. (b) Illustration of ground state geometry and time average flat structure of cyclic trimers ***c*-5a$_2$** and ***c*-5b$_2$** (▬ represents Cp above the plane of paper, ⋯ represents Cp ring below the plane of paper and — represents Cp on the paper plane).

They display fast, degenerate *anti*-to-*anti* isomerization. Similarly, *anti*-to-*anti* isomerization occurs in solutions of tin-bridged [1.1]FCPs ***c*-5a$_2$** and ***c*-5b$_2$**. As illustrated in Figure 3-4-5b, *anti* isomers of ***c*-5a$_2$** and ***c*-5b$_2$** can be visualized as an expanded cyclohexane in chair conformation and *anti*-to-*anti* isomerization of ***c*-5a$_2$** and ***c*-5b$_2$** is similar to chair-to-chair isomerization of cyclohexane. This fast isomerization results in a structure similar to a flat cyclohexane, which contains D_{2h} point group symmetry with group order of $h = 8$. Therefore, all 16 Cp protons appear as 2 ($16/h = 2$) signals.

The ^{1}H NMR spectra of the cyclic trimers ***c*-5a$_3$** and ***c*-5b$_3$** revealed interesting features. At r.t., species ***c*-5a$_3$** showed a singlet for Me groups in the aliphatic range and 2 broad peaks and a sharp peak in the range of Cp protons (Figure 3-4-6c). However, species ***c*-5b$_3$** displayed 4 peaks for *n*Bu groups and 4 broad peaks of equal intensities for all 16 Cp protons. In addition to sharp peaks, ^{13}C NMR spectra also displayed broad signals. Broad signals in NMR spectra of ***c*-5a$_3$** and ***c*-5b$_3$** indicated dynamic behavior. Therefore, variable temperature (VT) NMR measurements was performed for ***c*-5a$_3$** ($CDCl_3$, -20 °C to 50 °C) and ***c*-5b$_3$** (toluene-D_8, -40 °C to 90 °C) (Figure 3-4-6). Both species displayed four sharp singlet at low temperature (-20 °C for ***c*-5a$_3$** and 10 °C for ***c*-5b$_3$**). With increasing temperature, the peaks broadened and the two peaks in the middle exhibited coalescence (first coalescence temperature for ***c*-5a$_3$** is 13 °C and for ***c*-5b$_3$** is 47 °C). The other set of two peaks broadened even more with increasing temperature until the second coalescence temperature (***c*-5a$_3$**: 29 °C and ***c*-5b$_3$**: 70 °C) was reached. At higher temperature, all peaks for Cp protons merged and exhibited only one sharp singlet. Line shape analyses were also performed for species ***c*-5a$_3$** and ***c*-5b$_3$**.

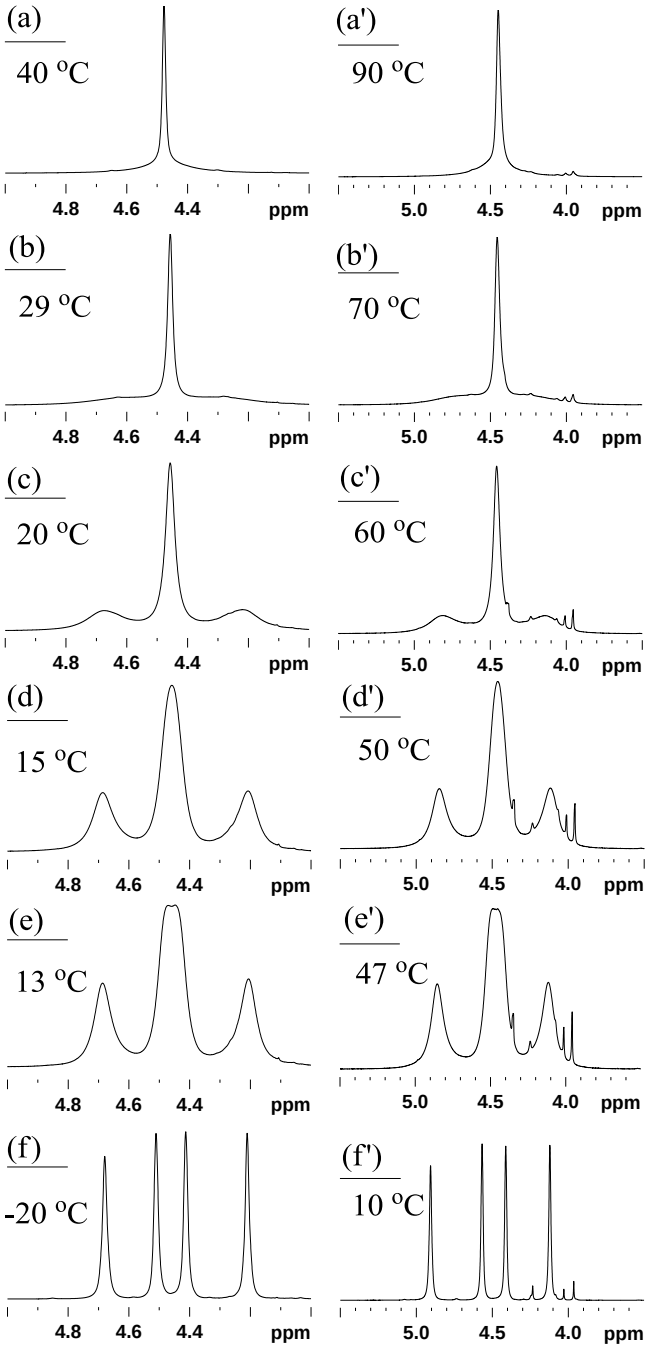

Figure 3-4-6. Variable temperature ^{1}H NMR of ***c*-5a$_3$** ((a) to (f)) and ***c*-5b$_3$** ((a') to (f')); only signals of Cp protons are displayed.

Species ***c*-5a$_3$** and ***c*-5b$_3$** exhibited four signals at low temperature and one signal at high temperature for 24 Cp protons of all 6 Cp rings. The crystal structures of ***c*-5a$_3$** and ***c*-5b$_3$** revealed that the ground state geometries are D_3 symmetric (group order $h = 6$). Species

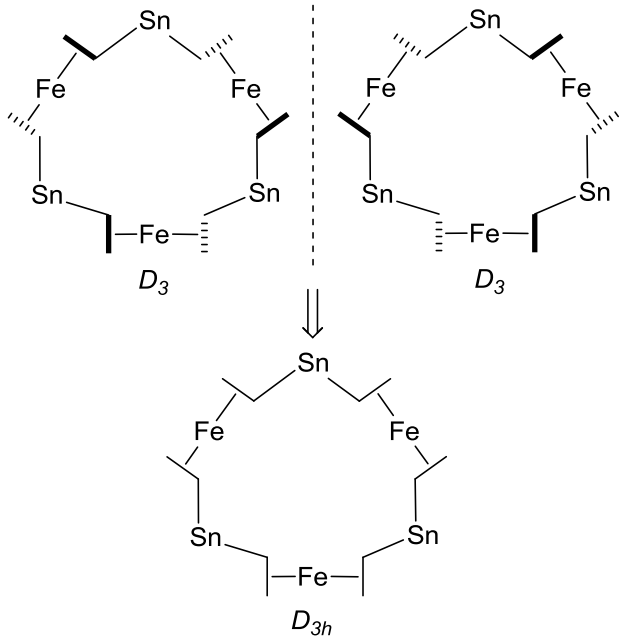

Figure 3-4-7. Illustration of ground state geometry and time average flat structure of cyclic trimers ***c*-5a$_3$** and ***c*-5b$_3$** (**—** represents Cp ring pointing up, ···· represents Cp ring pointing down and **—** represents Cp ring on the ring on the plane).

equipped with 1,1'-disubstituted ferrocene moieties, all Cp protons *must* be in general position (not on a symmetry element). That means that the number of Cp signals in ^{1}H NMR spectroscopy directly reveals the group order of the time-averaged symmetry of the species in question. For example, if compound ***c*-5a$_3$** would be D_3 symmetric in solution, each set of Cp protons (one for all α and one for all β protons) would give two signals; i.e., 4 siganls for all the 24 Cp protons (e.g., α protons: 12/h = 2 for D_3 symmetry). This is what was observed at low temperature (Figure 3-4-6f: ***c*-5a$_3$**, Figure 3-4-6f': ***c*-5b$_3$**) indicating that the structure in the solution is similar as in the solid state. As illustrated in Figure 3-4-7, the fast ring inversion at higher temperature introduces a pseudo mirror plane, which increases the symmetry of the molecule resulting in a time average flat structure with D_{3h} point group symmetry (h = 12), which is the highest possible symmetry of such a cyclic compound. Therefore, the time averaged flat structure with

group order of h = 12 should exhibit 2 signals (24/h = 2) for all 24 Cp protons at high temperature. However, the appearance of one peak for the Cp protons at high temperature therefore must be due to a coincidental overlap of two peaks.

The isolated linear oligomers were also characterized by ^{1}H, ^{13}C and ^{119}Sn NMR. In the ^{1}H NMR spectra, the species ***l*-5b$_2$** and ***l*-5b$_3$** displayed four peaks for *n*Bu-groups (see Supporting Information). However, the ^{1}H NMR spectrum of linear tetramer ***l*-5b$_4$** displayed two sets of four peaks with approximate intensity ratios of 1:2, which are either separated from each other or partially to completely overlapped (see Supporting Information). In the Cp range of ^{1}H NMR spectra, species ***l*-5b$_2$**, ***l*-5b$_3$** and ***l*-5b$_4$** displayed three peaks with intensity ratio of 4:4:10, five peaks with intensity ratio of 4:4:4:4:10 and six peaks with intensity ratio of 8:4:4:4:4:10, respectively. The large signals with relative intensity ratio of 10 in all three cases are due to two Cp end groups, which indicate a two-fold symmetry element. The other Cp signals are from the substituted Cp rings. The number of Cp signals for the linear species ***l*-5b$_2$** (number of peaks: 2), ***l*-5b$_3$** (number of peaks: 4), and ***l*-5b$_4$** [number of peaks: 6 (considering the peak with intensity ratio of 8 generated from an overlap of two peaks)] shows in all cases a time averaged point group of the order 4. This could either be C_{2v} or C_{2h} symmetry, which means that fast rotations around all Sn-Cp bonds occur in solution, which is not a surprise for these small, linear species. ^{13}C NMR data are consistent with ^{1}H NMR data.

Electrochemical studies of species *l*-5b$_2$, *l*-5b$_3$, *l*-5b$_4$, *c*-5a$_2$, *c*-5b$_2$, *c*-5a$_3$, *c*-5b$_3$, 6a, and 6b. The redox behavior of the isolated linear species, ***l*-5b$_2$**, ***l*-5b$_3$**, and ***l*-5b$_4$** and cyclic species ***c*-5a$_2$**, ***c*-5b$_2$**, ***c*-5a$_3$**, and ***c*-5b$_3$** were investigated by cyclic voltammetry and AC voltammetry (Table 3-4-3). In addition, we have studied the electrochemical behavior

of two previously reported [1.1.1.1]FCPs[17a] (**6a** and **6b**, Figure 3-4-8) with silicon and tin as alternating bridging elements by using cyclic voltammetry, AC voltammetry and rotary-disc voltammetry (Table 3-4-3). CH_2Cl_2 was selected as the solvent for all electrochemical measurements due to its inertness towards ferrocenium-type ions. [nBu$_4$N][PF$_6$] was used as supporting electrolyte.

Table 3-4-3. Measured Formal Potentials [V] of ***l*-5b$_2$**, ***l*-5b$_3$**, ***l*-5b$_4$**, ***c*-5a$_2$**, ***c*-5b$_2$**, ***c*-5b$_3$**, **6a**, and **6b** with respect to FcH/FcH$^+$ (0.1 M [nBu$_4$N][PF$_6$]; Scan Rate of 50 mV/s).

	$E_1^{o\prime}$	$E_2^{o\prime}$	$E_3^{o\prime}$	$E_4^{o\prime}$	$E_2^{o\prime} - E_1^{o\prime}$ ($\Delta E_1^{o\prime}$)	$E_3^{o\prime} - E_2^{o\prime}$ ($\Delta E_2^{o\prime}$)
***l*-5b$_2$**	-0.172	0.075	—	—	0.247	—
***l*-5b$_3$**	-0.214	-0.085	0.066	—	0.129	0.151
***l*-5b$_4$**	-0.168		0.025		—	—
***c*-5a$_2$**	-0.138	0.099	—	—	0.237	—
***c*-5b$_2$**	-0.099	0.100	—	—	0.199	—
***c*-5b$_3$**	-0.057		0.193	—	—	—
6a	-0.144	0.024	0.224	—	0.168	0.200
6b	-0.094	0.101	0.282	—	0.195	0.181

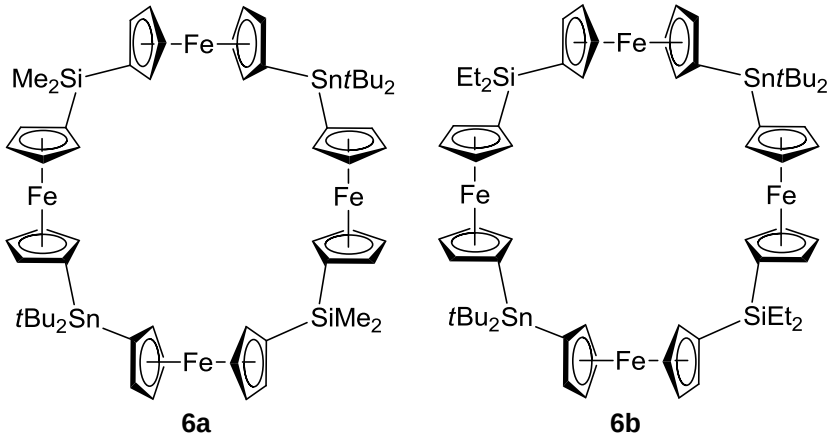

Figure 3-4-8. [1.1.1.1]FCPs, **6a** and **6b** with silicon and tin as alternative bridges.

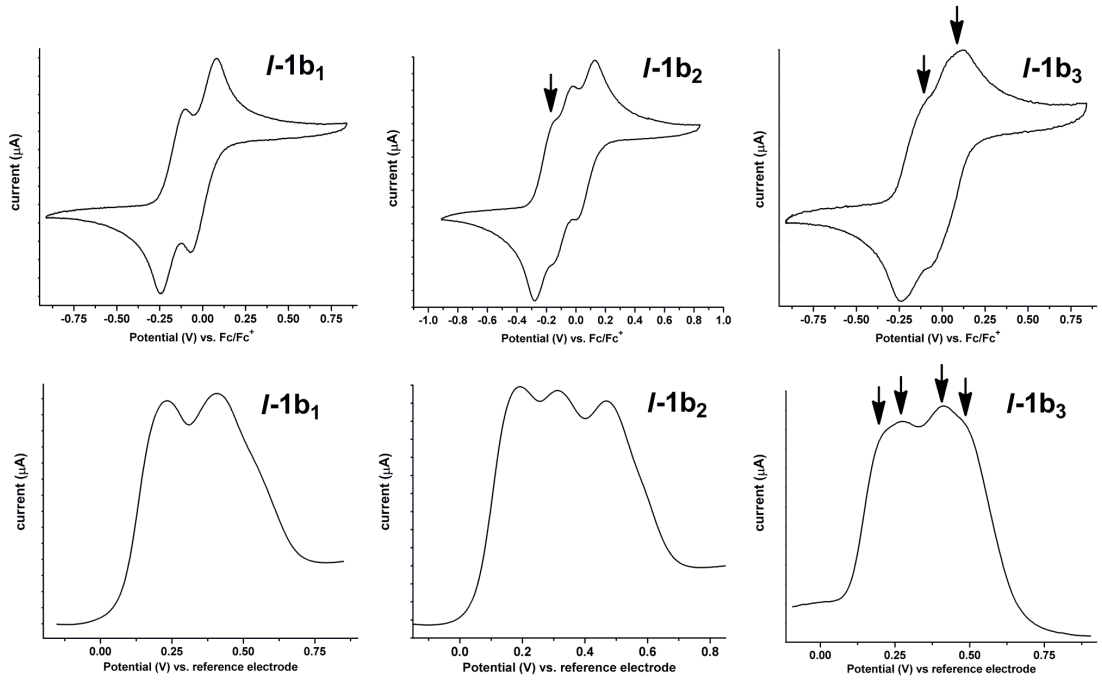

Figure 3-4-9. Cyclic voltammogram (upper row) and AC voltammograms (bottom row) of ***l*-5b$_2$**, ***l*-5b$_3$**, and ***l*-5b$_4$** using scan rates of 50 mV/s and 20 mV/s, respectively (CH_2Cl_2; 0.1 M [nBu$_4$N][PF_6]; r.t.).

The cyclic voltammograms and AC voltammograms of tin-bridged linear species ***l*-5b$_2$** and ***l*-5b$_3$** displayed two and three reversible redox waves, respectively (Figure 3-4-9). These results are consistent with ***l*-5b$_2$** and ***l*-5b$_3$** having two and three iron redox centers, respectively. Species ***l*-5b$_4$** with four iron centers exhibited two broad redox waves, indicative of two sets of two overlapping one-electron processes (Figure 3-4-9). The stepwise oxidation of each iron center in ***l*-5b$_2$**, ***l*-5b$_3$**, and ***l*-5b$_4$** is illustrated in equation 1. Similar to ***l*-5b$_2$**, related silicon-bridged bis(ferrocenyl) species Me_2SiFc_2 [Fc = $(C_5H_5)Fe(C_5H_4)$] showed two redox waves with $\Delta E_1^{o\prime}$ ($\Delta E_1^{o\prime} = E_2^{o\prime} - E_1^{o\prime}$) of 150 mV (measured in 1:1 mixture of CH_2Cl_2:CH_3CN using [nBu$_4$N][PF_6] as supporting electrolyte).[24] The higher analogues of Me_2SiFc_2 displayed significantly different

electrochemical behavior as compared to ***l*-5b$_3$** and ***l*-5b$_4$**.[24] Silicon-bridged linear species with three ferrocene moieties showed two well-separated peaks; one broad peak corresponding to a two-electron process and the other corresponding to a one-electron process. In contrast, the similar species ***l*-5b$_3$** with tin as bridging element showed three well-resolved redox waves. As compared to ***l*-5b$_4$**, analogous silicon-bridged species displayed a different redox behavior with three redox waves (relative intensities = 2:1:1).

$$\text{l-5b}_2 \underset{-e}{\overset{+e}{\rightleftharpoons}} \text{l-5b}_2^{+} \underset{-e}{\overset{+e}{\rightleftharpoons}} \text{l-5b}_2^{2+} \quad \text{(1a)}$$

$$\text{l-5b}_3 \underset{-e}{\overset{+e}{\rightleftharpoons}} \text{l-5b}_3^{+} \underset{-e}{\overset{+e}{\rightleftharpoons}} \text{l-5b}_3^{2+} \underset{-e}{\overset{+e}{\rightleftharpoons}} \text{l-5b}_3^{3+} \quad \text{(1b)}$$

$$\text{l-5b}_4 \underset{-e}{\overset{+e}{\rightleftharpoons}} \text{l-5b}_4^{+} \underset{-e}{\overset{+e}{\rightleftharpoons}} \text{l-5b}_4^{2+} \underset{-e}{\overset{+e}{\rightleftharpoons}} \text{l-5b}_4^{3+} \underset{-e}{\overset{+e}{\rightleftharpoons}} \text{l-5b}_4^{4+} \quad \text{(1c)}$$

Two reversible redox waves were observed in the cyclic voltammogram and AC voltammogram of the Me_2Sn-bridged [1.1]FCP, ***c*-5a$_2$**. The observed redox behavior of the *n*Bu_2Sn-bridged [1.1]FCP, ***c*-5b$_2$** ($\Delta E_1^{o\prime}$ = 199 mV) is very similar to that of published data ($\Delta E_1^{o\prime}$ = 200 mV).[23] This behavior of stepwise oxidations of two iron centers is typical for [1.1]FCPs with different bridging elements. Two previously reported tin-bridged [1.1]FCPs, *t*Bu_2Sn[1.1]FCP and Mes_2Sn[1.1]FCPs also displayed two redox waves with $\Delta E_1^{o\prime}$ of 270 and 280 mV, respectively (solvent: CH_2Cl_2; supporting electrolyte: [*n*Bu_4N][PF_6]).[13] The measured $\Delta E_1^{o\prime}$ of ***c*-5a$_2$** and ***c*-5b$_2$** are 237 and 199 mV, respectively. As shown in Table 3-4-4, the Fe···Fe separation in ***c*-5b$_2$**, *n*Bu_2Sn- and *t*Bu_2Sn-bridged [1.1]FCP are very similar. Therefore, it is surprising to see a significant difference of $\Delta E_1^{o\prime}$ for those species.

Table 3-4-4. Redox Splitting ($\Delta E_1^{o\prime}$) and Fe···Fe Separation in Tin-Bridged [1.1]FCPs.

	$\Delta E_1^{o\prime}$ [mV][a]	d (Fe···Fe)	reference
Me_2Sn-bridged [1.1]FCP (***c*-5a$_2$**)	237	5.4972(7)	this work
nBu$_2$Sn-bridged [1.1]FCP (***c*-5b$_2$**)	199[b]	5.50[c]	this work
tBu$_2$Sn-bridged [1.1]FCP	270	5.474(1)	Ref 13
Mes_2Sn-bridged [1.1]FCP	280	5.248(1)	Ref 13

[a] Values obtained by cyclic voltammetry. [b] $\Delta E_1^{o\prime}$ = 200 mV in Ref 23. [c] value taken from Ref 23.

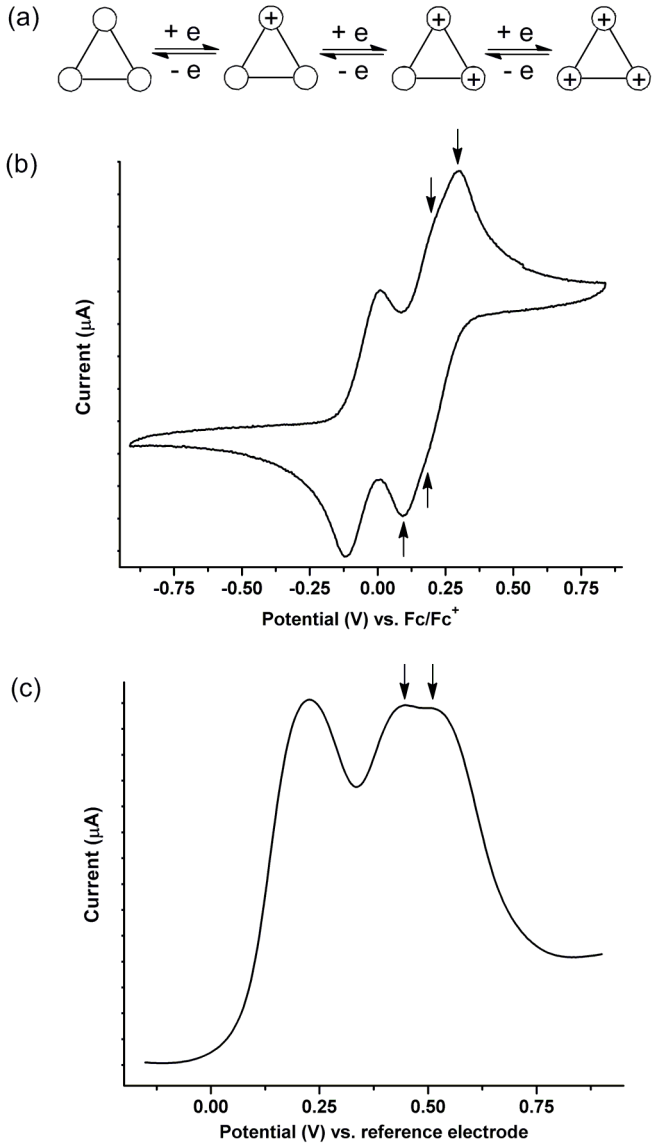

Figure 3-4-10. (a) Proposed redox events (each circle represents a ferrocene unit), (b) cyclic voltammogram, and (c) AC voltammogram of nBu$_2$Sn-bridged [1.1.1]FCP ***c*-5b$_3$**.

The cyclic voltammogram of the cyclic trimer, ***c*-5b$_3$** with nBu$_2$Sn bridging moieties displayed one sharp and one broad redox waves, indicative of one isolated and two partially overlapped one-electron processes (Figure 3-4-10b). This was further supported by AC voltammetry, which clearly showed three redox waves (Figure 3-4-10c). The known, analogous [1.1.1]FCP with Me$_2$Si-bridges showed a very similar electrochemical behavior with three well-resolved redox waves.[22] In contrast to ***c*-5b$_3$**, the cyclic trimer, ***c*-5a$_3$** with Me$_2$Sn-bridges exhibited a complicated behavior (Figure 3-4-11). Species ***c*-5a$_3$** displayed three oxidation waves of similar intensities in the cyclic voltammogram and AC voltammogram. However, species ***c*-5a$_3$** showed complex reduction waves. So far, the redox behavior of ***c*-5a$_3$** could not be explained.

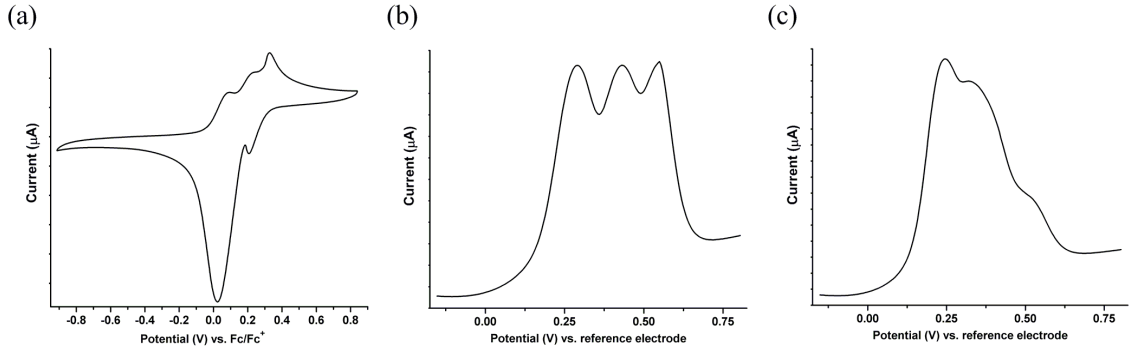

Figure 3-4-11. (a) cyclic voltammogram, (b) AC voltammogram (oxidation wave) (c) AC voltammogram (reduction wave) of Me$_2$-bridged [1.1.1]FCP ***c*-5a$_3$.**

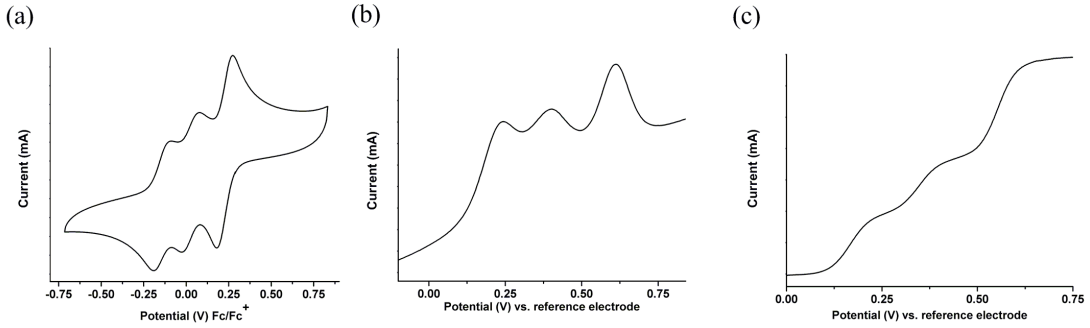

Figure 3-4-12. (a) Cyclic voltammogram, (b) AC voltammogram and (c) rotary-disc voltammogram of **6a**.

The silicon- and tin-bridged [1.1.1.1]FCPs **6a** and **6b** exhibited three reversible redox waves in the cyclic voltammograms and AC voltammograms (Figure 3-4-12 and Supporting Information). Rotary-disc voltammetry of both species showed three redox events with relative intensities of 1:1:2 (Figure 3-4-12 and Supporting Information), clearly revealing that the first two redox waves correspond to one electron, whereas the third wave corresponds to two electrons. An explanation is proposed in Scheme 3-4-2.

Scheme 3-4-2. Proposed redox events of [1.1.1.1]FCPs, **2a** and **2b**.

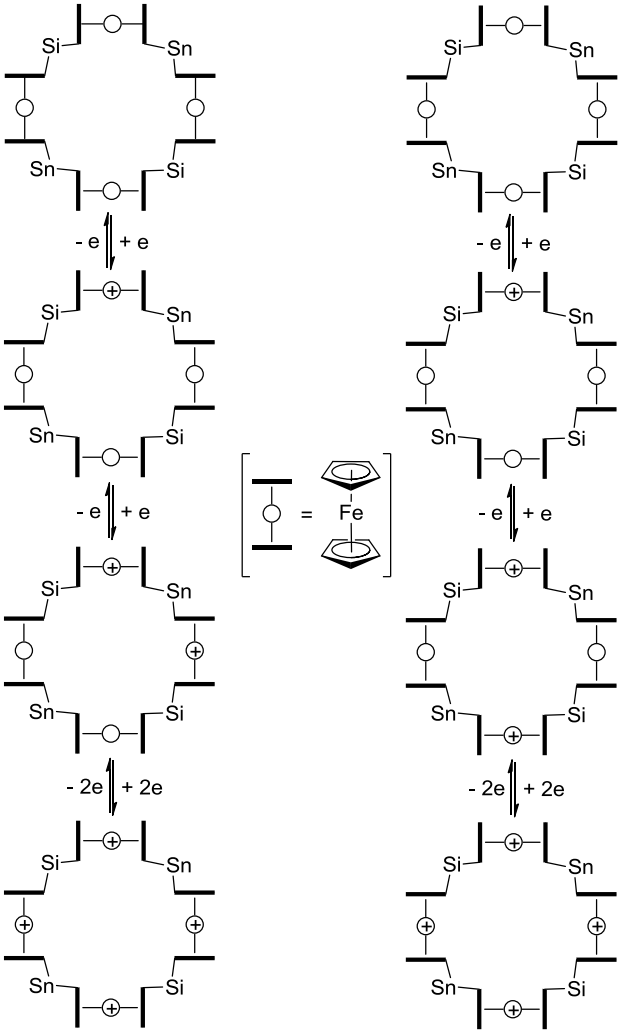

The first redox wave redox represents to the oxidation of one of the four irons. The second redox wave represents the oxidation of either the second iron (Scheme 3-4-2a) or the third iron (Scheme 3-4-2b). The remaining two irons, which are equivalent, are getting oxidized simultaneously at the same potential, and thus, the third redox event is a two-electron process. In contrast to the cyclic tetramers **6a** and **6b**, analogous [1.1.1.1]FCP with Me_2Si bridge displayed two broad peaks, which were interpreted as two sets of two overlapping one-electron processes.[22]

SUMMARY

As reported earlier, reactions of dilithioferrocene with Me_2SnCl_2 and nBu_2SnCl_2 yielded poly(ferrocenylstannane)s $\mathbf{5a_n}$ and $\mathbf{5b_n}$, respectively. The MALDI-TOF mass analysis of $\mathbf{5a_n}$ showed the presence of linear species ***l*-5a$_n$** with up to 18 ferrocene moieties and cyclic species ***c*-5a$_n$** with up to 13 repeating units. The MALDI-TOF mass spectrum of $\mathbf{5b_n}$ displayed smaller cyclic (***c*-5b$_n$**, n = 1-4) and linear species (***l*-5b$_n$**, n = 1-3) as well as some additional peaks, which indicates fragmentation. Some compounds, ***c*-5a$_2$**, ***c*-5b$_2$**, ***c*-5a$_3$**, ***c*-5b$_3$**, ***l*-5b$_2$**, ***l*-5b$_3$** and ***l*-5b$_4$** were isolated by using column chromatography. The isolated species were characterized by ^1H, ^{13}C and 119Sn NMR spectroscopy, mass analysis and elemental analysis. The molecular structures of Me_2Sn-bridged cyclic dimer ***c*-5a$_2$** and cyclic trimer ***c*-5a$_3$** were determined by single-crystal X-ray analysis. Species ***c*-5a$_2$** exists as an anti isomer in the solid state. The molecular structure of ***c*-5a$_3$** is very similar to the calculated structure of analogous [1.1.1]FCP with Me_2Si as bridging moieties. NMR spectra of ***c*-5a$_2$** exhibited fast, degenerate *anti*-to-*anti* isomerization in solution. [1.1.1]FCPs ***c*-5a$_3$** and ***c*-5b$_3$** also displayed dynamic behaviors

in solution as revealed by NMR spectroscopy. Line shape analyses were performed for species ***c*-5a$_3$** and ***c*-5b$_3$**. Different electrochemical techniques were employed to investigate the redox behaviors of the isolated species ***c*-5a$_2$**, ***c*-5b$_2$**, ***c*-5a$_3$**, ***c*-5b$_3$**, ***l*-5b$_2$**, ***l*-5b$_3$** and ***l*-5b$_4$** as well as two previously reported cyclic tetramers **6a** and **6b** with alternating silicon as tin as bridging elements. Species ***c*-5a$_2$**, ***c*-5b$_2$** and ***l*-5b$_2$** with two ferrocene units showed expected redox behaviors with two reversible redox waves. Three ferrocene-containing species ***c*-5b$_3$** and ***l*-5b$_3$** displayed three, partially overlapped redox waves. However, species ***c*-5a$_3$** showed complicated redox behavior, which could not be explained. The largest isolated species ***l*-5b$_4$** with four iron redox centers displayed two broad redox waves indicating two sets of two partially overlapped one-electron events.

EXPERIMENTAL SECTION

General information. Syntheses were carried out partly using standard Schlenk technique and partly in an air atmosphere. Dry solvents were used for reactions and solvents used for workup and purifications were used as received from suppliers. Solvents were dried using a MBraun Solvent Purification System and stored under nitrogen over 3 Å molecular sieves. All solvents for NMR spectroscopy were used as received from suppliers. Ferrocene, *n*BuLi, and nBu$_2$SnCl$_2$ were purchased from Sigma Aldrich, and Me$_2$SnCl$_2$ were purchased from Alfa Aesar and used as received. Silica gel 60 (EMD, Geduran®, particle size 0.040-0.063 mm) were used for chromatography. (LiC$_5$H$_4$)$_2$Fe·2/3tmeda was synthesized as described in literature.[25] ^{1}H, ^{13}C, and ^{119}Sn NMR spectra were recorded on a Bruker 500 MHz Avance NMR spectrometer at 25 ºC in C$_6$D$_6$ and CDCl$_3$, respectively. ^{119}Sn NMR values are referenced relative to tributyltin

chloride (δ 152.0 in $CDCl_3$). ^1H chemical shifts were referenced to the residual protons of the deuterated solvents (δ 7.15 for C_6D_6 and 7.26 for $CDCl_3$); ^{13}C chemical shifts were referenced to the C_6D_6 signal at δ 128.00 and the $CDCl_3$ signal at δ 77.00. Mass spectra were measured on a VG 70SE and were reported in the form *m/z* (%) [M^+] where "*m/z*" is the mass observed, the intensities are reported relative to the most intense peak, and "M^+" is the molecular ion or fragment; only characteristic mass peaks are listed. For isotopic pattern, only the mass peak of the isotopoloque or isotope with the highest natural abundance is listed. Elemental analyses were performed on a PerkinElmer 2400 CHN Elemental Analyzer using V_2O_5 to promote complete combustion.

MALDI-TOF Mass Spectrometry. MALDI-TOF mass spectra were collected on a 4700 Proteomics Analyzer (Applied Biosystems) equipped with a Nd:Yag laser, operating at 335 nm. Positive ion mass spectra were obtained in reflector or linear mode over a range of 500 – 5000 *m/z*. Each spectrum was an accumulation of 12500 laser shots over 100 points on the sample (125 shots/point). Laser intensity was varied for each sample. Solutions of the analytes (1 mg mL^{-1} thf solution) and dithranol (10 mg mL^{-1} thf solution) were prepared and then mixed in a 1:10 ratio. The resulting solutions were drop-cast by micropipette into sample wells and allowed to evaporate for 1 h prior to sample analysis.

Electrochemical measurements. A computer controlled system, consisting of a HEKA potentiostat PG590 (HEKA, Mahone Bay, NS, Canada) was used for the cyclic voltammetry and AC voltammetry experiments. Data was collected using a multifunction DAQ card (BNC 2090) and in-house software written in the LabVIEW environment. Glassy carbon (BAS, 3 mm) was used as the working electrode. The quasi-reference

electrode (QRE) was a silver wire and all measurements were made against the QRE. A loop of gold wire was used as the auxiliary electrode. The instrument for rotary-disc voltammetry was a Autolab PGSTAT302N, with an Autolab rotating disc electrode. Loop of gold wires served as the quasi-reference electrode (QRE) as well as the auxiliary electrode. Autolab control and data collection was done with the accompanying software, NOVA. Before each measurement, 1 mM solutions of samples were freshly prepared in dry organic solvent with 0.1 M $[Bu_4N][PF_6]$ as the supporting electrolyte. The electrolyte was dried overnight under high vacuum at 100 °C before. The scan rate for the cyclic voltammetry and rotary-disc voltammetry was 50 mV/s and for AC voltammetry was 20 mV/s. The measurements were conducted in air and taken at ambient temperature.

Synthesis of poly(ferrocenyldimethylstannane) ($\mathbf{5a_n}$). A solution of Me_2SnCl_2 (3.84 g, 17.5 mmol) in thf (110 mL) was added dropwise to a cold (-78 °C) slurry of $(LiC_5H_4)_2Fe{\cdot}2/3$tmeda (4.83 g, 17.5 mmol) in thf (110 mL). The reaction mixture was warmed up to r.t. and stirred for 16 h, resulting in a dark red solution. The following work up was performed in air. Water (2 mL) was added to the reaction mixture and stirred for 15 min. All volatiles were removed under high vacuum to yield a dark red paste, which was extracted with toluene (200 mL). The toluene solution was concentrated to ca. 30 mL and added dropwise to well-stirred hexane (200 mL), resulting in a dark red solution with little blackish precipitate. After the solid was filtered off, all volatiles were removed from the filtrate under high vacuum, resulting in $\mathbf{5a_n}$ as a dark red paste (5.36 g, 92%). Compound $\mathbf{5a_n}$ was further purified by filtration chromatography by using silica gel as column material and thf as eluent (4.16 g, 71%).

Isolation and identification of *c*-5a$_2$ and *c*-5a$_3$. Flash chromatography of **5a$_n$** was performed on silica gel using a solvent mixture of hexane and CH_2Cl_2 (8.5:1.5). Several orange bands of different compounds were separated into the column and were collected in separate vessels. Six fractions were collected which were identified as: ferrocene (first fraction), ***c*-5a$_2$** (second fraction), ***c*-5a$_3$** (third fraction), and a mixture of several compounds including species ***c*-5a$_3$** (fourth, fifth and sixth fractions). The crystallization of ***c*-5a$_3$** into column material prevented further separation of compounds from fourth, fifth and sixth fractions. Species ***c*-5a$_2$** (7.1%) and ***c*-5a$_3$** (6.7%) were further purified by crystallization into a mixture of hexane and CH_2Cl_2 (9:1). A major portion of **5a$_n$** was trapped into silica gel, which was further recovered by using thf as eluent.

***c*-5a$_2$.** Appearance: Dark red crystalline block or orange powder. ^{1}H NMR ($CDCl_3$): δ 0.36 (s, 12H, CH_3), 4.25, 4.45 (pst, 16H, C_5H_4). ^{13}C NMR ($CDCl_3$): δ -6.81 (CH_3), 68.85 (*ipso*-C of C_5H_4), 70.29, 74.42 (α-C and β-C of C_5H_4). ^{119}Sn NMR ($CDCl_3$): δ -20.93. MS (70 eV, EI): m/z (rel intens) 666 (47) [M^+], 651 (71) [M^+- Me], 368 (100) [$C_{15}H_{12}FeSn^+$], 304 (34) [$C_{10}H_8FeSn^+$]. HRMS (EI; m/z): calcd for $C_{24}H_{28}Fe_2Sn_2$, 665.8913; found, 665.8928. Anal. Calcd for $C_{24}H_{28}Fe_2Sn_2$ (665.59): C, 43.31; H, 4.24. Found: C, 43.26; H, 4.13. R_f (hexanes/CH_2Cl_2: 8.5/1.5) = 0.364.

***c*-5a$_3$.** Appearance: Orange crystalline niddle or orange powder. ^{1}H NMR ($CDCl_3$): δ 0.44 (s, 18H, CH_3), 4.00 - 4.40 (br. s, 8H, C_5H_4), 4.47 (s, 16H, C_5H_4), 4.50 - 4.90 (br. s, 8H, C_5H_4). ^{13}C NMR ($CDCl_3$): δ -7.97 (CH_3), 69.05 (*ipso*-C of C_5H_4), 70.50 – 72.00 (1 br. signal) and 72.50-76.50 (2 br. signals) (α-C and β-C of C_5H_4). ^{119}Sn NMR ($CDCl_3$): δ -20.02. MS (70 eV, EI): m/z (rel intens) 998 (100) [M^+], 650 (60) [$C_{23}H_{24}Fe_2Sn_2^+$], 620 (19) [$C_{213}H_{19}Fe_2Sn_2^+$]. HRMS (EI; m/z): calcd for $C_{36}H_{42}Fe_3Sn_3$, 997.8399; found,

997.8389. Anal. Calcd for $C_{24}H_{28}Fe_2Sn_2$ (665.59): C, 43.31; H, 4.24. Found: C, 43.01; H, 4.06. R_f (hexanes/CH_2Cl_2: 8.5/1.5) = 0.206.

Synthesis of poly(ferrocenyldibutylstannane) ($5b_n$). As described for the synthesis of compound $\mathbf{5a_n}$, the reaction of nBu$_2$SnCl$_2$ (5.32 g, 17.5 mmol) in thf (110 ml) and $(LiC_5H_4)_2Fe{\cdot}2/3$tmeda (4.83 g, 17.5 mmol) in thf (110 mL) afforded $\mathbf{5b_n}$ as a red oil (7.08 g, 97%). Compound $\mathbf{5b_n}$ was further purified by filtration chromatography by using silica gel as column material and thf as eluent (5.34 g, 73%).

Isolation and identification of *c*-$5b_2$, *c*-$5b_3$, *l*-$5b_2$, *l*-$5b_3$, and *l*-$5b_4$. Flash chromatography of $\mathbf{5b_n}$ was performed on silica gel using a solvent mixture of hexane and CH_2Cl_2 (8.5:1.5). Several orange bands of different compounds were separated into the column and were collected in separate vessels. Seven fractions were collected which were identified as: ***c*-$\mathbf{5b_2}$** (first fraction), ***c*-$\mathbf{5b_3}$** (second fraction), a mixture of several compounds including species ***c*-$\mathbf{5b_3}$** (third and fourth fraction), ***l*-$\mathbf{5b_2}$** (fifth fraction), ***l*-$\mathbf{5b_3}$** (sixth fraction), ***l*-$\mathbf{5b_4}$** (seventh fraction). The crystallization of ***c*-$\mathbf{5b_3}$** into column material prevented further separation of compounds from third and fourth fractions. Species ***c*-$\mathbf{5b_2}$** (5.4%) and ***c*-$\mathbf{5b_3}$** (6.0%) were further purified by crystallization into a mixture of hexane and CH_2Cl_2 (9:1). A major portion of $\mathbf{5b_n}$ was trapped into silica gel, which was further recovered by using thf as eluent.

***c*-$\mathbf{5b_2}$.** Appearance: Dark red crystalline block or orange powder. ^{1}H NMR (C_6D_6): δ 0.92 (t, 12H, CH_3 of nBu), 1.21 (t, 8H, CH_2 of nBu), 1.37 (m, 8H, CH_2 of nBu), 1.67 (p, 8H, CH_2 of nBu), 4.30, 4.35 (pst, 16H, C_5H_4). ^{13}C NMR (C_6D_6): δ 12.87, 13.91, 27.54, 29.34 (nBu), 68.57 (*ipso*-C of C_5H_4), 70.75, 75.03 (α-C and β-C of C_5H_4). ^{119}Sn NMR (C_6D_6): δ -28.46. MS (70 eV, EI): m/z (rel intens) 834 (43) [M^+], 777 (100) [M^+- nBu],

663 (21) [M^+- 3*n*Bu], 606 (16) [M^+- 4*n*Bu], 368 (63) [$C_{15}H_{12}FeSn^+$], 304 (28) [$C_{10}H_8FeSn^+$]. HRMS (EI; m/z): calcd for $C_{36}H_{52}Fe_2Sn_2$, 834.0839; found, 834.0806. Anal. Calcd for $C_{36}H_{52}Fe_2Sn_2$ (833.91): C, 51.85; H, 6.29. Found: C, 51.52; H, 5.91. R_f (hexanes/CH_2Cl_2: 8.5/1.5) = 0.756.

***c*-5b$_3$.** Appearance: Orange crystalline block or orange powder. ^{1}H NMR (C_6D_6): δ 0.93 (t, 18H, CH_3 of *n*Bu), 1.27 (br. m, 12H, CH_2 of *n*Bu), 1.41 (m, 12H, CH_2 of *n*Bu), 1.75 (br. m, 12H, CH_2 of *n*Bu), 4.17, 4.45, 4.63, 4.98 (br. signal, 24H, C_5H_4). ^{13}C NMR (C_6D_6): δ 12.32, 13.93, 27.57, 29.63 (*n*Bu), 69.40 (*ipso*-C of C_5H_4), 71.00, 71.97, 74.40, 75.86 (br. signals, α-C and β-C of C_5H_4). ^{119}Sn NMR (C_6D_6): δ -27.61. MS (70 eV, EI): m/z (rel intens) 1250 (90) [M^+], 847 (16) [$C_{34}H_{33}Fe_3Sn_2^+$], 777 (100) [$C_{32}H_{43}Fe_2Sn_2^+$], 661 (34) [$C_{24}H_{23}Fe_2Sn_2^+$], 604 (46) [$C_{20}H_{14}Fe_2Sn_2^+$], 545 (79) [$C_{15}H_{15}Fe_2Sn_2^+$]. HRMS (EI; m/z): calcd for $C_{54}H_{78}Fe_3Sn_3$, 1250.1210; found, 1250.1206. Anal. Calcd for $C_{36}H_{52}Fe_2Sn_2$ (1250.86): C, 51.85; H, 6.29. Found: C, 51.13; H, 5.99. R_f (hexanes/CH_2Cl_2: 8.5/1.5) = 0.649.

***l*-5b$_2$.** Appearance: Orange solid. ^{1}H NMR (C_6D_6): δ 0.96 (t, 6H, CH_3 of *n*Bu), 1.28 (t, 4H, CH_2 of *n*Bu), 1.46 (m, 4H, CH_2 of *n*Bu), 1.77 (p, 4H, CH_2 of *n*Bu), 4.08 (s, 10H, C_5H_5), 4.14, 4.28 (pst, 8H, C_5H_4). ^{13}C NMR (C_6D_6): δ 11.99, 13.95, 27.79, 29.58 (*n*Bu), 68.50 (C_5H_5), 68.76 (*ipso*-C of C_5H_4), 70.96, 74.73 (α-C and β-C of C_5H_4). ^{119}Sn NMR (C_6D_6): δ -28.35. MS (70 eV, EI): m/z (rel intens) 604 (51) [M^+], 547 (100) [M^+- *n*Bu], 490 (20) [M^+- 2*n*Bu], 370 (94) [$C_{15}H_{14}FeSn^+$], 305 (19) [$C_{10}H_9FeSn^+$], 185 (19) [$C_{10}H_9Fe^+$]. HRMS (EI; m/z): calcd for $C_{28}H_{36}Fe_2Sn$, 604.0555; found, 604.0538. Anal. Calcd for $C_{28}H_{36}Fe_2Sn$ (602.99): C, 55.77; H, 6.02. Found: C, 55.65; H, 5.99. R_f (hexanes/CH_2Cl_2: 8.5/1.5) = 0.410.

***l*-5b$_3$.** Appearance: Orange gummy material. ^{1}H NMR (C_6D_6): δ 0.98 (t, 12H, CH_3 of *n*Bu), 1.33 (t, 4H, CH_2 of *n*Bu), 1.48 (m, 4H, CH_2 of *n*Bu), 1.79 (p, 4H, CH_2 of *n*Bu), 4.08 (s, 10H, C_5H_5), 4.16, 4.21, 4.29, 4.39 (pst, 16H, C_5H_4). ^{13}C NMR (C_6D_6): δ 11.97, 13.99, 27.83, 29.62 (*n*Bu), 68.56 (C_5H_5), 68.80, 69.19 (*ipso*-C of C_5H_4), 70.99, 71.38, 74.77, 74.81 (α-C and β-C of C_5H_4). ^{119}Sn NMR (C_6D_6): δ -28.39. MS (70 eV, EI): m/z (rel intens) 1020 (100) [M^+], 604 (19) [$C_{28}H_{36}Fe_2Sn^+$], 546 (85) [$C_{24}H_{26}Fe_2Sn^+$]. HRMS (EI; m/z): calcd for $C_{46}H_{62}Fe_3Sn_2$, 1020.0964; found, 1020.0938. R_f (hexanes/CH_2Cl_2: 8.5/1.5) = 0.286.

***l*-5b$_4$.** Appearance: Orange gummy material. ^{1}H NMR (C_6D_6): δ 0.98 (m, 18H, CH_3 of *n*Bu), 1.34 (t, 8H, CH_2 of *n*Bu), 1.38 (t, 4H, CH_2 of *n*Bu), 1.49 (m, 12H, CH_2 of *n*Bu), 1.81 (m, 12H, CH_2 of *n*Bu), 4.09 (s, 10H, C_5H_5), 4.16, 4.21, 4.23, 4.29 (pst, 16H, C_5H_4), 4.41 (pst, 8H, C_5H_4). ^{13}C NMR (C_6D_6): δ 11.98, 14.00, 27.87, 29.63 (*n*Bu), 68.81 (C_5H_5), 69.22, 69.25, 69.56 (*ipso*-C of C_5H_4), 70.99, 71.40, 71.42, 74.78, 74.82, 74.85 (α-C and β-C of C_5H_4). ^{119}Sn NMR (C_6D_6): δ -28.39. MS (70 eV, EI): m/z (rel intens) 1436 (28) [M^+], 1020 (59) [$C_{46}H_{62}Fe_3Sn_2^+$], 604 (34) [$C_{28}H_{36}Fe_2Sn^+$], 547 (100) [$C_{24}H_{27}Fe_2Sn^+$]. HRMS (EI; m/z): calcd for $C_{64}H_{88}Fe_4Sn_3$, 1436.1386; found, 1436.1338. R_f (hexanes/CH_2Cl_2: 8.5/1.5) = 0.196.

Single-crystal X-ray analysis of *c*-5a$_2$ and *c*-5a$_3$. Single crystals of ***c*-5a$_2$** and ***c*-5a$_3$** were coated with Paratone-N oil, mounted using a Micromount™ (*MiTeGen* - Microtechnologies for Structural Genomics), and frozen in the cold stream of the Oxford cryojet attached to the diffractometer. All measurements were made on a Nonius KappaCCD 4-Circle Kappa FR540C diffractometer using monochromated Mo K_α radiation at -100 °C. An initial orientation matrix and cell was determined from 10

frames using ϕ-scans. Data =was collected using ϕ- and ω-scans.[26] Cell parameters were initially retrieved using the COLLECT[26] software and then refined with the HKL DENZO and SCALEPACK software.[11] Data reduction was performed with the HKL DENZO and SCALEPACK software,[27] which corrects for beam inhomogeneity, possible crystal decay, Lorentz and polarization effects. A multiscan absorption correction was applied (SCALEPACK).[27] The structure was solved using direct methods (SIR-2004)[28] and refined by full-matrix least-squares method on F^2 with SHELXL97-2.[29] The non-hydrogen atoms were refined anisotropically. Hydrogen atoms were included at geometrically idealized positions (C-H bond distances 0.95/0.98/0.99 Å) and were not refined. The isotropic thermal parameters of these hydrogen atoms were fixed at 1.2 times that of the preceding carbon atom. Neutral atom scattering factors for non-hydrogen atoms and anomalous dispersion coefficients are contained in the SHELXTL-NT 6.14 program library.[30]

All thermal ellipsoid plots were prepared using ORTEP-3 for Windows.[31]

ACKNOWLEDGMENT

We thank the Natural Sciences and Engineering Research Council (NSERC) of Canada for a Discovery Grant (J.M.). We thank the Canada Foundation for Innovation (CFI) and the government of Saskatchewan for funding of the NMR and XRD facilities in the Saskatchewan Structural Sciences Centre (SSSC). We thank K. Thoms for mass measurements.

ASSOCIATED CONTENT

Supporting Information. NMR spectra of ***c*-5a$_2$**, ***c*-5b$_2$**, ***c*-5a$_3$**, ***c*-5b$_3$**, ***l*-5b$_2$**, ***l*-5b$_3$** and ***l*-5b$_4$**; cyclic voltammograms and AC voltammograms of ***c*-5a$_2$**, ***c*-5b$_2$** and **6b**; rotary-disc voltammograms of **6b**.

REFERENCES

(1) Osborne, A. G.; Whiteley, R. H. *J. Organomet. Chem.* **1975**, *101*, C27-C28.

(2) Braunschweig, H.; Dirk, R.; Müller, M.; Nguyen, P.; Resendes, R.; Gates, D. P.; Manners, I. *Angew. Chem., Int. Ed.* **1997**, *36*, 2338-2340.

(3) (a) Schachner, J. A.; Lund, C. L.; Quail, J. W.; Müller, J. *Organometallics* **2005**, *24*, 785-787. (b) Schachner, J. A.; Lund, C. L.; Quail, J. W.; Müller, J. *Organometallics* **2005**, *24*, 4483-4488.

(4) Osborne, A. G.; Whiteley, R. H.; Meads, R. E. *J. Organomet. Chem.* **1980**, *193*, 345-357.

(5) Rulkens, R.; Lough, A. J.; Manners, I. *Angew. Chem., Int. Ed.* **1996**, *35*, 1805-1807.

(6) Seyferth, D.; Withers, Jr. H. P. *J. Organomet. Chem.* **1980**, *185*, C1-C5.

(7) Butler, I. R.; Cullen, W. R.; Einstein, W. B.; Rettig, S. J.; Willis, A. J. *Organometallics* **1983**, *2*, 128-135.

(8) Rulkens, R.; Gates, D. P.; Balaishis, D.; Pudelski, J. K.; McIntosh, D. F.; Lough, A. J.; Manners, I. *J. Am. Chem. Soc.* **1997**, *119*, 10976-10986.

(9) Foucher, D. A.; Tang, B.-Z.; Manners, I. *J. Am. Chem. Soc.* **1992**, *114*, 6246-6248.

(10) (a) MacLachlan, M. J.; Ginzburg, M.; Coombs, N.; Coyle, T. W.; Raju, N. P.; Greedan, J. E.; Ozin, G. A.; Manners, I. *Science* **2000**, *287*, 1460-1463. (b) Peter, M.;

Lammertink, R. G. H.; Hempenius, M. A.; Vancso, G. J. *Langmuir* **2005**, *21*, 5115-5123. (c) Ma, Y. J.; Dong, W. F.; Hempenius, M. A.; Möhwald, H.; Vancso, G. J. *Nature Mater.* **2006**, *5*, 724-729. (d) Lu, J.; Chamberlin, D.; Rider, D. A.; Liu, M. Z.; Manners, I.; Russell, T. P. *Nanotechnology* **2006**, *17*, 5792-5797. (e) Arsenault, A. C.; Puzzo, D. P.; Manners, I.; Ozin, G. A. *Nature Photonics* **2007**, *1*, 468-472.

(11) Zechel, D. A.; Foucher, D. A.; Pudelski, J. K.; Yap, G. P. A.; Rheingold, A. L.; Manners, I. *J. Chem. Soc. Dalton Trans.* **1995**, 1893-1899.

(12) (a) Foucher, D. A.; Edwards, M.; Burrow, R. A.; Lough, A. J.; Manners, I. *Organometallics* **1994**, *13*, 4959-4966. (b) Peckham, T. J.; Massey, J. A.; Edwards, M.; Manners, I. *Macromolecules* **1996**, *29*, 2396-2403. (c) Ieong, N. S.; Manners, I. *Macromol. Chem. Phys.* **2009**, *210*, 1080-1086.

(13) Jäkle, F.; Rulkens, R.; Zech, G.; Foucher, D. A.; Lough, A. J.; Manners, I. *Chem.−Eur. J.* **1998**, *4*, 2117-2128.

(14) Rulkens, R.; Lough, A. J.; Manners, I. *J. Am. Chem. Soc.* **1994**, *116*, 797-798.

(15) Ni, Y.; Rulkens, R.; Manners, I. *J. Am. Chem. Soc.* **1996**, *118*, 4102-4114.

(16) Gädt, T.; Ieong, N. S.; Cambridge, G.; Winnik, M. A.; Manners, I. *Nature Mater.* **2009**, *8*, 144-150.

(17) (a) Bagh, B.; Breit, N. C.; Dey, S.; Gilroy, J. B.; Schatte, G.; Harms, K.; Müller, J. *Chem.–Eur. J.* **2012**, *18*, 9722-9733. (b) Bagh, B.; Breit, N. C.; Gilroy, J. B.; Schatte, G.; Müller, J. Chem. Commun. **2012**, *48*, 7823-7825.

(18) Seyferth, D.; Withers, H. P. *Organometallics* **1982**, *1*, 1275-1282.

(19) Katz, T. J.; Acton, N.; Martin, G. *J. Am. Chem. Soc.* **1969**, *91*, 2804-2805.

(20) Dong, G.; Gang, H.; Chun-ying, D.; Ke-liang, P.; Qing-jin, M. *Chem. Commun.* **2002**, 1096-1097.

(21) (a) Grossmann, B.; Heinze, J.; Herdtweck, E.; Köhler, F. H.; Noth, H.; Schwenk, H.; Spiegler, M.; Wachter, W.; Weber, B. *Angew. Chem., Int. Ed.* **1997**, *36*, 387-389. (b) Köhler, F. H.; Schell, A. *Rapid Commun. Mass Spectrom.* **1999**, *13*, 1088–1090.

(22) Herbert, D. E.; Gilroy, J. B.; Chan, W. Y.; Chabanne, L.; Staubitz, A.; Lough, A. J.; Manners, I.; *J. Am. Chem. Soc.* **2009**, *131*, 14958-14968.

(23) Dong, T. Y.; Hwang, M.; Wen, Y.; Hwang, W. *J. Organomet. Chem.* **1990**, *391*, 377-385.

(24) Rulkens, R.; Lough, A. J.; Manners, I.; Lovelace, S. R.; Grant, C.; Geiger, W. E. *J. Am. Chem. Soc.* **1996**, *118*, 12683-12695.

(25) Butler, I. R.; Cullen, W. R.; Ni, J.; Rettig, S. J. *Organometallics* **1985**, *4*, 2196-2201.

(26) Nonius, B. V. *Nonius Collect*, (1998) Nonius BV, Delft, The Netherlands, Delft, The Netherlands.

(27) (a) Otwinowski, Z.; Minor, W. *Macromolecular Crystallography, Part A*. (b) Carter, C. W.; Sweet, R. M. *Academic Press, London*, **1997**, *276*, 307-326.

(28) Burla, M. C.; Caliandro, R.; Camalli, M.; Carrozzini, B.; Cascarano, G. L.; De Caro, L.; Giacovazzo, C.; Polidori, G.; Spagna, R. *J. Appl. Crystallogr.*, **2005**, *38*, 381-388.

(29) Sheldrick, G. M. *Acta Crystallogr., Sec A*, **2008**, *64*, 112-122.

(30) Bruker, *SHELXTL-NT 6.14: Program Library for Structure Solution and Molecular Graphics*, (2000-2003) Bruker AXS, Inc., Madison, WI.

(31) Farrugia, L. J. *J. Appl. Crystallogr.* **1997**, *30*, 565.

3.4.5. Selective Materials from Supporting Information of Contribution 4

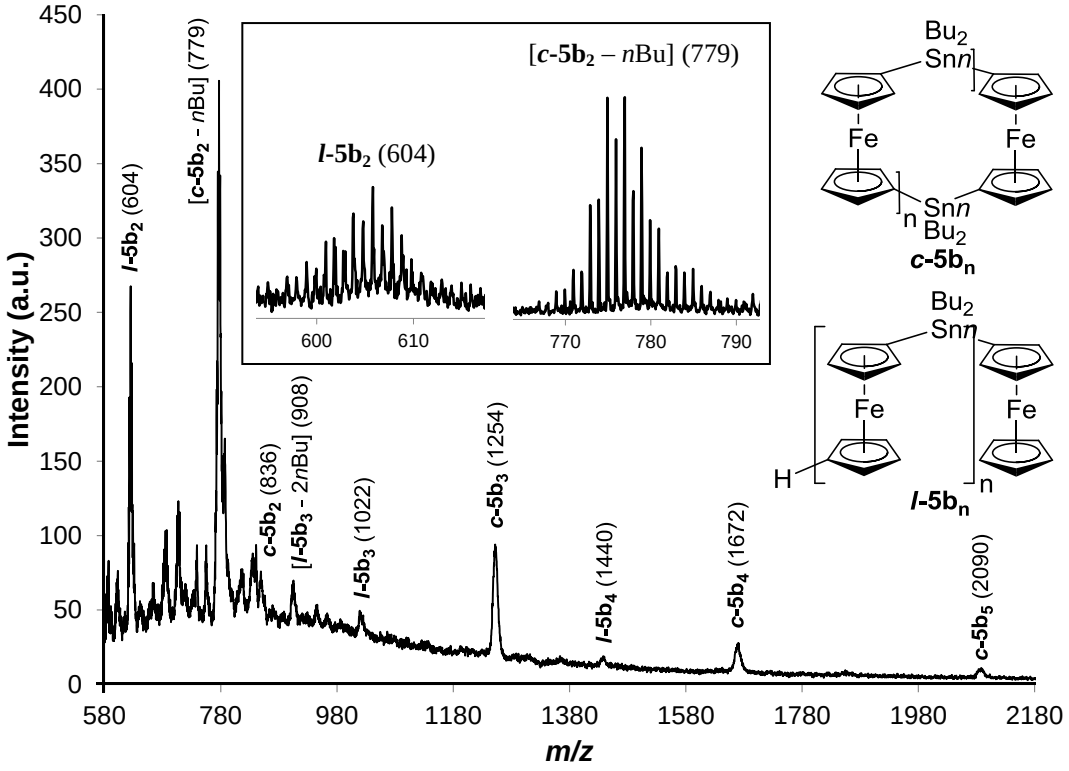

Figure 3-4-S2. MALDI-TOF mass spectrum (linear mode) of **5b$_n$** (box contains the cut out of MALDI-TOF mass spectrum (reflector mode) showing species ***l*-5b$_2$** and [***c*-5b$_2$** – *n*Bu]).

CHAPTER 4
SUMMARY AND CONCLUSIONS

Part A: The results, which have been discussed in Contribution 1, 2, and, 3 of Chapter 1, are summarized in this section.

The primary challenge of this Ph.D. work was to design suitable ligands for the synthesis of heavier group 13 dichloride complexes, which would yield reactive [1]metallocenophanes upon reaction with dilithio-sandwich complexes. My former group members found that heavier group 13 element dichloride decorated with intramolecularly coordinated, sterically bulky ligands such as Pytsi or Me_2Ntsi (Figure 4-1) resulted in strained [1]metallocenophanes. However, dichlorides with the slim ligand Ar′ (Figure 4-1) yielded [1.1]metallocenophanes, which turned out to be not suitable for ROP. Based on this knowledge, my research started with a search for a ligand that allowed the synthesis of strained compounds and, at the same time, wouldn't block its reactivity toward ROP. It began with the idea that increase of steric protection around group 13 elements in (Ar′)ECl_2 (E = Al, Ga, In) would result in a dichloride complex, which would be appropriate for the synthesis of strained [1]metallocenophane. Mamx ligand was choosen for the synthesis of heavier group 13 element dihalide complexes (Figure 4-1). We picked up this ligand because we wanted a group in *ortho* positon at Ar' as structural evidence suggested that this would likely block the formation of unwanted [1.1]FCPs. Therefore, I synthesized aluminum, gallium, and indium dichlorides equipped with the Mamx ligand. NMR spectroscopy suggested that these dichlorides are C_s symmetric on the NMR time-scale. Single-crystal X-ray analysis of (Mamx)$GaCl_2$ confirmed that the nitrogen of the amine arm is indeed coordinated to the group 13 element.

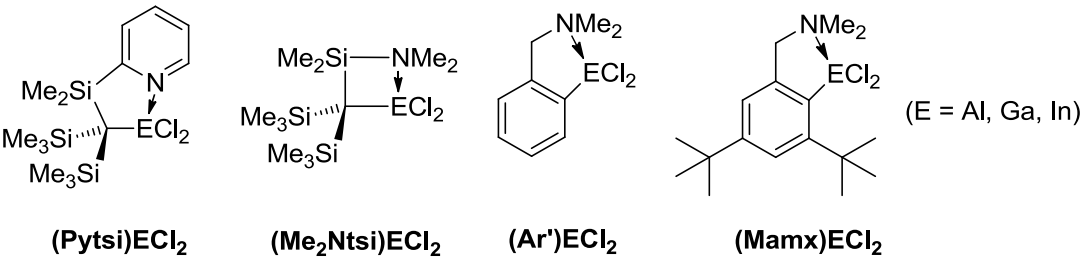

Figure 4-1. Heavier group 13 element dichlorides with intramolecularly coordinated ligands.

(Mamx)$AlCl_2$ and (Mamx)$GaCl_2$ were reacted with dilithioferrocene resulting in an alumina[1]ferrocenophane and a galla[1]ferrocenophane, respectively (Figure 4-2). However, all attemps to isolate these strained sandwich compounds failed as they ring-open polymerized under the reaction conditions of their formation reactions to yield high-molecular-weight poly(ferrocenylalumane) (M_w = 106 kDa) and poly(ferrocenylgallane) (M_w = 36.0 kDa). Similarly, the reaction of (Mamx)$AlCl_2$ with dilithioruthenocene resulted in a reactive alumina[1]ruthenocenophane (Figure 4-2), which spontaneously polymerized in the reaction mixture to give low-molecular-weight poly(ruthenocenylalumane) (M_w = 8.07 kDa). All of the reactive [1]metallocenophanes were characterized by ^{1}H NMR spectroscopy. Surprisingly, the galla[1]ruthenocenophane (Figure 4-2), which formed in the reaction of (Mamx)$GaCl_2$ and dilithioruthenocene, was isolable as a pure compound. It was polymerized using Karstedt's catalyst and yielded poly(ruthenocenylgallane) with M_w of 28.6 kDa. However, the reactivity of the gallium-bridged [1]RCP was not vastly different from the other three [1]metallocenophanes as it also spontaneously polymerized to poly(ruthenocenylgallane) (M_w = 10.1kDa), when it was left in solution for an extended amount of time (6 h). All attempts to crystallize (Mamx)Ga[1]RCP failed and, thus, important structural informations such as tilt angles

could not be obtained. The ^{1}H NMR spectrum of the poly(ferrocenylgallane) displayed some peaks with rich fine structures. As for example, the peak for the *t*Bu group *ortho* to gallium was split into 10 signals. This type of fine splitting arose from the tacticity of the polymer. A less prominent splitting was observed in the ^{1}H NMR spectrum of poly(ferrocenylalumane) and, the other two polymers did not show any fine structure. To gain some structural information of polymers, bis(ferrocenyl) species (Mamx)EFc_2 [E = Al, Ga; Fc = $(C_5H_5)Fe(C_5H_4)$; Figure 4-2] with aluminum and gallium as bridging elements was synthesized by the reaction of lithioferrocene and respective dichlorides. These bis(ferrocenyl) species can be imagined as the smallest repeating units of the respective polymers. They were structurally characterized by single-crystal X-ray analysis. The aluminum-bridged bis(ferrocenyl) species displayed two ferrocene units pointing in opposite direction, whereas the gallium analogue exhibited two parallel ferrocene units.

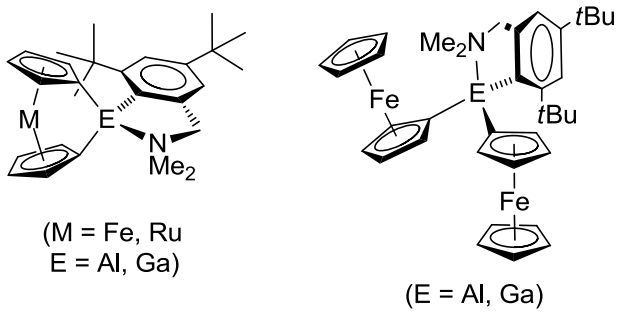

Figure 4-2. Aluminum- and gallium-bridged [1]metallocenophanes and bis(ferrocenyl) species.

We performed DFT calculations to understand the unexpected high reactivity of these new [1]FCPs and [1]RCPs as well as to get some structural informations. Particularly, we intended to find out the structural changes in the strained sandwich compounds caused by the *ortho*-*t*Bu group. The calculated structures showed that the tilt angle α varies in the

range of 13-16° for [1]FCPs, and between 19-23° for [1]RCPs (Table 4-1). These tilt angles are similar to the experimental tilt angles of the previously reported [1]FCPs and [1]RCPs with heavier group 13 elements as bridges. However, other structural informations such as the orientation of the bridging moiety with respect to the sandwich unit suggested that the bulky *ortho-t*Bu group indeed creates a tension in these compounds. The influence of the *ortho-t*Bu group toward the reactivity of the strained species was evaluated by selecting a hydrogenation reaction, where the strained species was transformed into an unstrained species. The average increase of enthalphy caused by the *ortho-t*Bu group was found to be 5.5 kcal/mol, which is a significant increase as compared to the ΔH^{ROP} of dimethylsila[1]ferrocenophane (ΔH^{ROP} = 19 kcal/mol). Therefore, a profound effect of the bulky *ortho-t*Bu group towards the structure and reactivity of [1]metallocenophanes with Mamx ligand was discovered. It is worth to mention that only (Mamx)Ga-bridged [1]RCP was isolable as a pure compound, while the other three [1]metallocenophane polymerized under the conditions of their formation reactions. This result was surprising because [1]RCPs are more strained than that of analogous [1]FCPs. However, we could not provide a reasonable explation.

Table 4-1. Tilt angles [°] of [1]Ferrocenophanes and [1]Ruthenocenophanes.

[1]Ferrocenophanes		[1]Ruthenocenophane	
Ligand/Element	α	Ligand/Element	α
Me_2Ntsi/Al	14.3	Me_2Ntsi/Al	20.3
Mamx/Al	13.2	Mamx/Al	19.4
Me_2Ntsi/Ga	15.8	Me_2Ntsi/Ga	20.9
Mamx/Ga	15.8	Mamx/Ga	22.9

The reaction of indium dichloride equipped with the Mamx ligand with dilithioferrocene was explored. The salt-metathesis resulted in an indium-bridged [1]FCP (19%), a [1.1]FCP (23%), and a poly(ferrocene) (32%) (Figure 4-3). In contrast, the reaction of (Mamx)$InCl_2$ with 1,1′-dilithio-2,2′-di(*iso*-propyl)ferrocene yielded inda[1]ferrocenophane exclusively (Figure 4-3). However, this indium-bridged [1]FCP could not be isolated as a pure compound as it ring-open polymerized under the condition of its formation reaction to give high-molecular weight poly(ferrocenylindane) (M_w = 27.9 kDa). These inda[1]ferrocenophanes are the first two examples of their kind. (Mamx)In-bridged [1.1]FCP displayed two well-separated reversible redox waves in the cyclic voltammogram, showing moderate electronic communication between the iron redox centers.

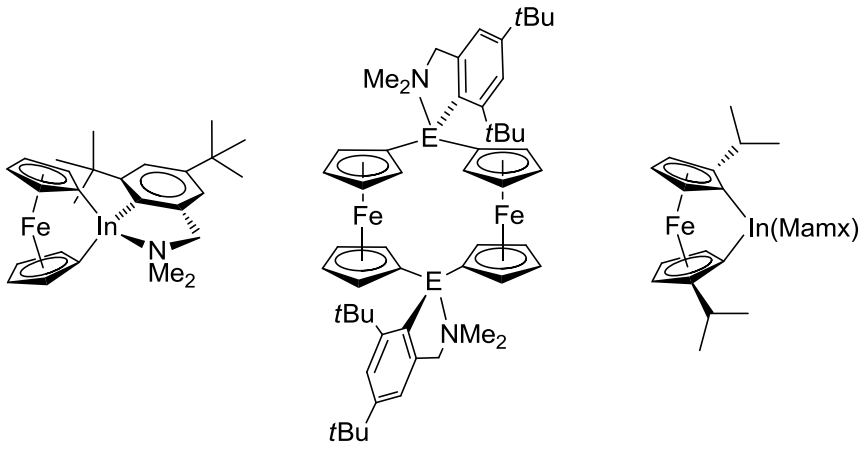

Figure 4-3. Indium-bridged [1]FCPs and [1.1]FCP.

Several conclusions can be drawn from this part of research. First of all, the sterically bulky Mamx ligand has been successfully employed for the synthesis of strained [1]metallocenophanes. It has been re-established that the steric requirements of the ligand connected to the heavier group 13 elements has a profound influence on the outcome of

the salt-metathesis reaction of dilithio-sandwich compounds and element dihalides. As illustrated in Scheme 4-1, the salt-metathesis reaction yields either strained [1]metallocenophane or unstrained [1.1]metallocenophane. In the first step of the reaction, a reactive intermediate (**A**) is formed, which can react intramolecularly to give [1]metallocenophane. Alternatively, the intermediate **A** can react with a second molecule of dilithio-sandwich compound to form an intermediate **B**, which can result in [1.1]metallocenophane. If the ligand R on the element E is bulky, the attack from the second molecule of dilithio-sandwich compound is blocked, and thus, the intramolecular pathway is favored. If the ligand R on the element E is a slim ligand, the intermolecular pathway is favored and [1.1]FCP can be formed. Of course, similar reaction paths can lead to higher oligomers.

Scheme 4-1. Proposed reaction pathways for the formation of [1]- and [1.1]metallocenophane.

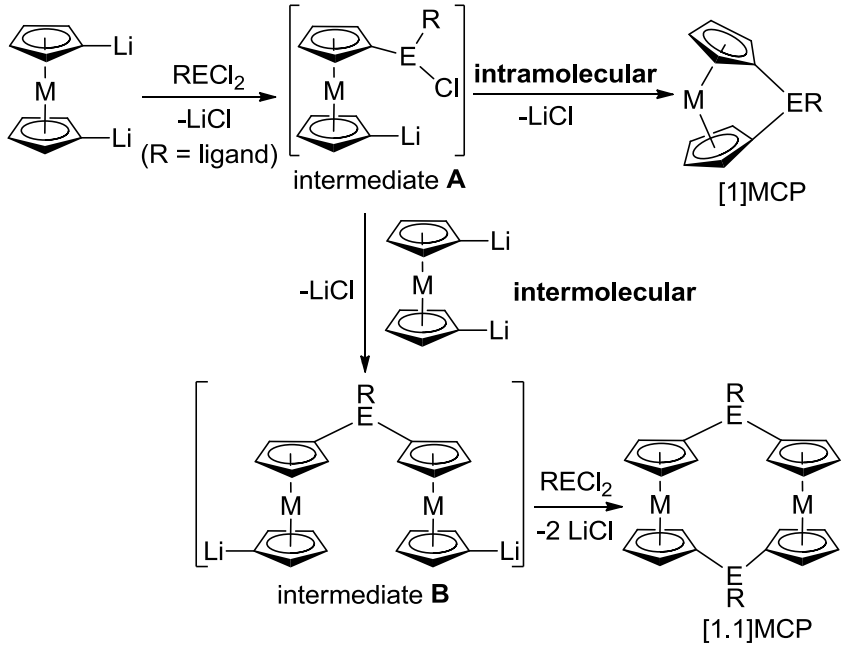

Secondly, the ligand plays a crucial role for the stability of [1]metallocenophane. The Mamx-containing [1]FCPs and [1]RCPs showed a very high reactivity toward ROP. However, previously reported [1]metallocenophanes bridged with heavier group 13 elements were resistant to ROP even though they showed similar tilt angles. We have shown that the *ortho-t*Bu group of the Mamx ligand increases the strain in [1]metallocenophanes.

Thirdly, the effect of the bulky ligand on the stability of the polymer was remarkable. Organometallic aluminum and gallium compounds are usually highly moisture sensitive. Therefore, it was expected that poly(ferrocenylalumane) and poly(ferrocenylgallane) are also moisture sensitive. It was not surprising that poly(ferrocenylalumane) with Mamx ligand degraded upon prolonged (ca. 2 months) storage in air. However, the gallium polymer displayed remarkable stability in air. ^{1}H NMR spectrum of the poly(ferrocenylgallane) did not indicate any sign of degradation after two years of storage in air. DLS analysis resulted in very similar particle size as observed two years ago. It is not surprising that the gallium-polymer is more stable than that of aluminum-analogue, because aluminum is much more Lewis acidic than gallium in general. However, the surprising stability of this gallium-polymer is likely because of the steric protection of the bulky Mamx ligand, which makes the gallium center inaccessible for the reaction with moisture. Due to its airstability, this poly(ferrocenylgallane) is a potential candidate for future applications.

In the context of the steric requirements of the ligand attached to heavier group 13 elements, a future work is proposed. It will be interesting to synthesize similar ligand frameworks, where the bulky *ortho-t*Bu group is replaced by a smaller group, such as a

Me group (Figure 4-4). The outcome of the reaction of dichloride complexes equipped with the proposed ligands and dilithio-sandwich compounds will be worth to find. The ligand with a smaller group might allow the formation of strained [1]metallocenophanes without putting too much pressure on the sandwich unit so that the species can be isolated. Thereafter, the isolated [1]metallocenophanes can be polymerized under controlled reaction conditions.

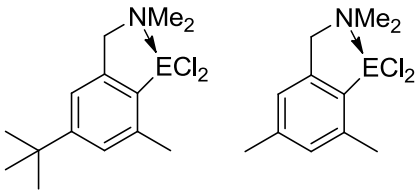

Figure 4-4. Proposed ligand frameworks with less steric protection around heavier group 13 elements.

In contrast to the the reaction of Al and Ga dihalides equipped with the Mamx ligand, the salt metatheis reaction of (Mamx)$InCl_2$ and dilithioferrocene gave mixtures of [1]FCP, [1.1]FCP and oligomer. It can be concluded that the steric requirement that is provided by the Mamx ligand alone, is not sufficient for a selective formation of an inda[1]ferrocenophane. Providing additional steric bulk from the ferrocene unit by two *i*Pr groups makes the salt metathesis reaction more selective, however, that indium-bridged [1]FCP was unstable. This instability might be a result of steric repulsion between the bulky groups on ligand and ferrocene unit. More effort is needed to isolate this In[1]FCP and analyse the molecular structure. The structural characterization could provide useful information regarding its stability. In this context, DFT calculation might again be a useful tool.

Part B: This section offers a summary of results shown in Chapter 2. The slim ligands *p*-$SiMe_3Ar'$ and Mpysm were selected for the synthesis of aluminum- and gallium-bridged [1.1]FCPs. At first, aluminum and gallium dichloride complexes equipped with these ligands were synthesized in good to moderate yields [(*p*-$SiMe_3Ar'$)$AlCl_2$: 73%, (*p*-$SiMe_3Ar'$)$GaCl_2$: 65%, (Mpysm)$AlCl_2$: 47%, (Mpysm)$GaCl_2$: 50%] (Figure 4-5). Thereafter, the dichlorides were reacted with dilithioferrocene to synthesize respective [1.1]FCPs. Though aluminum- and gallium-bridged [1.1]FCPs with the *p*-$SiMe_3Ar'$ ligand were only isolated in moderate yields (Al[1.1]FCP: 43%, Ga[1.1]FCP: 47%) (Figure 4-6), the species with Mpysm ligands could not be isolated at all. The molecular structures of (*p*-$SiMe_3Ar'$)Al- and (*p*-$SiMe_3Ar'$)Ga-bridged [1.1]FCP were determined by single-crystal X-ray analysis. Both species are isostructural to each other and crystallized as *anti* isomers. All dichloride complexes were also utilized for the synthesis of aluminum- and gallium-bridged bis(ferrocenyl) species [(*p*-$SiMe_3Ar'$)$AlFc_2$: 47%, (*p*-$SiMe_3Ar'$)$GaFc_2$: 41%, (Mpysm)$AlFc_2$: 21%, (Mpysm)$GaFc_2$: 33%; Fc = $(C_5H_5)Fe(C_5H_4)$] (Figure 4-6). Moreover, the two bis(ferrocenyl) species Me_2SiFc_2 and Et_2SiFc_2 were also prepared in good yields (Me_2SiFc_2: 70%, Et_2SiFc_2: 72%) (Figure 4-6).

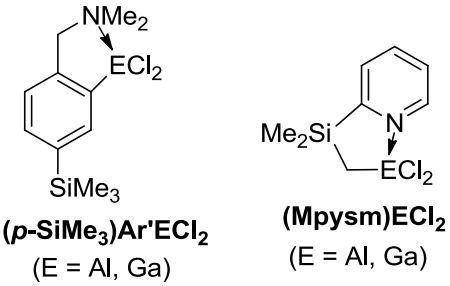

Figure 4-5. Aluminum- and gallium dichlorides with ligands *p*-$SiMe_3Ar'$ and Mpysm.

The electrochemical behavior of [1.1]FCPs [(*p*-$SiMe_3Ar'$)Al- and (*p*-$SiMe_3Ar'$)Ga-bridged [1.1]FCP] and bis(ferrocenyl) species [(*p*-$SiMe_3Ar'$)$AlFc_2$, (*p*-$SiMe_3Ar'$)$GaFc_2$,

(Mpysm)$AlFc_2$, (Mpysm)$GaFc_2$, (Mamx)$AlFc_2$, (Mamx)$GaFc_2$, Me_2SiFc_2, and Et_2SiFc_2] were investigated by cyclic voltammetry. The gallium-bridged [1.1]FCP displayed two reversible redox waves irrespective of solvents (thf and CH_2Cl_2). The separation of the two redox waves ($\Delta E^{\circ\prime}$) decreased from CH_2Cl_2 to thf, which is a well-established influence of solvent's donor ability already known in literature. The analogous aluminum species displayed two major redox waves in CH_2Cl_2 and complicated electrochemistry in thf. All of the gallium- and silicon-bridged bis(ferrocenyl) species exhibited two reversible redox waves in CH_2Cl_2 and one redox wave in thf. The electrochemistry of all aluminum-bridged bis(ferrocenyl) species were problematic with the only exception of (Mamx)$AlFc_2$. The cyclic voltammogram of (Mamx)$AlFc_2$ showed two reversible redox waves in CH_2Cl_2 and one redox wave in thf.

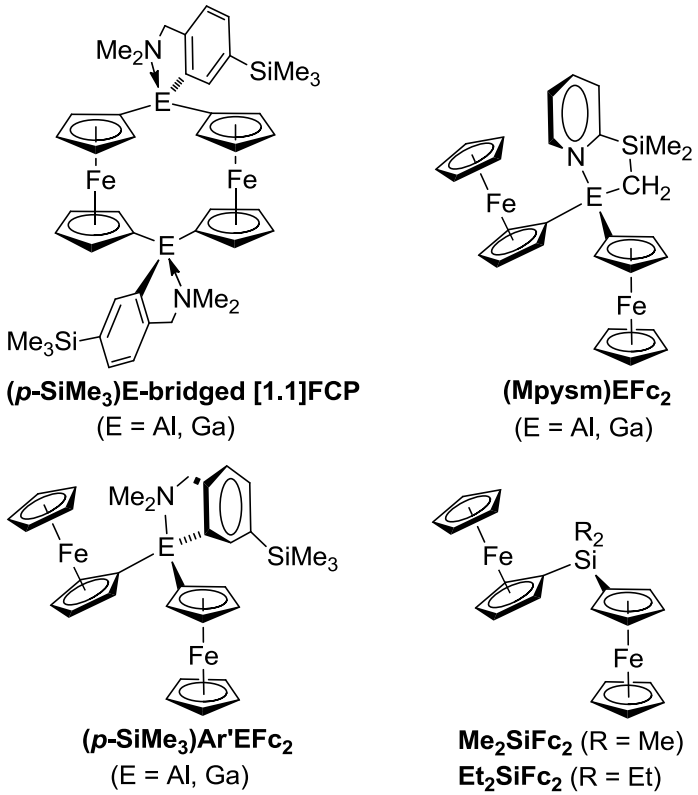

Figure 4-6. [1.1]FCPs and bis(ferrocenyl) species with aluminum, gallium and silicon as bridging elements.

To enrich the chemistry of [1.1]metallocenophanes, a new synthetic strategy was developed for the preparation of unsymmetrically bridged [1.1]FCPs that contain two different bridging elements in the same molecule (Figure 4-7). The starting materials, $Me_2Si(FcBr)_2$ and $Et_2Si(FcBr)_2$ [FcBr = $(C_5H_4Br)Fe(C_5H_4)$] were prepared in moderate yields [$Me_2Si(FcBr)_2$: 55%, $Et_2Si(FcBr)_2$: 69%] (Figure 4-7). The lithiation of those species followed by the addition of dialkyltin dichlorides (alkyl = Me, *n*Bu, *t*Bu) resulted in a mixture of poly(ferrocene)s that contained silicon and tin as alternative bridging elements. GPC and DLS analysis of those polymers suggested that they were low-molecular-weight oligomers (M_w: 2100 to 6300 Da). MALDI-TOF mass analysis revealed the presence of linear and cyclic species with up to 20 ferrocene units. Some species such as silastanna[1.1]ferrocenophanes and cyclic tetramers (Figure 4-7) were isolated in low yields from the oligomeric mixtures either by column chromatography or by crystallization. The molecular structures of those cyclic tetramers were determined by single-crystal X-ray analysis. Electrochemical analysis of those [1.1.1.1]FCPs displayed three reversible redox waves correspond to one, one and two electrons, respectively, which suggested stepwise oxidations of two iron centers followed by the oxidation of the remaining two irons.

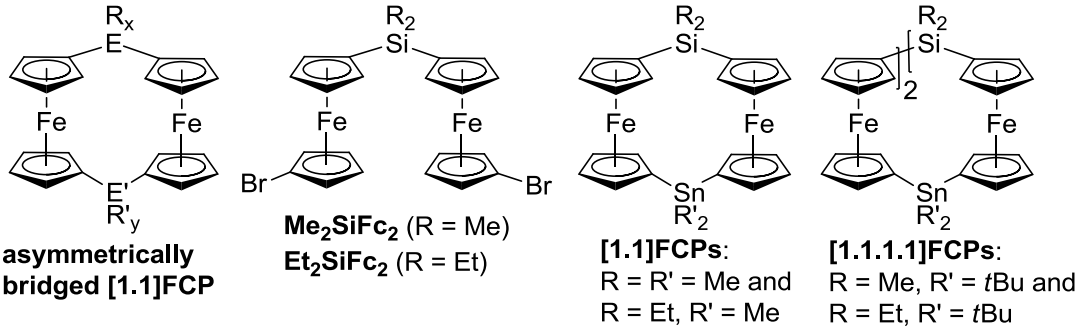

Figure 4-7. Ferrocene derivatives with silicon and tin as bridging elements.

Similarly, the lithiation of $Me_2Si(FcBr)_2$ followed by the addition of gallium dichlorides [(Ar′)$GaCl_2$ and (*p*-$SiMe_3$Ar′)$GaCl_2$] resulted in silagalla[1.1]ferrocenophanes (Figure 4-8) in moderate yields (29% and 41%) and oligomers were isolated from the reaction mixtures. MALDI-TOF mass analysis showed the presence of cyclic species and three different linear species with up to 16 ferrocene units. Single-crystal X-ray analysis of silagalla[1.1]ferrocenophanes revealed that they exist as *anti* isomers. The cyclic voltammograms of these [1.1]FCPs displayed two reversible redox waves, showing stepwise oxidation of two iron redox centers.

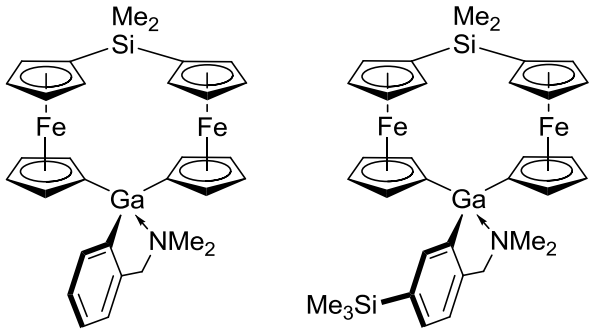

Figure 4-8. Silagalla[1.1]ferrocenophanes.

Two published reactions of Me_2SnCl_2 and *n*Bu_2SnCl_2 with dilithioferrocene were reinvestigated. As reported before, those reactions resulted in low-molecular-weight poly(ferrocenylstannane)s, which were analyzed by MALDI-TOF mass spectrometry. [1.1]FCPs and [1.1.1]FCPs (Figure 4-9) were isloated and their molecular structures were determined by single-crystal X-ray analysis. All these cyclic species show fluxional behavior in solution which was investigated by ^{1}H NMR spectroscopy. Some linear species were isolated as well. The metal-metal interactions in all isolated species were

studied by different electrochemical methods. All species displayed stepwise oxidation of the iron redox centers.

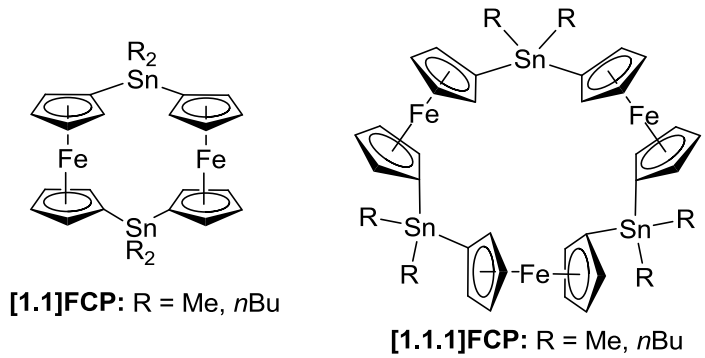

Figure 4-9. Tin-bridged [1.1]FCPs and [1.1.1]FCPs.

Several conclusions can be drawn from these results. All of [1.1]FCPs displayed moderate electronic communication between the two iron centers with two reversible redox waves, thus, they are classified as class II compounds according to Robin-Dey classification. Similarly, gallium- and silicon-bridged bis(ferrocenyl) species also belong to class II compounds as they displayed two well resolved redox waves in CH_2Cl_2. The problematic electrochemistry displayed by aluminum-bridged bis(ferrocenyl) species might be because of the instability of aluminum species under electrochemical conditions. It is well known that aluminum-species are much more reactive than analogous gallium species. However, (Mamx)$AlFc_2$ exhibited very similar electrochemistry as compared to the gallium analogue. The possible reason is that the aluminum center in (Mamx)$AlFc_2$ is sterically protected by the bulky Mamx ligand.

We have developed a synthetic method that allowed the formation of unsymmetrically bridged [1.1]FCPs. Though silastanna[1.1]ferrocenophanes were isolated in very poor yields (3 and 7%), the yields were improved by several times for

silagalla[1.1]ferrocenophanes (29 and 41%) by carefully selecting the ligand framework on the second bridging element. This novel synthetic method also allowed the formation of poly(ferrocene)s with linear and cyclic structures. The low-molecular-weight of these polymers is attributed to the early chain termination. More researchs need to be done to prevent premature chain termination, and thus, high-molecular-weights of this type of polymers can be achieved.